MITIGATION OF COMPARTMENT JET FIRES USING WATER SPRAYS

By

KHALID SAAD ALAGEEL

Thesis submitted to the University of Sheffield in partial fulfilment of the requirements for the degree of Doctor of Philosophy.

Department of Chemical and Process Engineering

The University of Sheffield

November, 1999

ACKNOWLEDGEMENTS

I would like to express my gratitude and sincere thanks to Dr BCR Ewan and Professor Jim Swithenbank for their invaluable and continual advice, supervision and support throughout this work, which would not have been completed without their help.

I am particularly grateful to Dr. P. J. Foster for his diligent help, encouragement and many helpful suggestions in the radiation modelling.

Special thanks also to Mr. Mike O'Meara and David Palmer from Buxton Lab for their help in the running of the experimental work.

Thanks are due to Mr. Djibril for proof reading the thesis.

I would like also to acknowledge the support of my colleagues.

The author is also indebted to the Ministry of Interior in Saudi Arabia for their financial sponsorship.

Last but not certainly the least, I would like to express sincere appreciation to my wife for being so supportive and understanding.

To The Memory of My Father

Who would have been very proud of this achievement

To My Mother

For her patient suffering while I was away

To Akeel

Who has always been a very kind brother_ I am proud of him

SUMMARY

The safe design and operation of Process plants requires an ability to predict hazard consequences reliably. One particular hazard is a jet fire that might arise from the ignition of an accidental release of pressurised gas or liquid. On offshore gas and oil production platforms and also on land-based gas facilities, accidental releases might occur of high pressure natural gas sometimes containing higher molecular weight components.

Industries continue to seek efficient and cost-effective means of protecting their plants and personnel from the hazards of fires. Following disasters which occurred in the past, the need for effective mitigation systems has, once again, been highlighted. Mitigation systems involving agents such as halons, which are perceived to be environmentally damaging, are currently out of favour and interest has revived in the use of water sprays.

The research work presented here addresses the problem of the suppression of a compartment jet fire by water sprays. This involved studying the interaction between water spray and a turbulent jet flame inside a compartment of dimension 6×2.4×2.4 m^3. The fuel used for the jet fire was propane emerging from a 2.0 cm diameter vertical nozzle and at a mass flow rate of 0.1 kg/s.

The objectives of the research are to investigate the mitigation of compartment jet fires by using water sprays by the application of a computational fluid dynamics (CFD) methodology incorporating

combustion and a radiation model to study the jet fire behaviour and the temperature distribution in a compartment. In order to achieve the above objectives, it is necessary to produce a workable CFD model of an offshore module.

The radiative heat exchange is considered in the modelling by using the Discrete Transfer Radiation Method (DTRM).

The study of the sprays requires details of the individual drops' sizes. The Malvern Particle Sizer was used to measure the drop size of water sprays from the different spray nozzles which have been investigated in this study. The obtained drop sizes of the spray nozzles investigated are used to model the spray in FLUENT, which is a well developed CFD package used in industry and university research.

The research started with the CFD modelling of the compartment fire, followed by experimental work done at the university laboratory at Buxton to validate the result of the modelling.

In contrast to previous studies in which the combustion reaction was treated as a simple heat source this CFD has included a model of the combustion reaction.

Comparisons are made between the experimental data and the predictions of different scenarios (i.e. steady state, different water spray arrangement and time dependent). The predicted temperature distributions from FLUENT, which includes radiation and surface heat transfer, are found to be in close agreement with the experimental data.

Modelling results showed that the current version of the CFD code is able to provide a satisfactory and practical means of modelling jet fire and extinguishment processes.

TABLE OF CONTENTS

Nomenclature

A	area [m^2]
a	absorption coefficient [m^{-1}]
C_ε	turbulence model constant
Ci',s	vapor concentration at the droplet surface [mol/m^3]
$C_{i',\infty}$	vapor concentration in the gas [mol/m^3]
c_p	specific heat capacity [J/kg K]
D_p	particle diameter [m]
$D_{i',m}$	binary diffusion coefficient [dimensionless]
F_j	external body forces [N]
G_k	rate of production of turbulent kinetic energy (equation 4.5)
g_j	gravitational acceleration [m/s^2]
h_c	convective heat transfer coefficient [W/m^2K]
h	enthalpy [J/kg]
h_{ext}	external heat transfer coefficient defined by the user [$W/m^2.K$].
h_f	fluid-side local heat transfer coefficient [$W/m^2.K$].
h_{fg}	vaporisation enthalpy [J/kg]
h_w	wall enthalpy, $c_w(T-T_{ref})$ [J/kg].
I	radiation intensity.
$J_{i'}$	flux of species i [kg/s m^2].
k	kinetic energy of turbulence [W].
κ	Thermal conductivity [W/m-K)
k_c	mass transfer coefficient (m/s)
M	molecular weight [kg/kmol].

$m_{i'}$	mass fraction of species *i'* [dimensionless].
m_p	mass of the particle [kg].
N	number of chemical species [dimensionless]
$N_{i'}$	molar flux of vapour [mol/m^2-s]
Nu	Nusselt number [dimensionless].
p	static pressure [Pa].
Pr	Prandtl number [dimensionless].
q	heat transfer rate, kJ per unit time.
q''	convective heat flux from the wall [W/m^2].
q''_{rad}	radiative heat flux [W/m^2].
$\dot{q}$	internal heat generation rate per unit volume
R	gas constant [J/kg K]
Re	Reynolds number
Sc	Schmidt number [dimensionless]
S_h	source term [W]
S_m	mass source term due to dispersed second phase [kg]
t	time [s]
T	temperature [K]
T_{cw}	local temperature of the conducting walls [K]
T_w	interior wall surface temperature [K].
T_{ow}	exterior wall surface temperature [K]
T_∞	is the temperature of the radiation source or sink on the exterior of the domain [K].
T_{ext}	external heat sink temperature defined by the user [K].
T_f	local fluid temperature [K].
u	axial velocity [m/s]

v	velocity in j direction [m/s]
w	velocity in k direction [m/s]
$\mathbf{v}$	velocity vector [m/s]
V_i	diffusion velocities [m/s]
X	mole fraction [dimensionless]

Greek Symbols

Δ	increment [dimensionless]
ε_p	particle emissivity [dimensionless]
ε_{ext}	is the emissivity of the external wall surface [dimensionless]
ε	dissipation of k [m^2/s^3]
μ	viscosity [N s/m^2]
μ_t	turbulent viscosity [N s/m^2]
θ_R	radiative temperature [K]
ρ	density [kg/m^3]
ρ_w	Wall density [kg/m^3].
σ	Stefan-Boltzmann constant [5.67×10^{-8} W/m^2 K^4]
τ_{ik}	viscous stress tensor [J]
Δn	distance between wall surface and the conducting wall cell-centre [m].
Δx	wall thickness [m]

Subscripts

cw	conducting wall
c	convection
p	particle
∞	continuous phase
f	fluid

p0	particle at initial conditions
r	radiation
R	reference
v0	volatile at initial conditions
w	wall

Superscripts

0	reference state
'	fluctuating component

CHAPTER 1
INTRODUCTION

Accidents involving fire have occurred ever since man began to use flammable liquids and gases as fuels (CCP, 1994). Fire is a main cause of loss in the process industries. In particular, fire causes extensive property damage. In fact most accidents with large loss of life which are reported in the loss prevention literature (Lees, 1991 and Vervalin, 1984) are explosions. Explosions are frequently followed by fires, but it is usually the former which are most lethal.

A list of some major fires in the process industries are listed in table (1.1) below:

Date	Location	Chemical involved	Consequences	
			Death	Injuries
1944	Cleveland, Ohio, USA	LNG	136	200-400
1962	Ras Tanura, Saudi Arabia	Propane	1	114
1966	Feyzin, France	Propane	18	90
1972	Lynchburg, VA., USA	Propane	2	3
1973	Austin, Texas, USA	NGL	6	2
1973	Staten Island, NY., USA	LNG	40	-
1978	San Carlos de la Rapita	Propylene	211	-
1978	Santa Cruz, Mexico	Methane	52	-
1984	Mexico City, Mexico	LPG	650	2500
1986	Lancaster, KY	Natural Gas	3	-
1987	Grangemouth, UK	Hydrogen	-	-
1988	Port Arthur, TX	Propane	-	-
1988	Piper Alpha, North sea	Oil, gas	167	-
1989	Richmond, CA	Hydrogen	-	-
1990	Denver, CO	Jet Fuel	-	-
1990	Warren, PA	LPG	-	-
1990	Stanlow, UK	Reaction Mixture	1	5
1991	Haifa, Israel	Chemicals	-	-
1994	Dronka, Egypt	Fuel	410	-
1995	Ukhta, Russia	Gas	-	-

Table (1.1). Some of the major fires [Lees, 1996 and ILO, 1990].

Losses from fire have escalated over the last century. Table (1.2) shows the losses in property damage within the hydrocarbon processing and chemical industries over the period 1953-1982 (Vervalin, 1984). During the first ten years covered in table (1.2), 12 fires and explosion losses only cost $316 million. Frequency of large loss almost tripled during the following decade. From 1973 to 1982 there were four times as many large losses as in the previous ten years. From 1983 to 1992 the total cost of the losses was $2,770,900,000 (Lees, 1996). In the forty-year period covered, trended value of the average loss in each decade has increased from $26,400,000 to $55,418,000, more than 100%.

YEARS	NUMBER OF LOSSES	TOTAL OF ALL LOSSES, TRENDED	AVERAGE LOSS, TRENDED
1953-1962	12	$316,799,000	$26,400,000
1963-1972	32	$841,549,000	$26,298,000
1973-1982	56	$1,900,417,000	$33,936,000
1983-1992	50	$2,770,900,000	$55,418,000
TOTAL	150	$3,058,765,000	$30,588,000

Table (1.2). Analysis of losses of the largest 150 losses [Vervalin, 1984 and Lees, 1996].

Jet fires have been involved in a number of accidents. Perhaps the most dramatic were the large jet flames from the gas riser on the Piper Alpha oil platform. In other

cases jet flames from pressure relief valves have caused adjacent vessels to overheat and burst, giving a boiling liquid expanding vapour explosion, or BLEVE; such was the case in Mexico City.

An understanding of the nature and scope of the fire loss problem is necessary to provide us with a basis for significantly reducing losses. Losses which have occurred offer valuable lessons because they provide the information needed to prevent or reduce the impact of a similar loss in the future.

It is essential, therefore, to understand the way in which fire can occur and develop. Normally, fire can take several different forms as a result of leakage or spillage of fluid from the plant.

Combustion of material which has leaked from a plant may take a number of forms. A leak of gas or liquid may be ignited at the point of issue so that it behaves like a flame on a burner. In some circumstances this flame may be directed like a blow torch at another part of the plant.

1.1 Some Major Incidents

Three incidents will be described in this section in order to show the consequences of these events.

1.1.1 Piper Alpha, North Sea (6 July 1988)

The initial cause of the accident was the tripping out of the operating condensate injection pump. The duty of the condensate system exceeded the initial design and

such problems were not uncommon. Staff started up the spare which had earlier been shut down for maintenance, during which the pressure relief cap had been removed and replaced by a cap that was not leak proof. Clearly there were failures in the communication of information at the change over of shifts in the evening. Gas escaped from the cap and ignited. The resulting explosion destroyed the fire control and communication systems and demolished most of the firewalls. The incoming gas pipeline was ruptured upstream of the emergency isolation valve and the gas burnt as if in a blowtorch and a fireball engulfed the platform. The adjacent rigs continued to feed gas and oil to Piper Alpha for over an hour. Other pipelines ruptured intensifying the fire and eventually most of the platform toppled into the water. The platform controller had tried to enact the practised emergency plan which involved mustering in the galley and then evacuation by helicopter. However the explosions made escape by helicopter impossible. Some survivors escaped by jumping into the sea from a height of up to 50 m or by climbing down knotted ropes, but 167 oil workers were killed, the platform totally destroyed and British hydrocarbon production dropped temporarily by 11%. The Piper Alpha explosion and fire was the worst accident which has occurred on an offshore platform (Lees, 1996).

1.1.2 Mexico City (19 November 1984):

Some 11000 m^3 of LPG was stored in six 1600 m^3 spheres and 48 horizontal cylindrical bullets, all in close proximity. The legs of the spheres were not fireproofed. There was a failure of the overall system of protection (water sprays or

deluge) of large LPG storage. A leak of LPG from 8 inch pipe between one of the spheres and cylindrical bullets formed a vapour cloud which was ignited by a plant flare. The storage area was bunded into 13 separate areas by walls about 1 m high. A fierce fire developed engulfing the spheres which went up one after the other in a series of BLEVEs. Nine explosions were recorded. This series of LPG explosions at the distribution centre resulted in 542 fatalities and over 7000 people being injured. Some 200,000 people were evacuated. The fireballs were up to 300 m in diameter and lasted as long as 20 seconds. Rain consisting of liquid droplets of cooled LPG fell over the housing area covering people and property. It was set alight by the heat from the fireballs. Since the construction of the plant some 100,000 people had settled in crowded housing on the valley floor and slopes. This had spread to within 130 m of the plant. The local housing was mainly of single storey and built of brick between concrete pillars. At least five people lived in each home. LPG was used for heating and cooking and each household had its own small bottles. Some 2000 houses at 300 m were destroyed and 1800 were badly damaged. Windows were broken at 600 m and missiles were thrown a considerable distance. One cylinder was thrown 1200 m (Lees, 1996).

1.1.3 Feyzin, France, (January, 1966)

A tank farm included eight spheres containing propane and butane. A routine drainage operation on a 1200 m^3 sphere was carried out using the wrong procedure. The isolating valves became inoperable and an uncontrolled leak from a propane sphere was ignited by a car on a nearby road. This flashed back to burn as a torch

directly under the sphere. Also propane snow had accumulated within the bund. The refinery fire brigade attempted to put out the fire but ran out of dry foam. The municipal fire company continued to fight the fire using fire water. After 30 minutes the safety valve lifted. An hour later a BLEVE ensued. The fire brigade had concentrated on cooling the other spheres and not the burning sphere on the assumption that the relief valve would provide protection. Approximately 340 m^3 of liquid propane was released and partially vaporised producing a large fireball and ascending mushroom cloud. This BLEVE resulted in over 100 people being killed or injured in its vicinity. One missile broke the legs of an adjacent sphere which contained 857 m^3 of propane. Another piece tipped over another sphere containing 1030 m^3 of butane. Another section travelled 240 m to the south and severed all the product piping connecting the refinery area to the storage area. One fragment broke piping near four floating roof tanks and fires were started in this area. Extensive minor structural damage was caused in the village of Feyzin, a distance centred about 500 m away. Some 2000 people were evacuated from the surrounding area. A further BLEVE and other explosions occurred as the fire spread. Fire fighting continued for a further 48 hours until the three spheres which were still intact and full of propane and butane were cooled to an appropriate level (Vervalin, 1984).

1.2 JET FIRE SCENARIOS

A jet fire is a turbulent diffusion flame resulting from the combustion of a fuel continuously released with some significant momentum in a particular range of directions (Cowley, 1992).

There is a wide variety of situations in which jet flame, or ejected flame, can occur in the process industries, either by design or by accident. The principal situations in which flames occur by design are in burners and flares.

Scenarios involving jet flames are not easy to handle, since a large jet flame may have a substantial 'reach', sometimes up to 50 metres or more.

If a leak forms a continuous jet of gas with significant momentum from process plant, this may ignite and cause a jet fire which would appear as a long narrow flame. Larger leaks may occur due to failure of a vessel, pipe or pump, and smaller ones from flanges, sample and disposing points and other small bore connections. These types of leak will form a jet of vapour containing liquid droplets. In addition to the jet fire arising from leakage in general, there are certain characteristic types of jet fire in process plant. These include well-head blowout fires which are a very large jet fire from a high pressure two-phase release, possibly accompanied by rain-out of burning liquid fuel which might form pool and running liquid fires. Also in offshore, jet fires might result from the failure of an oil riser or a high pressure gas riser.

If the leak forms a liquid pool on the ground this may ignite and burn. The flame may be substantial and may do damage by direct impingement or by radiation.

If the leak gives rise to a gas or vapour cloud which grows for a period before it is ignited, the resultant effect may be either an unconfined vapour cloud explosion or flash fire. In a flash fire the gas could rapidly burn back to the source, but does not explode.

Compartment fire is used to describe a fire burning within a structure where, compared with an open fire, there may be coupling between the fire and the structure, which influences the fire properties and vice versa (Cowley, 1992).

These and other types of fire characteristics of process industries will be described in more details in chapter 2.

1.2.1 European Community Programme

The Commission of the European Communities (CEC) sponsored a project JIVE (Jet-flame Interaction with VEssels) within the STEP programme. The general objective of the study is to assess the behaviour of jet fires impinging on or engulfing obstacles, especially vessels and pipework, and the response of the vessel or pipework and its contents to the fire. It included experimental and theoretical work on free and obstructed jet flames, thermal response of a vessel including the effectiveness of mitigation techniques, and failure modes including full-scale BLEVE trials (Duijm, (1994).

The main finding from the study was the characteristics of medium and large-scale natural gas and other hydrocarbon jet-flames from the measurement. The response of

engulfed vessels was measured. The catastrophic failure of unprotected two-tonne propane tanks, resulting in BLEVE, was studied. It was found that, for the scenario tested, water deluge and emergency release are ineffective in providing protection; however cementitious insulation was effective. No effective method was found to protect flange connections (Wicks and Cole, (1995) and Bennet, (1991).

1.3 FIRE EXTINGUISHING AGENTS:

Among the many Halons applications is the suppression of the flammable liquids and gases fires (DiNenno, 1993). Halons have been identified as stratospheric ozone-depletion agents. 'The Montreal Protocol on Substances that Deplete the Ozone Layer', an international agreement, requires a complete phaseout of the production of these halons by the year 2000 (Cote, 1992). Carbon dioxide is also used for this application as inert gas (DiNenno, 1993). However, because required concentrations are lethal (Cote, 1992), alternatives to halons and carbon dioxide are also sought. Water spray is an attractive option because the US Environmental Protection Agency has determined that it is an acceptable Halons substitute, and that using water spray poses no toxicological or physiological hazard and is safe for use in occupied areas (Bill, 1997). Water has zero ozone depletion potential, zero global warming potential, is non-corrosive and has tremendous cooling capacity (Back, 1996). The

primary hazards in offshore compartments are flammable-gas fires resulting from fractured gas lines. Because water spray is thought to extinguish fires primarily through heat extraction, oxygen displacement and blocking of radiant heat (Mawhinney, 1994), hazards with flammable-gas fires in enclosures would be expected to be a good candidate for water spray protection. Indeed, water spray protection has been shown to be effective for gas turbine enclosures which present similar hazards (Wighus, et al., 1993 and Ural et al., 1995).

It has been known that very small water droplets control or extinguish fires in several ways: cooling of the flame and fire plume; oxygen displacement by water vapour and radiant heat attenuation (Kim, 1997). The nature of a fire also has an influence on the ease with which water can extinguish the fire (Rashbash, 1985).

Other extinguishing agents include (Cote, 1992):

Dry chemical agents: a powder mixture that is used as fire extinguishing agent. It is efficient in extinguishing fires in flammable liquids;

Dry powder agents: mainly used to extinguish the fire of the combustible metals;

Foam agents: an aggregate of gas-filled bubbles formed from aqueous solutions of specially formulated concentrated liquid foaming agents. Foams are used to diminish or halt the generation of flammable vapours.

1.4 WATER SPRAY SYSTEM

In 1812, the first prototype water spray system was installed in the Theatre Royal, Drury Lane, London (Nash, 1973). Its life safety and property protection potential were quickly recognised and developed. Today the water spray system is widely accepted as the most efficient form of automatic fire extinguishment.

Historically, the world has experienced many tragic fires (table 1.1). Most of these unfortunate experiences led to changes in the codes concerning fire and life safety.

In the nineteenth century the newly formed insurance companies, like the Mutual Fire Insurance company, were the driving force behind the development and subsequent setting of the rules and regulations for water spray systems installation (Hoffmann, 1990). Today research and testing into every aspect of the fire phenomena, from collecting fire statistics, understanding the physical and chemical interactions to examining the process involved in activating and subsequent working of spray systems are carried out at different research organisations such as Fire Research Establishment in UK, Building and Fire Research Laboratories in USA, SINTEF NBL in Norway and The Technical Research Centre of Finland.

The characteristics of the water spray determines the mechanism by which it suppresses fire. Those characteristics are dependent upon the method of spray production, different spray systems producing water spray with different characteristics. The important parameters that define the characteristics of the spray are drop size distribution, spray flux density, spray angle and spray momentum.

1.5 OBJECTIVES OF THE PRESENT STUDY

The objectives of this research are:

1. To study experimentally the behaviour of jet fire in a compartment of substantial size.
2. To study the temperature distribution inside the compartment and at the compartment surfaces.
3. To prepare a CFD model of the combustion reaction and compare it with experimental results.
4. To include radiation and heat transfer at the compartment surfaces in the CFD model.
5. To test existing water-spray technologies in extinguishing or controlling the compartment jet fires. An assessment of water spray design parameters (i.e. flow rates, drop size, nozzle location, nozzle numbers and spray angle) was also conducted investigating their effects in extinguishing or controlling fires, and in understanding the mechanism of extinguishment.
6. To compare the measured with the predicted results for both fire steady state and water sprays.

In order to achieve the above objectives, it is necessary to produce a workable CFD model of an offshore module and to carry out an experimental programme on compartment jet fire. A total of 58 fire tests were done in two phases. Final numerical calculations will be performed to help interpret the experimental data and understand the suppression mechanisms.

1.6 LAYOUT OF THESIS

A general introduction to fire has just been given in this first chapter; the remainder of the work is set out as follows. In chapter two the context of the problem is explored and the action of the water spray in various burning environments, compartment fires and jet flames is reviewed. Chapter three describes the experimental setup. Experimental apparatus, sampling gas analysis system and data acquisition system are described in this chapter. Experimental procedures and conditions are discussed as well as the safety requirement and the risk assessment for running the rig. For completeness, outlines of the physical and mathematical modelling of a steady-state within a compartment are provided in chapter four. This includes the single-phase governing partial differential equations along with the auxiliary equations, such as heat losses to the walls, turbulence and boundary conditions. The two-phase steady state and transient fire-spray modelling are

presented in this chapter as well. Due to the more complex nature of the phenomena investigated, the auxiliary equations now also include interphase heat and mass transfer. Chapter five is devoted to the setup of the numerical modelling and to the results of the single-phase fire modelling and the preliminary results of fire extinguishment by water spray. Chapter six presents the measurement of the droplet sizes using Malvern Particle Analyser. The successful modelling of the extinguishment of the compartment jet fire by water sprays is reliant on accurate data of the droplet diameters of the different spray nozzles used. Chapter seven is devoted to the result analysis of the test data and includes discussion of the jet fire behaviour; comparing the different temperature measurement instruments; investigating the different temperature measurement locations; effect of different spray angles; effect of spray numbers and locations and the optimum water flow rate. The predictions obtained by implementing the fire models are presented in chapter eight. For the steady state simulation a jet fire within a compartment was used. The cases considered transient studies when the water spray was activated for the two phase modelling. The results obtained by implementing the two-phase models are detailed in this chapter as well. The effect of different droplet sizes, spray angles, droplets velocity, spray number and locations on reducing the overall temperature of the compartment are discussed here. Chapter nine contains validation of the measured and predicted results. Finally, chapter ten deals with the conclusions and recommendations for future work. This chapter presents the main conclusions derived from this study. Recommendations for the future design of water spray system with the optimum water flow rate are included here (optimum characterisation, i.e. water flow rate, droplets diameters, spray angle, etc.).

Recommendations for the future studies are also included in this chapter. A reference section at the back contains papers and texts which are of primary importance to this work.

CHAPTER TWO

LITERATURE REVIEW AND RELATED THEORY

2.1 INTRODUCTION

A study of the subject of this work is undertaken in this chapter. In general terms, the problem is that of suppressing fires or mitigating their destructive effects. Although several means are available by which such mitigation may be achieved, the interest here lies primarily in suppression or the mitigation by sprays of water.

For at least the last five decades, researchers have sought to maximise the efficiency of using water spray for fire suppression (Mawhinney, 1997).

Interest in water sprays for fixed fire suppression systems was vigorously renewed with the beginning of the phase-out of halon fire extinguishing agents, which followed the signing of the Montreal Protocol in 1987.

Over the last ten years, there has been great deal of activity in the field of water spray research and development. In early 1996, development continued rapidly (Mawhinney, 1997). Activities occurred on a variety of fronts from theoretical investigations into extinguishing mechanisms, computational fluid dynamics modelling, and the development, patenting, and manufacturing of spray generating equipment.

2.2 THE COMBUSTION PROCESS

The term 'Combustion' usually refers to an exothermic or heat producing, chemical reaction between some substance and oxygen. Chemical analysis of the combustion products would show the presence of certain molecules involving combinations of oxygen atoms with other types of atoms, such as CO_2 and H_2O.

A flame is gaseous oxidation reaction which occurs in a region of space much hotter than its surroundings and which generally emits light.

Combustion requires a high temperature, and the reactions must proceed fast enough at this high temperature to generate heat as fast as it is dissipated, so that the reaction zone will not cool down. If any thing is done to upset this heat balance, such as introducing a coolant, it is possible that the combustion will be extinguished. It is not necessary for the coolant to remove heat as fast as it is being generated because the combustion zone in a fire is already losing some heat to the cooler surroundings. In some cases, only a modest additional loss of heat is needed to tip the balance toward extinguishment.

Extinguishment can be accomplished by cooling either the gaseous combustion zone or the solid or liquid combustible.

As an alternative to removing heat from the combustion zone to slow the reactions, it is also possible to reduce the temperature of the flame by modifying the air which supplies the oxygen. Air contains 21 % by volume of oxygen, the remainder being almost entirely the inert gas nitrogen. The nitrogen, which is drawn into the flame along with the oxygen, absorbs heat, with the result that the flame temperature is much lower than it would be in a fire burning in pure oxygen. If additional nitrogen or some other chemically unreactive gas, such as steam, carbon dioxide or a mixture of combustion products, were to be added to the air entering the flame, the heat absorbed by these inert molecules would cause the flame temperature to be even lower.

The types of fire characteristic of the process industries will be discussed in this section, in particular, the main features of large process jet fires.

2.2.1 JET FIRE:

Jet fire is a turbulent diffusion flame resulting from the combustion of a fuel continuously released with some significant momentum in a particular range of directions (Cowley, 1992). Loss of hydrocarbon containment can arise from mechanical failure damage or procedural failures. The leakage rates and their time dependence, the hydrocarbon type, storage and discharge conditions greatly influence the nature and extent of a fire.

Hydrocarbon fires can have very varied characteristics and encompass a very extensive range of site. Fire properties are influenced by surrounding structures and equipment. Fires might be followed by an explosion causing damage to structures, process plant, or fire protection systems and thereby affecting the extent of air access and subsequent fire development. The consequences of fires and explosions and the strategies to mitigate them must therefore always be considered together.

Jet fires vary considerably in their characteristics. Their behaviour depends on the source momenta and fuel type. Near the release point, the source momentum is usually the dominant effect, and further downstream the buoyancy of the hot gases and the forces due to cross flows have an increasingly greater influence.

2.2.2. Jet Flame Length

The flame length is the distance from the release point to the defined end of the flame. A reasonable measure of the progress of burning of a diffusion flame is its height. A jet fuel is assumed to issue from a nozzle of known diameter in a vertical direction upward into an ambient medium containing an oxidant. The changes in the flame length and shape during this transition are diagrammatically illustrated in Figure (2.1). It can be seen that, as long as the flame remains laminar, its length

increases with the increase in the velocity of the fuel gas at the burner nozzle up to a maximum level; and after reaching this point, a slight flow instability appears at the flame tip. With further increase of the fuel velocity at the nozzle the transition point moves closer to the nozzle and the flame becomes shorter. When the fuel flow from the nozzle reaches a certain velocity, the transition length and the flame length become almost constant and the flame length continues to increase with flow velocity until a critical Reynolds number is reached. It has been suggested by Hottel and Hawthorne (1949) that the propane Reynolds number criteria to determine transition from laminar flame to turbulent flame is 8500.

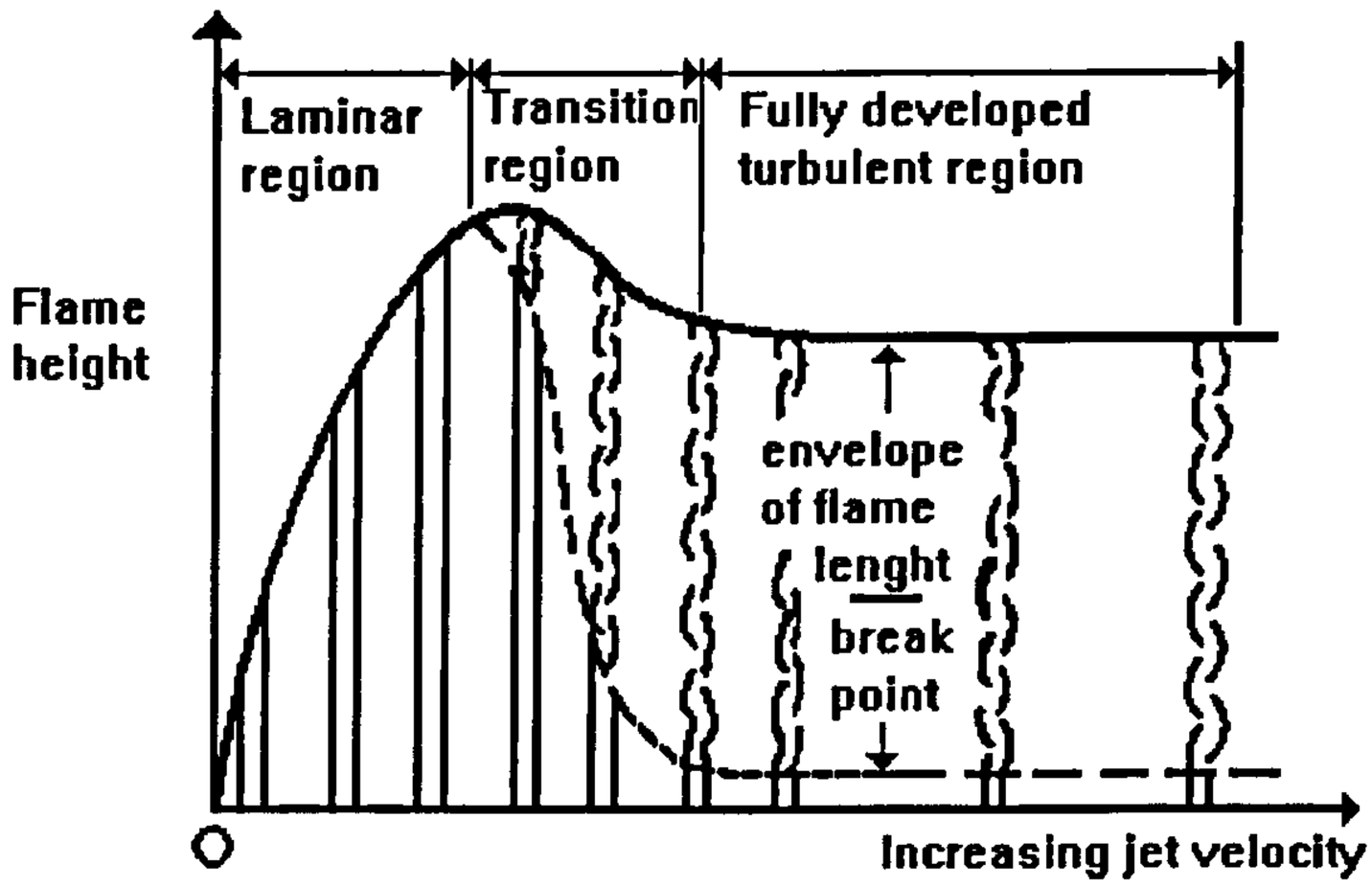

Figure (2.1). Progressive change in flame type with increasing jet velocity (DiNenno, 1988).

2.2.3 Flame Lift-off:

Jet flames are generally lifted, the base of jet flame is not attached to the release point. This occurs because the high velocities, strain rates and the richness of the fuel near the source make it difficult to maintain a flame. (Phylaktou, 1996).

McCaffrey (1989), using data from 7 MW methane flames out of a 30 mm orifice, determined that the correlation due to Peters and Williams (1983) predicted the distance to blue flame L_f reasonably well.

$$L_f = 0.0036\ U \qquad (2.1)$$

Therefore, L_f is independent of jet nozzle diameter, U is the exit gas velocity in m/s.

2.2.4 Radiation

Thermal radiation in fires involves energy exchange between surfaces (i.e. walls, ceiling, floors) as well as emission and absorption by various gases and soot particles. Among those gases of great practical importance to fire are water vapour and carbon dioxide, which are strongly absorbing-emitting in the major thermal radiation spectrum.

It has been recognised that radiation is the dominant mode of heat transfer in flames with characteristic lengths exceeding 0.2 m (Tien et al, 1988).

2.2.5 The European Union Programme

A project JIVE was carried out on the hazard consequences of jet fire interactions with a vessel containing pressurised liquids. The Commission of the European Communities sponsored the project. The different research subjects within the JIVE project are summarised below (Wicks and Cole, (1995), Bennet et al, (1991) and Duijm, (1994)).

A. Modelling of unobstructed jet fires.

A one-dimensional model to describe the behaviour of unobstructed jet fires was developed. This work was a further development of the one-dimensional codes UPMFIRE and TORCIA.

Jet fire stability and the lift-off distance of the flame from the release nozzle as well as sonic and two-phase release were important parameters for extending the models. Methane jet flame contents were not significantly changed by adding butane up to 40% (mass). Radiation levels were proportional to the release rate and are nearly independent of wind speed.

B. Modelling of obstructed jet fires.

Heat transfer to the obstacles was considered. Distinction was made between jet fires engulfing relatively small objects and large obstacles. The work was carried out experimentally from impingement and wind tunnel tests.

The main finding from the study of heat transfer from jet fires to obstacles such as pipework and vessels was as follows: the maximum heat flux from methane jet fires did not exceed 350 kW/m^2, the heat flux distribution on obstacle surfaces was non-uniform, dependent on the distance between the obstacle and the origin of the flame. The effects of the non-uniformity on the obstacles resulted in thermal stresses on the surface of the obstacles and obviously affected the resistance of the obstacles to the fire, which could cause failure of the obstacle to occur sooner than if the obstacle was fully engulfed by fire (Duijm, 1994).

Radiative heat transfer to obstacles was often under-predicted, possibly due to turbulence or incorrect use of averaging. The maximum heat flux to an obstacle was well predicted. Temperature distribution and sizes of jet fires were well predicted by one-dimensional and three-dimensional models.

C. Modelling of the thermal response of a pressure vessel.

Local heat fluxes and wall temperatures, temperature distribution in the contents, pressure build-up, and flow characteristics of the vent flow due to partial heating by jet fire impingement on vessel containing pressurised liquids and on nearby flange connections, were investigated.

At this stage the code ENGULF for investigating the response for vessels which are fully engulfed by fire was extended to investigate partially heated obstacles.
Experiments of full-scale failure were performed on unprotected two-tonne propane tanks engulfed by a liquid propane jet flame. Time to failure was found of the order of 5 minutes irrespective of the fill level. In some cases, vent operation prolonged the life of the tank by increasing the volume of the two-phase region, so improving the heat transfer from the formerly dry wall. All unprotected vessels test resulted in complete failure and BLEVE.

D. Assessment of the effectiveness of mitigation techniques.

Water spray cooling and insulation of obstacles were considered in this research. Water spray was only investigated theoretically. The mitigation by insulation was made experimentally with flange connections and storage vessels (Duijm, 1994).
It was found that the water spray cooling of obstacles is less effective for jet fires than pool fires. In addition to the water being deflected by the jet, once the tank surface became too hot it became partially insulated from the water by a layer of water vapour.
On the other hand, experiments involving a 40 mm thick cementitious coating and a 13 mm thick epoxy intumescent material showed them to be effective in protecting the two-tonne propane tank. The wall temperatures of the tank remained below 250°C for 80 minutes.

E. Modelling failure modes of pressure vessels.

The failure mode of pressure vessels under jet fire attack was investigated experimentally. The results were compared with cold vessel failures and small-scale laboratory trials results and were included in a model describing the thermal response of pressure vessel up to failure.

Increasing vapour pressure inside the vessel triggered a relief valve causing a sudden pressure drop which resulted in rapid boiling and frothing. This pressure reduction as a result of the relief valve opening was only temporary. Soon after that, failure occurred and the fuel ignited causing BLEVE with 100 m high cylindrical fireball containing most of the remaining liquid contents (Wicks and Cole, 1995).

2.3 COMPARTMENT FIRE:

Compartment fire is a fire burning within a structure where, compared to an open fire, there may be coupling between the fire and the structure that influences the fire properties and vice versa.

When a fire is burning inside a compartment, the combustion starts as though the fire were in the open. If the compartment openings are sufficiently large, and there is enough air already present to satisfy the stoichiometric requirement for complete combustion, the fire size and intensity are controlled by the fuel burning rate (Cowely, 1992). The flame burning under these conditions may impinge on the ceiling. The fire is deflected sideways and the plume spreads out into a so-called ceiling jet. This jet continues to burn until all the fuel is consumed, and may extend beyond the opening if the ceiling is relatively small and shorter than the ceiling jet flame extension. There is a net outflow of material through the compartment openings as the gases heat up and expand. After a short time a hot gas layer of combustion products builds up in the upper part of the compartment which grows and descends as gases continue to flow into it. A relatively well-defined interface normally forms between the upper hot layer and cool air below. When this interface descends below an opening there is a sudden outflow of smoke, combustion products or flame. If the compartment openings are small, the fire may not be able to entrain

enough air for complete combustion of the fuel inside the compartment. The fire is then said to be ventilation-controlled.

The air supply rate is controlled mainly by the geometry of the opening. In a short time, dependent on burning rate and vent size, a steady state is reached in which hot combustion products flow out of the top of the opening and ambient air flows in at the bottom. There normally exists a well-defined boundary between the hot layer in the ceiling and the colder air at the floor.

The major hazards associated with compartment fires include all those normally associated with open fires. However, additional hazards exist due to the effect of confinement. For personnel these include:

- The extent of external flaming;
- Impaired visibility along escape route through smoke obstruction;
- Increased hazard from carbon monoxide (CO);
- Explosion hazard from unburned fuel if the fire extinguishes due to insufficient oxygen.

Heat loading onto vessels, pipework and structures can be greater in compartment fires due to the effects of increased soot formation during ventilation-controlled conditions, and additional heat radiated from the hot surroundings or walls.

The primary physical parameters affecting compartment fire behaviour include (Persaud, 1997):

1. Geometry and size of compartment, position and size of vents, and degree of thermal insulation present on the boundaries.
2. Type of fire (jet or pool) and fuel involved.
3. Release conditions of fuel-mass flow rate, orifice/ nozzle diameter or pool diameter, flow regime, orientation of release for jet fire.
4. The mass transfer from the fire feeding the smoke layer and losses to the outside environment through vents.

The amount of air present and available for combustion is the controlling factor in determining soot and CO production and flammability of the smoke layer.

5. Radiation and convection heat fluxes to impinged roof, walls and objects.
6. Mitigating circumstances, such as passive fire protection coatings on objects inside the compartment and/or the roof and walls.
7. Water spray system.

The processes discussed above are not independent, but are coupled together such that a change in any one process can have an immediate effect on all others. (Persaud et al., 1997).

High pressure gas discharges are likely to produce jet fires that are substantially distorted by impingement onto large objects or compartment boundary surfaces. The impinged area may be much greater than that predicted from overlaps of the free flame idealisation with the impinged surface. The flame distortion, local turbulence and induced large scale air/product flows within the compartment may produce via increased velocities heat transfer to surface different form values encountered in relatively unperturbed open flames (Cowely, 1992).

The flame distortion, induced turbulence, large scale circulation and momentum modification via impingement may also modify the internal flame conditions themselves because different aeration and turbulent combustion was found by Chamberlain (1994) who carried a series of compartment jet fires at large scale to study the compartment jet fire behaviour which was part of programme designed to provide data on fire severity and smoke emission suitable for hazard model validation and guidance on risk assessment, for a range of fire scenarios to be carried out by Shell Research Centre (Brightwell, 1995). A large compartment was used with size of 135 m^3. The fuel flow rate used was 0.3 kg/s. The geometry of the compartment and jet characteristics was varied systematically. The jet was directed at a 0.27 m diameter pipe target. It was also found gas temperature may be increased or

decreased in particular flame regions because the air supply could be enhanced or alternatively vitiated.

The partial products from a ventilation-controlled fire include carbon monoxide in concentration which may pose a hazard at a downwind refuge. Under favourable conditions of composition and temperature, these products may become flammable. A flame may propagate from the fire plume into the hot smoke layer and create flames external to the compartment. The sudden increased aeration and high temperatures in the external flame then reduce the CO concentration to levels more typical of open flames. Therefore, it is important to know the conditions which determine the onset of external burning and the extent of the new hazard posed by the external flame. Under-ventilation Jet fire could lead to high CO levels, even exceeding those from pool fires because of the potential for generating higher temperatures in jet fires.

Persaud (1997) developed a physically based zone model, enabled the hazards of compartment fires to be estimated at steady state and at a scale representitive of offshore modules. The model was able to estimate global smoke layer properties at steady state, such as depth and temperature, radiative heat and mass transfer losses, and the extent of external flaming. The results compare favourably with experiments.

2.3.1 USE OF CFD IN COMPARTMENT FIRE

The numerical modelling of fires and its use for the assessment of fire hazards in compartment presents very attractive alternative to experimental measurements in fire research, because of its easy use and relative low cost. A number of recent studies have concentrated on the gaseous flow field characteristics in compartment (Kumar et al, 1991, Kerrison et al, 1994a and 1994b and Mawhinney et al, 1994b), and tunnels enclosing a fire (Woodburn and Bitter, 1996a and 1996b and (Bennardo et al, 1997), with effects of turbulence, chemical reaction and radiation (Lewis, 1997) included.

The exact equations governing the turbulent flow of hot fluids are known; however, their solution for practical purposes is not possible. The problem lies in the very nature of turbulence. The physical process controls the growth and decay of turbulent motion occurring on scale much smaller than the overall flow scales. To overcome this problem semi-empirical turbulence models have been developed, which consist of differential or algebraic equations and associated constants. One such model, the two-equation k-ε model (Jones and Whitelaw, 1992) is generally applied to simulate the re-circulating turbulent flow conditions occurring during fire scenario.

Combustion process is very complex, due to the number of intermediate reactions and the formation of short lived species taking place. Turbulence further complicates this situation by mixing reactants and products. A single fluid approach was used and both the eddy break-up model proposed by Spalding (1971) and the Magnussen and Hjertager (1976) model suggested for diffusion flame systems were employed. However, combustion reaction is often entirely omitted (Kerrison, 1994a and 1994b, Lewis, 1997 and Mawhinney et al, 1994b) in favour of a simply prescribed heat source.

Numerical simulation of the interaction between sprinkler spray and a fire plume introduces one more complexity into the already complicated subject (Nam, 1996).

The numerical modelling of a water spray can be divided into two categories depending on how drops in the spray are traced. The gas flow is always treated in an Eulerian coordinate system, but the liquid flow can be treated in either Eulerian (Hoffmann and Galea, 1991 and Hoffmann et al 1989) or Lagrangian systems (Alpert, 1984 and 1985), Chew and Fong (1991), Bill (1993), Fthenakis et al (1993) and Berlemont (1991)).

2.4 EXTINCTION MECHANISM

To suppress a fire, which is burning with a continuous supply of fuel and oxygen, the suppression agent must limit either the fuel or the oxygen supply or reduce the temperature of the flame zone.

The mechanisms of extinction of flames in a fire situation have been investigated as early as 1955 by two authors, Braidech (1955) and Rasbash (1956 and 1960). Research conducted four decades later has not altered the accuracy of this description and the results are in general agreement.

Mawhinney (1993a) and (1993b) described three mechanisms which act together to extinguish fire. These mechanisms of extinction of flames are grouped below:

i. heat extraction (cooling);
ii. oxygen displacement by water vapor;
iii. Blocking of radiant heat.

Wighus (1994, 1991a and 1991b) and Hanauska (1993) described the mechanisms as gas phase cooling and steam inerting, but made no reference to radiant heat attenuation. Although all three mechanisms are involved to some degree in every extinguishment.

For engineering design purposes of reliable water spray fire suppression systems, and for computer modelling purposes, it may be sufficient to understand all the extinguishing mechanisms.

Wighus (1991a) and (1991b) carried out a series of experiments to investigate the extinguishment of an enclosed 1 MW propane fire. A ventilated enclosure of size $2.5 \times 2.5 \times 5$ m^3 with various nozzle was used to run the fire test. The main results from these sets of tests were that the absorption of heat from a fire by water spray is dependent on the rate of water applied and droplet size distribution.

A water flow rate of 1.3 lit/min/m^2 was sufficient to extinguish this 1 MW fire when the mean droplet diameter was 600 μm. However when the droplet diameter was greater than 1000 μm the application rate increased to 3.5 lit/min/m^2.

The main finding from Rasbash (1956 and 1957) tests were the extinction time was directly proportional to the drop size of the spray and to the preburn time, and inversely proportional to the rate of flow of water per unit of fire area, and also to the difference in temperature between the fire point and ambient temperature raised to the power 1.75, with the importance of spray momentum being critical to the spray penetrating the fire plume, hence extinguishing the fire.

The local application of water spray, if successful, will bring about the suppression of a fire very quickly. Due to the speed of extinction, it can be concluded that the main mechanisms, which bring about extinction, are dependent on the evaporation of water droplets in the flame. The evaporation of a water droplet can, depending on droplet diameter, occur in the time it takes the water droplet to pass through the reaction zone.

The evaporation of water droplets, and the resulting suppression effects from this, occurs regardless of the enclosure condition of a fire. For this reason the local application of a spray to extinguish a diffusion fire can be regarded as independent of the enclosure conditions.

Ndubizu et. al. (1996) carried out a study on the suppression mechanisms of small diffusion and premixed flames by water spray and noted that the real fire condition is such that the spray interaction with fire is influenced by the imposed aerodynamics. Such aerodynamics would be greatly affected by the fire size, enclosure geometry, opening, imposed flows i.e. ventilation system. These complexities have made it difficult to acquire a detailed understanding of the physics of water spray fire suppression.

2.4.1 HEAT EXTRACTION (COOLING OF THE FLAME):

The predominant mechanism by which a diffusion fire will be suppressed by a locally applied water spray is by the extraction of the heat from the flames.

The heat absorbed by the water spray can be divided into tow categories (Rasbash, 1957):

i. The heat to raise the temperature of the water droplets to their boiling point.

ii. The heat to evaporate the water droplets from their boiling point.

Although the heat extracted by the spray to raise the temperature of droplets to boiling point is one sixth of the heat extracted by evaporating the droplets, there have been no investigations (Rasbash, 1957) to compare the competing effects of raising the temperature of water used to produce a spray.

The competing effects would be a reduction in the heat extracted by raising water droplets to their boiling point, and an increase in the heat extracted by increasing the number of larger droplets which would be fully evaporated. Such an investigation may provide valuable information for situations where complete penetration of the flames, therefore residence time of droplets in flames, may be sufficient for the full evaporation of larger droplets at ambient temperature. Situations in which this occurs are predominantly the total flooding situations.

Water absorbs heat when it is applied to a fire in three areas: from the hot gases and flames; from the fuel; and from the objects and surfaces in the vicinity of the fire (Mawhinney, 1995). Fuel and nearby objects cooling contributes to reducing fire spread, but it does not necessarily require fire drop sizes. In fact, solid fuels wetting and cooling is easier to achieve by using larger droplets (> 400 microns)

The amount of heat removed by the water is dominated by the amount of water which is evaporated. The proportion of heat necessary to bring the water from the normal ambient water temperature to the boiling point to the heat of evaporation is 1:6.

$$\Delta h = c_{P\,(water)} \times \Delta T \qquad (2.2)$$

where Δh: change in enthalpy (kJ/kg),

c_p: specific heat capacity (kJ/kg K)

ΔT: temperature difference (K)

For example the heat extracted from the compartment fire to heat water from 25°C (ambient) to 100°C (boiling point) is equal to $\Delta H_{100\text{-}25} = 4.2 \times 75 = 315$ [kJ/kg]. And the heat extracted to evaporate this water is 1890 [kJ/kg]. So, the most effective way of taking heat out of a compartment fire is to evaporate the water inside the compartment (Wighus, 1991).

2.4.2 OXYGEN DISPLACEMENT:

Water droplets expand approximately 1600 fold upon evaporating (at 95°C, 1 atmosphere pressure). Due to the latent heat needed to vaporise the water, evaporation of the droplets allow very large amounts of heat to be removed from the surface. Most of the produced steam will follow the combustion gases through the ventilation opening. If evaporation occurs rapidly, the water vapour will displace a proportion of the air from the vicinity of the drop. However, injection of a finely divided water spray into a hot compartment results in rapid evaporation, which may cause blocking of the air supply by the expansion of the evaporation, displacing the air in the compartment by steam. And the air drawn into the combustion zone may be recirculated from the upper part of the room. This can lead to oxygen starvation in the combustion zone, and consequently to extinction. This process is transient, and the location of the fire relative to the spray nozzle, the air supply and to outlet openings will dominate the result. If the amount of oxygen available for combustion

is reduced below a critical level, the fire burns inefficiently and will be easier to extinguish by cooling (Mawhinney, 1994a).

Researchers such as Braidech (1995), Wighus et al. (1994), Mawhinney (1994a) and Hanauska and Back (1993) who made tests on diesel and heptane pool and spray fires, confirmed that the displacement of oxygen within the region of the fire plays a more predominant role in the extinction of a fire than the extraction of heat, both in compartments and in open-area pool fires.

In certain experimental conditions this is true. Certain experiments have taken place where the fire size in relation to the enclosure volume was insufficiently large, or where the positioning of ventilation openings were not conducive to natural draught (Orr, 1996).

The minimum amount of free oxygen needed to support combustion varies with the type of fuel. In general, hydrocarbon gases and vapours cease burning at oxygen concentrations below 13 %, while charring solid fuels may burn with oxygen concentration as low as 7 % (Mawhinney, 1994a). This explains why it is easier to extinguish hydrocarbon fires than wood crib fires.

The effect of oxygen displacement also explains why it is easier to extinguish large fires than small fires in a compartment. Large fires release more heat into a compartment in the early stages than small fires, so that more heat is available to evaporate the fine water droplets. A small fire will have a continuos source of fresh combustion air at normal oxygen concentrations. A large fire will reduce the ambient oxygen concentration to the point that combustion efficiency will be reduced, prior to introducing the water spray (Mawhinney, 1994a).

2.4.3 BLOCKING RADIANT HEAT:

Blocking radiant heat was included as a third mechanism of extinguishment which stops the fire from spreading to unignited fuel surfaces, and reduces the evolution of flammable vapours which would decrease the burning rate of the fire (Orr, 1996).

Blocking of radiant heat transfer is not taken into account by most researchers, studying extinction mechanisms of water spray (Braidech, 1955, Rashbash, 1960, Wighus, 1993 and Log, 1996). Mawhinney (1994a) studied the problem in depth and stressed the potential of reducing thermal feedback to burning and unburned fuel surfaces by water sprays.

The radiation attenuation provided by water spray protects objects and personnel in a space from radiant heat damage, whether or not extinguishment occurs. On that account, radiant heat blocking is an important benefit of water spray in fires both in compartment and in open areas. This heat, radiated to the surroundings, can be attenuated by applying a water spray. Mawhinney (1994a) records attenuation levels of over 50 % for droplets of around 50 μm diameter, and only 10% for droplets of 100 μm diameter. However, not all of this heat is absorbed by the spray, an unknown quantity will be reflected, or deflected back to the fuel.

Theoretical considerations suggest that spray or steam that enters the space between a flame and the fuel surface will reduce the radiant heat flux to that surface (Jones et al 1993).

Recent theoretical work on radiation attenuation by water sprays (Coppalle, 1993 and Ravigururajan, 1989) indicates that the attenuation of radiation depends very much on drop diameter and mass density of the droplets.

2.4.4 OTHER EXTINGUISHING MECHANISMS

Some other extinguishing mechanism discussed in this section includes dilution of vapour air mixture. Entrained air which is to be used for combustion will entrain water droplets when the compartment was filled with water droplets because the water spray will follow the flow pattern dominated by the fire inside the compartment used. So air entrained into the compartment contaminated by water droplets may dilute the vapour air mixture to below the lean flammability limit. This mechanism depends on the fuel type; in some fuels it is difficult to reduce the fuel air mixture to

below its lean flammability limit because of the low flash point temperature and high vapour pressure, i.e. heptane (Mawhinney, 1995).

Another extinguishing effect is due to inert gas production, mainly CO2, water vapour and oxygen consumption by the fire itself, and recirculation of fire products, water vapour and droplets into the fire plume.

Speeding up flow velocity to a level where the residence time of fuel and oxygen in combustible mixture is less than needed by the chemical reaction (blow off) is one of the extinguishing mechanism which could be used as well as adding components in the combustion zone which breaks the chain of chemical reactions by substitution with endothermal reaction.

Finally, self-extinguishment condition can be considered here. It will be achieved in an air tight compartment. Realistic compartments are seldom totally air-tight, and some supply of air is normal. The temperature increases as the fire burns and the oxygen concentration decreases until a critical limit is reached. The reason for self-extinguishment is that the fire itself consumes oxygen and produces inert gases, mainly CO2 and water vapour. The circulation of fire products into the flames and the smoke plume leads to self-extinguishing due to lack of oxygen. The rate of oxygen consumption is decided by the fire size.

The inerting of the enclosure requires a certain total amount of water applied into the enclosure, and the application rate influences the time to extinguishment only.

To optimise the effect of a fire suppressant system, a combination of extinguishing mechanisms, i.e. cooling and inerting, is favourable.

2.5 EFFECT OF COMPARTMENT CONDITIONS ON FIRE EXTINGUISHMENT

The compartment conditions of a fire influence not only the development of the fire, but also the mode in which a fire can be suppressed. The ventilation properties of a compartment are an influential factor in determining the method of suppression which should be used. In a well-ventilated fire the principal mechanism of suppression is heat extraction (Orr, 1995).

The problem of engineering design of a water spray system is to design nozzles which produce water spray with optimum droplet size distribution, throw length and coverage or density (Wighus, 1995).

The two main approaches found in the literature (i.e. Wighus, 1995) for designing a spray system are:

- Local application, relevant for well ventilated fires.
- Total flooding of an enclosure, relevant to compartment fire when air supply may be restricted.

2.5.1 LOCAL APPLICATION

Instantaneous extinguishment by direct application of water and total coverage of the fire area with the spray, and by creation of an inert environment to prevent combustion from taking place is the local application. Once the water is vaporised the fuel is isolated from the ignition source followed by rapid cooling of the radiated heat generated by the surrounding hot surfaces.

A local application system design is a function of the environmental conditions, the type of hazard or fuel and the equipment being protected (Gameiro, 1995). In order to compensate for the small mass of the water droplets, hence low momentum, the nozzle location must be such to ensure direct delivery of the water spray to the fire. This is to ensure that a large number of nozzles should be installed around the hazard,

and to compensate for losses due to wind conditions and mostly to offset the increased supply of oxygen encountered in an outside scenario.

2.5.2 TOTAL FLOODING OF AN ENCLOSED FIRE

Oxygen displacement is the principal mode of suppressing compartment fires with restriction to ventilation, where locally applied water sprays are unsuitable. In these situations total flooding of the enclosure is required. The activation of a total flooding system within the enclosure complements the fire oxygen consumption, and its production of inert diluents by obstructing the ingress of air into the enclosure; this can be illustrated by Figure (2.2) which shows the result obtained by Wighus (1994) from the suppression of 130 m^3 enclosure.

The first curve in Figure (2.2) marked "self extinguishment" represents the oxygen level in a compartment resulting from a large fire relative to the size of the compartment. If the compartment is air-tight, the fire eventually consumes sufficient oxygen to bring its level below that required to sustain combustion.

The second curve of Figure (2.2) marked "not extinguished", represents a small fire in a large enclosure. This type of fire cannot be extinguished, or is difficult to, because the heat source is not large enough to cause a significant production of inerting gases such as steam, CO and CO_2. If the compartment is airtight, eventually the fire will become extinct due to a combination of oxygen starvation and build-up of steam, etc. If the compartment is previously permitting entry of sufficient oxygen to sustain the flame, the fire can be controlled but not necessarily extinguished.

The third curve in Figure (2.2) marked "extinguishment with water spray" represents medium size fire. The small droplets will cool the gases inside the enclosure, and water vapour will be produced. A combination of the water vapour and the gases produced by the combustion result in an inert situation, with oxygen level below 15%. The combined effect of cooling and inerting leads to extinguishment. The continued application of water spray after extinguishment further cools down the

ambient air inside the compartment and scrubs the air from toxic particles and smoke. It should also be noted that the oxygen concentration after extinguishment with fine water spray is higher than in the case of self-extinguishment.

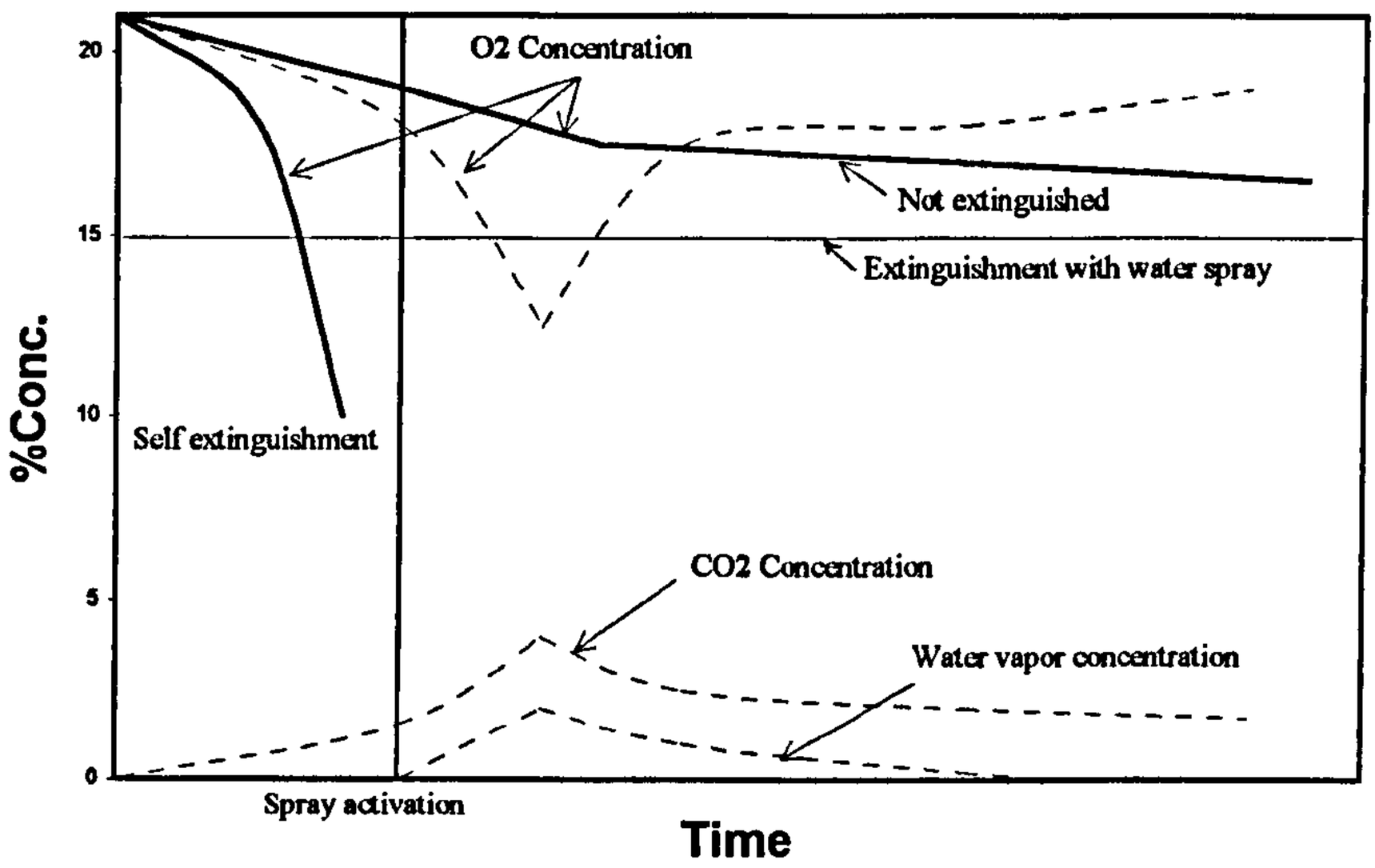

Figure (2. 2). Typical gas concentrations in an enclosure with large fire (self-extinguished), Medium size fire (Extinguished by water spray) and small fire (Not extinguished) [Wighus, 1994].

2.6 CONTROLLING AND EXTINGUISHING CRITERIA

A number of investigations have been carried out to examine the suppression effect of extracting heat from the flame of a diffusion fire. From these a number of studies have set down requirements for the proportion of heat to be extracted by the water spray to achieve extinction.

The process of conversion of water droplet to steam in a diffusion flame absorb heat from the flame and fire plume. If sufficient heat is withdrawn, the gas-phase temperature can be dropped below that necessary to sustain the combustion reaction Figure (2.3) and flame will be extinguished. Theoretical considerations suggest that the combustion reaction in a diffusion flame will cease if the flame temperature drops below approximately 1600° K (Drysdale, 1985). Various authors constitute sufficient heat absorption as it is not necessary to absorb all of the heat generated in a combustion reaction to stop it.

The criterion of extinction of a flame by heat abstraction inside the flame found by Burgoyne and Richardson (1949) is that the combustion products as they leave the reaction zone should not exceed the temperature they would have for lower limit flames; this temperature is about 1580° K for a wide range of flammable vapours and gases. A decrease in temperature approximately to this value is obtained when extinction is obtained by adding extinguishing agent to flames in stoichiometric mixtures.

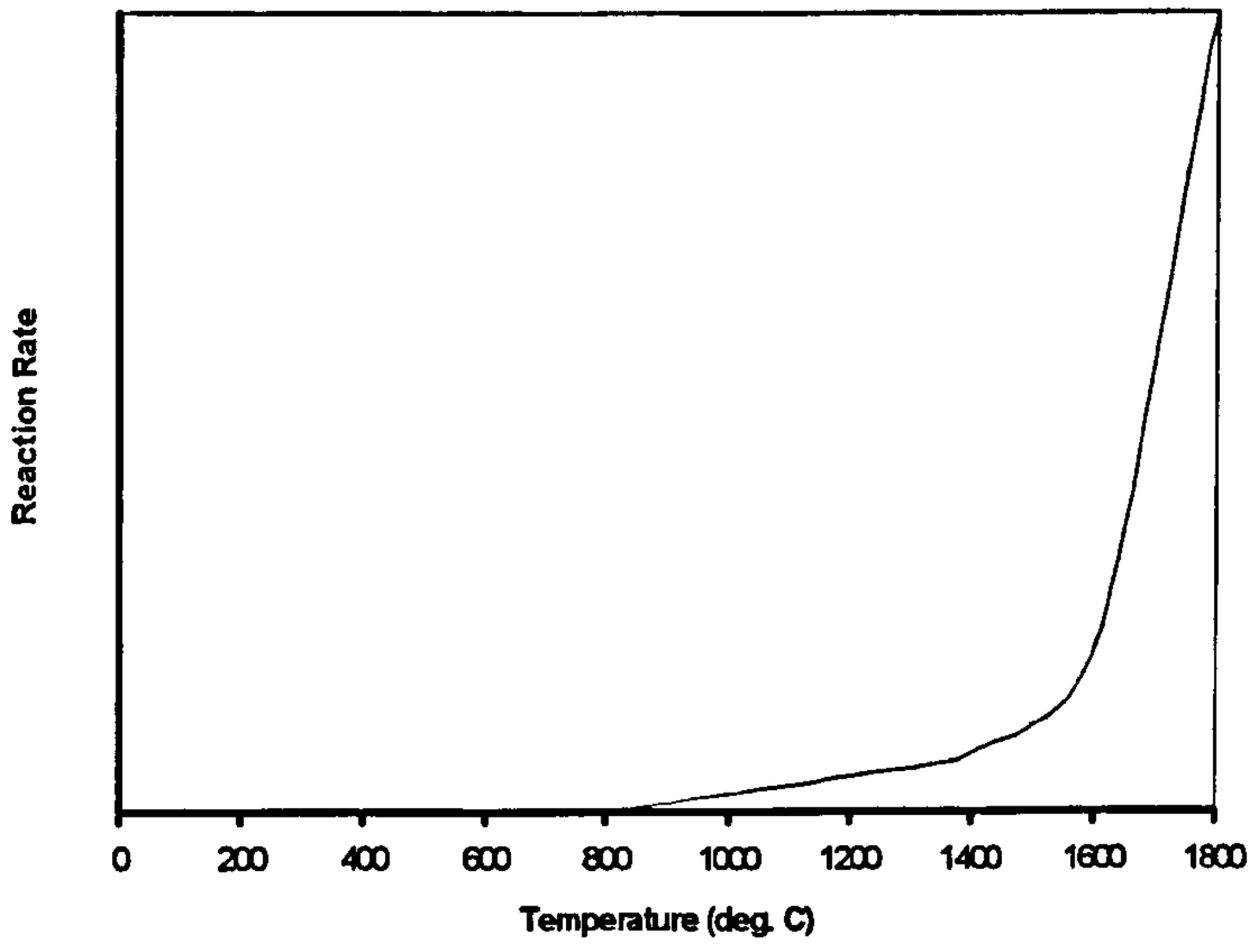

Figure (2. 3). Temperature Dependence of Reaction Rate (Typical for hydrocarbon fuel), Wighus, 1995.

Rasbash (1964) found that the amount of heat which needs removing from the flame to accomplish extinction, is the difference in heat of combustion of stoichiometric and lower limit mixtures. For most flammable organic compounds it is about 45 % of the heat of combustion of the fuel. It is important, however, that this heat be removed either from the reactants or the reaction zone. In a turbulent diffusion flame it is very difficult to differentiate between the reactants, the reaction zone and the combustion products. However, it would be expected that if a spray is capable of removing all the heat of combustion from the flame, then the flame will be extinguished.

Wighus (1991a), (1991b) and (1994) showed that extracting 30 to 60 percent of the heat produced by the fire may be enough to cause burning to stop. Wighus (1995) discovered an important experimental finding which is: if 1/3 of the heat produced by the fire is removed by water spray, extinguishment of well ventilated fires is possible. However, Wighus (1993) suggests that this is a minimum temperature, in practice temperature higher than this can extinguish a fire. This can occur if critical combination between the flame temperature and local oxygen concentration is obtained.

The minimum amount of free oxygen needed to support combustion varies with the type of fuel. In general, hydrocarbon gases and vapours cease burning at oxygen concentrations below 13 percent (Mawhinney, 1994a). On the other hand, SINTEF (1994) found the critical oxygen concentration for extinguishment with water spray system was between 15% and 18%. This means that as much as 30 % of the original oxygen in the compartment was replaced by an inert mixture.

Another engineering correlation for local application of water mist is to consider the ratio of water-to-fuel necessary to achieve extinguishment. In the SINTEF experiments a ratio of approximately 5-6 was found for extinguishment of gaseous propane fires. McCaffrey (1984) found the extinguishment occurs with a water spray into diffusion jet methane flames at a water-to-fuel ratio less than 10. The spraying time to obtain extinguishment by local application is short, in the order of seconds.

2.7 HEAT TRANSFER AND BALANCE

2.7.1 COMPARTMENT HEAT BALANCE

The heat generated by the fire within a compartment is either accumulated in the compartment: a major part is absorbed by the compartment boundaries and any other structural surfaces, by the surfaces of the fuel, by incoming air and any excess fuel; or

transported to the exterior of the compartment in the flame and hot gases that exit from the openings: a smaller part is radiated through the openings and the greater part will be conducted through the boundaries to the ambient. Steady state occurs when the heat absorbed by the compartment surfaces goes to zero as shown in Figure (2.4).

Activation of water spray systems will change the heat balance in the compartment. The water spray systems will generate droplets which will enter the compartment and will be heated by the hot gases. The droplets may be fully or partly evaporated or survive in the hot gas environment, depending on some factors such as the droplets velocity, spray angle and droplets size. But when droplets survive they will hit the boundary and maybe evaporate or form a water film which is taking heat out of the surface, or run off the surface.

The heat transfer from the fire to the compartment and the surrounding may be influenced by the water spray. The temperature of the gases inside the compartment and in the effluent gases may be reduced by the water spray as well. This leads to less heat transfer to the walls, the ceiling, the floor and to objects hit by the smoke. Direct cooling of the compartment boundary is obtained when water droplets hit it. The content of water droplets and vapor increases the absorptivity of the gases inside the compartment, and consequently this may lead to reduced radiation from the flames to surfaces.

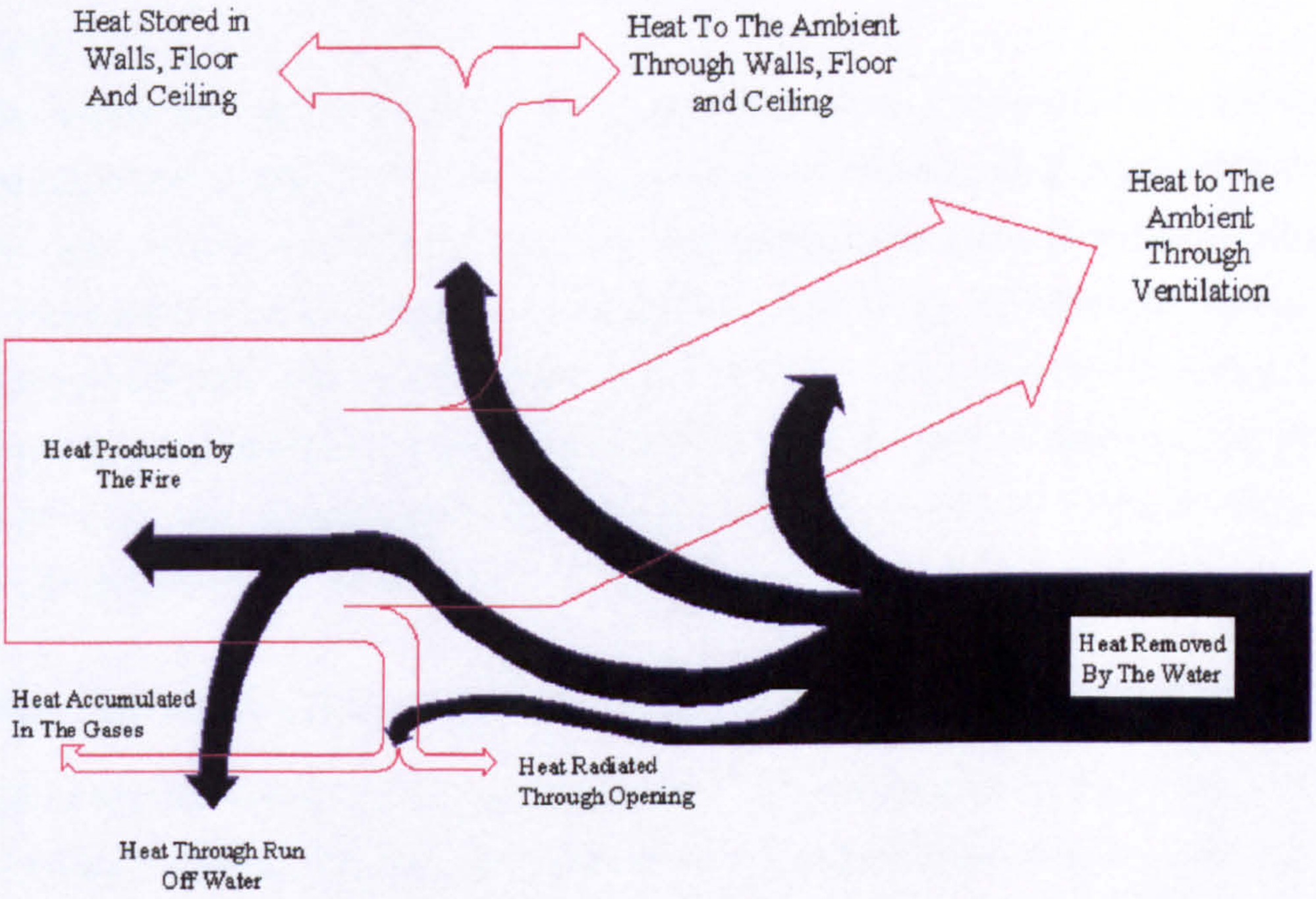

Figure (2. 4).Heat balance of a compartment fire, with water introduced for extinguishment and control (Wighus, 1991).

2.8 INTERACTION BETWEEN DROPS AND HOT GASES

2.8.1 DROP BEHAVIOUR AND MOVEMENT

When a water jet comes out and breaks up into droplets, the droplets will continue to fall. Water drop particles moving in air with an initial velocity are subject to an

accelerating gravitational force and retarding drag forces (Lapple and Shepherd, 1940).

The drag force is due to the surface friction and pressure drag. Viscous friction of the gas at the drop surface will cause the surface friction. Pressure drag is caused by the aerodynamic shape of the drop producing back eddies in the wake of the drop owing to the separation of the boundary layer (Jackman, et al, 1993). If initially the velocity is low, it will accelerate because of gravitational force. As the droplet accelerates, its drag increases, and soon it will reach the condition where the gravitational force will balance the drag of the droplet. The resultant velocity is called the terminal velocity for the droplet (Yuen, 1974).

2.8.2 DROP EVAPORATION

The evaporation of drops in a spray involves simultaneous heat and mass transfer processes in which the heat for evaporation is transferred to the drop surface by conduction and convection from the surrounding hot gas, and vapour is transferred by convection and diffusion back into the gas stream. The rate of evaporation is mainly governed by the temperature difference between the droplets and the surrounding gases, by the pressure, transport properties of the gas; volatility, and diameter of the drops in the spray; and the velocity of the drops relative to that of the surrounding gas.

The primary purpose of atomisation is to increase the surface area of the fuel and thereby enhance the rate of heat transfer from the surrounding gases to the fuel. As heat transfer takes place the drops heat up and, at the same time lose part of their mass by vaporisation and diffusion into the surrounding air or gas. The rate of heat and mass transfer is markedly affected by the drop Reynolds number, whose value varies throughout the lifetime of the drop, since neither the drop diameter nor the drop velocity remains constant. The history of the drop velocity is determined by the relative velocity between the drop and the surrounding gas and also by the drop drag

coefficient. The latter again depends on the Reynolds number. After a certain time has elapsed each drop attains its steady-state temperature corresponding to the prevailing conditions.

The larger drops take longer to attain equilibrium conditions, and their trajectories are different from those of the smaller drops since they are less influenced by aerodynamic drag forces. However, the smaller drops supplied in the hot zone of the fire evaporate faster and produce a cloud of vapour that moves along with air, and this will cause the fire to be cooled faster.

2.8.3 DROP-GAS INTERACTION

The cooling effect of the drop on the hot gases causes an increase in density, which consequently causes a decrease in gas velocities (assuming a constant mass flow rate). The gas velocity is also altered by the momentum of the dorps as they pass through the gas stream. The subsequent change in velocity is found by using the energy balance equation (Welty, Wicks and Wilson,1984).

2.8.4 EFFECT OF WATER DROPLET SIZE:

The smaller the droplet diameter is, the faster it will evaporate in a hot gas environment. A large number of very small droplets will have a larger surface area than fewer large drops. Presentation of such a large surface area of water within a combusting region allows more of the heat generated to be abstracted from the reaction and hence improves the chances of extinction. The residence time of a water droplet from the spray nozzle till it hits a surface or is blown out of the compartment, is the effective time where heat can be absorbed from the flames and the hot gases. Small droplets will evaporate before they reach the base of the fire, and they will evaporate in the upper part of the compartment, and most of the steam can follow the smoke through the exhaust opening.

The effect of evaporating water droplets will be cooling of the gases, which may consequently lead to extinction of flames.

However, rapid evaporation of water leads to an increase of volume of the water by a factor of about 1600. This may block the air supply to the enclosure. Smoke and products from the combustion zone may be recirculated from the upper part of the enclosure. This may lead to oxygen starvation in the combustion zone, and consequently to extinction.

However, a counter-argument can be raised over small droplets, which is that large water drops are preferred for some applications such as combating fires with higher-velocity plumes; this is mainly because the larger drops will have greater momentum, and be able to penetrate the fire plume and hit the fuel and the floor without being totally evaporated, for the purpose of cooling surfaces to prevent spread of flames. There is also a concern that very fine droplets will be carried away on the strong convection currents associated with certain types of large fires. These fine droplets will thus be transported away from the source of the fire and become unavailable for fire control.

It has been claimed that the optimum droplet size in a spray is 300 μm (Thomas, 1992). This is based on a theoretical analysis of the trade-off between the cooling effect which increases as droplet size reduces, and the throw which decreases as droplet size reduces.

2.8.5 PENETRATION OF DROPS INTO A RISING FIRE PLUME

Once the water droplets have been discharged from a spray, they finds themselves in a hot buoyant fire plume that has been produced by a growing fire. The rising fire plume, consisting of flame, hot products of combustion, and entrained air, is a region of fairly high velocities and temperature.

For a spray to be able to exert a useful effect on a fire, it is usually necessary for the spray to penetrate to the seat of the fire, particularly to the burning fuel. To do this

the spray must be either formed near the fuel or have sufficient forward force to prevent too much of the spray being either deflected by or evaporated in the flame and hot gases associated with the fire.

The factors which control the penetration of spray to the seat of a fire are the drop size and thrust of the spray, the thrusts of the flames and wind, gravity, and the evaporation of spray in the flames (Rasbash, 1964).

2.8.6 Experimental and Numerical Spray-Fire Interactions

In an effort to determine the cooling that occurs in a room fire due to the presence of water spray, Kung (1977) devised an experiment utilising a pool fire in a room enclosed on all sides with the exception of one open window. The sprinkler was located in the centre of the ceiling and the orifice size, water pressure, and flow rate were varied throughout the tests. Even though the fire was towards one corner of the room, the sprinkler was close enough to the fire to provide direct sprinkler-fire interaction. Three important parameters were found in the extinguishment and cooling of room or enclosure fires: one was the fire size and the amount of fuel burned in a given time, another was the flow rate of the water through the sprinkler, and finally the nozzle orifice diameter which can control the droplet size was found to be important. Large flow rates and small droplets were found the best for fire suppression. The study also found that the mole fraction of steam present was good indicator of whether or not a fire could be extinguished, the more steam the better. Also noted was the fact that smaller droplets evaporate more, increasing the mole fraction of steam as compared to large droplets.

An experiment on the air entrainment into water sprays was conducted by Heskestad et al (1976). An array of 32 downward-facing nozzles was set up in rows of four, two rows to each height level, with the bottom level being at 2.13 m from the floor. They studied the air entrainment in the case of one nozzle operating, then with multiple nozzle forming a curtain. In the single nozzle case air velocities were measured at

distances of 1.52, 3.05 and 5.79 m below the nozzle and at radii 0.31, 0.61 and 1.22 m from the nozzle centreline. Droplet sizes were also measured by freezing them in liquid nitrogen at a distance of 5.8 m below the nozzle, which resulted in a 0.4 mm Sauter Mean diameter. Performing an integration of the air velocity profiles obtained enabled the authors to find flow rates of the entrained air. The nozzles used produced a solid cone type spray and it was found that the greatest air entrainment flows occurred along the nozzle centreline (vertically beneath the nozzle) with the velocity dropping off, slowly at first, then more rapidly at greater radii. The airflow was also found to increase with increasing vertical distance from the nozzle. The same trends were also found when multiple nozzles were used but with larger airflows obtained. The authors also used a theory based on the aerodynamic drag of each droplet in the spray of given cross sectional area (and droplet density), droplet velocity, and droplet size- this theory produced results within 17% of the experimental values obtained. Using this theory it was found that wide sprays entrain far more air than narrow ones. It was also found that the air flow was sensitive to changes in water pressure holding the nozzle orifice diameter constant, but insensitive to increased flow rates obtained through orifice variation with pressure constant.

In order to predict the interaction between a downward directed water spray and buoyant plume induced flow, Alpert (1984) made use of numerical methods in order to simulate the situation. In the simulation the sprinkler was located at a height of ten meters above the floor and directly above the buoyant plume. Even with the water spray having its greatest momentum, the buoyant upward plume along with the continuation of the plume above the nozzle and cross the ceiling existed throughout the tests. The spray however did cause a widening of the upward plume along with downward deflection of the ambient air approaching at the lower levels. The droplets in the innermost section of the spray were found to be turned back towards the ceiling by the plume at a height of around two meters from the source. The simulated velocities and diameters of the droplets were varied to obtain information on the

reaction to a change in momentum of the spray. It was found that with greater water spray momentum the heat absorption increased, temperature decreased, and the ceiling plume velocities were decreased. It was concluded that the properties of the flow appear to be dependent on the ratio of the droplet momentum to the buoyant sources momentum.

Chow and Fong (1991) also used a computer model to simulate a fire in an enclosure with the effect of water sprinkler activation being assessed. The interaction of one, two, then three sprinklers was simulated in the vicinity of the fire with direct fire-sprinkler interactions. The temperature-time curve predicted by the model did not decrease at the very end of the time period simulated as in the experimental results, but the temperature trends were otherwise quite similar. The temperatures predicted were also slightly higher than in the experiment. The authors attributed these discrepancies to their model not simulating the fire suppression of the fuel.

Hoffman and Galea (1993) used a Eulerian-Eulerian fire sprinkler model to simulate fire-sprinkler interaction. It was found their simulation followed previous experimental data quiet well near the sprinkler, deteriorating in the far field. The authors stressed the need for detailed experimental data on fire-sprinkler interaction.

Nam (1993) simulated the interaction of one fire sprinkler located directly over a fire source. Different drop sizes from 0.29 to 1.1 mm were used for the simulation of the spray. It was found that the model produced results close to previous experiments along the centre region but proved less satisfactory in the outer plume area. The model predicted higher penetration of droplets in the outer plume area than the experiments, which was attributed to possibly inaccurate initial spray conditions.

Nam (1999) conducted numerical simulation to investigate the interaction between ESFR sprinkler sprays and three heat release rates (500, 1000 and 1500 kW) under two different ceiling heights, 3 and 6.1 m. The water flow rates used vary from 1.9 to 9.48 lit/sec. Actual delivered densities (ADD) and penetration ratios were computed to a target area. The effect of water penetration into a fire plume that could have

reduced the fire intensity was not taken into account. It was found that the actual delivered density always increases as the flow rate increases, that the actual delivered density under the 6.1 m ceiling is generally lower than the corresponding ones under the 3.0 m ceiling but the penetration ratios are higher. Also, the results suggested that large drops are more important for the penetration capability of spray under the 6.1 m ceiling than that under the 3.0 m ceiling.

Interaction of a water spray with the smoke layer is an important issue for study (Morgan, (1979) and Hinkley, (1986) and (1989)). This is so because the fire-induced buoyant smoke layer might be cooled down significantly by the water spray. Therefore, it could lose buoyancy and fall to a lower level. The occurrence of smoke logging reduces the efficiency of smoke extraction systems, causing hazards to building occupants.

It is interesting to know whether the sprinkler water spray obtained under certain operating conditions is able to confine a fire. With such knowledge, the minimum amount of water can be discharged from an appropriate sprinkler head in order not to overflood the compartment and cause water damage. A good understanding of the interaction between the fire-induced flow and sprinkler water spray enables engineers to improve the present design for sprinkler layout, by applying a reasonable amount of water, and giving guidance for modifying the physical features of the sprinkler head itself. The sprinkler system can then be designed to perform more efficiently in controlling a fire. Solving this problem is very difficult, however, because many physical phenomena such as direct cooling of the smoke, air entrainment into the spray and water evaporation (Kung, (1977) and You, (1986)) have all to be considered concurrently.

2.9 WATER SPRAY SYSTEMS

Water spray systems, often referred to as deluge systems, consist of open spray nozzles fed by a network of small diameter piping, connected through a control valve to the fire protection water supply. The control valve may be manually actuated, but automatic actuation is preferred. Automatic actuation requires the addition of fire detection and automatic control circuits (pneumatic or electrical). Water spray systems are commonly provided in areas where rapidly developing, high-intensity fires are likely to occur. Depending upon the effect desired (i.e. extinguishment, control of fire or exposure protection) the water application rates may vary.

In design of the water spray systems, the most commonly followed standard is NFPA 15 "Standard For Water Spray Fixed Systems For Fire Protection" (NFPA, 1994). The selection and placement of nozzles must be based upon their characteristics such as discharge pattern, drop size.

Sprinkler systems differ from water spray systems in that all of the sprinkler heads, or nozzles, are sealed by a heat-sensitive mechanism. Each head will open individually to begin flowing water when exposed to the heat of a fire. There are basically two types of sprinkler systems, referred to as wet pipe and dry pipe. Wet pipe systems are used in areas which are not subject to freezing. Dry pipe systems are used in unheated areas which may occasionally freeze.

2.9.1 Spray Nozzle Types

There are different types of spray nozzles commercially available which can be fixed in water spray systems. Some of these are discussed below (Cote, 1991):

1. High velocity spray nozzles, generally used in piped installations, discharge in the form of a spray-filled cone.

2. Medium velocity spray nozzles designed to produce a solid cone spray.
3. Low velocity spray nozzles usually deliver a much finer spray in the form of a spray-filled spheroid or cone.
4. Internally impinging type of spray nozzles produce spray by giving the water streams a rotary motion in spiral passages inside the nozzles. These rotating streams are mixed internally with a centre stream to project a solid cone of water spray from the nozzle.
5. Another type of water spray nozzle uses the deflector principle of a sprinkler. The water discharge orifice projects a solid, cylindrical stream of water onto a deflector which breaks it up mechanically into a conical distribution of water spray.
6. Spiral-type water spray nozzles which are characteristically different from all the others discharge water along the axis of a spiral of diminishing inside diameter. This spiral continuously peels off a thin layer of water from the surface of the cone, and breaks into spray as it leaves the spiral.

The selection of spray nozzles should take into consideration such factors as the character of the hazard to be protected, the purpose of the system, and the possibility of severe winds or drafts.

2.10 WATER SPRAY CHARACTERISATION

A spray is generally considered as a system of liquid droplets in a fluid continuous phase. Examples of common sprays are rains, fogs and waterfall mists. Other artificial sprays are fountain spray and atomiser sprays. Figure (2.5) indicates the range of drop sizes as they occur in certain natural phenomena and also as commonly produced by atomisers.

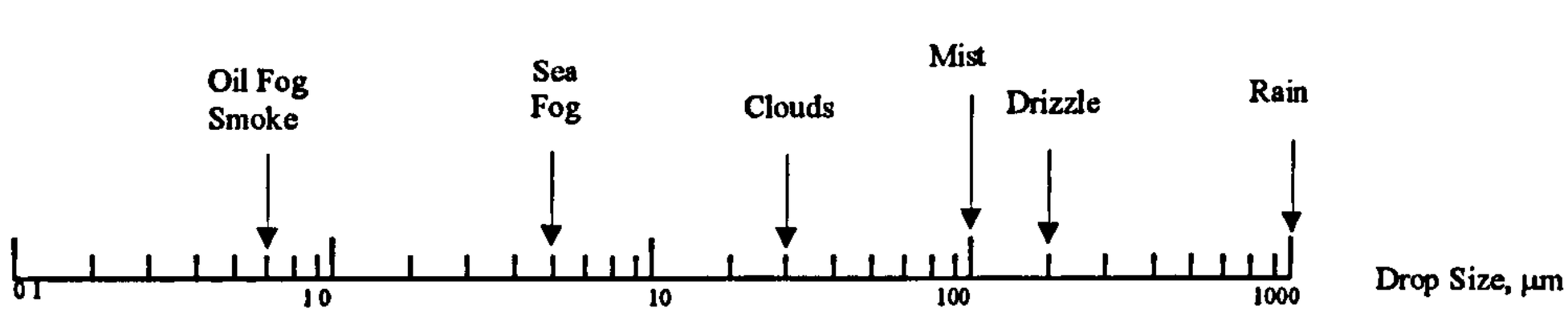

Figure (2. 5). Spectrum of droplet diameters (μm) [Lefebvre, 1989].

The characteristics of the water spray determines the mechanisms by which it suppresses fire. Those characteristics are dependent upon the method of spray production, different water spray systems producing water sprays with different characteristics.

The characterisation of the spray can be described with four factors for the fire suppression purposes; those are:

- Drop size and distribution (Diameter and range)
- Spray angle
- Spray momentum
- Spray flux density
- Droplets velocities

2.10.1 Drop Size and Distribution

A more complete picture of any spray can be gained using a distribution function (Lefebvre, 1989).

Drop size distribution refers to the percentage of the total liquid volume contained in drops of different diameters, measured at specified location in a spray. A drop size distribution is not a constant for spray, it varies with location e.g. closer or farther from the nozzle, near the centre or the outer edge of the cone (Lefebvre, 1989 and Mawhinney, 1993a).

Different designs on spray nozzles will produce sprays with different proportions of larger and finer drops (Mawhinney, 1993b).

ASTM E799 describes a number of representative diameters such as Volume Median Diameter (VMD), or the Sauter Mean Diameter (SMD), which could be used to give an industry standard for the description of a spray diameter distribution. Representative mean diameters can be defined in terms of simple diameter, droplet surface area or volume.

For modelling the interaction of water spray and fire using computational fluid dynamics, the distribution of drop sizes in the spray is represented as a function of two parameters, one of which is representative diameter and the other a measure of the range of drop sizes (Mawhinney, 1993b).

A number of drop size distributions have been proposed, some are theoretically based, others are purely empirically based. Some of these distributions are briefly described below (Mugele,1951, Lefebvre, 1989 and Jones, 1995);

Rosin-Rammler Distribution Function

One of the best known empirically-based distribution functions, and widely used expression for drop size distribution is one that was originally developed for powder. It is frequently quoted in the cumulative form:

$$1-Q=\exp\left[-(D/\overline{D})^{q}\right] \qquad \textbf{(2. 3)}$$

Where Q is the fraction of the total volume occupied by drops of diameter less than D, $\bar{D}$ the representative diameter and q the measure of the distribution of the droplet sizes. $\bar{D}$ and q are constants.

The higher the value of q, the more uniform is the spray. If q is infinite, the drops in the spray are all the same size. For most sprays q usually takes values between 1.5 and 4. The representative diameter, $\bar{D}$, is defined such that 63.2% of the spray's liquid is found in droplets of smaller diameter. A slight modification of this Rosin-Rammler distribution function involves using the logs of the droplet diameter and mean diameter. So, re-writing the Rosin-Rammler equation in the form of volume distribution equation:

$$\frac{dQ}{dD}=q\frac{(\ln D)^{q-1}}{D(\ln\overline{D})^{q}}\exp-(\frac{\ln D}{\ln\overline{D}})^{q} \qquad \textbf{(2. 4)}$$

generally provides a good fit to the data.

However, it is desirable to work only with average diameters instead of the complete drop size distribution (Mugele, 1951). Lefebvre (1989) usefully divides the possible diameters into two types: these are **mean diameters** and **representative diameters,** each type has its own attributes and applications. Mean diameters are defined according to the general formula (Mugele,1951, Lefebvre, 1989 and Jones, 1995);

$$(D_{mn})^{m-n} = \frac{\int_{Do}^{D_m} D^m (dN/dD) dD}{\int_{Do}^{D_m} D^n (dN/dD) dD} \qquad (2.5)$$

Where D is droplet diameter, D_m the maximum droplet diameter, D_o the minimum droplet diameter and dN/dD the variation in droplet numbers according to their diameters. The integers m and n may take on any values between 0 and 4 depending on the particular mean being investigated; and the sum $(m+n)$ is called the order of that mean diameter. The integer m is greater than n. Examples of m and n of the important mean diameters are given in the table below:

m	n	$m+n$	symbol	Name of mean diameter
1	0	1	D_{10}	Length
2	0	2	D_{20}	Surface area
3	0	3	D_{30}	Volume
2	1	3	D_{21}	Surface area-length
3	1	4	D_{31}	Volume-length
3	2	5	D_{32}	Sauter (SMD)
4	3	7	D_{43}	De Brouckere or Herdan

Sauter mean diameter, SMD

An example of mean diameter is a 5th order mean: m = 3, n = 2: the volume-surface mean diameter (also called the Sauter mean diameter, SMD):

$$D_{32} = \frac{\int_{D_0}^{D_m} D^3 (dN/dD) dD}{\int_{D_0}^{D_m} D^2 (dN/dD) dD} \qquad \textbf{(2. 6)}$$

Mean diameters can provide an estimation of the quality of the spray. The Sauter Mean Diameter (D_{32}) is often used as an indicator of the fineness of a spray, since it is heavily weighted by the smaller droplets in a given distribution (Jones, 1995).

2.10.2 FLUX DENSITY

The ability of water mist to extinguish a fire depends on more than its drop size distribution (Mawhinney, 1993a). Flame suppression with fine spray requires that a certain minimum mass of water droplets be suspended as spray. Therefore, a spray must have a density, or mass flow rate, that is appropriate for the fire scenario and compartment conditions. Whether the extinguishment mechanism is due to heat extraction as fire droplets evaporate, or to displacement of oxygen by steam expansion, a certain minimum number of droplets per volume of space will be required to accomplish suppression.

The water spray droplets that actually interacts with the fire must be sufficient to absorb a significant proportion of the heat given off by the fire.

Spray flux density is therefore an important characteristic of water spray for fire suppression systems. The flux density is the mass of water which is discharged over a defined area per unit time (Orr, 1996).

The initial spray density must be high enough to allow for losses of spray due to drops falling out or depositing on the surfaces of obstructions, and still have enough suspended water droplets per unit volume of air to be able to extinguish a fire.

The flux density, most commonly described by the term "nominal flux density, N_{fd}", was introduced to establish an initial spray flux density that a (full cone only) nozzle is capable of delivering (Mawhinney, 1993a), where:

$$N_{fd} = Q_N / A_C \qquad (2.7)$$

Q_N being the nozzle discharge in lit/min and A_C the area of a circle with diameter equal to the diameter of the spray cone, measured 1 metre from the nozzle tip.

2.10.3 SPRAY ANGLE

The spray angle is usually the angle formed between the outer limits of the spray core (Lefebvre, 1989 and Lev, 1991). The spray angle governs parameters which can control the interaction between the water spray and the flame (Kim, 1997). Therefore, it is necessary to understand its significance in defining appropriate sprays for fire suppression applications. Spray angle directly affects the velocity and direction of the droplets leaving the spray nozzle. Therefore, for modelling with computational fluid dynamics at least, the range of directions of initial droplet trajectories is of interest. Spray angle is a critical factor in determining nozzle spacing to ensure a relatively uniform distribution of spray, without large void area between nozzles. Finally, spray angle is very significant in determining the initial velocity and momentum of the spray, which in turn determines its ability to penetrate obstructions in the compartment (Mawhinney, 1993b).

Spray angle will determine the ability to penetrate the flame. The spray momentum therefore is highly affected by the spray angle of the nozzle.

In general, a narrow spray angle of a nozzle will produce higher spray momentum and penetrate further than wide spray angle nozzle (Mawhinney, 1993a) and (Lefebvere, 1989).

2.10.4 SPRAY MOMENTUM

The ability of the spray to penetrate the fire plume and push the water droplets towards the fire in the compartment, and to interact with the flame, depends on the spray momentum. This momentum must come from the spray nozzle.

The spray angle of the nozzle partly participates in the projection ability: the wider spray angle of a nozzle has a lower projection than the narrower spray angle. Another factor affecting the projection ability is the mechanism for producing the spray (Mawhinney, 1993a and 1993b). To maximise spray momentum higher nozzle pressure and reduced spray angle are needed.

Indirect indication of the momentum provided by a nozzle is studied experimentally by Mawhinney (1993a) by measuring the horizontal distance of spray nozzle projection.

2.11 WATER DROPLET CHARACTERISATION TECHNIQUES

The various techniques for drop characterisation can be classified as mechanical, electrical and optical methods (Lefebvre, 1989).

The mechanical techniques depend on the collection of drops. The electrical techniques rely on the detection and analysis of electronic pulses produced by drops, i.e. use indirect probing method; some electrical methods include hot wire technique and charged wire technique.

The optical methods can be divided into imaging, single drop counting and light diffraction techniques. There are two main methods of sampling the spray in optical drop sizing method in order to determine its droplet size distribution, one

representing spatial averaging (light diffraction and imaging methods) and the second temporal averaging (single drop analysers) (Bayvel, 1993).

2.11.1. IMAGING TECHNIQUES

Imaging techniques include microscopy, photography and holography. In these techniques, incandescent lights, mercury vapour lamps, flash and laser light are used as light sources.

The longest established and most inexpensive imaging method is photography. This technique involves direct photography of a spray followed by analysis of processed film. After development, the negative can be projected at greatly increased magnification to obtain direct measurement of particle size.

Photographic characterisation is able to measure non-spherical drops, and analyses events like drop coalescence, break up and oscillations. This technique does not disturb the sample and is able to measure in harsh environments (Jackmann et al, 1992).

Manual analysis of photographs is very time-consuming and subject to operator fatigue and bias. Automatic image analysis is an improvement but must be used with care, and the cost of equipment is significantly increased (Chigier, 1983).

2.11.2. SINGLE PARTICLE ANALYSER

The theory of phase/Doppler particle analysers was described in Bachalo (1980) who developed this method. Two beams of laser light with different angles of approach incident on a drop undergo a phase shift. The detection at off-axis angles, the spatial frequency of the scattered interference fringe pattern is inversely related to the particle diameter.

The drop velocity of a single particle can be measured by using crossed-beam. When these two beams intersect, stationary interference fringes appears. As the particle traverses the fringes, a modulated scattered light signal is produced.

Three detectors are used to reduce measurement ambiguity, add redundant measurements to improve reliability, and provide high sensitivity over a large size range (Lefebvre, 1989). The instrument can measure drop size in the range 0.5 to 3000 microns.

2.11.3. DIFFRACTION OF LIGHT

For average size distribution measurement of clouds of droplets in sprays, the particle analyser based on Fraunhofer diffraction is proving to be one of the most effective, simple and reliable instruments.

It is particularly useful for testing global (ensemble) characteristics of sprays from a wide variety of nozzles. The instrument is easy to use and very little knowledge of its basic principles is required for operation.

The instrument is based on well known optical principles (Chigier, 1980) to be discuss in chapter six. The instrument owes its development to Swithenbank et al (1977) at Sheffield University and now is commercially available through Malvern Instrument Ltd, England.

The positive points of the Malvern instrument: it is easy to set-up, very versatile and requires no calibration; the measurement is non-intrusive, there is no probe to disturb the flow and introduce sampling errors and can be used in many environments; it gives accurate and repeatable results from large number of drops sampled.

2.11.4. THE CHOICE OF A TECHNIQUE

The choice of a technique and instrument for drop size distribution measurements that are most appropriate should have the following characteristics:

a) Make no disturbance to the spray pattern

b) Give rapid means of sampling and counting

c) Good size range capability

d) Continuous sampling

It is clear that no single instrument is completely satisfactory and can fulfil all the above criteria.

2.12 FIRE MODELLING

Modelling is a means of presenting some facets of reality for purposes of explanation, manipulation and analysis. (DiNenno, 1988). Modelling are used in many areas of fire protection design, including suppression system design, smoke control system design, and egress analysis. (DiNenno, 1995). Two model-building strategies have evolved for calculating the effects of fire in enclosure (Cox, 1995).

These are zone model and field model which differ in their concepts, computational requirements and potential power.

2.12.1 ZONE MODELLING:

Zone modelling is the traditional approach to compartment fire modelling, whereby the compartment is subdivided into a series of zones, for example a hot upper layer, a cool lower layer, a rising plume of hot gas, a ceiling, upper walls, lower walls, floor, fuel source, and an external environment connected via a ventilation opening. This is a "three gas zone" model. Some of the zone models programmes are ASET & ASET-B, Harvard, FIRST, CCFM, COMPF2, CSTBZ1, FAST and OSU (Ohio State University Compartment Fire Computer Program).

2.12.2 FIELD MODELLING:

Field modelling represents a completely different approach to compartment fire modelling compared to zone models. Advances in computer power and fundamental research over the last decade have made it feasible to directly model turbulent combustion phenomena using computational fluid dynamic (CFD). The incentive for this approach of detailed models of combustion chemistry, turbulent flow and radiative heat transfer, removes much of the dependence of the fire hazard models on expensive, large scale experiments. Instead, validation of the CFD turbulent combustion model can be made with smaller laboratory, or medium scale experiments, and then confidently extended to a larger scale or to more complicated release geometries. In addition, CFD calculation can provide insight for the development of new robust, simple to use, prediction tools. Field models can be difficult for potential users to assess. They are often treated as black boxes perhaps with associations of 'fundamental' approaches complexity, sophistication and user friendly graphics output. Users need a deeper knowledge of the contents of individual models. Some of the field models programs are JASMINE (FRS) for Smoke Movement Model, and for general purpose CFD models are PHOENICS (CHAM Ltd), FLOW3D (AEA HARWELL), FLUENT (CREARE), and TEACH/CINAR (IMPERIAL COLLEGE).

2.13 COMPUTATIONAL FLUID DYNAMICS APPLICATIONS

The importance of CFD as design tools for architects can be seen in the paper by Waters (1986). A general purpose computer code was used to study air and smoke movement generated by a fire within very large buildings, such as airport terminals or

department stores. The environmental conditions within a building and hence the life safety aspect in the event of a fire could be assessed with the aid of this model.

A computational fluid dynamics model designed specifically for aircraft cabin fires was developed by Galea and Markatos (1987). It is a steady state and time-dependent, three-dimensional model which uses a body-fitted co-ordinate (BFC) to accurately model the interior of an aircraft. It has been partially validated and is now used as a research tool to investigate design features of aircraft such as the effect of the air-conditioning system on the temperature distribution within a burning fuselage (Galea and Markatos, 1989).

Computational fluid dynamics (CFD) simulations are increasingly used to estimate the effects of fires in tunnels and corridors investigating the effects of turbulence models, model constants, differencing schemes (Bennardo et al, 1997 and Woodburn et al, 1996), fuel pan size, fuel inflow profile, upstream smoke layer radiative heat transfer, grid refinement on mine gallery fire (Fletcher et al, 1994), ventilation schemes (Fletcher et al, (1994) and Brandeis and Bergmann (1983)) and radiation modelling (Fletcher et al, (1994), Kumar and Cox, (1988) and Woodburn et al, (1996 a and b)).

The CFD was used to investigate the fire accidents that occurred in the past, such as the King's cross station fire (Simcox, 1989).

CFD simulation was carried out on enclosed gas fire extinguishment by water spray (Alper, 1984 and Novozhilov et al, 1996) discussed in section (2.8.6). Significant effort has been devoted to the modelling of sprinkler interaction with a smoke layer because of the important effect of smoke knockdown (Chow and Fong (1993), Hoffmann et al (1993 and 1989) and Chow and Cheung (1995)).

The interaction of fire plume (Hoffmann, (1993), Downie, (1995) and Nam (1996)) and the hot air layer (Chow and Fong (1991), (1993)) with water sprays and the process of heat and mass transfer in the droplet and the parameters that impact the evaporation (Butz, 1992) are other applications of the CFD.

Computational fluid dynamics was utilised to investigate the penetration capability of sprinkler sprays above a fire source (Nam, 1999).

Though computational fluid dynamics provided a useful investigation tool, the accuracy obtained is paid for by the excessive amount of CPU time required to perform the modelling. Partly due to the overheads involved in the calculation of the models and the limited amount of experimental data available, thorough validation of these models still needs to be carried out.

2.14 CONCLUSION

Although there are a number of research studies that have been reported on the compartment fire, the behaviour of jet fires and spray-fire interaction, most compartment fire research has concentrated on fires in buildings rather than on the specialised situation of the oil and gas industries. The EU programme JIVE concentrated on the behaviour of jet fires impinging on or engulfing obstacles, especially vessels and pipework, and the response of the vessel or pipework and its contents to the fire.

The previous work of spray-fire interaction provided useful information concerning some important aspects of droplets emanating from spray systems and the spray-fire interaction. However, there are some major points of concern where a compartment jet fire scenario could produce entirely different results. In some of the studies, strong convective currents and an extreme heat source are not taken into account.

A review of early work, including its computational fluid dynamics and application was given which, however, showed that much less attention has been given to CFD modelling of extinction phenomenon and comparison between numerical and

experimental results. In addition, the combustion reaction is often entirely omitted in favour of a simply prescribed heat source.

Water spray systems show much potential as effective and safe fire suppression systems. There is however general lack of detailed and quantified information regarding spray suppression mechanisms for jet fire.

CHAPTER 3

EXPERIMENTAL SETUP

3.1. INTRODUCTION

This chapter describes the experimental set-up, which includes the experimental rig, apparatus, data acquisition systems and sampling gas analysis systems. This chapter also describes the experimental condition and experimental procedures. Safety requirements and risk assessment are also described in this chapter.

3.2 EXPERIMENTAL RIG

The overall experimental apparatus is schematically shown in Figure (3.1). A propane jet nozzle was located at the centre of 6×2.4×2.4 m^3 compartment. The

water spray nozzles were located at the top of the compartment and could be moved any where on the top plane. The compartment was equipped with various forms of instrumentation that will be described in detail in the following sections. The rig was initially built by Shell specifically for jet fire research and the mitigation which includes the use of standard water deluge systems. The results found by Shell were not available in the published literature and therefore the data were confidential and restricted to Shell's own use.

3.2.1. Compartment

The test were performed in a test compartment of 35 m^3, located at the University of Sheffield Buxton Laboratories at Harpur Hill, near Buxton in Derbyshire. The dimensions of the compartment are 6 m long, 2.4 m wide and 2.4 m high. The compartment was elevated 1 m above the ground. The walls, floor and ceiling were made of 1.5mm thick corrugated steel plate (channel), shown in Figure (3.2). The figure also shows the main dimensions of the compartment. Originally the compartment was built as small-scale model of a typical offshore module.
The air inlet opening covers the width of the enclosure, and is 600 mm high at the bottom of the front side. The outlet opening is located at the top of the front side and covers the width of the compartment and height of 600 mm too.

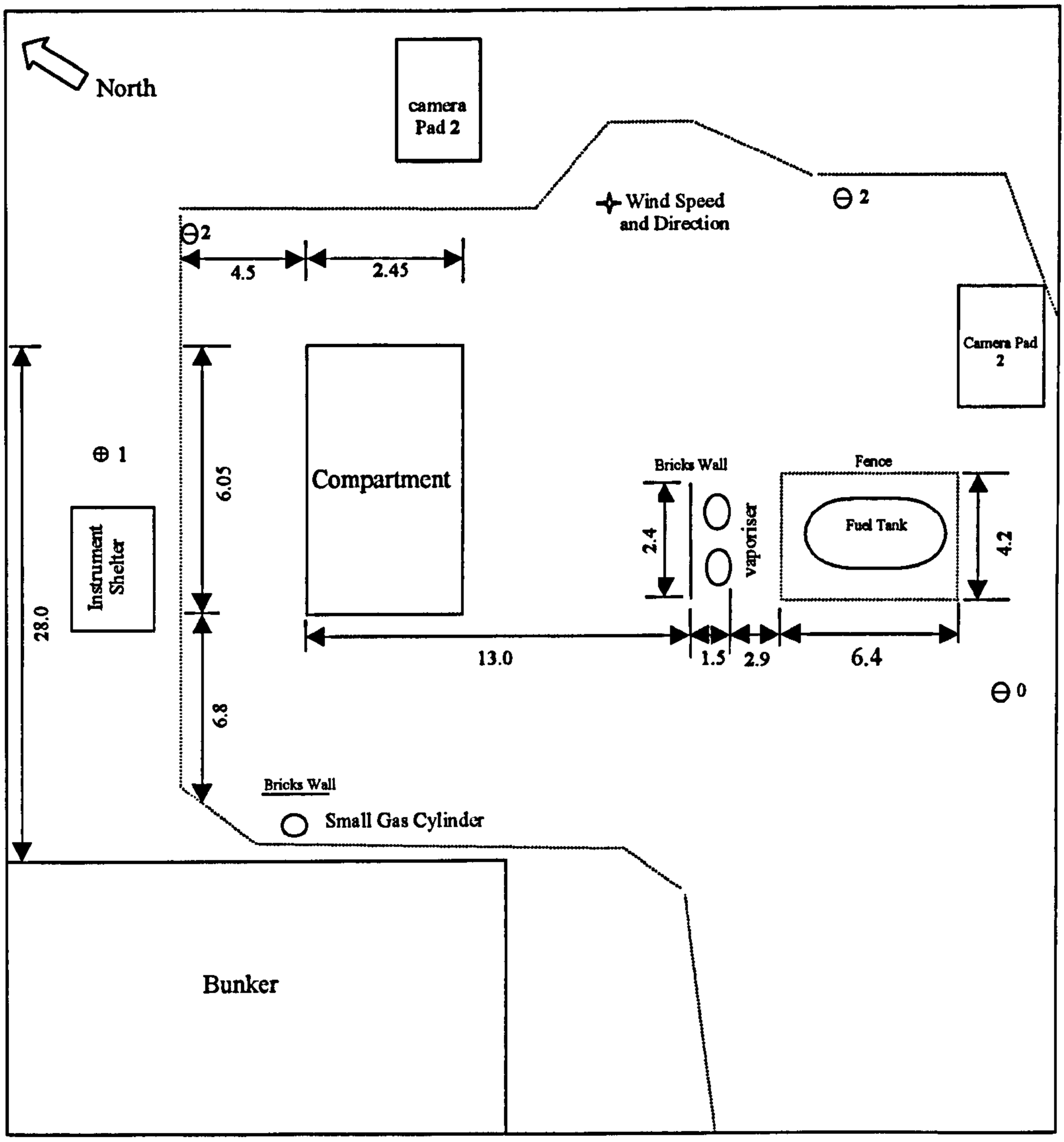

Figure (3.1). Plan View of the Field General Layout (dimensions in metre).

3.2.2. Ventilation

The compartment has an opening at its front (Northeast) side to provide ventilation. There is a baffle in the opening which was used to block half of the opening area. It was fixed in the centre of the opening, dividing it into two equal vents. Previous experience of Shell indicated that the size of the baffle was adequate to reduce the air entrained and limit the ventilation. Figure (3.2) shows the baffle dimensions and position in the compartment.

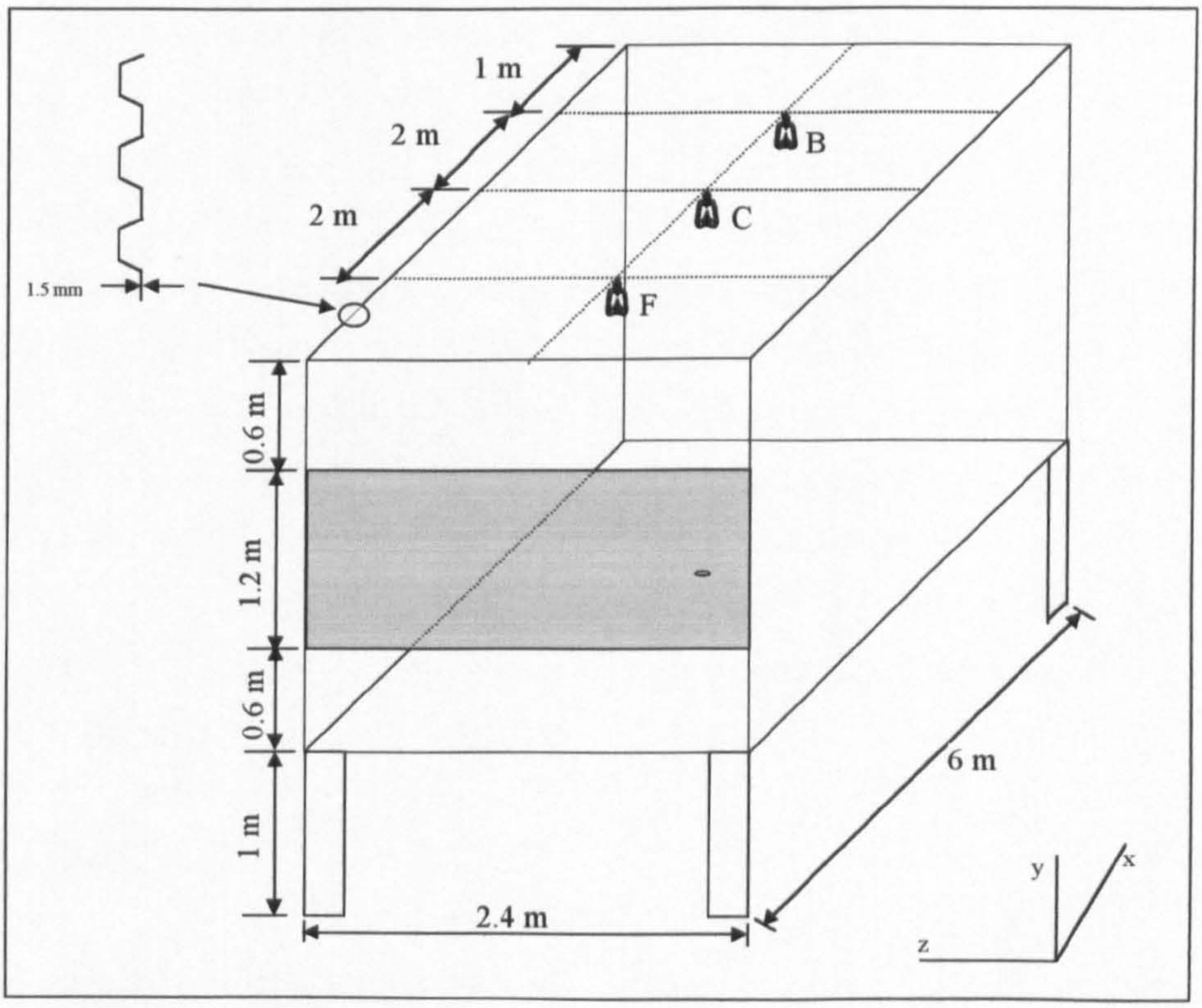

Figure (3.2). Schematic of Compartment and Cross Sectional of wall Panel

3.2.3. Jet Fire Systems

The propane jet nozzle used in the experiments is 20mm diameter steel pipes flowing along the centre of the module. The propane flow rate is 0.1 kg/s; the heat release rate of the jet was about 4.6 MW in all the tests.

- **Propane Gas Flow Control:**

A schematic diagram of the propane flow control system is shown in Figure (3.3). The gas line was equipped with a main manual shutoff ball valve, and directly down stream a pressure regulator was installed. The pressure regulator assured that fluctuations in the main line pressure would not affect the flow through the jet nozzle. A solenoid valve used in conjunction with the safety system (see section 3.2.5) was used to stop the gas flow should the flame go out. The pilot flame gas supply was taken directly from a small propane cylinder see Figure (3.3). The solenoid did not control the flow through the pilot. The gas lines passed through two vaporisers before it goes to the jet nozzle (see the figure). Another valve was next on the line with the flow meter directory following. The flow meter had a valve type flow controller allowing for flow rate adjustment, from the flow meter the gas then proceeded directly to the jet nozzle. The instruments used were as follows: The pressure regulator, The flow meter and the pressure gage manufactured by Platon Instrumentation. All control valves are numbered for ease of operation.

- **Vaporiser:**

Two vaporisers were installed three metres away from the propane vessel (see Figure 3.3). Two liquid inlet control valves are fitted to vaporisers directly connected to the process gas. The controller shuts off the liquid automatically if the bath heat exchange fluid temperature falls to a level where vaporisation will

not occur. This prevents low temperature vapour or liquid from entering the process system. The vaporisers used were 30 kW FGS.

- **Propane Storage Tank:**

The propane storage tank was located 15 m away from the compartment (see Figure 3.1). The capacity of the tank was 2 tonnes of liquid propane. For safety reasons the storage tank was protected by a fence all around. The tank was connected to one supply line connected to a pump and one return line for the excess fuel to be returned to the tank.

- **Pilot Flame:**

In order to start the jet fire; it is necessary to have a pilot light to ignite the jet flame. The pilot nozzle was adjacent to the jet nozzle and supplied by propane gas through a 75 kg cylinder see Figure (3.3). The pilot nozzle was fixed at an angle (inclined) to the jet nozzle to make sure that the flame crosses the jet nozzle. An ignition source was required to ignite the pilot light. This was provided by a 4 metre hand-held gas torch.

3.2.4. Water Spray Systems

The water system to the spray nozzle consisted of a main water line, which was supplied from a pressurised hydrant. The water flow rate and pressure were measured before the spray nozzle head. Water was supplied through large diameter pipe work with a shut-off solenoid valve controlled from the control room. The main water line was then connected to 4" pipe which consisted of three 2" branches for the spray nozzle heads to be fitted. Flow rate was monitored by means of flow meters fixed on each one of the pipe branches. Pressure was measured for the water supply on the main by a pressure transducer and the signal was sent to the computer through a data channel. A schematic drawing is shown in Figure (3.4).

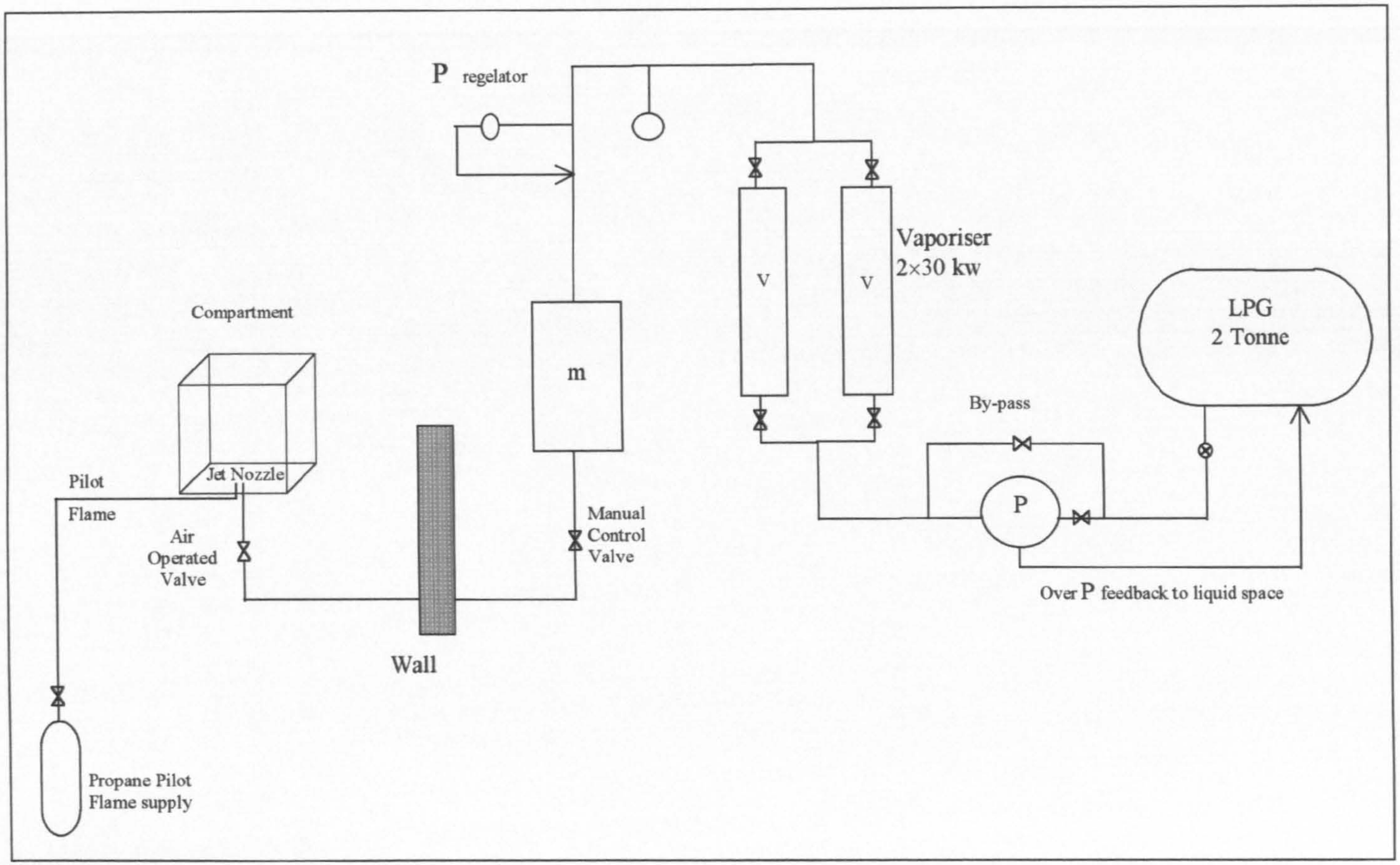

Figure (3.3). A Schematic Diagram of LPG/Gas Flow Control System.

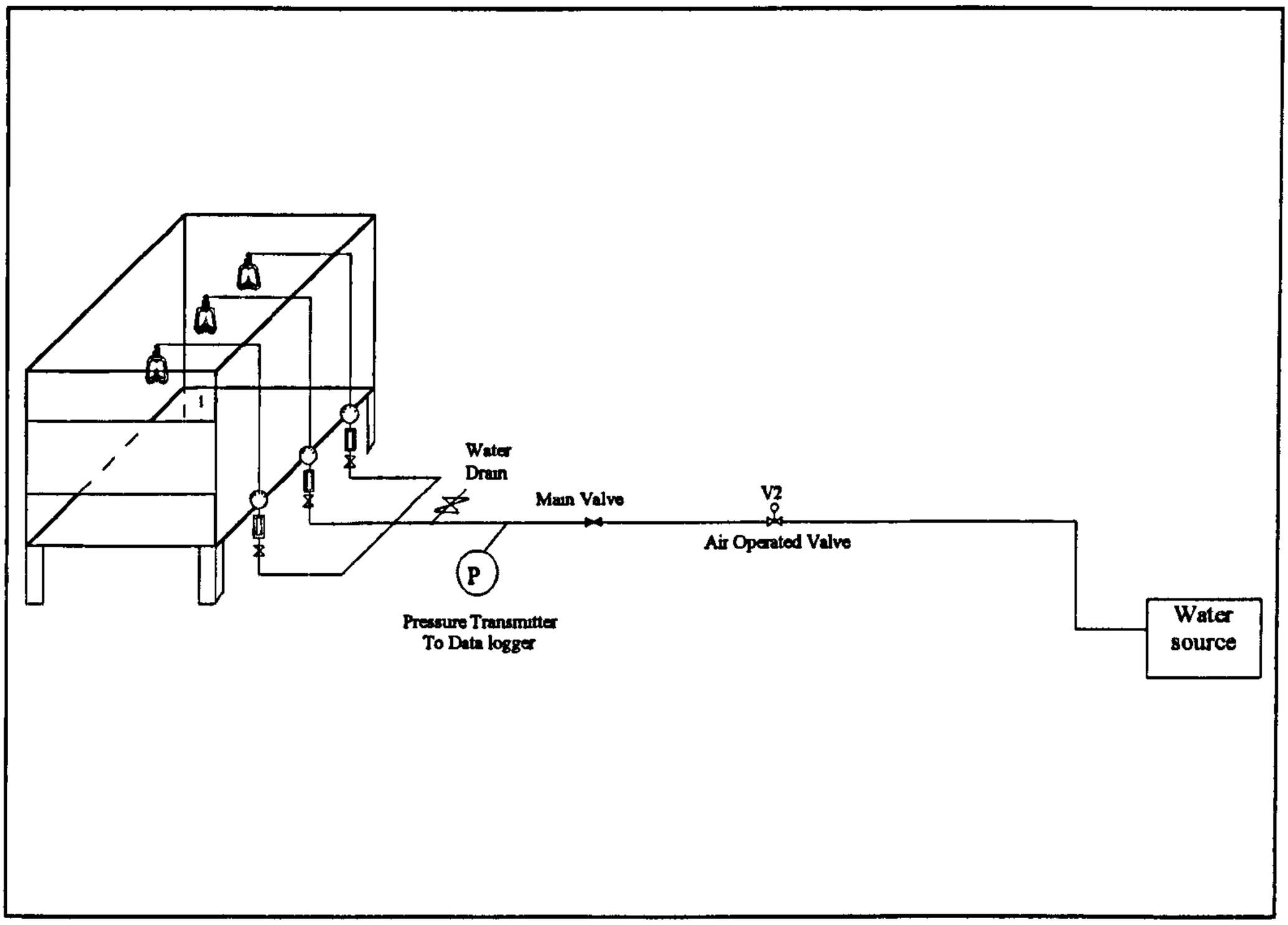

Figure (3.4). Water Flow System Diagram.

SPRAY CHARACTERISTICS

The spray nozzle consists of an orifice or nozzle and deflector. The deflector is designed to break up the solid jet of water issuing from orifice into small drops, which are re-distributed uniformly in a hemispherical pattern below the deflector. Four geometrically different nozzles were used for the purpose of this study. Different spray angles were used which were 60°, 90°, 120° and 150°. Figure (3.5) shows the spray pattern for three sprays and 150° spray angle. The nozzles were installed at the centreline of the ceiling with the orifice 100 mm below the ceiling and pointing vertically down. The nozzles used in the experiments are the

ANGUS Thermospray medium velocity 'open pendant' water spray nozzles. A schematic of one nozzle is shown in Figure (3.6). The models used are K50 150D, K50 120D, K50 90D and K50 60D (ANGUS, 1991).

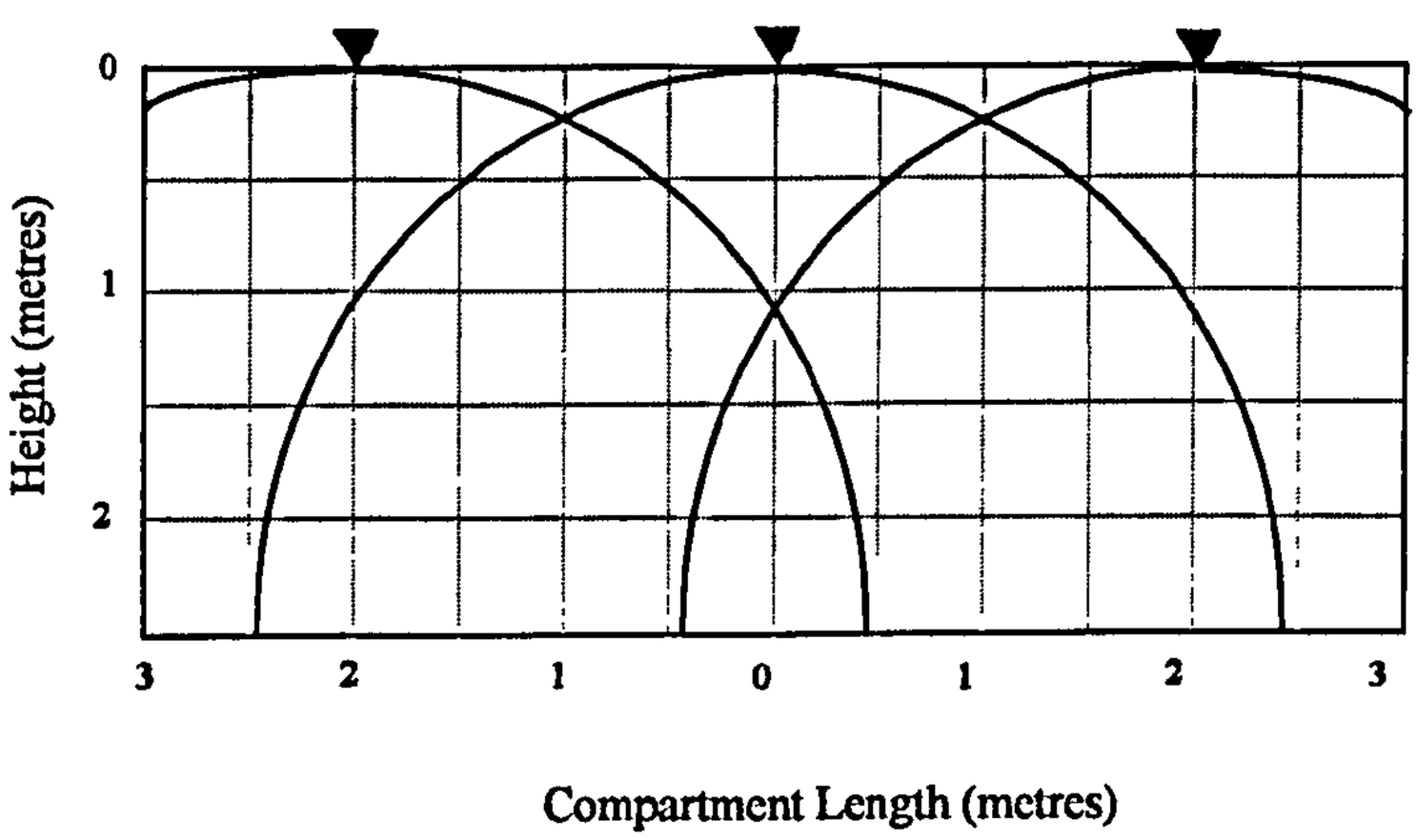

Figure (3.5). Water Spray Pattern for nozzles with 150° spray angle, 'K' Factors of 50 and 9.3 mm bore size.

- **Drop Size**

The most surprising observation was how little manufacturers have focused on the properties of the water spray; there is for instance hardly any information available on the drop size distribution that affects the vaporisation rate.

- **Bore Size:**

Water passes through a hole cylindrically bored before it travels towards the strike plate. The pipe fitting of sprays is 1/2 inch. The bore sizes most commonly used are between 6 and 14 mm. The orifice diameter, D, of the nozzles used in the tests was 9.3 mm. Each spray is given a K-factor, which relates the pressure at the spray head to the water flow rate leaving the spray.

$$\dot{m} = K\sqrt{P}$$

Where:

$\dot{m}$: Flow rate (litres/min)

P : Pressure at head (bar).

Angus data sheet 102/4/91 shows the K-factor for the ANGUS Thermospray (bore size 9.3 mm) is 50, for nozzles with larger bore sizes the K-factor is larger and hence the required pressure for the flow rate is lower.

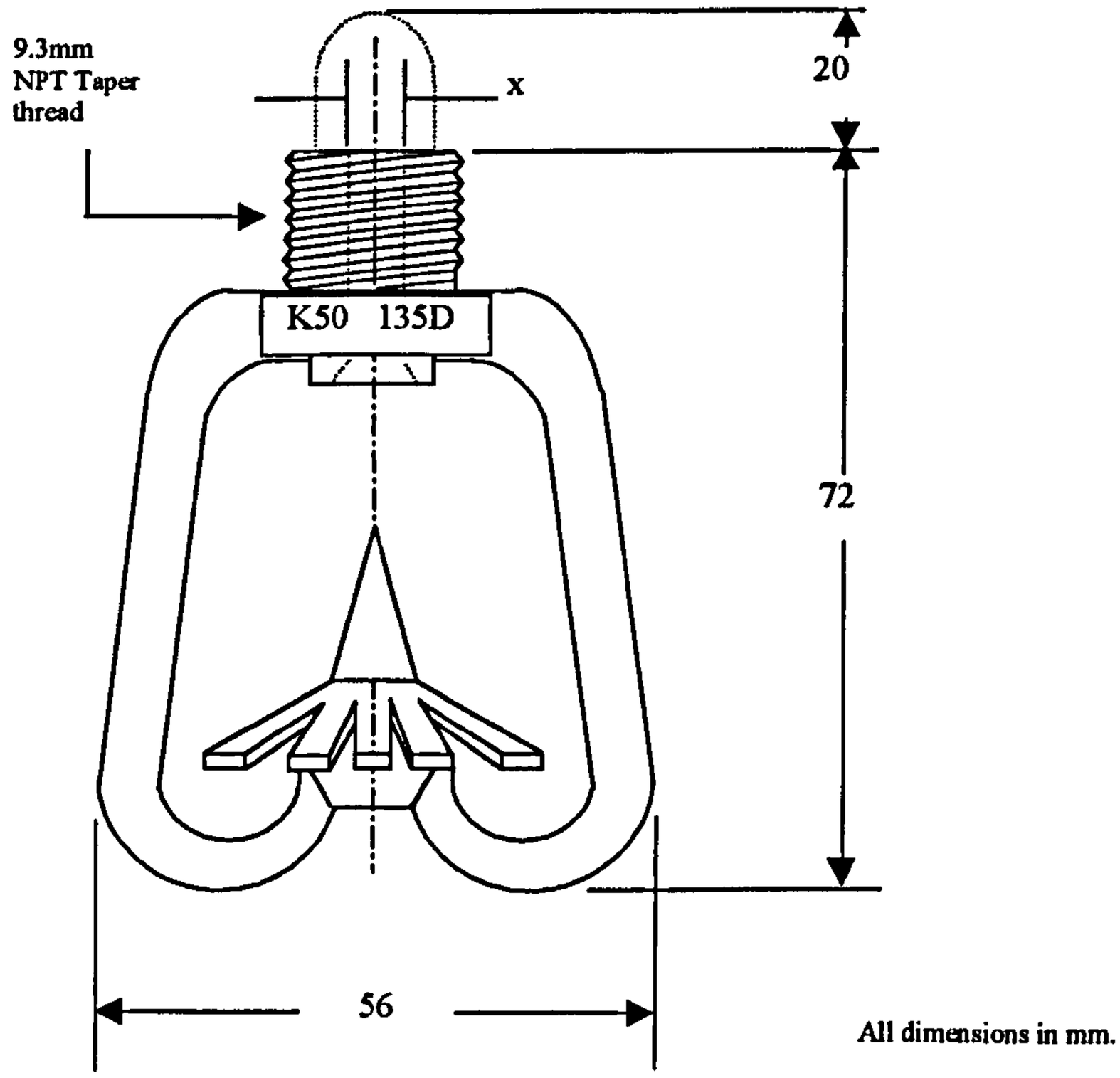

Figure (3.6). The nozzle used in the experiment (ANGUS, 1991).

- **Water velocity:**

The ANGUS THERMOSPRAY is a medium velocity water spray nozzle. The water velocity at the nozzle exit lies between 15 m/s and 25 m/s (ANGUS, 1991).

- **Spray Selection:**

The criteria for the selection of spray were primarily based on their water distribution. The preliminary spray studies found that each spray at each flow rate produced a unique water distribution. The selection criteria were also made with regard to spray head characteristics.

- **Spray nozzle Set-up:**

Each spray nozzle was located 10 cm. below the ceiling. Different spray locations were used as in Figure (3.2) along the centre line of the compartment. The water was released from different flow rate, see section (3.6). Different spray angles were used in the experimental programme, see tables (3.1) and (3.2) for further details of the different parameters used in the tests.

The locations of the spray nozzles are:

NOZZLE	X	Y	Z
F	1190	2300	1170
C	3180	2300	1170
B	5080	2300	1170

All dimensions in mm.

3.2.5 Safety Systems

The safety system as shown in Figure (3.7) was placed in operation mainly to assure that if for some reason the propane gas flow was not ignited during the start up or the flame blew out during a test, the gas flow to the jet nozzle would be stopped, preventing a dangerous build-up of non-combusted propane gas within the compartment. Once the main on/off switch was activated, the emergency button could be used for shutting off most of the equipment to stop any further gas flow.

An observer was assigned to announce "test abort" in case the propane gas flow was not ignited during the start up or in case the flame blew out during a test, and he was ready to act in an emergency. All control valves were numbered for ease of operation.

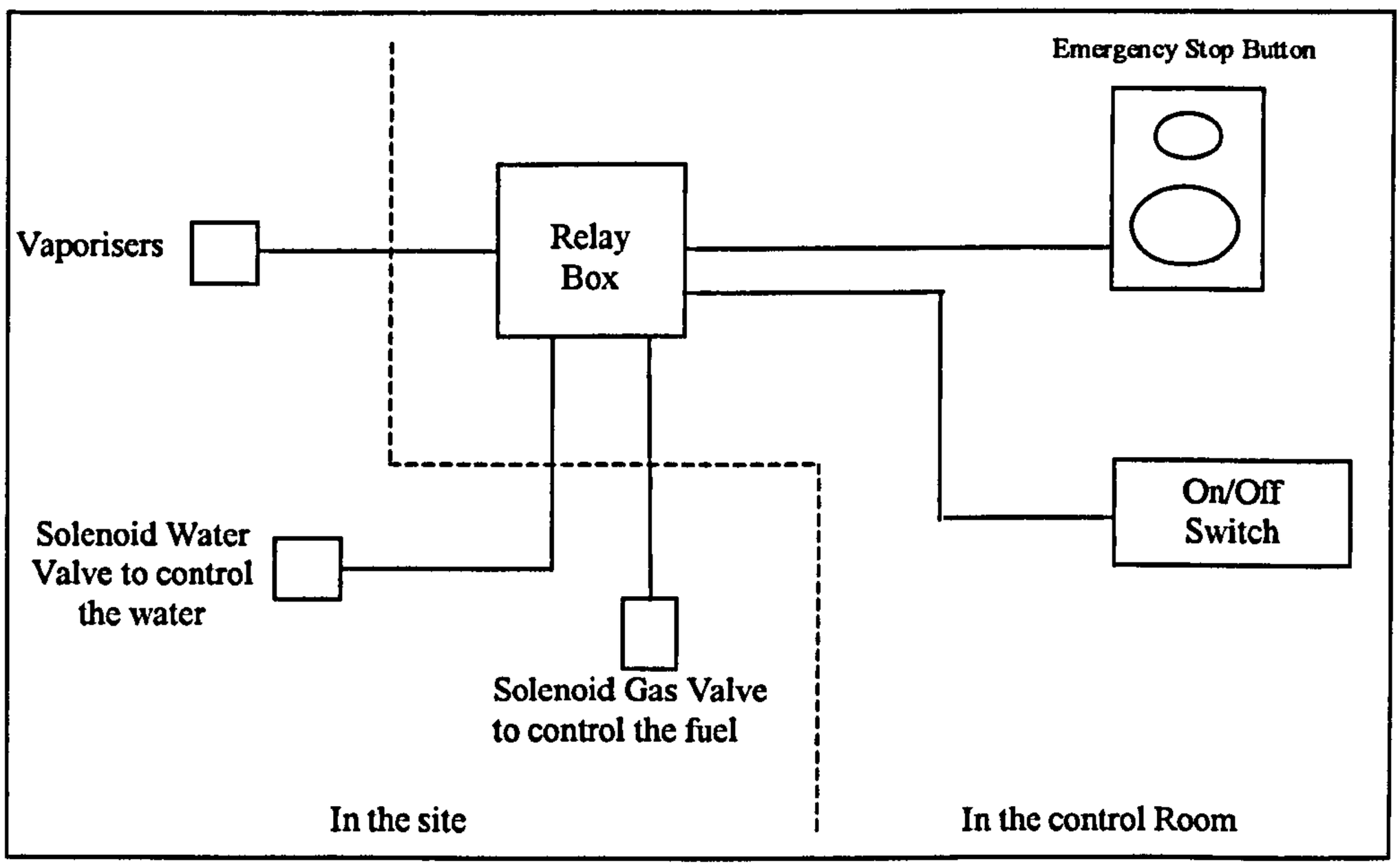

Figure (3.7). Safety System Schematic.

The solenoids valves were connected in such a way that in the event of either the Emergency shut off being operated or an electrical supply failure, the system would "fail safe".

To enhance the visualisation of the extinguishing process, two 1 kW halogen arc lamps were placed above the intermediate instrument shelter and above camera pad 1, see Figure (3.1). Their height and intensity were adjusted to give maximum visibility.

3.3. EXPERIMENTAL APPARATUS AND DATA ACQUISITION SYSTEMS

3.3.1. Temperature Measurements

The compartment has been instrumented with a total of 139 data channels, see Figure (3.8); these includes 35 aspirated thermocouples, 22 unshielded thermocouples, 19 wall temperature 4 mm washer type thermocouples, one gas temperature thermocouples.

Of the 35 aspirated thermocouple, 25 were positioned at the open side, the remaining thermocouples were placed in two vertical strings in the centreline inside the compartment. The thermocouples were evenly distributed in position, and covered both the flame zone, the inflowing air and the smoke. The first string (Northeast) was located two metres from the compartment opening and one metre from jet nozzle, the second string (Southwest) was located one metre away from the jet nozzle and two metres from the back wall; their location is shown in Figure (3.9).

One thermocouple was installed on the fuel nozzle before it went to the compartment to measure gas temperature.

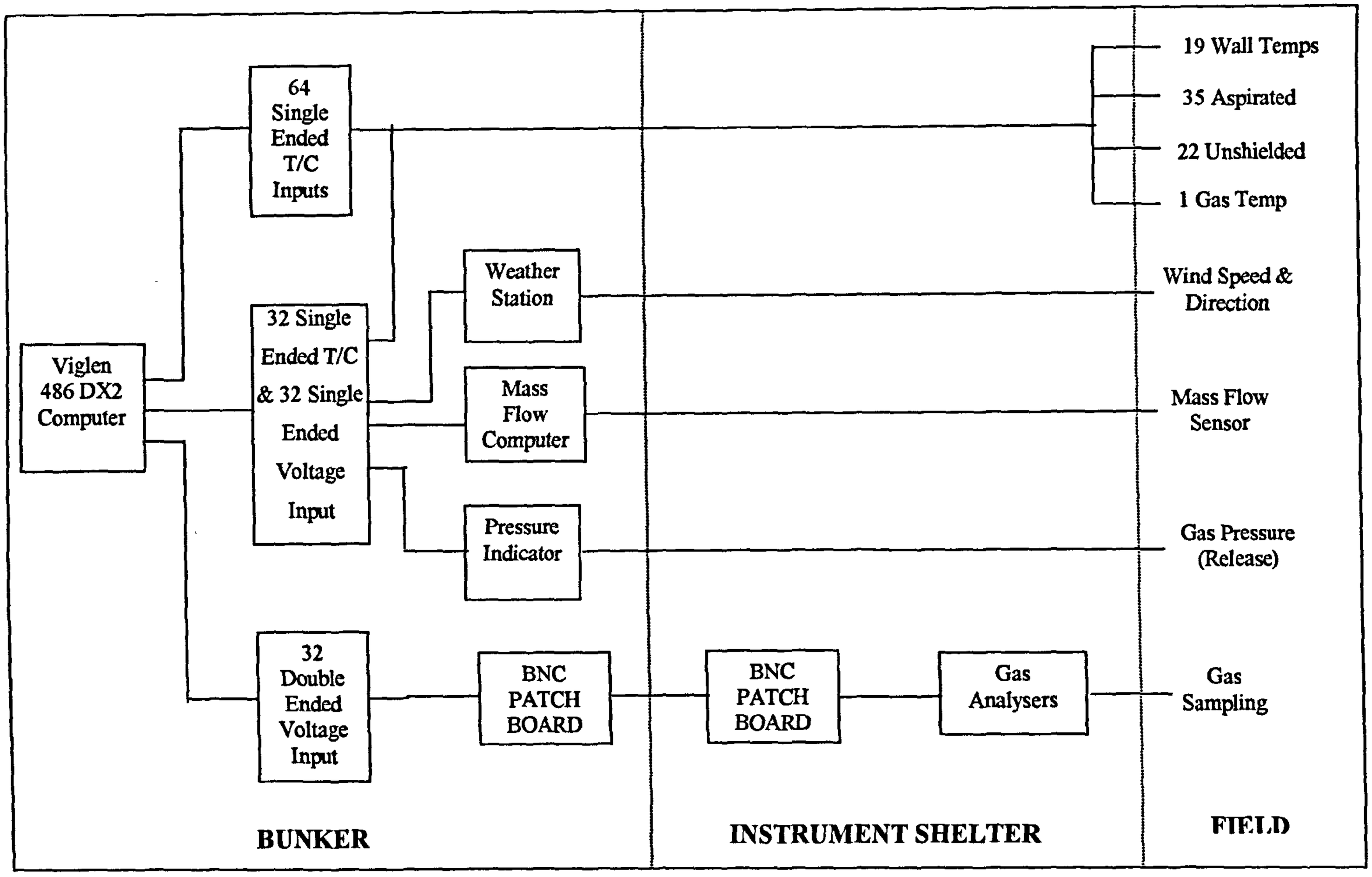

Figure (3.8). Instrumentation Arrangement.

FRONT ARRAY

1	2	3	4	5
21	22	23	24	25
16	17	18	19	20

SIDE VIEW

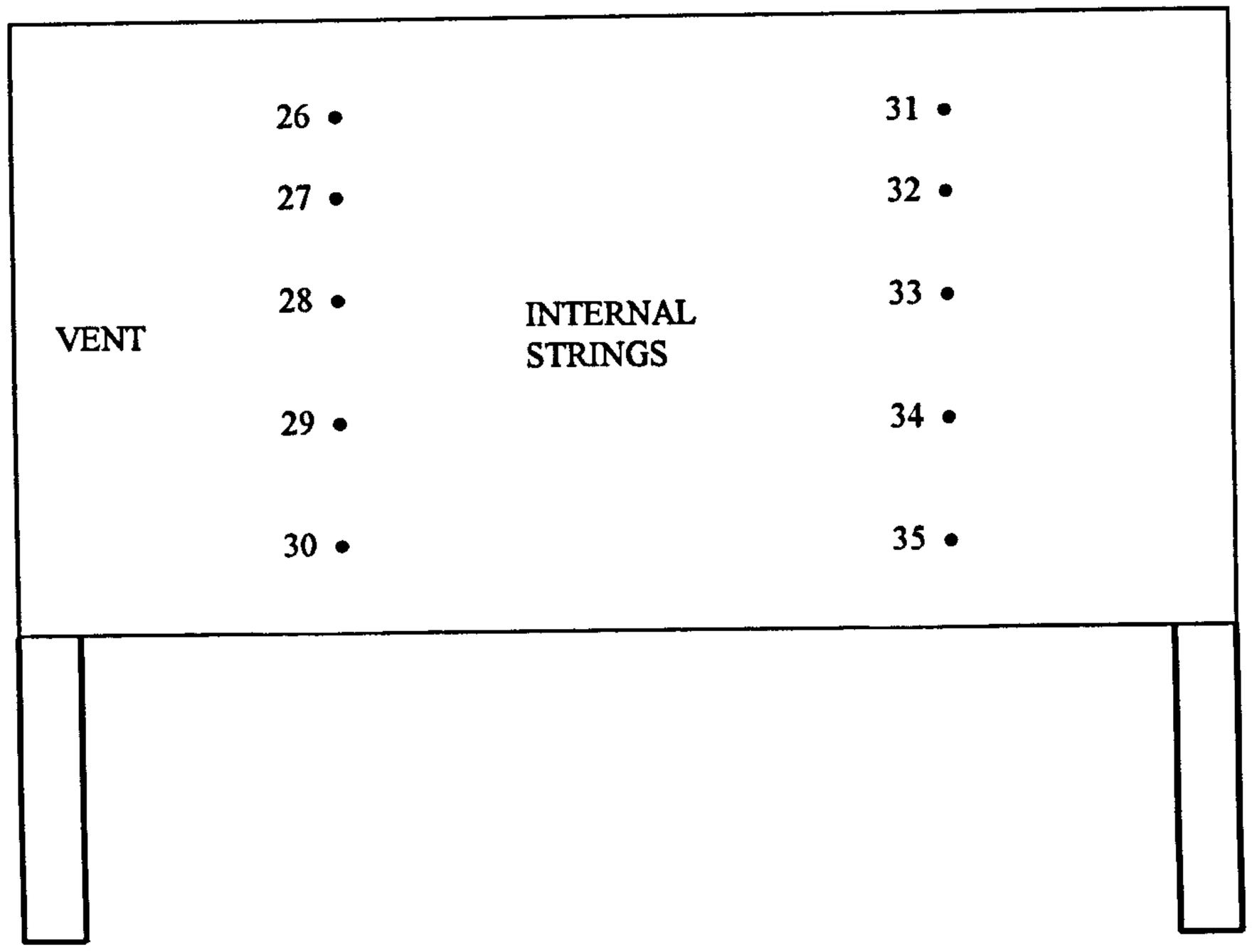

FIGURE (3.9). ASPIRATED THERMOCOUPLE POSITIONS

Figure (3.10) and (3.11) show the unshielded and wall temperature thermocouples arrangements and locations. A 4-mm washer type thermocouple, which was used as wall thermocouples, is shown in Figure (3.12). Figure (3.13) shows the aspirated thermocouples connected to the ejector.

All thermocouples were type K, fabricated from 30-gage chromel-alumel wire.

The thermocouples measuring the surface temperatures of the walls, ceiling, and floor were mounted in shallow grooves (25 mm long).

The thermocouple inside the compartment should be shielded from direct water

During the tests, a continuous flow rate measurement of the propane flow rate was made.

The 139 data signals were monitored by a data acquisition system with Viglen 486 DX2 computer inside the control room. Every 4 seconds the system scanned each of the 139 data channels ten times within a half second and logged the average value of each data channel on a magnetic tape.

Measurement of CO, CO2 and O2 concentration at different location in the opening was made.

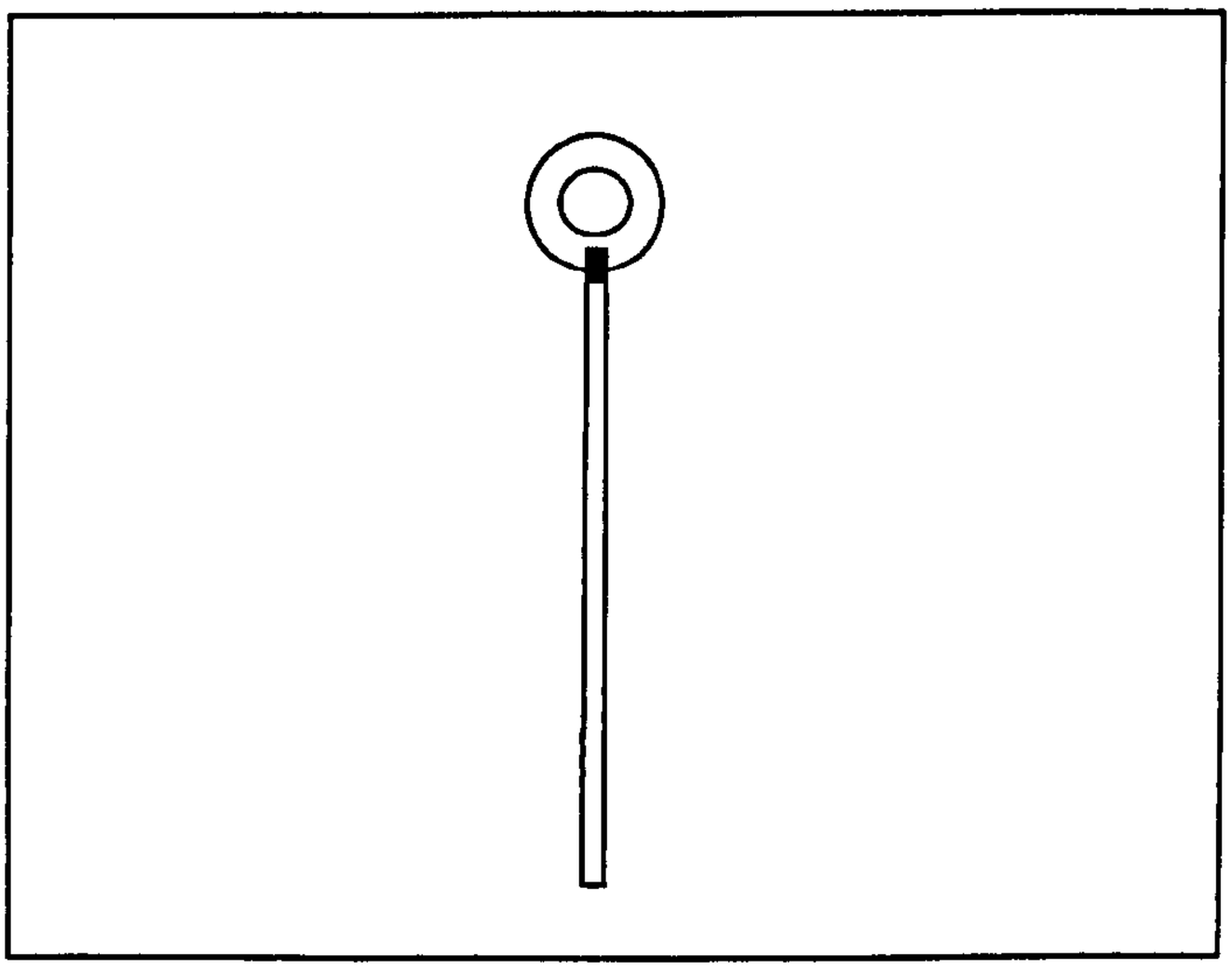

Figure (3.12). Showing 4 mm Washer Type Thermocouple.

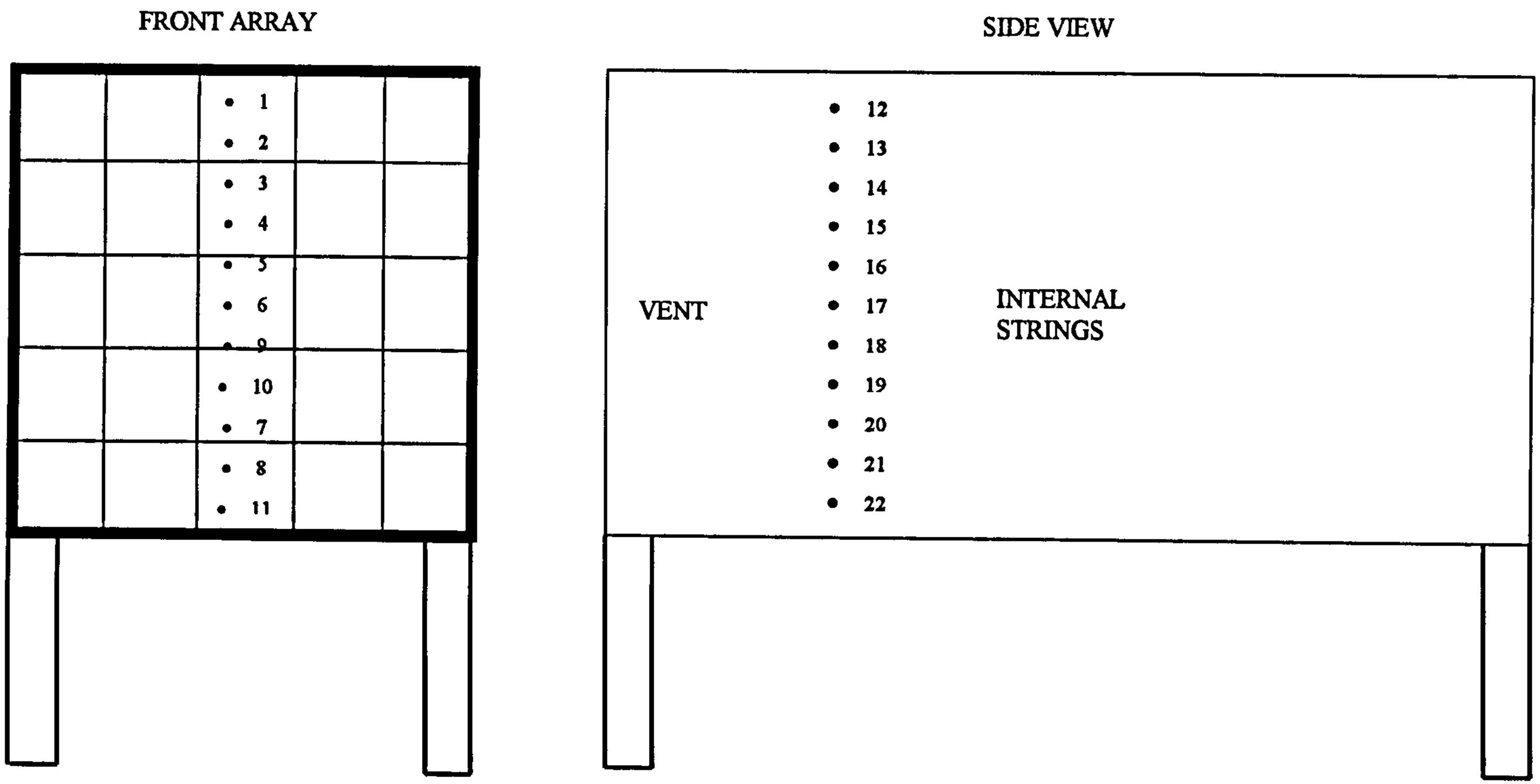

FIGURE (3.10). Unshielded Thermocouple Positions

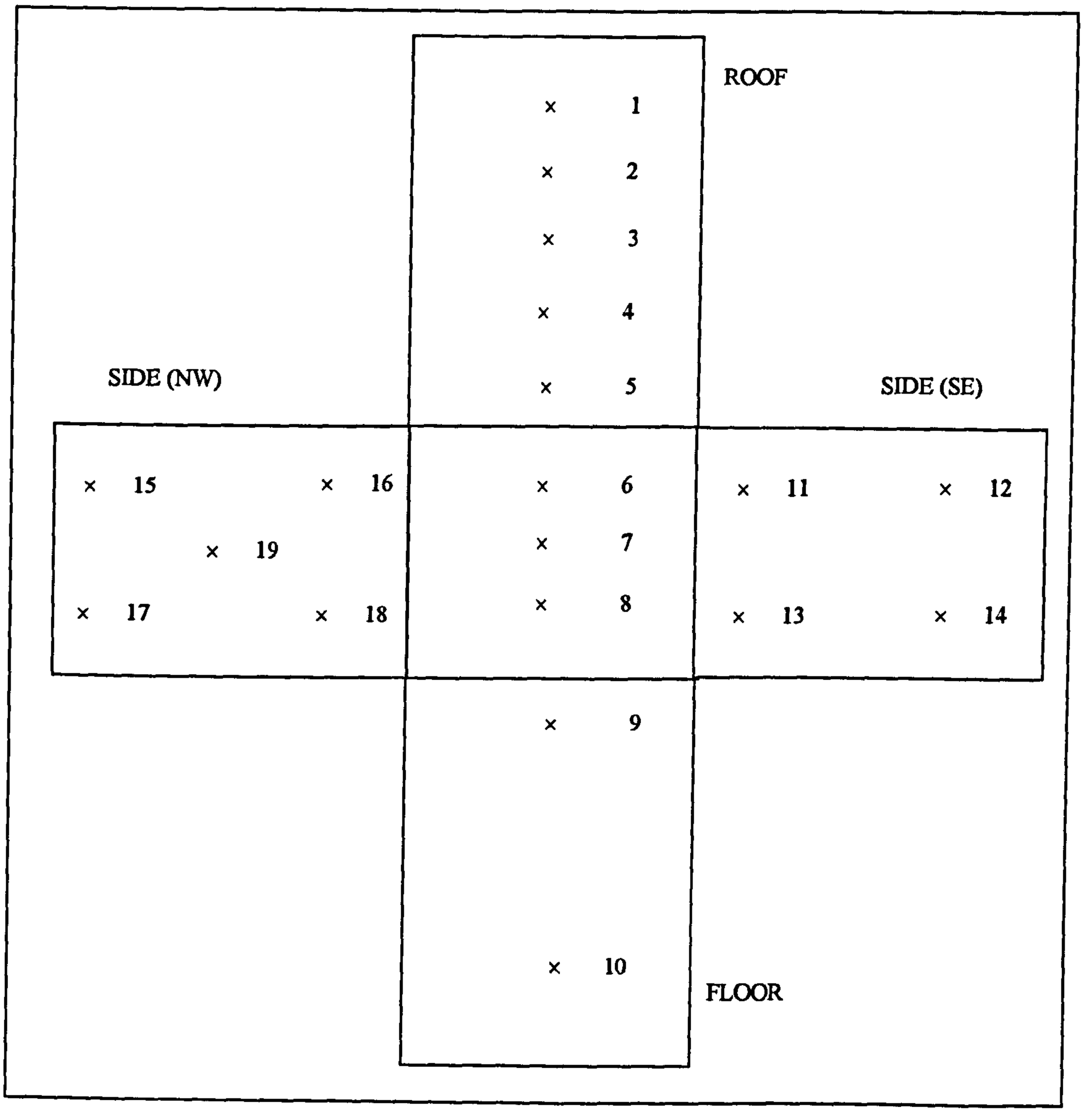

FIGURE (3.11). Wall Temperature Thermocouples

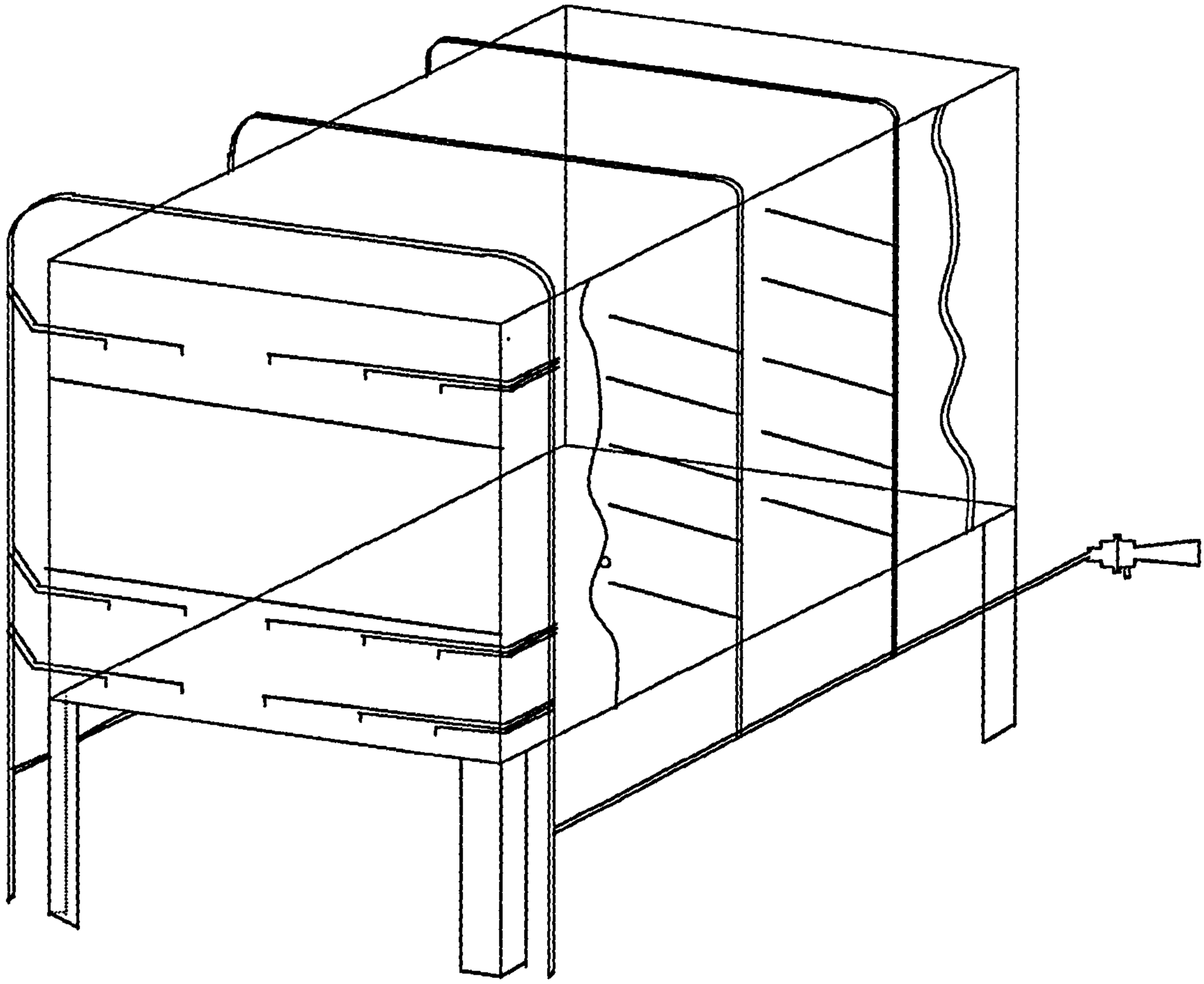

Figure (3.13) Aspirated Thermocouple connections.

- **Aspirated Thermocouple**

The measurement of the temperature of a gas by aspirated thermocouples is subjected to errors for different reasons (Mullikin, 1941); Direct impingement of water droplets during water spray operation to the gas-temperature measuring thermocouples inside the compartment may be one reason for temperature measurement error (Shell, 1974 and Kung, 1977). Another reason is that when a thermocouple immersed in a gas receives heat by convection from the gas, but there will also occur radiant-heat exchange with the compartment walls which it can see. If the wall surfaces seen are at the same temperature as the gas, the thermocouple will read the true temperature of the gas, because no radiant-heat exchange will take place. On the other hand, if the compartment walls are hotter than the gas they will radiate heat to the thermocouple which, because of the extra heat received, will read higher than the true gas temperature. If the walls are at a lower temperature they will absorb radiant heat from the thermocouple and hence the thermocouple will read lower than the true gas temperature (Mullikin, 1941).

Since radiation is proportional to the fourth power of the absolute temperature, the radiant-heat transfer will be very great at high temperature where the wall temperature is quite different from the gas temperature.

Shields were placed around the thermocouple hot junction so that it cannot see the colder surfaces. In this case the shield assumes a temperature between that of the thermocouple and the cold walls. This decreases the radiation errors but unless the gas flows through this shield with an appreciable velocity, a considerable error still exists (Mullikin, 1941).

The thermocouple element is surrounded by one or more concentric tubes so that flue gas can be drawn over the thermocouple and through the concentric tubes. When the flue gas is withdrawn at a high rate, the thermocouple closely approaches the true gas temperature whilst it is protected from radiation heat loss to the cold walls, by the concentric tubes which themselves approach the flue gas temperature.

The probe of this instrument consists of a 6.5 outer diameter stainless steel tube with a 1.5 mm.

- **Calibration of the Aspirated Thermocouple**

One way to calibrate the aspirated thermocouple is by measuring the rate of the air flowing -aspirated- through the thermocouple. This can be done by inserting the aspirated thermocouple using a small cylinder connected to the output pipe of a flow meter as in Figure (3.14) and by gradually increasing the air flow rate. The indicated temperature with no suction, i.e., no gas flow past the thermocouple junction, shows a considerable error because of the poor convection heat transfer from the gases to the thermocouple. As the suction or gas flow is increased, the temperature indicated rises, until a value is reached where the convection heat transfer from the gases to the thermocouple is so great that the heat losses of thermocouple by conduction and radiation is relatively negligible. A further increase in gas flow results in no appreciable temperature rise, thus showing that the true temperature has been reached. Figure (3.15) shows a typical temperature curve for a different flow rate. It suggests that the aspirated thermocouples requires a high suction rate at least 20 lit/min in order to represent the correct temperature of the gas entering the probe.

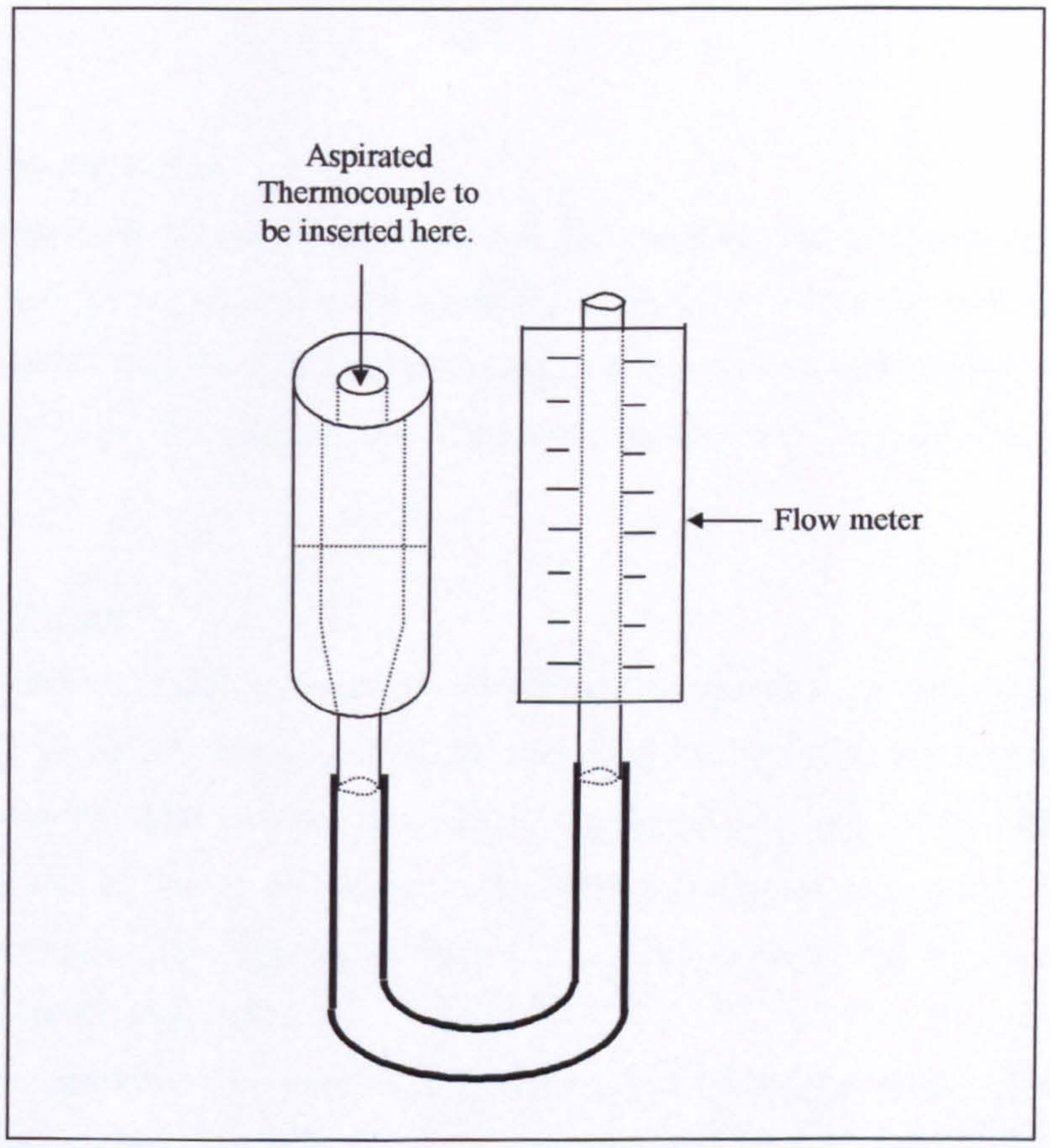

Figure (3.14). Aspirated Thermocouples calibration apparatus.

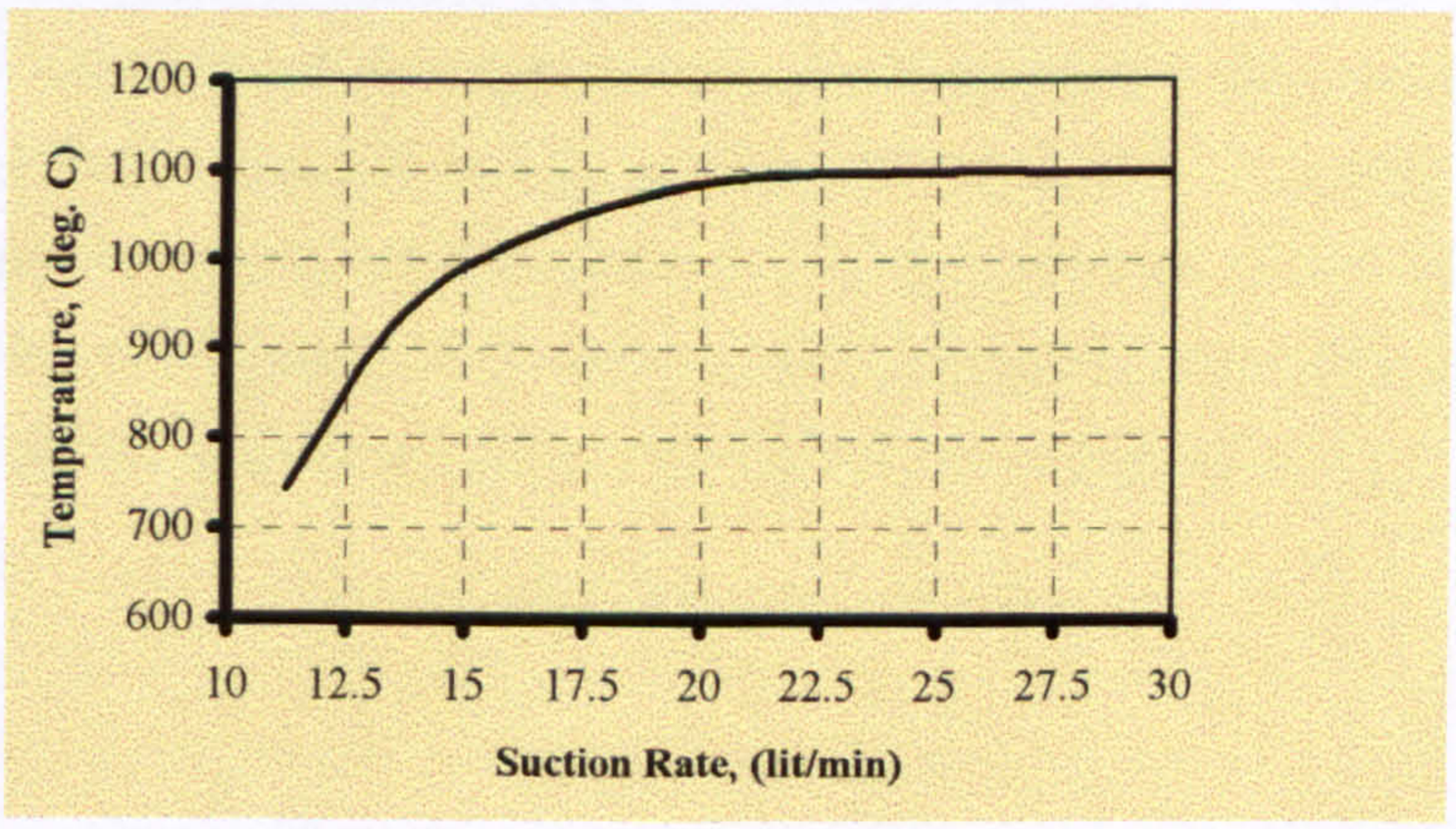

Figure (3.15). Relation between temperature indication and airflow rate through the Aspirated Thermocouple.

- **Compressed Air**

Compressed air for control purposes and for powering the airmovers is provided by the compressor located in the workshop welding bay. The solenoids valves are connected in such a way that in the event of either the Emergency Shut Off being operated or an electrical supply failure, the system will "fail safe" to the vent mode.

- **Air Mover**

The air mover used is operated by compressed air. Its effect is to produce a high velocity jet of air, which is ideal for operating the aspirated thermocouple. In generating the high velocity jet a negative pressure is created at the inlet which enables the air mover to extract combustion gases from around the aspirated thermocouple. The diagram in Figure (3.16) below shows the air mover used throughout the experiments.

Since the air mover is compressed air driven, when low pressure air passes over an aerofoil surface it both clings to the surface and accelerates. When the primary compressed air enters the manifold through a radial connection and is released through an annular gap where it accelerates over an aerofoil surface, then a secondary ambient air is sucked into the throat of the airmover to fill the vacuum created by the accelerating compressed air, which causes the induced secondary air mixes with the expanding primary air in the divergent tube. As a result of that the high-velocity air emitted from the outlet entrains additional tertiary into a jet stream which can be directed to extract combustion gases through the aspirated thermocouple connections which have been discussed in section (3.3.1).

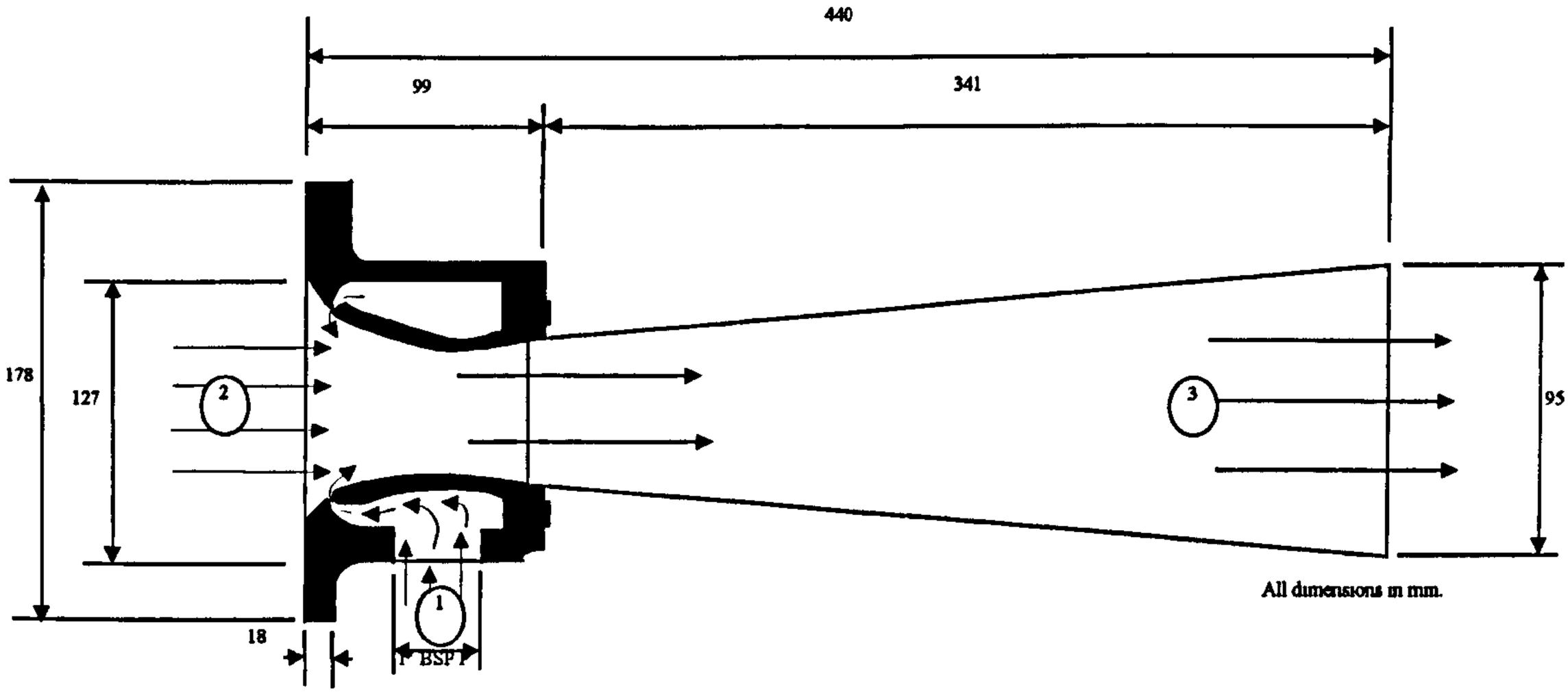

1. The primary compressed air inlet.
2. The secondary ambient air sucked into the airmover to fill the vacuum
3. The induced secondary air mixes with the compressed air in the divergent tube near outlet

Figure (3.16). Diagram of the airmover used in the experiments.

3.3.2. Gas Sampling and Analysis

Sampling of the combustion gases products were achieved using the flow set up outlined in Figure (3.17). The combustion product oxygen, carbon monoxide, and carbon dioxide concentrations at the vent plane were monitored by continuously drawing samples for analysis from the upper portion of the gas stream emerging from the vent. Sample points were chosen at three positions and the streams combined in an attempt to obtain representative gas concentrations in the emerging products. The gas samples were cooled, dried from the moisture content and filtered from any particles before they go to the units.

The output from the sampling unit was recorded through the data acquisition unit. The units used to sample the combustion gases were ADC 7000 for measuring

propane and carbon monoxide, Rotork Analysis NDIR ANALYSER MODEL 401 for measuring CO_2, Servomex 1400B4 O_2 Analyser for measuring O_2. The ADC 7000 was capable of measuring propane concentrations up to 15% and measuring Carbon monoxide up to 10%, the CO_2 analyser was capable of measuring up to 20% and the O_2 analyser was capable of measuring oxygen up to 25%. The complete sample line length was 15 metres and the tubing outer diameter was 6 mm.

Gas sampling flow and calibration gases pass through a set of valves and manifolds prior to analyser's connections. The reason for this arrangement was to ease the control of the flow and the quantity of the gas required according to the analysers requirements. This arrangement is shown in Figure (3.18).

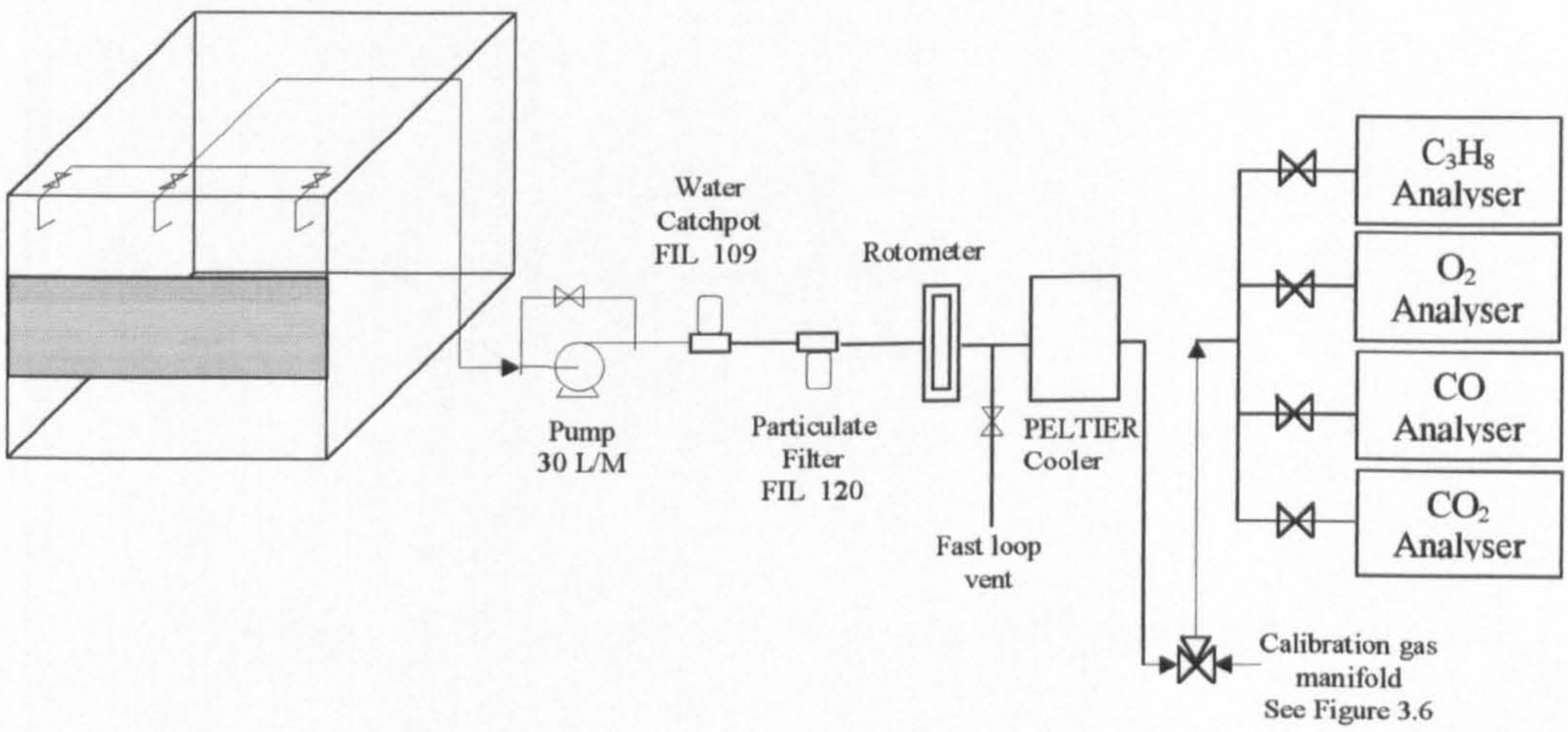

Figure (3.17). Showing gas Sampling Flow set up.

The analysers were checked and calibrated to examine their stability and accuracy. The analysers were calibrated at the beginning of each test day using suitable zero and span gas for each analyser.

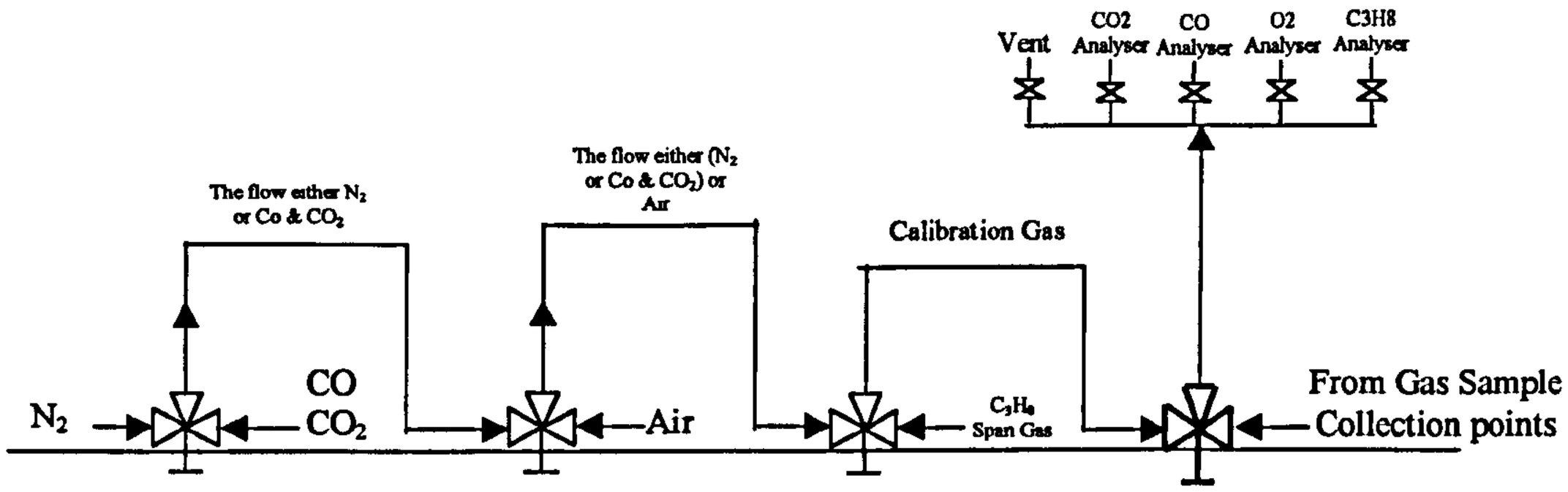

Figure (3.18). Calibration and Sampling Gases Flow Arrangement

3.3.3. Wind Speed and Directions

The wind speed and direction and rain affect the test running, therefore when the weather conditions were very windy no experiments were done and some of the tests were repeated because the wind affected the results. Measurement of wind speed and direction was logged to the computer. Figure (3.8) shows the arrangement of the measurement.

3.4. EXPERIMENTAL PROCEDURES

A number of procedures were carried out before doing any test:

3.4.1. START-UP PROCEDURES

- **PRE-TEST CHECKLIST:**

1. All critical instruments deemed operational and fit to use, non-operational items should be logged.

2. Availability of sufficient fuel for the test should be checked as well as the vaporiser liquid level.
3. Atmospheric conditions should be suitable for test; i.e. wind speed, pressure stable and no likely rain.
4. Radios and portable gas monitor must be in working order and charged.

- **PRE-TESTS PROCEDURE**

1. Pre-test checklist should be completed
2. Water spray position set according to appropriate test in experimental programme.
3. Water supply to be connected to the spray system.
4. Zero and span gas calibration should be done to the analysers in any test day, gas bottles should be switched off after zero and span calibration completed.
5. Start air compressor in the workshop.
6. Start main compressor; Charge air tank (100 psi.).
7. All in correct positions knowing what to do.

   Controller: inside the control bunker, operating computer and data acquisition programme.

   Observer: Checking for propane gas inside compartment, starting pilot light, maintaining over site watch.

   Operator 1: Providing additional safety cover and assistance, opening the manual propane valve and closing the pilot light valve when the flame is stable.

   Operator 2: - Maintaining watch over test site
8. Check manual valve is fully closed and V1 is off (closed).
9. Open valves in liquid propane line to allow vaporiser to fill.
10. Switch on vaporisers 30 min before test (check compressor already up to pressure).
11. Start gas analysers, chiller and associated external pumps 30 min before test is on, check volumetric flow rate.

12. Set up computer, check signal lines critical to control of test, and that acquisition software is set up with proper test reference code in filename.
13. Perform 'cold run' data acquisition and note defective channels.
14. Transfer data to Excel 5.0 template and save. Transfer these values to a new Excel 4.0 format file and save onto hard disk.
15. Move data files to Sheffield (label disk for return).
16. Record test reference code and all defective channels on instrument checklist.
17. Enter test reference code into data acquisition software and logbook (with link to test number in experimental programme).
18. Switch on hazard warning lights.
19. Check vaporisers up to temperature.
20. Start aspirated probe air-mover (P=80 psi).
21. Check for gas inside box.
22. Ignite pilot light and check stability.
23. Check test area clear of personnel.
24. Record atmospheric data on test data sheet: wind velocity & direction, ambient temperature and pressure.
25. Complete test data sheet.

3.4.2. TEST RUNNING PROCEDURES

Before every test a number of procedures were carried out. All the thermocouples were cleaned while the wall thermocouples were brushed to remove the rust as well. Also on the pre-test checklist were numerous activities to prepare the instruments for a test, such as:

1. Set up the water spray flow meter to the desired flow according to the test number in the experimental programme.
2. When target flow achieved, close auto valve.
3. Announce beginning of test.
4. Confirm target fuel mass flow rate (0.1 kg/s).
5. LPG pump on, announce standby for countdown (All confirm 'READY').

6. Countdown to test (3,2,1,GO).
7. At GO- open gas release valves (manual and auto V1), adjust manual mass flow control valve according to the reading from LCD.
8. Check flame stability, check instruments (Abort test if flame goes out).
9. When desired stable mass flow (0.1 kg/s) is achieved, note and announce time on internal microphone.
10. Shut down and isolate pilot light system.
11. Run until steady thermal state is achieved, then open water spray auto valve.
12. When the flame goes out, close the fuel auto V1 and the water auto valve.
13. Shut manual fuel mass flow control valve.
14. Shut manual water mass flow valve.
15. Terminate data acquisition.
16. Announce "END OF TEST".

3.4.3. SHUTDOWN PROCEDURES

There are certain procedures to be done for shutting down the test safely and correctly either normally or in case of emergency:

- **Normal shut Down Procedure**

1. Switch off LPG pump.
2. Shut down the vaporisers, electrically and manually.
3. Close all manual propane valves.
4. Close auto and manual valves of the water systems.
5. Stop air mover.
6. Hazard light off.
7. Stop compressor and shut down.
8. Do not approach compartment for at least 30 min or while compartment is hot.
9. Check compartment is cool, with thermocouple data indicating no hot spot (i.e. below 40°C).
10. If gas analyser out put levels below:

CO	0.1%
CO_2	5.0%
C_3H_8	0.5%

11. Announce "Safe to manually check compartment gas level".
12. When gas level falls below:

CO	0.005% (50 ppm)
CO_2	0.5%
C_3H_8	20% LEL

13. Announce "safe to work in compartment".
14. Shut down all remaining systems (including chiller and all pumps).
15. Drain the water system to avoid freezing the water inside the system, which may cause damage to the flow meters.
16. Transfer raw ASCII digital data into Excel 5.0 template format for SI conversion, and save file as Excel 5.0 format under test reference code.
17. Open new Excel file, transfer values from Excel.

- **Emergency shut Down Procedure**

To shut down the test in case of emergency, there is an emergency stop button located at centre of release control panel in the bunker. This will shut down:

1. All field instrumentation inside the compartment and instrument shed
2. Gas mass flow measuring system
3. All video equipment in the field and inside the bunker (if available)
4. All automatic valves (i.e. gas release valve V1 will fail safe)
5. Computer and all other instruments inside the bunker
6. This will also shut down the auto gas alarms.

After emergency has passed, to start up again safely:

1. Ensure all valves in the LPG/gas line are closed.
2. Personnel are clear from the site
3. Reset emergency button - All power will be restored to instruments
4. Reset Gas alarm timers
5. Check instruments

- **ABORTED TEST PROCEDURE**

1. Switch off auto-valve 'V1' and close manual flow control valve.

3.4.4. DATA ACQUISITION

Data were sampled every 4 seconds and logged by means of the data acquisition system DAS1800, and stored as ASCII file on computer. After data processing, the calculation should be readily performed using Excel 97 programmes. Extensive use was made of video and still photography. These were invaluable for recording flame development inside and outside the compartment.

3.5. EXPERIMENTAL CONDITIONS

3.5.1. External Conditions

Pressure:	Atmospheric
Wind:	Calm or very light
Rain:	No likely rain

3.5.2. Jet Burner

Gas Flow Rate:	0.1 kg/s
Exit Gas Velocity	250 m/s
Jet Nozzle Diameter	20 mm

3.5.3. Water Spray

Flow Rate	variable
Number of Nozzle	Variable either one, two or three sprays.

3.6. SAFETY REQUIREMENTS AND RISK ASSESSMENT

The apparatus has to be operated as a three-man experiment. It is essential that good communication is maintained. Portable intrinsically safe radios on a discrete frequency are available for this purpose and communication between all working parties is encouraged. They were used by all parties operating at the test site. All control valves are numbered for ease of operation.

3.6.1. SAFETY REQUIREMENTS

These rules must be read in conjunction with COSHH assessment related to this work.

1. It is most important all operations are carried out with due regard to all safety regulations and common sense.
2. All fuel gas piping should be checked for leaks and gas supplies should be turned off at the storage tank after finishing the test (before leaving the site)
3. All personnel involved in the operation of the test should present before starting any test.
4. Before igniting the pilot light, check the fuel level inside the compartment from the output of the analyser is less than 20% LEL.
5. All work must be performed with the correct protective clothing and equipment.
6. When any work not specified in this procedure is being carried out measures should be taken to eliminate any hazard at source. If this is not possible the hazard should be minimised and the appropriate protective equipment used.
7. Before commencing work consider if there is any hazard to other workers in the vicinity.

3.6.2. RISK ASSESSMENT

1. Propane gas is used to create the fires in the compartment. Any uncontrolled release of propane results in an obvious hazard. The consequences of such an event could result in damage to the compartment and surrounding shed and possible injury to near-by personnel. However this event is unlikely to occur as all gas piping is checked periodically.

2. A 50 kg propane gas cylinder is used to create a pilot flame in order to ignite the jet fire. The propane gas is placed in the gas cylinder rack behind a protection wall near the compartment (see Figure 3.1). The hazard and consequences from the cylinder are as above and the same precautions are adopted to remove the risk.

3.6.3. SITE LOCATION AND TRAVEL

The Buxton test facility site is on a remote area in the Derbyshire Hills and is operated by Sheffield University. Access to the site is restricted by a boundary fence and controlled by the Health & Safety Executive (HSE) gatehouse.

During tests period access to some areas which may be hazardous was barred. An "exclusion area" around the immediate vicinity of the compartment apparatus is clearly marked with warning signs. The site is rough and largely unpaved.

3.6.4. COMMUNICATIONS

Three hand-held radios and one base station were used for running the tests. These are very important for providing safe operation of the rig, reducing the possibility of any error happening.

3.7. TEST PROGRAMME

The test programme was divided into two phases. Fifty-eight tests were needed in order to complete this programme. The tests were done as follows:

3.7.1. Phase One

Twenty tests were done in this phase with different flow rates, which were 18, 36, 54, 72 and 90 litres/minute. These water flow rates were chosen because they fall below the maximum NFPA standard requirements which were 20 lit/min/m^2 (NFPA, 1994). Four spray angles were selected for these investigations namely 60°, 90°, 120° and 150° spray angles. One spray location was used in this phase. All notations are given in table (3-1). The objectives of this phase were to study the jet fire behaviour and the temperature distributions, and to study the effect of different spray angles which produce different mean droplet sizes in order to find the nozzles which perform the best, based on these conditions. The results from this phase were used as basis for further investigation in phase two.

3.7.2. Phase Two

Based on the tests which were done in phase one, and after detailed data analysis (see chapter 7), it was decided to do further investigation with the nozzles which have 150° spray angle for different locations and different flow rates, because this angle was found to perform the best. Table (3-2) illustrates the notations used for the second phase of the programme. The objective of this phase was to study the effect of different water flow rates, different nozzle locations and number.

Table (3-1). Phase One Experimental Programme.

Test No	No. of nozzle	Spray Locations			Water Flow Rate				Spray Angle
					For each Spray		Total		
		Back	Centre	Front	kg/s	lit/min	kg/s	lit/min	
Comp 01	1		✓		0.3	18	0.3	18	150
Comp 02	1		✓		0.6	36	0.6	36	150
Comp 03	1		✓		0.9	54	0.9	54	150
Comp 04	1		✓		1.2	72	1.2	72	150
Comp 05	1		✓		1.5	90	1.5	90	150
Comp 11	1		✓		0.3	18	0.3	18	60
Comp 12	1		✓		0.6	36	0.6	36	60
Comp 13	1		✓		0.9	54	0.9	54	60
Comp 14	1		✓		1.2	72	1.2	72	60
Comp 16	1		✓		1.5	90	1.5	90	60
Comp 19	1		✓		0.3	18	0.3	18	90
Comp 20	1		✓		0.6	36	0.6	36	90
Comp 21	1		✓		0.9	54	0.9	54	90
Comp 22	1		✓		1.2	72	1.2	72	90
Comp 23	1		✓		1.5	90	1.5	90	90
Comp 26	1		✓		0.3	18	0.3	18	120
Comp 27	1		✓		0.6	36	0.6	36	120
Comp 28	1		✓		0.9	54	0.9	54	120
Comp 29	1		✓		1.2	72	1.2	72	120
Comp 30	1		✓		1.5	90	1.5	90	120

Table (3-2). Phase Two Experimental Programme.

Test No	No of nozzle	Spray Locations			Water Flow Rate				Spray Angle
					For each Spray		Total		
		Back	Centre	Front	kg/s	lit/min	kg/s	lit/min	
Comp 08	1	✓			0.3	18	0.3	18	150
Comp 09	1	✓			0.6	36	0.6	36	150
Comp 10	1	✓			0.9	54	0.9	54	150
Comp 33	1	✓			1.2	72	1.2	72	150

Comp 34	1	✓			1.5	90	1.5	90	150
Comp 15	1			✓	0.3	18	0.3	18	150
Comp 37	1			✓	0.6	36	0.6	36	150
Comp 38	1			✓	0.9	54	0.9	54	150
Comp 39	1			✓	1.2	72	1.2	72	150
Comp 40	1			✓	1.5	90	1.5	90	150
Comp 43	3	✓	✓	✓	0.3	18	0.9	54	150
Comp 44	3	✓	✓	✓	0.6	36	1.8	108	150
Comp 45	3	✓	✓	✓	0.9	54	2.7	162	150
Comp 46	3	✓	✓	✓	1.2	72	3.6	216	150
Comp 47	3	✓	✓	✓	1.5	90	4.5	270	150
Comp 50	2	✓		✓	0.3	18	0.6	36	150
Comp 51	2	✓		✓	0.6	36	1.2	72	150
Comp 52	2	✓		✓	0.9	54	1.8	108	150
Comp 53	2	✓		✓	1.2	72	2.4	144	150
Comp 54	2	✓		✓	1.5	90	3	180	150
Comp 57	3	✓	✓	✓	0.4	24	1.2	72	150
Comp 58	3	✓	✓	✓	0.5	30	1.5	90	150
Comp 59	2	✓		✓	0.45	27	0.9	54	150
Comp 60	2	✓		✓	0.75	45	1.5	90	150
Comp61	2	✓	✓		0.3	18	0.6	36	150
Comp62	2	✓	✓		0.45	27	0.9	54	150
Comp63	2	✓	✓		0.6	36	1.2	72	150
Comp64	2	✓	✓		0.75	45	1.5	90	150
Comp65	2	✓	✓		0.9	54	1.8	108	150
Comp66	2	✓	✓		1.2	72	2.4	144	150
Comp67	2	✓	✓		1.5	90	3	180	150
Comp70	2		✓	✓	0.3	18	0.6	36	150
Comp71	2		✓	✓	0.45	27	0.9	54	150
Comp72	2		✓	✓	0.6	36	1.2	72	150
Comp73	2		✓	✓	0.75	45	1.5	90	150
Comp74	2		✓	✓	0.9	54	1.8	108	150
Comp75	2		✓	✓	1.2	72	2.4	144	150
Comp76	2		✓	✓	1.5	90	3	180	150

CHAPTER 4
NUMERICAL MODELLING THEORY

4.1. INTRODUCTION

In most flow systems of engineering importance, considerable flow complexity is commonly encountered and an analytical solution is not possible. For the past several decades, engineers and scientists have developed numerical methods and computer software to solve complex systems of partial differential equations numerically. Many computer programmes or computer codes, as they are called, have been developed specifically to solve flow equations. Each different code tends to have certain strengths and is best suited to particular types of flow. In this work, a code called FLUENT was chosen and used to perform solutions of the governing equations and for modelling the combustion process of jet fire in a large scale combustion chamber.

The equations of fluid dynamics can be solved numerically with the aid of modern computers. The set of techniques and procedures to achieve this has led to the development of what is known as computational fluid dynamics (CFD). Although it

is not possible to leave out real experiments, numerical experiments using CFD allow the determination of certain trends and give an insight into the physics of complex problems that would be impractical to study experimentally. The subject has now advanced to the point where commercial packages are available and can be used to simulate or predict fluid dynamics problems using CFD as a black box. These codes should not be used as such since any discrepancy between predictions and experiments can only be explained in terms of the assumptions made in the development of the code. For this reason the code FLUENT is described in some detail in this chapter. It is worth emphasising that not all the available options of FLUENT are mentioned here, but only those which were used in this work.

The approach used by FLUENT, to model gas fuel combustion, is to solve the basic equations of fluid dynamics to be presented later, accounting for the interaction with the droplets of water spray through the inclusion of source terms. The water spray droplets, referred to as the second or disperse phase, in turn, interact with the fluid phase through the processes of momentum, heat and mass exchange, as described below.

4.2. Choice of the CFD package

There are several commercial CFD packages available at present in the market which have the capability to handle a wide range of fluid flow problems. These are FLUENT, PHOENICS, FLOW3D and STAR-CD, each offering similar capabilities. The choice of a package will depend on a number of factors:

1. Its appropriateness to the problem in question;

2. The easy use of the package and help facilities;

3. The cost of software and hardware required;

4. Technical user support services.

The present work required facilities for two-phase flow, three-dimensional spray modelling and particle tracking. Fluent has these facilities and was already available on site (work station, University network and University network remote access) with technical user support services. Experience and previous knowledge of the research supervisors in FLUENT also was taken into account. Since the CFD is advancing rapidly to keep the code up to date The University of Sheffield has an agreement with FLUENT Europe for supplying the latest version of FLUENT to the University's academic purposes. There was no published work found in the literature for modelling spray in a fire environment using FLUENT. Therefore, FLUENT was chosen as a basic tool for this work.

4.3. BASIC CONSERVATION EQUATIONS

The first step in numerical modelling is to establish the basic conservation equations based on the principles of fluid mechanics, heat transfer, combustion and the relevant fields of science. These equations constitute a system of non-linear simultaneous partial differential equations which can be solved by numerical methods. The equations used in this numerical modelling are presented here. It is worth emphasising that not all the available models of FLUENT are mentioned here, but only those which were used in this work.

The main problem of fluid dynamics is the determination of the velocity and state of the fluid subject to certain imposed conditions. Throughout this work it has been assumed that the fluids are gases at ambient pressure which behave ideally. In

addition to the fluid dynamics problem, consideration is given to the case when several gases are present and chemical reactions occur. The equations that allow the solution of the most general case of a multicomponent, reacting, ideal gas mixture are the following:

- Mass conservation:

$$\frac{\partial \rho}{\partial t} + \frac{\partial}{\partial x_i}(\rho u_i) = S_m \tag{4.1}$$

The source S_m is the mass added to the continuous phase from the dispersed second phase i.e. due to vaporisation of liquid droplets.

- Momentum conservation:

$$\frac{\partial}{\partial t}(\rho u_j) + \frac{\partial}{\partial x_i}(\rho u_i u_j) = \frac{\partial}{\partial x_i}\left[\mu\left(\frac{\partial u_i}{\partial x_j} + \frac{\partial u_j}{\partial x_i}\right)\right] - \frac{\partial p}{\partial x_j} + \rho g_j + F_j \tag{4.2}$$

The left hand side represents the convection term, and the terms in the right hand side represent in sequence the diffusion, pressure body forces, and the momentum interaction between forces.

The continuity and momentum equations are non-linear partial differential equations and, together with appropriate boundary conditions, provide a complete description of flows for which the density is uniform.

4.4. TURBULENCE MODELLING

Turbulence is one of the remaining unsolved theoretical problems in fluid mechanics (Yang, 1989). Nevertheless, there are different approaches in dealing with engineering problems. Obviously, the most rigorous treatment is needed for predicting complex turbulent flows, such as the three-dimensional jet flow, required by this study. In the modelling concerned with this work, the k-ε turbulence model was used.

4.4.1. The k-ε model

The above equations describe the time-averaged flow when applied to a finite number of discrete control volumes. The effects of turbulence can be included by substituting an 'effective' viscosity in the equations consisting of the molecular viscosity augmented by its turbulent counterpart, μ_t. The differential transport equations for the kinetic energy of turbulence k and its dissipation rate ε are:

$$\frac{\partial}{\partial t}(\rho k)+\frac{\partial}{\partial x_i}(\rho u_i k)=\frac{\partial}{\partial x_i}\frac{\mu_t}{\sigma_k}\frac{\partial k}{\partial x_i}+G_k-\rho\varepsilon \tag{4.3}$$

And

$$\frac{\partial}{\partial t}(\rho \varepsilon)+\frac{\partial}{\partial x_i}(\rho u_i \varepsilon)=\frac{\partial}{\partial x_i}\frac{\mu_t}{\sigma_\varepsilon}\frac{\partial \varepsilon}{\partial x_i}+C_{1\varepsilon}\frac{\varepsilon}{k}G_k-C_{2\varepsilon}\rho\frac{\varepsilon^2}{k} \tag{4.4}$$

Where G_k is the generation term of k and is given by:

$$G_k = \mu_t\left(\frac{\partial u_j}{\partial x_i}+\frac{\partial u_i}{\partial x_j}\right)\frac{\partial u_j}{\partial x_i} \tag{4.5}$$

The turbulent viscosity, μ_t, is related to k and ε, by

$$\mu_t = \rho C_\mu \frac{k^2}{\varepsilon} \tag{4.6}$$

Where $C_{1\varepsilon}$, $C_{2\varepsilon}$, C_μ, σ_k and σ_ε are empirical constants, with values, 1.44, 1.92, 0.09, 1.0 and 1.3 respectively.

4.5 THERMAL AND REACTING FLOWS

- Conservation of Energy:

FLUENT solves the energy equation in the form of a transport equation for enthalpy, *h*, and can be written as:

$$\frac{\partial}{\partial t}(\rho h) + \frac{\partial}{\partial x_i}(\rho u_i h) = \frac{\partial}{\partial x_i}\frac{(\kappa + \kappa_t)}{c_p}\left(\frac{\partial h}{\partial x_i} - \sum_j h_j \frac{\partial X_j}{\partial x_i}\right) - \frac{\partial}{\partial x_i}\sum_j h_j J_{ji} +$$

$$\frac{Dp}{Dt} - \tau_{ik}\frac{\partial u_i}{\partial x_k} + S_h \tag{4.7}$$

Where the source term S_h includes heat of reaction, radiation and any interphase exchange terms, $\kappa+\kappa_t$ is the mixture thermal conductivity. Enthalpy *h* is defined as

$$h = c_p T \tag{4.8}$$

- Conservation of species:

FLUENT predicts the local mass fraction of each species, $m_{i'}$, through the solution of a convection-diffusion equation for the *i'* th species. The conservation equation takes the following general form:

$$\frac{\partial}{\partial t}(\rho m_{i'}) + \frac{\partial}{\partial x_i}(\rho u_i m_{i'}) = \frac{\partial}{\partial x_i} J_{i',i} + R_{i'} + S_{i'} \tag{4.9}$$

where $R_{i'}$ is the mass rate of creation or depletion by chemical reaction and $S_{i'}$ is the rate of creation by addition from the dispersed phase. The reaction rates are computed by FLUENT from Arrhenius rate expressions or by using the eddy dissipation concept due to Magnussen and Hjertager (1976). In turbulent flows, FLUENT uses the mass diffusion in the form:

$$J_{i',i} = \left(\rho D_{i',m} + \frac{\mu_t}{Sc_t}\right)\frac{\partial m_{i'}}{\partial x_i} \tag{4.10}$$

where Sc_t is the effective Schmidt number (with a default setting of 0.7).

The source of chemical species *i* due to reaction, $R_{i'}$, is computed as the sum of the reaction sources over the k reactions that the species may participate in:

$$R_{i'} = \sum_k R_{i',k} \tag{4.11}$$

where R_{ik} is the rate of creation-destruction of species *i* in reaction *k*. The reaction rate, R_{ik}, is controlled either by an Arrhenius kinetic rate expression or by the mixing of the turbulent eddies containing fluctuating species concentrations.

The Arrhenius reaction rate is computed as:

$$R_{i',k} = -\dot{\nu}_{i',k} M_{i'} T^{\beta_k} A_k \prod_{j\,reactants} C_{i'}^{\nu' i'k} \exp\left(-E_k/RT\right) \tag{4.12}$$

where $\nu'_{i',k}$ is the molar stoichiometric coefficient for species *i'* in reaction *k* (positive values for reactants, negative values for products) [dimensionless]

$M_{i'}$ is the molecular weight of species *i'* [kg/kmol]

β_k is the temperature exponent [dimensionless]

A_k is the pre-exponential factor [m^3/kg K]

$C_{j'}$ is the molar concentration of each reactant species j' [kmol/m^3]

$\nu_{j'k}$ is the exponent on the concentration of reactant j' in reaction k [dimensionless]

And

E_k is the activation energy for the reaction [J/kmol]

The influence of turbulence on the reaction rate is taken into account by employing the Magnussen Hjertager model. In this model, the rate of reaction $R_{i',k}$ is given by the smallest limiting value of the two expressions below:

$$R_{i',k} = -\nu'_{i',k} M_{i'} A\rho \frac{\varepsilon}{\kappa} \frac{m_R}{\nu'_{R,k} M_R} \tag{4.13}$$

$$R_{i',k} = \nu'_{i',k} M_{i'} AB\rho \frac{\varepsilon}{\kappa} \frac{\sum_P m_P}{\sum_P \nu'_{P,k} M_P} \tag{4.14}$$

where m_P is the mass fraction of any product species, P [dimensionless]

m_R is the mass fraction of particular reactant, R [dimensionless]

R is the reactant species giving the smallest value of $R_{i',k}$ [dimensionless]

A is an empirical constant [dimensionless]

And

B is an empirical constant [dimensionless].

4.6 SOLUTION OF THE FLUID PHASE EQUATIONS

The equations mentioned above are transformed into a set of algebraic equations that can be solved iteratively. This transformation, also called discretisation, involves the following.

- The domain is assumed to be divided into cells or control volumes.
- The governing equations are integrated over each cell.

The algebraic equations so obtained are solved by iteration as described later. In this section consideration is given to the discretisation procedure.

4.7. PHYSICAL AND COMPUTATIONAL DOMAIN

In order to perform the discretisation of the governing equations the physical space must be subdivided into a number of cells by means of a structured grid. The grid can be constructed using a rectangular, a cylindrical or a body-fitted coordinate system. In this research, a Cartesian grid was generated directly form FLUENT. The cells generated are defined by the node points, i.e. the points where the grid lines intersect. It is possible to enumerate the grid nodes, so that instead of working with the physical coordinates of the nodes, the integer numbers of the enumerated nodes are used. The space where the integers numbers are used is called the computational domain, and it is said to be mapped to the physical domain once a one-to-one relation has been established. The mapping process essentially performs a transformation between the integer indices and the physical

coordinates of the nodes and additionally gives weighting factors to each of the faces of the cells in order to compute correctly the fluxes and gradients.

4.8. DISCRETISATION OF THE EQUATIONS

The discretisation procedure consists of the integration of the conservation equations over each control volume assuming uniform values of the variables over the cell. This results in a set of algebraic equations which relate the values of the variables at discrete points (assumed to be the centres of the cells) and at the faces of the cell, the fluxes across the faces of the cell and the dimensions of the cell. It is this set of algebraic equations which is actually solved by the code.

The values of the variables at the centres of the cells become the unknowns. The values of the variables at the faces of the cells need to be interpolated between the values at the centres of two adjacent cells. This interpolation procedure is an important part of the solution scheme and is discussed in the following section.

4.9. INTERPOLATION SCHEMES

There are several interpolation procedures, among which the power law, the Quadratic Up-wind (QUICK) and the second-order-upwind are used by FLUENT.

The power-law scheme utilises the solution to a one-dimensional convection-diffusion type of equation to interpolate the values at the cell faces. FLUENT actually uses a piece-wise approximation to this solution known as the power-law (Patankar, 1980). This scheme works well only where the flow can be considered locally as one dimensional, and aligned with the grid. The advantage of the

interpolation method is its stability and that it always leads to a physically realistic solution.

The QUICK and second-order-upwind can only be used with the cylindrical velocity formulation.

4.10. SOLUTION PROCEDURE

The three momentum equations and the continuity equation provide four equations to determine the three components of the velocity vector and the pressure. The way in which the pressure appears in the equations after discretisation, however, prevents a direct solution being obtained. This is because the pressure appears evaluated not at the nodes, but at the cell faces, and simple interpolation can lead to the well known checkerboard problem [Patankar, (1980)].

FLUENT uses either the SIMPLE or the SIMPLEC algorithms in which an equation is derived for a pressure correction term to replace the continuity equation. This equation is then used to update the (guessed) pressure field and this updated pressure is in turn used to update the velocity field when the momentum equations are solved. The difference between the algorithms just mentioned is the neglect of a term that relates the correction term at the node under consideration and the correction terms at the neighbour nodes. The algorithm SIMPLEC is said to improve convergence. More details can be found in the FLUENT user's guide (1996).

4.11. BOUNDARY CONDITIONS

FLUENT allows for a number of different types of boundary conditions. Of special interest to this work are the following:

- **Inlet type**: the velocity, turbulence, temperature and composition of the flow at this type of boundary must be specified.
- **Outlet type**: at an outlet boundary the normal velocities are adjusted to satisfy an overall mass balance and no velocity gradients should exist.
- **Wall type**: at these boundaries, the normal velocity component vanishes and the non-slip condition is observed. Temperature, conduction or heat flux can be specified. No species mass flux can occur. The pressure gradient is zero. The log-law is used to calculate wall shear stress, in terms of a roughness parameter and a dimensionless distance, assuming turbulence equilibrium conditions in the turbulent boundary layer. If the dimensionless distance becomes less than a certain value, then a laminar expression is used instead.

4.12. THE ITERATIVE SOLUTION PROCEDURE

The equations are not solved simultaneously at all nodes. The line-by-line solution procedure is employed. The last step in the calculation is the inclusion of the interaction terms between the second phase and the fluid phase, as discussed in the next section.

4.13. DISPERSED PHASE

A second phase is necessary to simulate the water spray. The droplets have their own equations of motion and physical evolution which are treated separately from the fluid phase but accounted for the interaction between the phases. In this section, the equations of motion are briefly described as used in FLUENT. In addition, the equations that describe the physico-chemical process undergone by the droplets are described more extensively as these are particularly important for this study. The equations used by FLUENT are presented and, where appropriate, the modifications made for this particular work are explained.

4.13.1 The equations of motion

The equations of motion for a single droplet are considered in a Lagrangian frame. The particle inertia is equated to the forces acting on the droplet in accordance with Newton's second law. When all external effects, except drag, are neglected, the equations of motion in Cartesian coordinates can be written as:

$$\frac{du_p}{dt} = -F_D(u_p - u_\infty)(\rho_p + \rho_\infty)/\rho_p \tag{4.15}$$

$$\frac{dv_p}{dt} = -F_D(v_p - v_\infty)(\rho_p + \rho_\infty)/\rho_p \tag{4.16}$$

$$\frac{dw_p}{dt} = -F_D(w_p - w_\infty)(\rho_p + \rho_\infty)/\rho_p \tag{4.17}$$

The equation of trajectory takes the form

$$\frac{dx}{dt} = u_p \tag{4.18}$$

$$\frac{dy}{dt} = v_p \tag{4.19}$$

$$\frac{dz}{dt} = w_p \tag{4.20}$$

where the subscript p refers to the particle and ∞ to the gas flow. The term F in the equation is written as

$$F_D = \left(\frac{18\mu_g}{\rho_p D_p^2}\right)\frac{C_D R_e}{24} \tag{4.21}$$

where μ_g is the molecular viscosity of the gas, D_p is the particle diameter. R_e denotes the relative Reynolds number defined as:

$$R_e = \rho_g D_p \left| v_p - v_\infty \right| / \mu_g \tag{4.22}$$

The drag coefficient, C_D, is a function of the relative Reynolds number given as:

$$C_D = a_1 + a_2 / R_e + a_3 / R_e^2 \tag{4.23}$$

Where the a's are constants which are applicable over several ranges of R_e given by Morsi and Alexander (1972).

4.13.2. Thermal history of a water droplet

Modelling of water spray droplets in fire environment undergoes a series of heat and mass transfer laws which essentially involve the following process: heating of droplets; evaporation of droplets; droplets boiling.

The duration of each law is governed by the following user inputs: the boiling point, the evaporation temperature and the non-volatile fraction.

The time history of a given droplet starts with the law of heating, which is applied until the droplet temperature reaches the vaporisation temperature. Vaporisation then follows while the temperature of the droplet lies between the vaporisation and

the boiling point values. Boiling continues when the temperature of the droplet has reached the boiling temperature until the remainder of the water is consumed; and finally, the inert particle is tracked until the end of the calculation steps. Each of the above stages is described in detail in the following paragraphs.

- **heating of a water droplet**

When a droplet enters the combustion chamber the first process it undergoes is heating. The droplet receives heat from various sources and in different ways, namely, radiation from walls, radiation from hot gases and ignited jet, and convection from hot gases. The relative importance of each of them depends strongly on the conditions of the whole system, particularly on the temperature and the flow pattern. Since very often such conditions are not known *a priori*, or they vary sharply within the same system, it is convenient to develop as comprehensive a model as possible. FLUENT V4.4 uses the following heat balance on the droplet:

$$m_p c_p \frac{dT_p}{dt} = h_c A_p (T_\infty - T_p) + \varepsilon_p A_p \sigma (\theta_R^4 - T_p^4) \qquad (4.24)$$

Equation (4.24) assumes that the droplet is at a uniform temperature throughout. Radiation heat transfer to the droplet is included only when P-1 radiation model has been activated.

The heat transfer coefficient, h_c, is evaluated using the correlation of Ranz and Marshall (1952):

$$Nu = \frac{h_c D_p}{\kappa_\infty} = 2.0 + 0.6\,\mathrm{Re}_D^{\frac{1}{2}}\,\mathrm{Pr}^{\frac{1}{3}} \qquad (4.25)$$

Finally, the heat lost or gained by the particle as it traverses each computational cell appears as a source or sink of heat in subsequent calculations of the continuous

phase energy equation. During this heating process, the droplets do not exchange mass with the continuous phase and do not participate in any chemical reaction.

- **droplet vaporisation**

This process is initiated when the temperature of the droplet reaches the vaporisation temperature ($T_p < T_{bp}$), and continues until the droplet reaches the boiling point, or until the droplet's volatile fraction is completely consumed ($m_p > (1-f_{v0})m_{po}$).

During the application of this law, the rate of vaporisation is governed by gradient diffusion, with the flux of droplet vapour into the gas phase related to the gradient of the vapour concentration between the droplet surface and the bulk gas:

$$N_{i'} = K_c (C_{i',s} - C_{i',\infty}) \tag{4.26}$$

FLUENT treats the droplet as inert when $N_{i'} = 0.0$.

The concentration of vapour at the droplet surface is evaluated by assuming that the partial pressure of vapour at the interface is equal to the saturated vapour pressure, $P_{sat,}$ at the particle droplet temperature, T_p:

$$C_{i',s} = \frac{P_{sat}(T_p)}{RT_p} \tag{4.27}$$

where P_{sat} = saturated vapour pressure (Pa)

The concentration of vapour in the bulk gas is known from the solution of the transport equation for species *i'*:

$$C_{i',\infty} = X_{i'} \frac{P_{op}}{RT_\infty} \tag{4.28}$$

where P_{op} = operating pressure (Pa)

The mass transfer coefficient in equation (4.26) is calculated from a Nusselt correlation:

$$N_{uAB} = \frac{k_c D_p}{D_{i',m}} = 2.0 + 0.6\,\mathrm{Re}_D^{\frac{1}{2}}\,Sc^{\frac{1}{3}} \tag{4.29}$$

The mass of the droplet is reduced according to:

$$m_p(t+\Delta t) = m_p(t) - N_i\,A_p\,M_i\,\Delta t \tag{4.30}$$

And finally, the droplet temperature is updated according to a heat balance that relates the sensible heat change in the droplet to the convective and latent heat transfer between the droplet and the gas:

$$m_p\,c_p\,\frac{dT_p}{dt} = h_c A_p\,(T_\infty - T_p) + \frac{dm_p}{dt}\,h_{fg} + A_p\,\varepsilon_p\,\sigma(\theta_R^4 - T_p^4) \tag{4.31}$$

where $\frac{dm_p}{dt}$ = rate of evaporation (kg/s)

- **droplet boiling**

When the droplet temperature reaches the boiling point, the following boiling rate equation is applied:

$$\frac{dD_p}{dt} = \frac{4\kappa_\infty}{\rho_p c_{p,\infty} D_p}\left(1 + 0.23\sqrt{\mathrm{Re}_D}\right)\ln\left[1 + \frac{c_{p,\infty}(T_\infty - T_p)}{h_{fg}}\right] \tag{4.32}$$

where h_{fg} = latent heat of vaporisation (J/kg)

Equation (4.32) has been derived assuming steady flow at constant pressure. The model requires that $T_\infty > T_{bp}$ in order for boiling to occur and that the droplet remains at a fixed temperature (T_{bp}) throughout the boiling process.

When radiation heat transfer is active, FLUENT uses a slight modification of equation (4.32), derived by starting from equation (4.24) and assuming that the droplet temperature is constant.

$$-\frac{dm_p}{dt} h_{fg} = h_c A_p (T_\infty - T_p) + \varepsilon_p A_p \sigma (\theta_R^4 - T_p^4) \tag{4.33}$$

Or

$$-\frac{dD_p}{dt} = \frac{2}{\rho_p h_{fg}} \left[\frac{\kappa_\infty Nu}{D_p} (T_\infty - T_p) + \varepsilon_p \sigma (\theta_R^4 - T_p^4) \right] \tag{4.34}$$

Using equation (4.25) for the Nusselt number correlation and assuming a Prandtl number of 0.45 in the fluid, equation (4.34) becomes:

$$-\frac{dD_p}{dt} = \frac{2}{\rho_p h_{fg}} \left[\frac{2\kappa_\infty \left(1 + 0.23\sqrt{\mathrm{Re}_D}\right)}{D_p} (T_\infty - T_p) + \varepsilon_p \sigma (\theta_R^4 - T_p^4) \right] \tag{4.35}$$

In the absence of radiation, this result matches that of equation (4.32) in the limit that the argument of the logarithm is close to unity.

FLUENT uses equation (4.35) when radiation is active and equation (4.32) when radiation is not active.

The droplet is assumed to stay at constant temperature while the boiling rate is applied.

4.14. HEAT TRANSFER

Fluent allows to include heat transfer within the fluid and at walls in the model. This section describe the various options that are available for defining heat transfer in the fluid and thermal boundary condition at wall cells.

4.14.1. Radiation modelling

Fluent provides two radiation models, termed the Discrete Transfer Radiation Model (DTRM) and the P-1 Radiation Model, which allow you to include radiation model.

The Discrete Transfer Radiation Model:

The main assumption of the DTRM is that the radiation leaving the surface element in a certain range of solid angles can be approximated by a single ray.

Fluent provides the DTRM for prediction of surface-to-surface radiation heat transfer with or without participating medium.

The primary advantages of the DTRM are threefold: it is a relatively simple model, you can increase the accuracy by increasing the number of rays, and it applies to a wide range of optical thickness.

On the other hand, DTRM has some limitations which are: the effect of dispersed second phase of particles or droplets can't be included or considered here, solving a problem with a large number of rays is CPU intensive, and the effect of scattering is not included. Finally the radiation file which will contain a description of ray traces (path-lengths, cells traversed by each ray, etc) requires large disk memory.

Constant or variable absorption coefficient can be used with DTRM in FLUENT based on local concentrations of CO_2 and H_2O species in the gas phase. Two variable absorption coefficient models are available in FLUENT; the Weighted-Sum-Of-Gray-Gases Model (WSGGM) and Modak's model. WSGGM has a wider range of applicability and is especially recommended for optically thick media or temperatures greater than 2000K.

In the case of the effective gray gas approximation, the equation for the change of radiant intensity, *dI*, along a path, *ds*, can be written as:

$$\frac{dI}{ds} + aI = \frac{a\sigma T^4}{\pi} \tag{4.36}$$

Fluent includes an option that allows the influence of the temperature of the gas and the walls beyond the inlets or outlets boundaries to be taken into account, and specify different temperatures for radiation and convection at inlets and outlets. This can be useful when the temperature outside the inlets or outlets differ considerably from the temperature in the compartment.

4.14.2. Heat transfer at walls

Thermal boundary conditions at wall boundaries tell Fluent the conditions at the wall that impact on the rate of heat transfer between the wall and the adjacent live or conducting wall cells. These conditions may be defined in terms of:

- Set Temperature at the wall and live or conducting wall cell interface.

- Set Heat flux at the wall and live or conducting wall cell interface.
- Set External heat transfer coefficient at the wall and live or conducting wall cell interface.
- External radiation boundary condition at the wall and live or conducting wall cell interface.
- Combined external radiation and external convective heat transfer at the wall and live or conducting wall cell interface.
- Set emissivity of the wall.

Temperature Boundary Conditions:

A set temperature is to be defined at the wall surface when a temperature boundary condition at wall was used. When the wall borders a live cell, Fluent computes the heat transfer to the wall as:

$$q'' = h_f(T_w - T_f) + q''_{rad} \tag{4.37}$$

Fluent computes the fluid-side heat transfer coefficient based on the local flow-field conditions (e.g. turbulence level, temperature, and velocity profiles).

When the wall borders a conducting wall cell, Fluent computes the heat transfer to the wall boundary as;

$$q'' = \frac{\kappa_{cw}}{\Delta n}(T_w - T_{cw}) + q''_{rad} \tag{4.38}$$

Heat Flux Boundary Conditions:

A set heat flux is to be defined at the wall surface when a heat flux boundary condition at wall is used. When the wall borders a live cell, Fluent computes the heat transfer to the wall as:

$$T_w = \frac{q'' - q''_{rad}}{h_f} + T_f \tag{4.39}$$

When the wall cell borders a conducting wall cell, the wall surface temperature is computed as:

$$T_w = \frac{(q'' - q''_{rad})\Delta n}{\kappa_{cw}} + T_f \tag{4.40}$$

Adiabatic wall can be defined via input of a zero heat flux boundary condition.

External Heat Transfer Coefficient Boundary Conditions:

The external heat transfer coefficient boundary condition at a wall is the resistance to heat transfer starting from the wall/live cell interface (or wall /conducting-wall cell interface) out of heat sink temperature which has been defined.

Fluent uses the input of the external heat transfer coefficient and external heat sink temperature to compute the heat flux to the wall as:

$$\begin{aligned} q'' &= h_f(T_w - T_f) + q''_{rad} \\ &= h_{ext}(T_{ext} - T_w) \end{aligned} \tag{4.41}$$

External Radiation Boundary Conditions:

If a radiation heat transfer from the exterior of the physical model is of interest, the external radiation option can be used. When this boundary condition option is used, Fluent computes the wall heat flux as:

$$q'' = h_f(T_w - T_f) + q''_{rad}$$
$$= \varepsilon_{ext}\sigma(T_\infty^4 - T_w^4) \quad (4.42)$$

Combined External Convective and Radiation Boundary Conditions:

Fluent computes the heat flux in the case of combined external heat transfer condition as:

$$q'' = h_f(T_w - T_f) + q''_{rad}$$
$$= h_{ext}(T_{ext} - T_w) + \varepsilon_{ext}\sigma(T_\infty^4 - T_w^4) \quad (4.43)$$

The input of the external heat transfer condition will include the external heat transfer coefficient h_{ext}, the temperature of the external medium T_{ext}, the external emissivity ε_{ext}, and the radiant heat sink temperature T_∞.

4.14.3. Modelling conduction using conducting walls

If conduction in solid regions is to be modelled, the solid is represented via conducting wall cells, with thermal boundary conditions supplied at the edge of the conducting region via wall thermal boundary conditions. The thermal treatment of conducting wall cells is thus not as a boundary condition, but via solution of a transport equation. For this reason, conducting walls cannot lie on the periphery of the domain and Fluent issues a warning if this situation is detected during an attempt to solve the governing equations.

Fluent solves a multi-dimensional conduction equation in conducting solid regions, which can be written as:

$$\rho_w \frac{\partial h_w}{\partial t} = \nabla \cdot \kappa_w \nabla T_w + \dot{q} \qquad (4.45)$$

Equation (4.45) is solved in conducting wall cells, with a special treatment at the wall-fluid interface where the heat flux is computed via a harmonic mean "conductivity" that correctly incorporates the thermal resistance change at the interface.

4.15. Limitations of FLUENT to this application:

Solving Discrete Transfer Radiation Model (DTRM) problem with a large number of rays is CPU-intensive. The ray tracing technique used in the DTRM can provide a prediction of radiation heat transfer between surfaces without explicit view-factor calculations. The accuracy of the model is limited mainly by the number of rays traced and the computational grid chosen. Therefore, the issue of the number of

rays, which involves computational economy, uniformity and accuracy of coverage, was investigated in this study and explained in section (8.4.3).

Radiation heat flux at outlet was computed in the same manner as at walls, by using the compartment outlet cells temperature for this computation. This caused a considerable error, because the temperature beyond outlet boundaries was much lower than the outlet temperature. To avoid this problem and to account for the influence of the temperature beyond the outlet by specifying different temperature for radiation at outlet, a correction factor was applied.

When the DTRM was included, a radiation file was created to store all the parameters controlling the model (properties, geometry, boundary conditions and solution control parameters). The storage requirement in terms of memory and disk to run and hold the data for the simulation was very large.

The computational time to run the simulation until convergence criteria was reached when radiation model and dispersed second phase were activated was unacceptable. Therefore, reduced convergence criteria was considered.

Other limitations such as: the effect of scattering in the DTRM used was not included and the radiation heat transfer to the particles was not included in the DTRM. Access to FLUENT source code for alteration and to minimise this limitation was not possible as it is proprietary product and was beyond the objective of this research.

In FLUENT the user does not have a control over the colour-filled contours plots, especially when the maximum number of contour lines is requested. As a consequence the values of the plotted variables represented in the colour range are not the same in the different graphs.

4.16. Uncertainties in CFD

The overall uncertainty involved in CFD modelling can be due to several sources of errors such as (i) modelling error (the inaccuracy inherent in the mathematical model of certain physical phenomena), domain dependency errors (i.e. errors arising from finite representation of a domain, (ii) errors due to inaccurate implementation of the boundary and initial conditions, (iii) iterative convergence errors (e.g. incomplete convergence), (iv) truncation convergence errors (errors due to insufficient grid refinement, i.e. discretisation errors).

4.16.1. Reduction of Numerical errors

For a solution to be acceptable, the total error must be reduced to tolerable level. Unfortunately, cost may limit the resources that can be brought to bear on a problem. It is possible that the problem cannot be solved to the desirable accuracy at acceptable cost. In such a case, compromise or another approach is necessary.

Rapid reduction of convergence error requires methods that converge in few iterations at low cost per iteration. Reduction of discretisation error can be accomplished through the use of finer grids and/or a more accurate approximation of derivatives (higher order methods).

4.17. CONCLUSIONS

The basic equations of fluid dynamics constitute a set of simultaneous non-linear partial differential equations and its solution can only be achieved numerically in the general case. Furthermore, when the problem at hand involves turbulence, the

problem needs to be solved through the turbulence approaches, none of which is completely satisfactory, especially for three dimensional problems.

This chapter has outlined the physical relationship and the correlation necessary to mathematically simulate the environment created by a compartment fire for steady state and time dependent situations using field approach.

CHAPTER 5

NUMERICAL SETUP AND PRELIMINARY RESULTS

5.1 INTRODUCTION

The simulation of compartment jet fire suppression by using water spray included the following steps:

Phase I: Single Phase Jet Fire Modelling

- Compartment construction, geometry set up and the generation of the computational grid.
- Completion of the problem definition.
- Solution of the problem.

Phase II: Dispersed Phase (Two Phase) Modelling

- Water spray setup
- Solution of the problem and coupling both solutions

The two phases are coupled using the Lagrangian frame.

The reacting flow was solved neglecting transport of energy by thermal radiation. The effect of radiation on the flow field and heat losses from the compartment are explored in chapter 8.

FLUENT requires defining and inputting many parameters in order to complete constructing and setting up the model; these are memory allocation and definition

of the size of the computational domain, the number of cells, physical models, and boundary conditions selection.

Once the model construction and setting up is completed, the next stage is to start the solution process by setting the solution parameters, the number of iterations or time steps of the solver and by controlling the display of the solution residuals during the calculation. Most of the important steps to set up the model are covered in details in the following sections. However, example of the completed model definition and construction listing is given in appendix II.

This task of CFD fire modelling required a considerable amount of time and effort in order to get a reliable prediction, because it incorporated sub-models such as turbulence, chemical reaction, radiative heat transfer and dispersed phase. This modelling requirement also places great demands in terms of storage and speed on currently available computer systems.

5.2. GEOMETRY AND GRID SET-UP

This shows the general procedure that was employed when setting up a model in the initial stage of the project. It describes how the geometry was set up, the specification of the boundary conditions and physical constants and then explains the results that were achieved. It contains many flaws as it is the first of many trial calculations but, as always, they are used as a learning process and are improved in the subsequent specifications of the calculations.

The philosophy is to carry out the flow simulations at successive levels of detail of application in order to understand the calculation at each step. Calculations of the flow field in this chapter are made for adiabatic walls and without thermal radiation. They establish the method and the calculation for a spray of water droplets at a manageable level of complexity for a 3-D simulation. However, they are not suitable for direct accurate comparison with the experimental data which is

approached in a further step, in chapter 8, by adding the radiation field which has further complexity.

5.2.1 Construction of the Compartment:

On setting up the initial geometry of the compartment (Figure 3.2) it was discovered that in order to investigate the flow at the exit, it was not recommended to include the compartment only, another reason being that FLUENT would not allow live cells on the edge of a domain; it was also found in the previous fire simulations (Markatos et al 1986b, Cox and Kumar 1987 and Galea and Markatos 1987) that the flow domains are extended outside the compartment of interest for computational purposes only.

It was therefore necessary to situate the compartment within a larger environment chamber, allowing the cells at the compartment opening to be live, and the flow to become fully developed. This outer environment chamber could then have an inlet for air and an outlet for all the gases to exit, without affecting the flow in the compartment.

It was necessary to start running the model for the flow field in order to examine the air movement inside the compartment. The environment was extended six meters to the front of the compartment and two meters on each side from the compartment walls in order to have no effect on the flow also, from experience obtained from previous fire simulations (Markatos et al 1986b, Cox and Kumar 1987, and Galea and Markatos 1987).

Most of the diagrams of the geometry, grid spacing and results are illustrated by showing a slice of the actual compartment through x-y, x-z and y-z planes. The outline of the geometry of this design is shown in Figure (5.1) which illustrates the compartment within a larger environment.

The result of examining the flow field showed that the lower opening entrains air at higher velocity than the others, so it acted like an inlet . The out-flow attached itself to the upper opening as it progressed in the compartment.

The problem under consideration had a rectangular physical boundary, so the domain was modelled in three dimensions. FLUENT grid-based geometry was used, in which the geometry of the compartment is determined by control volumes defined by the grid. Cartesian coordinates have been used in which the grid lines are aligned with the Cartesian (x, y, z) coordinates.

The geometry of the compartment was created by defining the number of dimensions and overall domain size (overall physical dimensions of the compartment and uniform grid size desired in terms of number of control volumes).

The computational time and accuracy was improved by the use of a non-uniform grid. Therefore, a uniform grid structure (one with a fixed cell size through the domain) would have been unacceptable. A non-uniform grid allowed the grid to cluster more densely in areas where the flow is complex or of interest, such as jet nozzle and water spray locations; it also allowed the use of grid lines more sparingly in regions that are of lesser interest. In addition, non-uniform grid was required in order to capture the geometric dimensions of flow inlets and solid regions. In this study, the high velocity jet is in a fixed position at the centre of the compartment. Therefore, non-uniform grid lines are required along the radial and the circumferential directions in order to specify the inlet conditions for the high-velocity jet as its dimension is very small, being only 0.0177 metre. The area of the jet nozzle has a fixed value of 314.2 mm^2. The area of the propane inlet was very small compared to the area of the whole domain, and the activity in and around this entrance was important to the solution of the problem. In order to create the necessary propane inlet dimension it was necessary to alter the grid spacing so that it was concentrated at the propane inlet, in both the x- and z-directions. A single cell was used as the inlet of 0.0177 m, the cells to the left of the inlet were contracted, and the cells to the right gradually expanded in order to create a smooth transition between cell sizes. This was necessary, as FLUENT calculates the properties of one cell and uses them as an approximation to the next cell. It would have caused great problems if adjacent cells were vastly different in

size. It can be observed that the grid line becomes narrower near the jet fire nozzle.

The expansion factor (f) which was required for each segment can be calculated from the equation below which is related to segment length (L), the starting cell size (a), and the number of cells in the segment (N), by the following relationship:

$$N = \frac{\ln\left[\left(\frac{L}{a}\right)(f-1)+1\right]}{\ln(f)} \qquad (5.1)$$

The grid generated was checked mathematically to see if there were some bad gridlines, such as skewed or having a high cell aspect ratio (the ratio of the sizes of the cell generated). It was also examined graphically to see if a good distribution of gridlines had been created. The calculations reported in this chapter 5 were carried out on the grid illustrated in Figure (5.2). The grid was further refined when making calculation of radiation and the final grid is shown in Figure (8.9).

The actual circular shape of the jet nozzle could not be accurately modelled under the Cartesian coordinates. Therefore, the circular inlet of the central jet nozzle was replaced by a square inlet having the same cross sectional area. However, it was found by Liu (1990) that the flow field in the main chamber cannot be greatly affected by this inaccurate setup of jet nozzle.

5.3 BOUNDARY CONDITIONS.

In order to complete the numerical model once the geometry set up was completed, initial boundary conditions need to be specified which take into account the flow rates, species and temperature.

5.3.1 Inlet boundaries:

In order to define the air inlet, only oxygen mass fraction of 23% need to be defined for the specified inlet. On the other hand, the fuel injected to the compartment need to be specified at the jet nozzle as 100% propane gas (the fuel supply was specified at the burner as 100% propane). In FLUENT the mass flow rate of the fuel must be input in terms of the velocity which is equivalent to 0.1 kg/s and 10% turbulent intensity. The boundary conditions specified for the input-cells are given in table (5.1).

	Velocity (m/s)	Temperature (K)	Chemical Species %
Air inlet (IA)	1	298	$O_2 = 23$ $N_2 = 77$
Fuel inlet (IJ)	193	298	$C_3H_8 = 100$

Table (5.1). Boundary Conditions for Inlet Cells.

5.3.2 Wall conditions

The nozzle wall surrounding the propane jet was specified as an adiabatic (zero heat flux) surface.

Initially the wall enclosing the compartment was treated as adiabatic wall. Then heat transfer and conduction were introduced to the compartment walls with proper thermal conductivity set accordingly.

5.4 COMPLETION OF THE PROBLEM DEFINITION

Specifying the physical models and constants and boundary conditions for the continuous and dispersed phase completed the problem definition.

5.4.1 Continuous Phase Set-up

The scope of the problem definition included:

- Turbulent flow
- Heat transfer
- Chemical species transport and reaction
- Dispersed Phase

Therefore, the relevant basic physical models and governing equations were activated by inputting 'yes' to CALCULATE TEMPERATURE, TURBULENT FLOW and to CALCULATE SPECIES. TURBULENT FLOW defined the problem as turbulent and activated FLUENT's turbulence models. CALCULATE TEMPERATURE added heat transfer and thermal mixing to the model, and activated the solution of energy equation. Discrete Transfer radiation model (DTRM) was switched on for the radiation heat transfer calculations. CALCUALTE SPECIES added chemical species transport and chemical reaction to the model and activated the species transport equations. The combustion of propane in air was modelled using the following stoichiometric equation,

$$C_3H_8 + 5\,O_2 \Rightarrow 3CO_2 + 4\,H_2O$$

The stoichiomety of the reaction and the number of species were defined in the model. Species included were C_3H_8, O_2, CO_2, H_2O and N_2. The reaction rate in the species conservation equation was determined from the rate expression, which

took account of turbulence rather than the Arhennius kinetic rate expression since the reaction is most likely to be diffusion-controlled.

Physical properties of the fluid were input and they included molecular weights, viscosity, heat capacity, thermal conductivity, mass diffusion coefficients, formation enthalpies. Properties were temperature and/or composition dependent with temperature dependence based on a polynomial or piece-wise linear function and individual component properties. They were taken from Perry's Chemical Engineers Handbook (6^{th} edition, 1984), David (1997) and Roger and Mayhew (1921).

The information on flow/thermal conditions at the boundaries of the physical model was provided to FLUENT through boundary conditions. The Cartesian velocity components, chemical species concentration, turbulence intensity/length scale inlets were given through cell types defined as INLET boundaries. There were two inlet boundaries, specified as IJ and IA which presented jet nozzle and air inlet respectively.

Flow exit was modelled using cells specified as OUTLET boundaries. FLUENT assumes that at the outlet boundary layer there was no change in the flow properties between the live cell upstream of the OUTLET and exit plane.

The boundary conditions at the wall including wall temperature and diffusion of chemical species were specified through WALL boundaries. The wall boundaries of the domain were named with different names so that the temperature distribution at the wall boundaries of the compartment would be specified. This was also necessary since it was aimed at determining where the particles were trapped. Zero flux boundary condition (cut link) was defined for each chemical species, i.e., no diffusion of chemical species from the fluid to the wall. The shear stress and heat transfer between the fluid and the wall were computed based on the flow details in the local flow field.

5.4.2 Physical Constants

The gas law was used, so FLUENT calculated the density as a function of local composition and temperature throughout the flow field. Therefore the molecular weights of each species had to be entered for this calculation to work.

The viscosity and thermal conductivity were all given values which were appropriate for this situation.

To calculate the required thermodynamic quantities, the specific heat for each species is first defined by a third order polynomial in temperature:

$$c_P\,(C_3H_8) = -4.195 + 6.442\,T - 2.8\times10^{-3}\,T^2 + 5\times10^{-7}\,T^3$$

$$c_P\,(O_2) = 6.924\times10^{2} + 4.647\times10^{-1}\,T - 1\times10^{-4}\,T^2 + 1\times10^{-8}\,T^3$$

$$c_P\,(CO_2) = 5.613\times10^{2} + 8.064\times10^{-1}\,T - 2\times10^{-4}\,T^2 + 2\times10^{-8}\,T^3$$

$$c_P\,(H_2O) = 1.276\times10^{3} + 1.294\,T - 3\times10^{-4}\,T^2 + 2\times10^{-8}\,T^3$$

$$c_P\,(N_2) = 7.688\times10^{2} + 5.05\times10^{-1}\,T - 1\times10^{-4}\,T^2 + 1\times10^{-8}\,T^3$$

The coefficients are found by curve fit of the data tabulated in reference (Perry and Green, 1984 and Sinnott, 1996).

The formation enthalpy for each of the species is shown in the table (5.2) below:

SPECIES	FORMATION ENTHALPY (J/KMOL)
C_3H_8	-1.039×10^{8}
O_2	0
CO_2	-3.937×10^{8}
H_2O	-2.419×10^{8}
N_2	0

Table (5.2). Formation enthalpies for species used in the modelling

5.5 DISPERSED PHASE SET-UP

The dispersed (particle) phase was setup by providing initial conditions that define the particle type (inert), starting positions (x, y, z), velocities (U, V, W), temperature (T), particle size distribution and mass flow rate of particles. A total number of 75 injections were defined. A Rosin-Rammler size distribution was used to define the water particle size distribution with different spread parameter. The Rosin-Rammler size distribution function is given as:

$$m_D = \exp\left(-\left(\frac{D}{\bar{D}}\right)^q\right) \tag{5.2}$$

where:

m_D	Mass fraction of particles greater than D.
q	the spread parameters.
D	droplet diameter
$\bar{D}$	representative diameter

When a particle reached a physical boundary WALL or an INLET, a dispersed phase boundary condition ESCAPE was applied to determine the fate of the trajectory at that boundary. ESCAPE reported those particles that escaped when it encountered the boundary in question. Trajectory calculations were then terminated.

The spray angle used for each of the spray heads is represented by 25 injection directions with each direction having the possibility of an independently defined size and velocity range.

Physical property inputs for the dispersed phase to predict particle trajectories and heat transfer included initial density, thermal conductivity, specific heat and binary diffusivity. After the model definition was completed it was saved as a CASE-FILE.

5.6. ADOPTED SOLUTION PROCEDURE

With the model definition completed, the governing equations were solved in order to predict the flow fields of velocity, temperature, composition and particle trajectories. Two techniques were used to get the calculation off to a good start. These include starting with guessed values for some flow variables at all locations along the domain (patching), and solving the problem in stages. Because in the absence of initial guess, all of the flow variables are assumed to have a value of 0 throughout with the exception of temperature which has default value of 273 K (0°C). The model created included fluid flow, heat transfer, chemical reaction and the interaction of two phases, continuous gas phase and dispersed particle phase. Therefore, it was a complex problem. To speed up the convergence for the problem a step by step solution was adopted. These two techniques were used to get converged solution for the governing equations as follows:

i. An isothermal velocity flow field was obtained by considering only mass and momentum conservation equations by turning off the energy and species conservation equations and the coupling between the two phases. Flow variables including velocity of the fuel through the jet nozzle of 100 m/s and air velocity through the air inlet 0.3 m/s, temperature 300 K, mass fraction of the oxygen 0.23 and 0.1 mass fraction of the fuel in the centreline of jet nozzle, values were patched. The iterations were performed until residual values less than 1×10^{-5} for velocity components were obtained. Residuals

are a measure of how closely each finite equation is balanced. This required about couple of thousands of iterations.

ii. The non-isothermal flow field was obtained by activating the energy and species conservation equations. Here an initial guess of 2000 K for temperature was patched along the jet nozzle to ignite the fire. Patching of temperature was essential since it was needed to overcome the activation energy barrier of propane so that the combustion reaction would take place. More iterations were performed till residuals of flow variables were less than 1×10^{-5}.

iii. The coupling between the two phases and its impact on both the dispersed and continuous phase flow patterns was included. The particle trajectories were based on the mean gas velocity and calculated once after every 5 iteration of continuous phase. The iterations were performed until the residual for the enthalpy equation was less than 1×10^{-4}. Cases solved for small particle sizes were found difficult to converge. Thus, the number of iterations required to get a converged solution changed between 30000 and 50000. The results of the calculation were saved in a DATA-FILE.

iv. After the converged solution was achieved, the results were used for post-processing.

It was found that the optimum strategy was to start the calculation with under-relaxation factors of typically 0.4 for the velocities and to reduce these as the calculation progressed to allow the stratified flow to develop.

When DTRM radiation sub-model was included in the model, to be discussed in detail in chapter 8, care had to be taken to under-relax the radiation source term and to allow the solution to stabilise between calls to the radiation sub-model by performing typically 3-6 flow iteration per radiation call.

5.7 CONVERGENCE

The calculation is terminated when the residuals are less than 1×10^{-5} in the case of steady state. On the other hand, in a transient mode, a few-thousand time steps are required before reaching the solution.

5.7.1 FLUENT RESIDUALS REPORT

The process of obtaining a converged solution is of great importance in FLUENT simulations. FLUENT provides a running report of the residuals for each equation at each iteration, hence this process was monitored very carefully. The residuals are a measure of how closely each finite difference equation is balanced, given the current state of the solution. A typical FLUENT residuals report is given in appendix III.

5.7.2 FLUENT GRAPHICS OUTPUT

Graphics of the colour-filled contours created by FLUENT which are presented in the thesis use the same colour coding range. In the colour scale red represents the maximum variable plotted and blue represents the minimum for all the graphics shown in this chapter and chapter 8. However the values of the plotted variables represented in the scale are not the same in the various graphs.

5.8 DESCRIPTION OF THE PRELIMINARY STUDY

In order to combat fire it is necessary to understand the nature of the interaction between the hot combustion products and the liquid water. Different cases

modelled can be classified under five main groups depending on the parameters being investigated. Factors which need to be considered include water flow rate, spray pattern, droplet size and the number and location of spray heads.

5.8.1 Determination of Optimum Spray Locations

The simulation started by studying the effects of a single spray located at different positions in the roof of the compartment. This will give a chance to better understand the fire–spray interaction and evaluate the best spray location(s) to be used to carry out a more detailed investigation.

Three spray locations were examined. In the first, a single spray is located above the propane nozzle. The remaining two were placed on the front/rear axis and 2.0 m on each side of the centre (Figure 5.3).

5.8.2 Determination of Optimum Mean Droplet Diameters

The mean droplet diameters could be chosen within the range from 100 to 600 μm.

5.8.3 Determination of Optimum Droplet Velocities

In addition to the condition simulated above, another experimental condition was studied, this was the droplets' velocities. In these studies the velocities of the droplets used varied between 5 and 25 m/s.

5.8.4 Determination of Optimum Spray Angles

The spray angle used for each of the spray heads is represented by 25 injection directions with each direction having the possibility of an independently defined size and velocity range.

5.8.5 Determination of Optimum Water Flow Rates

It is important also to find out the maximum amount of water that can be discharged from an appropriate spray head in order not to flood the compartment and cause water damage.
The total water flow rate for each of these arrangements was varied from 0.1 to 2.7 kg/s.

5.9 RESULTS AND DISCUSSION

5.9.1 STEADY STATE RESULTS

The steady state simulation of the flow field was performed using the compartment layout discussed in chapter 3, which represents an offshore compartment module but with no heat transfer through the walls, i.e. adiabatic and no thermal radiation, which are considered in chapter 8. Using the above description of the physical setup. The following results were obtained.
To examine the three dimensional flow structures inside the final compartment geometry, the predicted velocity vector distributions of the gas flow field are shown on different x-y, y-z and x-z planes through various locations inside the compartment. The upper part of the plume can clearly be identified as well as the other features such as plume entrainment, the escape of the hot gases through the opening and the wall effects on the upper layer's flow as shown in Figures (5.4) to (5.10). Whereby Figures (5.4) and (5.5) show flow fields through vertical slice at (x-y) and (y-z) planes, respectively at the centre of the jet fire section (z =1.2 and x =3 m). These indicated the very strong rising fire plume which, after hitting the ceiling, is forced to spread outwards along the ceiling, creating the upper layer. The gases are able to escape through the upper opening of the compartment. The

way in which the fire plume entrains gases, both hot and cold, is also demonstrated. Examination of velocity vectors on vertical planes showed recirculation of partial combustion products back into the flame. Two circulation zones were observed to the right and the left of the jet flow. These are due to the movement of the air entrained by the fire plume upward and downward movement of layer. The flow field of further slice position can be seen in Figure (5.6). The entrainment of cold air through the lower part (region) of the opening into the compartment and subsequently into the base of the fire is clearly shown in horizontal x-z plane (y =0.2 meter). The process of air entrainment into the fire, vertical acceleration of the plume, formation of a ceiling jet and the establishment of recirculation in the cell are clearly evident. The effect of the upper opening and the strong flow established by the upper layer, spreading out along the ceiling can also be clearly seen in Figure (5.7). The hot fire gases that hit the roof and surrounding walls are re-directed towards the upper part of the opening through which the hot and subsequently lighter air can leave the compartment whereas colder and denser air is entrained into the compartment from the lower part of the opening. These two sections are divided by the neutral plane which is predicted to be around 0.6 metre above the compartment floor as shown in Figure (5.4). The downward movement along the walls by the hot gases can be more clearly seen in Figure (5.8) where slices across the compartment are shown. The strong upward movement by the plume created circulation fields in the top corners of the compartment as shown in Figure (5.9).

The flow field which occurred on the side of the compartment near the opening is shown in Figure (5.10) whereby it should be noticed that the gases are leaving the compartment through the upper part and the cooler air is entrained through the lower part of the opening.

The mean flue gas velocity in the compartment was predicted as 8.65 m/s which was slightly higher than the one reported in Brightwell and Chamberlain (1997) which was 8 m/s.

The temperature distribution obtained for the whole domain and close to the jet nozzle location in adiabatic conditions are given in Figures (5.11) to (5.15). These are presented in Kelvin degrees where the temperature contours predicted close to the jet nozzle section in the x-y and y-z plane are shown in Figure (5.11) and (5.12) respectively. Most of the combustion took place above the jet nozzle where the higher temperatures were predicted. Due to the attachement of the velocity to the top wall, the temperature flow field also attached to the top wall. The temperature of the gas at the location where the flue gas temperature was measured for the experimental study was 1900° C. as shown in Figure (5.13).

Some of the temperature distributions obtained can be seen in Figures (5.14) and (5.15). The reason for this temperature pattern becomes more apparent from the velocity vectors shown in Figure (5.4). From these it can be seen that air is entrained from the outside through the lower part opening and attracted towards the fire plume. However, due to the hotter gases being pushed downwards along the walls a certain amount of this fresher and cooler air is mixed in with these hotter gases.

The predictions of mole fraction of fuel, oxygen and the combustion products on the vertical plane through the centre of the jet nozzle are shown in Figure (5.16) to (5.19). Inspection of these shows that the neutral plane occurs around 0.6 meter above the floor with oxygen mole fraction above this height being gradually decreased from 21 to less than 1 percent and the combustion products CO_2 and H_2O concentrations gradually increased to 11.7 and 15 percent respectively. The unburnt fuel mole fraction is everywhere very low, except at the jet nozzle .

The results of a single-phase simulation are used as the initial conditions of the gas phase for the fire-spray simulations which will be described later. Having developed a one-phase fire model capable of predicting temperature, species concentration, etc., the next stage is to activate the spray.

5.9.2 WATER SPRAYS: PRELIMINARY RESULTS AND DISCUSSION

Initially, the steady state behaviour of the compartment fire was evaluated and used as the starting condition for the subsequent two-phase calculation.

Prior to the spray activation, the fire plume was able to rise straight upwards and spread outwards along the ceiling. For the case of a single spray located above the propane jet and at a low flow rate less than 1 kg/s, two major flows were apparent after the solution fully developed. The first, generated by the water spray, was downwards whilst the second, generated by the fire, was along the ceiling. These two currents met towards the centre of the upper layer of the compartment, aiding the mixing and cooling process.

The value for temperature used in the calculations throughout this section is the average temperature from the upper two-third of the compartment. Because of the configuration of the inlet to the compartment, realistic values of temperature are only obtained above this cooler inlet region.

From the modelling of different spray locations, the results show that less water is needed to extinguish the flame in the case of a single spray located centrally above the jet nozzle. For most of the flow rate, this location also gave lowest temperatures as shown in Figure (5.20). Subsequent modelling therefore used a single spray located in the centre of the compartment above the jet nozzle.

Figure (5.21) shows the average temperature in the compartment as function of mean droplet diameter of 100, 200, 300, 400, 500 and 600 μm. The curve is nearly parabolic and the lowest temperature was found with mean droplet diameters of 300 μm. Subsequent modelling was therefore carried out using mean diameters of 300 μm. It is likely that the minimum arises from the competing effects of droplet penetration which increases with droplet diameter and total droplet surface area for evaporation.

Modelling different spray angles of 30, 60, 75, 90, 100, 120, 135 and 150° indicated that using spray angle of 60° or 75° was most effective in reducing the

overall temperature as can be seen in Figure (5.22). Subsequent examination of the effect of spray droplet velocity has therefore used this optimised 60° spray angle. The effect on average temperature of varying this velocity from 5 to 25m/s is shown in Figure (5.23). This shows the limiting behaviour due to the effectiveness in penetrating the flame and indicates that for this geometry, velocities in excess of 18 m/s should be used.

For those cases where the water flow rate produced large reduction in average temperature, it was considered that the assumption of steady state was invalid since extinguishment was the likely outcome. For these cases, a time-dependent calculation was performed which has the capability of predicting the change in combustion variables with time during this process. This will be taken into consideration in chapter 8.

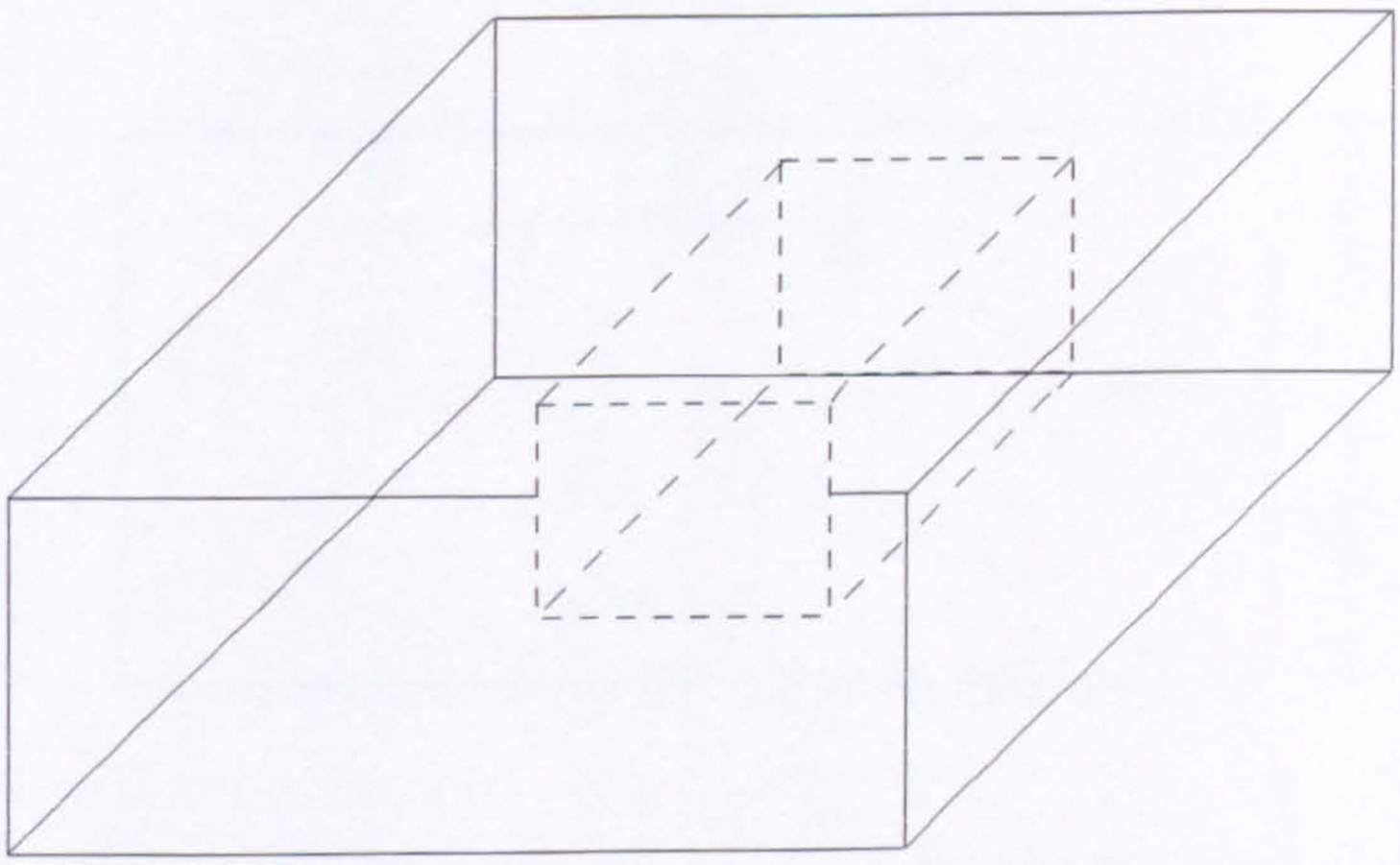

Figure (5.1). The initial geometry of the compartment with extended environment.

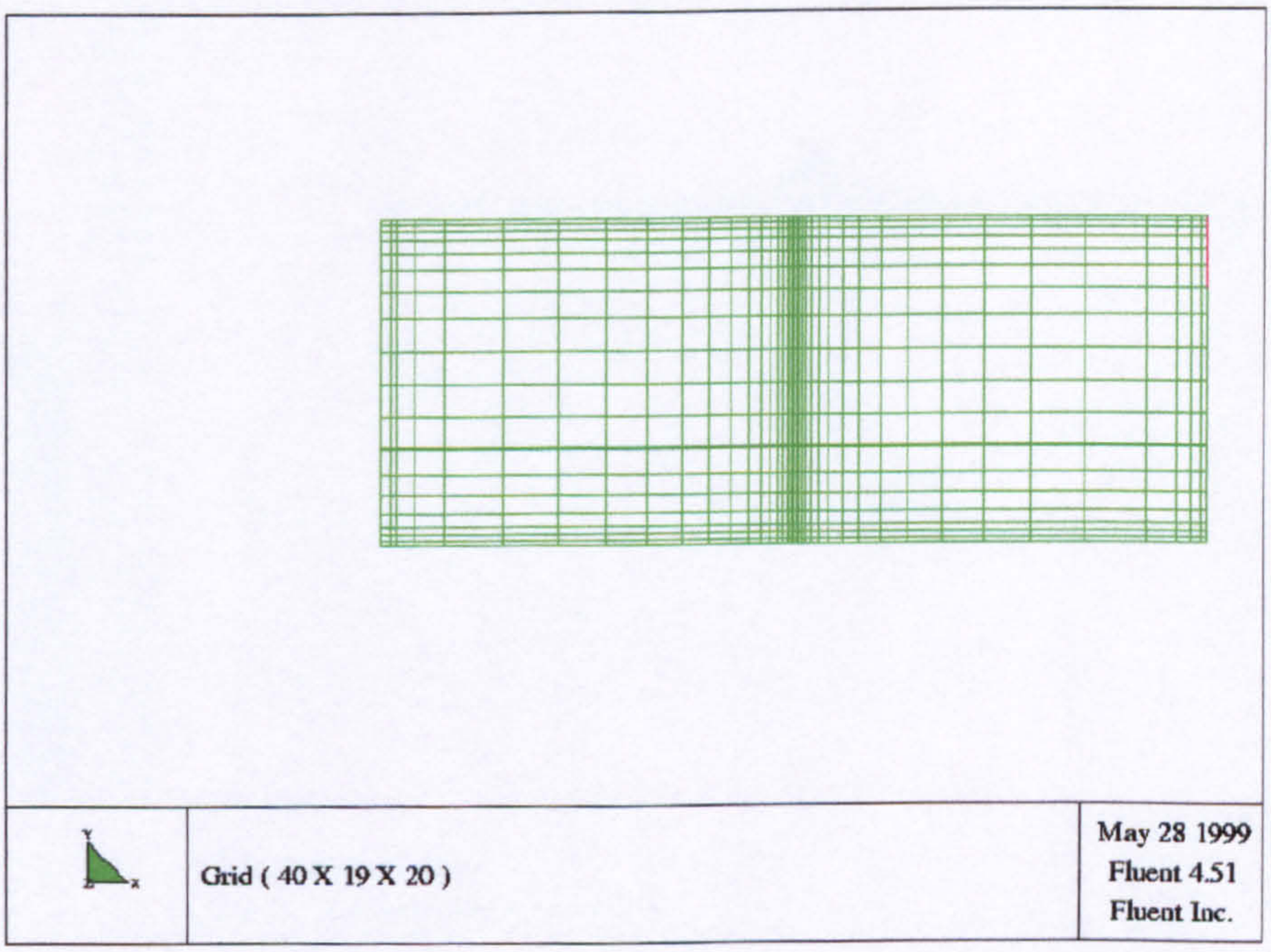

Figure (5.2). Grid distribution in the compartment.

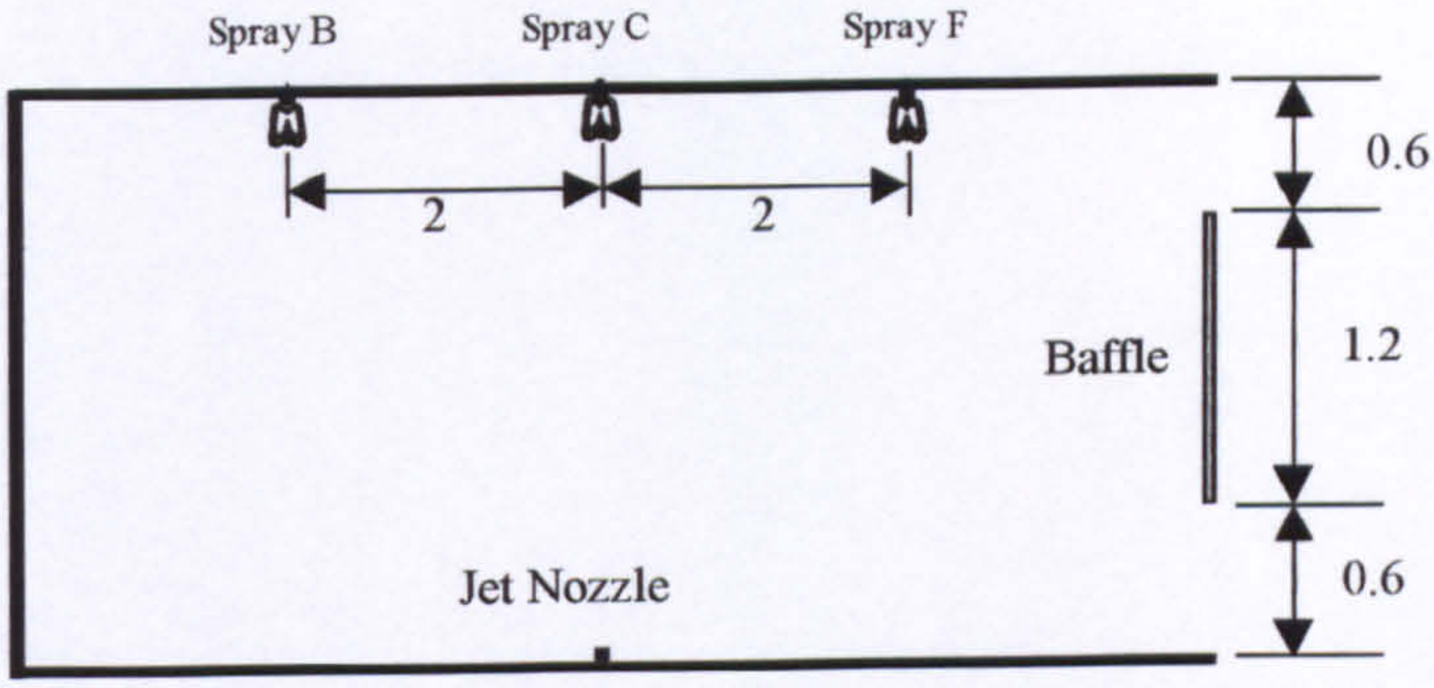

Figure (5.3). Compartment Schematic showing the spray locations (dimensions in meter).

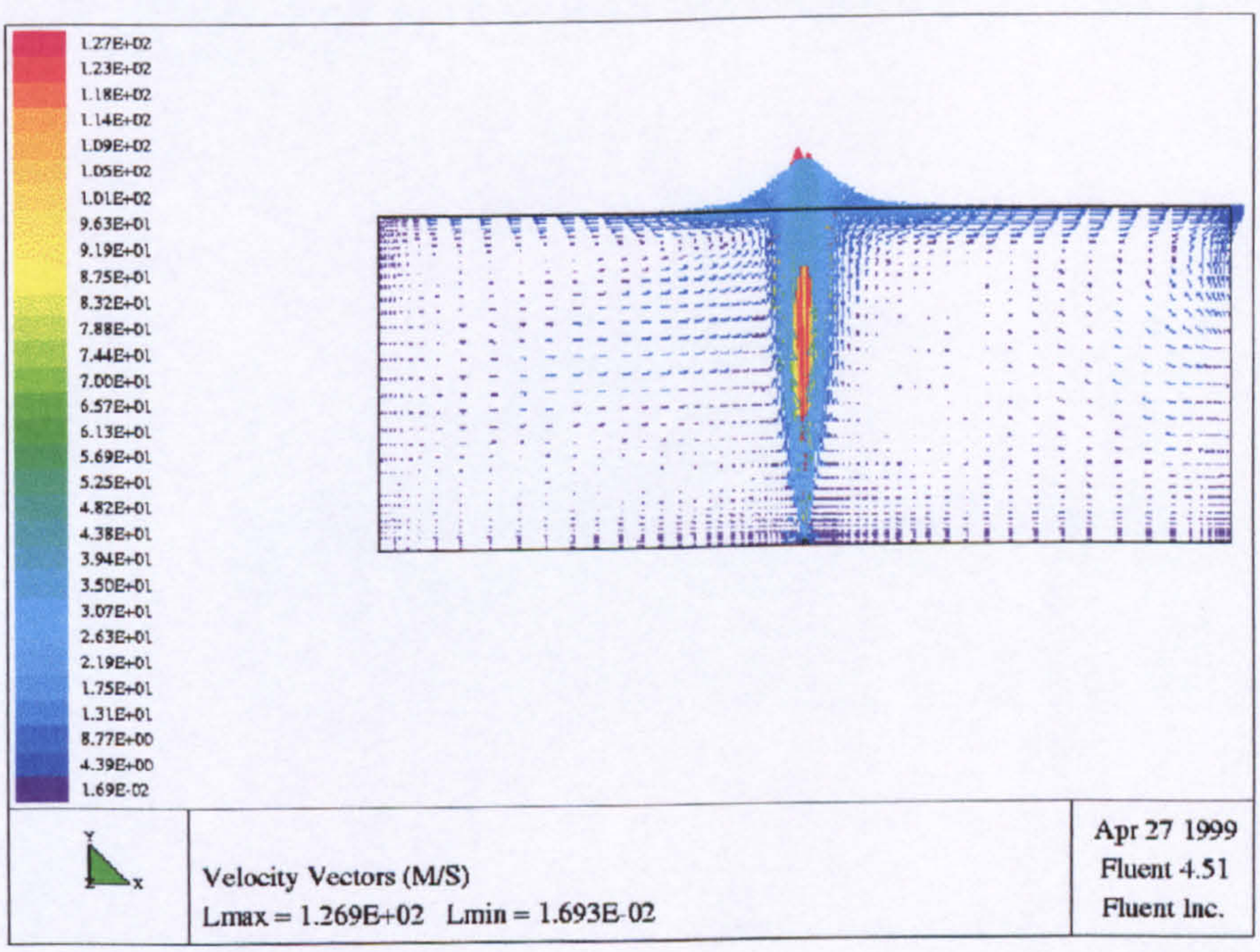

Figure (5.4). Predicted gas velocity vector through the longitudinal x-y plane at the centre of the jet fire section.

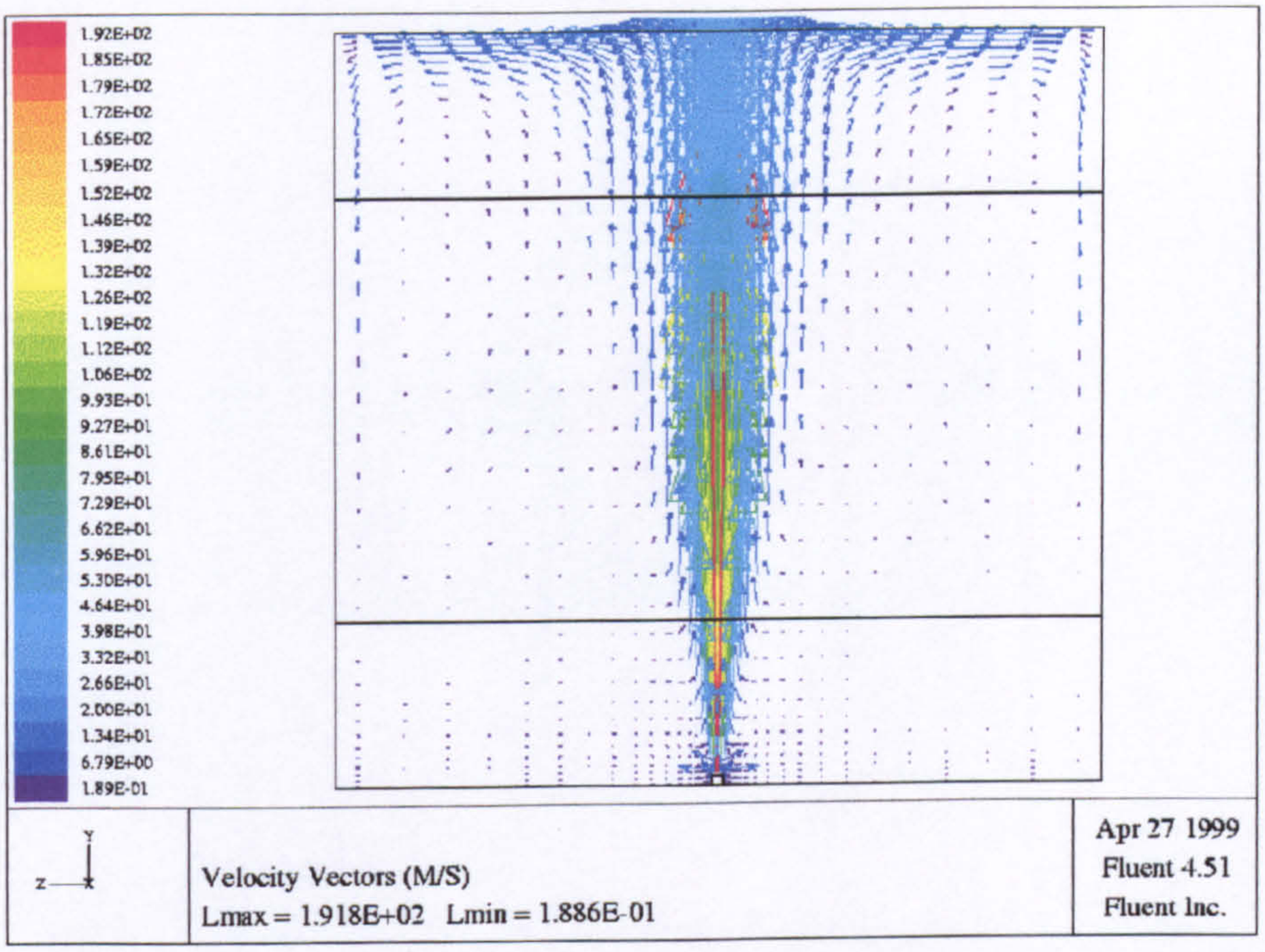

Figure (5.5). Predicted gas velocity vector through the lateral y-z plane at the centre of the jet fire section (I=40).

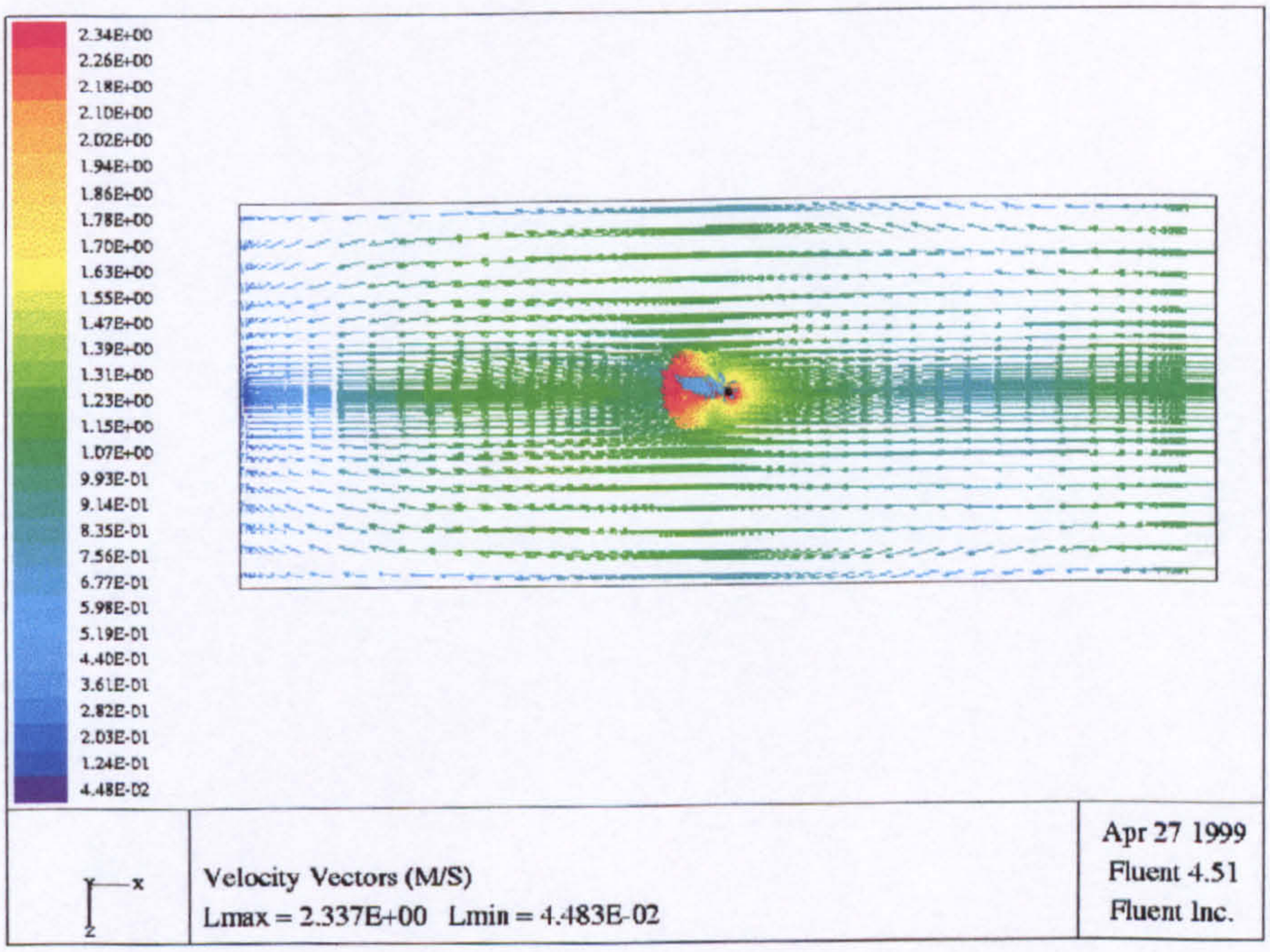

Figure (5.6). Plan view of the predicted gas velocity vector through x-z plane at 0.2 m above the floor.

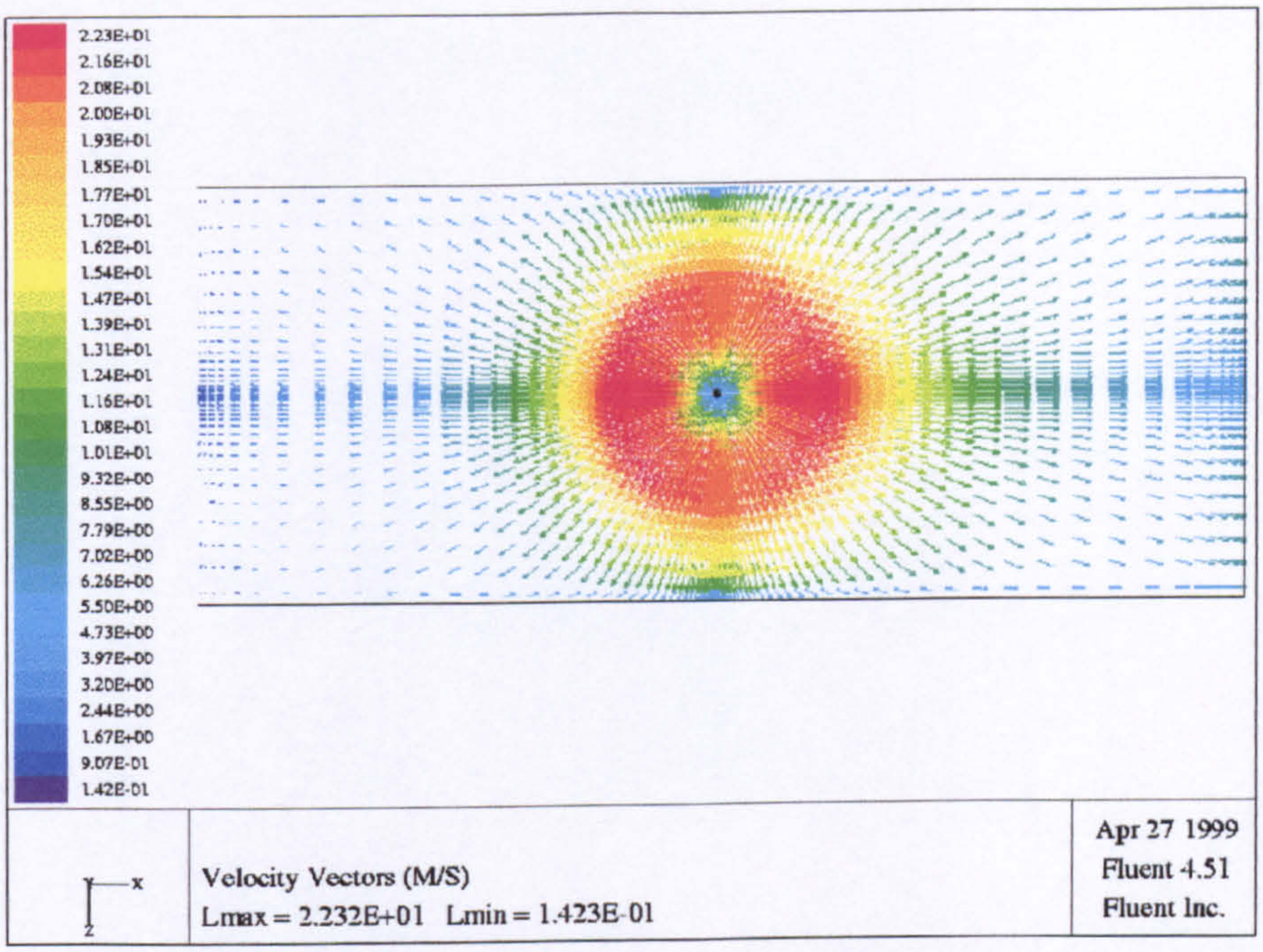

Figure (5.7). Plan view of the predicted gas velocity vector through x-z plane 0.1 metre below the roof.

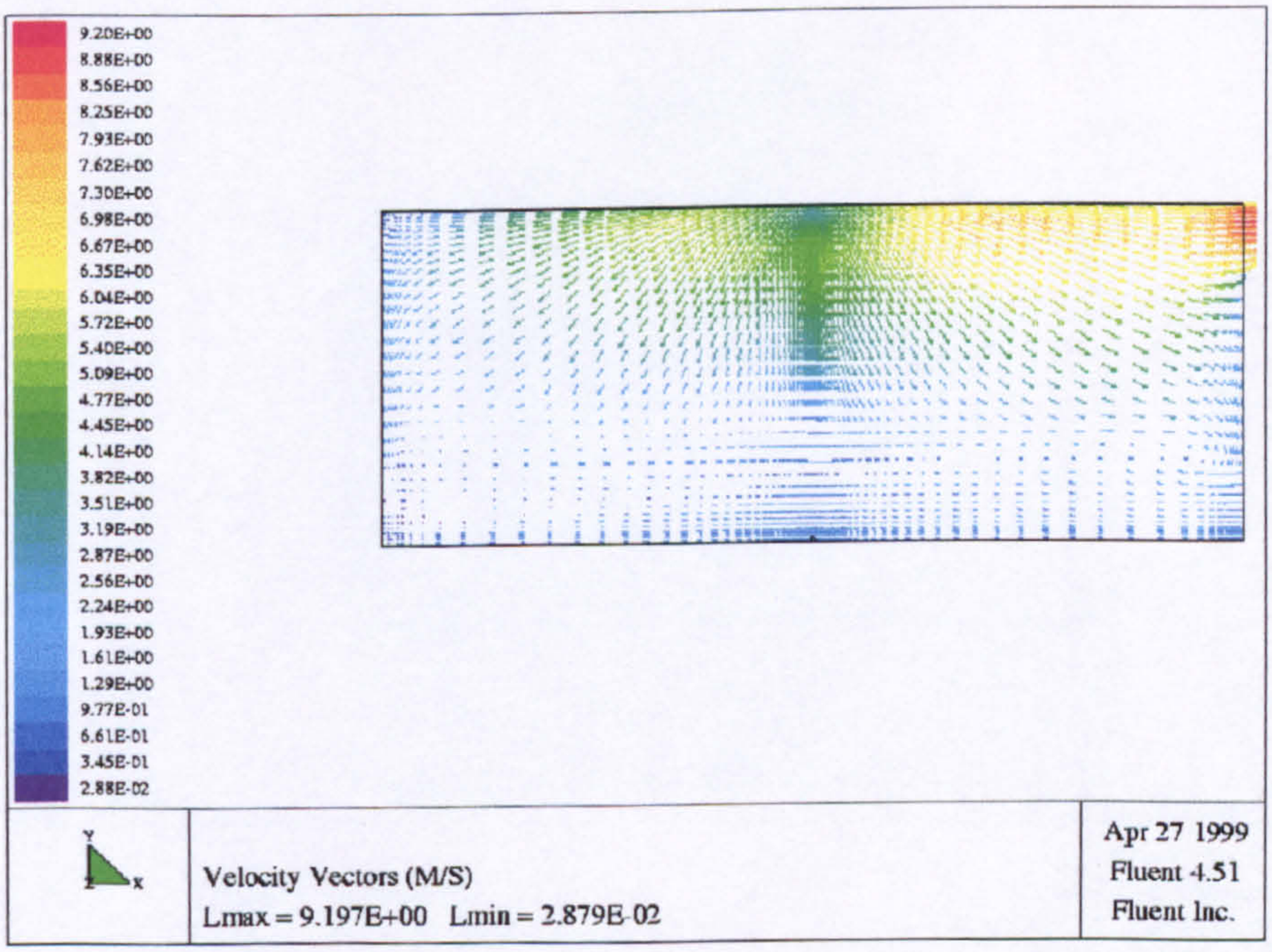

Figure (5.8). Predicted gas velocity vector through longitudinal x-y plane near the side wall.

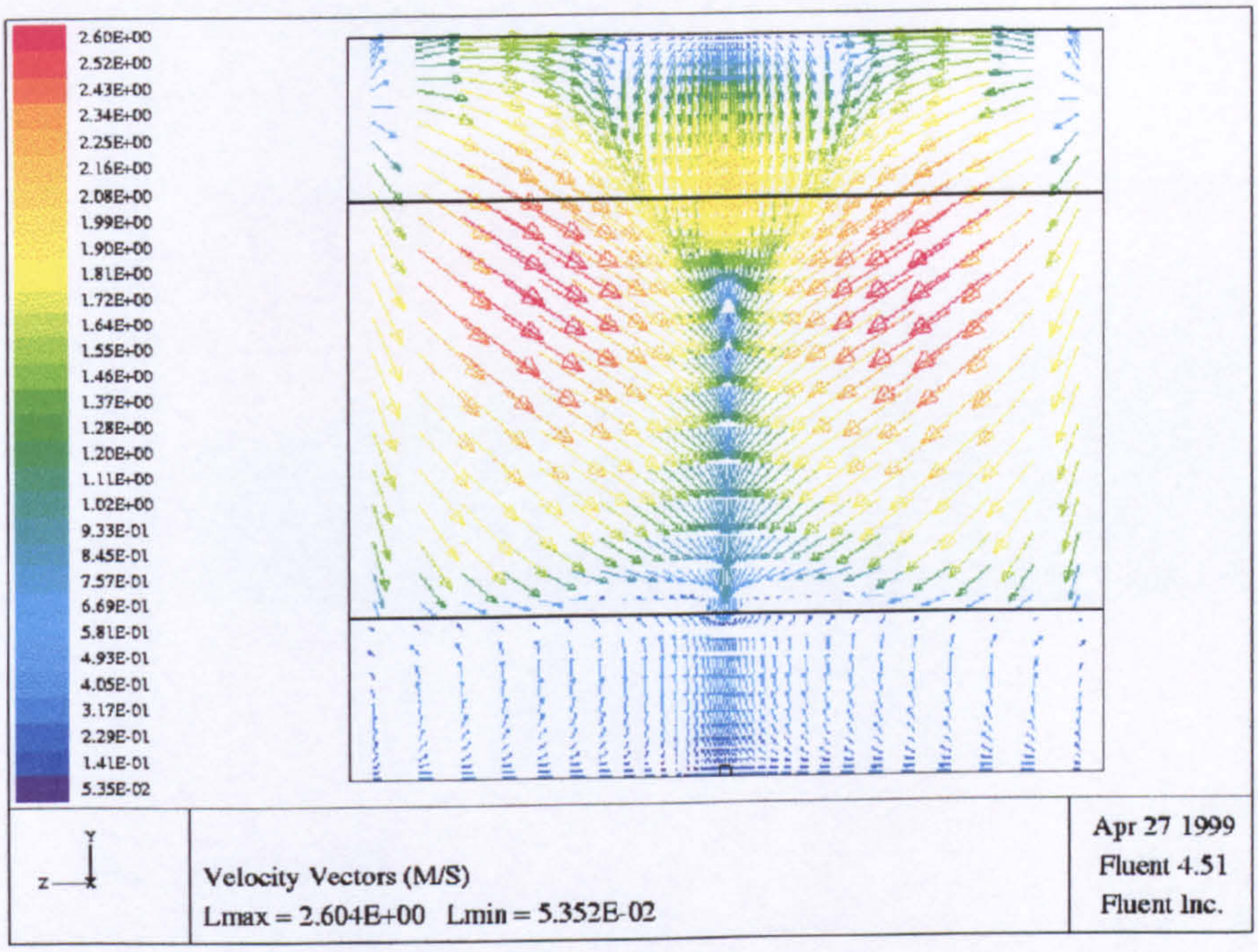

Figure (5.9). Predicted gas velocity vector through lateral y-z plane 3 cm from the back wall (I=2).

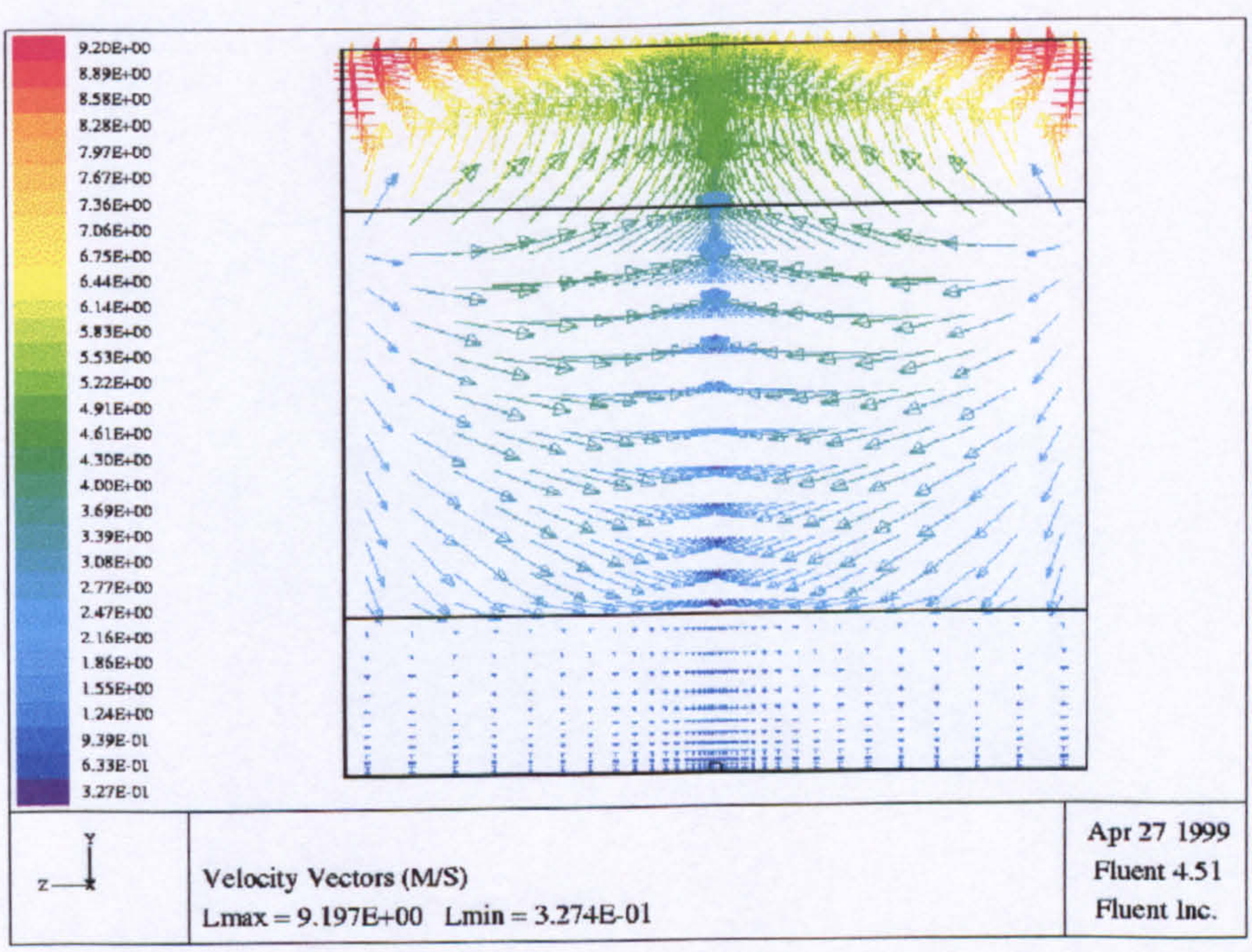

Figure (5.10). Predicted gas velocity vector through lateral y-z plane 1.3 cm from the baffle, showing the inlet and exit flow (I=80).

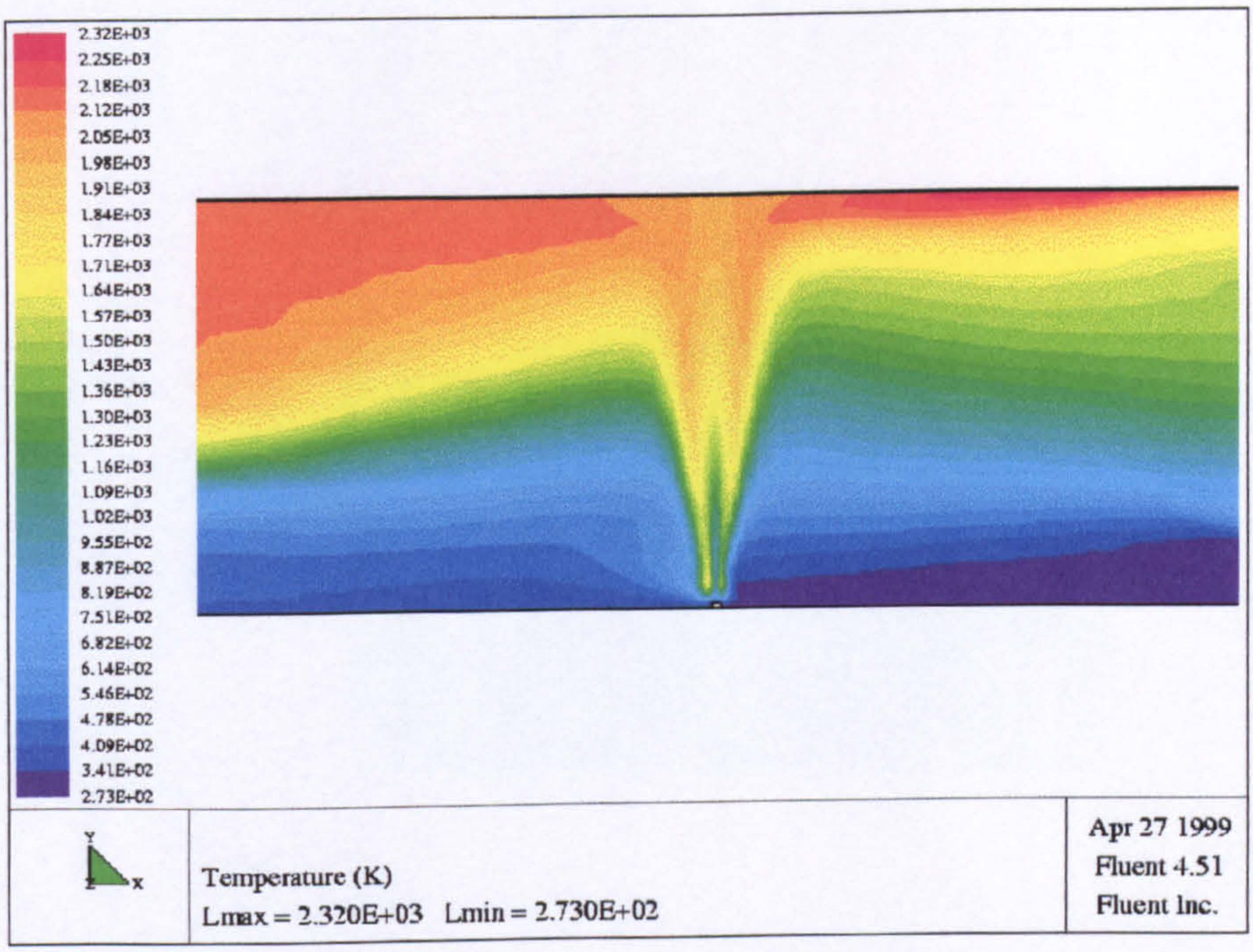

Figure (5.11). Predicted temperature contour through longitudinal x-y plane through the jet fire using adiabatic conditions.

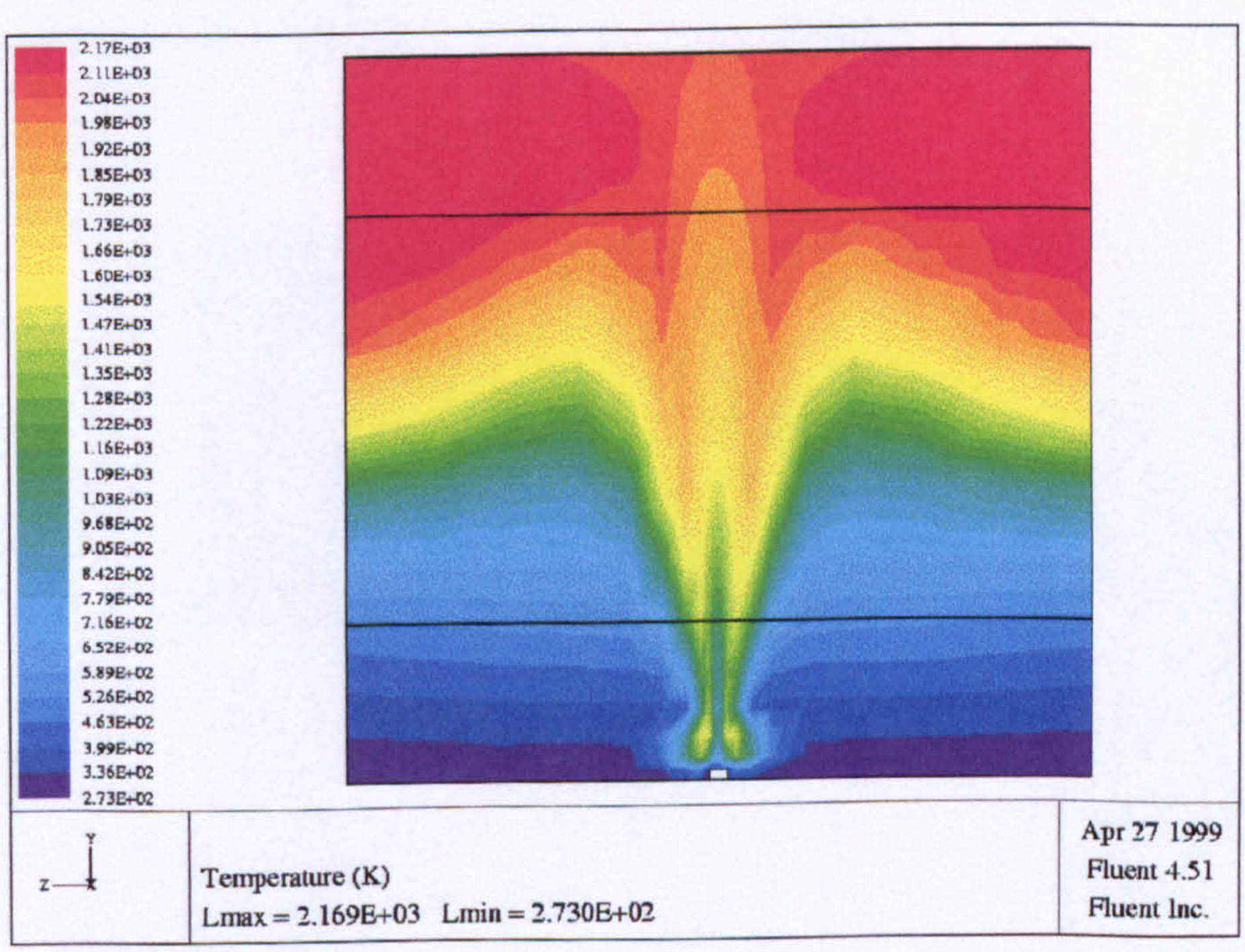

Figure (5.12). Predicted gas temperature contour through the lateral y-z plane through the jet fire nozzle using adiabatic conditions.

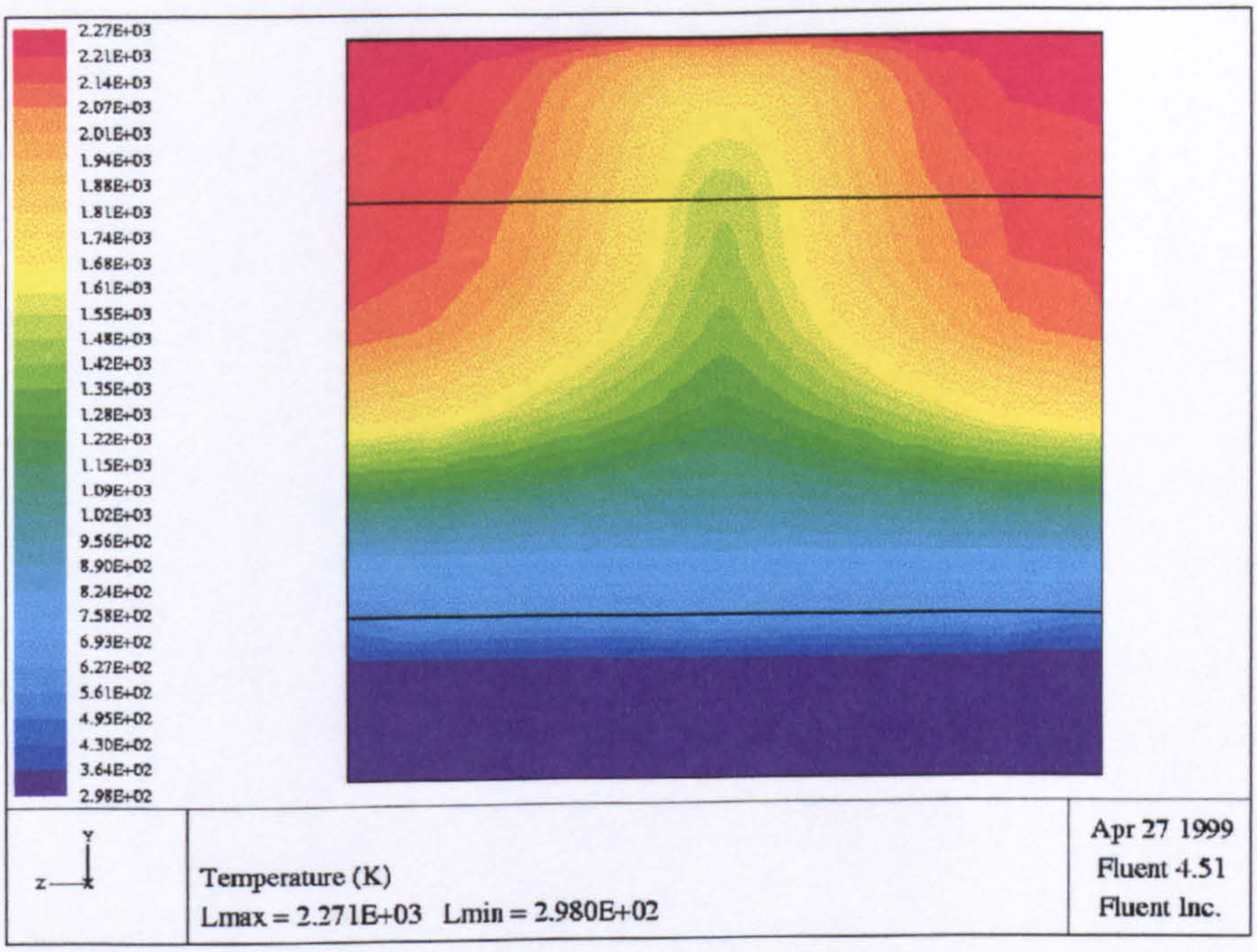

Figure (5.13). Predicted gas temperature at the lateral y-z plane 1.3 cm from the baffle, showing the temperature of the inlet and exit flows.

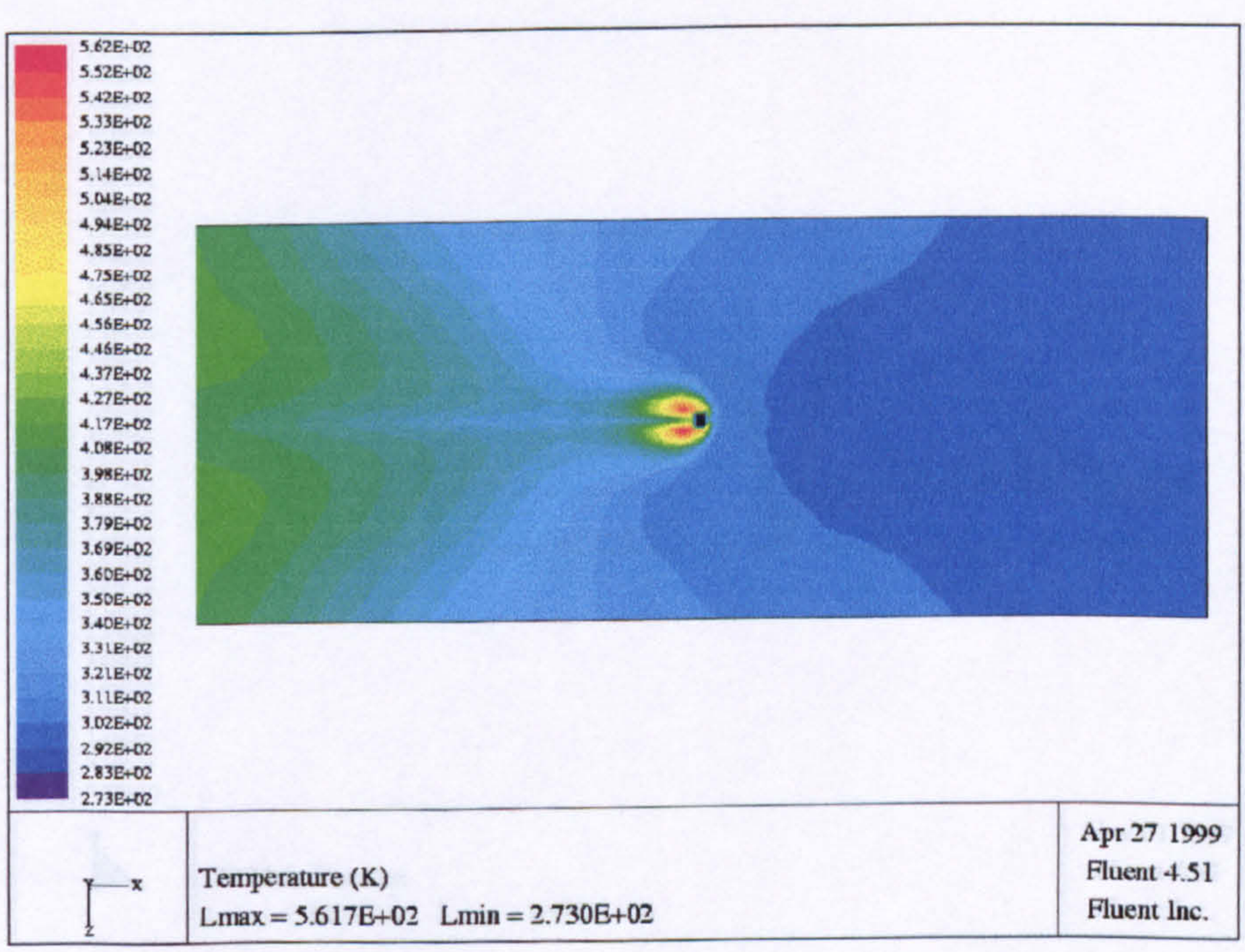

Figure (5.14). Plan view of the predicted gas temperature contours in the x-z plane 2 cm above the compartment floor.

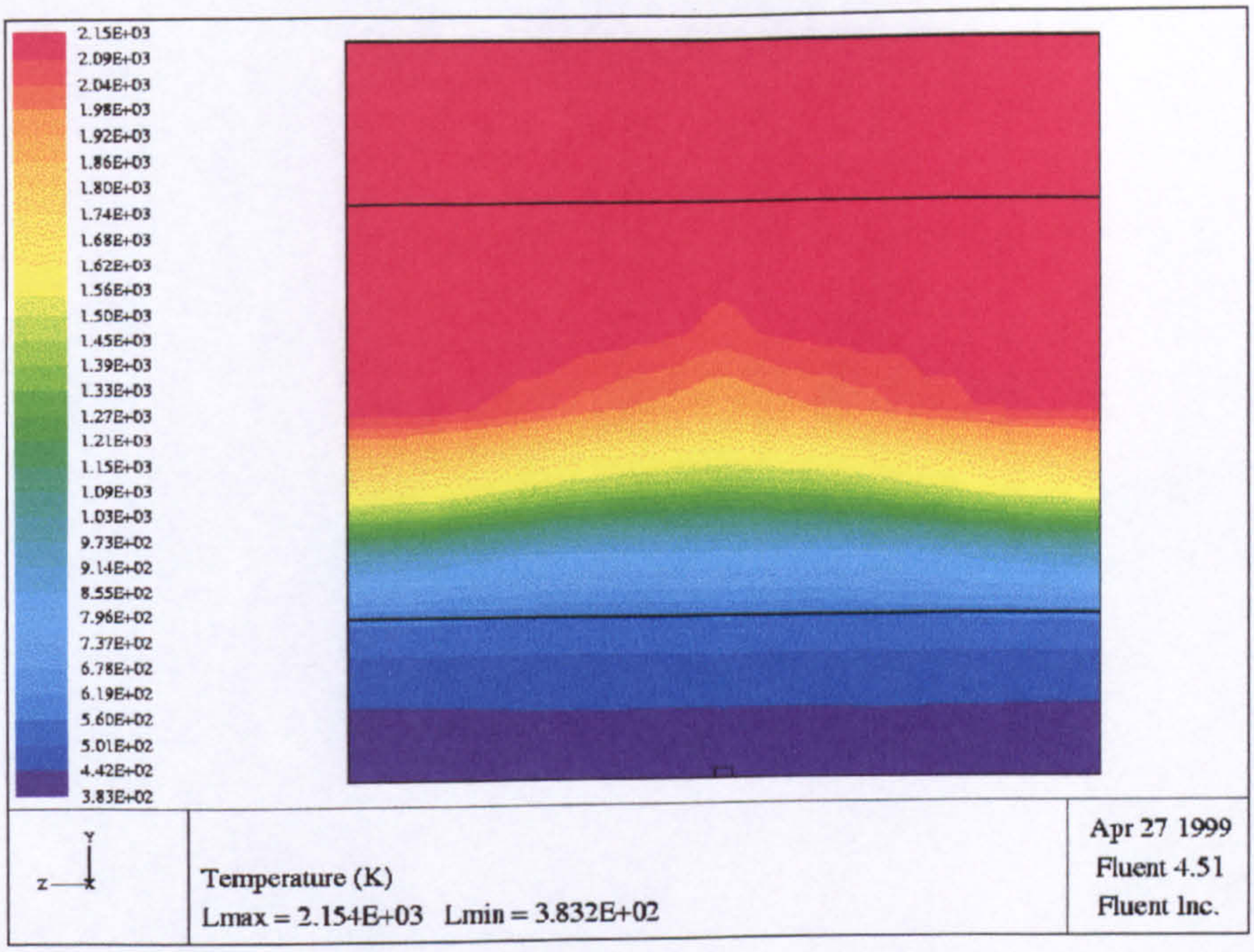

Figure (5.15). Predicted gas temperature contours in the lateral y-z plane 3 cm from the back wall of the compartment.

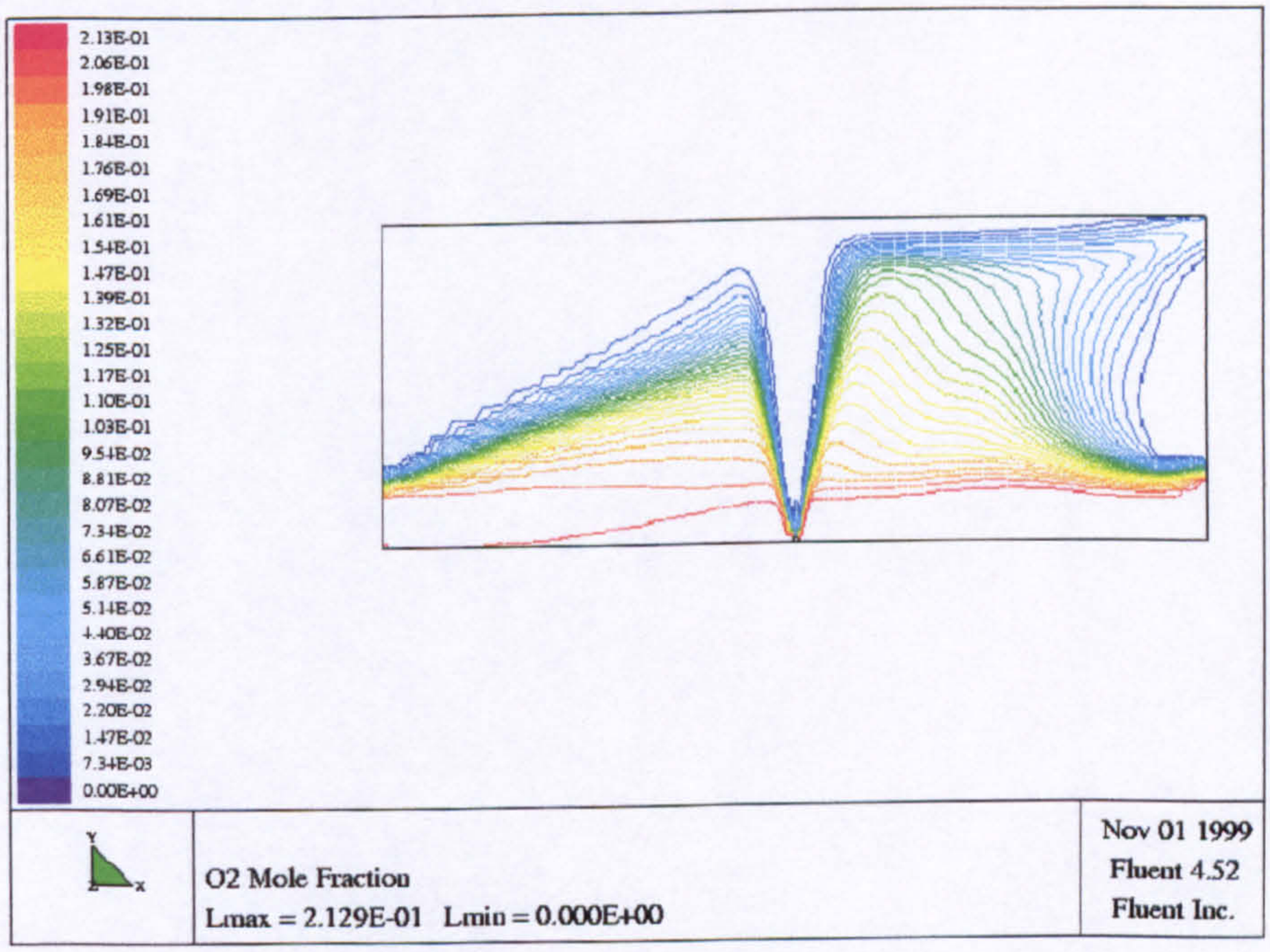

Figure (5.16). Predicted mole fraction contours of oxygen at longitudinal x-y plane through the jet fire centre.

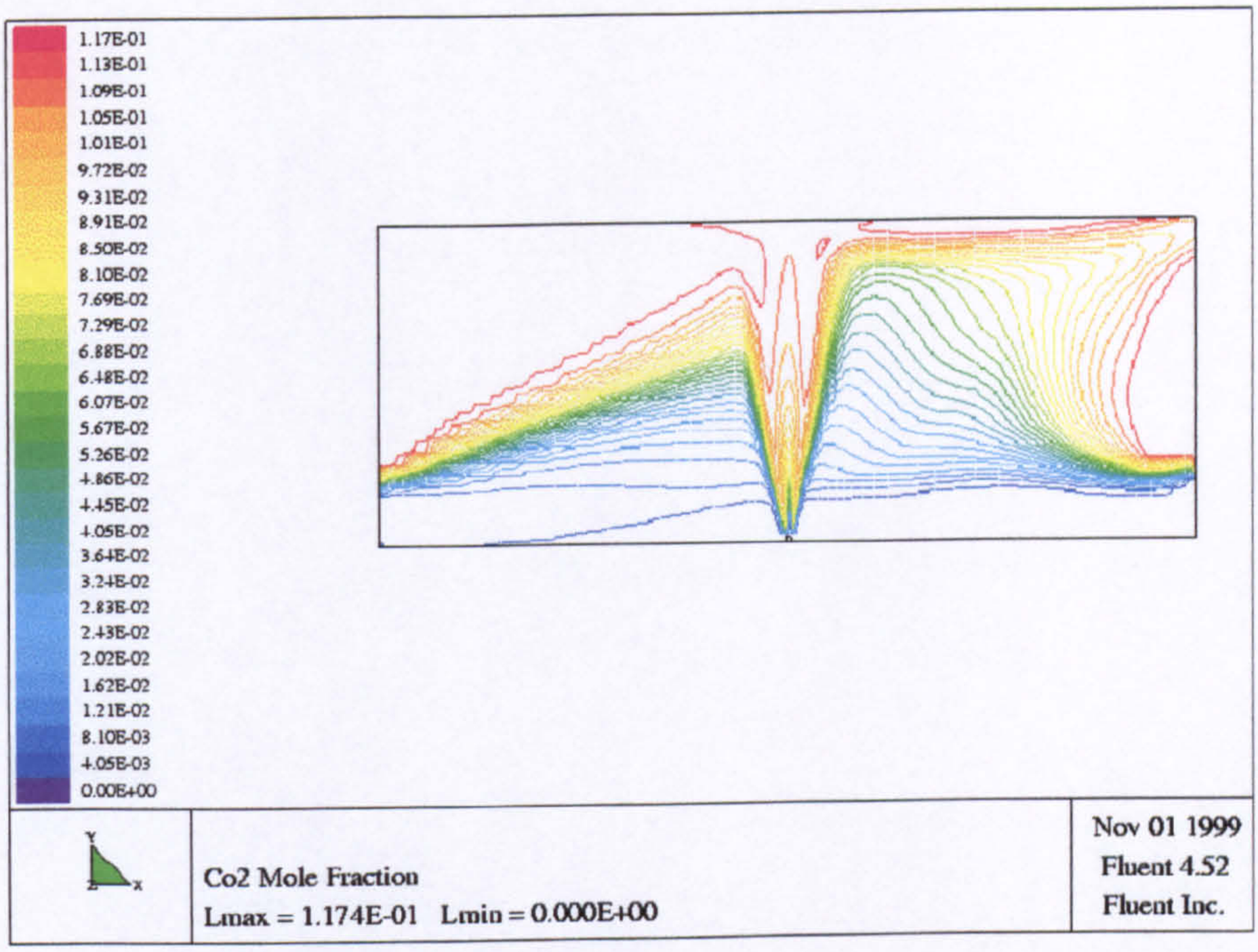

Figure (5.17). Predicted mole fraction contours of CO_2 at the longitudinal x-y plane through the jet fire centre.

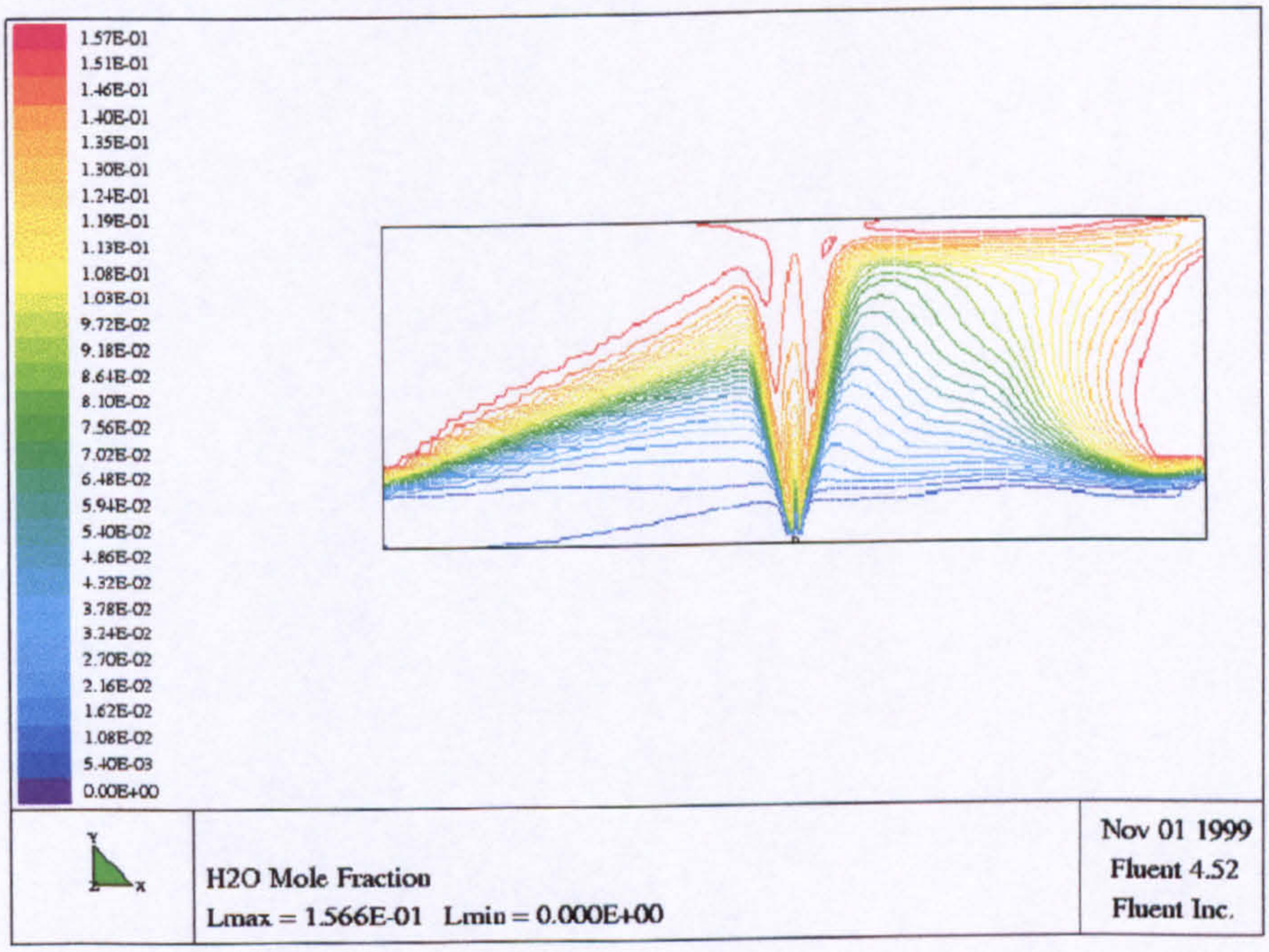

Figure (5.18). Predicted mole fraction contours of H_2O at the longitudinal x-y plane through the jet fire centre.

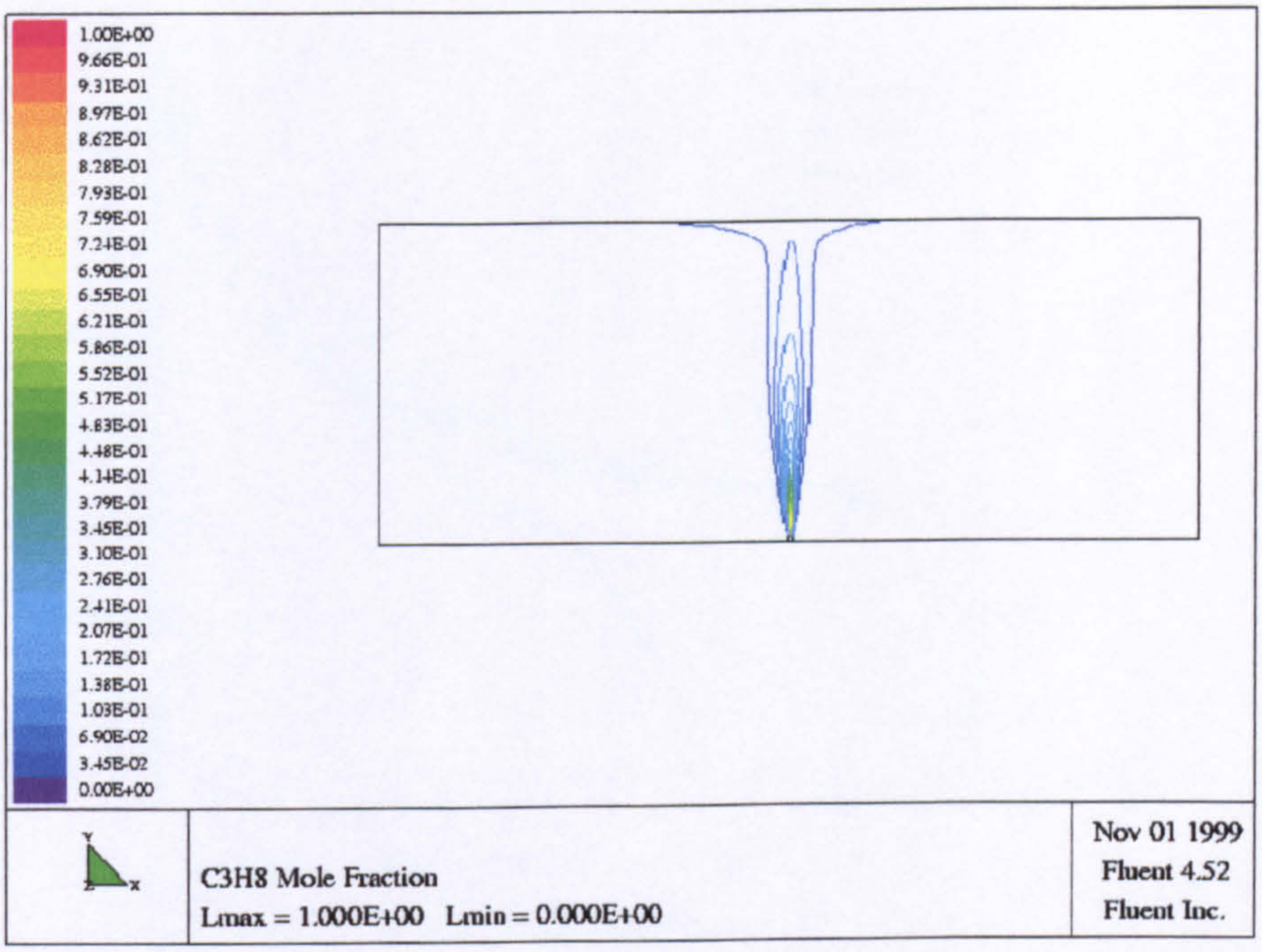

Figure (5.19). Predicted mole fraction contours of the fuel (C_3H_8) at the longitudinal x-y plane through the jet fire centre.

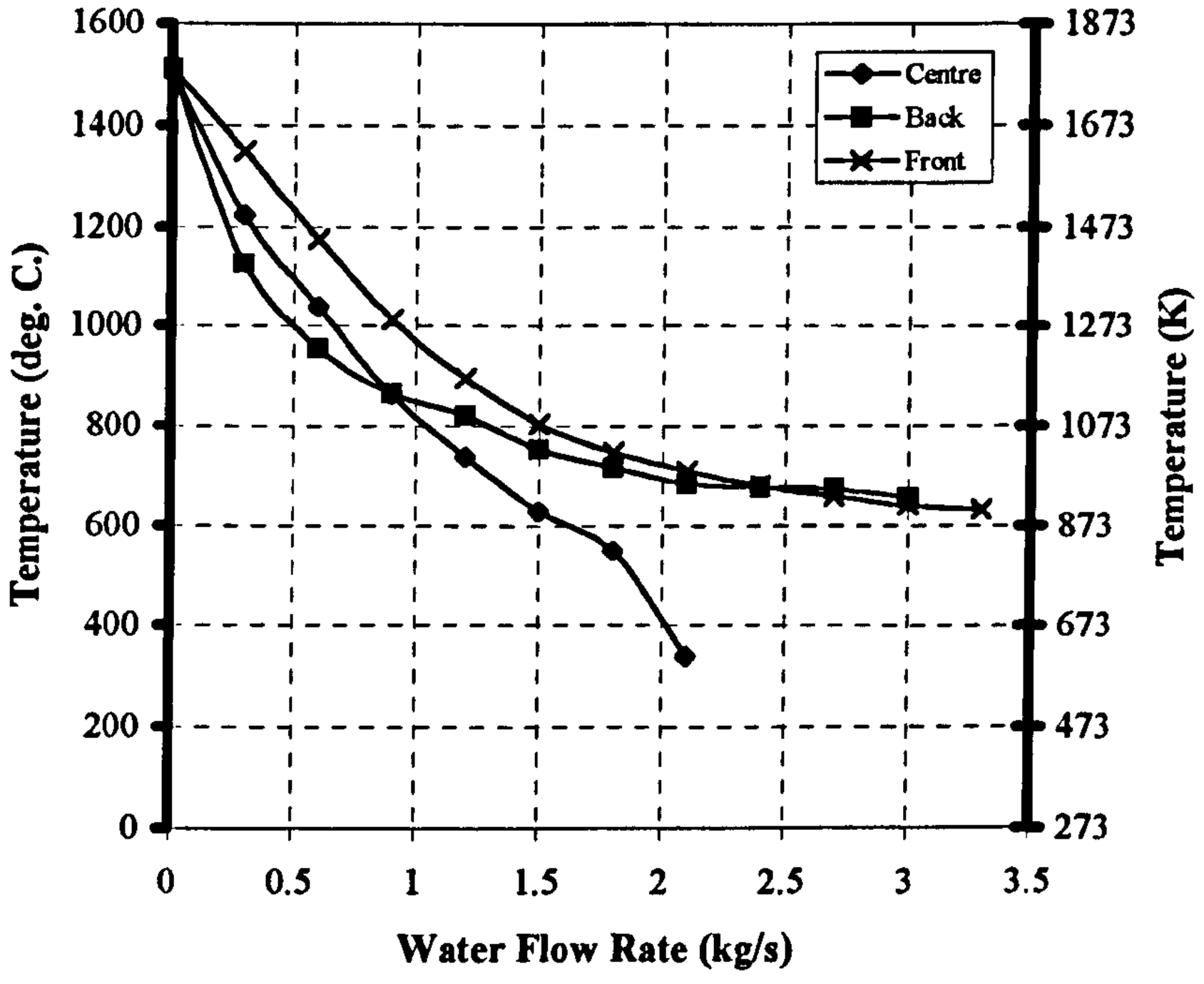

Figure (5.20). Comparison of different flow rates with different spray locations.

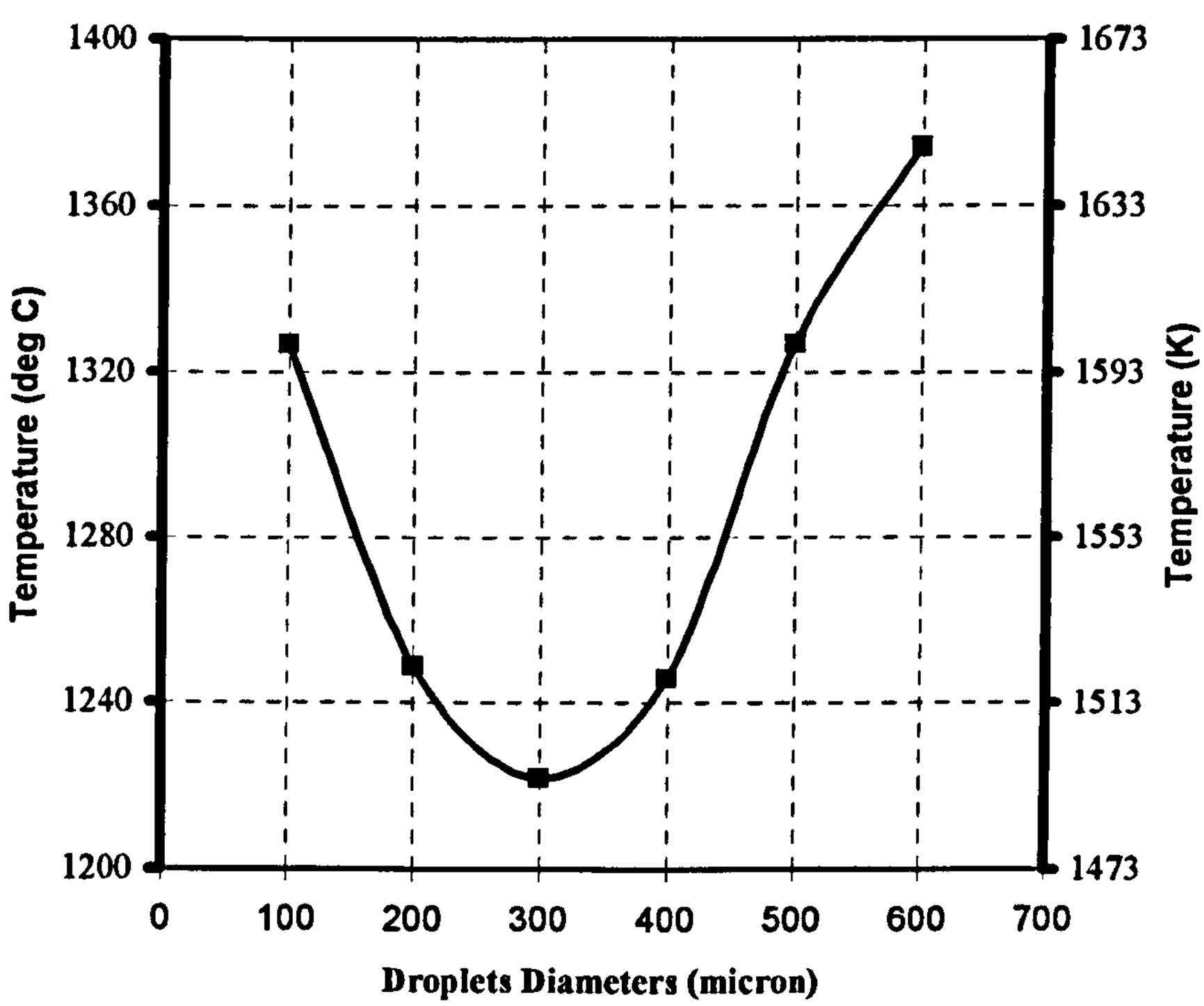

Figure (5.21). Comparison of different droplets diameters.

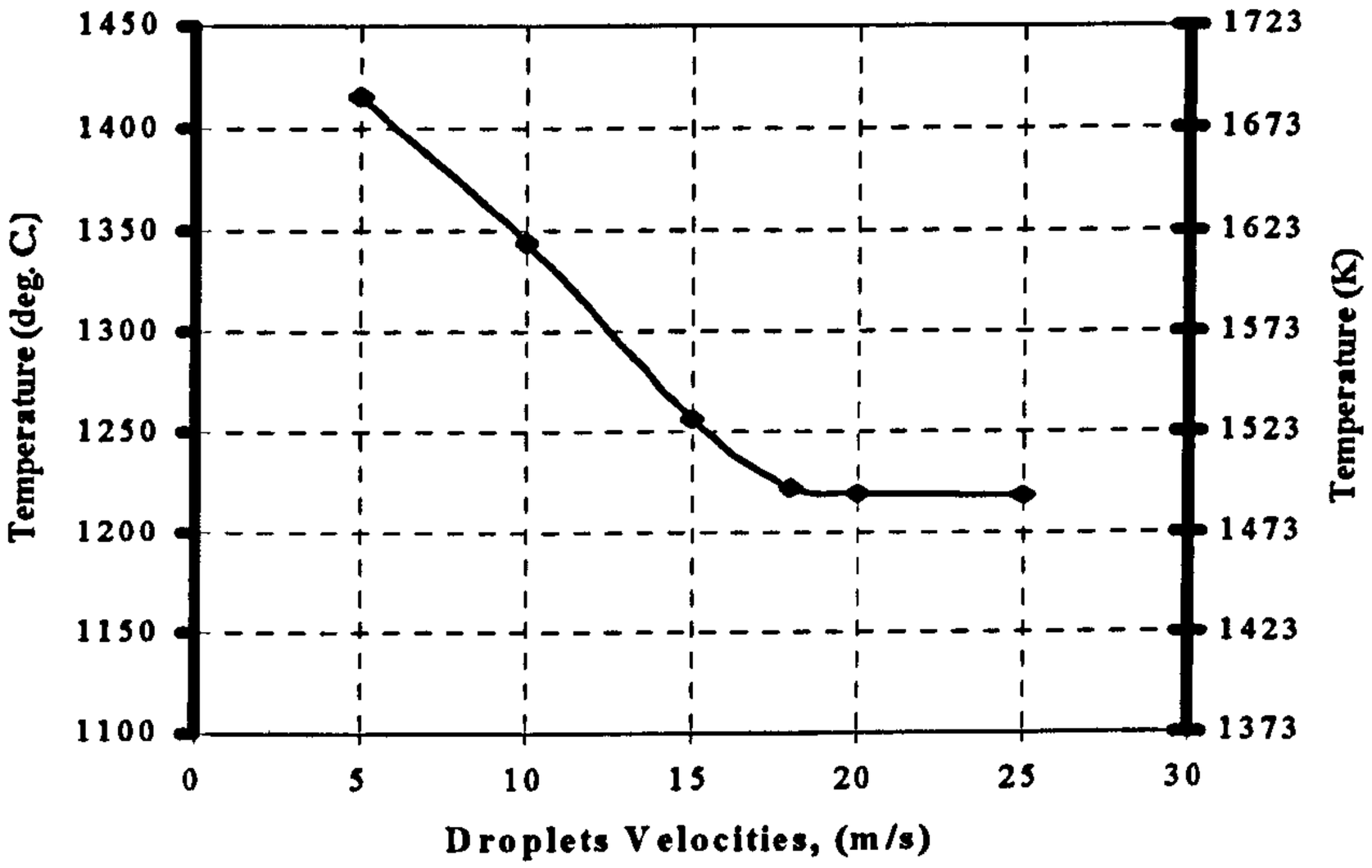

Figure (5.22). Comparison of different spray angles at 54 lit/min water flow rate.

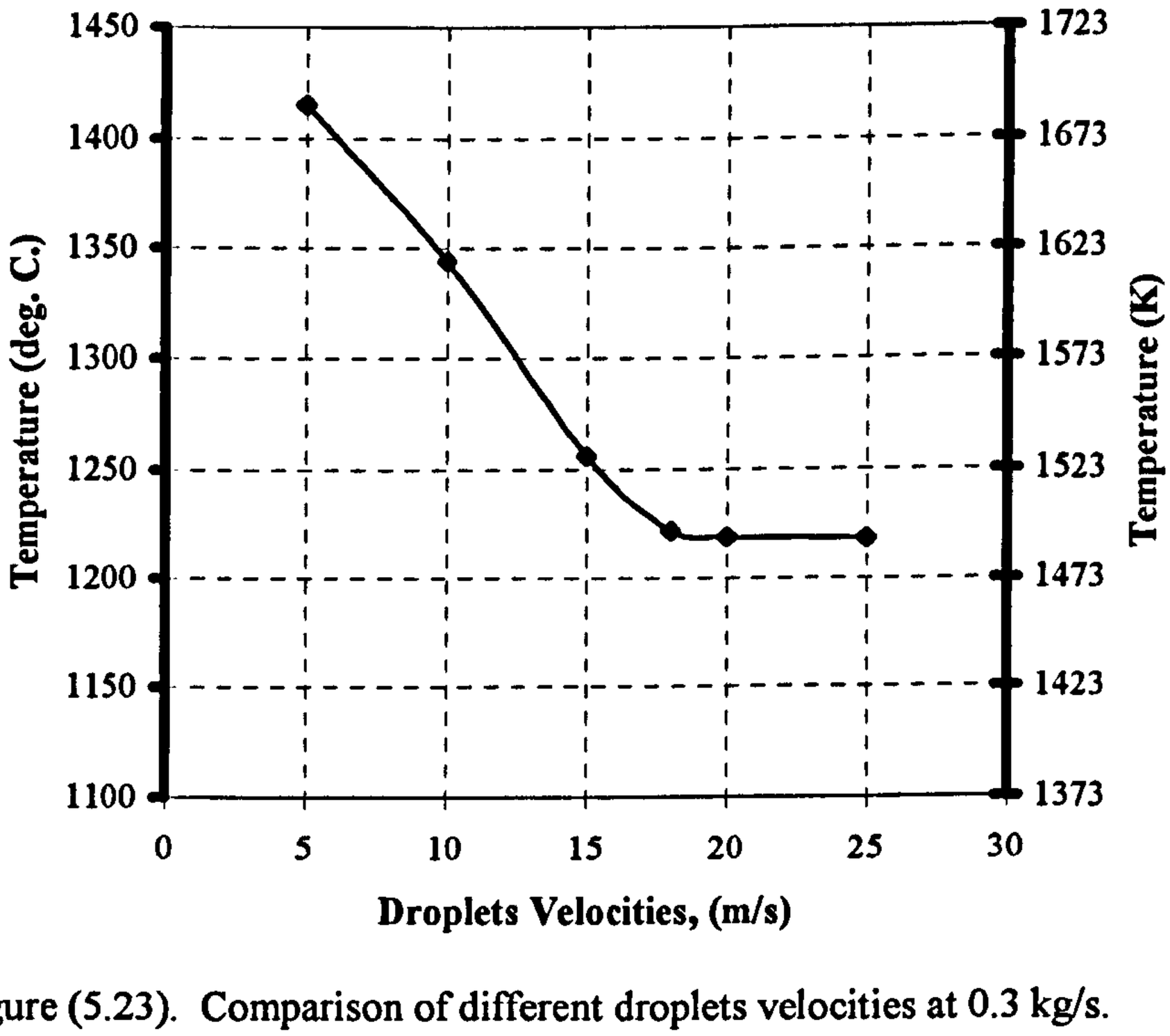

Figure (5.23). Comparison of different droplets velocities at 0.3 kg/s.

CHAPTER 6

DROPLETS SIZE MEASUREMENTS

6.1 INTRODUCTION

For the successful modelling of the extinguishment of the compartment jet fire by water sprays and for the study of the interaction between sprays and jet fires, it is necessary to define the initial conditions with as great accuracy as possible. The successful modelling of spray is reliant on accurate experimental data of the droplet diameters of the different spray nozzles used. So one of the intended uses of this information is for inclusion within FLUENT.

The most surprising observation was how little manufacturers have focused on the properties of the water spray; there is for instance hardly any information available on the drop size distribution that affects the vaporisation rate.

Different designs on spray nozzles will produce sprays with different proportions of larger and finer drops (Mawhinney, 1993).

The Malvern Particle Sizer was used to measure the drop size of water spray from four different spray nozzles which have been intensively investigated for different water flow rates.

6.2 MALVERN PARTICLE SIZER

Effort has been devoted to measuring the drop size distribution of spray discharge under a non-fire condition. The Malvern Particle Sizer is currently one of the most effective, simple, and reliable methods that is commercially available. It is easy to use. This instrument uses the principle of diffraction from the particles for the analysis of the particle size distribution. A low power visible laser transmitter produces a parallel monochromatic beam of light which illuminates the particles by use of an appropriate sample cell or other measurement technique. The incident light is diffracted by the particle movement. As the particles enter and leave the illuminated area the diffraction pattern "evolves", always reflecting the instantaneous size distribution in this areas. Thus, by integration over a suitable period and using a continuous flux of particles through the illuminated area a representative bulk sample of particles contributes to the final measured diffraction pattern. Figure (6.1) shows the optical arrangements employed in Malvern particle sizer.

A Fourier transform lens focuses the diffraction pattern onto a multi-element photo-electric detector which produces an analogue signal proportional to the incident light intensity. This detector is directly interfaced to a computer, which reads the diffraction pattern and performs the necessary integration digitally.

Having measured a diffraction pattern the computer used a non-linear least-square analysis to find the size distribution which gives the most closely fitting diffraction pattern.

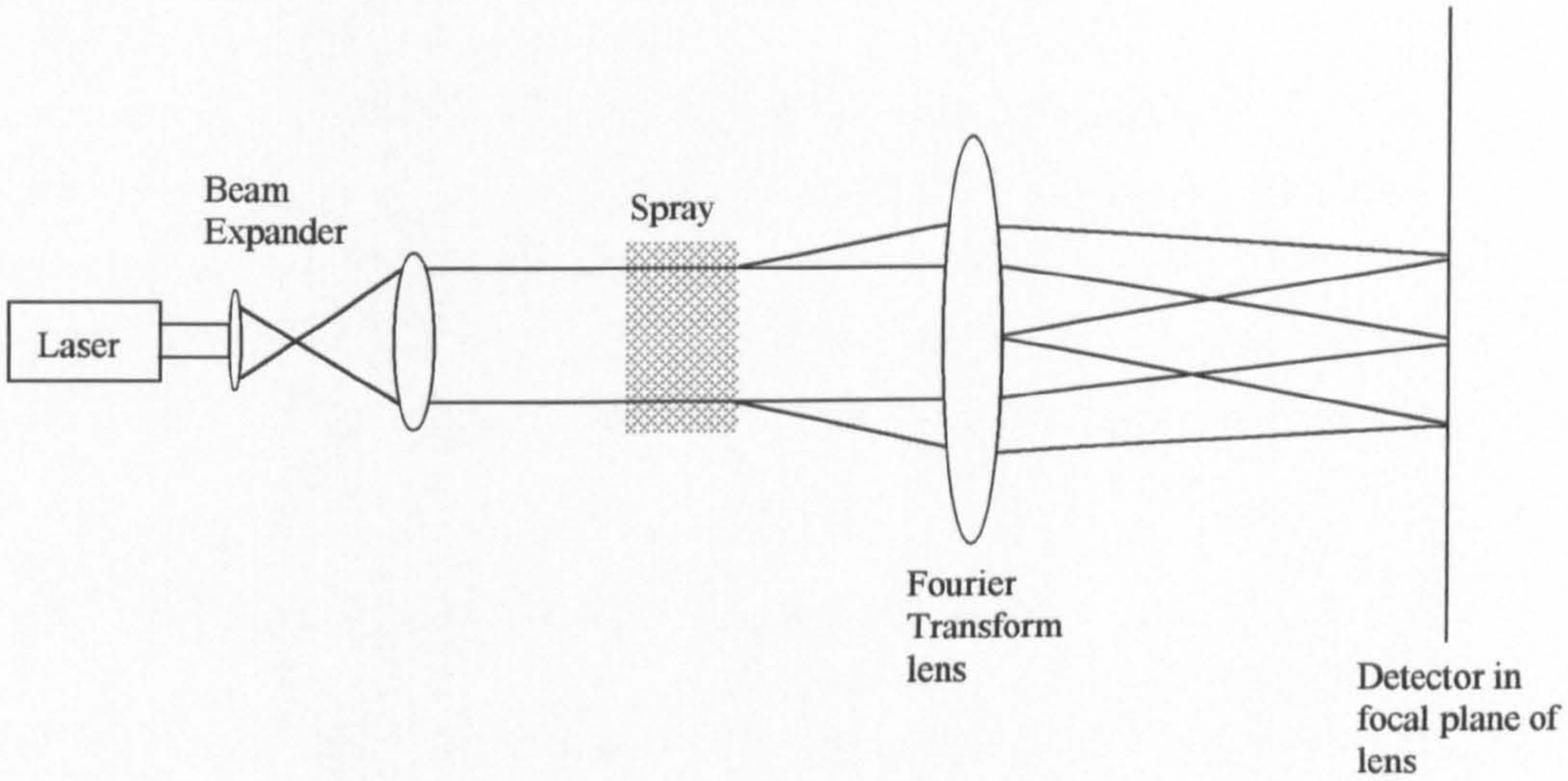

Figure (6.1) Optical arrangement employed in Malvern Particle sizer.

6.3 Limitation of Malvern instrument

As is the case in all drop size measuring instruments, Malvern Particle Sizer has certain limitations. Among them are (Lefebvre, 1989 and Bayvel and Orzechowski, 1993):

Multiple Scattering: light that is scattered by a drop may be scattered by a second drop before reaching the detector when the spray densities are high. This multiple scattering introduces error in the computed size distribution.

Vignetting: it is important to limit the maximum distance between the spray and the receiving optics. This maximum distance depends on the focal length and diameter of the receiver lens. When this distance is exceeded, this will result in vignetting of

the signal on the outer detector rings, which causes skewing of the measured size distribution toward the larger diameters.

Beam steering: thermal gradients in the hot air refract the laser beam in a random high frequency pattern, resulting in a spurious reading on the innermost detectors.

It is not possible to use the technique when the transmittance is low (Chigier, 1983). Among other problems that have arisen with the Malvern Particle Sizer are ambient light level restrictions and coarse resolution due to the line of sight of measurement.

6.4 EXPERIMENTAL SETUP

The aim was to obtain droplet size data for the spray configuration used in jet fire tests. Since the measurement was required within the spray injection region, it was necessary to find some means of positioning the Malvern sizer relative to the nozzle.

For the purpose of comparing the dorps sizes produced by different nozzles, it is stated in the NRC (National Research Council of Canada) Design Guide that a drop size is best measured at a distance of 1 meter from the nozzle, along the central axis of the spray cone (Mawhinney, 1993).

Due to the considerable weight of the analyser, and to get a good level, it was decided to build a solid platform on which to rest it, and to construct adjustable mechanism with which to move the spray nozzle to direct it to the suitable position for measurement depending on the spray angle to be used.

The spray nozzle was connected directly to the same fire water source used for the compartment jet fire tests. The nozzle was fixed with pressure gauge and water flow metre to accurately record the flow rate readings. A manual valve had been fixed on the pipe as well to control the amount of the water to be discharged.

The orientation of the analyser meant that stringent re-aligning of the laser beam had to be taken before measurement could proceed.

A supporting platform was used which consisted of two steel channels which were used to position and clamp the lens on it.

Since the spray nozzle would discharge an excessive amount of water in the measurement region, which might cause some damage to the laser or the receiving unit, Polythene sheets were used to protect the Malvern units from the water sprayed by covering and isolating the spraying region from the rest of the setup, except for the analyser beam path.

To take a set of measurements, the beam alignment was checked, a background measurement was taken without the spray and then the actual measurement was taken with the spray in operation. The analyser's software proceeded to calculate the droplet size distribution, taking account of the background reading, and copies of the result files were obtained for further analysis.

6.5 USE AND PRESENTATION OF SPRAY DATA

The frequency data collected by instrument is converted by software to include occurrence percentage, surface area percentage, volume and cumulative volume percentage, which can be tabulated and plotted. A number of representative mean diameters for the spray can be tabulated as well. For this study of sprays for fire suppression purposes, the volumetric mean diameter (VMD or $D_{v0.5}$) and Sauter Mean Diameter (SMD or D_{32}) were selected as the most meaningful representative mean diameters. $D_{v0.5}$ is defined as the diameter of a drop such that 50% of total liquid volume is in drops of smaller diameter. On the other hand D_{32} is defined as the diameter of the drop whose ratio of volume to surface area is the same as that of the entire spray (Lefebvre, 1989). These data were analysed by using model independent program. This program does not assume a particular drop size distribution function. Instead it has 15 adjustable parameters corresponding to the 15 size bands of the

volume distribution. These parameters are varied systematically until the best fit to the experimental data is obtained.

A useful picture of drop diameters can be obtained by plotting histograms of drop data. Additional information can be found from further plots of different spray angles and different flow rates to help formulate correlation. The plot of cumulative volume percentage curve versus drop diameter was selected as more informative than single representative diameter for comparing the characteristics of sprays.

Droplet data can be used either in their raw form, i.e. drops of various description were recorded. Alternatively the drops of various descriptions can take their diameters from distribution curves. As Lefebvre (1989) explains a number of functions which have been proposed are based on either probability or purely empirical considerations. This includes the empirical relationship most widely used in the Rosin-Rammler distribution.

In the CFD modelling part of this study, the mean droplet diameters to be used in FLUENT is taken from Rosin-Rammler distribution as well as the spread parameters. The Rosin-Rammler distribution was seen to provide an adequate fit when experimental data was compared with a number of other distribution functions such as normal, log-normal, Nukiyama-Tanasawa and upper limit distributions. It also has the virtue of simplicity (Lefebvre, 1989).

6.6 EXPERIMENTAL MEASUREMENTS

The first set of experimental measurements were conducted on a 9.3 mm ANGUS spray nozzles (K50 150D), spray angle of 150 degrees was used and seven different water flow rates were used as well.

The second set of experimental measurements were conducted with the same type of spray but different spray angle (K50 120D) which was 120 degrees and four different water flow rates.

Experiments in group three collected data at the same water flow rates as experiments in group two but the spray angle used was 90 degrees with the same type of spray (K50 90D).

Experiments in group four measure the droplets size of the same type of spray and same water flow rates, again the spray angle used was changed to 60 degrees (K50 60D).

Full details of the experimental measurement programms are given in table (6.1). The measurement experiments completed the study of the spray used in the fire experiments and the modelling.

The data collected from the above experiments were intensively analysed and used to calculate some of the statistical mean values. These values are used to compare different extinguishing strategies and to find the optimum droplets diameter for jet fire extinguishment based on the water flow rates and spray angle used.

Water Flow Rate (lit/min)	Spray Angle			
	60	90	120	150
90	✓	✓	✓	✓
72	✓	✓	✓	✓
54	✓	✓	✓	✓
45				✓
36	✓	✓	✓	✓
30				✓
24				✓

Table (6.1). Droplet Measurement Tests Programme.

6.7 MEASUREMENT RESULTS AND DISCUSSION

To characterise fully, a spray nozzle that is to be used for fire extinguishment purposes requires measurement of all the characteristics of the drops in the spray.

The experiments produced a complete picture of drops from the spray nozzles. Table (6.2) shows the calculated values of Sauter Mean Diameter (SMD) and Volume Mean Diameter (VMD) for each of the sampling tests. Considering the spray vertical angles 150°, 120°, 90° and 60°, the Sauter Mean Diameters are closely grouped, their overall mean values are minimum in 150° spray angle nozzle which is 172 μm. Likewise the Volume Mean Diameter has the same trend as SMD with 258 μm.

The results of the measurements are summarised in figures (6.2 to 6.12) which show the droplets distributions of the drop diameters as a series of histograms. Each histogram shows the spectrum of observed droplet sizes at each of the test investigated according to table (6.1). The Malvern analyser gives the percentage of the spray's volume (i.e. mass) observed in each of 32 size band. These bands are not uniform but their widths increase logarithmically with increasing diameter. The mean of each band is calculated and used to represent that band on histograms and curves.

Investigating the effect of increasing water flow rates, the recorded diameter range becomes smaller at increased water flow rates. The mean diameter supports this with decreasing values at increasing water flow rates (see Figures 6.2 to 6.12).

The droplets diameters increased with the decreasing of the spray angles for similar water flow rates.

Cumulative frequency plots of each spray type, for all the pressure used in the measurements, have been plotted in Figures (6.13) to (6.17) which compare the distributions of the drop sizes for different water flow rates in which each curve in the

graph represented a different water flow rate plotted against cumulative percentage volume.

The Sauter mean diameter of the spray is presented as a function of the water flow rates in Figure (6.18) and the spray angle one of the parameters which can determine spatial distribution of water droplets. In Figure (6.19) shows the spray angle as a function of the Sauter mean diameter of the spray.

Table (6.3) shows the Rosin-Rammler distribution data such as the mean droplet diameter (x) and the spread parameter (n).

Some sprays are finer than others, and this generally corresponds to higher flow rate, which are caused by higher pressure and the spray angle.

6.8 CONCLUSIONS:

1. The higher the water flow rate of the spray nozzle at any angle, the lower the droplet diameter size.
2. From the measurements, it is clear that nozzle K50150D that has spray angle 150° gives the finest spray, especially when the flow rate is high such as 90 lit/min.
3. The K50150D nozzle has reasonably fine initial drop size distribution, wide spray angle and good projection, especially when the water flow rates higher than 72 lit/min.

Test No.	Spray angle (deg.)	Water Flow rate(lit/min)	Sauter Mean Diameter (μm), D_{32}	Volumetric Mean Diameter (μm), $D_{v0.5}$
MALV-1	150	90	172	258
MALV-2	150	72	190	294
MALV-3	150	54	307	389
MALV-4	150	45	357	450
MALV-5	150	36	405	644
MALV-6	150	30	638	704
MALV-7	150	24	716	910
MALV-8	120	90	190	263
MALV-9	120	72	193	273
MALV-10	120	54	378	487
MALV-11	120	36	474	590
MALV-12	90	90	264	352
MALV-13	90	72	317	407
MALV-14	90	54	371	476
MALV-15	90	36	550	723
MALV-16	60	90	230	298
MALV-17	60	72	267	347
MALV-18	60	54	519	676
MALV-19	60	36	769	947

Table (6.2). Mean values of drop diameter at each test, output data from Malvern Particle Sizer.

Test No.	Spray angle (deg.)	Water Flow rate(lit/min)	Mean Diameter, X (μm)	Spread Parameter, (N)
MALV-1	150	90	295	2.09
MALV-2	150	72	342	2.15
MALV-3	150	54	417	2.6
MALV-4	150	45	489	2.73
MALV-5	150	36	755	2.76
MALV-6	150	30	706	4.97
MALV-7	150	24	965	3.8
MALV-8	120	90	295	2.15
MALV-9	120	72	302	2.08
MALV-10	120	54	552	2.45
MALV-11	120	36	658	2.66
MALV-12	90	90	386	2.66
MALV-13	90	72	451	2.47
MALV-14	90	54	513	2.66
MALV-15	90	36	827	2.4
MALV-16	60	90	334	2.39
MALV-17	60	72	380	2.31
MALV-18	60	54	760	2.47
MALV-19	60	36	1084	3.64

Table (6.3) Mean values of drop diameter at each test based on Rosin Rammler distribution, output data from Malvern Particle Sizer.

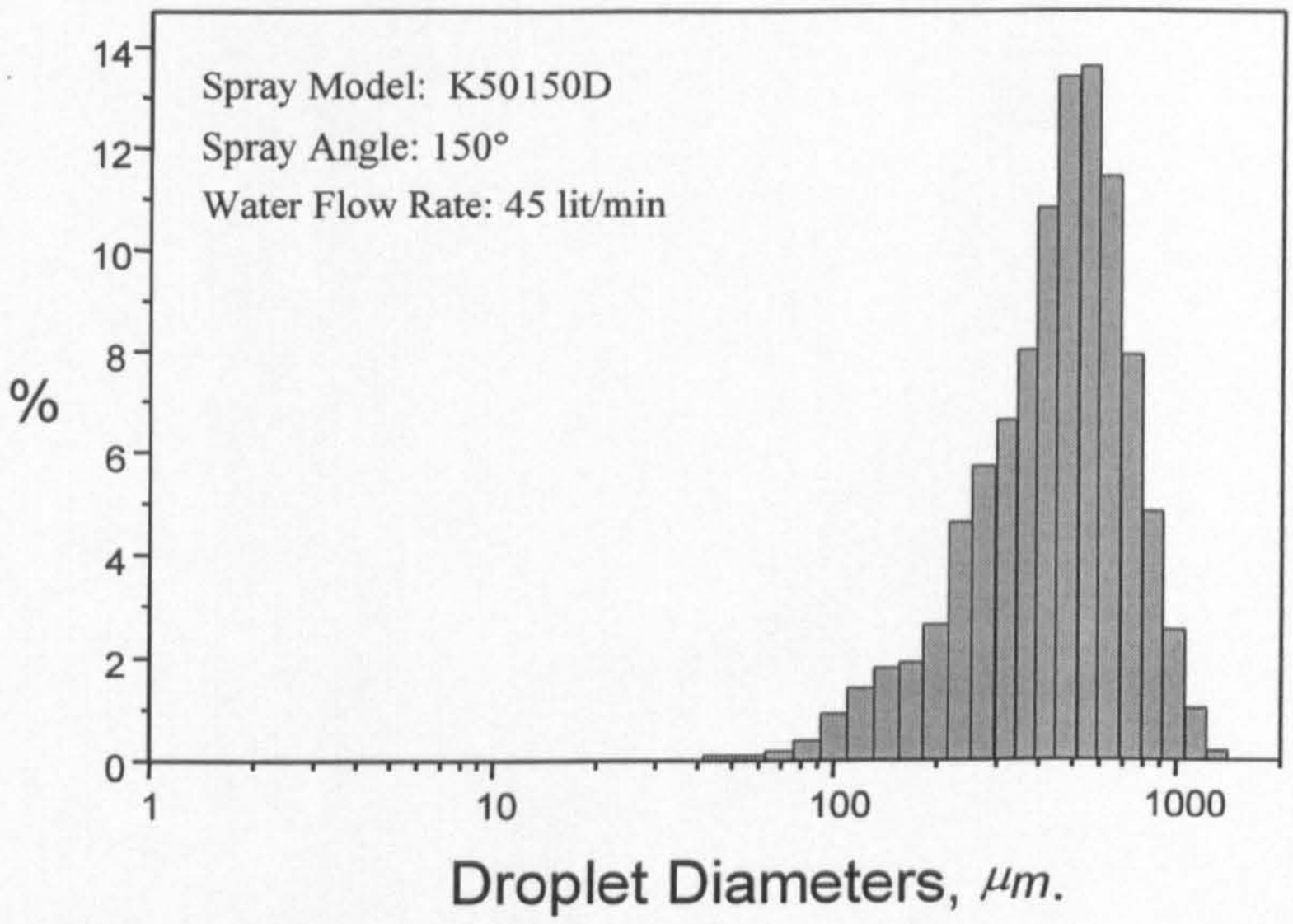

Figure (6.2). Droplet diameter histogram measured by Malvern particle sizer.

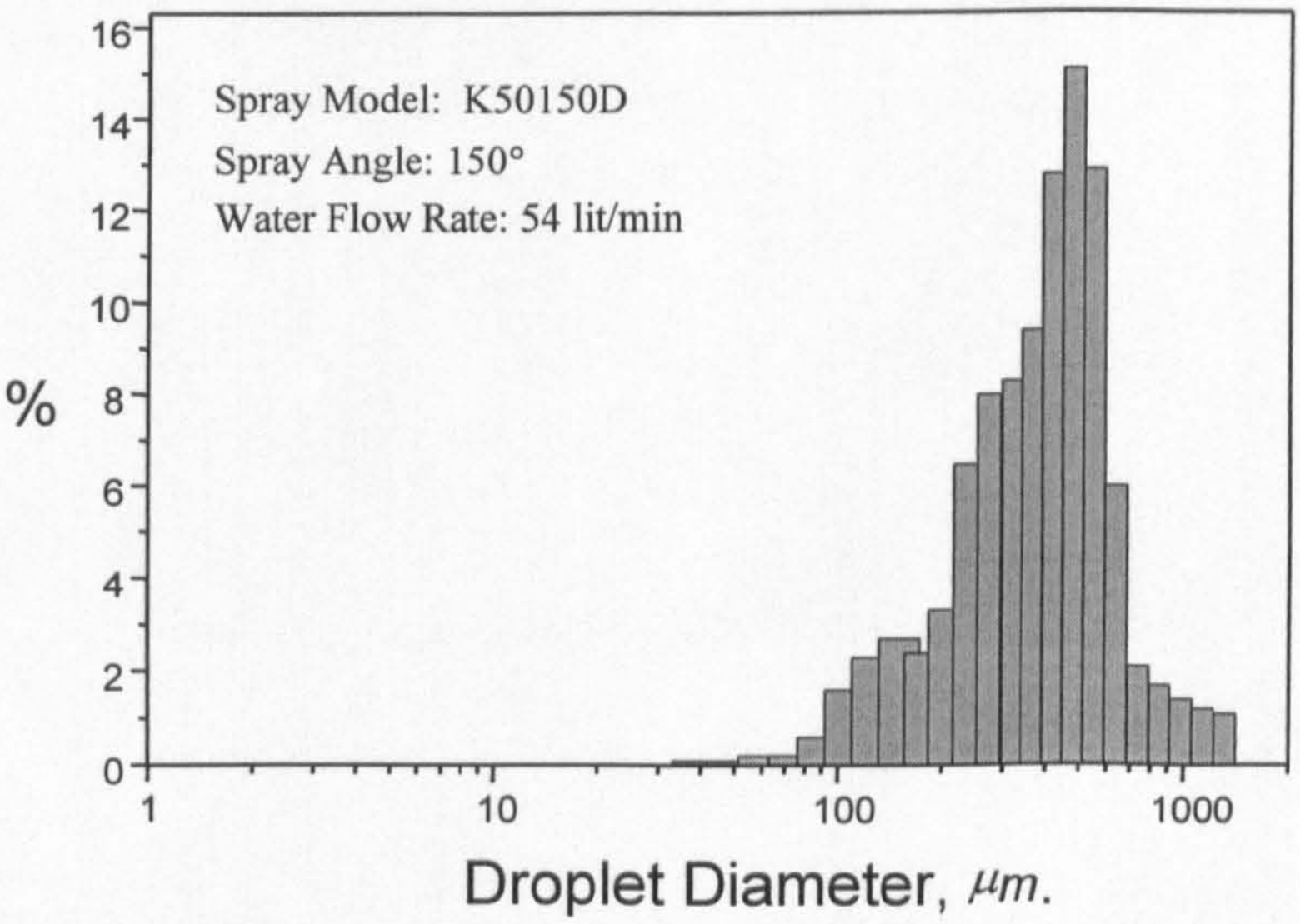

Figure (6.3). Droplet diameter histogram measured by Malvern particle sizer.

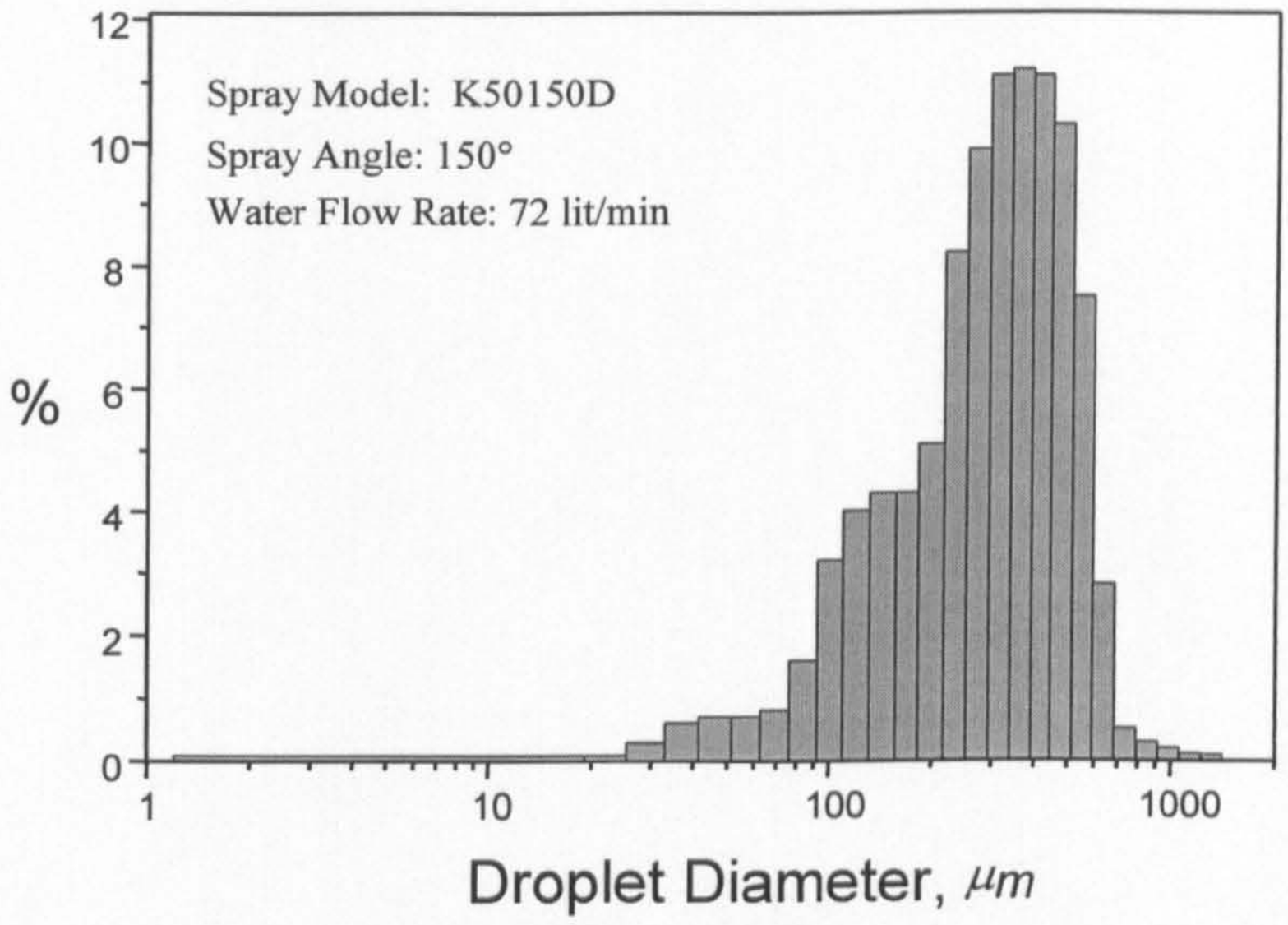

Figure (6.4). Droplet diameter histogram measured by Malvern particle sizer.

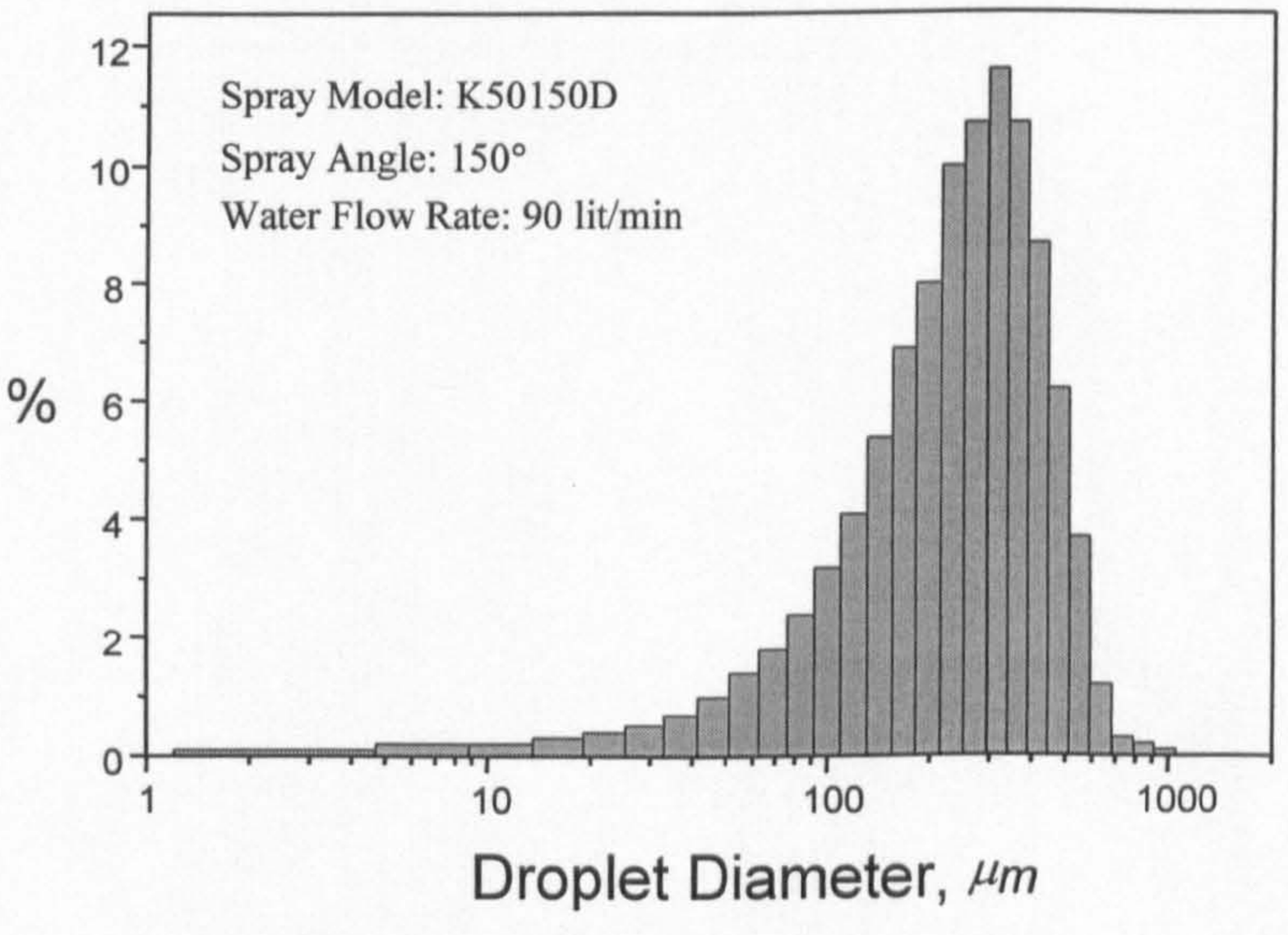

Figure (6.5). Droplet diameter histogram measured by Malvern particle sizer.

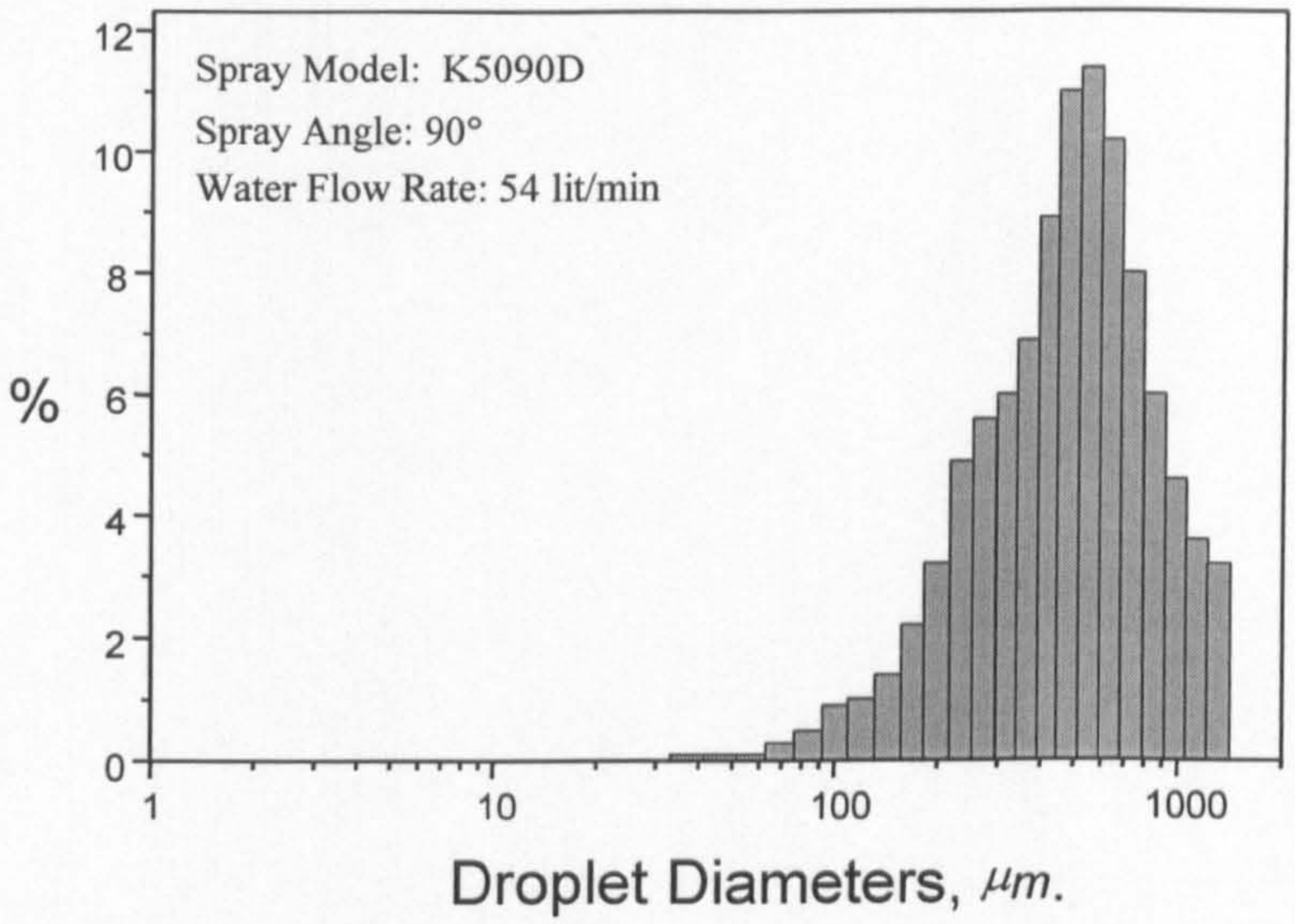

Figure (6.6). Droplet diameter histogram measured by Malvern particle sizer.

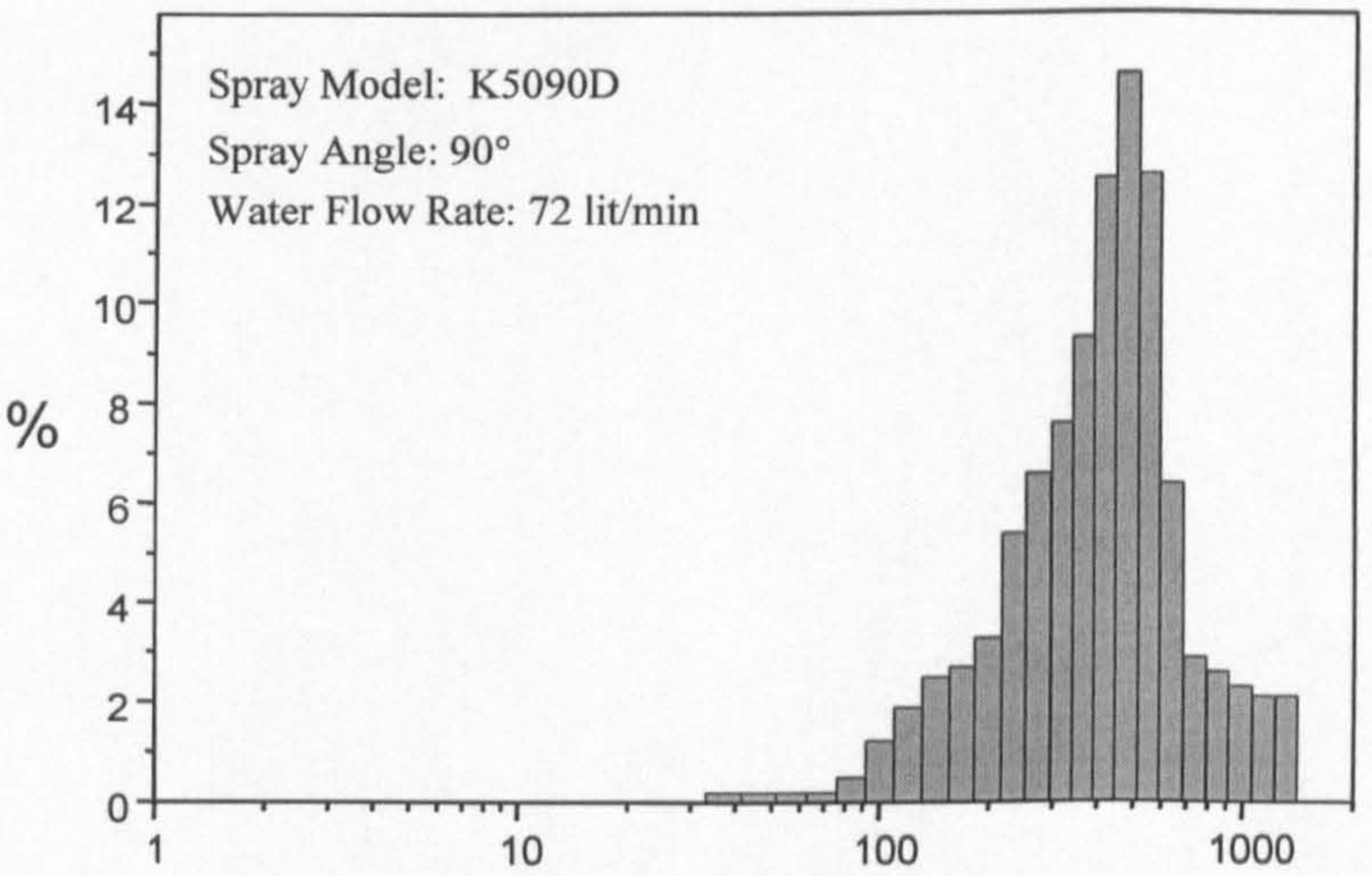

Figure (6.7). Droplet diameter histogram measured by Malvern particle sizer.

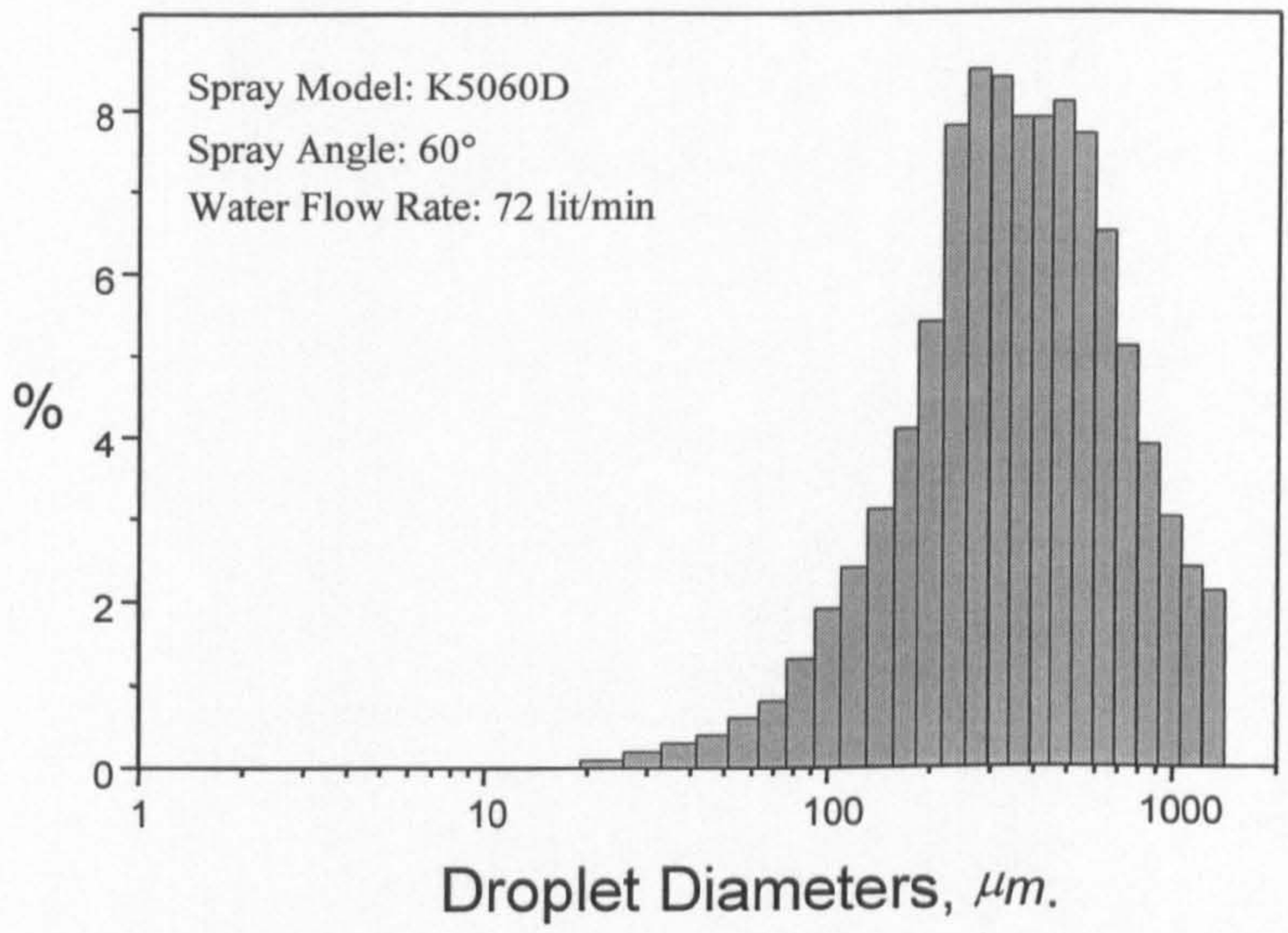

Figure (6.8). Droplet diameter histogram measured by Malvern particle sizer.

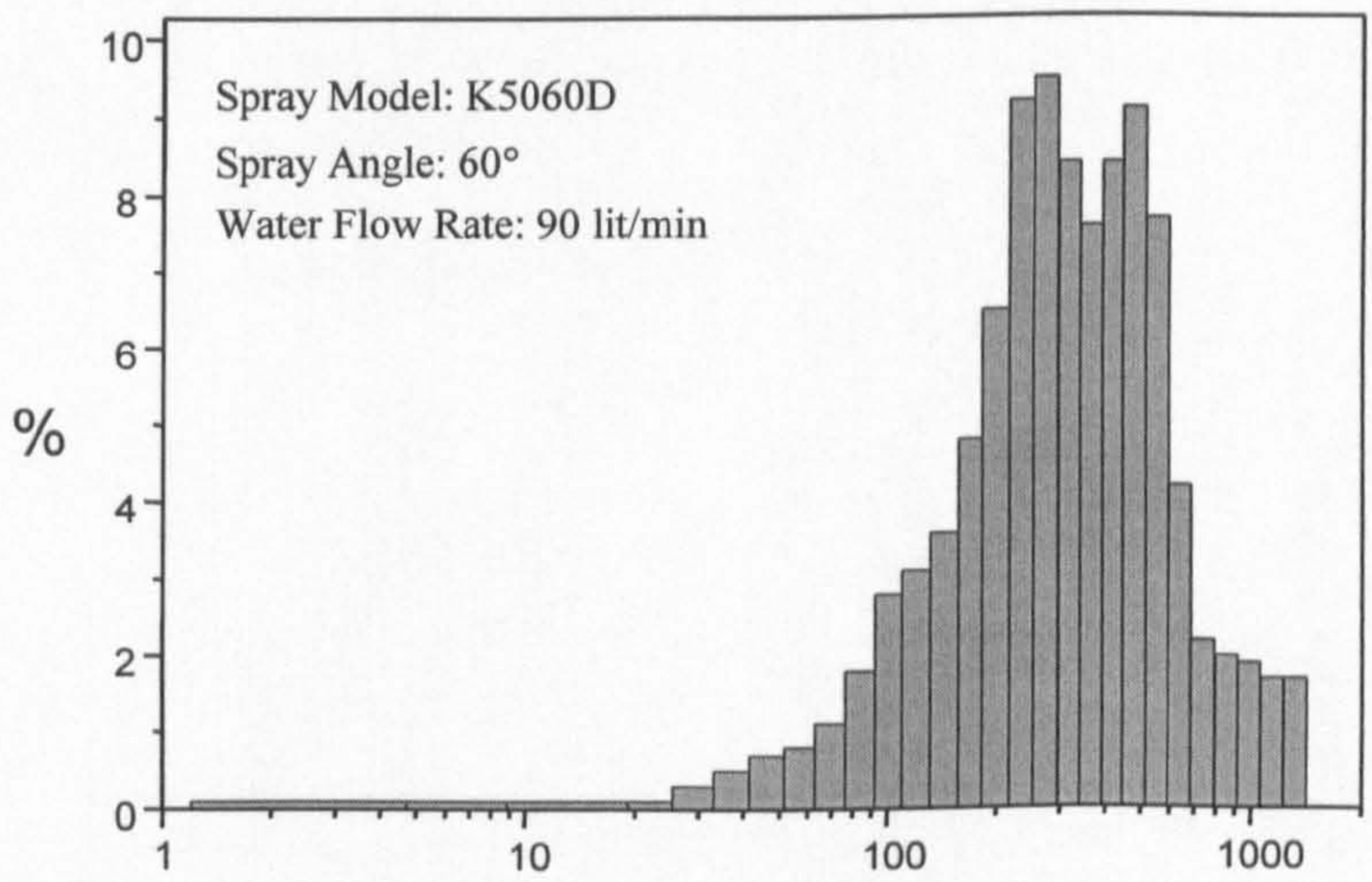

Figure (6.9). Droplet diameter histogram measured by Malvern particle sizer.

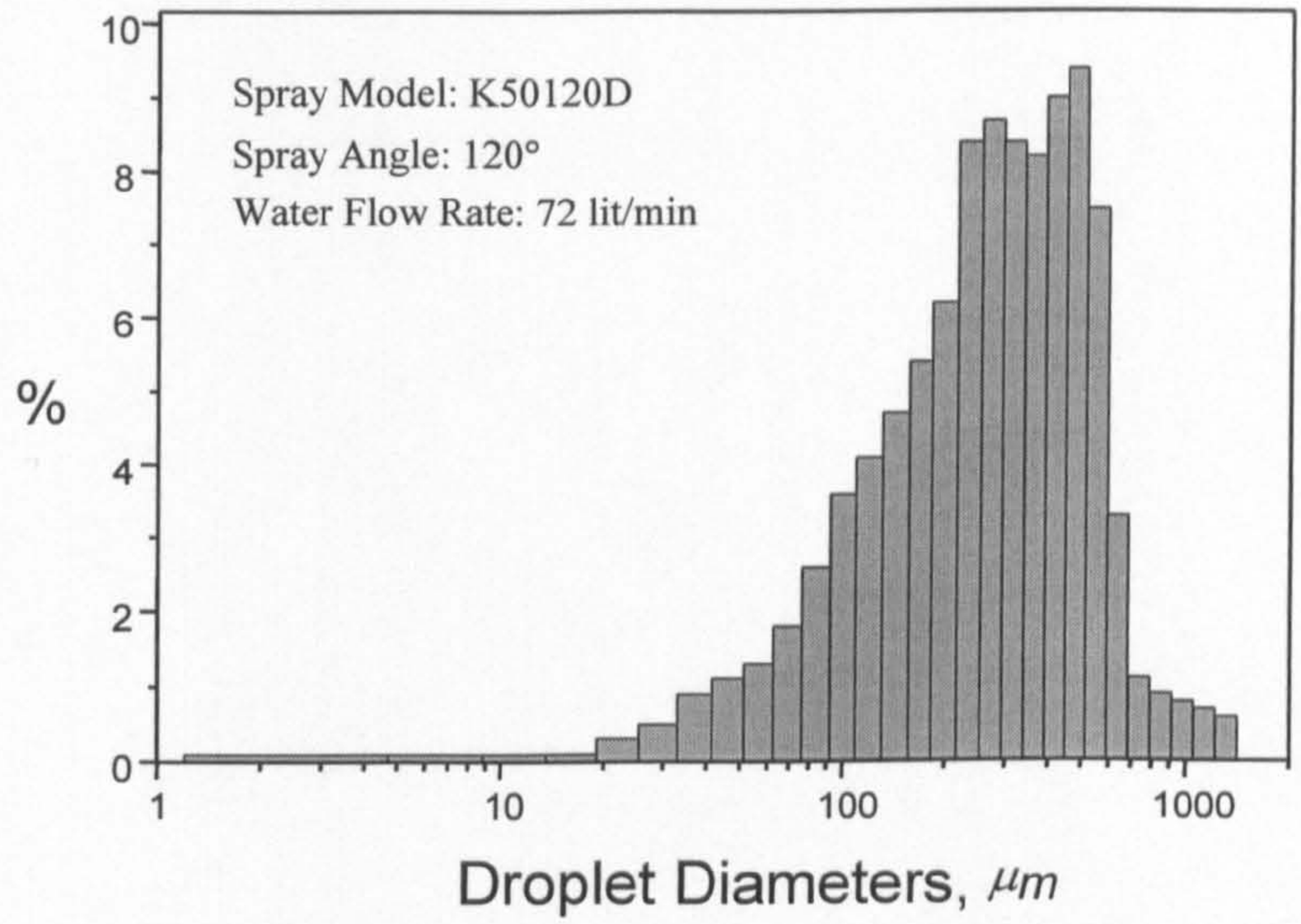

Figure (6.10). Droplet diameter histogram measured by Malvern particle sizer.

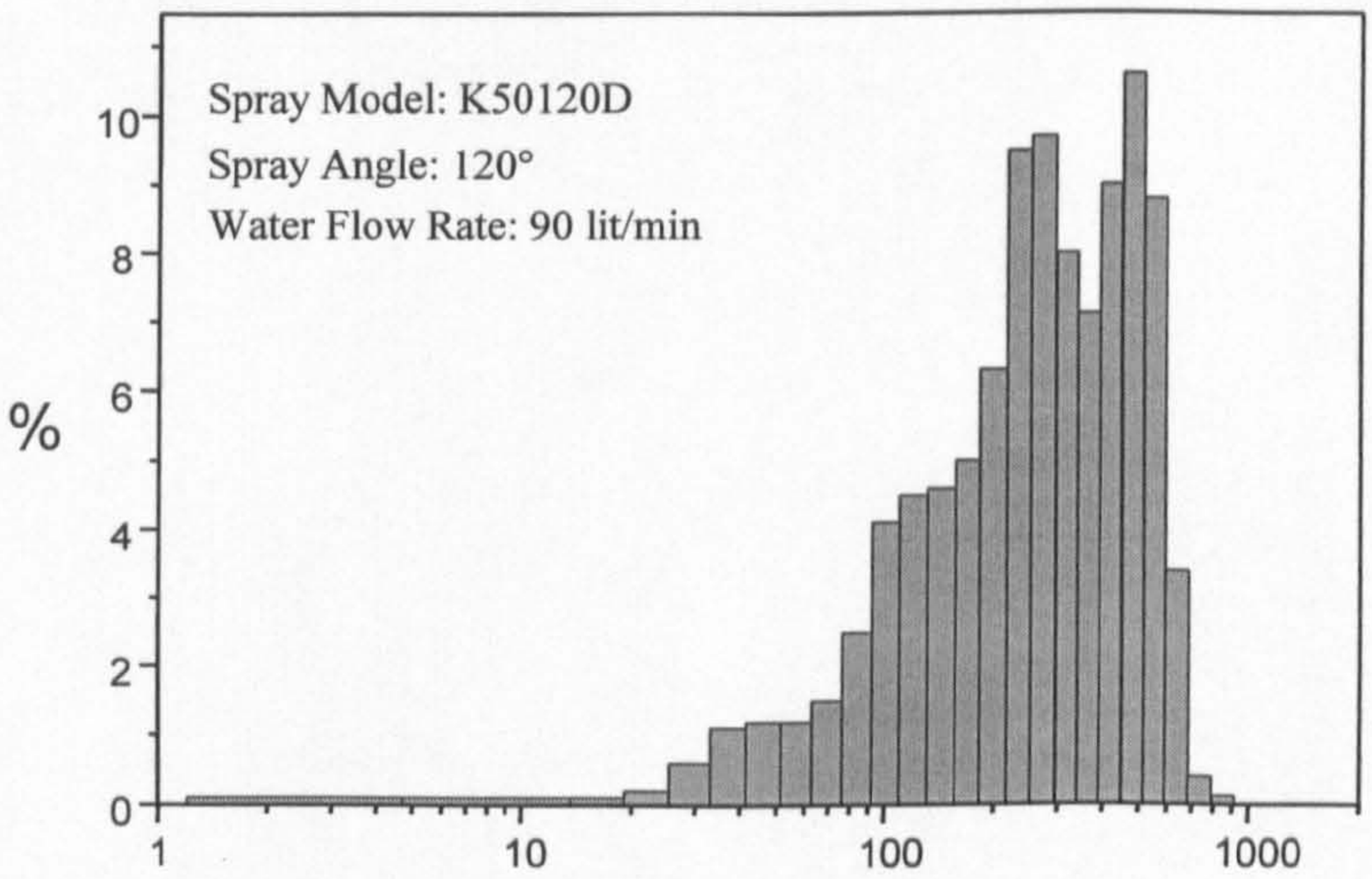

Figure (6.11). Droplet diameter histogram measured by Malvern particle sizer.

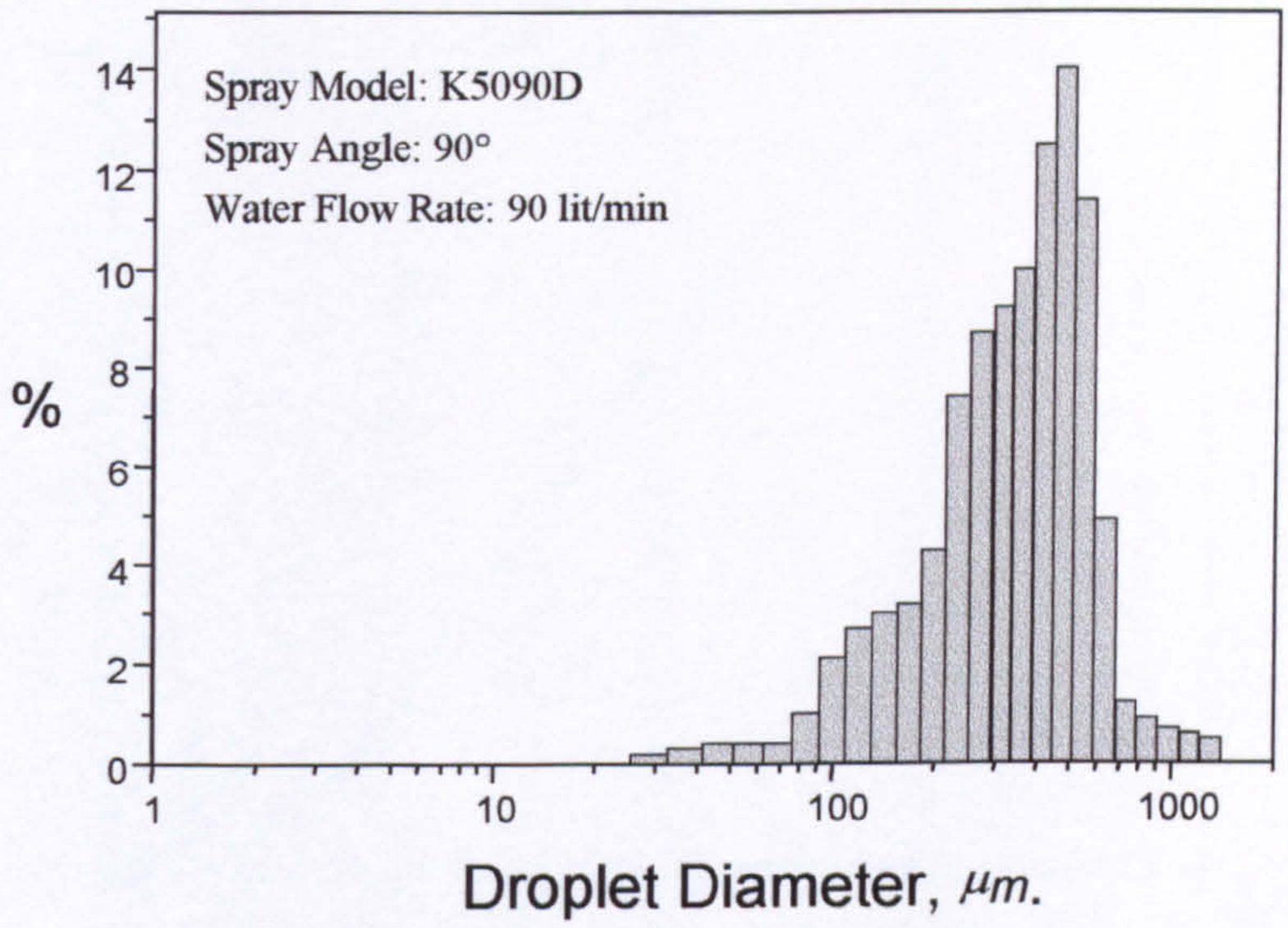

Figure (6.12). Droplet diameter histogram measured by Malvern particle sizer.

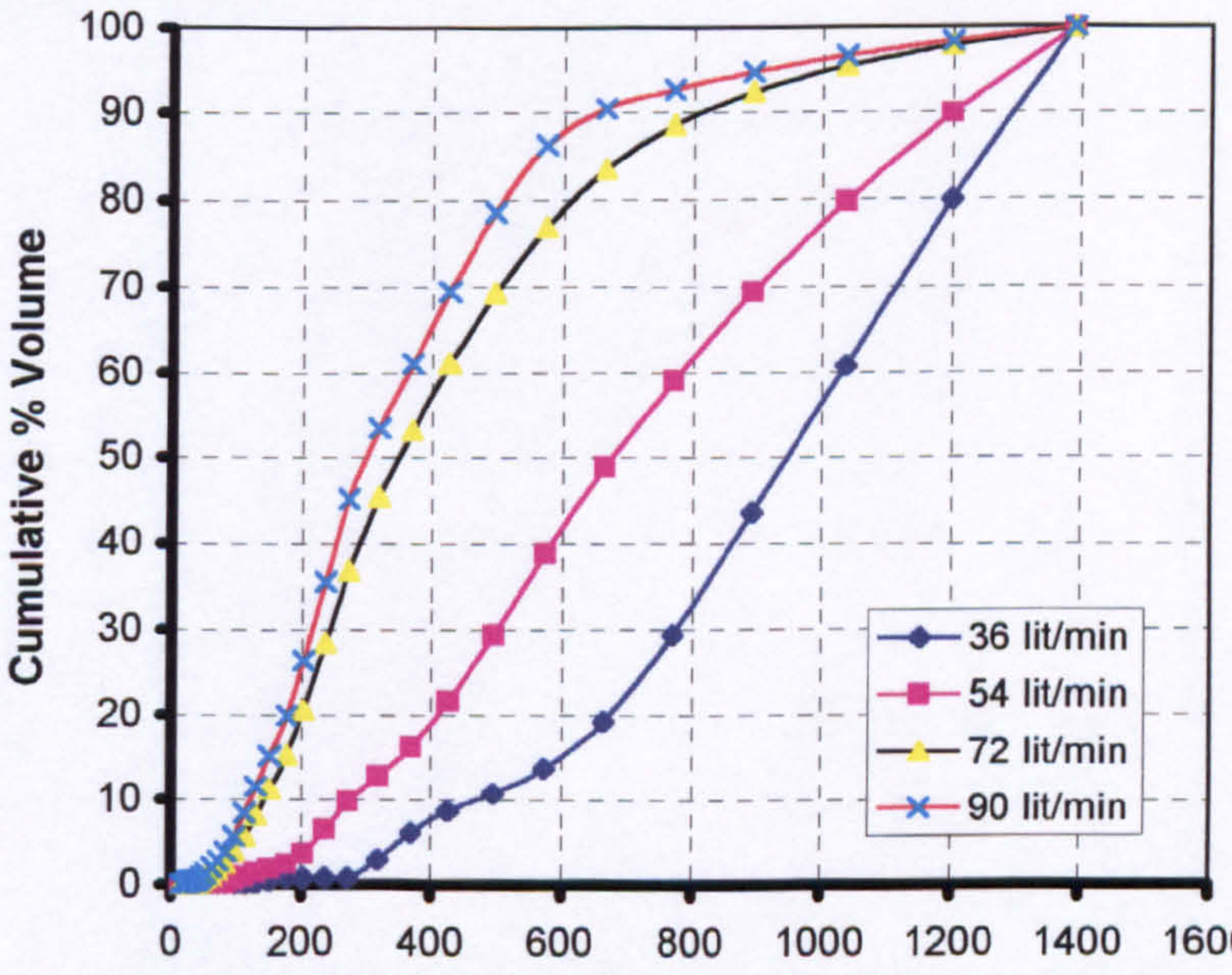

Figure (6.13). Comparison of spray distribution curves for spray nozzle K5060D for different flow rates.

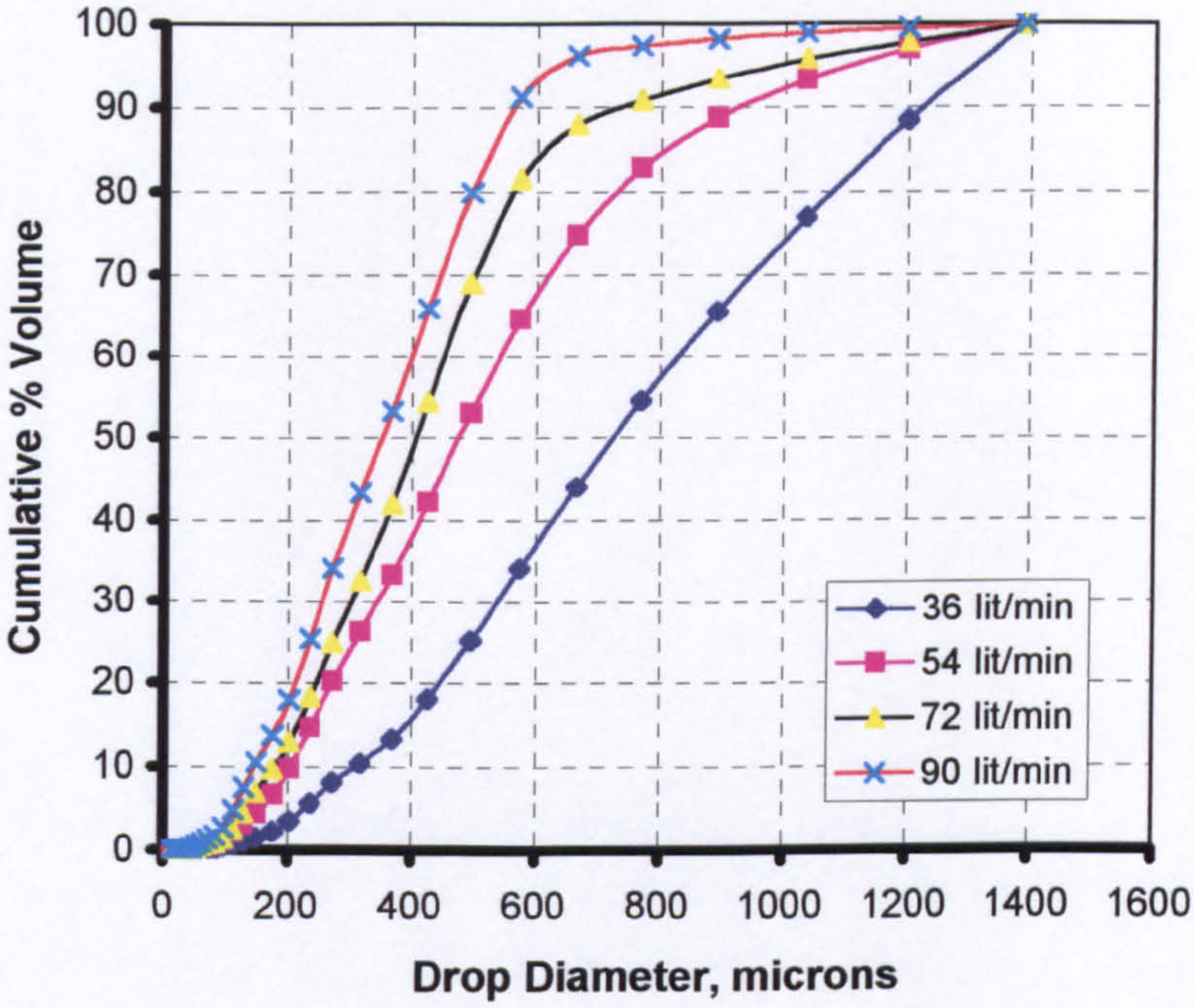

Figure (6.14). Comparison of spray distribution curves for spray nozzle K5090D for different flow rates.

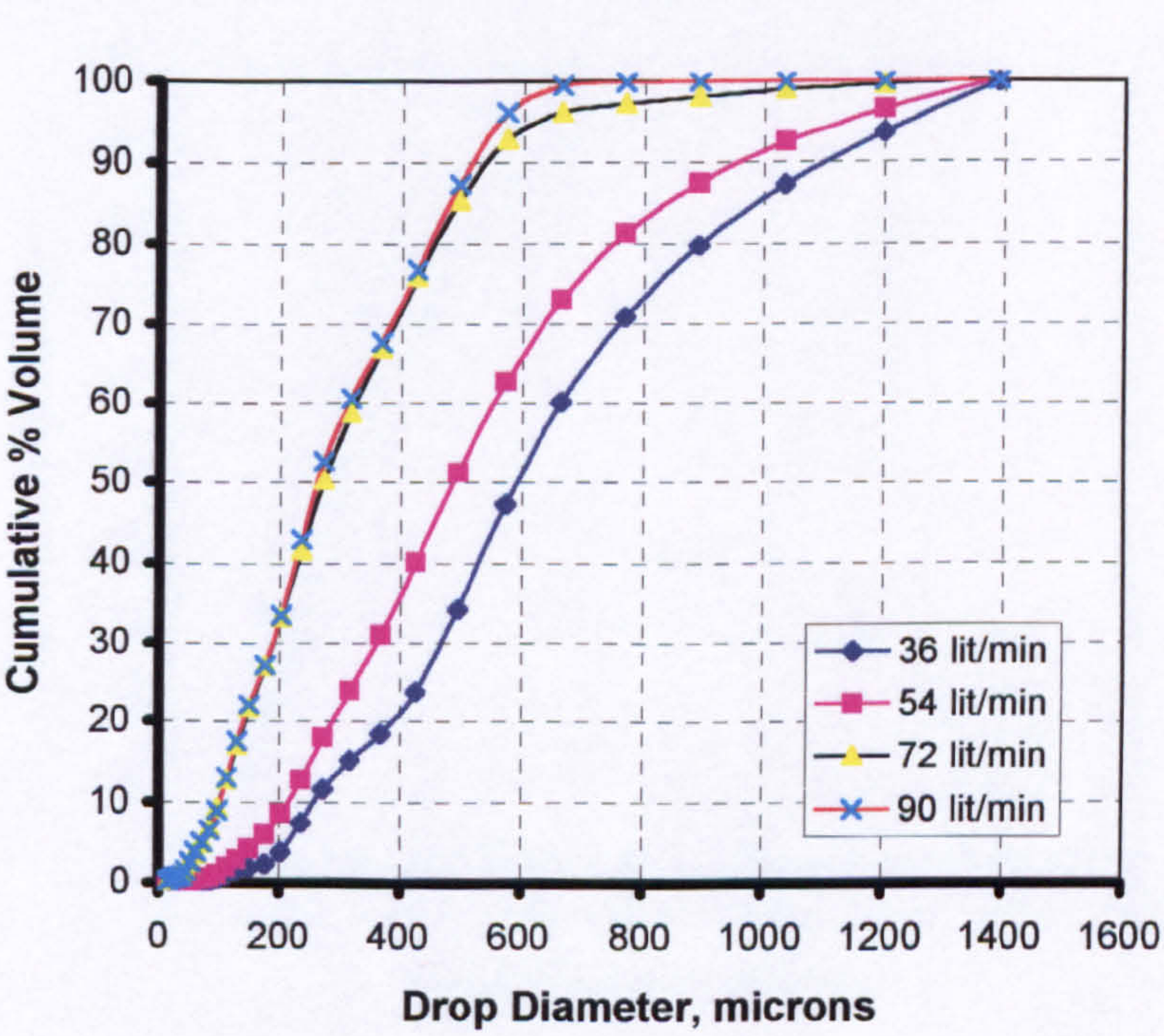

Figure (6.15). Comparison of spray distribution curves for spray nozzle K50120D for different flow rates.

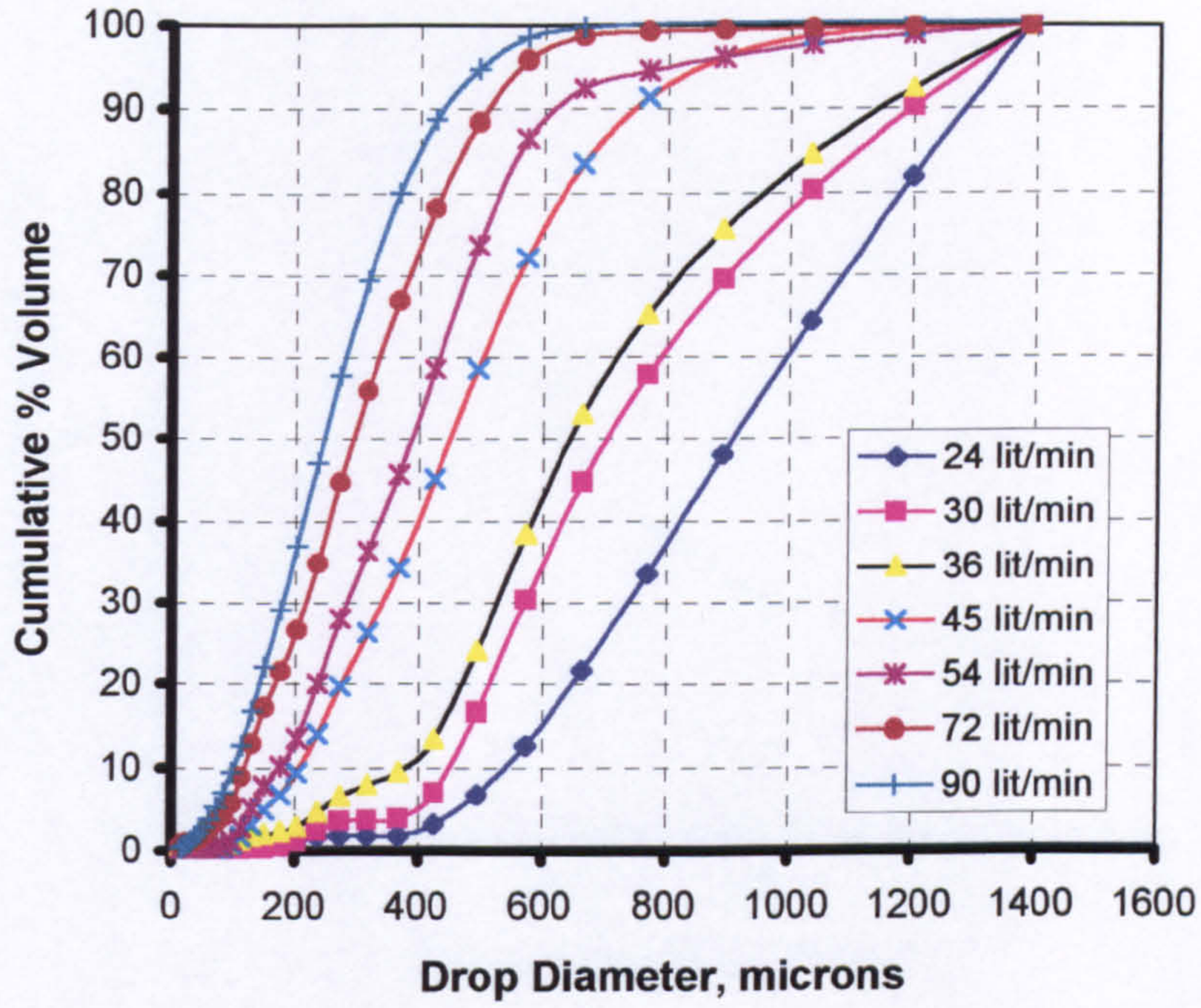

Figure (6.16). Comparison of spray distribution curves for spray nozzle K50150D for different flow rates.

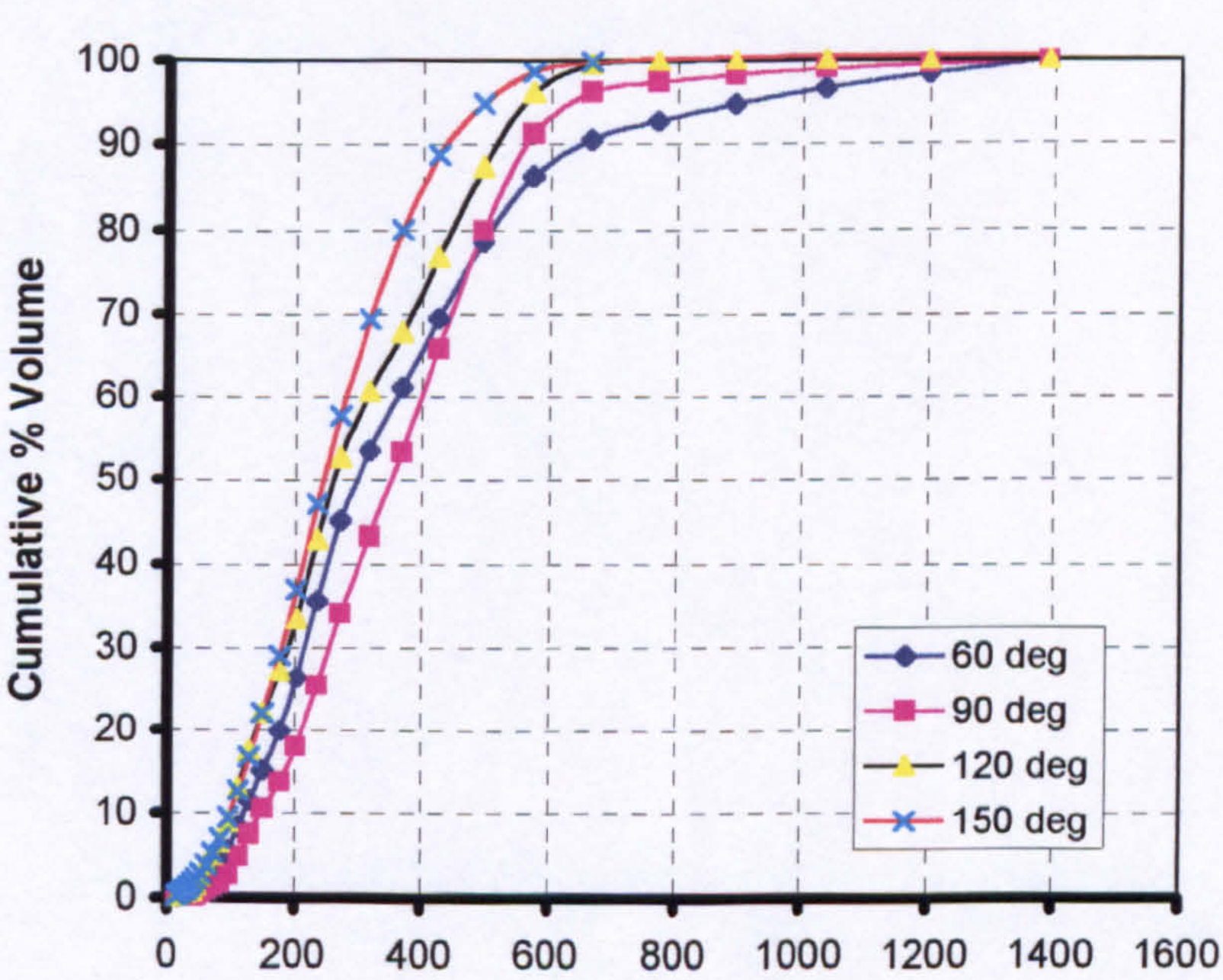

Figure (6.17). Comparison of spray distribution curves for different spray nozzles at 90 lit/min water flow rates.

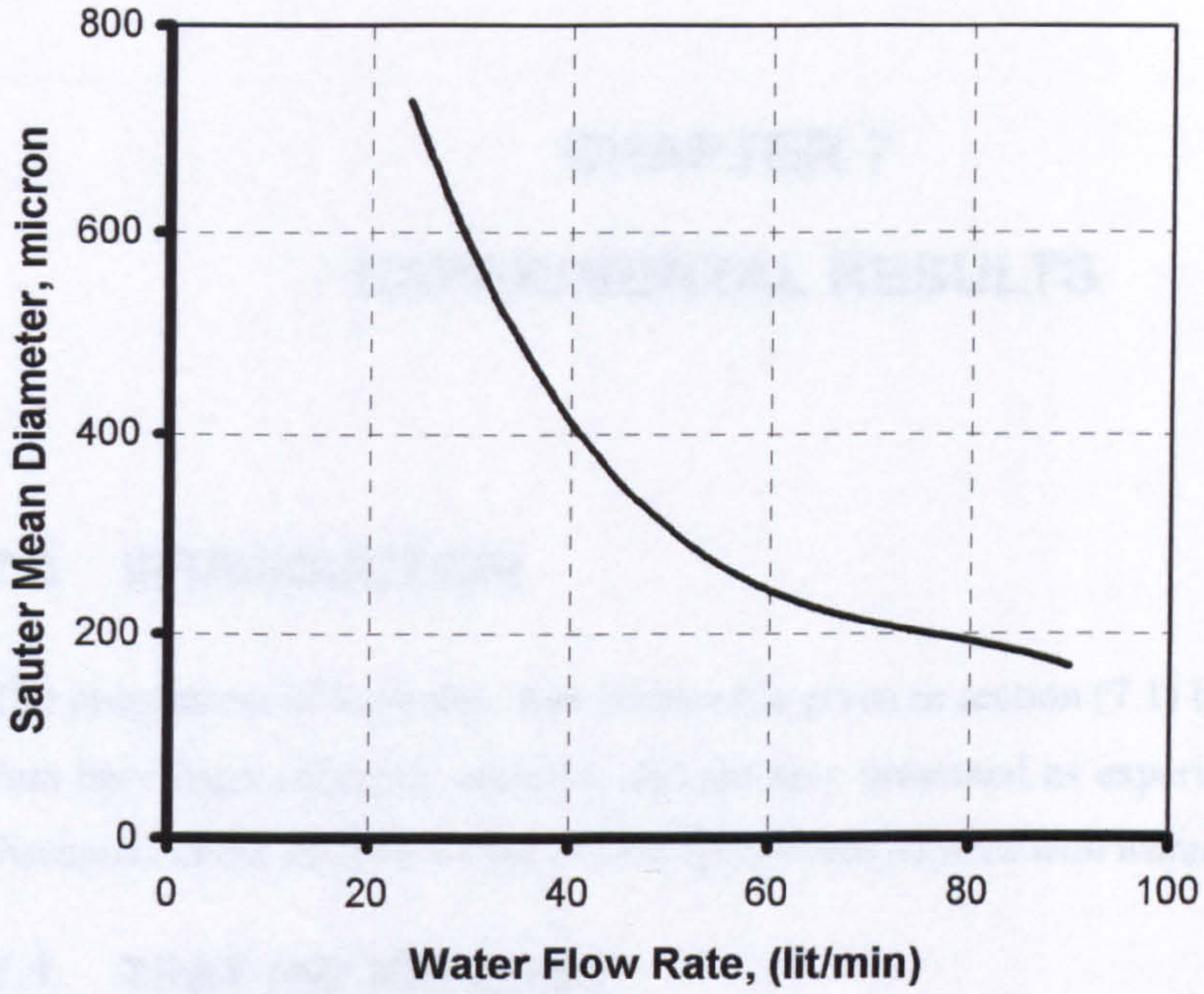

Figure (6.18). The Sauter mean diameter versus the water flow rate at 150° angle.

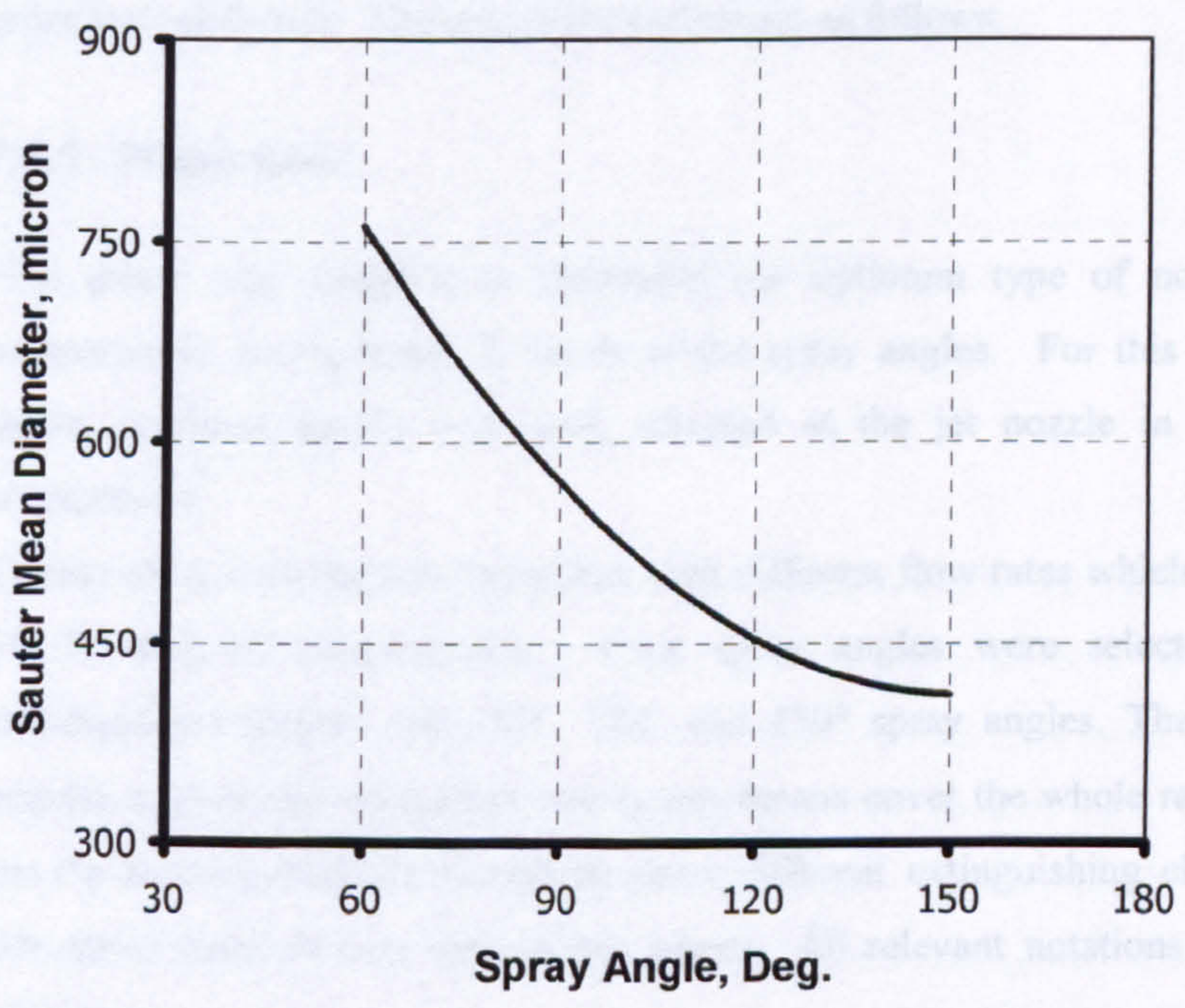

Figure (6.19). The Sauter mean diameter versus the spray angle.

CHAPTER 7

EXPERIMENTAL RESULTS

7.0 INTRODUCTION

The programme of work that was followed is given in section (7.1) below. All the data have been collected, collated, and are now presented as experimental results discussed under *jet fires without water sprays* and *jet fires with water sprays.*

7.1 TEST PROGRAMME

The test programme was divided into two phases. Fifty-eight tests were needed in order to complete it. The tests were performed as follows:

7.1.1 Phase One:

First phase was designed to determine the optimum type of nozzle for this compartment arrangement, in terms of the spray angles. For this purpose, one single overhead nozzle was used, directed at the jet nozzle in a downward arrangement.

Twenty tests were done in this phase with different flow rates which were 18, 36, 54, 72 and 90 litres/minutes. Four spray angles were selected for these investigations namely, 60°, 90°, 120° and 150° spray angles. The selection of nozzles used in this study does not by any means cover the whole range of types, but the nozzles differed enough to show different extinguishing characteristics. One spray location was used in this phase. All relevant notations are given in table (7-1).

Test No	No. of nozzle	Spray Locations			Water Flow Rate				Spray Angle
					For each Spray		Total		
		Back	Centre	Front	kg/s	lit/min	kg/s	lit/min	
Comp 01	1		✓		0.3	18	0.3	18	150
Comp 02	1		✓		0.6	36	0.6	36	150
Comp 03	1		✓		0.9	54	0.9	54	150
Comp 04	1		✓		1.2	72	1.2	72	150
Comp 05	1		✓		1.5	90	1.5	90	150
Comp 11	1		✓		0.3	18	0.3	18	60
Comp 12	1		✓		0.6	36	0.6	36	60
Comp 13	1		✓		0.9	54	0.9	54	60
Comp 14	1		✓		1.2	72	1.2	72	60
Comp 16	1		✓		1.5	90	1.5	90	60
Comp 19	1		✓		0.3	18	0.3	18	90
Comp 20	1		✓		0.6	36	0.6	36	90
Comp 21	1		✓		0.9	54	0.9	54	90
Comp 22	1		✓		1.2	72	1.2	72	90
Comp 23	1		✓		1.5	90	1.5	90	90
Comp 26	1		✓		0.3	18	0.3	18	120
Comp 27	1		✓		0.6	36	0.6	36	120
Comp 28	1		✓		0.9	54	0.9	54	120
Comp 29	1		✓		1.2	72	1.2	72	120
Comp 30	1		✓		1.5	90	1.5	90	120

Table (7-1). Phase One Experimental Programme.

7.1.2 Phase Two:

Based on the tests which were done in phase one, and after detailed data analysis, it was decided to do further investigation with the nozzles which have 150° spray angle for different spray numbers, locations and different flow rates, because these nozzles were found to perform best over all other nozzles used with different spray angles (to be discussed further in section 7.5). Approximately 38 tests were conducted in this phase. Table (7-2) illustrates the notations used for the second phase of the programme. It was important to observe the effectiveness of the water spray under these conditions.

Test No	No of nozzle	Spray Locations			Water Flow Rate				Spray Angle
					For each Spray		Total		
		Back	Centre	Front	kg/s	lit/min	kg/s	lit/min	
Comp 08	1	✓			0.3	18	0.3	18	150
Comp 09	1	✓			0.6	36	0.6	36	150
Comp 10	1	✓			0.9	54	0.9	54	150
Comp 33	1	✓			1.2	72	1.2	72	150
Comp 34	1	✓			1.5	90	1.5	90	150
Comp 15	1			✓	0.3	18	0.3	18	150
Comp 37	1			✓	0.6	36	0.6	36	150
Comp 38	1			✓	0.9	54	0.9	54	150
Comp 39	1			✓	1.2	72	1.2	72	150
Comp 40	1			✓	1.5	90	1.5	90	150
Comp 43	3	✓	✓	✓	0.3	18	0.9	54	150
Comp 44	3	✓	✓	✓	0.6	36	1.8	108	150
Comp 45	3	✓	✓	✓	0.9	54	2.7	162	150
Comp 46	3	✓	✓	✓	1.2	72	3.6	216	150
Comp 47	3	✓	✓	✓	1.5	90	4.5	270	150
Comp 50	2	✓		✓	0.3	18	0.6	36	150
Comp 51	2	✓		✓	0.6	36	1.2	72	150
Comp 52	2	✓		✓	0.9	54	1.8	108	150
Comp 53	2	✓		✓	1.2	72	2.4	144	150
Comp 54	2	✓		✓	1.5	90	3	180	150
Comp 57	3	✓	✓	✓	0.4	24	1.2	72	150
Comp 58	3	✓	✓	✓	0.5	30	1.5	90	150
Comp 59	2	✓		✓	0.45	27	0.9	54	150
Comp 60	2	✓		✓	0.75	45	1.5	90	150
Comp61	2	✓	✓		0.3	18	0.6	36	150
Comp62	2	✓	✓		0.45	27	0.9	54	150
Comp63	2	✓	✓		0.6	36	1.2	72	150
Comp64	2	✓	✓		0.75	45	1.5	90	150
Comp65	2	✓	✓		0.9	54	1.8	108	150
Comp66	2	✓	✓		1.2	72	2.4	144	150
Comp67	2	✓	✓		1.5	90	3	180	150
Comp70	2		✓	✓	0.3	18	0.6	36	150
Comp71	2		✓	✓	0.45	27	0.9	54	150
Comp72	2		✓	✓	0.6	36	1.2	72	150
Comp73	2		✓	✓	0.75	45	1.5	90	150
Comp74	2		✓	✓	0.9	54	1.8	108	150
Comp75	2		✓	✓	1.2	72	2.4	144	150
Comp76	2		✓	✓	1.5	90	3	180	150

Table (7-2). Phase Two Experimental Programme.

7.2 PARAMETER VARIATIONS

The main variables in the experiments were the nozzle type (spray angle), the water flow rate and the number and location of the nozzles. The compartment itself with two openings, one air inlet at the floor level of the front wall, and an outlet at the ceiling level on the same side, was not altered throughout the experiments. A list of parameter variations and some key numbers for identification of each test are given in tables (7.1) and (7.2).

The fire condition was similar in all the experiment, except for some tests when the wind speed was high, which caused the jet flame to have stabilisation problem. Therefore, these tests were repeated on other days when the weather conditions improved.

7.2.1 Pre-burn Time

The pre-burn time (steady state) of the fire in the compartment is to be found and used for all the subsequent tests. After the steady state burning time is reached, the spray is then to be activated according to the test programme.

The pre-burn time of the fire before spray activation determines the available heat accumulated in the compartment.

7.2.2 Spray Angle

The spray angle is more a characteristic of the nozzle than the spray, but it is nonetheless important to understand its significance in defining appropriate sprays for fire suppression applications. Spray angle is a critical factor in determining nozzle spacing to ensure a relatively uniform distribution of spray, without large void areas

between nozzles. The spray angle is very significant in determining the initial velocity and direction of the droplets leaving the nozzle, which in turn determines its ability to penetrate obstructions in the compartment (Mawhinney, 1993).

7.2.3 Drop Size

The drop size produced is a very important parameter in that droplets are the form that the water takes as it interacts with the fire. Droplet size affects heat absorption and also the spray's ability to slow the progress of the fire by extinguishment and dilution of unburned fuel.

7.2.4 Water Flow Rates

Water flow rates are also very important parameter to be concerned with. The extinguishing effectiveness of a fire is dependent on the absorption of heat from a fire by water spray which is a function of the water flow rate.

Water was applied through one, two or three nozzles mounted in the ceiling, heading directly at the propane nozzle according to the test programme. The nozzles produced full cone spray, totally covering the jet nozzle area.

Water sprays for fire protection requirements are usually stated in terms of water discharge density and total area of demand or total water volume needed over a time period.

7.2.5 Spray Location and Numbers

The location of the fire related to the spray nozzles, wall and objects would influence the interaction between water droplets and the flame zone. This will decide the time before extinguishment.

Some combinations of nozzle locations and fire may promote quick extinguishment, as other combinations may work against rapid extinguishment.

The nozzles were mounted along the Northeast-Southwest centre line of the ceiling. The distance between the nozzles was 2 metres.

7.3 JET FIRES WITHOUT WATER SPRAY: STEADY STATE RESULTS

The experiments were carried out in the $35m^3$ compartment. For all the experiments, the jet nozzle configuration location in the compartment and fire size were the same. The jet nozzle was supplied with propane at a steady state rate for the duration of the experiment.

The heat release rate in these experiments is based on the measured fuel consumption. The flow rate of the propane is measured, and the heat release is calculated from the mass flow and the heat of combustion. Figure (7.1) shows the heat release rate based on the fuel consumption measured in the experiments.

All the temperatures presented in this chapter are measured from different locations of aspirated thermocouples in the compartment. The location details of the thermocouples were discussed in chapter 3. For each experiment, all the measured steady state temperatures were calculated from time averages over the last 2 minutes of the experiment pre-burn time before water spray activation.

During the experiment, the ambient wind velocity in the test site was low and the wind direction was opposite to the compartment opening. Experiments were repeated on some tests on different days to avoid the effects of the wind direction and speed.
A propane jet fire was flowing along the vertical central axis, from the floor to the ceiling. A lifted conical flame, typical of open flames, but impinging on the ceiling, persisted throughout the experiments. The large fire almost filled the compartment.
The steady flow induced by jet fire in the compartment was viewed in terms of the model illustrated in plate (7.1). Air flowed into the compartment from the lower vent. Some gases from the hot upper layer were entrained to the air flow and mixed with it in the lower layer. The fire plume entrained gas from lower layer and pumped it to the upper layer.

7.3.1 Pre-burn Time

The effect of pre-burn time was studied by varying the length of the test. It was found that the fuel for jet fire was continuously released, that the compartment reached a steady state situation after approximately 5 minutes. Continuing the burning of the jet fire after the first 5 minutes showed no significant increase in the temperature of the gases inside the compartment as shown in Figure (7.2) or the temperature of the compartment surfaces as shown in Figure (7.3). After that the compartment reached a steady state condition in which there were no significant changes.
Therefore, five minutes was considered as the pre-burn time in all the tests programme.

7.3.2 Temperature Distributions

The temperatures in the compartment and at the outlet opening are shown in Figures (7.4) to (7.6). Following the first minute of ignition and after the full mass flow rate

of the fuel was reached, the maximum temperature inside the compartment rose high quickly to reach 900 °C before increasing slowly to 1100°C. Finally it reached steady state conditions 4 minutes later with a maximum temperature of 1140 °C. The same trend was found for the other temperature measurement locations as shown in Figures (7.4) and (7.5).

A steady ceiling temperature of 700 °C was reached in the centre of the compartment opposite to the jet nozzle location in the floor after nearly 4 minutes. Then the temperature decreased as the distance from the centre of the ceiling increased in both directions. The lowest temperature found in the ceiling was 580 °C, as clearly shown in Figures (7.7).

The fact that the front of the compartment was hotter than the back shows the effect of the opening on the ceiling jet. It is possible that the dominant flame-flow pattern existed towards the front of the compartment as shown in plate (7.2). This caused the external flame to be burning at the upper opening at the front of the compartment, which would increase the temperature of the front part of the compartment.

The Southeast side wall temperatures were nearly the same as the Northwest wall temperatures.

The maximum temperature at the Southeast and Northwest walls was 740°C at the front upper part of the side wall and 610°C and 660°C at the rear upper part of the Southeast and Northwest walls respectively. At the bottom of the side walls the maximum temperatures found for both Northeast and Southwest walls were similar. The temperature found at the bottom side walls was 485°C. The temperature found in the middle of the Northwest wall was 625°C. The temperature distribution is shown in Figures (7.8) and (7.9).

The floor temperature was low compared to the ceiling and other wall surfaces of the compartment. The front half floor was found to have a lower temperature than the rear half floor. The temperatures found in the front half floor were 114°C and 203°C

for the rear half floor. The explanation for this is that the air entrained to the jet was flowing over that front part of the floor and caused it to be cooler. Figure (7.10) shows the temperature measured at the floor of the compartment.

The temperature measured at the back wall is shown in Figure (7.11). It shows that the temperature increased as the height increased.

The average temperature distribution in the top half of the vent as in Figure (7.12) shows the maximum temperature found near the corners to be 1050 °C. In the figure the temperature decreased as the distance increased until it reached the centre where the minimum temperature found in the top half vent reached 800°C. Thereafter the temperature started to increase again until it got to the other side's corner. Typical opening temperature data are included in Figure (7.13). For clarity, the centreline temperature within the opening and the East corner are shown. Nevertheless, this profile is representative of most off-centreline profiles.

The average temperature of the gas inside the compartment measured from the Southwest string increased as the height of the compartment increased. This is shown in Figure (7.14). The maximum steady-state temperature measured inside the compartment can be found in the upper layer of the front half of the compartment due to the flow of the hot combustion gases leaving the compartment through the top half vent. The lower temperature in the compartment was found in the lower front part of the opening in which the air for the combustion entrained and this in turn cooled the lower part of the compartment. The lower part of the rear half of the compartment was found to be hotter than the front one. This can be proved very clearly by Figure (7.15) which shows the measured temperature from the bottom thermocouples in both the Southwest and Northeast strings.

7.3.3 Combustion Gases

Carbon monoxide concentration measured in the compartment jet fire without water spray was in the range from 0.5 to 4%. A plot of the concentration of CO versus time for the three different sampling points is given, by way of example, in Figure (7.16) measured in COMP64. It has been showed that there was very little smoke produced in the tests and CO level reached up to 3.5 % at the top half of the vent.

The oxygen concentration in dry air is normally around 21%. In the tests the minimum oxygen concentration at the upper part of the outlet opening was in the range from 1% to 3%. This depletion of oxygen was caused by the combustion itself. This minimum oxygen concentration corresponded to maximum CO2 concentration, which was in the range from 11-15%. Figures (7.17) and (7.18) show examples (COMP64) of oxygen and carbon dioxide concentrations versus time for the three different sampling points. In these figures the oxygen concentration is 2% and carbon dioxide concentration 12%.

It is clear that at this stage the fire was burning in under-ventilation regime i.e. there was not enough air to meet the stoichiometric flame requirement.

7.4 JET FIRES WITH WATER SPRAY RESULTS

7.4.1 Phase I Results: Effect of Spray Angles at Different Water Flow Rates

In order to establish the impact of the water spray on the compartment jet fires different water flow rates between 18 and 90 lit/min were considered. Four different spray nozzles were tested in this phase, having different spray angles of 60, 90 120 and 150°. One spray nozzle location was used in this phase. The spray nozzle

location used was in the centre of the compartment located directly above the jet nozzle. The objective of this phase is to find out the optimum spray angle to be used for further investigations, knowing that larger spray angle with higher water flow rates will produce smaller drops (it was discussed in detail in chapter 6). The minimum water application rate required for extinguishment is to be found for each nozzle type.

The spray was activated to the required water flow rate approximately 5 minutes after the fire ignition and after the full capacity of the fuel flow rate was reached. The water flow was kept at a constant rate throughout the whole experiment period, an example is shown in Figure (7.19). Each experiment was terminated when extinguishment due to the water spray activation or steady state non-extinguishment had occurred.

Figure (7.20) shows the average temperature development for different water flow rates at 150° spray angle. Test COMP5, which had a spray angle of 150° and 90 lit/min water flow extinguished the flame almost immediately, approximately after 10 seconds. However, COMP4 which had 72 lit/min water flow rate and same spray angle extinguished the flame in around 12 seconds.

After spray activation in COMP3, where the water flow rate of 54 lit/min and 150° spray angle were used, the average temperature inside the compartment decreased by 550° C in test where the water flow rate was insufficient for extinguishment. Figure (7.21) shows the average temperature reduction after the water spray activation for different water flow rates at 150° spray angle when the water was insufficient for extinguishment.

A typical temperature development for compartment jet fire tests of phase I are shown in Figures (7.22) to (7.24) which show the average temperature development in the compartment after the water spray activation for different water flow rates at different spray angles such as 60, 90 and 120°.

The figures generally show the temperature reduction increases as the water flow rate increases. The fire was not extinguished when smaller spray angles such as 60° and 90° were used, but was at the maximum water flow rate when 120° spray angle was used.

In the case of small droplets with higher water flow rate test (> 72 lit/min), when the spray (150° spray angle nozzle) was activated the flame was distorted and blown sideways. The water spray penetrated down to the base of the fire, which affected the air entrainment to the jet. The fire was still burning, but with more flickering performance. Also, the small droplets were carried with the air entrained to the jet which then mixed with the fuel in the lift off distance.

In this experiment the flame was lifted off the jet nozzle - more than before - when the spray was activated, but there were still flames out of the outlet openings. The flame became bluish, and was not visible in the vicinity of the jet nozzle. This blue flame flickered around in the compartment, then suddenly disappeared, and the fire was extinguished.

In the medium water flow rates (≈ 54 lit/min), after ~ 30 seconds spray activation, grey smoke was flowing through the openings of the compartment through the upper part of the openings and the upper part of the lower vent. The overpressure inside the compartment forced the smoke and water vapour to leave the compartment.

The entrained air of the spray mixed with the combustion gases and also pushed the flame downwards.

The difference in the performance of these tests could be from the difference in spray momentum when it hit the flame, and in the droplets' sizes. Water spray lost its momentum as it travelled through hot fire gases which were flowing in counter direction to strong jet momentum.

From Figures (7.20) to (7.24) plotted from the present tests series in phase I, and which show the average temperature of different location in the compartment, it was found that the spray reduced the temperature more at 150° spray angle; this is very

clear in Figure (7.25a) which shows the average temperature reduction after the water spray activation for different spray angles for 72 lit/min water flow rate. So the larger the spray angle is, the greater temperature reduction will result. The temperature reduction at 60° spray angle was less than any other spray angle.

The test results with a single spray, located directly above the fuel jet nozzle, indicated that the effectiveness of the water spray in extinguishing a fire depended on the spray momentum and coverage. With the low flow rates below 54 lit/min., a single nozzle located at 2.2 m above the fire reduced the flame size substantially; however it failed to extinguish the fire for a period of 5 minutes after the spray activation. But for higher flow rates greater than 72 lit/min., the spray quickly reduced the flame size and pushed the flame back to the jet fuel nozzle, eventually extinguishing it in approximately less than 12 seconds. Therefore, it can be concluded that the 72 lit/min for the nozzle type K50 150D with spray angle 150° is the minimum water flow rate used in order to have extinguishment situation.

The difference in extinguishment time between test COMP4 and COMP5 is probably due to the lower flow rate in COMP4 and the smaller water droplets' sizes in COMP5. This experiment shows the lowest water application rate with extinguishment.

Table (7.1) summarises the combination of tests variables used and indicates whether extinguishment occurred or not. The fire was either extinguished by the water from the spray, continued to burn or was controlled to 600°C or less.

Table (7.1). Effectiveness of different spray heads and water flow rates in extinguishing or controlling jet fire - Number indicates time in seconds to extinction; 'c' indicates the temperature was controlled to 600°C or less.

Water Flow Rates (lit/min)	Spray Angle			
	150°	120°	90°	60°
90	10	20	100	c
72	12	30	c	c
54	c	c	c	c
36	c	–	–	–
18	–	–	–	–

7.4.2 Effect of Drop Sizes

The droplet diameter is very dependent on the water flow rate and on the spray angle as shown earlier in chapter 6.

To determine the relationship between droplet size and extinguishing effectiveness, experiments were conducted with 4 different spray nozzle angles. The test nozzle was located in the centre of the compartment directly above the jet nozzle. Similar types of nozzles were used that produced Sauter mean droplet sizes (SMD) ranging from 170 to 770 μm. The results indicate that the extinguishing effectiveness of the water spray decreases with increasing droplet diameter, as shown in Figure (7.25b).

7.5 EFFECT OF SPRAYS NUMBER AND LOCATIONS AT DIFFERENT WATER FLOW RATES

The experiments were carried out in the same 35 m^3 compartment as used in phase I, and with the same propane nozzle. One, two or three spray nozzles, using water only, operating at different water flow rates from 18 to 90 lit/min for each nozzle were tested. Three different spray locations with seven spray combination arrangements were used. A minimum water flow rate required for extinguishment was found for each arrangement. The different spray arrangements were characterised by different water flow rates, spray number, locations relative to the jet flame and mean droplet diameters, based on data found from previous measurements for different spray characterisation and presented in chapter 6.

The results from phase one showed that the best spray angle to be used for further investigation with this arrangement of compartment jet fire was spray angle of 150°.

7.5.1 Effects of One Spray Nozzle

Figure (7.26) shows the average temperature reduction due to water spray activation when one spray nozzle positioned at different locations inside the compartment was used for water flow rate of 72 lit/min and 150° spray angle in three different tests. The figure shows the spray located in the centre (C) was more effective in reducing the average temperature from the compartment, followed by spray located in front position (F).

In similar test, but using lower water flow rate like 18 lit/min, one spray located either in front (F) or back (B) locations, it was observed that there was not much difference in fire behaviour and temperatures during suppression as compared to the test without water spray as shown in Figures (7.27) and (7.28). However, for 90 lit/min water flow rate, it was found from Figures (7.27) and (7.28) that when the

spray in the front was used, it caused the flame to extinguish; in the other hand, the spray in the back position was not able to extinguish the flame when the same water flow rate was used. However, for lower water flow rates (less than 54 lit/min) the temperature reduction was nearly the same when either one of them was used.

7.5.2 Effects of Two Sprays Nozzles

When tests were conducted with two-spray nozzle combinations, either positioned in the front and the back (F+B), in the front and the centre (F+C) or in the centre and the back (C+B) locations which were 2 metres apart and 2.2 metres above the jet nozzle, the total water flow rate of 72 lit/minute for both sprays controlled the fire and reduced the average temperature by 200° C for the front and centre (F+C) nozzle location, which was not enough to extinguish the flame. This can be seen clearly in Figure (7.29) which also shows that the temperature for the front and the back (F+B) spray nozzle position was reduced by only 160° C.

The results of tests conducted with the jet fire placed in the middle of two nozzles, (F+B), with the total water flow rate of 90 lit/min and less for both sprays showed that this arrangement controlled but did not extinguish the flame. However, with similar water flow rate and less, such as 72 lit/min, the jet fire was extinguished by using one spray located in the centre of the compartment. On the other hand, water flow rate of 90 lit/min and greater for two spray nozzles located in the centre and front (C+F) nozzle position extinguished the jet flame. But with the same water flow rate for the other spray locations such as the back and the centre (B+C) nozzle position, this quantity of water flow rate was not able to extinguish the flame. For combinations (F+B) and (B+C), which were not able to extinguish the flame at a total of 90 lit/min, the minimum water flow rate required to extinguish the flame was found to be 108 lit/min. Figures (7.30) to (7.32) show the different temperature

profiles after water spray activation when two sprays located at different nozzle positions were used.

As discussed previously, the two nozzles system produced lower spray flux density at the center of the space where the fire was located, compared to a single nozzle located directly above the fire.

A temperature development for the compartment is shown in Figures (7.33) and (7.34). When 72 and 90 lit/min from two spray nozzles located at the front and the centre (F+C), the front and the back (F+B) and centre and the back (B+C) were activated, then the temperature dropped relatively fast in around 12 second by about 200° C, then decreased more slowly by 100° C. The fire was extinguished after about 60 seconds when two spray nozzles were located at the centre and the front (F+C) position at flow rate of 90 lit/min.

7.5.3. Effect of Three Spray Nozzles

Figure (7.35) shows the temperature profile for different water flow rates when three sprays were used. The results show that using three sprays at the same time was one of the three worst cases of spray location arrangement. It was found that the minimum water flow rates to extinguish the jet flame by using three sprays was 108 lit/min. However, in the worst case scenario of two sprays, the minimum water flow rate required for extinguishment was 108 lit/min. In the optimum case where two sprays were used the minimum water flow rate required to extinguish the jet flame was 90 lit/min. So the worst case scenario found for any spray locations arrangement was the use of two spray nozzles positioned at the back and front (B+F) or at the centre and the back (C+B) of the compartment, and the use of three sprays (F+C+B) at the same time.

7.5.4 Spray Locations, Numbers, and Water Flow Rates

One effect of the spray when extinguishment occurred was that the flames became blue, flickering about, from one part of the compartment to another before disappearing totally. The duration of this period was less than 12 seconds in experiments with small droplets sizes and high water flow rates, and up to 60 seconds with the relatively larger droplets and less water flow rates.

When different water flow rates were used for one spray located in one of the spray nozzles, either centrally, back or in front inside the compartment, it was noticed that the flame was extinguished when the nozzle positioned either in the centre or front was used, with different minimum water flow rates for each location.

From comparing these locations together it was found that using the nozzle located in the centre reduced the average temperature more than any of the other positions. However, using the front (F) nozzle reduced the temperature more than the back (B) nozzle position. The reason for that was that, when using the nozzle in the front (F) position, the spray pattern covered the external flame burning near the upper vent as well as part of the jet flame. Another reason was that the front (F) nozzle sprayed the water to the space near the opening, which created a water curtain which, in turn obstructed the air entrainment to the jet flame which was necessary for the combustion continuation. Also, the water curtain obstructed the combustion gases from leaving the compartment through the upper opening. This forced the combustion gases produced to recirculate back to the jet flame, which inerted the compartment.

It appeared that water vapour from evaporated drops was pushed towards the fuel nozzle where it displaced the oxygen and perhaps interrupted radiant feedback to the fuel flow, and the air flow to the jet flame.

The behaviour of the flame when the spray was activated for medium water flow rates and no extinguishment occurred, was that no flame was seen above the jet

nozzle; but the fire, which was burning at the top of ceiling as shown in plate (7.3), then engulfed the entire compartment from inside, disappeared for 3 seconds and then re-ignited.

There was appreciable change in visible mean flame height upon activation of the spray for tests with water flow rates higher than 36 lit/min.

From the tests series in phase I and II, the main result found was that for similar water flow rate and when using one spray in any location, the test with one spray located centrally gave the overall best result of temperature reduction. Also, the one in the back (B) will be the worst location to be used due to its being farthest from the vent. However, the test with one spray in the front gave reasonable temperature reduction .

A minimum water flow rate of 72 lit/min using one spray nozzle located centrally above the jet nozzle with spray angle of 150° was found to extinguish a 4.5 MW jet fire in this type of arrangement in 12 sec.

However, the minimum water flow rate required for jet fire extinction with multiple spray nozzles resulting from phase II tests was found in COMP73 which was 90 lit/min, with only 2 nozzles activated at front and centre (F+C) locations. When the same experiment arrangement with the same water flow rate but different spray nozzle locations (back and centre (B+C) and front and back (F+B)) was tested in COMP60 and COMP64, extinguishment was not obtained. The time of extinguishment for COMP73 was found to be in the order of 60 seconds.

Table (7.1) summarises the combination of tests variables used and indicates whether extinguishment occurred or not. The fire was either extinguished by the water from the spray (E), continued to burn (N) or was controlled to 600°C or less (c).

Table (7.2). Effectiveness of different spray numbers and locations and water flow rates in extinguishing or controlling jet fire- 'E' indicates extinguished, 'N' not extinguished, 'c' indicates temperature was controlled to 600°C or less and 'N/A' not applicable.

Water flow rates for each spray (lit/min)	Spray Numbers and Locations						
	One spray			Two sprays			Three Spray
	C	F	B	F+C	C+B	F+B	C+F+B
90	E	E	N	E	E	E	E
72	E	E	N	E	E	E	E
54	c	N	N	E	E	E	E
45	N/A	N/A	N/A	E	c	c	N/A
36	c	N	N	c	N	N	E
18	N	N	N	N	N	N	N

C: The spray nozzle positioned at the centre of the compartment
F: The spray nozzle positioned at the front of the compartment
B: The spray nozzle positioned at the back of the compartment

7.5.5 Combustion Gases

Examination of the resulting trends of gases concentrations shows that the minimum oxygen measured was found before water spray was turned on . This can be seen very clearly in Figure (7.36). The oxygen concentration in the out-flowing gases at the upper part vent rose from 4% in test COMP29 to about 13% indicating that the

combustion had become fuel-controlled. Figures (7.37) and (7.38) show carbon monoxide and carbon dioxide concentrations. These figures show that the jet fire had decreased the carbon dioxide concentration after the activation of the water spray from 14% to about 5%, and decreased the carbon monoxide to about 0.62 %. When the water flow rate was insufficient for extinguishment the oxygen concentration increased for the first 30 second and then the jet fire started to stabilise and to consume the oxygen available in the compartment and produced carbon dioxide as shown in Figure (7.39).

7.5.6 Compartment Surfaces Temperature

Temperature of the compartment surfaces from Figure (7.40) showed that it was difficult to reduce the temperature from 18 lit/min water flow rate during the extinguishing time. The reduction of the temperature required more time than the ten minutes extinguishing time as in COMP1 in order to reduce the temperature below the re-ignition temperature inside compartment and to avoid re-ignition in case of extinguishment occurrence. Maximum temperature reduction in this test was 50°C in the roof and 100°C in the other sidewalls.

In test with higher water flow rates, when the water flow rate was insufficient for fire extinguishment, the surface temperature was reduced by average of 150°C on the ceiling and 250°C on the side walls when 72 lit/min in COMP57 was used, and reduced by 50° C and 100° C in the roof and side walls respectively when 54 lit/min in COMP71 was used as shown in Figures (7.41) and (7.42). However, when the water flow rate was sufficient for extinguishment as in COMP4, which uses 72 lit/min, there was no temperature reduction in the compartment surfaces as shown in Figure (7.43).

The spray angle affected the surfaces temperature reduction. The larger the spray angle, the more the temperature was reduced, because the larger spray angle had large coverage area in which the water drops hit a bigger area of the walls. Also, smaller drops were produced from a larger spray angle for similar water flow rate than from smaller spray angle, and this enhanced the rapid evaporation of the drops and the cooling of the compartment. The comparison in the surfaces temperatures reduction of a jet fire with one spray nozzle located centrally (C) having spray angles of 60 and 150° is shown in Figure (7.44).

7.6 DISCUSSION

The fire in the compartment showed two different results, depending on the characteristics of the spray. The first 60 seconds of the spray action was very critical regarding extinguishment or not. The water spray acted on the flames from the propane nozzle by deflecting and shortening them, and the evaporated water entered the combustion zone. In the first critical phase there was a fight between the flames and the spray, where the flames became bluish and were replaced by steam. The flames may however survive in other parts of the enclosure, even burn at the outlet opening only. If the spray has an efficiency to remove the flames at the centreline of the jet nozzle for more than 10 seconds, there is a good chance of permanent extinguishment of the fire. If not, the flames re-enter the compartment and more or less stabilise, influenced only by the flow induced by the spray. The fire is now controlled, but not extinguished.

Extinguishment of flames take place when the conditions in the flaming zone of a fire reach a critical combination of temperature and mixture of oxygen, the so-called inert condition. To extinguish a gas fire it is normally sufficient to keep the critical combination for a very short time, and/or one may denote this as instantaneous

extinguishment. If the fuel can be isolated from all ignition sources after instantaneous extinguishment, permanent extinguishment is obtained.
Therefore, the fire was considered permanently extinguished when no re-ignition in the compartment occurred within 20 seconds.

So, inerting of a whole compartment requires that the conditions of the total enclosure reach the critical combination. The principle of inerting the whole compartment is to keep the atmosphere of the enclosed space at inert condition as long as the risk of re-ignition exists.
However, because extinction is not the only measure for the success of suppression on arbitrary control criteria, the fire was deemed to be under control when both a) the average temperature at thermocouples strings was reduced to reach 600°C and surface temperatures decreased by 200°C, and b) the flame length in any direction decreased permanently below the ceiling and there was no external flame. The flame length was determined from the visual observation.
In practical terms all the tests with medium water flow rates such as 36 lit/min (at 150° spray angle) or higher at smaller spray angles can be regarded as controlled because the fire was always limited to the fuel nozzle and the temperature of the surrounding structure was generally reasonable, which posed no danger of destroying the surrounding structures.
It was noticed that the water flow rate required for temperature reduction for controlling the jet fire changed with the different conditions used (i.e. spray angle and droplets diameters). When the spray angle of the nozzle changed, the droplets diameters changed, hence the water flow rate required had to be changed to meet the new condition. Figure (7.45) shows the temperature reduction effect for the different water flow rate recommended for controlling the jet fire in the compartment. It can be seen that the reduction in temperature for the different conditions is almost the same. The water flow rate required for controlling the fire for different conditions is increasing as the spray angle decreases, starting as minimum as 36 lit/min when 150°

spray angle was used and ending at 90 lit/min water flow rate when 60° spray angle was used.

Figure (7.45) suggests that the amount of cooling due to vaporisation of the entrained water droplets, and subsequent dilution due to the addition of water vapor, was not sufficient to cause significant changes in the flame temperature and hence extinguishement, but was enough to control the fire.

Figure (7.46) shows the temperature profile after the spray activation for the optimum combination of the spray characterisation for a total of 72 lit/minute water flow rate, 150° spray angle and the optimum spray number and locations arrangement which was found previously for each arrangement. The result showed that using the one spray located in the centre of the compartment gave the overall best results from the point of maximum temperature reduction with the lowest water flow rate.

A more efficient spray may then be one with larger proportion of smaller droplets. With this in mind, the optimum drop size ($D_{v\,0.5}$) is found in Figures (7.25b) to (7.35) to extinguish a compartment jet fire which was 295 μm (SMD=190 μm). This was based on the cooling effect which increased as the water flow rate and spray angle increased, hence the droplets size was reduced.

Finally, the water flow rate 72 lit/min delivered from the spray nozzle located in the centre of the ceiling was found in this study as the optimum to extinguish the jet fire issued from the centre of the compartment floor. But when the jet nozzle location changes, this optimum will not be useful for extinguishing the fire in the new jet position. From this, one can conclude that this optimum water flow rate can be used to determine the water flow rate required to extinguish the fire from any jet nozzle location. Therefore, all the water spray nozzles should be activated, with water flow rate for each of them similar to the optimum found earlier, hence the resulting total water flow rate required to extinguish the jet fire, irrespective of the location of the fire nozzle, is 216 lit/min. As the protection requirements are usually stated in terms

of water discharge density and total area of demand or total water volume needed over a time period the water flow rate required is 15 lit/min/m^2.

7.7 CONCLUSIONS

The heat produced by the fire ended up partly in the compartment itself and was partly being transported to the surroundings. The time to heat the compartment walls and ceiling to steady state temperature where almost all the heat transported into the compartment was convected to the surroundings was 5 minutes. So the pre-burn time of the fire before water was applied was chosen to be 5 minutes, to assure equal initial conditions in every experiment.

One main part of the heat lost was leaving the compartment as hot combustion gases through the outlet opening. The other part of the heat lost was to the walls and the ceiling, and then a fraction to the floor.

The water spray tests were planned to find the limit for extinguishment for one, two or three nozzles producing different droplet sizes. To characterise the spray action in a situation without extinguishment, several tests with low water flow rate were studied as well. Before water spray was activated the large fire almost filled the compartment. Each experiment was terminated when extinguishment due to the water spray activation or steady state non-extinguishment occurred.

Experiments were conducted at different water flow rates, using different spray nozzles, to determine if water flow rate had an effect on extinguishment. Each nozzle was tested with increasing pressure, which led to higher water flow rate and lesser mean droplet diameter. The results of the flow rate experiments showed a slight decrease in the time to extinguish the fires when the water flow rate increased, in the cases when the water flow rates were able to extinguish the flame.

It became apparent early in the experimental programme that the amount of water necessary for extinguishment varied greatly with the types of spray.

The use of 72 lit/min was found to produce the best overall results in terms of water usage for extinguishment. A further increase in application rates produced a significantly higher water usage with negligible decrease in extinguishment time. An application rate of 36 lit/min with spray angle of 150° proved to be the most effective in terms of minimum water usage for control of fire.

The varying of spray patterns produced significant differences in the results. However, that of 150° spray angle gave the best overall performance. This is probably due to the generation of a larger number of smaller droplets at higher flow rate.

Comparing the different spray angle tests has shown that increasing the spray angle will reduce more temperature.

The water droplets follow the air flow pattern in the vicinity of the fire. To extinguish a fire, the water droplets have to reach the flame zone by supplying it with the air going to the flame.

The presence of droplets increases the total amount of water present in the plume, and the local distribution of water vapor within the plume is expected to influence the flame chemistry. The temperature decrease is due to evaporative cooling from water droplets.

Generally, for two sprays nozzle system, the highest temperature reduction was found when the nozzle was located in the front and the centre (F+C) positions. Then the next temperature reduction occurred with the sprays located in the centre and back (C+B) and in the front and back (F+B). However, for the same water flow rate, the overall optimum arrangement to be used for any combination was found to be one spray nozzle located centrally.

These experiments showed that it is possible to extinguish fires in compartment without direct hit, but with higher water flow rate as compared to direct hit, provided that the fire and the spray create sufficiently effective mixing of water droplets with the flames.

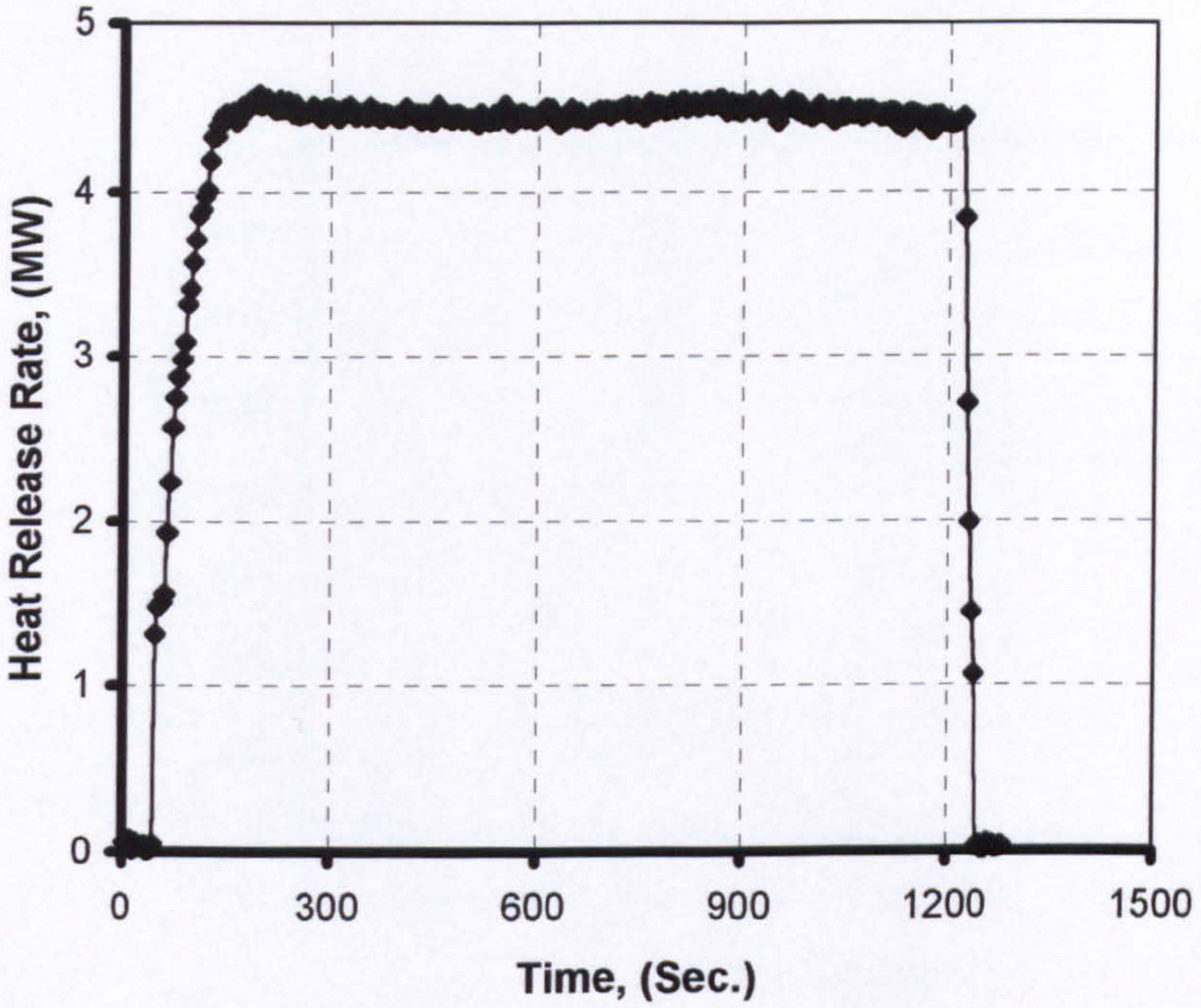

Figure (7.1). Heat release rate based on the measured fuel consumption.

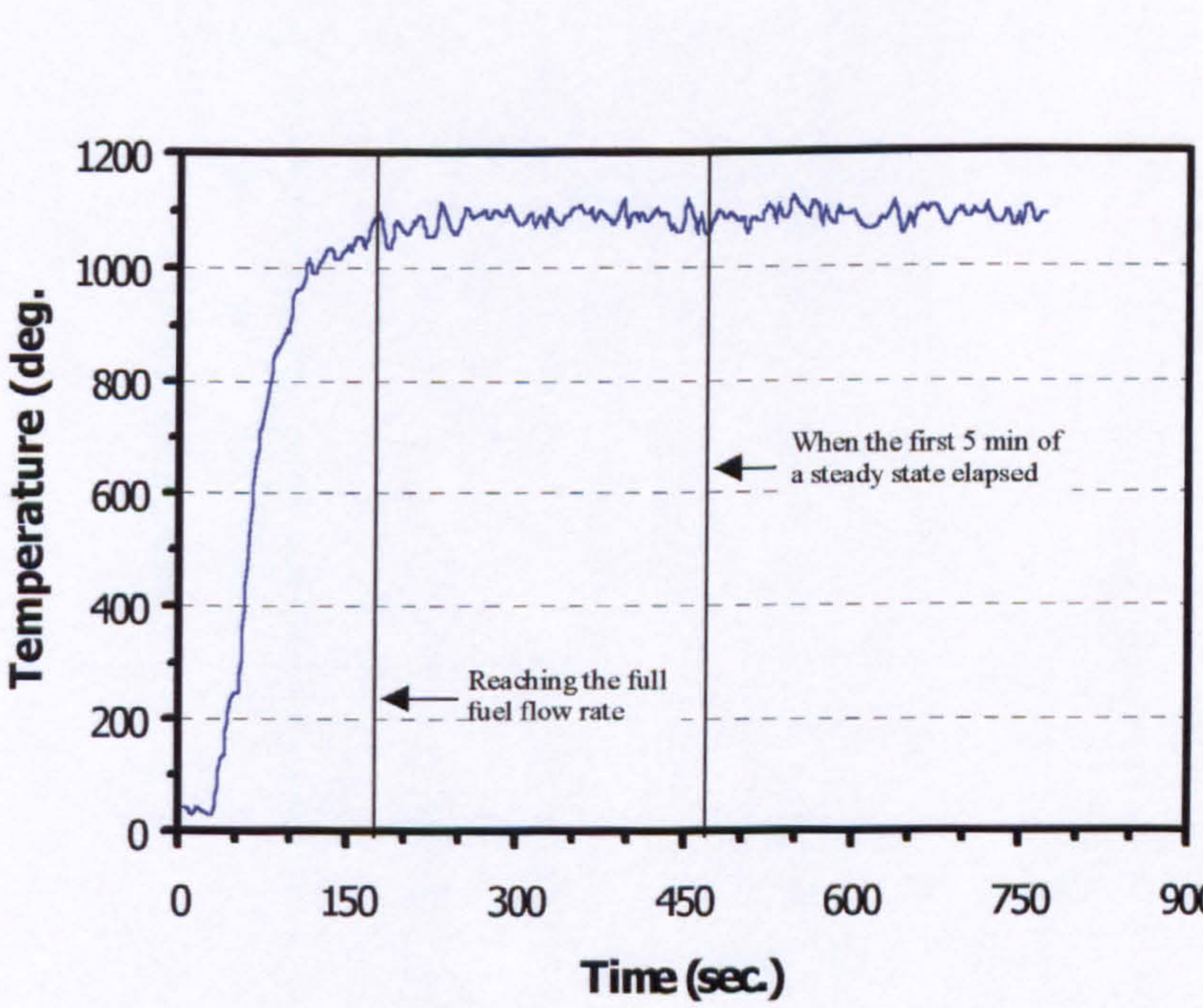

Figure (7.2). Temperature profile to show the pre-burn time for ASP-1 (COMP1).

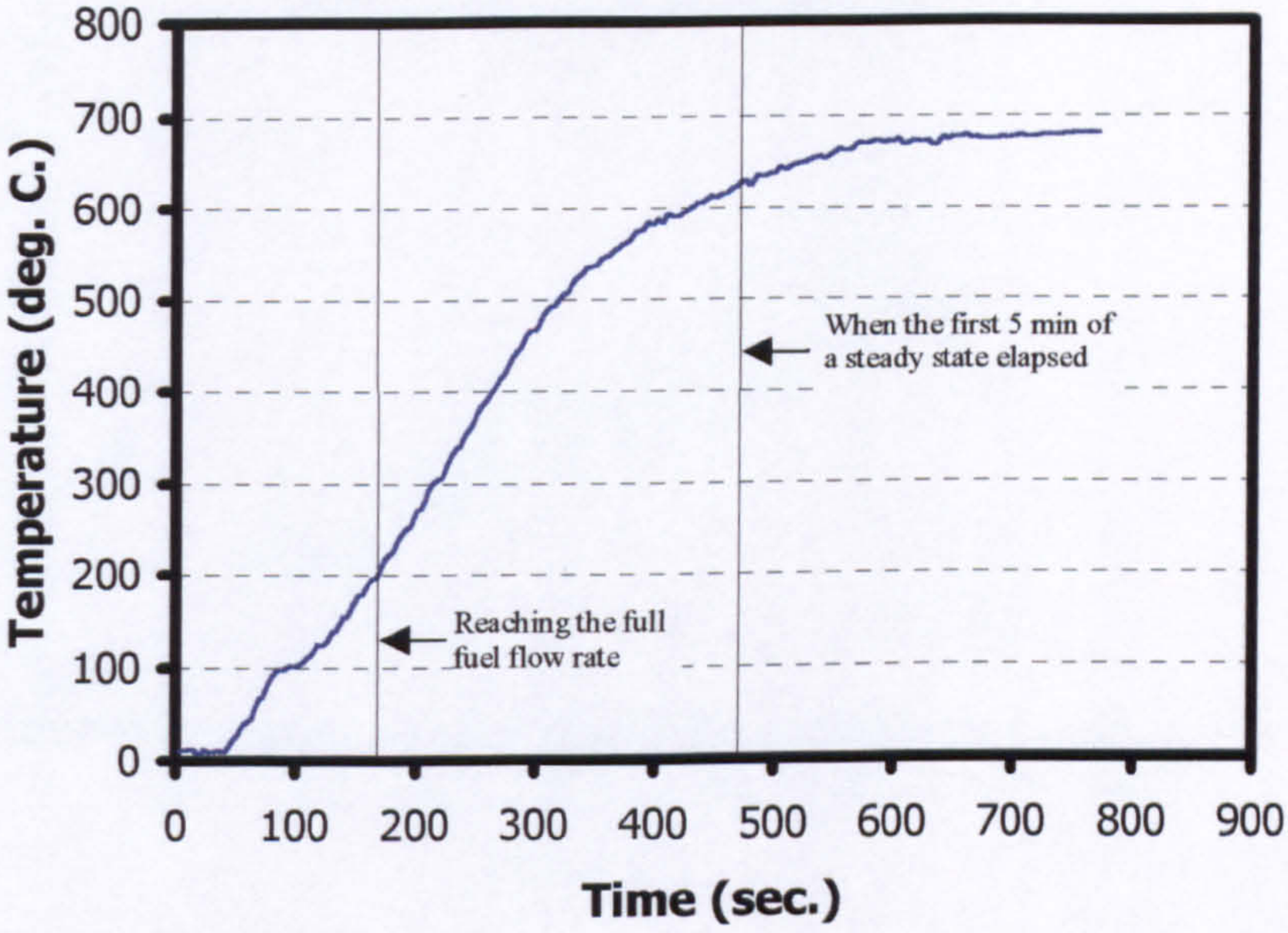

Figure (7.3). Temperature profile to show the pre-burn time for WAL-2 (COMP1).

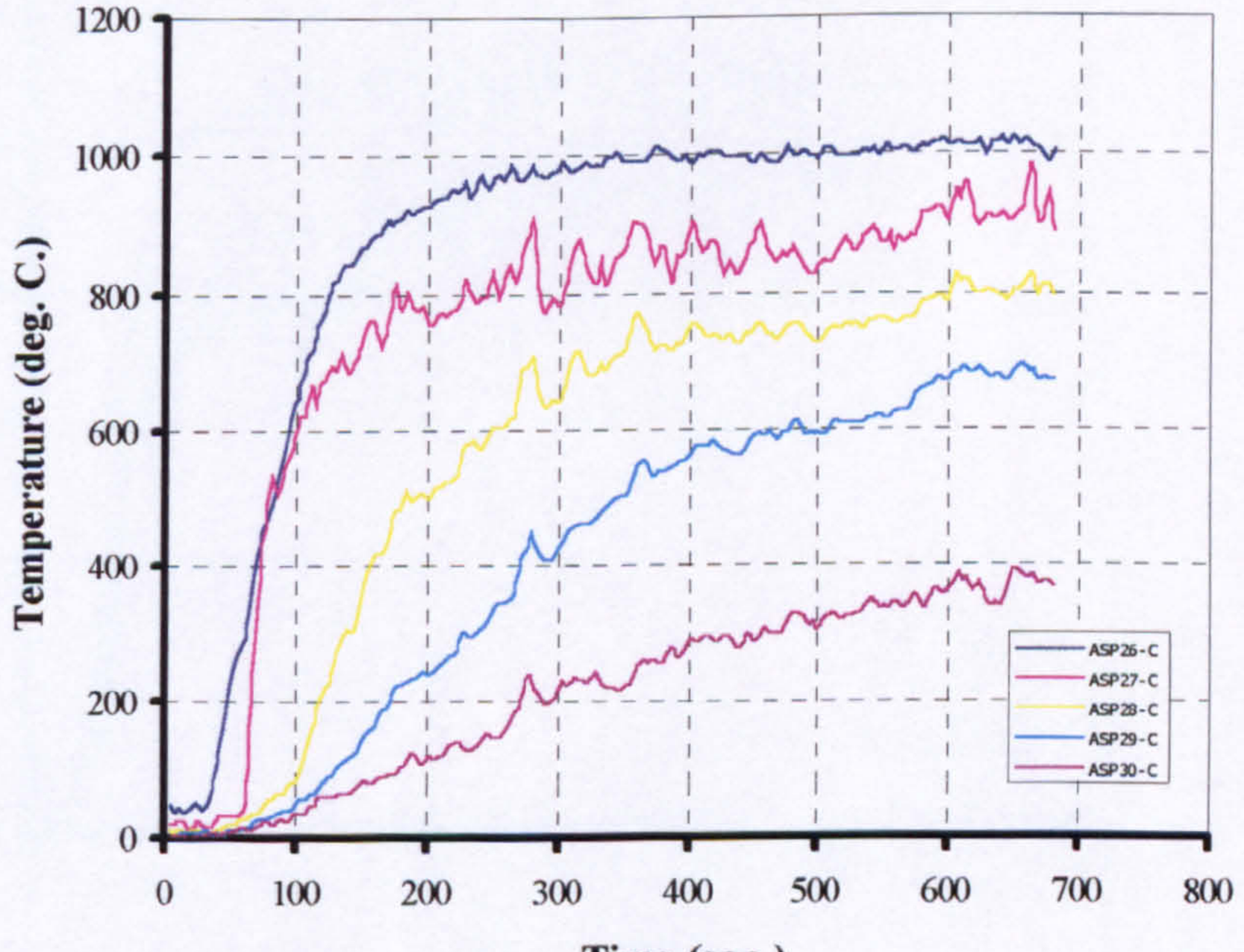

Figure (7.4). Temperature development in the Northeast string for different thermocouples.

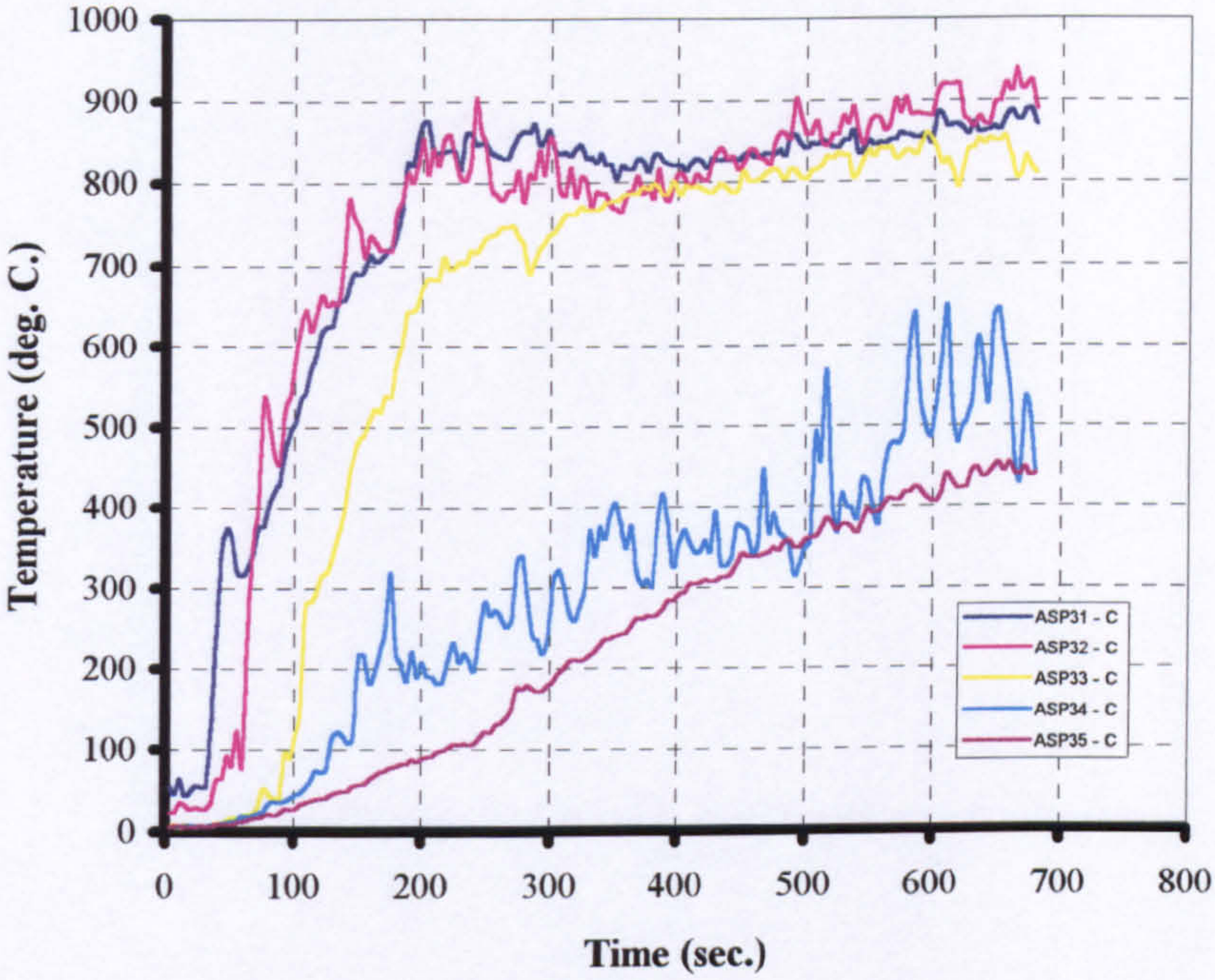

Figure (7.5). Temperature development in the Southeast string for different thermocouples.

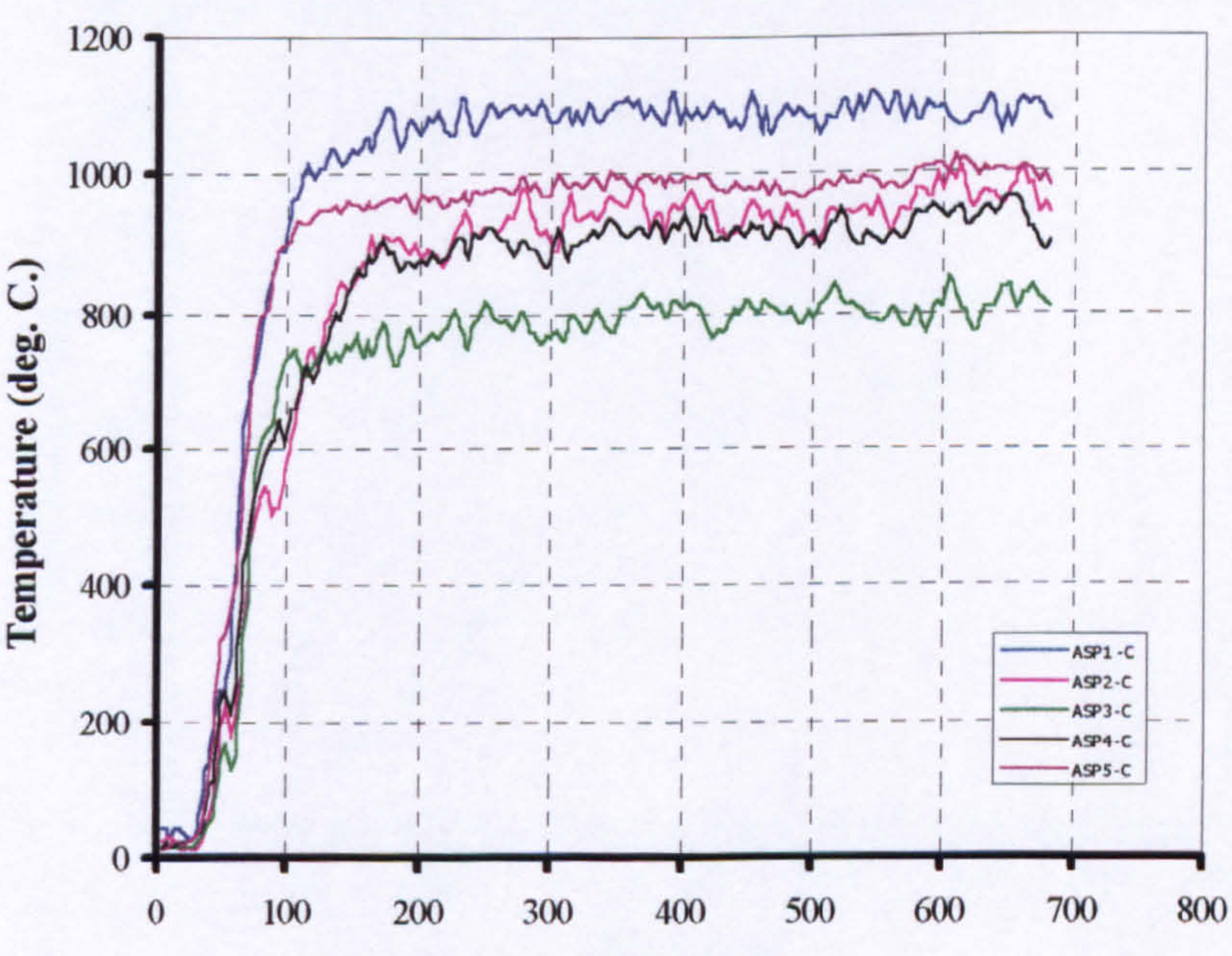

Figure (7.6). Temperature development in the outlet opening for different thermocouples.

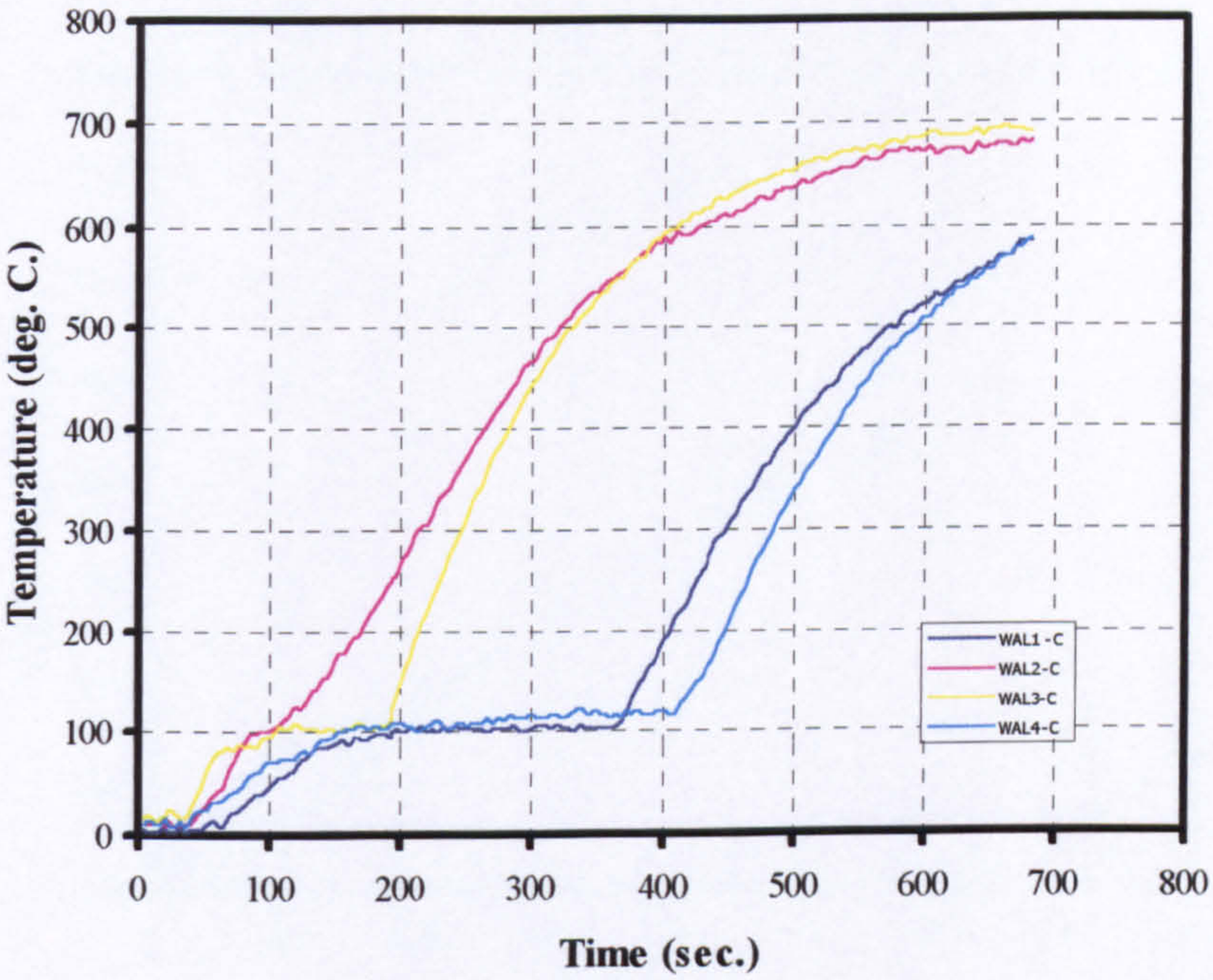

Figure (7.7). Temperature development in the ceiling for different thermocouples.

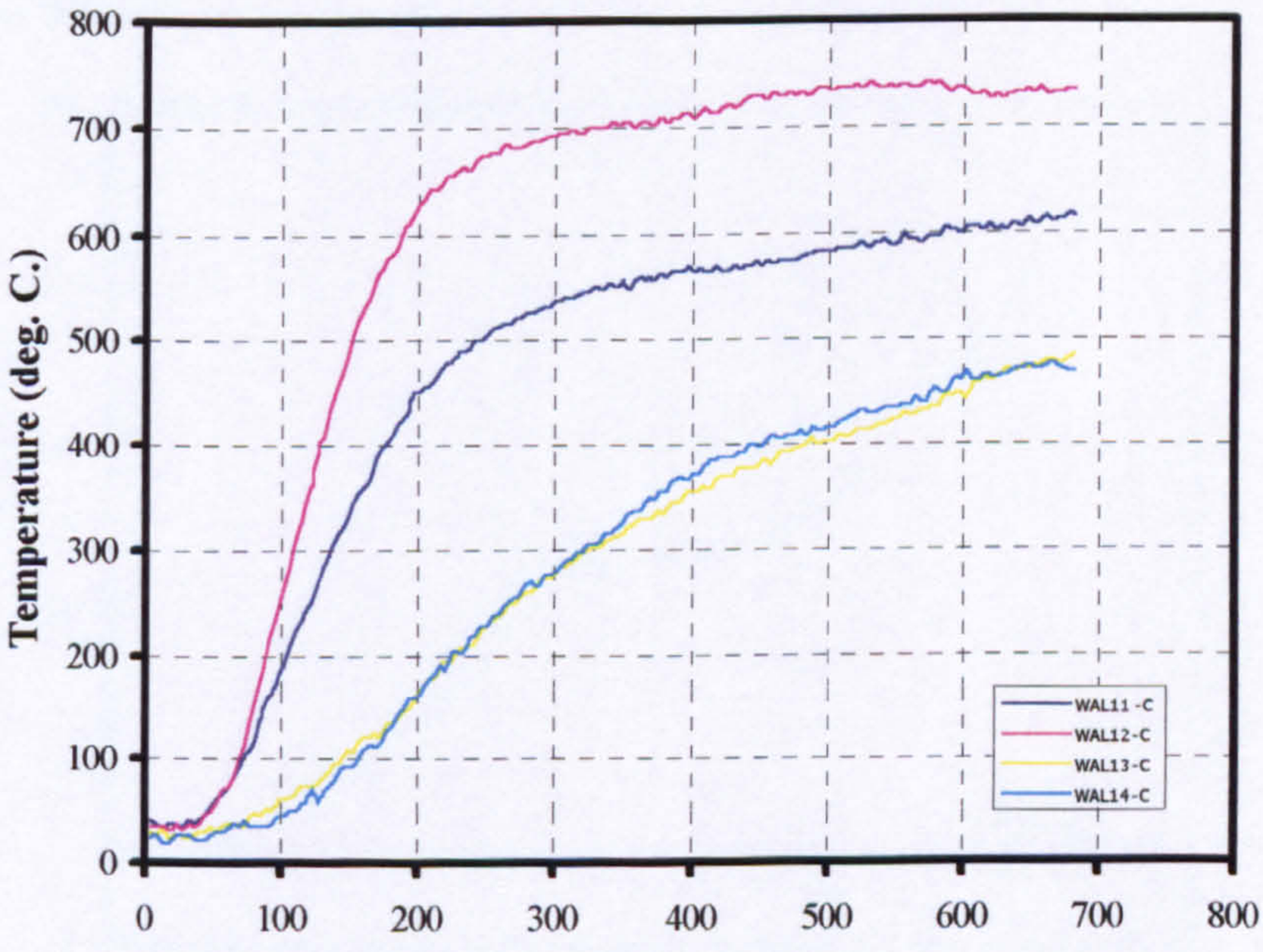

Figure (7.8). Temperature development in the Southeast wall for different thermocouples.

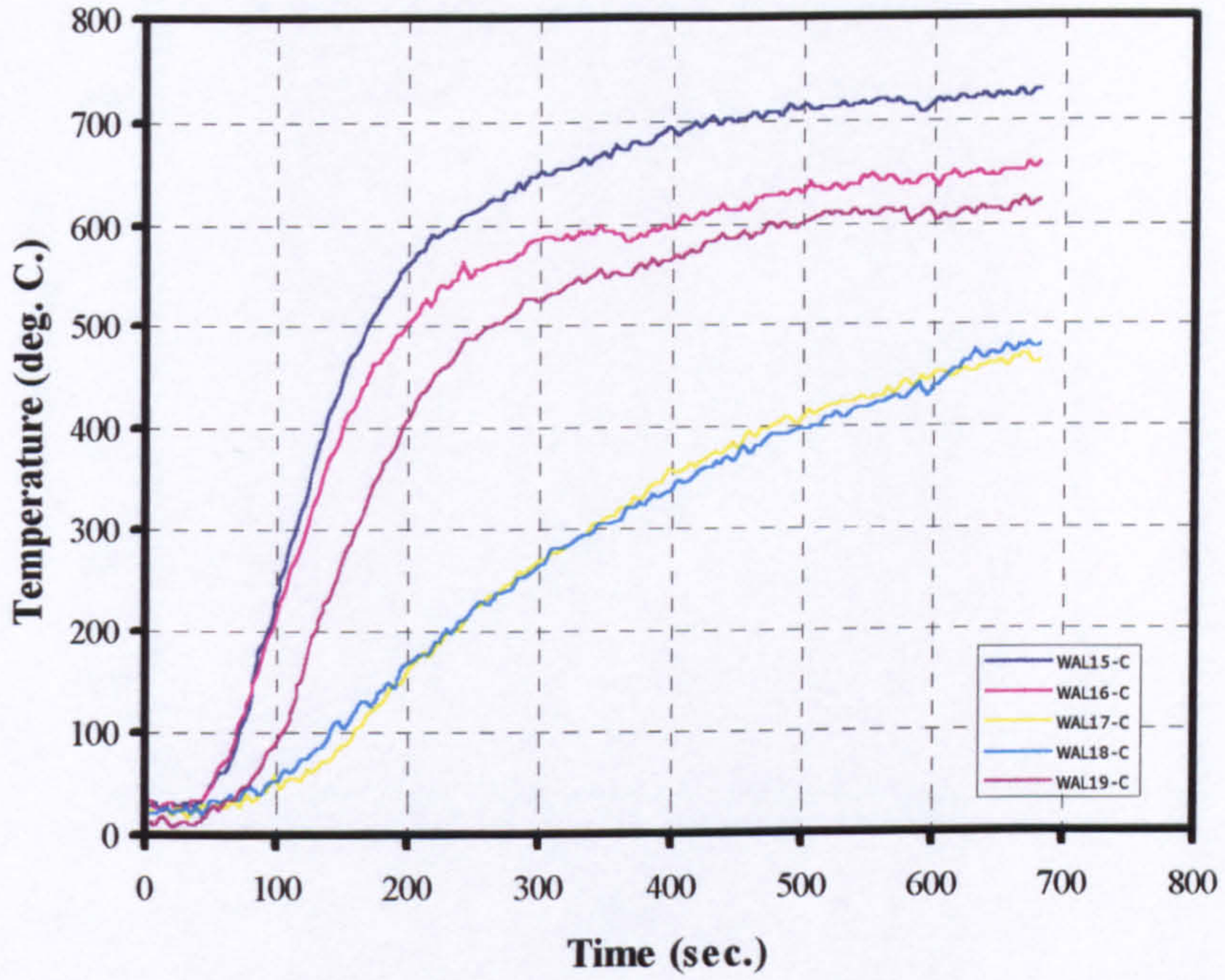

Figure (7.9). Temperature development in the Northwest wall for different thermocouples.

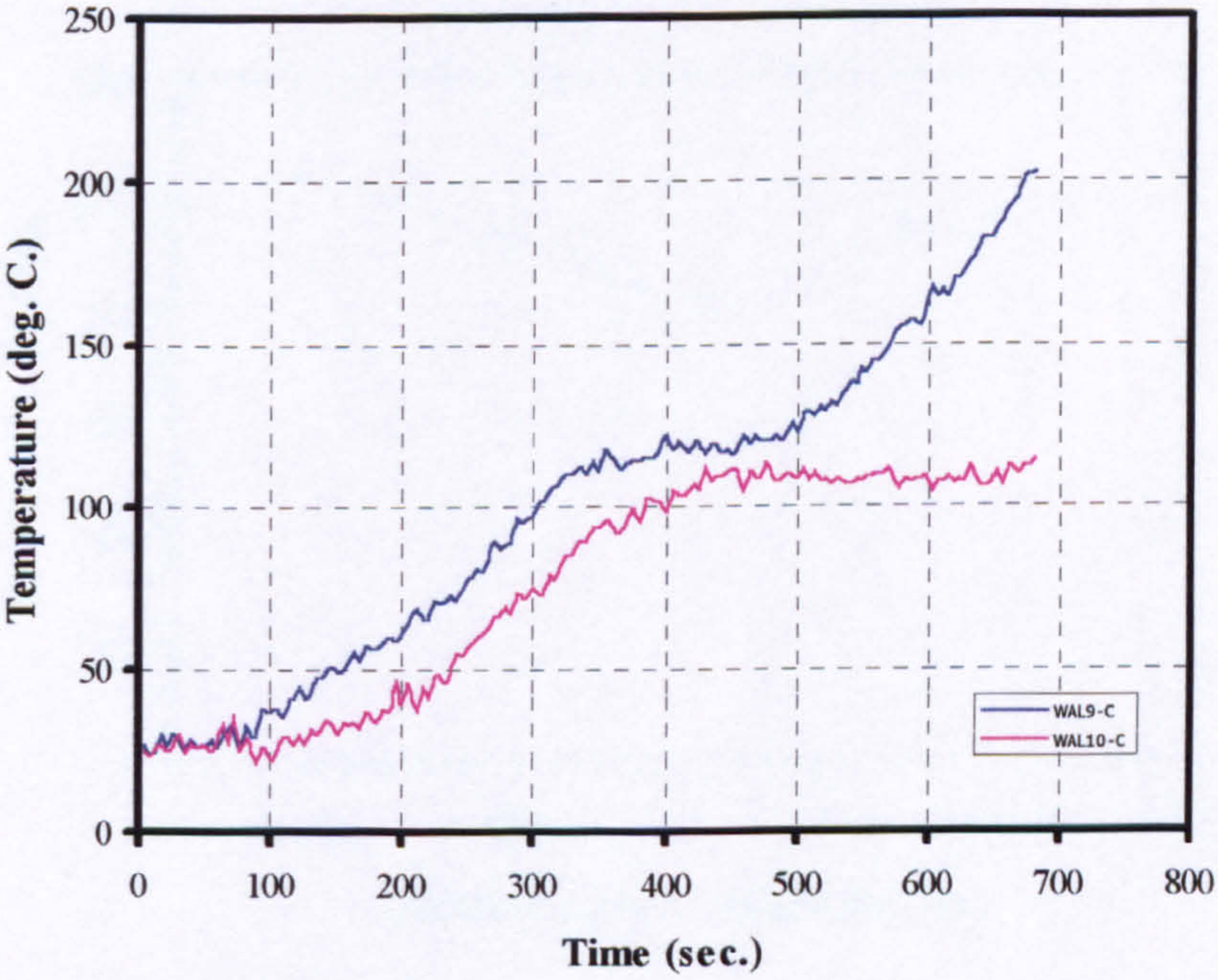

Figure (7.10). Temperature development in the floor for different thermocouples.

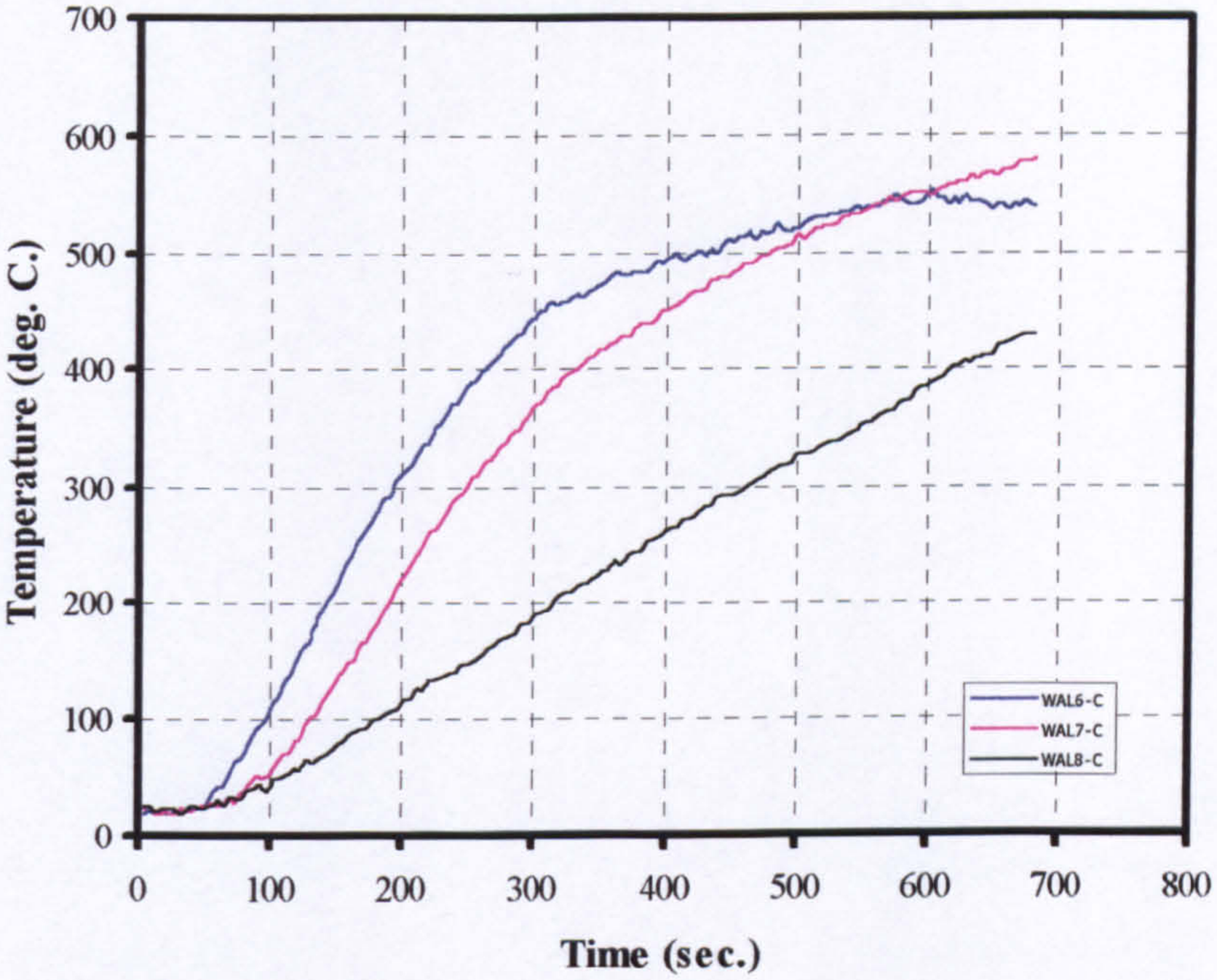

Figure (7.11). Temperature development in the back wall for different thermocouples.

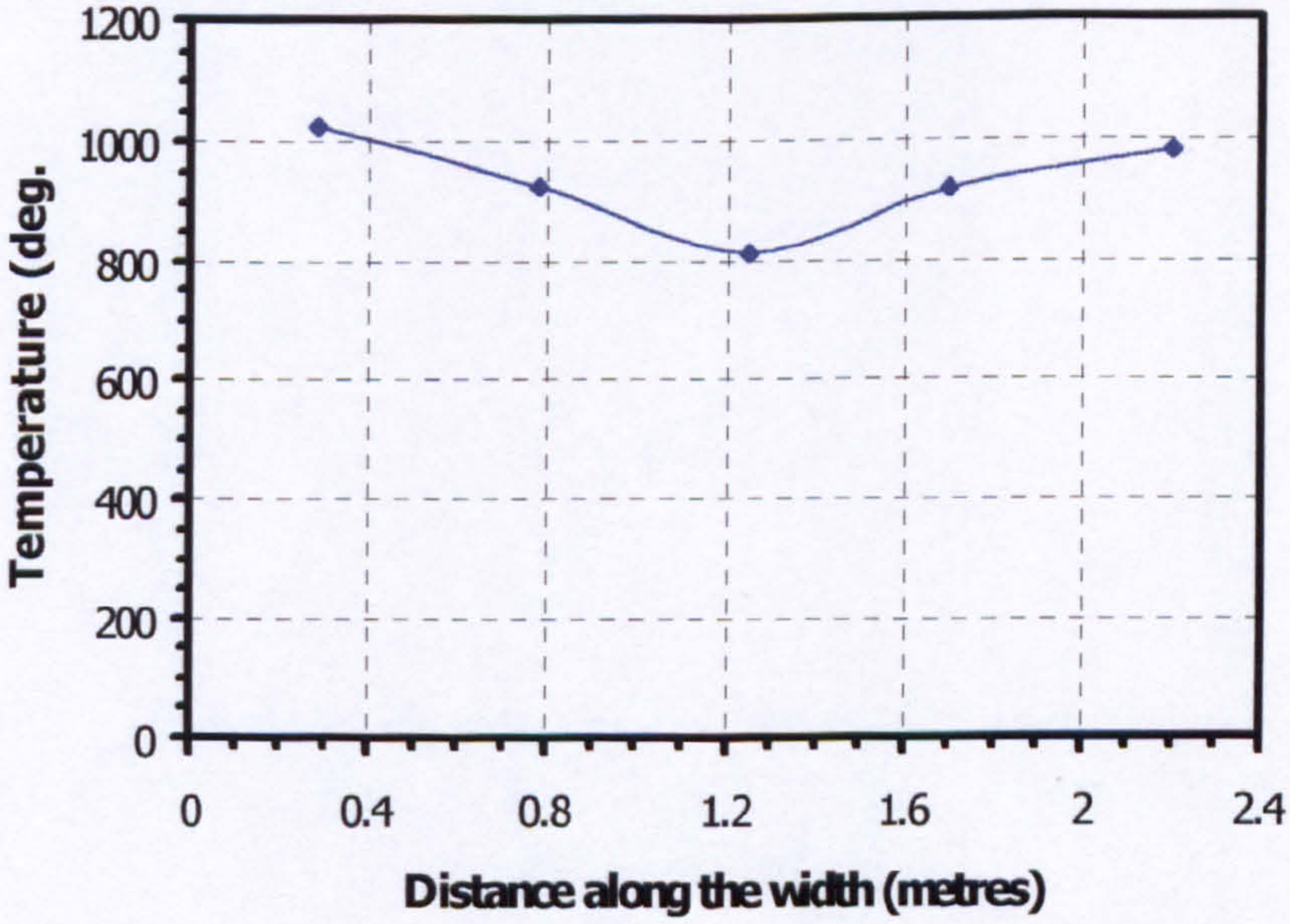

Figure (7.12). Temperature distribution at the upper vent of the compartment (COMP1).

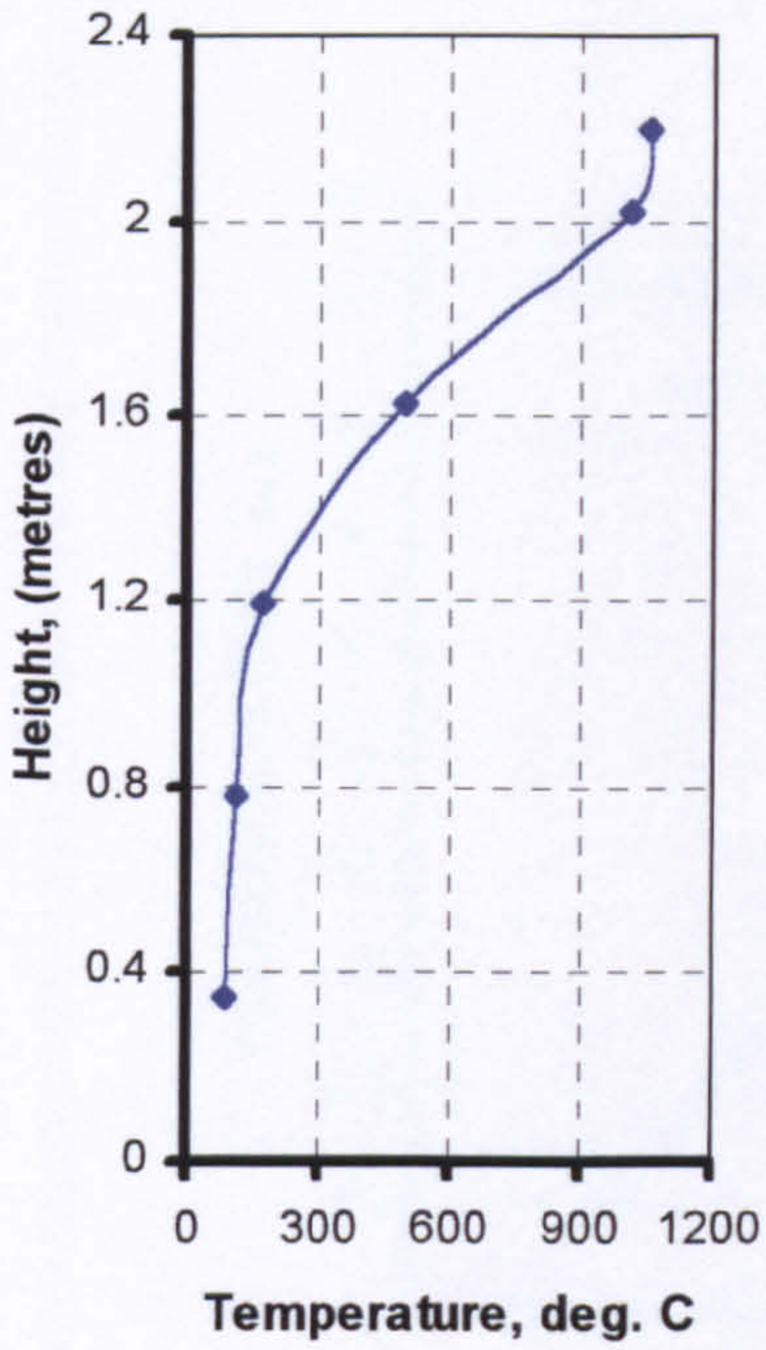

(At the opening East corner)

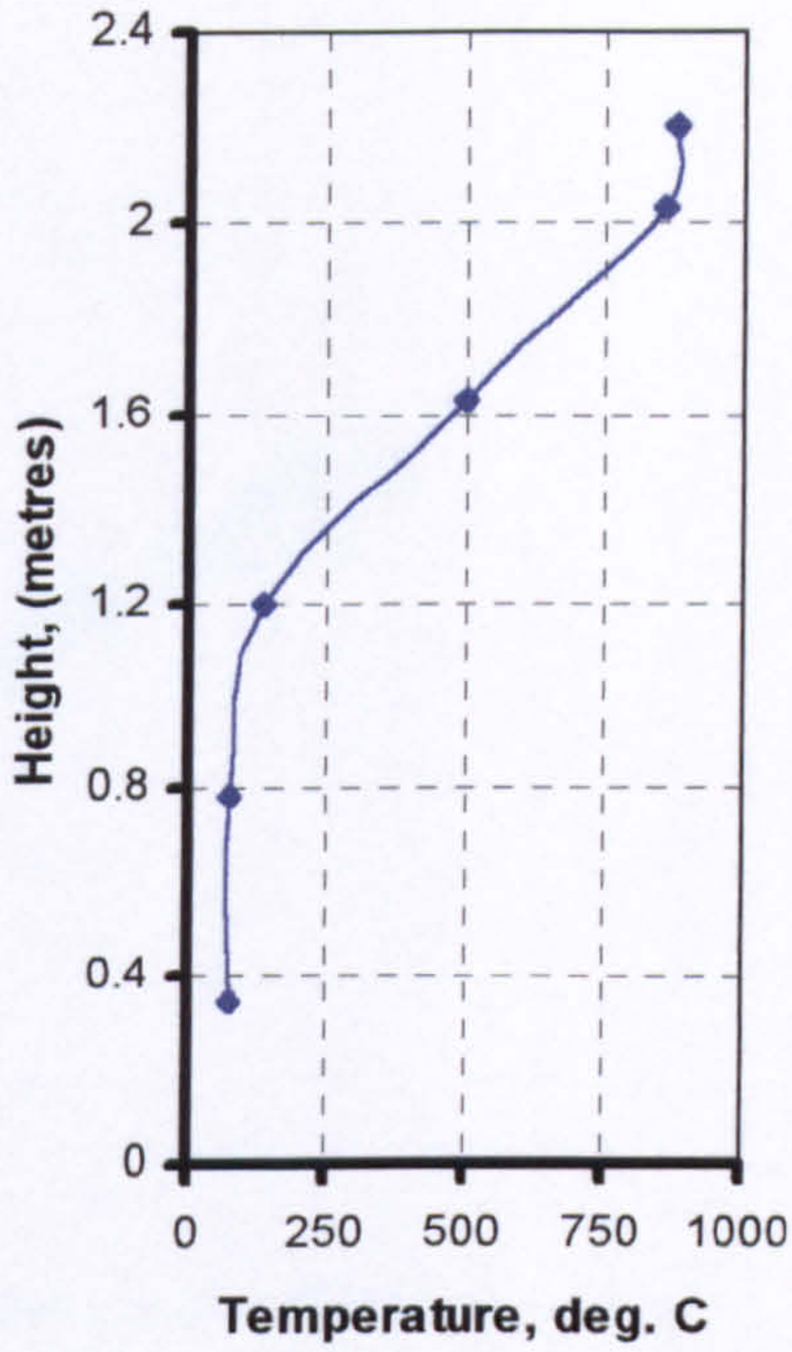

(At the opening centreline)

Figure (7.13). Gas temperature profile at the opening of the compartment.

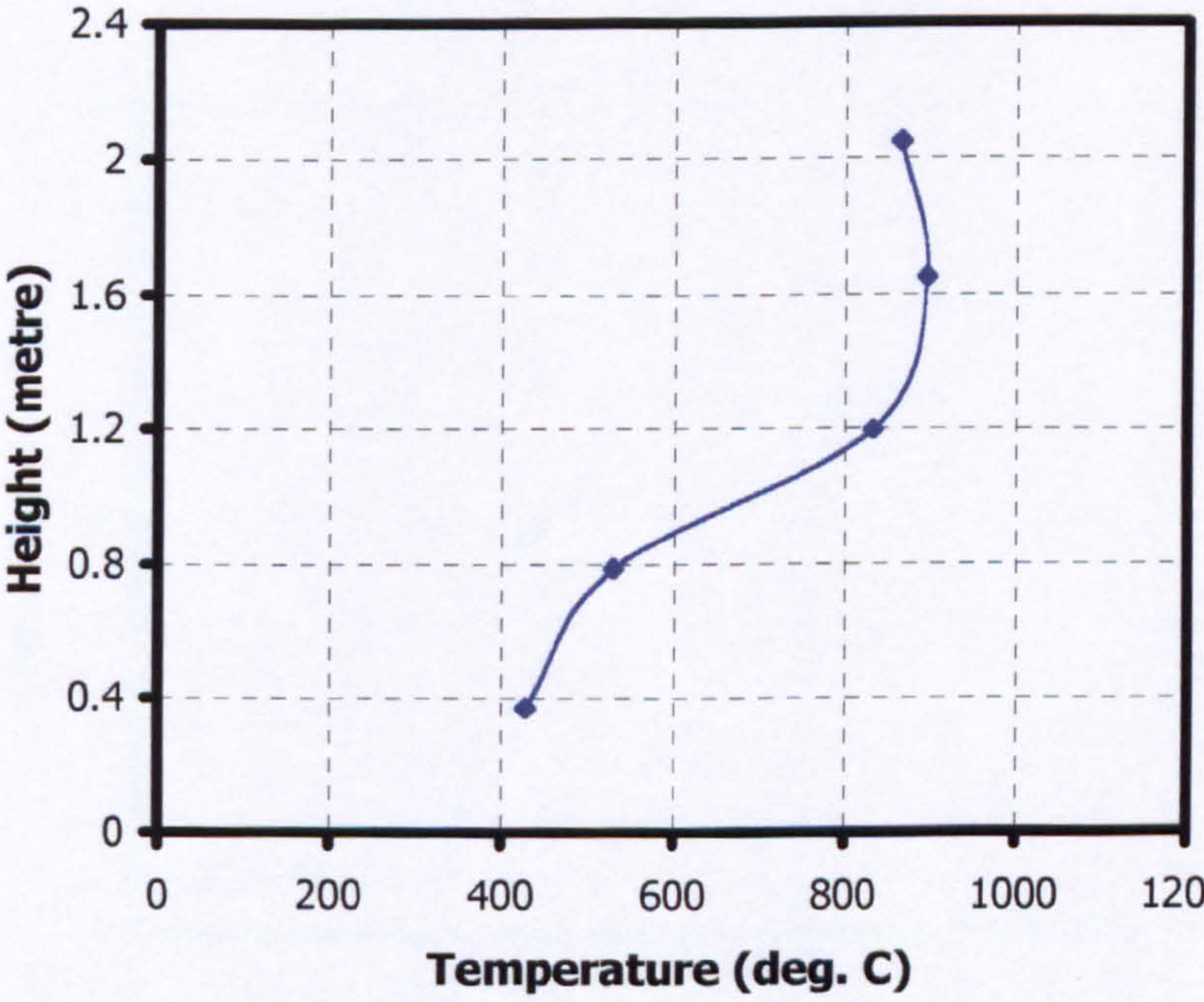

Figure (7.14). Gas temperature profile at the Southwest string inside the compartment (COMP1).

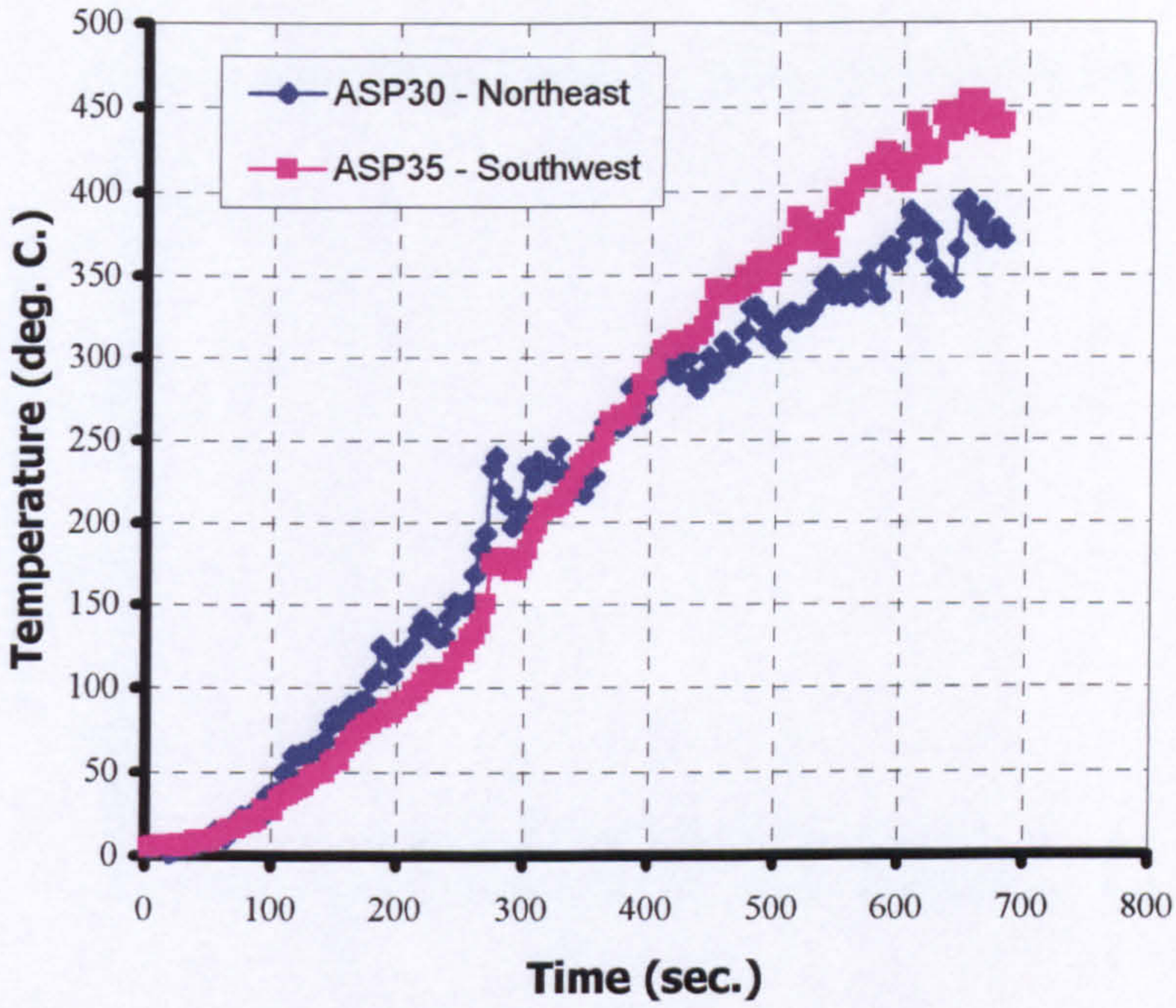

Figure (7.15). Gas temperature comparison for two thermocouples at the Southwest and Northeast string inside the lower part of the compartment (COMP1).

Figure (7.16). Carbon monoxide concentration for steady state (COMP64C).

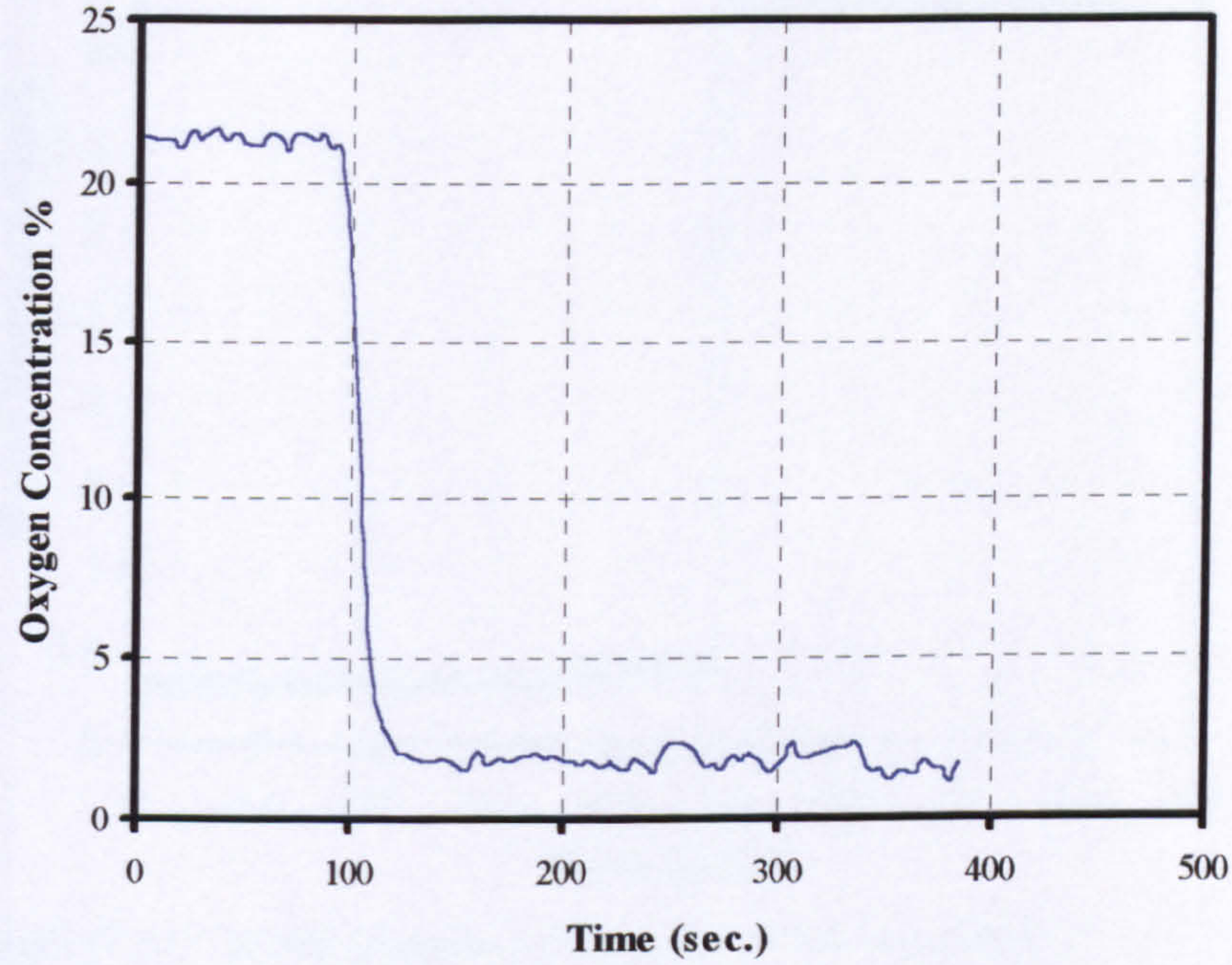

Figure (7.17). Oxygen Concentration for steady state (COMP64C).

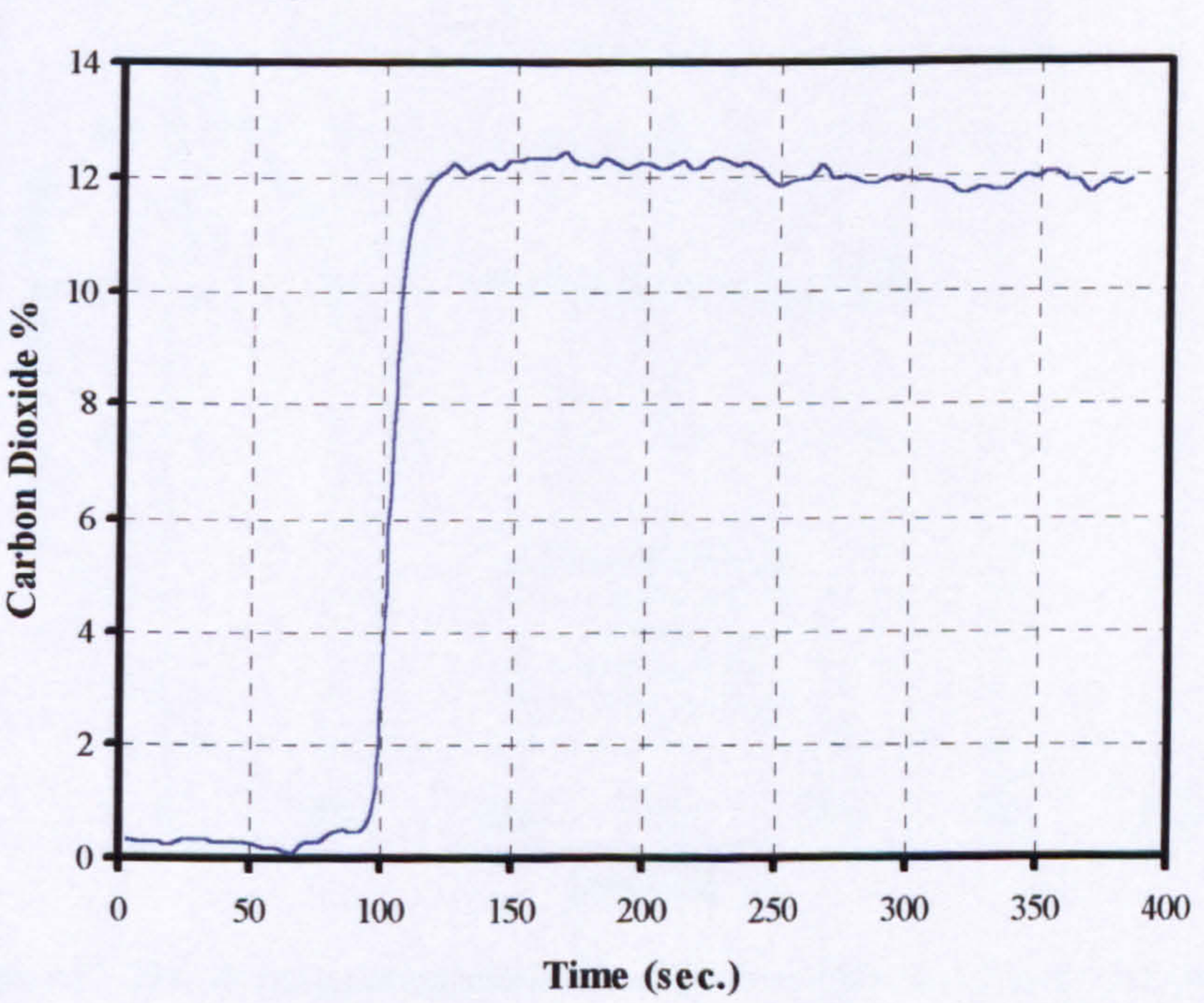

Figure (7.18). Carbon dioxide concentration for steady state (COMP64C).

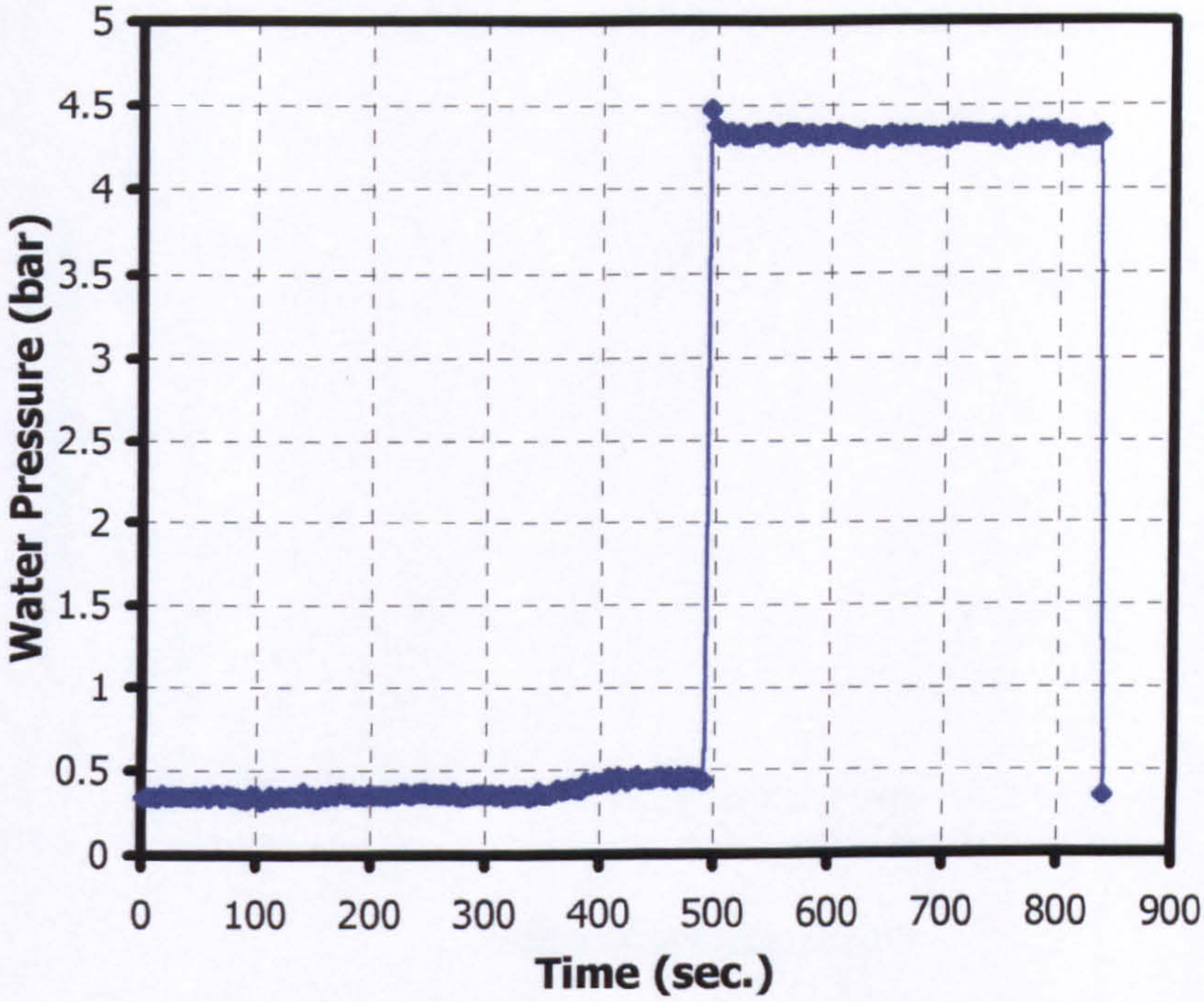

Figure (7.19). Water pressure profile at one of the experiments.

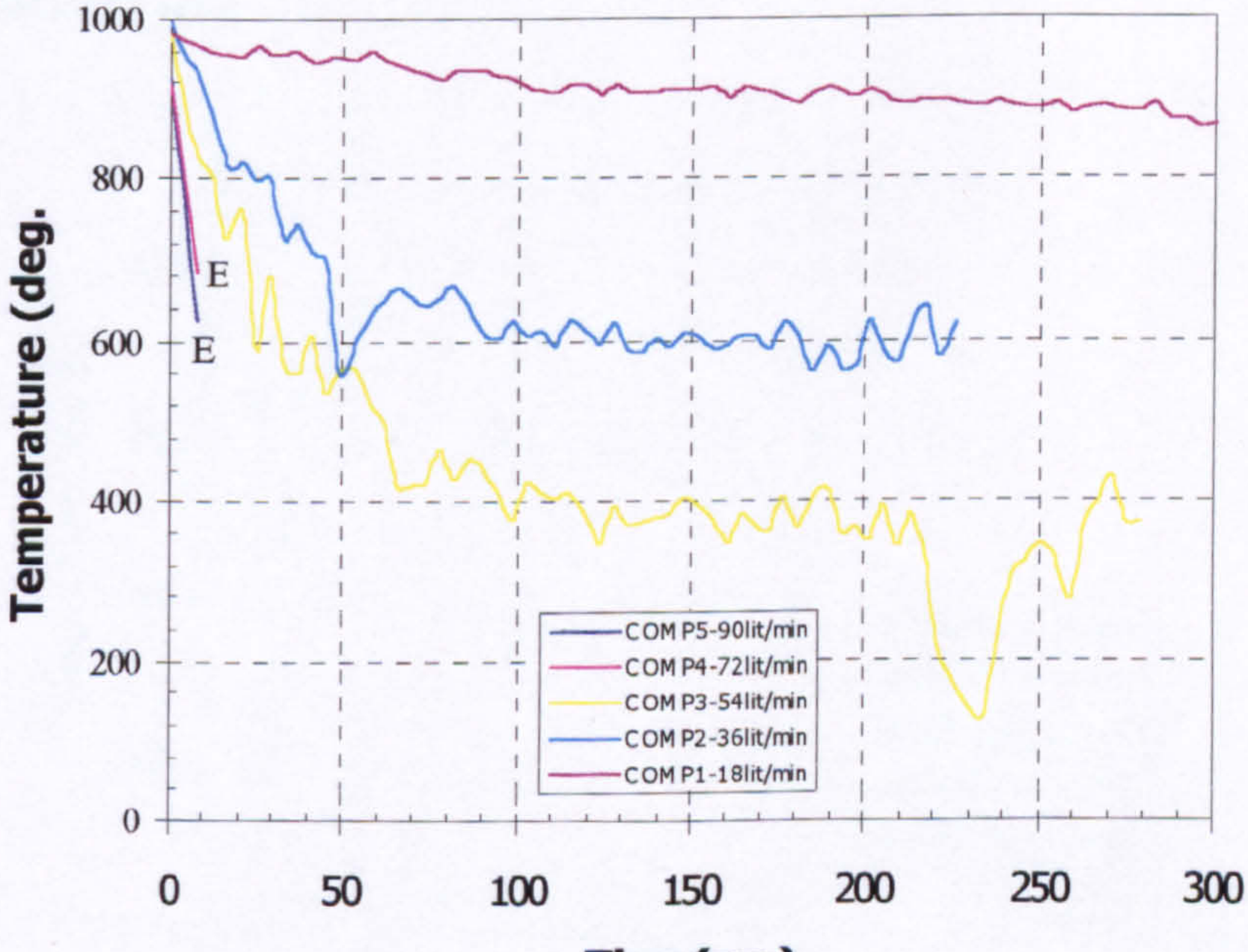

Figure (7.20). Average temperature development after water spray activation for different water flow rates at 150° spray angle for one spray located at the centre of the compartment (E = extinguished).

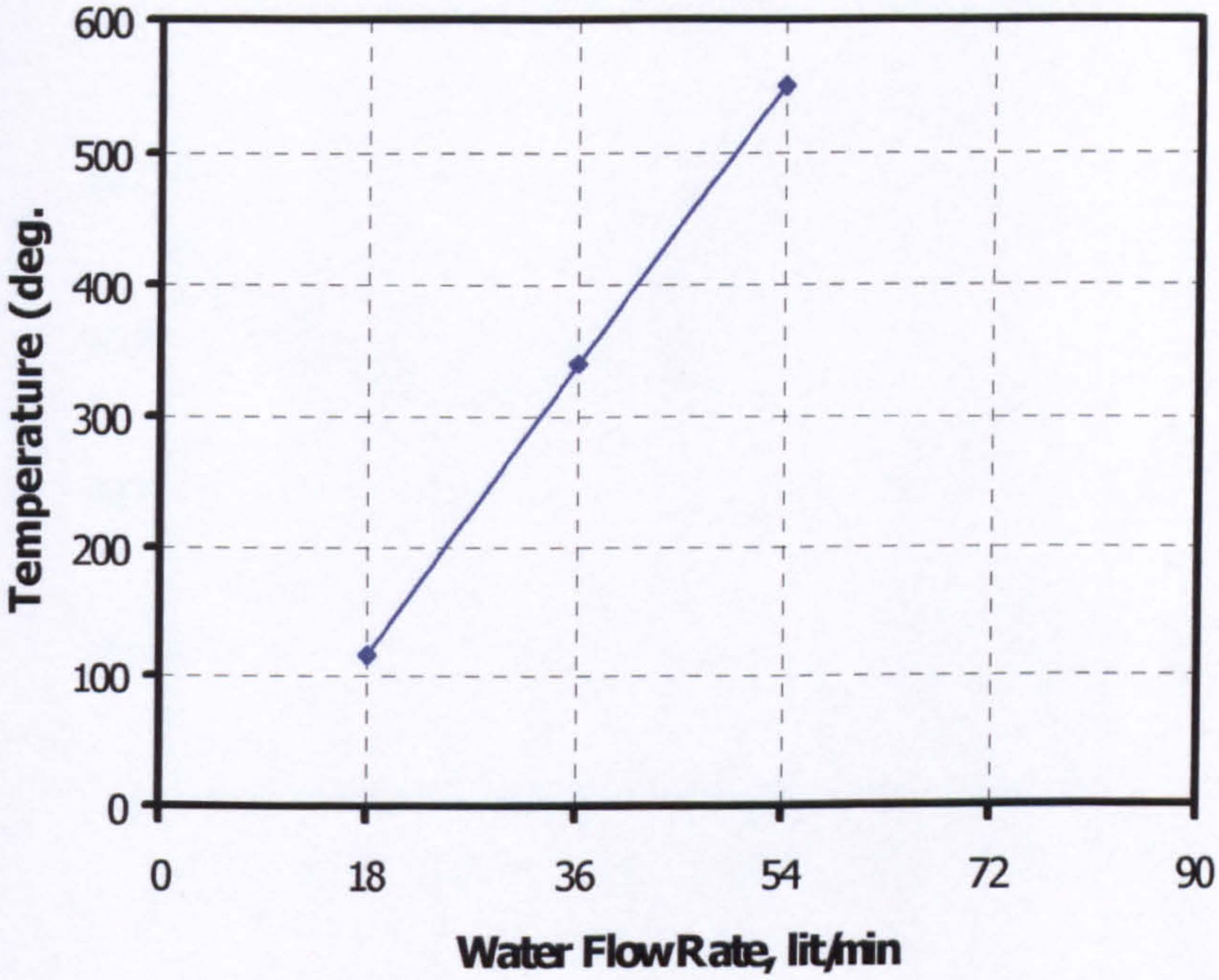

Figure (7.21). Average temperature reduction (drop) after water spray activation for different water flow rates at 150° spray angle when the water was insufficient for extinguishment.

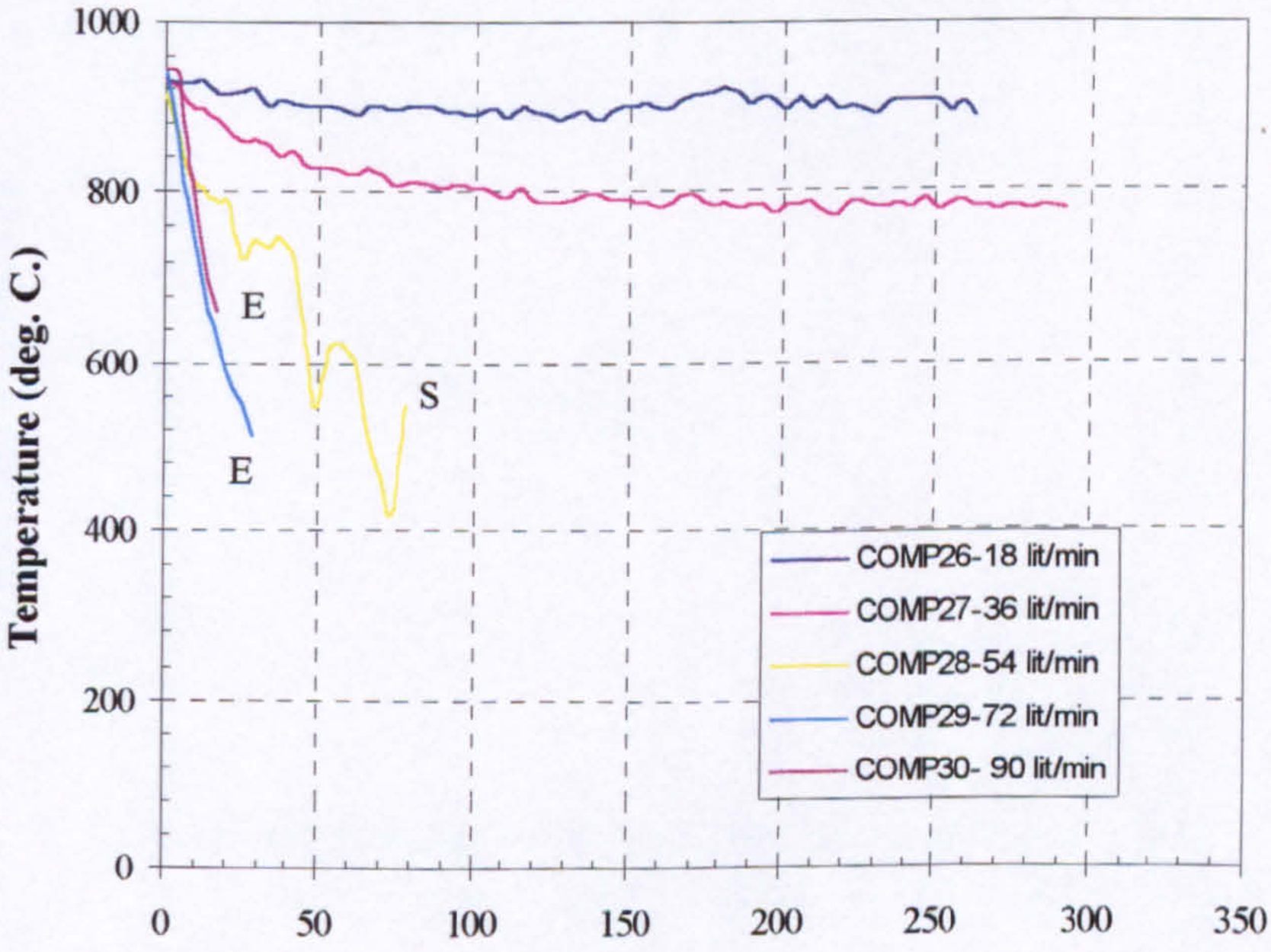

Figure (7.22). Average temperature distribution after water spray activation for different water flow rate at 120° spray angle for one spray located at the centre of the compartment (E = extinguished and S= test stopped).

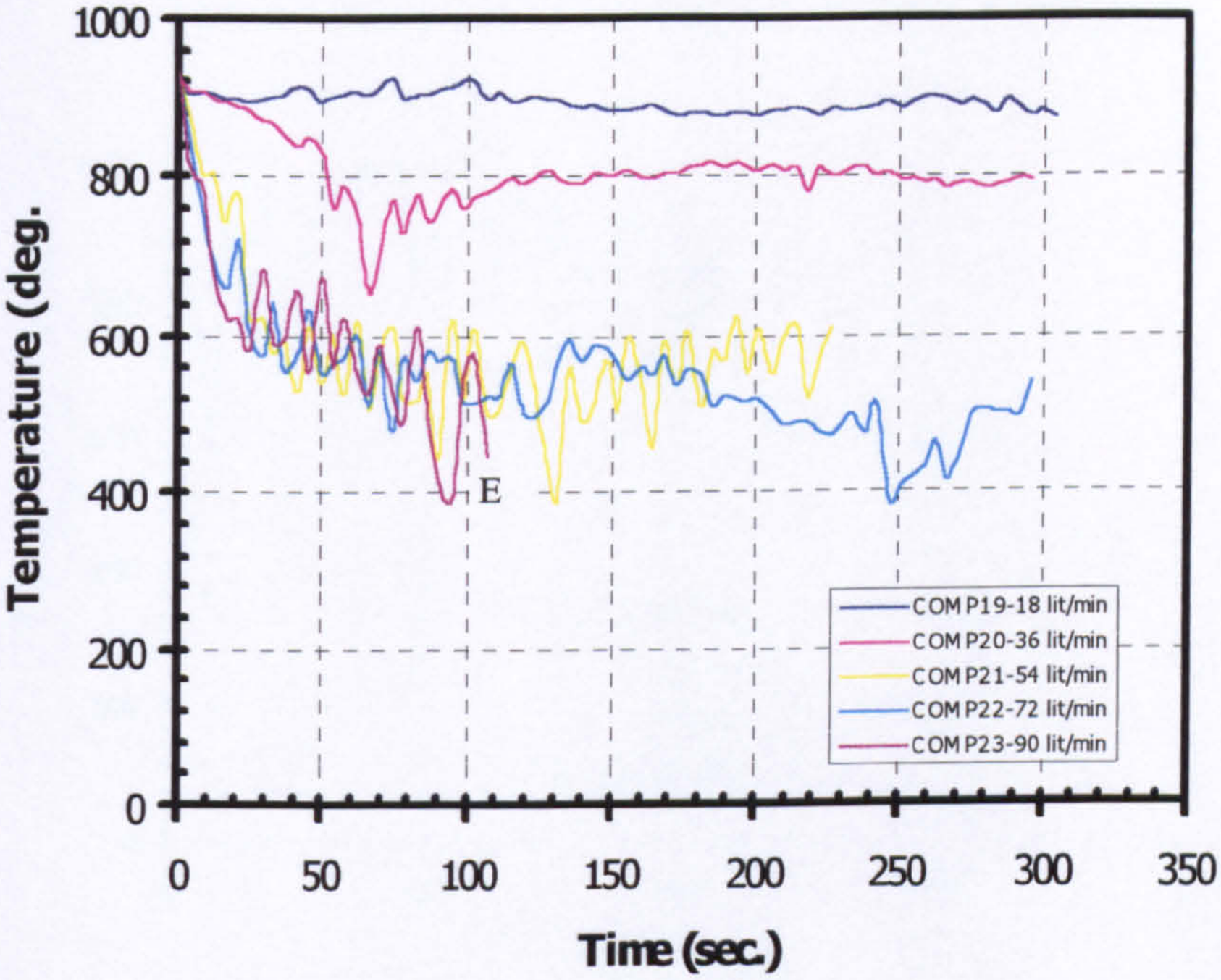

Figure (7.23). Average temperature development after water spray activation for different water flow rates at 90° spray angle for one spray located at the centre of the compartment (E = extinguished).

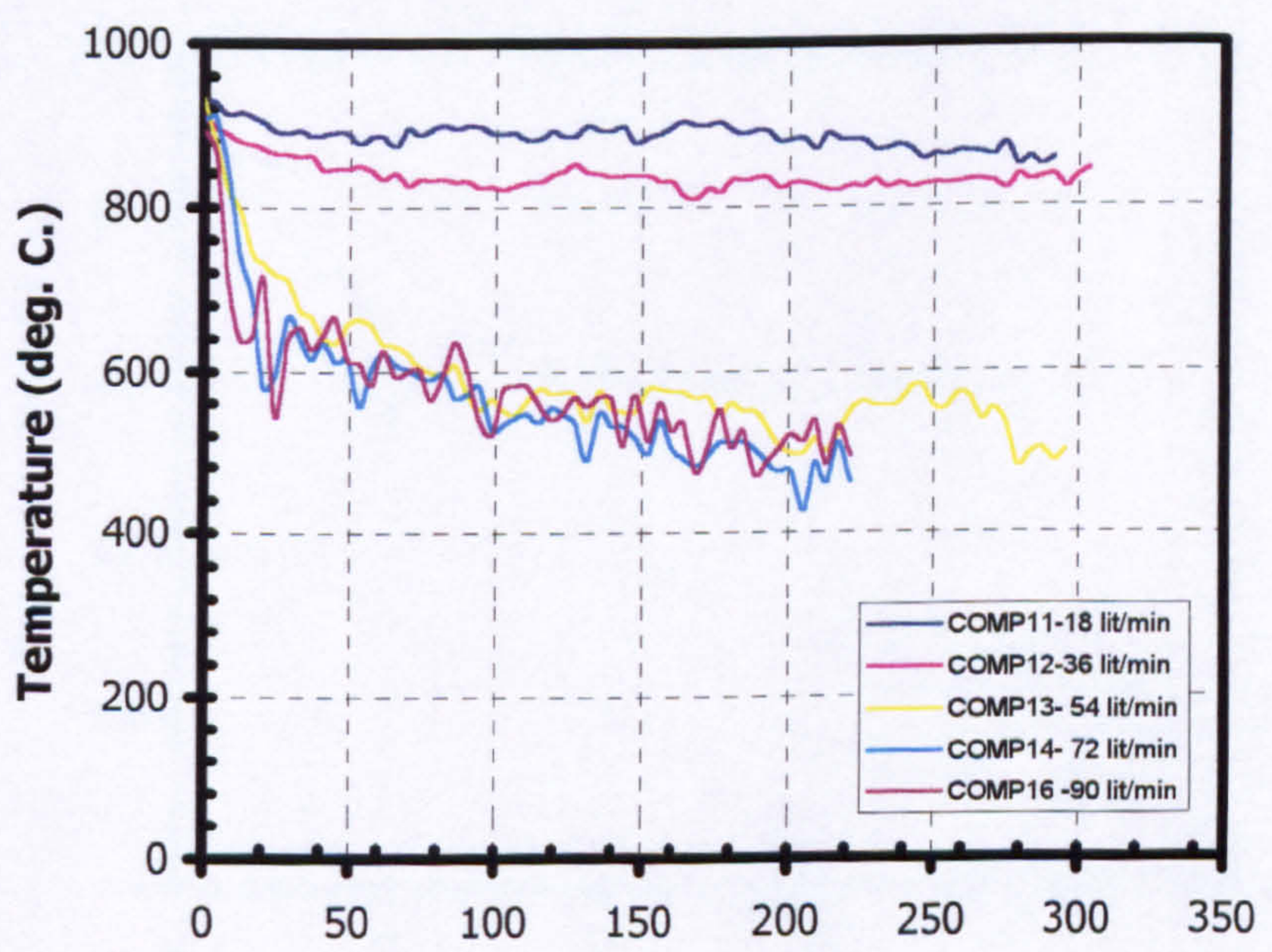

Figure (7.24). Average temperature development after water spray activation for different water flow rates at 60° spray angle for one spray located at the centre of the compartment.

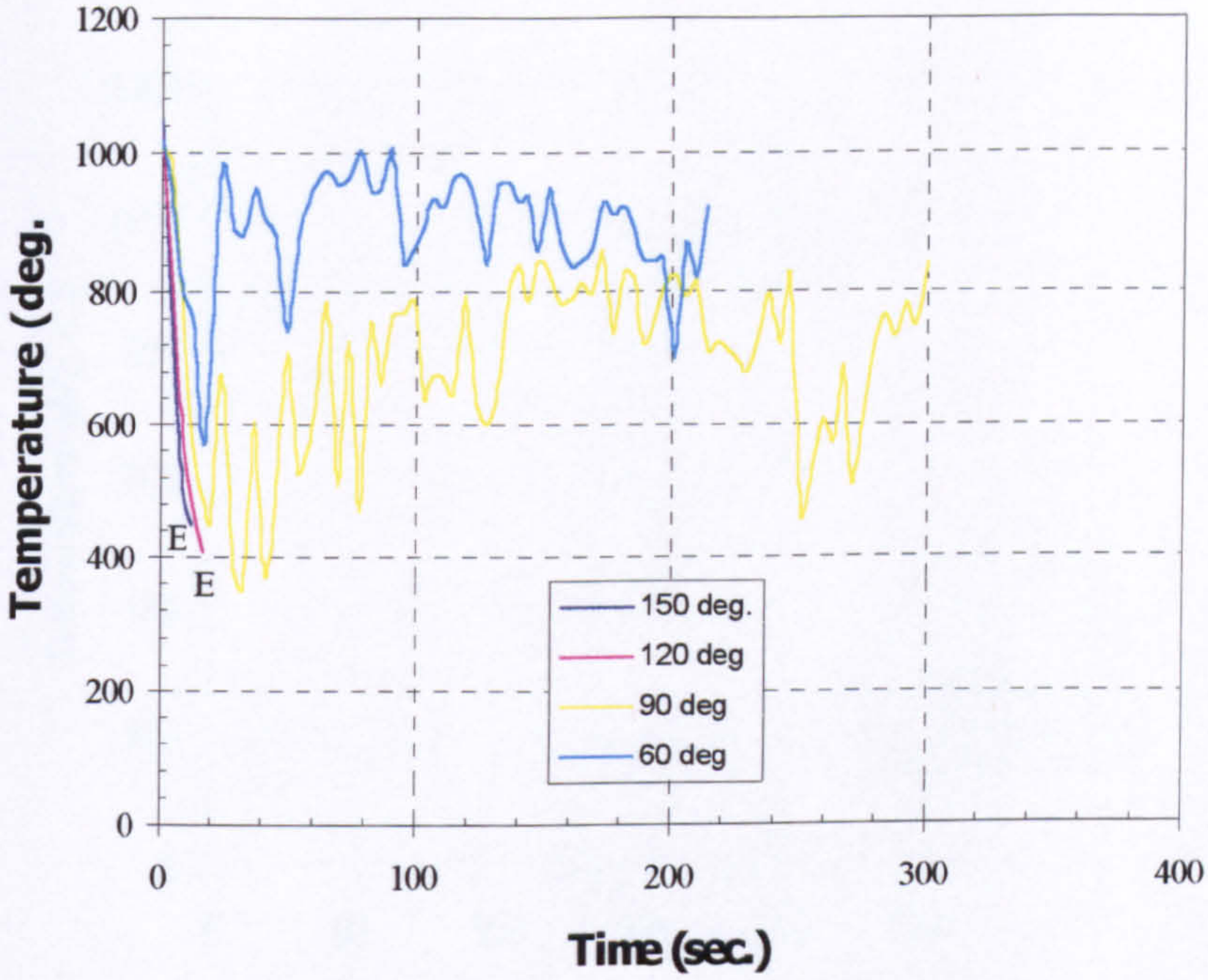

Figure (7.25a). Temperature development after water spray activation for different spray angles for 72 lit/min water flow rates and one spray located centrally measured by ASP-1 (E = extinguished).

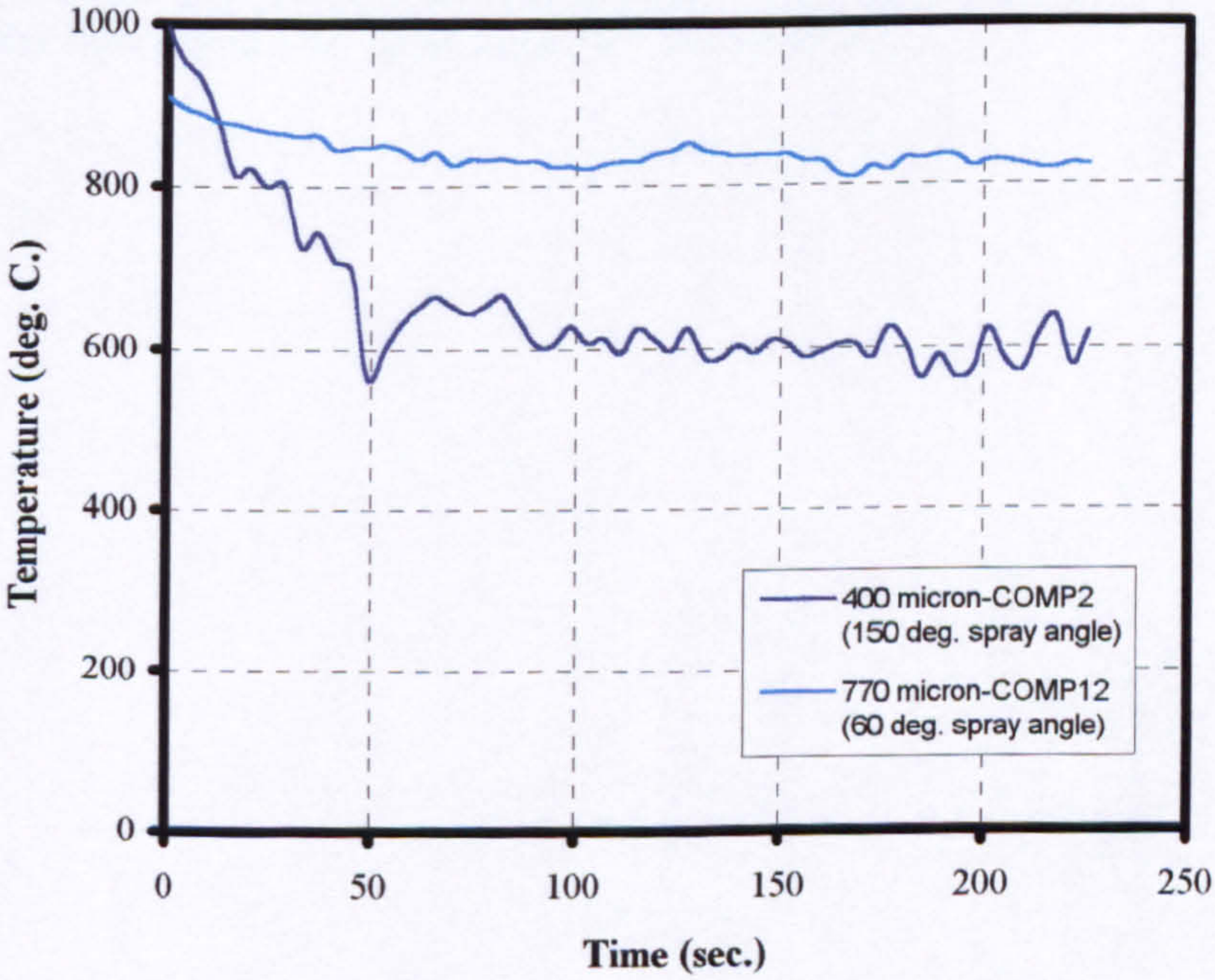

Figure (7.25b). Average temperature profile for different Sauter mean droplet diameters and different spray angles at 36 lit/min water flow rate.

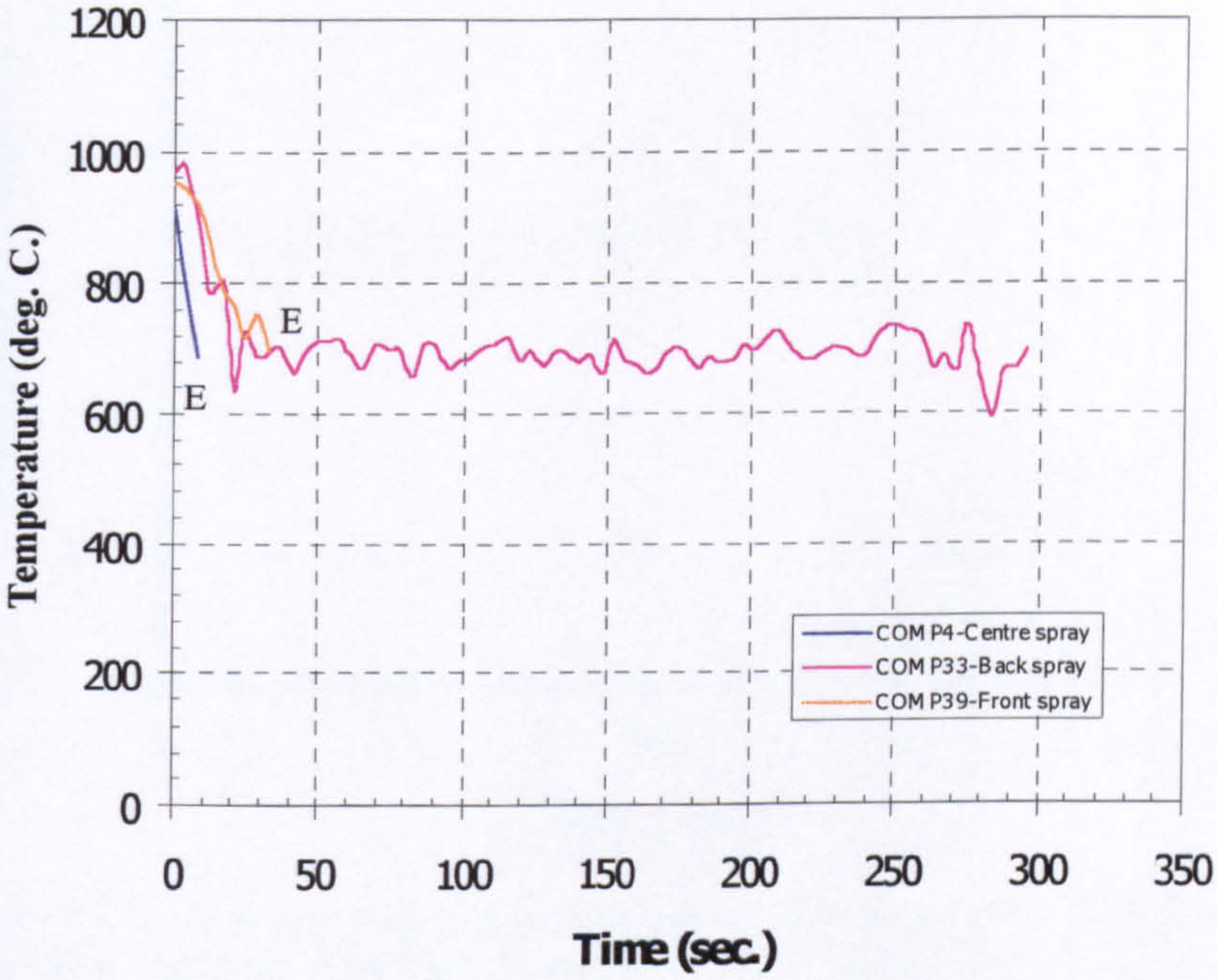

Figure (7.26). Average temperature distribution after water spray activation for one spray nozzle positioned at different locations inside the compartment for 72 lit/min water flow rate at 150° spray angle (E = extinguished).

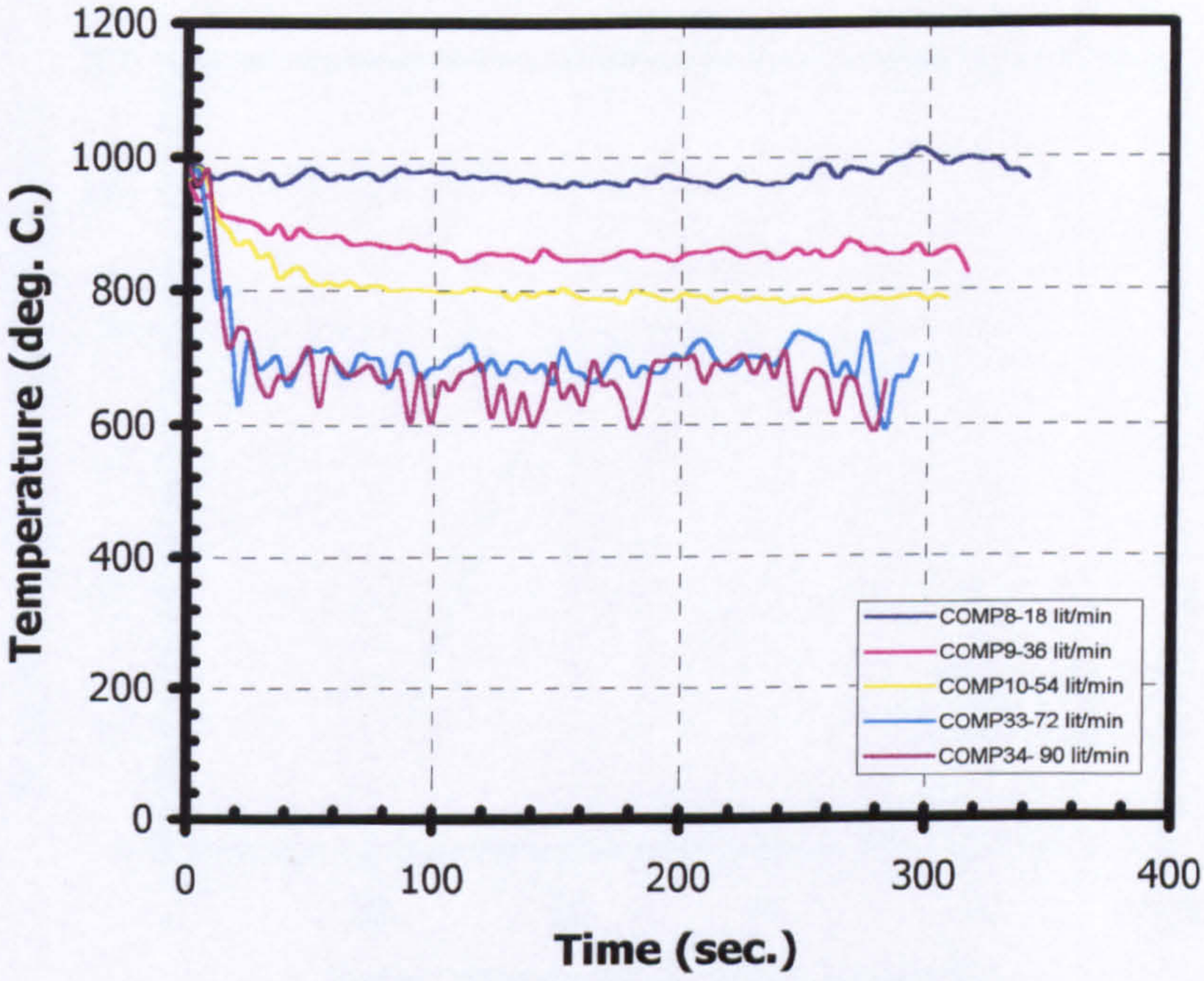

Figure (7.27). Average temperature distribution after water spray activation for different water flow rates at 150° spray angle for one spray located at the back of the compartment.

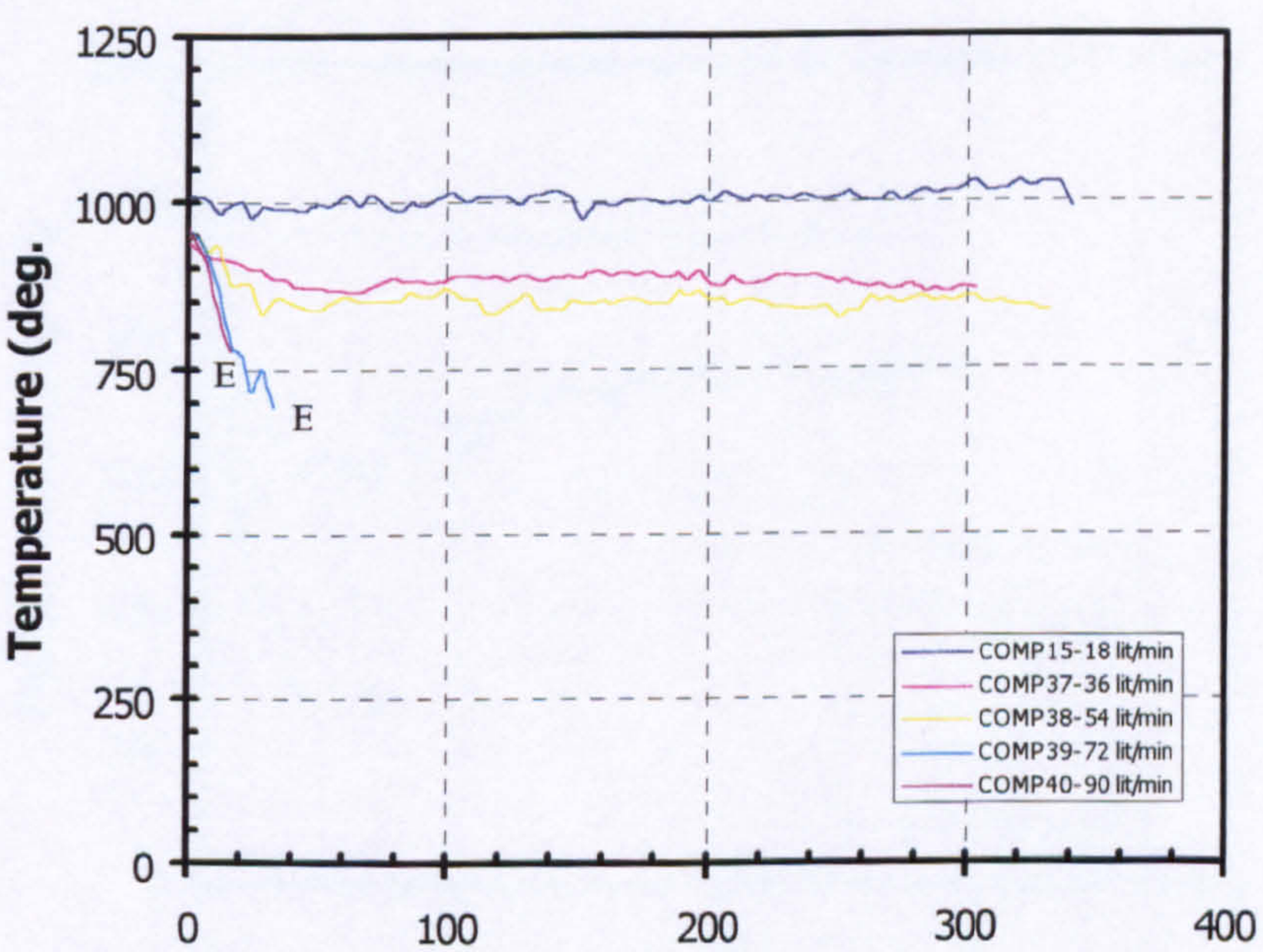

Figure (7.28). Average temperature distribution after water spray activation for different water flow rates at 150° spray angle for one spray located at the front of the compartment (E = extinguished).

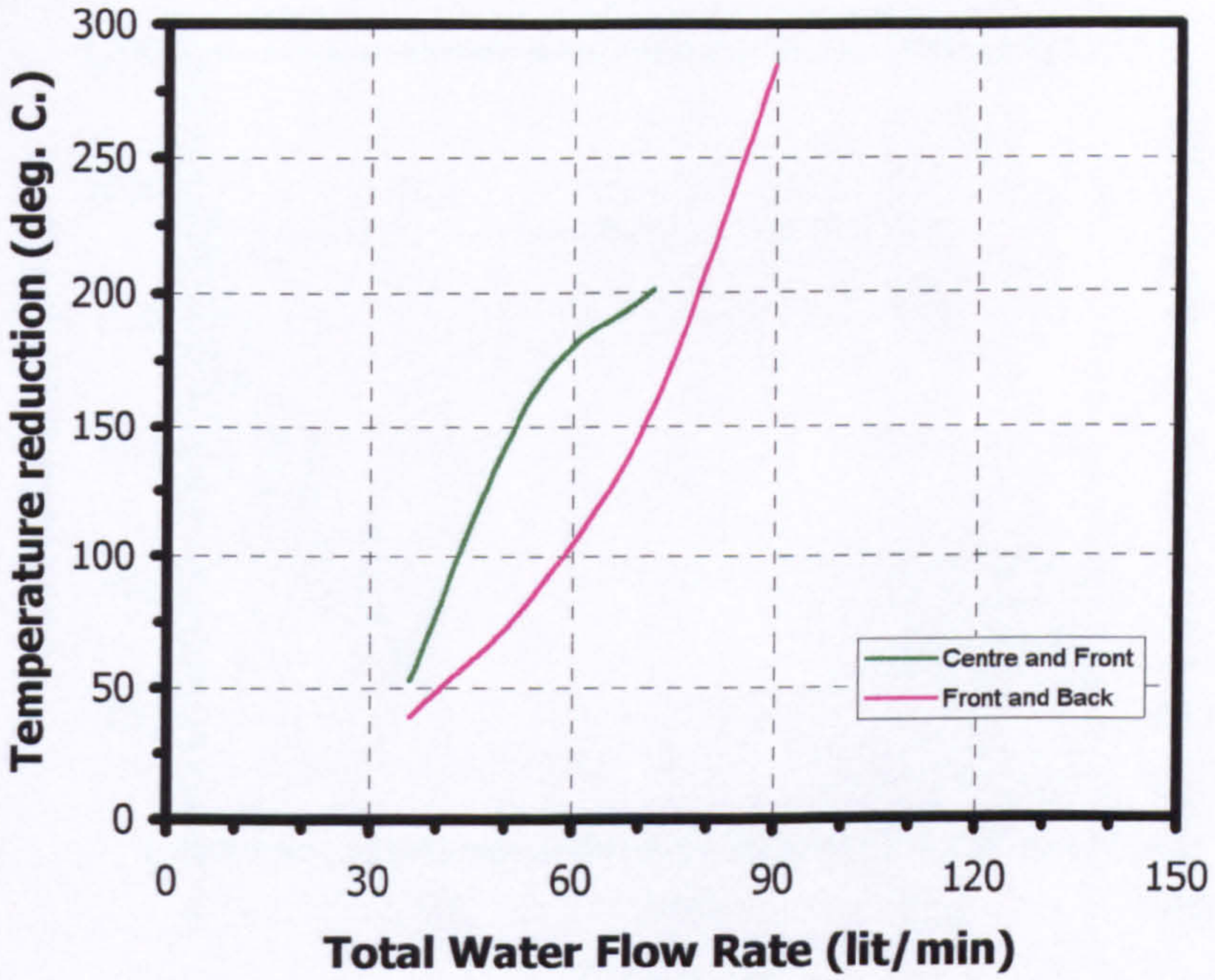

Figure (7.29). Average temperature reduction (drop) after water spray activation for two-spray nozzle for different locations and different water flow rates at 150° spray angle when the water was insufficient for extinguishment.

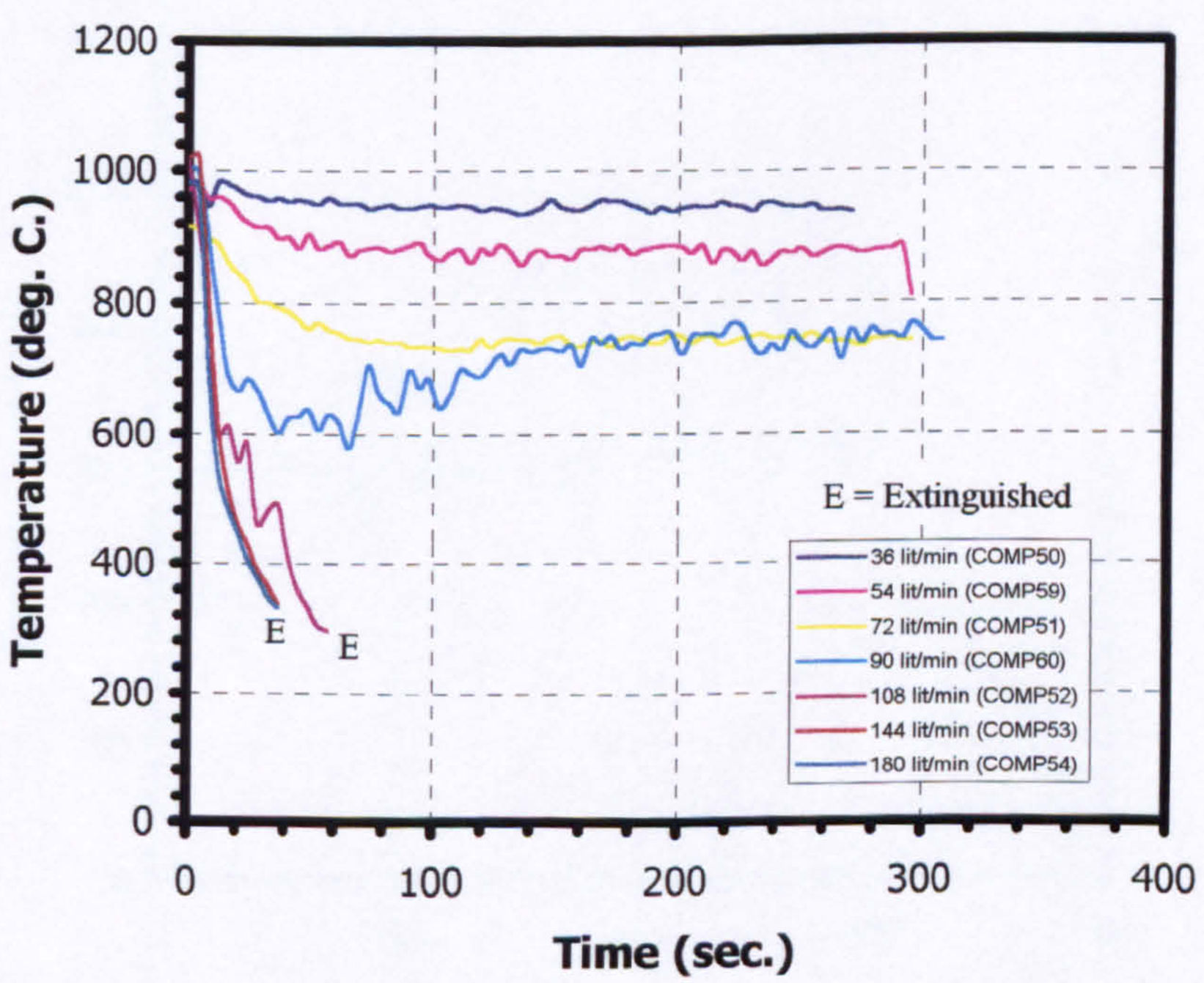

Figure (7.30). Average temperature distribution after water spray activation for two-spray nozzle used (front and back) for different water flow rates at 150° spray angle.

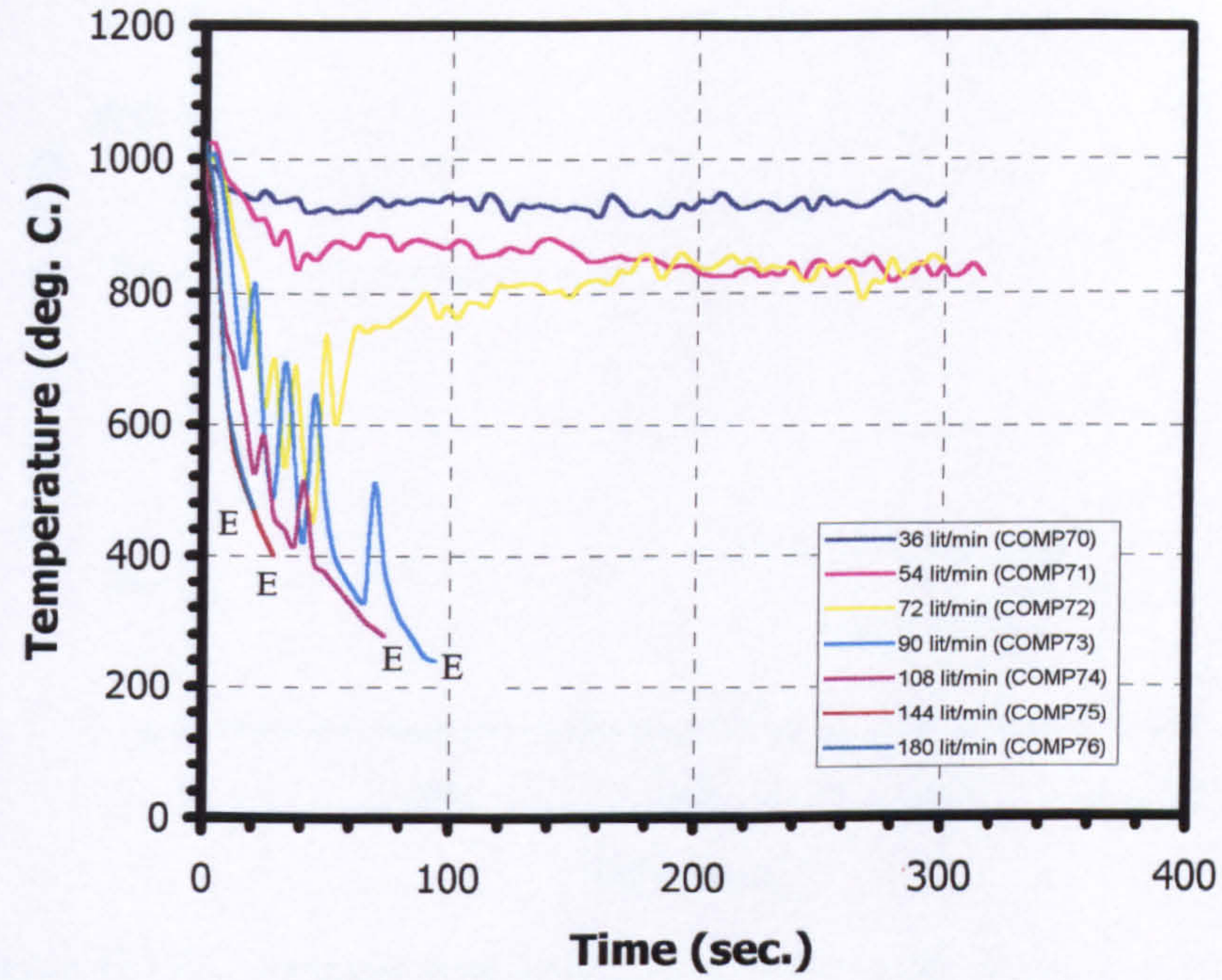

Figure (7.31). Average temperature distribution after water spray activation for two-spray nozzle used (front and centre) for different water flow rates at 150° spray angle (E=extinguished).

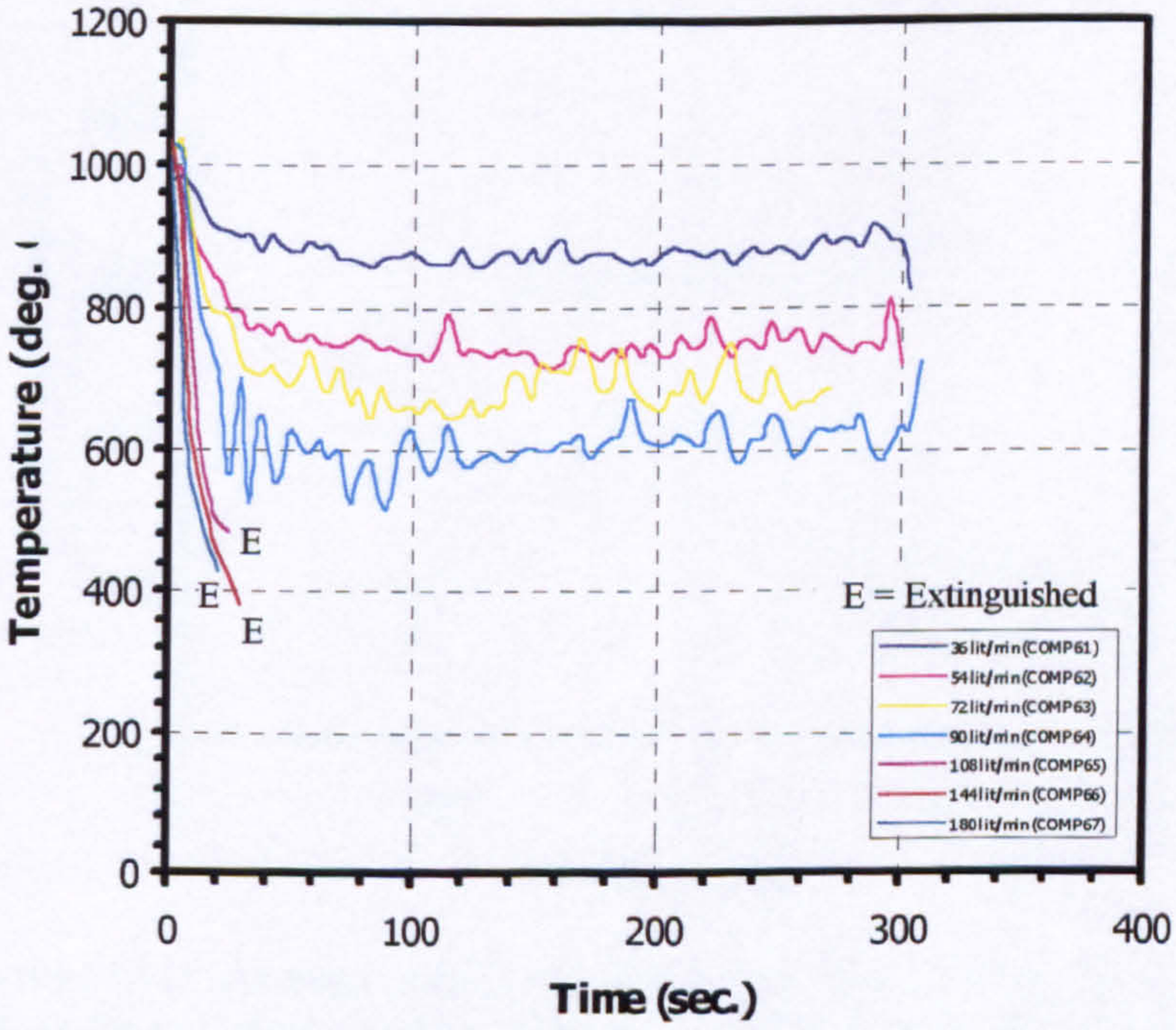

Figure (7.32). Average temperature distribution after water spray activation for two-spray nozzle used (centre and back) for different water flow rates at 150° spray angle.

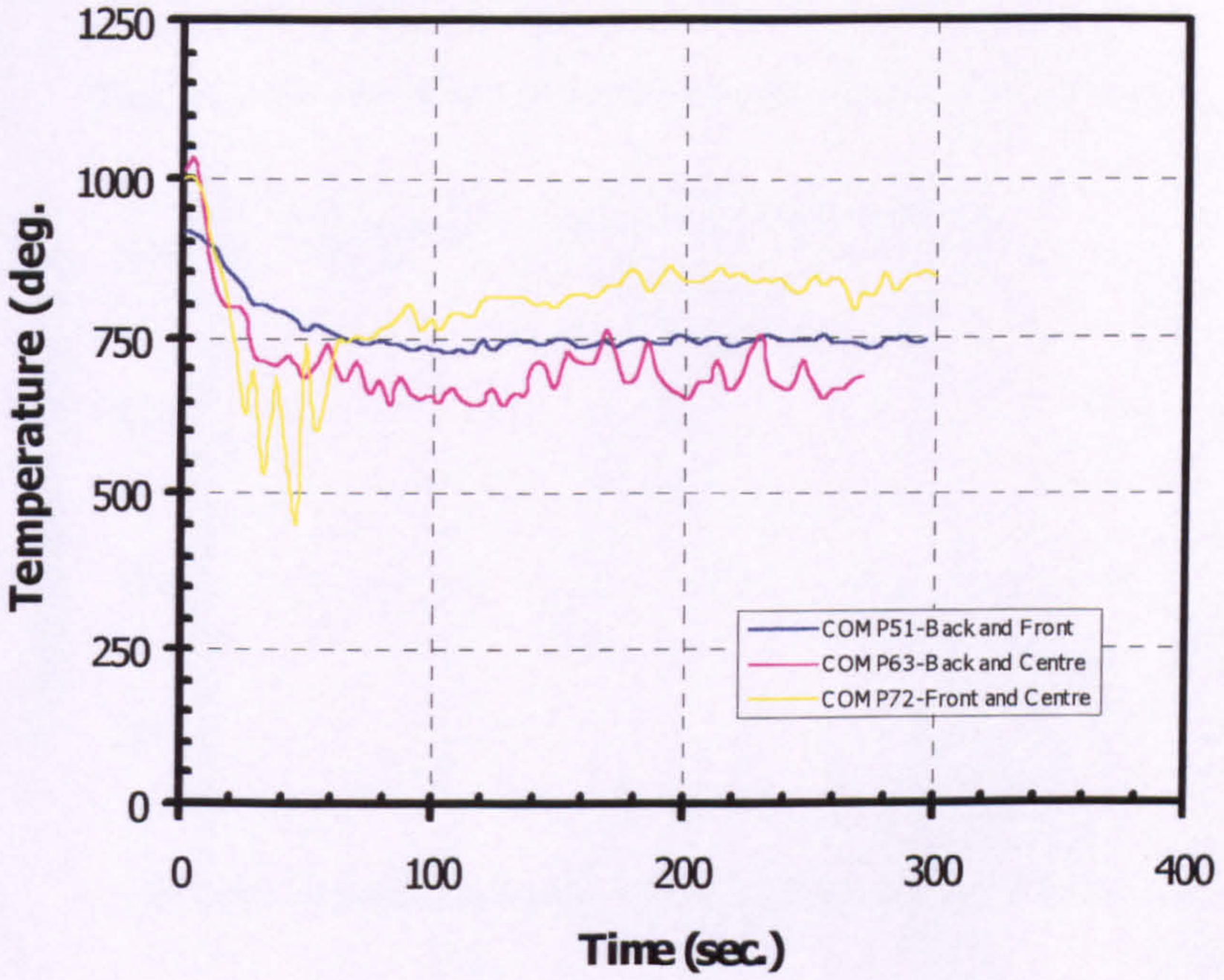

Figure (7.33). Average temperature distribution after water spray activation of 72 lit/min for two-spray nozzle at different spray locations in the compartment at 150° spray angle.

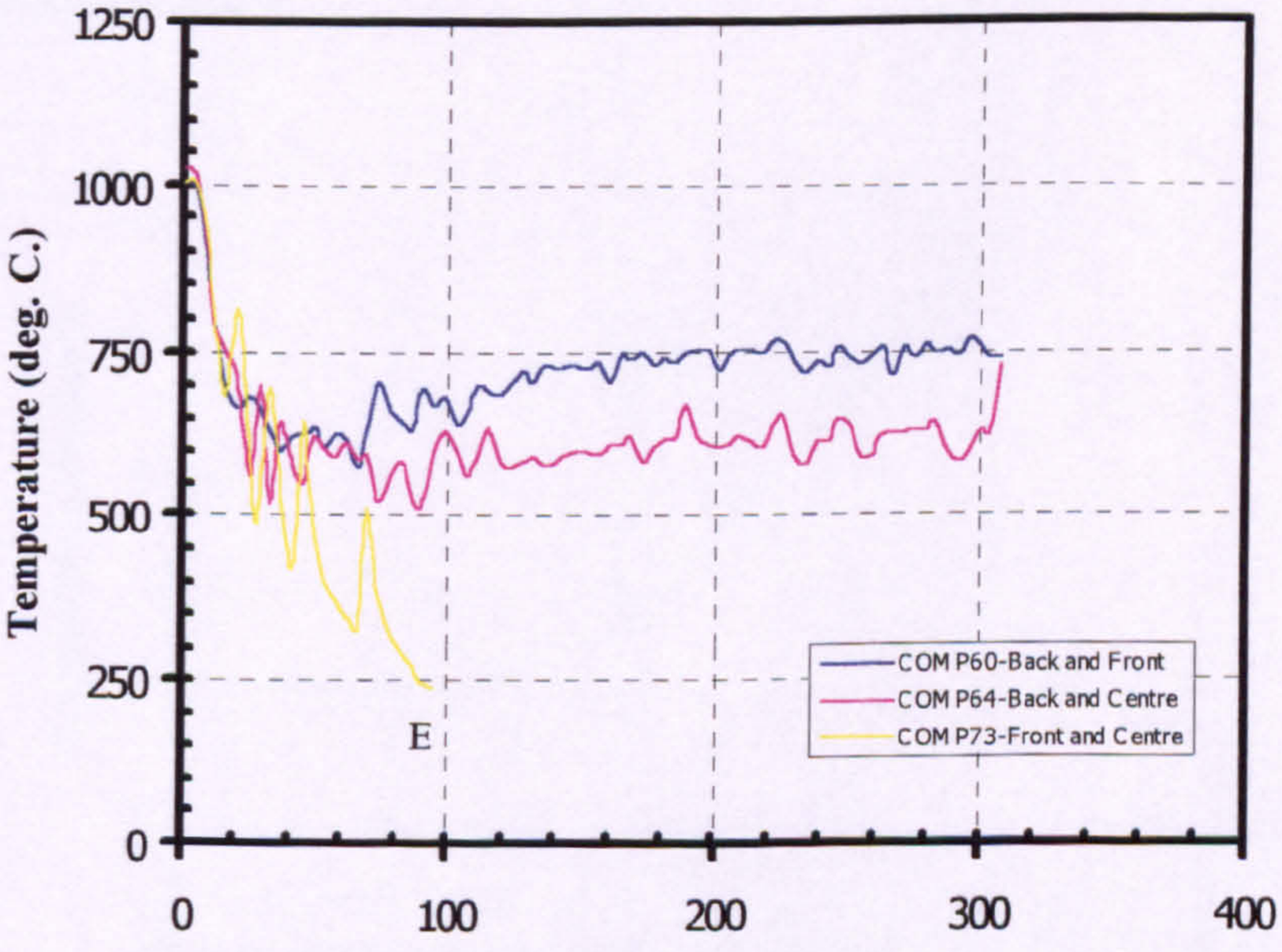

Figure (7.34). Average temperature distribution after water spray activation of 90 lit/min for two-spray nozzle at different spray locations in the compartment at 150° spray angle (E = extinguished).

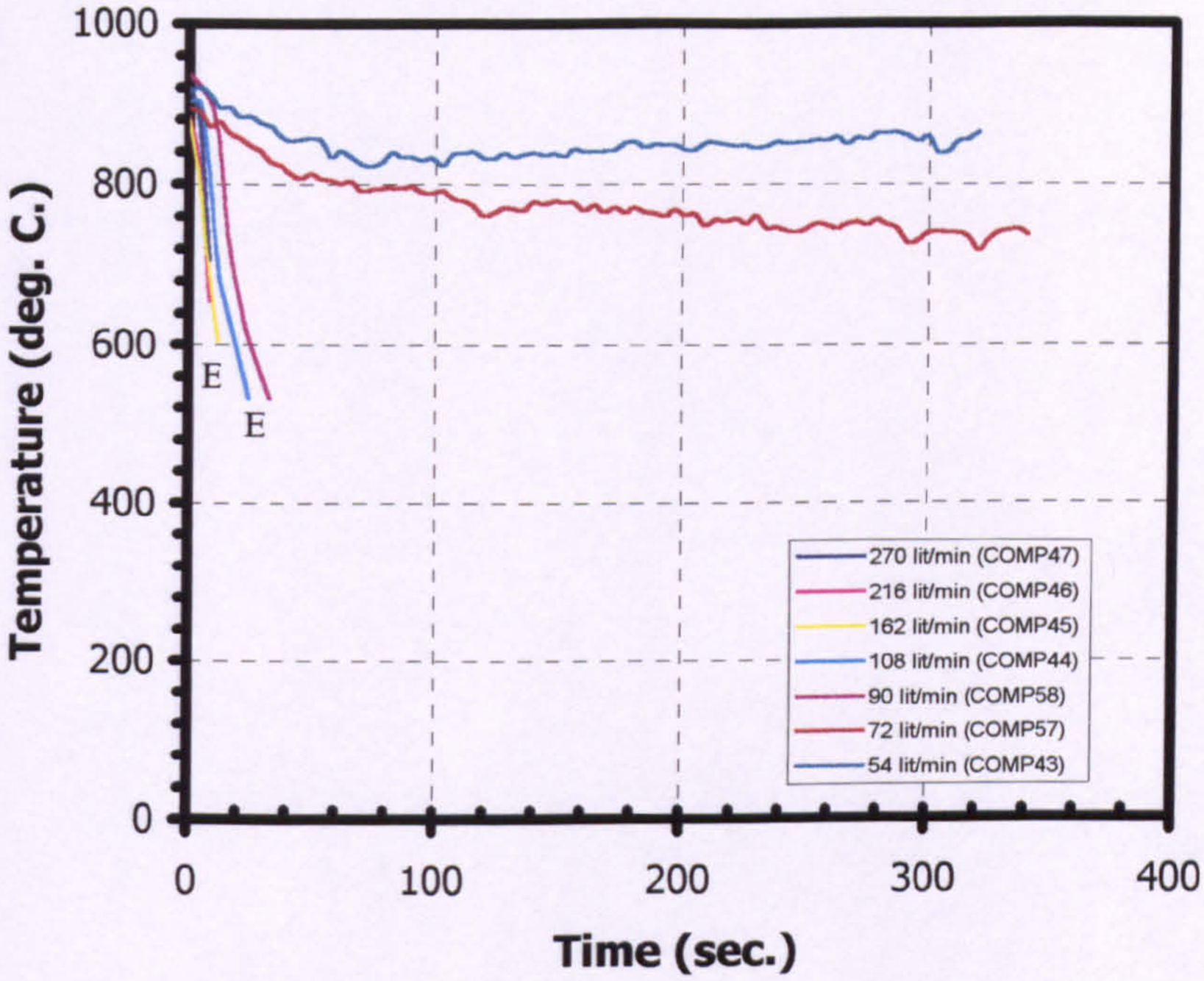

Figure (7.35). Average temperature distribution after water spray activation for three-spray nozzle inside the compartment for different water flow rates at 150° spray angle (E=extinguished).

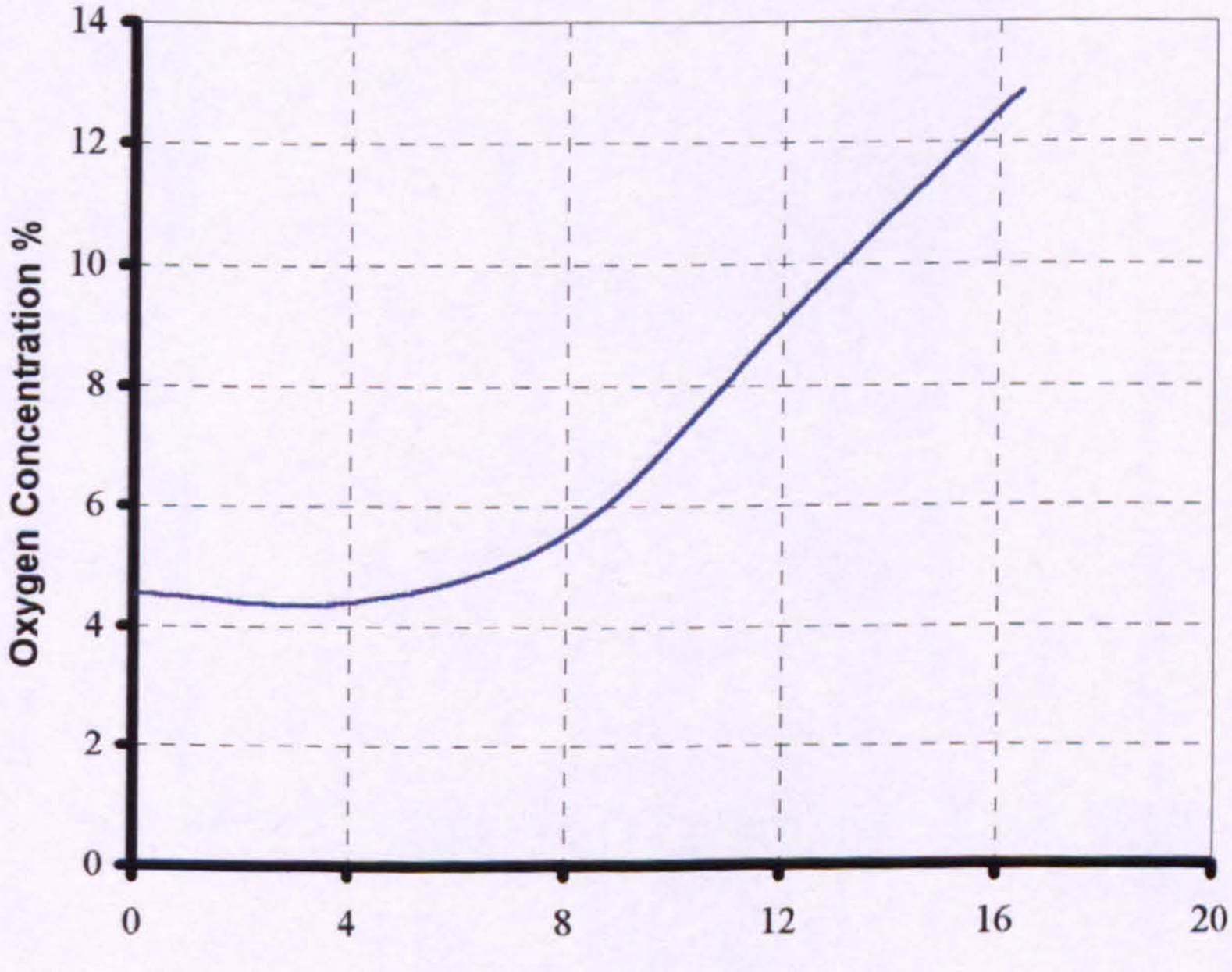

Figure (7.36). Oxygen Concentration after water spray activation for 72 lit/min for one spray nozzle at 120° spray angle (COMP29).

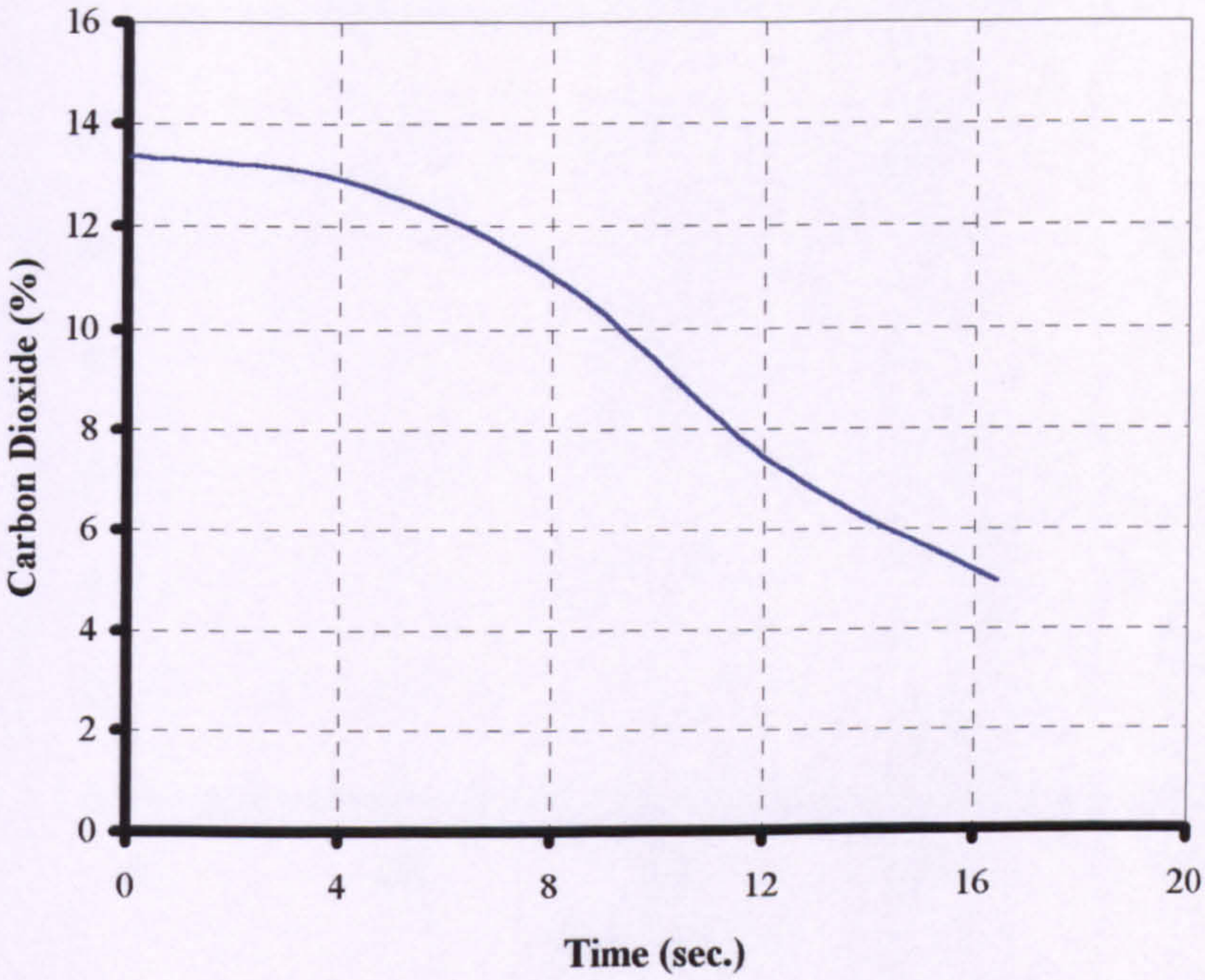

Figure (7.37). Carbon dioxide concentration after water spray activation for 72 lit/min for one spray nozzle at 120° spray angle (COMP29).

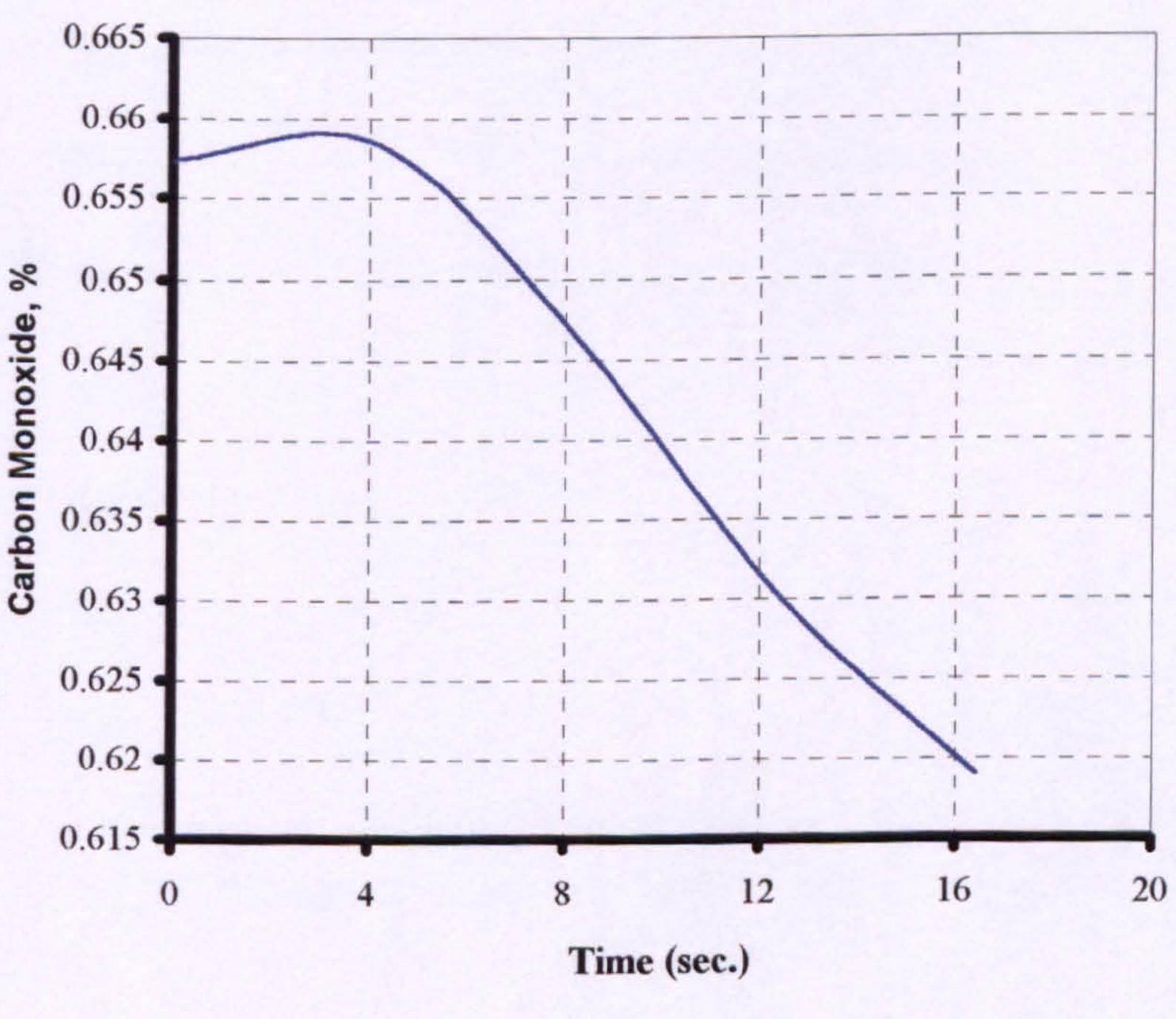

Figure (7.38). Carbon monoxide concentration after water spray activation of 72 lit/min for one spray located centrally at 120° spray angle (COMP29).

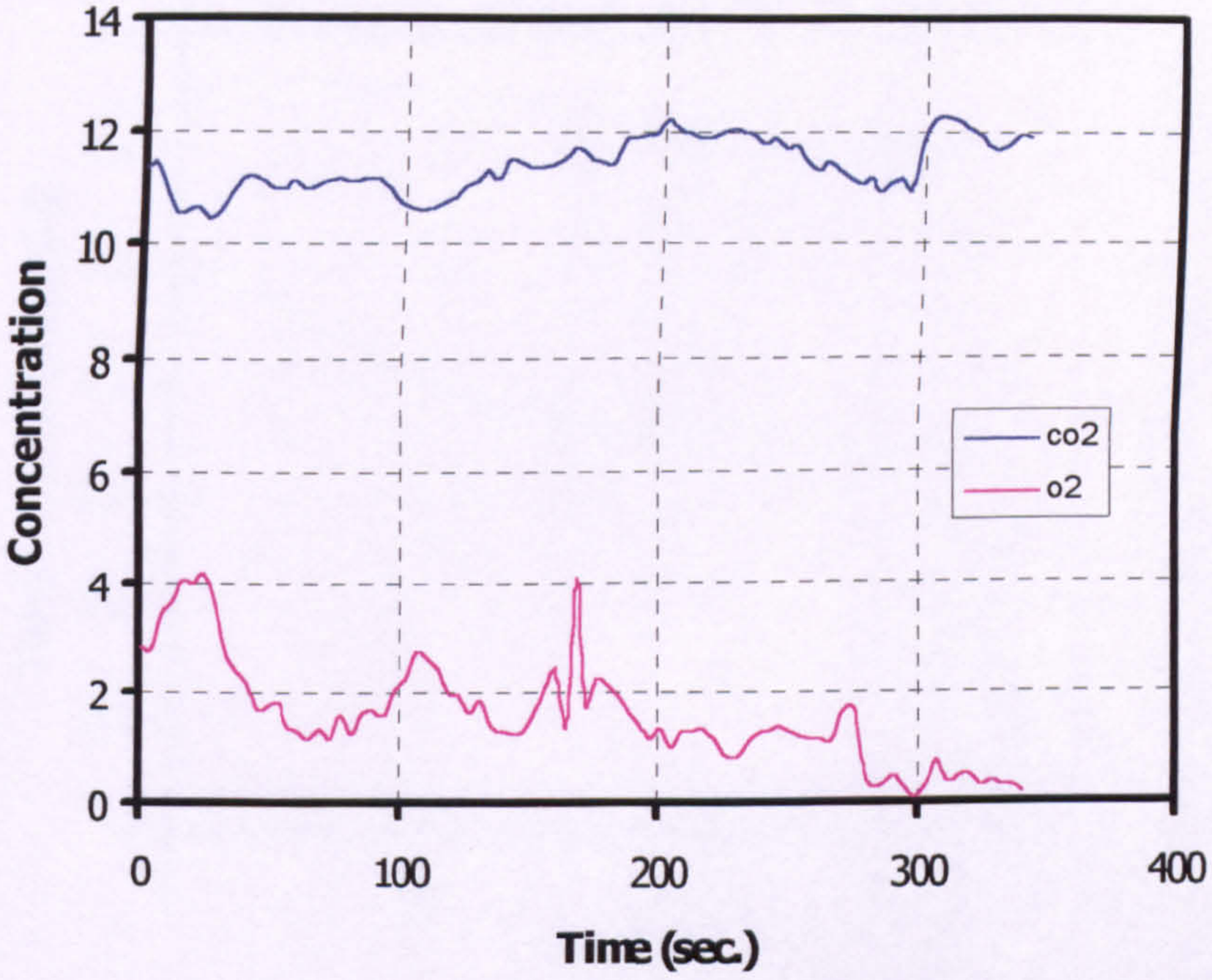

Figure (7.39). Oxygen and Carbon dioxide concentrations after water spray activation of 72 lit/min for three sprays at 150° spray angle (COMP57).

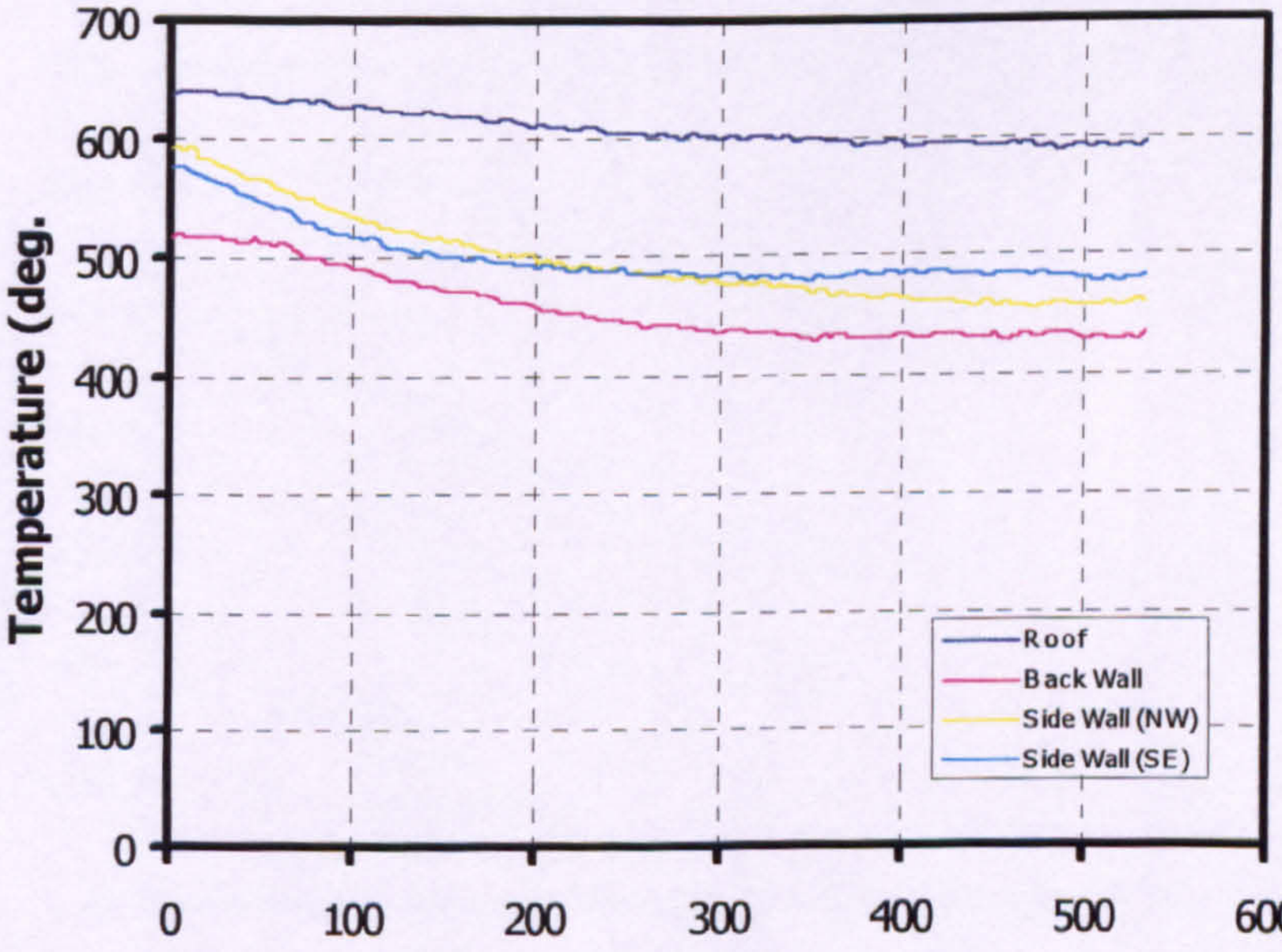

Figure (7.40). Average wall temperature profile after water spray activation for 18 lit/min one spray nozzle located at the centre of the compartment (COMP1).

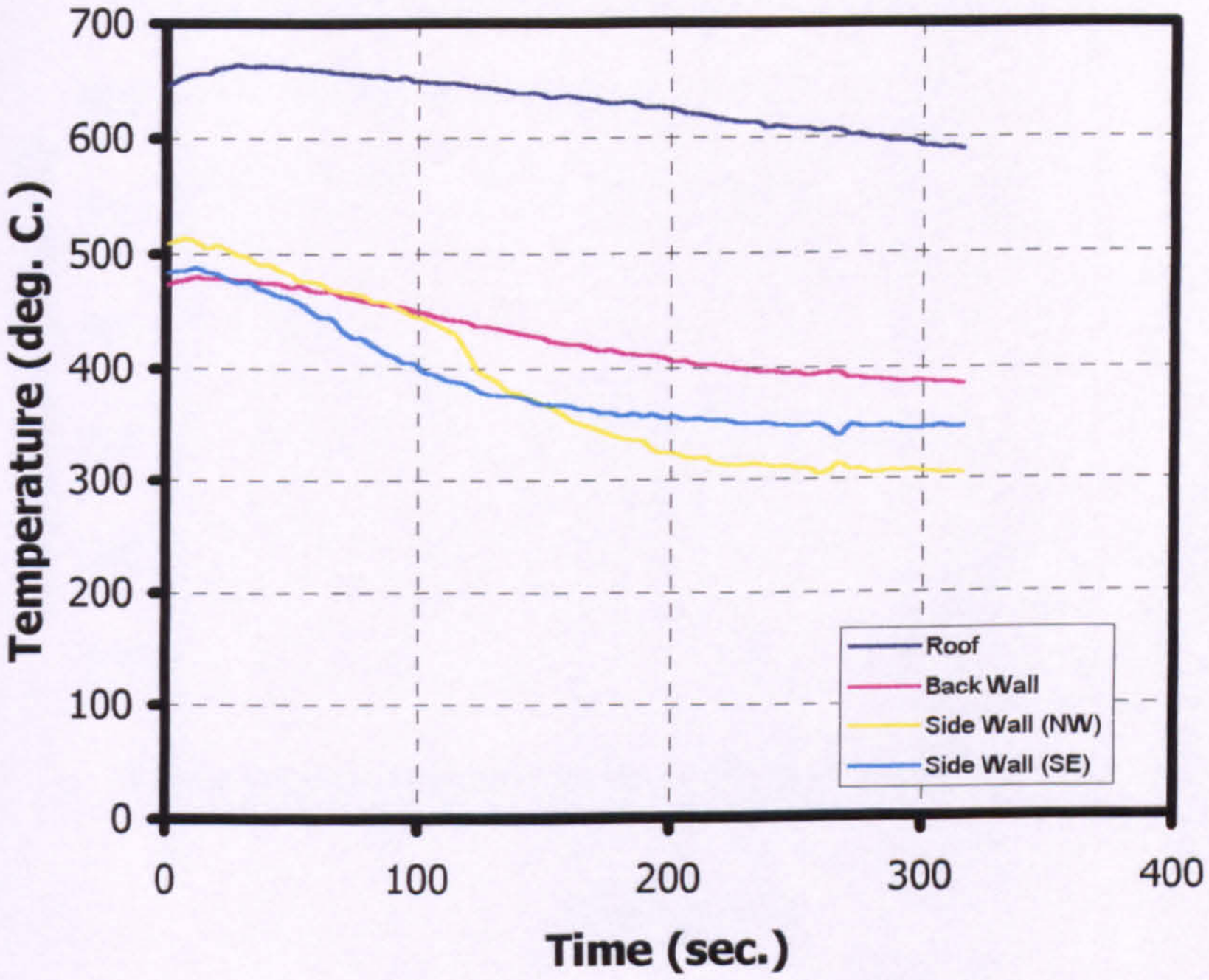

Figure (7.41). Average wall temperature profile after water spray activation for 54 lit/min for two spray nozzles located at the front and the centre of the compartment (COMP71).

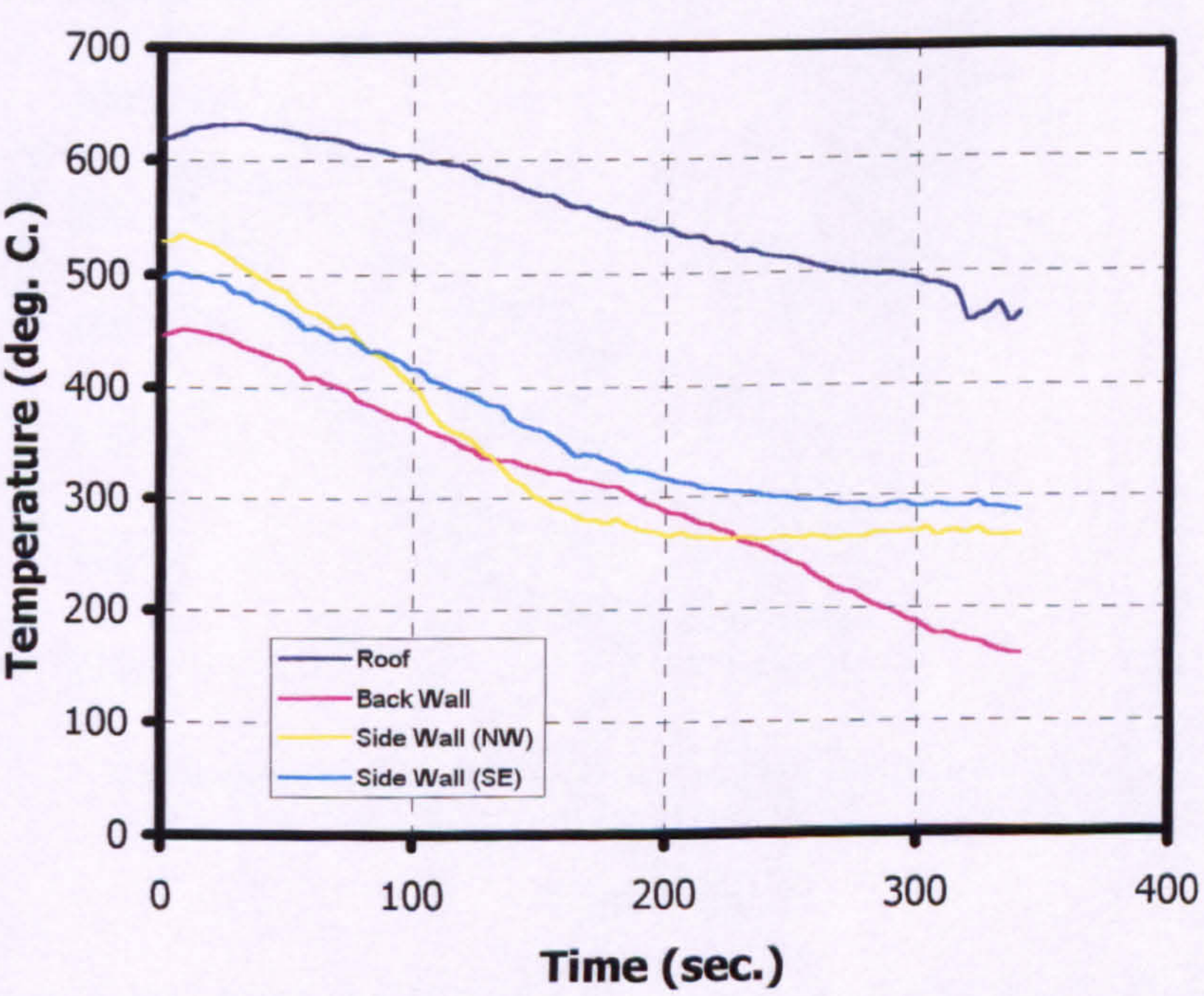

Figure (7.42). Average wall temperature profile after water spray activation for 72 lit/min for three spray nozzles (COMP57).

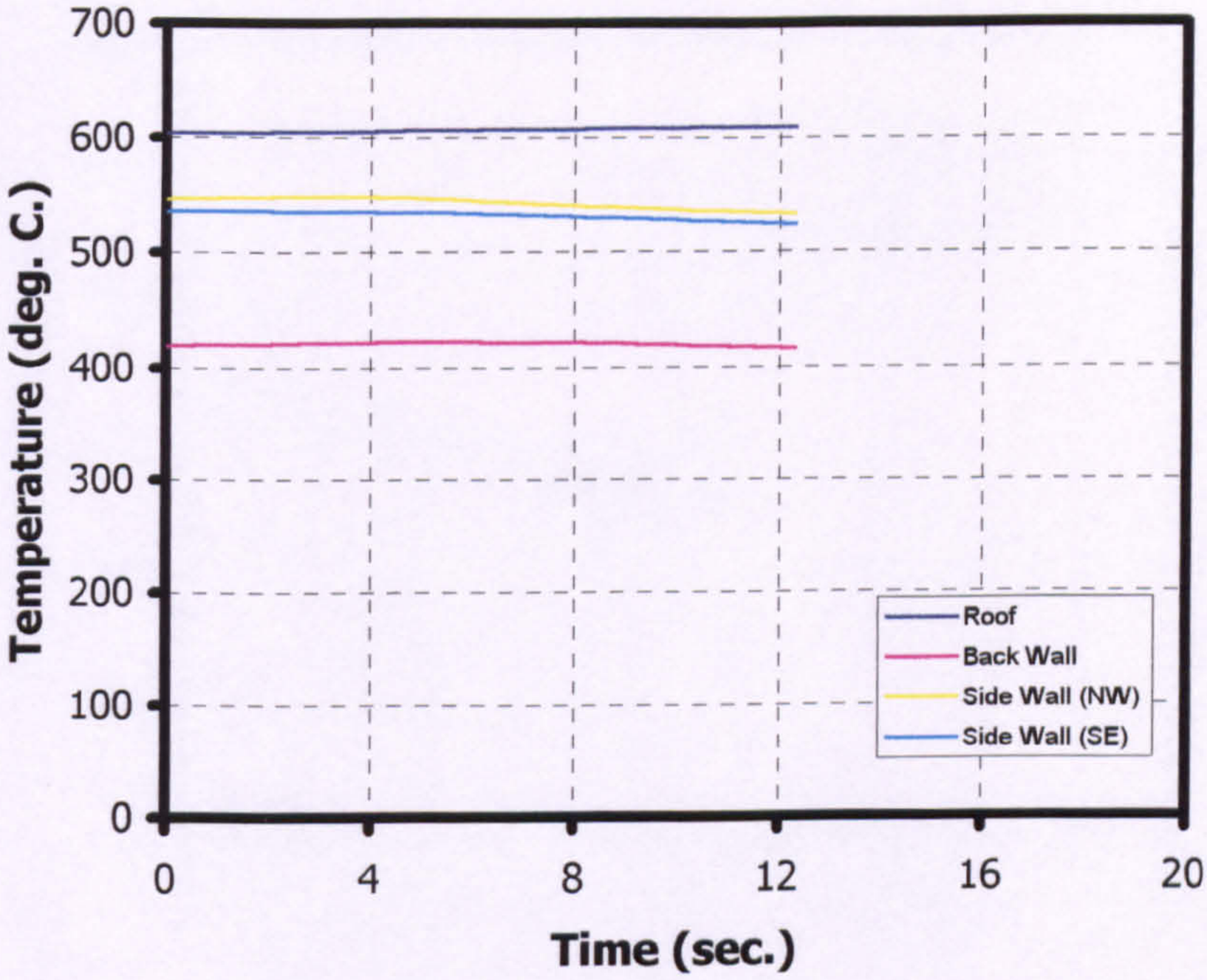

Figure (7.43). Average wall temperature profile after water spray activation for 72 lit/min one spray nozzle located at the centre of the compartment (COMP4).

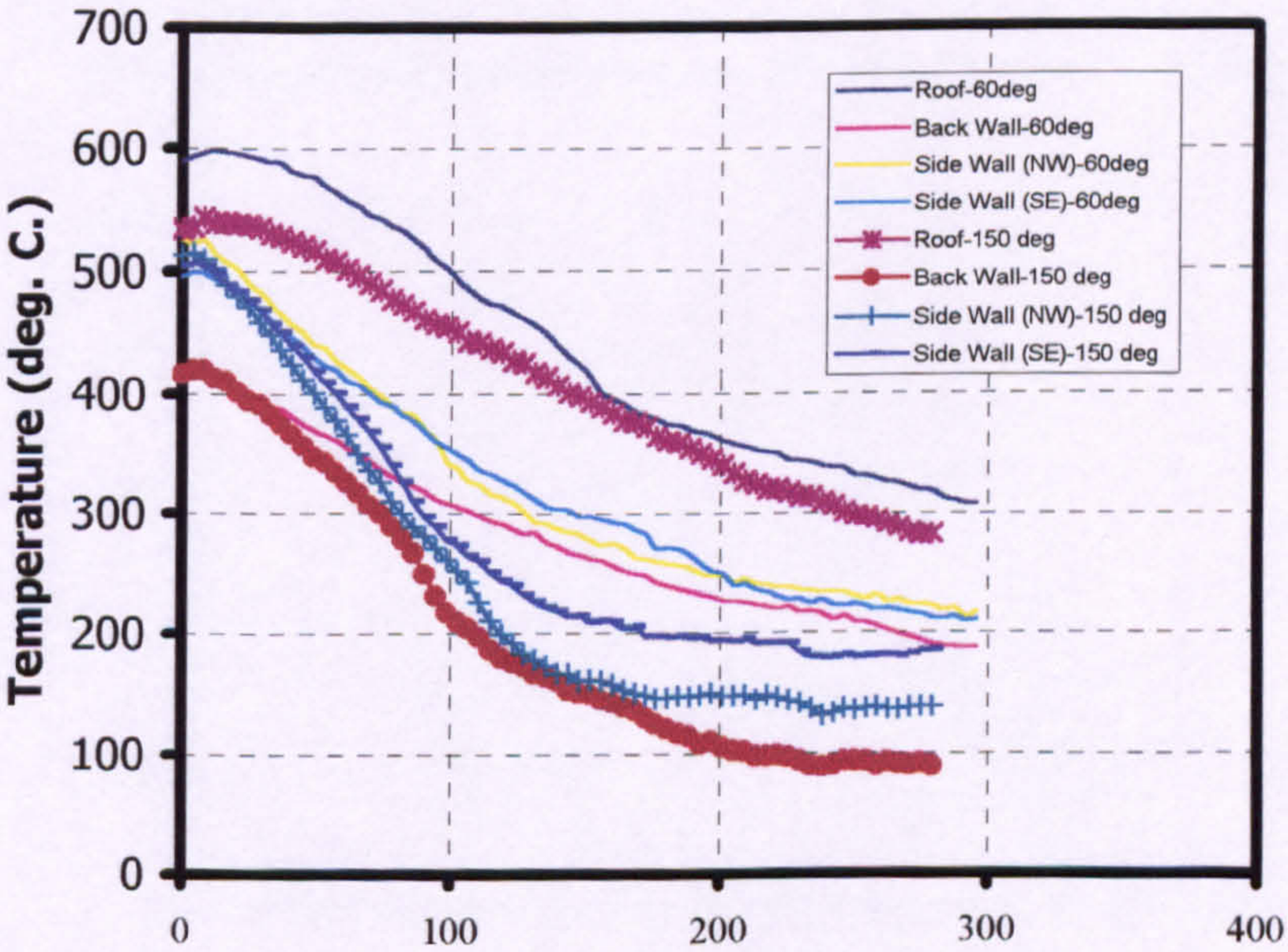

Figure (7.44). Average wall temperature profile after water spray activation for 54 lit/min for 60° and 150° spray angle for one spray nozzle located centrally (C) (COMP3 &13).

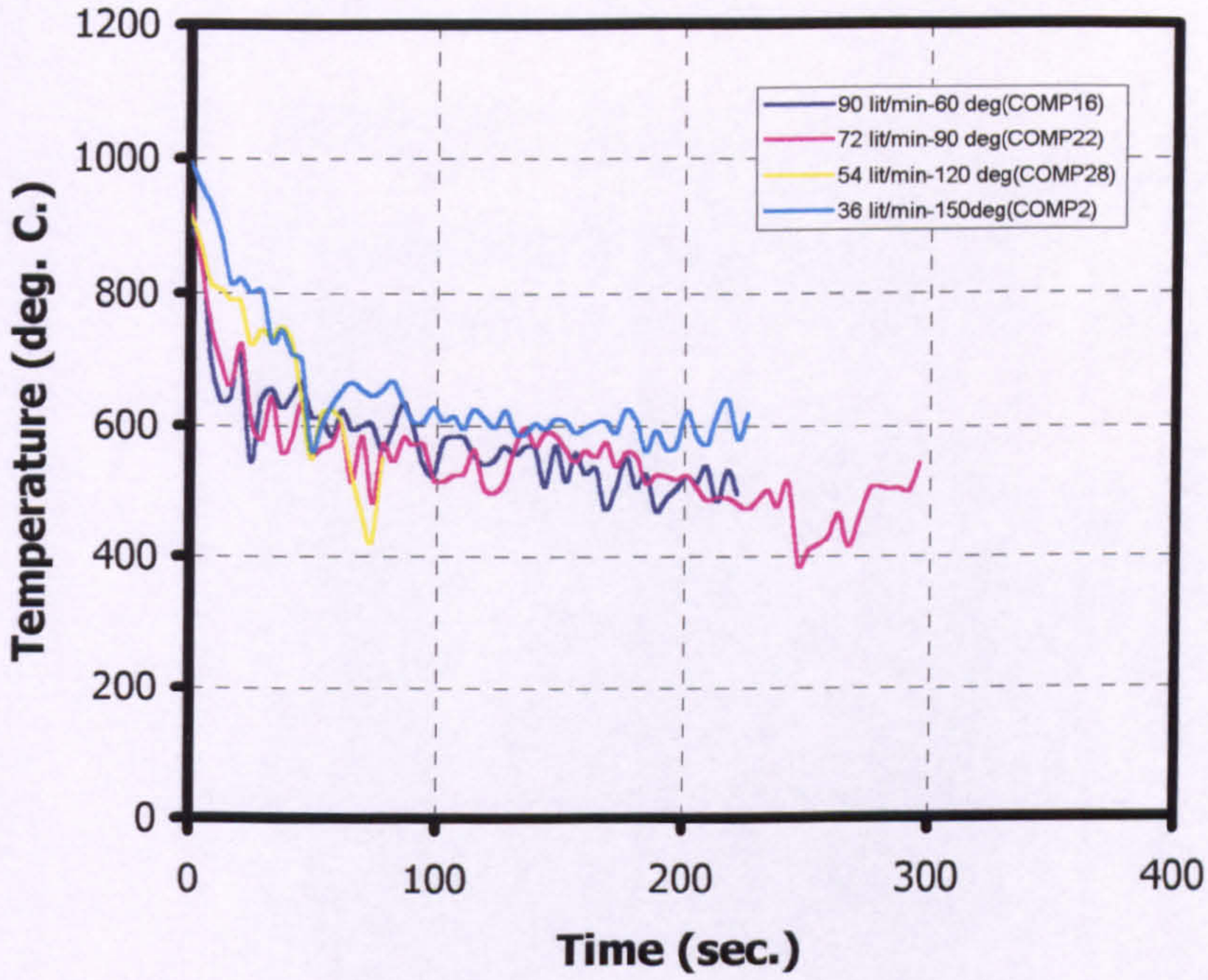

Figure (7.45). Average temperature profile after water spray activation for different water flow rates for one-spray nozzles located at the centre of the compartment and different spray angles which show similar temperature reduction.

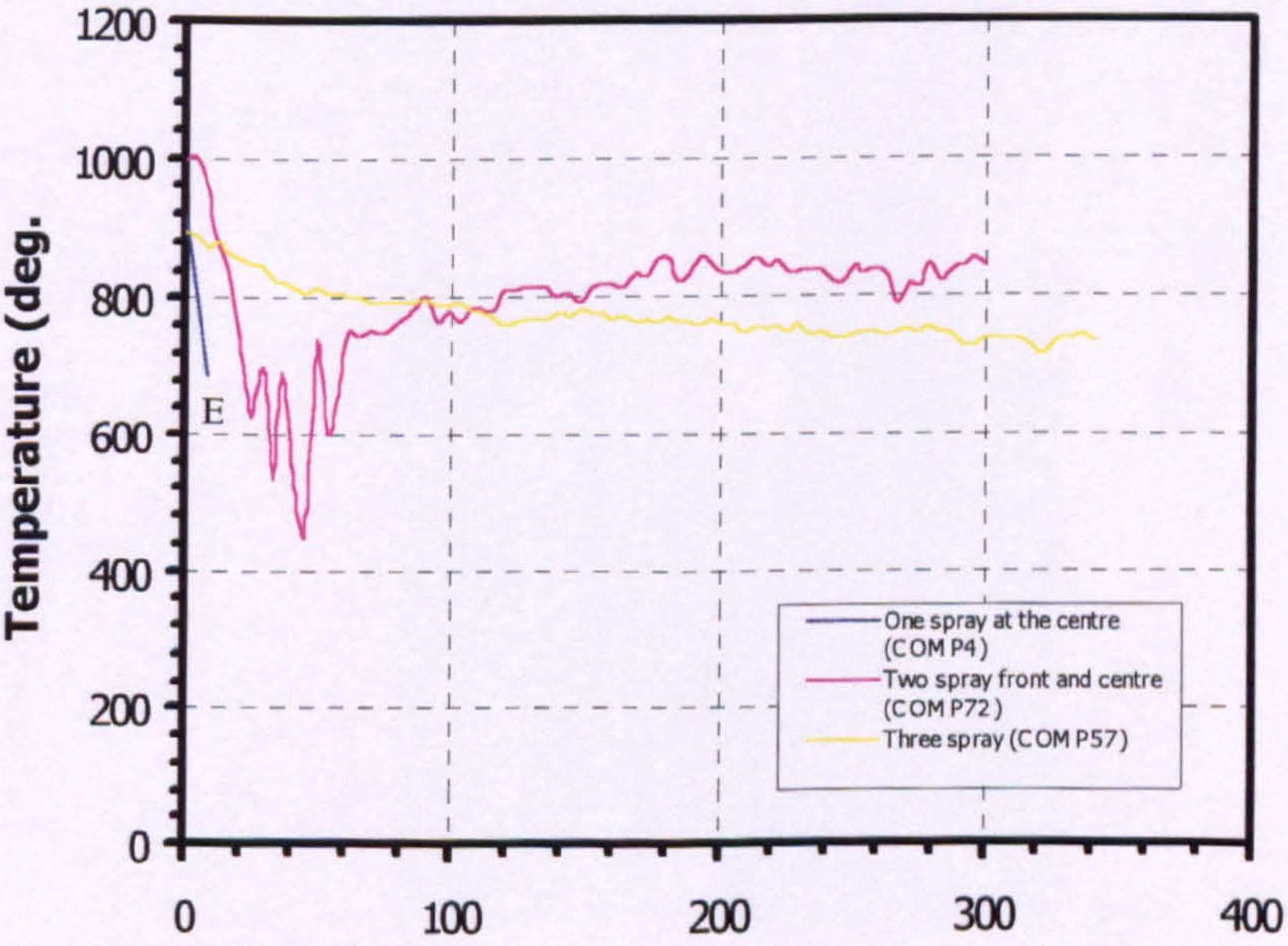

Figure (7.46). Average temperature distribution after water spray activation for different spray arrangements (number and locations) inside the compartment for 72 lit/min water flow rate at 150° spray angle (E = extinguished).

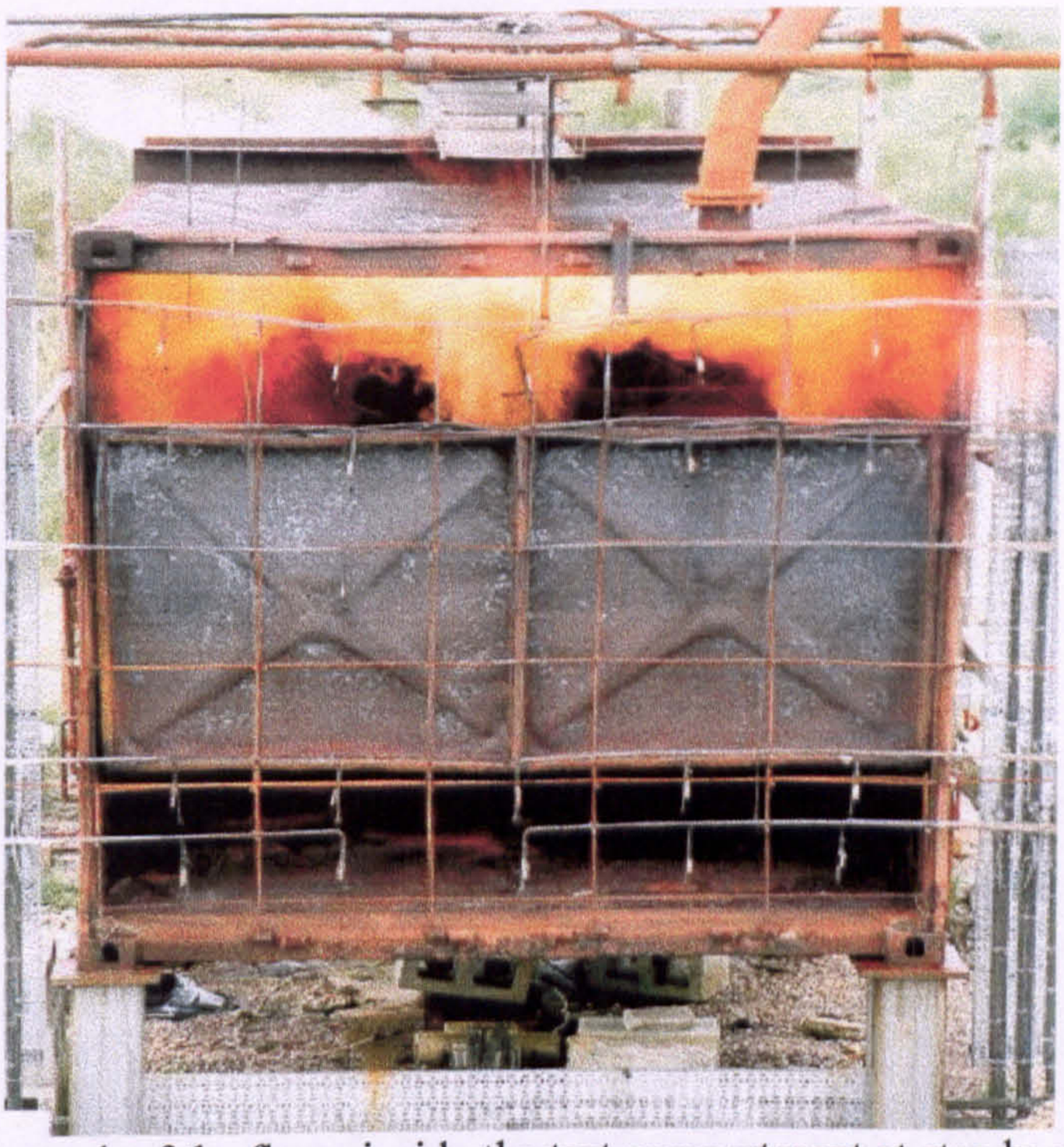

Plate (7.1). Photograph of the flame inside the test compartment at steady state.

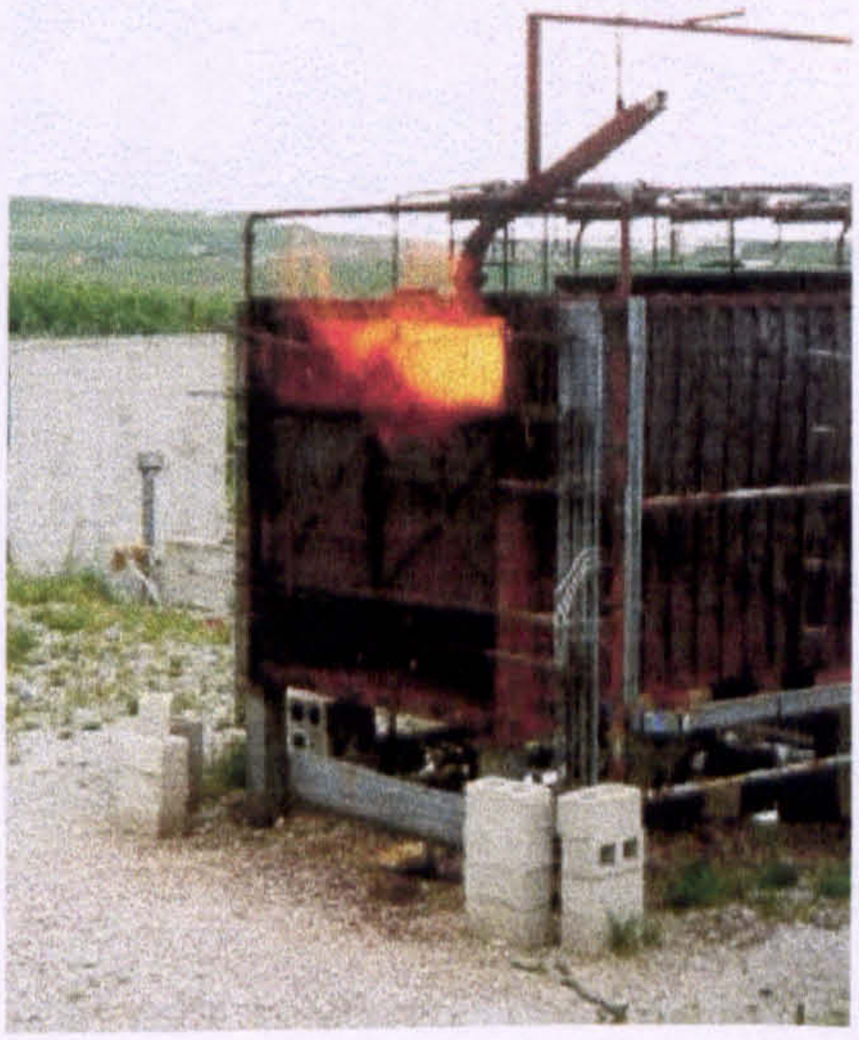

Plate (7.2). Photograph of the test compartment showing the external flame burning at the upper opening.

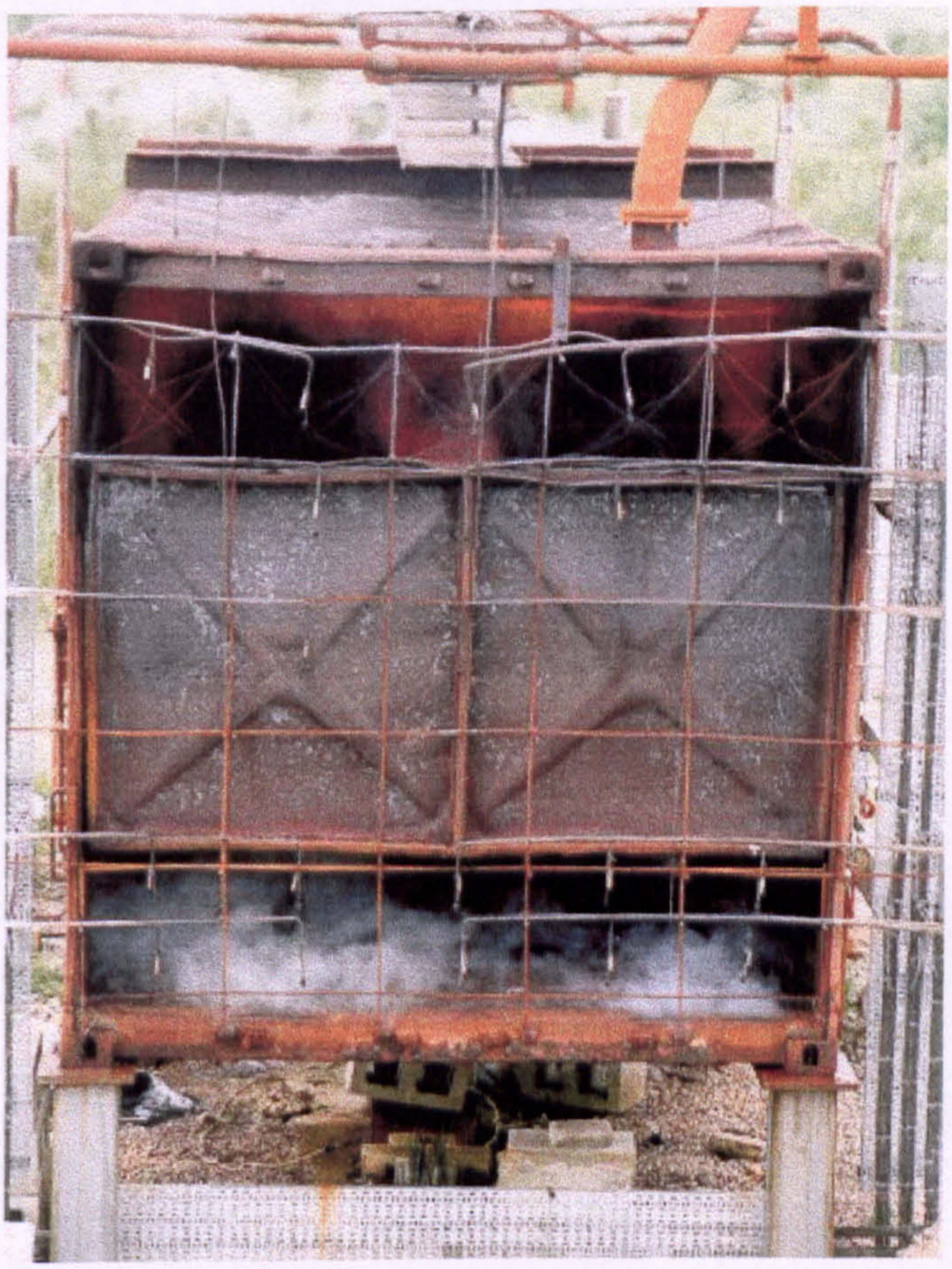

Plate (7.3). Photograph of test compartment when the water spray was activated, showing no flame shape was clearly noticed.

CHAPTER 8

NUMERICAL RESULTS BASED ON EXPERIMENTAL CONDITIONS

8.1 HEAT TRANSFER MODELLING

In order to simulate the heat transfer in the compartment, different modelling strategies have been used. To demonstrate and validate the model, a simple 2D steady state system was modelled. With this simple geometry, several tests were done to check the applicability of some sub-models (i.e. radiation) to the existing study, and to find the correct parameters to be used in the final solution. Then the system was modelled on 3-D geometry.

8.1.1 Conditions at the walls

The modelling went through different stages. Initially, an adiabatic condition was used to model the fire in the compartment. The outside wall surfaces were assumed to be adiabatic. The temperature contours on longitudinal plane along the jet nozzle are shown in Figure (5.11). From the figure the maximum temperature was found to be 2320 K.

Then heat transfer through the walls was applied by using the combined external convective and radiation boundary condition. The average combined (convection and conduction) heat transfer coefficients for the compartment external surfaces were determined and used. Experience has indicated that satisfactory solutions may be obtained by combining the heat loss effects together in an overall heat transfer coefficient, h_{ext}. A simplified approach was used to estimate the heat transfer coefficient as in the following (Foster, 1999):

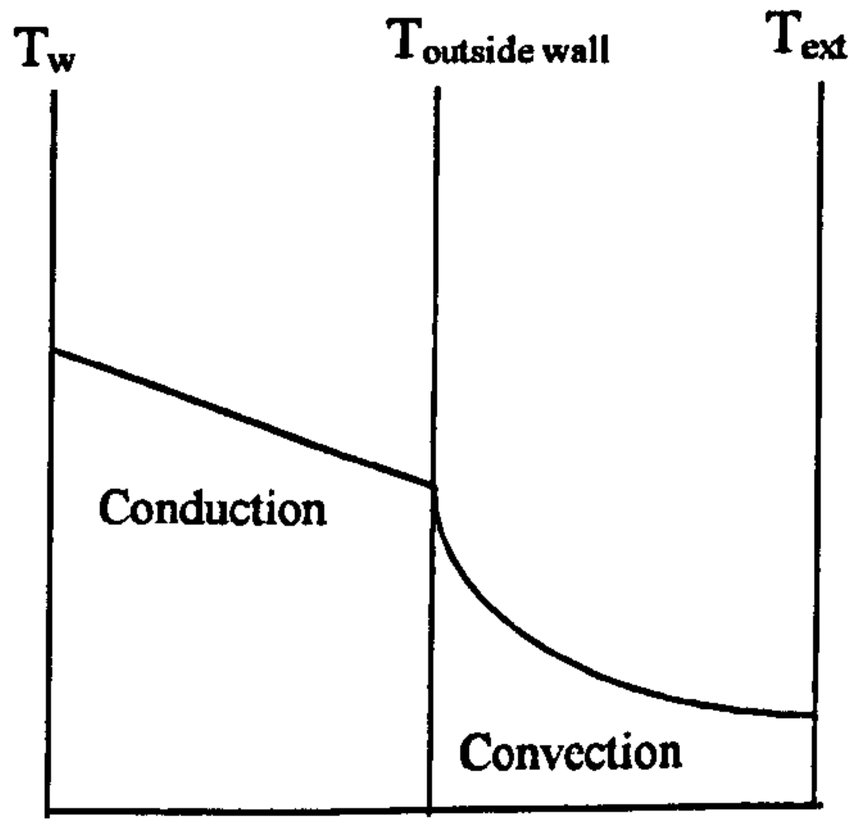

Figure (8.1) Overall heat transfer through a plane wall.

From Figure (8.1):

$$\frac{q}{A}\frac{\Delta x}{\kappa} = T_w - T_{ow} \tag{8.1}$$

$$\frac{q}{A}\frac{1}{h_o} = T_{ow} - T_{ext} \tag{8.2}$$

$$\frac{q}{A}\left[\frac{\Delta x}{\kappa} + \frac{1}{h_o}\right] = T_w - T_{ext}$$

$$\frac{q}{A} = \frac{T_w - T_{ext}}{\frac{\Delta x}{\kappa} + \frac{1}{h_o}}$$

$$\frac{q}{A} = h_{ext}(T_w - T_{ext})$$

$$h_{ext} = \frac{1}{\frac{\Delta x}{\kappa} + \frac{1}{h_o}}$$

$\kappa = 50$ W/m K [Smithells, 1983].

$h_o = 10$ W/m^2 K [Foster, 1999]

$\Delta x = 1.5$ mm

$$h_{ext} = \frac{1}{\frac{1.5\times10^{-3}}{50} + \frac{1}{10}}$$

$$h_{ext} = \frac{1}{0.10003}$$

$$h_{ext} = 10 \text{ W/m}^2 \text{ K} \tag{8.3}$$

The calculations above assume that the fire is fully developed and a design value of about 10 W/m^2 k is recommended for the coefficient of heat transfer. However, better results are obtained if h_{ext} is assumed to change linearly from zero at the start of combustion to a maximum value when the temperature of the gases and the steel element become equal. Unfortunately, since FLUENT did not have the facility to input h_{ext} as function of temperature, a constant value of h_{ext} is the only way to be used in FLUENT.

The results from this model are shown in Figures (8.2) and (8.3) which show the maximum temperature was 2100 K.

Since the model used combined external convective and external radiation boundary condition, it was decided to use heat transfer coefficient (h_r) to substitute for the external radiation boundary condition.

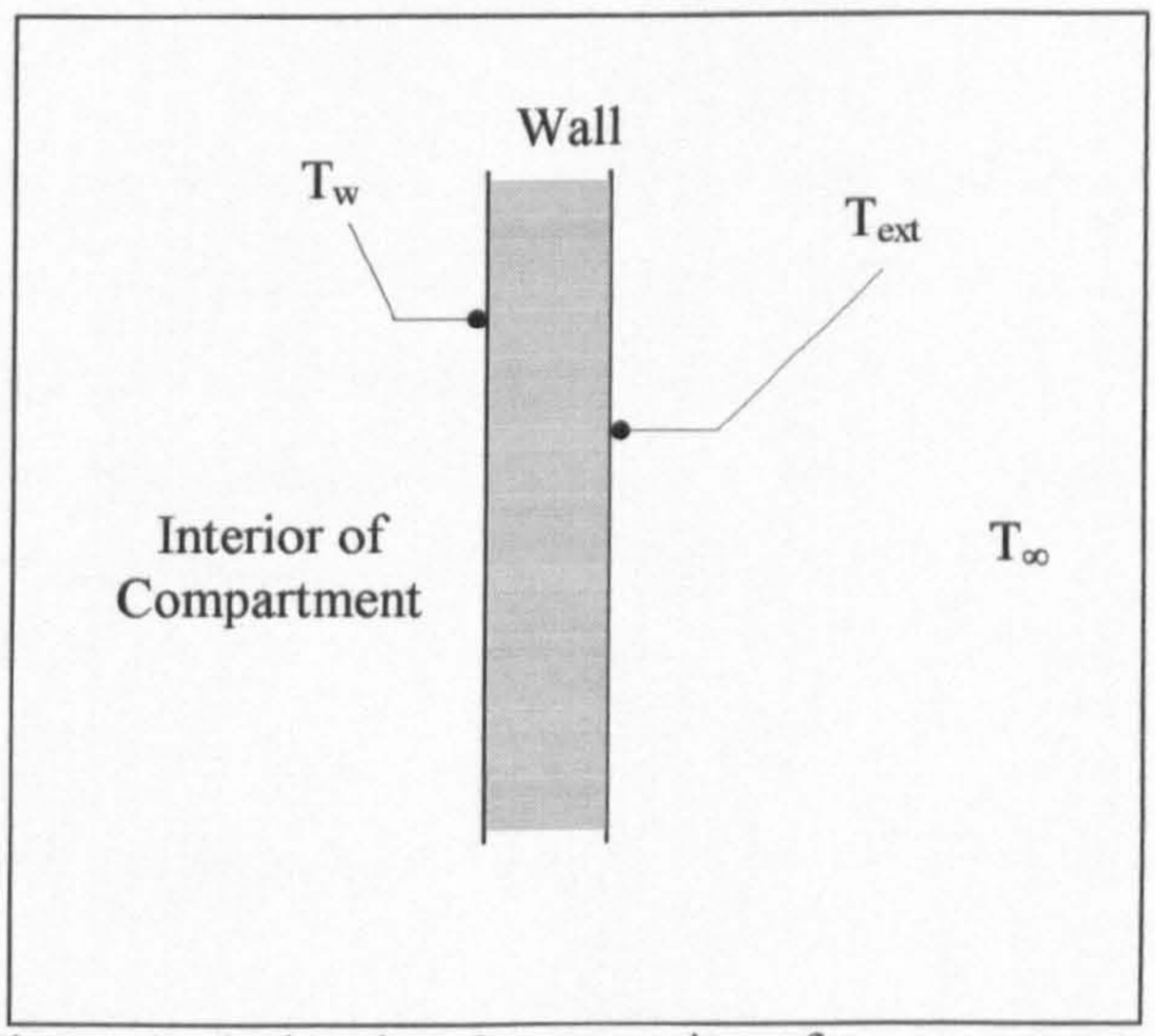

Figure (8.4) showing Cross section of compartment wall panel

From Figure (8.4)

$$q_c = (h_c + h_r)(T_\infty + T_{ext}) \tag{8.4}$$

$$q_c = h_c(T_\infty - T_w) \tag{8.5}$$

$$q_r = h_r(T_\infty - T_{ext}) \tag{8.6}$$

$$= 0.8\sigma(T_*^4 - T_{ext}^4)$$

$$= 0.8\sigma(T_\infty - T_{ext})(T_\infty + T_{ext})(T_\infty^2 + T_{ext}^2) \tag{8.7}$$

From equation (8.6) and equation (8.7):

$$h_r = 0.8\sigma(T_\infty + T_{ext})(T_\infty^2 + T_{ext}^2)$$

$$h_r = 0.8\times5.672\times10^{-8}(873+295)((873)^2+(295)^2)$$

$$h_r = 45\ W/m^2\ K. \tag{8.8}$$

From equation (8.3) and equation (8.8):

$$h_{Total} = h_c + h_r$$

$$h_{Total} = 55\ W/m^2\ K.$$

The results show that there is no difference between both cases as can be seen in Figures (8.5) and (8.6). Using either of these cases will give the same result; however using heat transfer coefficient for external radiation boundary condition will reduce the computational time, although this way will assume constant external radiation over the whole of the surfaces, which is not true.

8.1.2 Choice of radiation model

The next stage is to introduce the radiation model to the system. Radiative heat transfer plays an important role in the modelling of the combustion system. It shares

an equal role with convection for the transfer of heat within a turbulent diffusion flame. Radiation heat transfer is a demanding calculation because many coupled processes contribute. At a particular position within a flame, the local cooling due to the loss of radiative heat depends on the local absorption coefficient and the local temperature. However, the local temperature partly depends on the local heating from absorbed radiation which has emanated from other regions of the flame. The absorption coefficient is related to the local mass fractions of carbon dioxide and water vapour which themselves depend partly on the local temperature.

The discrete Transfer Radiation Model (DTRM) was chosen for use in these calculations because it is suitable for moderate optical thicknesses and also data are available for CO_2, H_2O and soot mixtures in Nitrogen. It employs a ray tracing procedure in which the radiative transfer equation is solved along paths generated by the angular discretisation of boundary cell faces. The radiative loss (or gain) of an individual control volume is then evaluated as a balance between emission and absorption for all the rays traversing that control volume. Summation of the final intensity at the end of a line of sight from rays in all directions intersecting a wall cell yields the incident flux.

In the present study, the radiation properties along the non-homogeneous ray paths have been computed using the weighted sum of grey gases method (FLUENT, 1996).

8.1.3 Choice of Number of Rays

Radiative exchange in the compartment fire studied was computed for 6 and 8 rays, fired from the solid surface of each boundary cell. Figure (8.7) and (8.8) show the filled temperature contours for two different cases simulated with radiation in the flow. The radiation was computed for two different ray numbers to test the effect of the ray numbers on the accuracy of the prediction. The ray numbers used were 6 and

8. From these figures it can be seen that the temperatures are not affected by the changing of the ray numbers. The result shows that 6 is to be used for the number of rays of both (θ and ϕ). This value reflects a compromise between computational economy, uniformity and accuracy of coverage. The wall emissivity used (McAdams, 1954) was 0.8.

8.1.4 Radiation Correction Factor

The radiation boundary temperature correction was used to solve the problem of the outlet in the radiation calculation. It has been noticed when investigating details of the radiation calculation that the outlet radiates back to the compartment, which causes a temperature increase. FLUENT used the inlet and outlet cells temperature to compute the radiation heat flux while the actual temperatures beyond the outlet boundary are less than the outlet temperatures. FLUENT includes an option that allows the influence of the gas temperature beyond the inlet and outlet boundaries to be taken into account, and to specify different temperatures for radiation at inlet and outlet. FLUENT will not take into account the influence of the temperature of the ambient beyond the outlet boundary without specifying the radiation boundary temperature correction option.

8.1.5 Conduction Modelling

Alternatively, modelling conduction can be performed by using conducting wall. A combined external convective and external radiation boundary condition was modelled on the exterior wall with a thin layer of conducting wall placed next to it. The discrete transfer radiation model (DTRM) was activated to ensure both

convection and radiation was calculated during the process in the compartment. The thermal conductivity of all structure components was modelled by temperature dependent profiles.

8.2 STEADY STATE FIRE RESULTS

The refined grid distribution which was used to model the steady state flow reported in this section is shown in Figure (8.9). The temperature distribution obtained for the whole domain and close to the jet nozzle location when using the radiation sub-model, combined external heat transfer and external radiation is given in Figures (8.10) to (8.14). This clearly shows that approximately 20% of the peak temperature has been reduced from the adiabatic values in excess of 2350 K to approximately 2000 K.

Figure (8.10) shows the temperature predicted through the jet nozzle section in (x-y plane). It is clear in this figure that the maximum temperatures in this section were predicted above the jet nozzle. The cooling effect of the air entrainment from the lower opening is also clearly presented in this figure which displays the minimum temperature in the whole compartment. Also this can be seen very clearly in Figure (8.11) which shows the predicted temperature through the side view of the jet nozzle (y-z plane). This figure also shows the flame shape which is consistent with the experimental observation.

Figure (8.12) shows the filled contours of the temperature through a (x-z plane) below the ceiling. The maximum temperature was found in the centre where the jet hit the ceiling.

The average predicted temperature of the gas exiting at the upper opening was 1373K (1100° C) as shown in the Figure (8.13) which shows the temperature filled contours

at (y-z plane) at the compartment opening. The figure also shows the cooler lower opening through which the air was entrained.

Back wall filled contours temperature obtained from the prediction can be seen in Figure (8.14). The figure shows the maximum temperatures were found in two circles in the upper middle of the back wall. This can be explained by Figure (8.15) which shows the velocity vector of the slice next to the back wall. In this slice, it has been found that in a position coinciding with the two hot circles the flow of the hot combustion gases hits the position which cause the circles to increase in temperature. The figure shows that gases flow towards the centreline of the slice from the sidewalls, which causes two small circulation zones to the left and right of the centre line. Also there were two circulation zones in the bottom corners.

Figures (8.16) to (8.19) show the predicted velocity vectors in different slices of the compartment, with Figure (8.16) showing the velocity vector below the ceiling in the x-z plane. After hitting the roof the jet fire spread outward along the ceiling. Most of the flow which was directed towards the vent escaped through the upper opening and a little mixed with the entrained air and recirculated back toward the flame. On the other hand, the flow directed towards the back wall was circulated back to the flame. This also can be seen in Figures (8.17) and (8.18). These figures show the x-y plane and the y-z plane of the compartment through the jet fire section respectively.

The velocity vector predicted at the compartment opening is shown in Figure (8.19). The figure clearly shows some of the flow escaping through the upper opening and the other part mixing with the entrained air through the lower opening and circulated back to the flame.

Finally, The predicted temperature filled contours of the side wall (x-y plane) and the slice next to it were shown in Figure (8. 20) and (8.21) respectively. It shows the maximum temperature was found in a circle below the ceiling in the centreline and to the right in the opening direction. The reason for that can be explained by Figure (8.22) which shows the velocity vectors for the (x-y plane) next to the wall, and

Figure (8.18). The flow of the jet hits the ceiling and then flows outwards along the ceiling at the same time as the jet flow hits the upper side wall at the centreline, which will affect that area by increasing its temperatures.

8.3 TWO-PHASE STEADY STATE

Using the field modelling approach it is possible to simulate the action of water sprays in a fire compartment. As this scenario is a continuation of the earlier steady state fire simulation presented in the previous section, the compartment temperatures and flow field for the steady state modelling was used as an initial condition for the water spray modelling.

FLUENT approximates the nature of sprays by calculating trajectories of droplets with five different diameters. The water spray is represented by distribution of droplets of varying sizes and initial projectile angles projected into the fire field from a chosen starting point. The droplet size distribution was described by the Rosin-Rammler distribution function. Each group of droplet sizes was further discretised by considering a distribution of initial projectile angles in order to represent a full spray cone. For each spray 25 injections were specified, covering an initial angle range represented by a range of initial droplet velocities. The mass flow along each trajectory is distributed to provide an initial mass distribution which is proportional to the solid angle. When using FLUENT four characteristics of the spray must be specified; the droplet diameters, the total water flow rate, the initial position and the injection velocity which represents the initial velocity and spray angle. The injection velocity specified is constant for all the drop sizes.

Using the description of the physical set-up and the outlined mathematical model described in chapter 4, the following results for steady state and time-dependent water spray modelling to be discussed were obtained.

In this study the spray locations were chosen so that they would provide a good coverage of the whole compartment.

The spray behaviour depends greatly on the initial angles of the droplet trajectories and the drop sizes. The initial angles were chosen so that a wide variety of angles can be used in such a way that, in the absence of the fire, all droplets fell within the jet fire source and the surrounding area.

The trajectory of particles obtained for the mean particle tracking are shown in Figures (8.23) to (8.26) for the different spray angles used without fire. The effect of the jet on droplets motion can be seen in Figures (8.27) to (8.30) in which trajectories of different mean droplets diameters with different spray angles are shown when the jet fire is fully developed. As can be seen from the figures some of the water is collecting along the floor and some is escaping through the upper and lower opening. The remaining part is shown with "+" at the end of the trajectories, representing the point at which complete evaporation has occurred.

An inspection of the trajectories of all droplets reveals that smaller droplets (less than 330 μm) do not actually penetrate the jet and are deflected by the effect of the jet and then evaporated. On the other hand, larger droplets (larger than 330 μm) penetrate the fire and hits the floor. It is clear that the droplets with diameter of 330 micron or less do not have sufficient momentum to penetrate the jet near the centreline.

Therefore, the spray must have sufficient forward force so that too much of it is not deflected by the flame and hot gases associated with the fire and then escapes through the upper opening. The factors which control the penetration of sprays to the centre of the flame are the drop size and thrust of the spray, the thrust of the flames, the gravity and the evaporation of spray in the flames.

The results on the flow field and the particle trajectories indicated that both the water trajectories and the air flow pattern were affected by the water flow rate and the droplet projectile angles. If the water flow rate and spray angle were increased, the drag (throw) force would increase.

In addition, the downward motion of the spray with the deflected smaller drops created a type of water barrier which tended to obstruct the upper opening and to confine the hot gases to the far end of the compartment as can be seen in Figures (8.28) and (8.30). The hot gases were initially flowing below the ceiling and escaped through the upper portions of the outlet. Meanwhile, cooler gases were entrained at the lower levels. However, the spray churned up this stable process by mixing the hot gases with the cold water droplets as they were forced out and downwards by the spray, as can be seen in Figures (8.32) and (8.33).

Figure (8.31) clearly shows some of the drops which fall in the air entrainment path will be carried and pushed with the air currents towards the jet fire which will enter the lower flame region and then evaporated.

Figures (8.32) and (8.33) show the predicted velocity vectors at the centre of the compartment. Figure (8.32) depicts the interaction between the jet fire and the 90 lit/min spray. It indicates that the overall flow is dominated by the jet and the presence of spray seems to make almost no impact on the jet flow. Figure (8.33) shows the interaction of the jet fire with 36 lit/min spray. Prior to the spray activation, the jet fire was able to rise straight upwards and spread outwards along the ceiling. After the spray activation (one single spray case) two major flows were apparent. The first, generated by the water spray, was downwards. The second, generated by the fire, was upward and hit the ceiling. These two currents met towards the centreline of the compartment, 0.4 metre below the ceiling, aiding the mixing and cooling process.

In Figures (8.34) and (8.35) two planes through the spray (y-z planes) illustrate the effect of the spray on the overall gas flow field. The spray forces the gases downwards as well as entraining air from its surroundings. The subsequent circulation pattern causes the air to be forced upwards along the walls.

The resulting flow field near the back wall is illustrated in Figure (8.35). It is worth noting how the air and gases are pushed upwards along the outside walls as well as forced downwards by the entrainment of the spray.

The hot gases created by the fire are also confined and further pushed back to their source. Therefore, the flame length was shortened due to the momentum of the spray drops as shown in Figure (8.36). However, the newly generated circulation pattern causes the lower levels to be slightly warmed up due to mixing of the hot upper layer gases and the colder lower layer gases.

Some of the resulting gas temperature distributions are shown in Figures (8.37) to (8.40). These clearly show the effect of the spray conditions on the gas temperatures.

An application of water flow rate to the jet fire in a compartment when steady state condition has been reached produces a temperature drop; however this temperature drop varies according to the spray condition used. These conditions include water flow rates, droplets diameters, spray angle, spray location and number of sprays used.

The same conditions previously used in the experiments will be used for the modelling, which will promote the validation and comparison of these results.

In order to investigate the effect of the spray angles alone on the average gas temperature reduction different spray angles were studied at 54 lit/min water flow rate. It was found that the maximum reduction in the gas temperature was reached when 150 degree spray angle was used.

Figure (8.36) clearly shows the reduction of average temperature from around 1520K before water spray activation to maximum reduction of 730 K in COMP18 after water spray activation; it also shows that steady state condition was reached. However, the minimum reduction for one spray nozzle was found when smaller spray angle and larger droplet sizes were used. Initially hot gases were rising from the jet nozzle. They were entrained by the spray, then forced downward and cooled down.

An application rate of 90 lit/min for one spray was the maximum water flow rate at any spray angle to be used in the modelling. Therefore the maximum drop in

temperature after the application of this water flow rate at 150 degree spray angle was found to be 600 degrees.

Figure (8.41) illustrates the maximum reduction in the average temperature for different spray numbers and locations at fixed total water flow rate. The results show a higher reduction in the temperatures when the total flow rate for one spray is used. However, the spray located in the centre reduced higher temperatures.

One finds in general that as the water application rate is increased, keeping all other conditions fixed, the maximum reduction in the average temperature is consistent with the increased water flow rates until 72 lit/min water flow rate has been reached when the drop in the temperature occurs abruptly above a certain increment as shown in Figure (8.42). The rapid drop of flame temperature in this case may be due to the penetration of the water drop into the flame and the relatively smaller drops produced with this flow rate, which increases the predicted evaporated mass flow. However, when the water flow rate further increases, the reduction in the temperature is not significant compared to the total large water usage.

The higher reduction in the temperature observed is in the path of the water injections.

Figures (8.43) and (8.44) taken through horizontal and vertical planes across the wall and the floor show the water mass fraction.

The wall surface temperatures, appear to be little affected by the water spray as after steady state condition is reached. The temperatures of the side walls have higher effects when using 150 spray angle. On the other hand the lower part of the side walls have higher temperature reduction when smaller spray angle was used.

The resulting compartment temperature distribution of water flow rate with 36 lit/min, 60° spray angle with mean drop diameters 1084 μm at slice x-y plane across the jet nozzle is shown in Figure (8.39). It clearly shows the reduction in the average temperature from 1520 to 1456 K. It also shows that the water flow rate and drop

diameters used were not affecting the temperature because the low flow rate and larger drops produced made evaporation difficulties.

The temperature stratification within the compartment was disturbed by the injected water spray. The water spray had cooling effect on the temperature of gases which existed in the spray region. As the hot gases were initially accumulating in a layer below the ceiling, when the water spray got activated and the flow rate was at 108 lit/min, the maximum drop in average temperature occurred (800 K). The lowest temperature was in the corner (opposite to the ventilation opening).

Table (8.1) shows the predicted evaporation rate for different cases modelled. Prediction of the evaporation rate when using a total of 90 lit/min water flow rate for different arrangements of spray nozzle number and locations has been studied. It is clear that using one spray nozzle with 90 lit/min will give the highest predicted evaporation rate. However, there is no significant changes in the predicted evaporation rate between 90 lit/min and 72 lit/min for the same conditions. But the use of the same water flow rate for three or two sprays located at any position arrangement such as the centre and front (F+C), centre and back (C+B) or front and back (F+B), will yield less evaporation rate than one spray. This can be attributed to the fact that with higher water flow rate the nozzle will produce relatively smaller droplet sizes than spray with lower water flow rates. Therefore, the smaller the droplet diameter is, the faster it will evaporate in a hot gas environment. On the other hand, larger drops take longer to attain equilibrium conditions, and their trajectories are different from those of the smaller drops since they are less influenced by aerodynamic drag forces.

As far as the evaporation is concerned, spray angle makes less significant contribution to the evaporation of the drops. From table (8.1) it was found that for the same water flow rate of 54 lit/min used for different spray angles with one spray located centrally, a spray angle of 150 degrees will produce the highest evaporation rate. There are two reasons for that, because of the spray angle effect which controls

the velocity of the drops relative to that of the surrounding gas, and the smaller drops produced with the 150 degrees. However, less momentum and mixing characteristics can be found with this spray angle.

When these arrangements were used to find the highest predicted evaporation rate for different spray locations it was found that the highest evaporation rate occurred when the spray was in the centre of the compartment. The reason for that is that the rate of evaporation depends on the temperature of the surrounding hot gases. Since the spray nozzle is located above the jet fire which has the maximum temperature. Therefore, the water drops injected from the central position will face the highest temperature in the compartment. The evaporation of drops involves simultaneous heat and mass transfer processes in which the heat for evaporation is transferred to the drop surface by conduction and convection from the surrounding hot gas, and vapour is transferred by convection and diffusion back into the gas stream. This will cause cooling and inerting of the flame and the combustion area.

Some of the cases modelled show very low evaporation rate, which means most of the drops didn't evaporate completely. However, the drops heat up and, at the same time lose part of their mass by vaporisation and diffusion into the surrounding air or gas as they travel until they hit the floor or the walls.

The above results for the steady state clearly demonstrate the significant effect an active spray has. Not only have the gas temperatures considerably decreased, but also the complex circulation pattern which aids this process has been captured. However, the important factor is that it provides initial guidelines as well as confidence for the design of a time-dependent two-phase fire-spray model. The results of the study for time dependent models are presented below.

In view of the effect of larger water flow rates on chamber temperatures, it was clear that a time-dependent approach would be more representative, since extinguishment would be associated with time dependence of the main variables.

Test No.	Spray location	Spray angle	Mean drop diameter μm	Spray number	Total water flow rate lit/min	Predicted evaporated mass %	Predicted evaporated mass flow lit/min
COMP3	C	150°	417	1	54	31	16.8
COMP4	C	150°	342	1	72	42.4	30.5
COMP5	C	150°	295	1	90	41	36.9
COMP10	B	150°	417	1	54	28.6	15.4
COMP13	C	60°	761	1	54	17.8	9.6
COMP14	C	60°	380	1	72	39.7	28.6
COMP21	C	90°	335	1	54	29.5	15.9
COMP23	C	90°	386	1	90	35.4	31.9
COMP28	C	120°	553	1	54	23.1	12.5
COMP38	F	150°	417	1	54	26.3	14.2
COMP51	F+B	150°	756	2	72	10.1	7.3
COMP57	F+B+C	150°	966	3	72	4.3	3.1
COMP58	F+B+C	150°	706	3	90	6.9	6.2
COMP63	C+B	150°	756	2	72	12.6	11.3
COMP72	C+F	150°	756	2	72	11.6	8.4

Table (8.1) Predicted evaporation rate in the compartment for different spray arrangements.

8.4 TIME DEPENDENT

For the time-dependent simulation, the general description and conditions of the compartment previously given for the steady state water spray modelling were not altered for this current simulation. As already mentioned, the predictions made and discussed in section (8.2.1) are used as the initial conditions for this simulation.

The time-dependent option in FLUENT was activated at the same time as the water sprays activation after the single-phase steady state simulation was reached.

The simulation was performed initially with one millisecond time step for time dependent cases, then was increased to 0.1 second. During these steps iterations across the domain were carried out until convergence criteria of the variables solved were satisfied; typically, residuals fall between 10^{-4} and 10^{-6} . The number of iterations required during each time step calculation was set to be 500.

Results from these for the one spray case located centrally above the jet fire with 72 lit/min water flow rate and 150 degree spray angle are shown in Figures (8.45) and (8.46) which illustrate the general conditions within the compartment and the way in which they vary in time. Gas temperature filled contours are used to show the effect of the spray on the temperature reduction and at (y-z) planes cross the jet fire at distinct time within the compartment. The time intervals shown are 0 and 12 seconds after spray activation, whereby Figure (8.45) is used to show more clearly the effect of the spray. In these figures the reduction in the flame height was very clear. The gas temperatures were reduced as the time increases.

The peak gas temperatures in the compartment, Figure (8.47), initially, after 5 seconds, appeared to be hardly affected. However, after 12 seconds they showed a

reduction of only 125°C. Temperatures in the upper portion of the flame are lowered by the heating and evaporation of water spray in the flame.

Figures (8.46) and (8.47) clearly show how the stable temperature stratification is quickly disturbed by the addition of the cooling water particles which are injected downwards through their centre. Hence, cooler gas is generated and pushed downwards resulting, with time, in a form of water curtain. This in turn confines the hot gases which are still generated by the fire, whilst cooling down the gases near the escape opening.

Figure (8.48) shows average temperature prediction in the compartment against time. In this figure a large drop in the average temperature occurred in the first second after the activation of the water spray. Thereafter, the temperature decreases slowly as the time increases.

Figures (8.49) and (8.50) show the prediction of the gas temperature at the centreline of the compartment in two different grid locations in the x-axis, within different layers at the compartment height. The two x-axis locations at 1.5 meter downstream and upstream the flame, ASP-26 to ASP-30 and ASP-31 to ASP-35, respectively. Detailed investigation of the results showed that a rapid drop in the gas temperature occurred in the first second after the water spray activation within the upper layer downstream the flame at locations ASP-26 and ASP-27 in Figure (8.49). Therefore, the interesting feature to point out is that after 8 seconds, the peak gas temperature reduction has occurred above 1.6 meter from the floor, indicating the overall cooling effect within the upper layers. A slight increase in gas temperature observed in location ASP-34 below that height illustrated the initial mixing of the hot and cold gases as they were pushed downwards by the spray as well as an overall cooling in the upper level. These characteristics were also observed for locations ASP-35 and ASP-29 when the gas temperatures almost remained unchanged.

Figure (8.51) shows the prediction of the gas temperature varying with time at different grid points along the compartment upper opening, ASP-1 to ASP-5. It was observed that the gas temperature was drastically reduced within the upper opening 1 second after the water spray activation, a characteristic similar to the prediction made inside the compartment within the upper layer. The overall cooling effect within the upper layer had reduced the external flame length which was burning near the compartment upper opening. The trend of the gas temperature reduction was similar for all locations along the compartment opening ASP-1 to ASP-5.

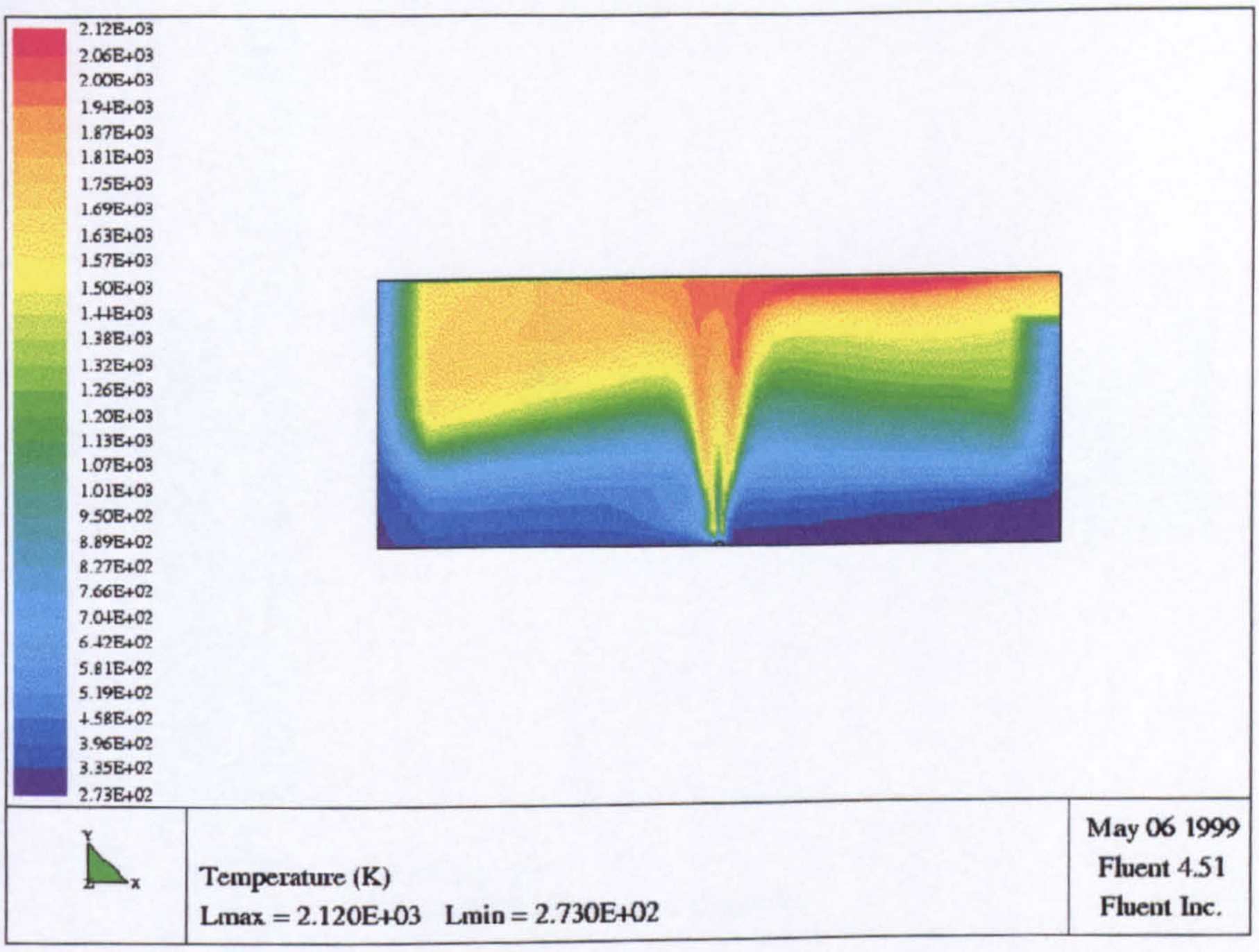

Figure (8.2). Predicted gas temperature contours through the longitudinal x-y plane at the centre of the jet fire with external convective heat loss, h_{ext} of 10 W/m^2 K, and no radiation, either external or in the flow. Showing the effect of a coarser grid.

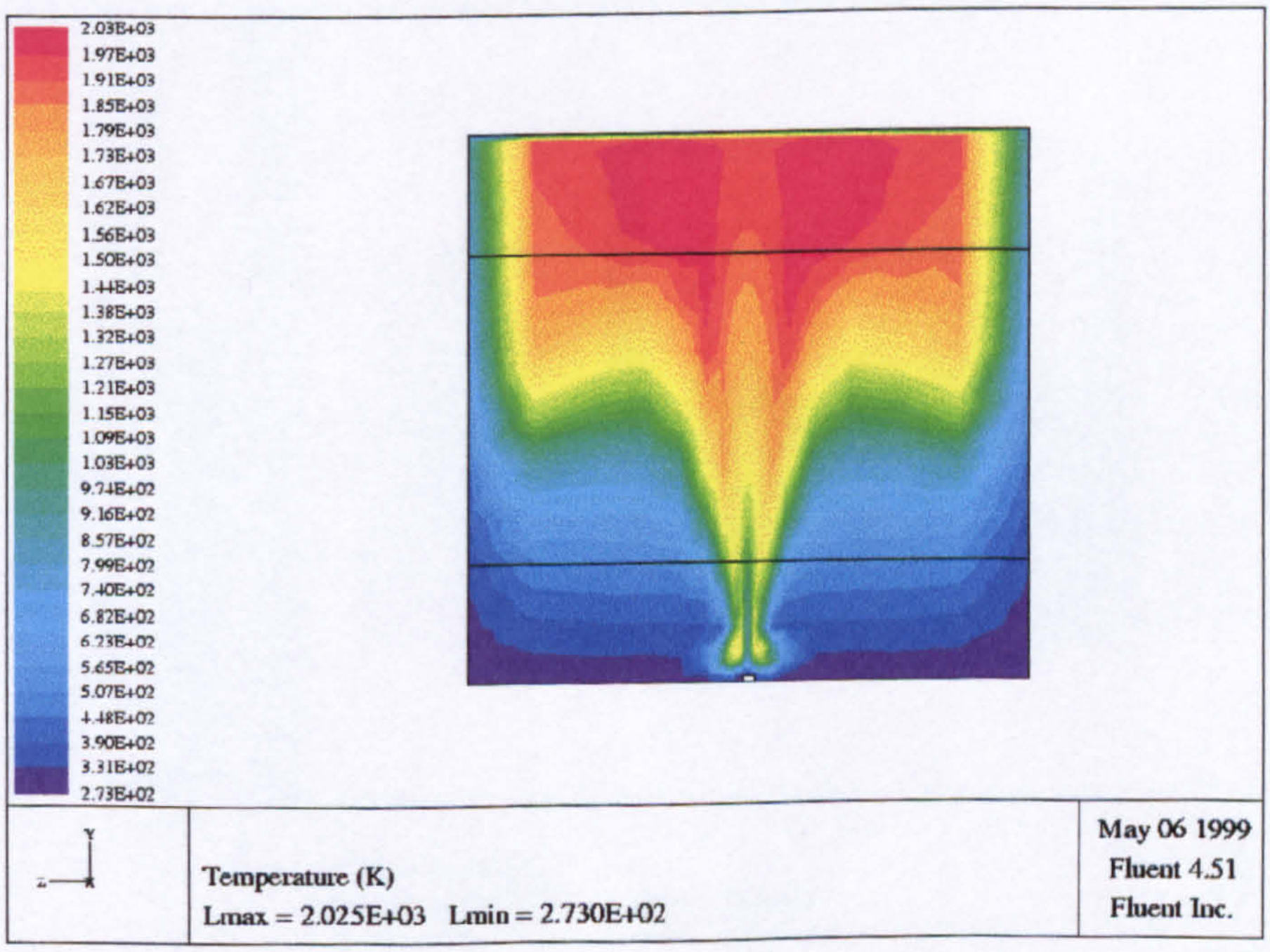

Figure (8.3). Predicted gas temperature contours through the lateral y-z plane at the centre of the jet fire with external convective heat loss, h_{ext} of 10 W/m^2 K, and no radiation, either external or in the flow. Showing the effect of a coarser grid.

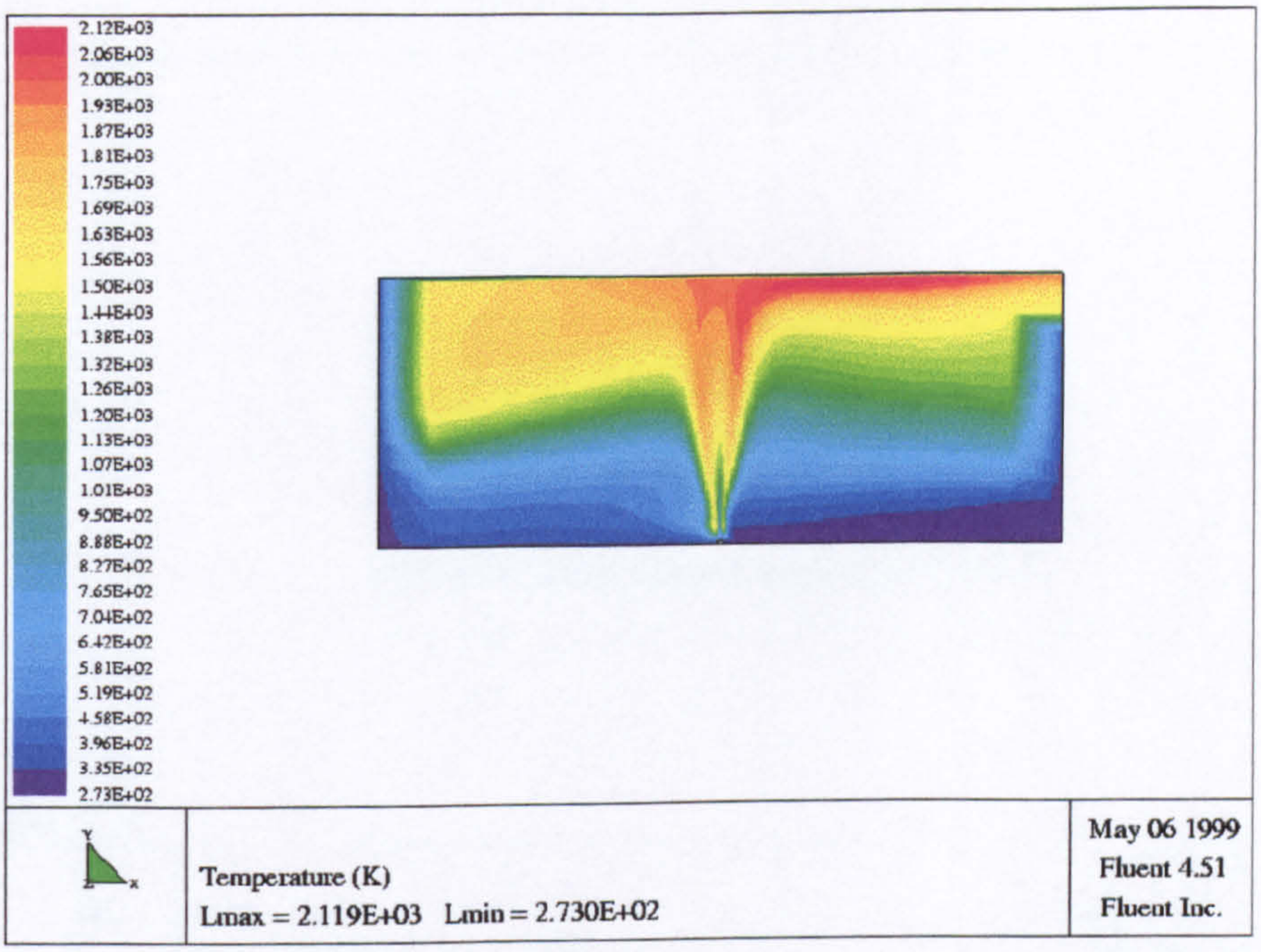

Figure (8.5). Predicted gas temperature contours through the longitudinal x-y plane at the centre of the jet fire with no radiation in the flow, but with both convective and radiative external heat loss when h_{ext} = 55 W/m^2 K has been used.

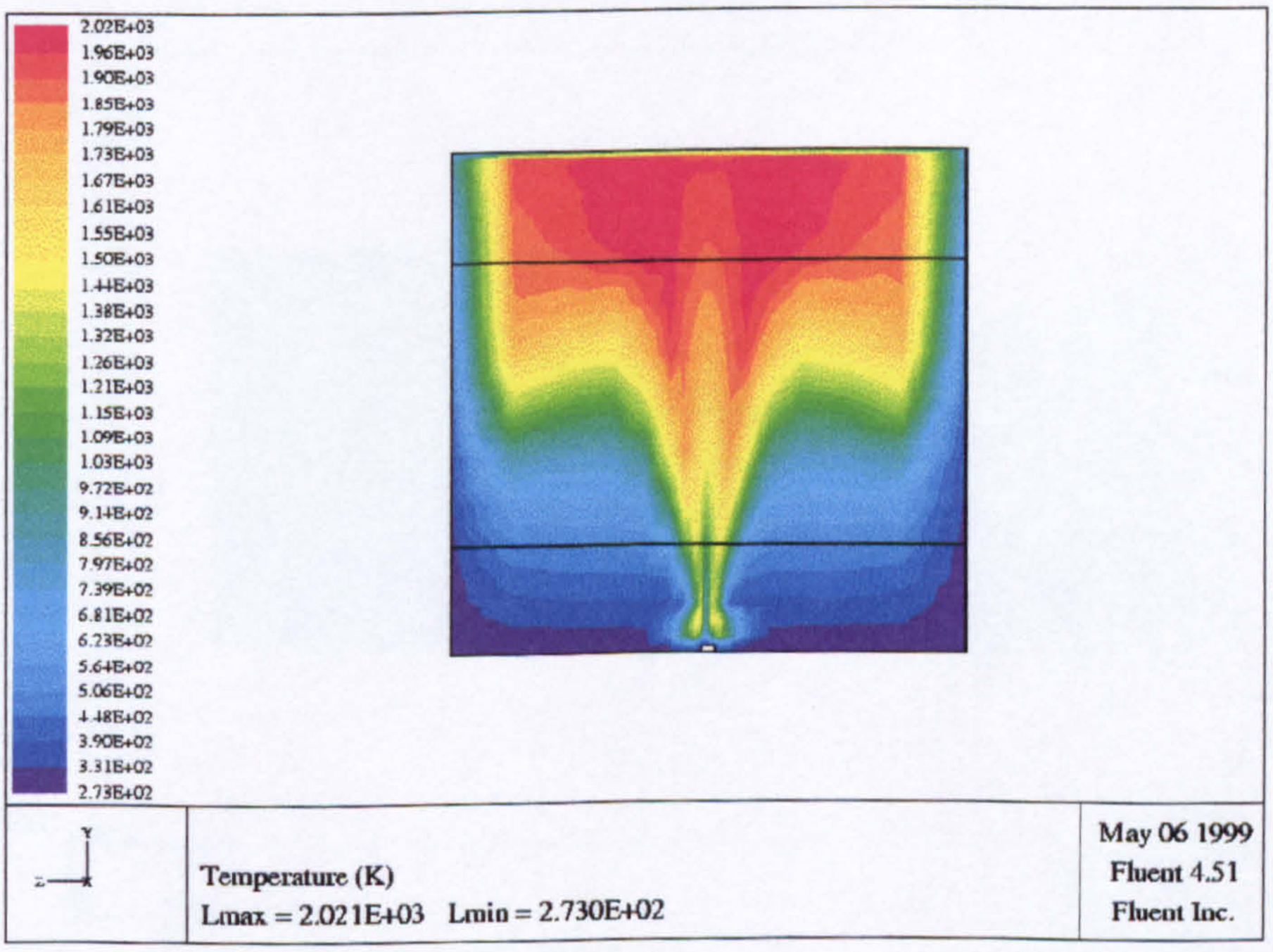

Figure (8.6). Predicted gas temperature contours through the lateral x-y plane at the centre of the jet fire with no radiation in the flow, but with both convective and radiative external heat loss for when h_{ext} = 55 W/m^2 K has been used.

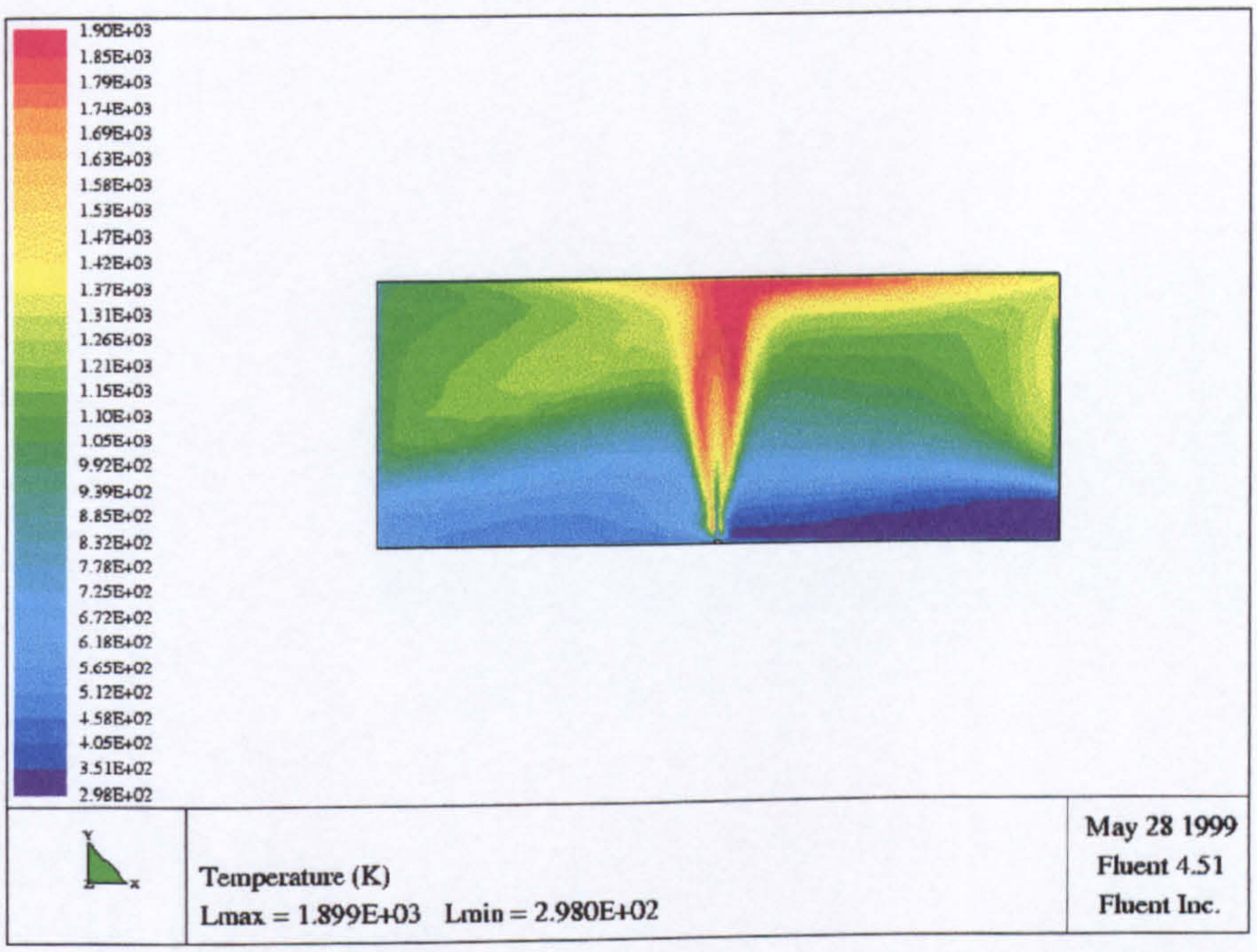

Figure (8.7). Predicted gas temperature contours through the longitudinal x-y plane at the centre of the jet fire using the DTRM radiation model in the flow and both external convective and radiation heat loss, the number of rays used, θ=8 and ϕ=8.

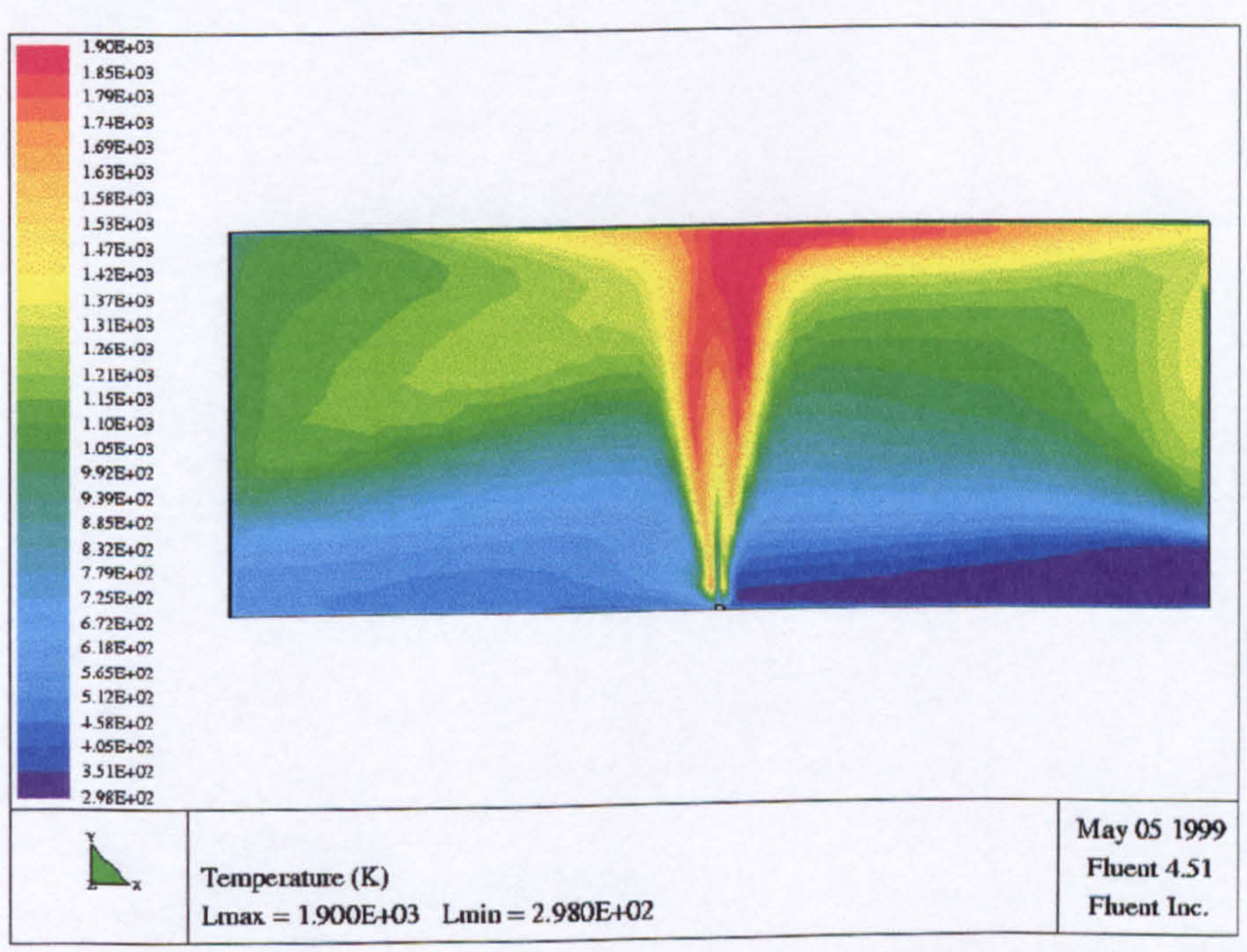

Figure (8.8). Predicted gas temperature contours through the longitudinal x-y plane at the centre of the jet fire using the DTRM radiation model in the flow and both external convective and radiation heat loss, the number of rays used, θ=6 and ϕ=6.

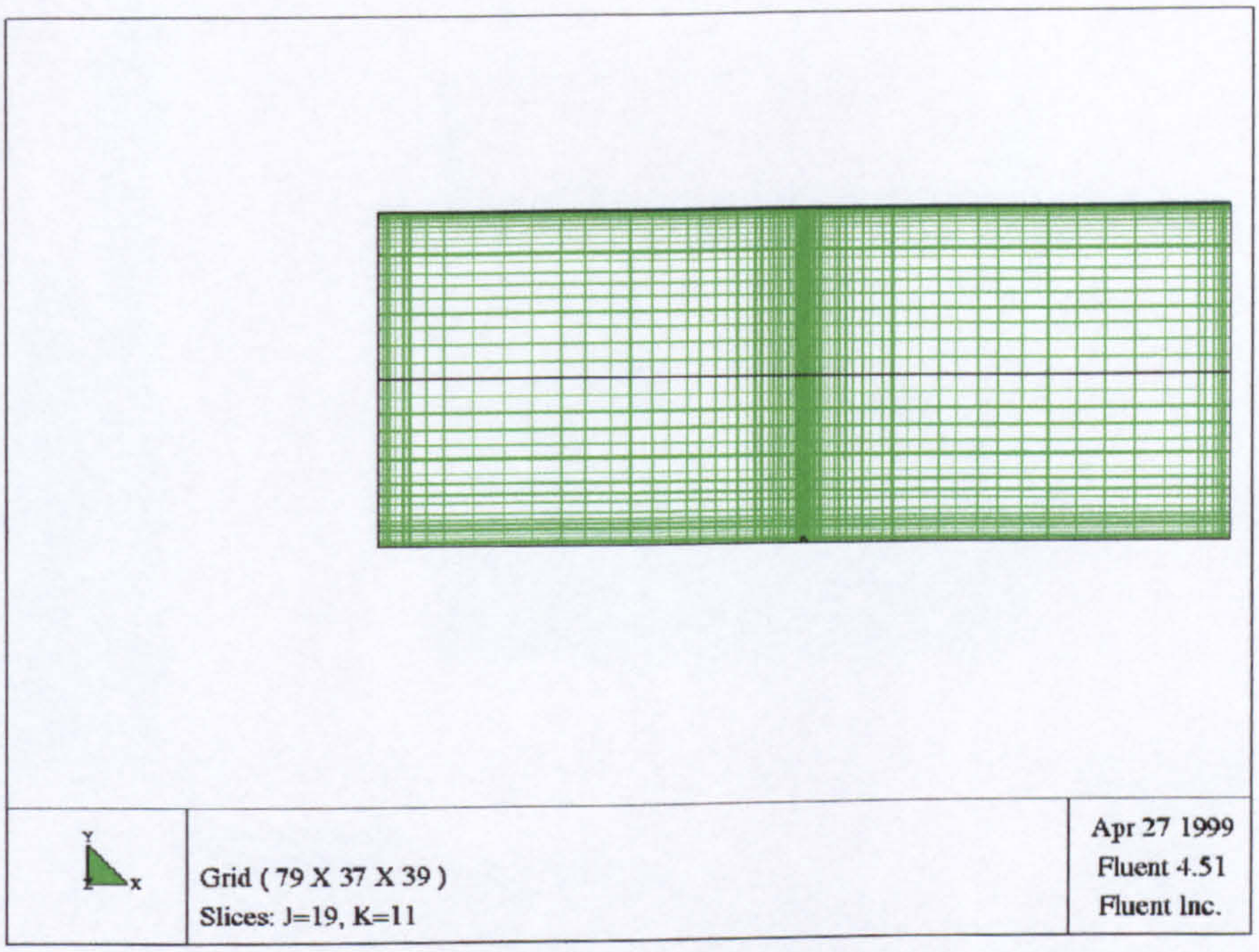

Figure (8.9). Refined grid distribution in the compartment.

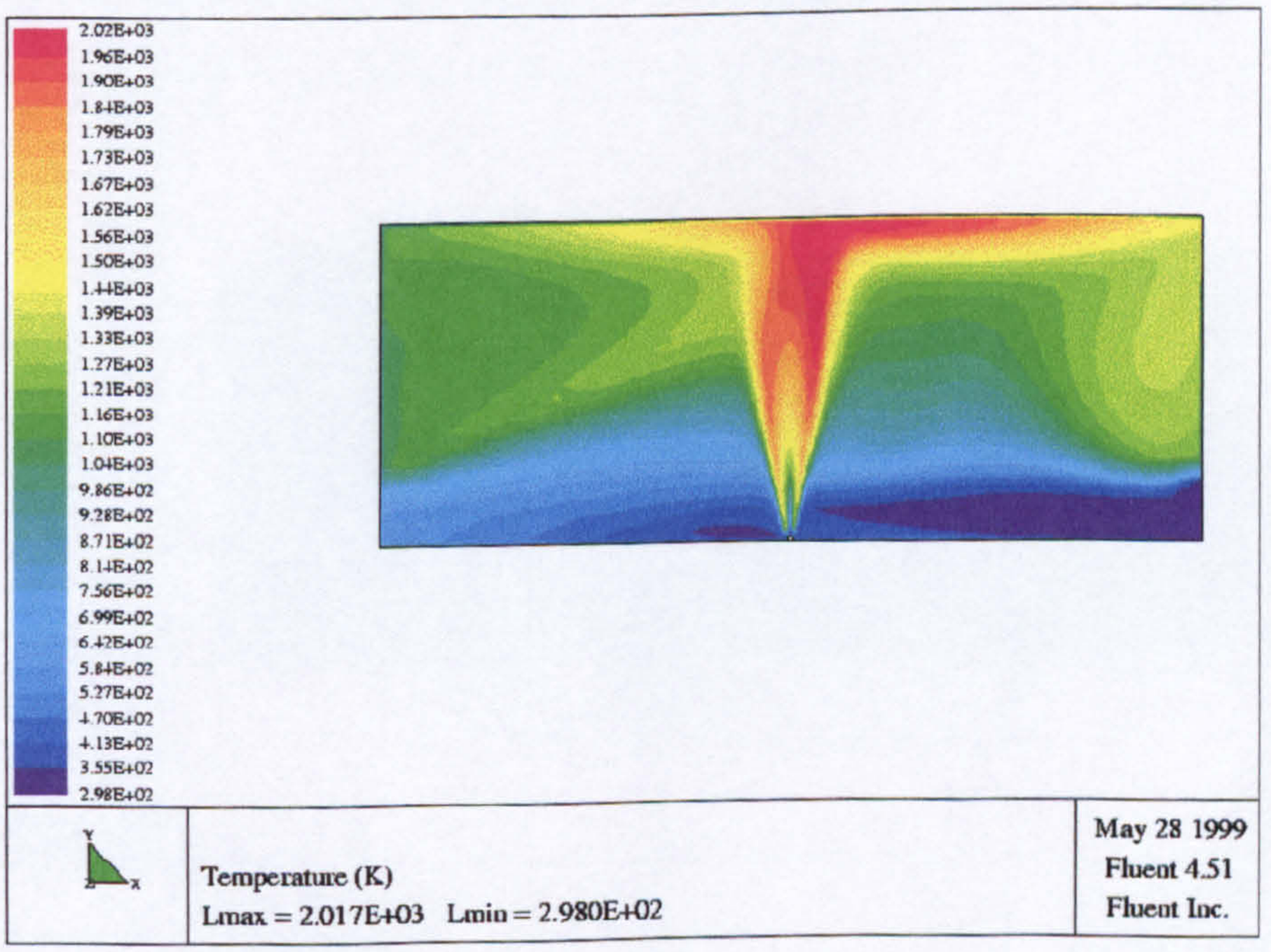

Figure (8.10). Predicted gas temperature contours through the longitudinal x-y plane through the jet fire section using the DTRM radiation model in the flow and both external convective and radiation heat loss, with a refined grid (see Figure 8.9).

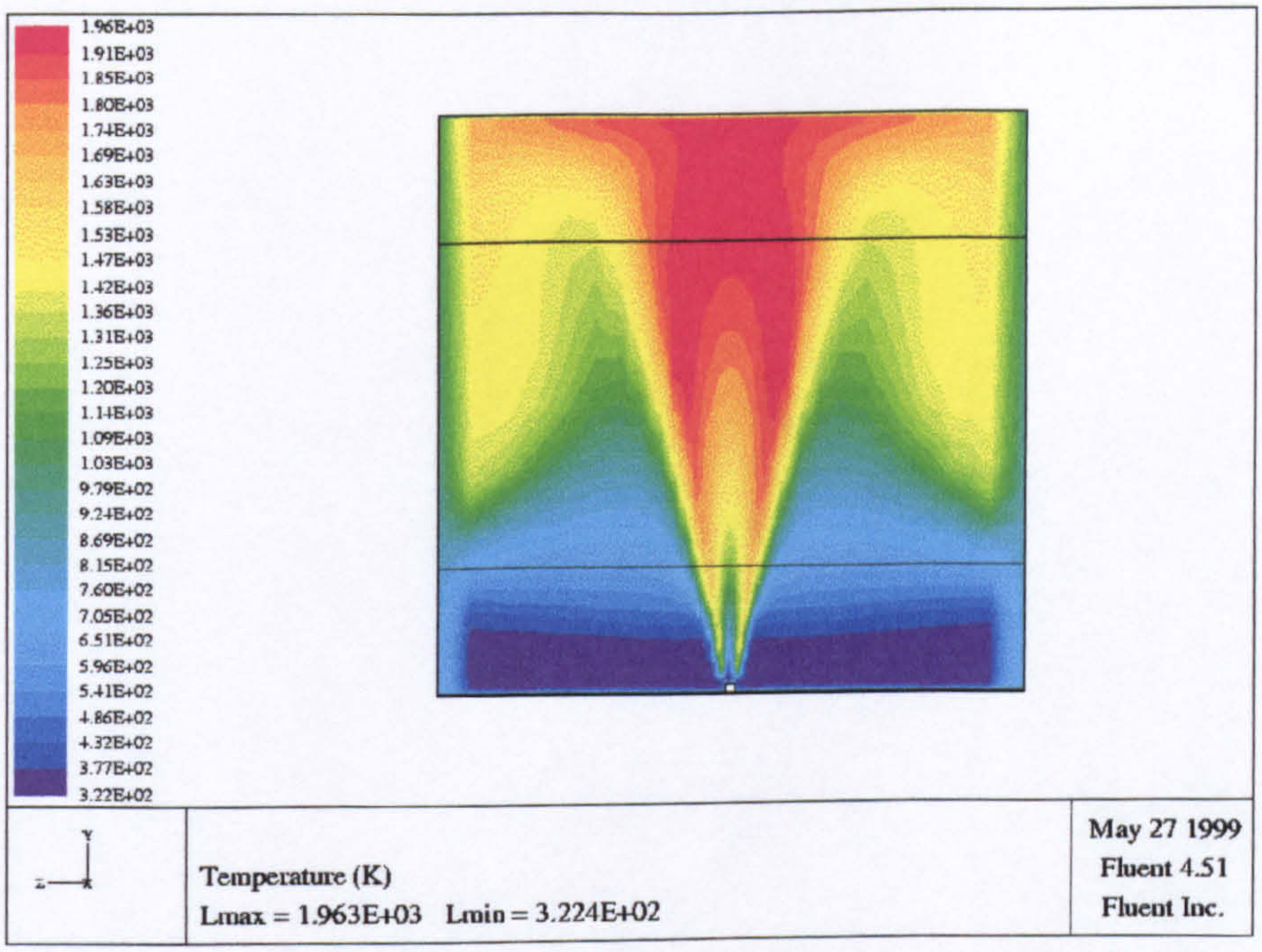

Figure (8.11). Predicted gas temperature contours through the lateral x-y plane through the jet fire section using the DTRM radiation model in the flow and both external convective and radiation heat loss, with a refined grid (see figure 8.9).

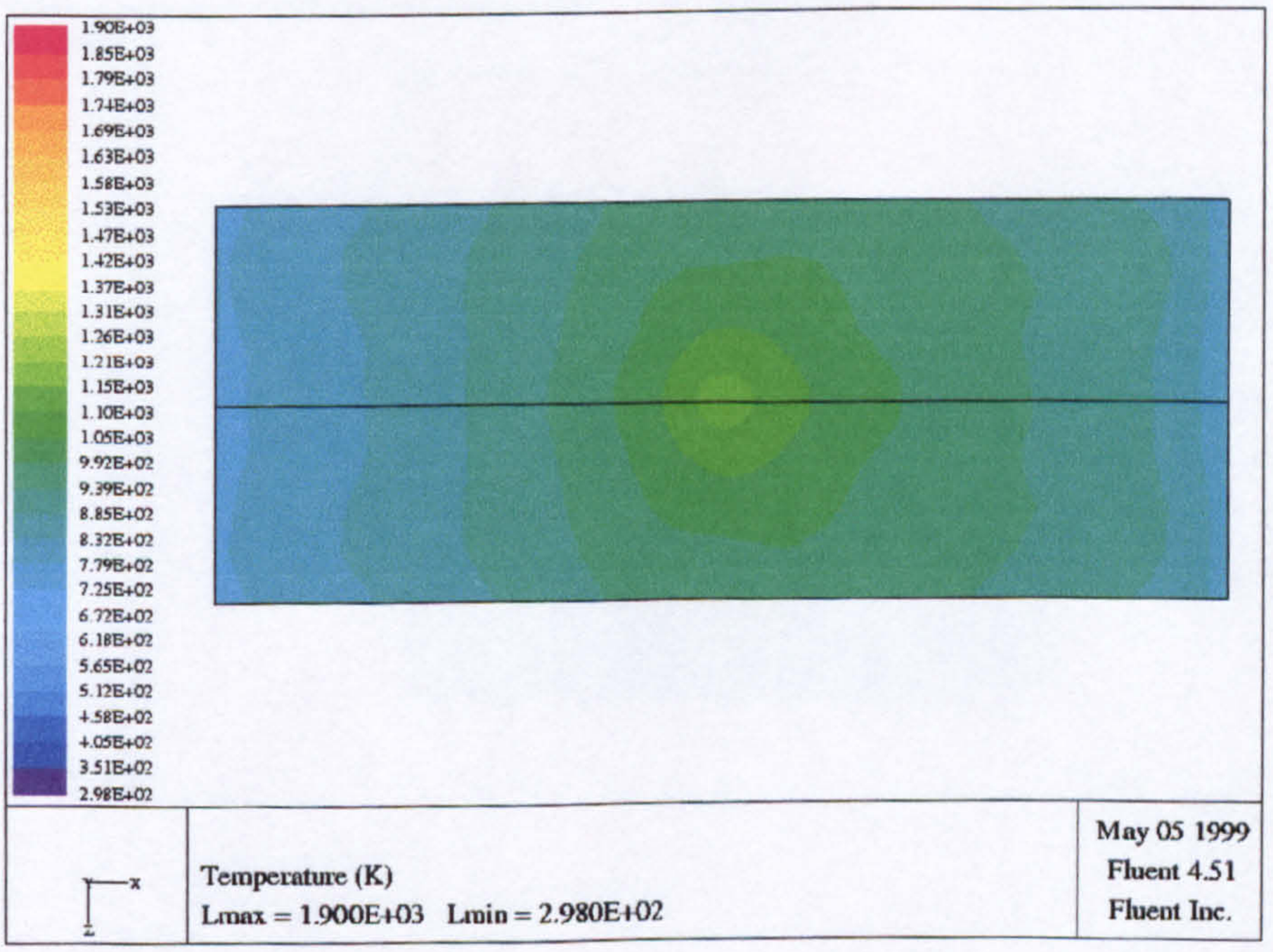

Figure (8.12). Plan view of the predicted gas temperature contours in the x-z plane 1 cm (1 cell) below the ceiling when DTRM radiation model has been used.

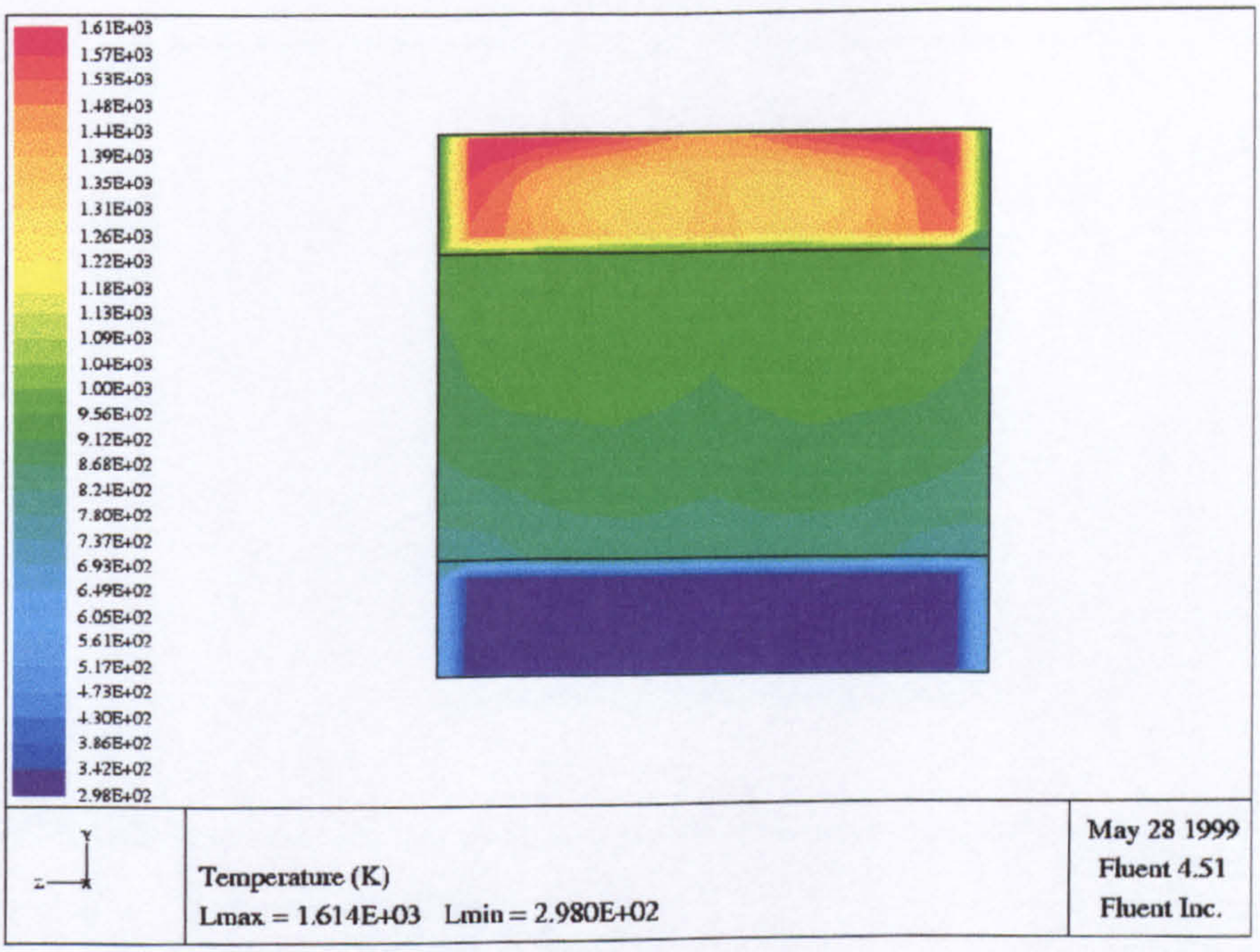

Figure (8.13). Predicted gas temperature contours with radiation at the flow at the lateral y-z plane 1.3 cm from the baffle, showing the temperature of the inlet and exit flows.

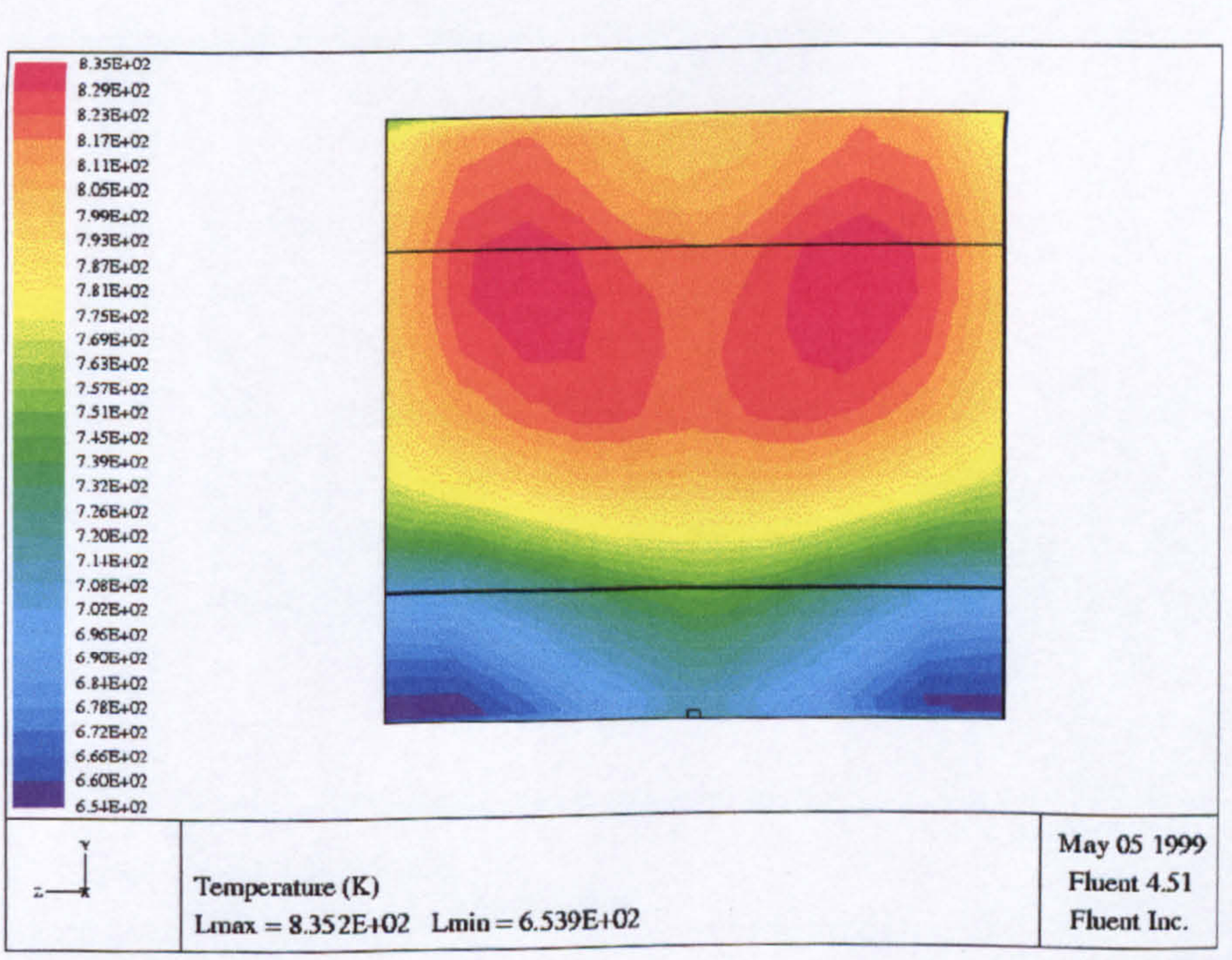

Figure (8.14). Predicted wall temperature contours (y-z plane) of the back wall when the DTRM radiation model with external convection and radiation.

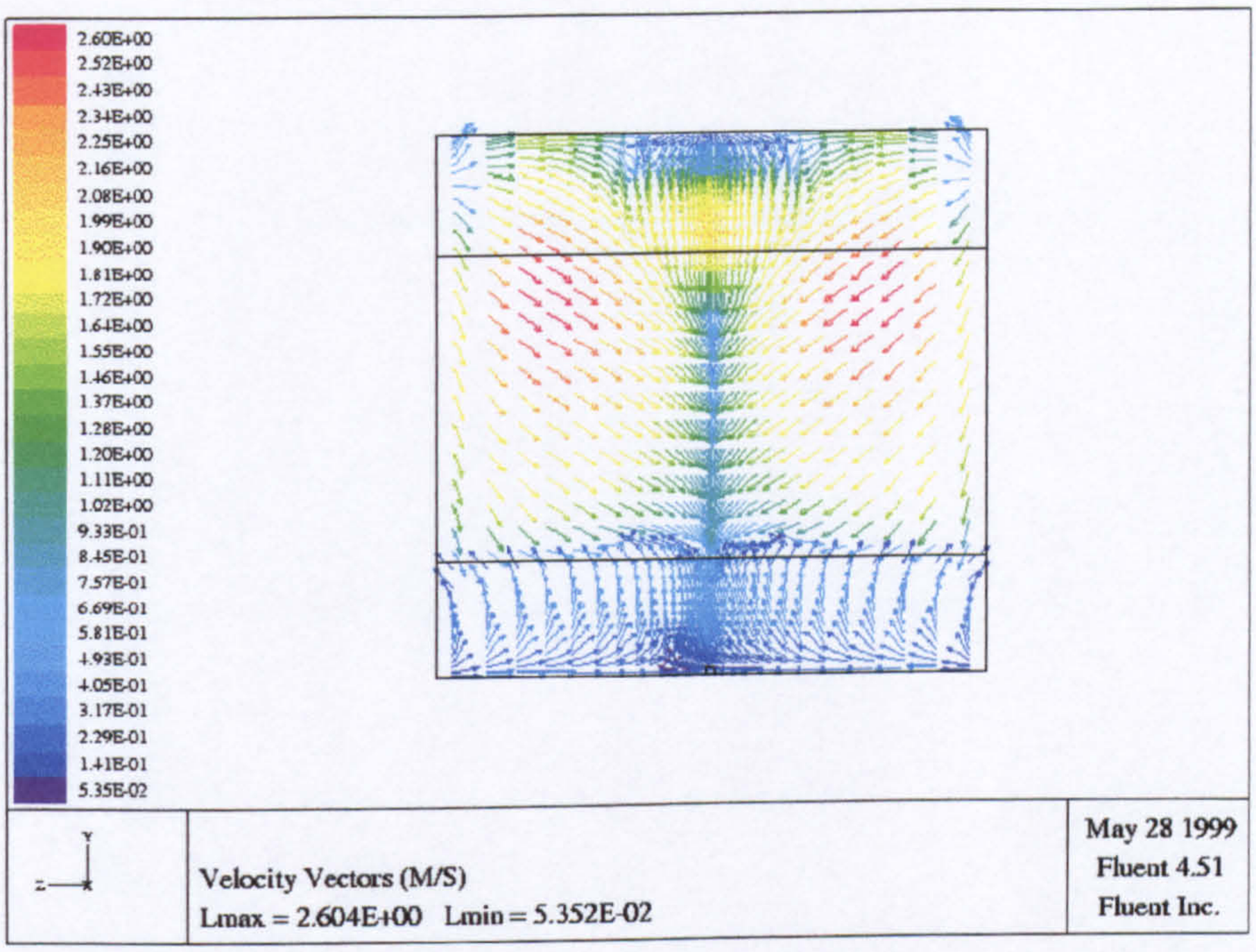

Figure (8.15). Velocity vectors predicted in the lateral y-z plane 3 cm from the back wall.

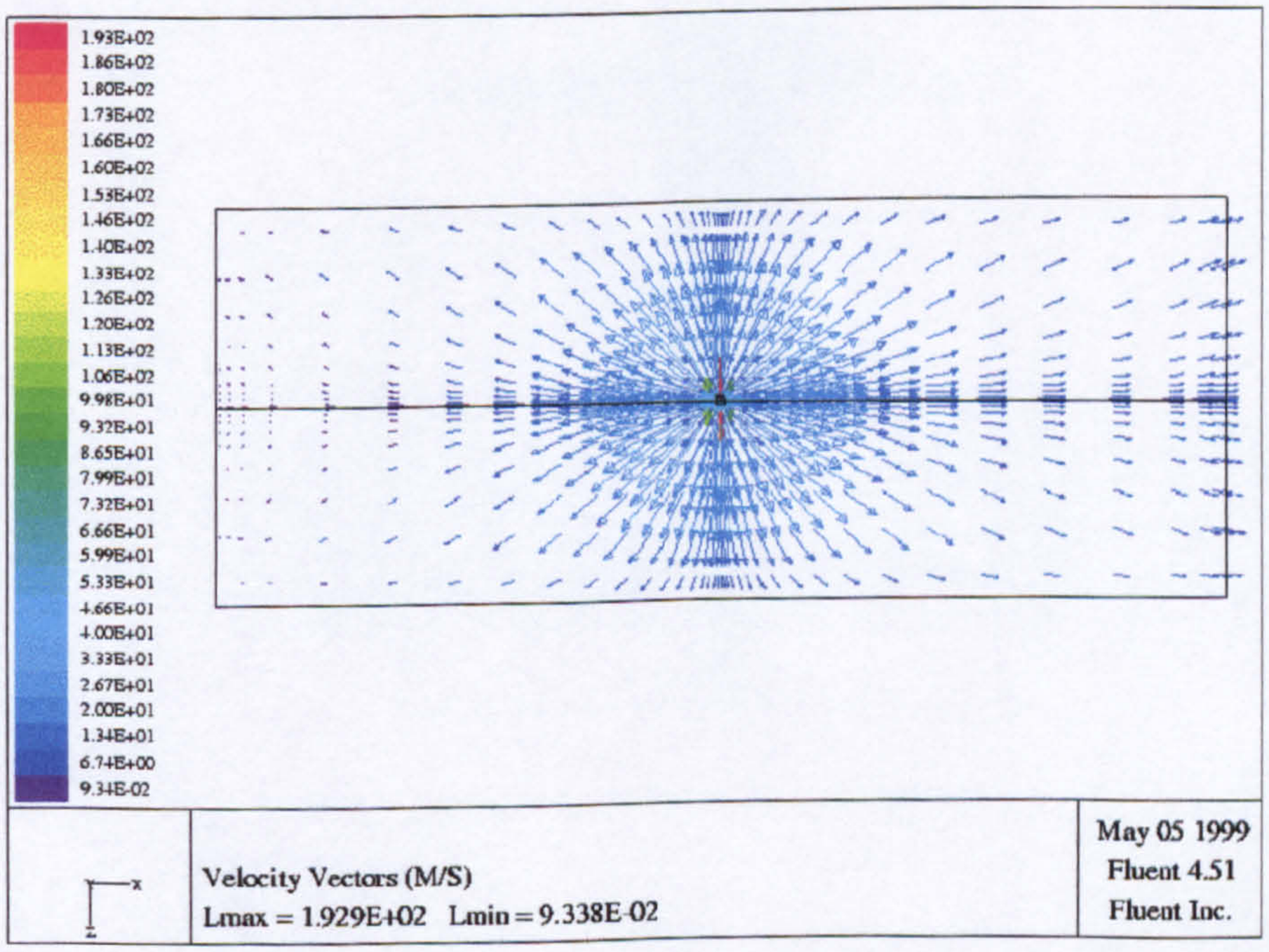

Figure (8.16). Predicted velocity vector 2 cm below the ceiling (1 cell) in x-z plane.

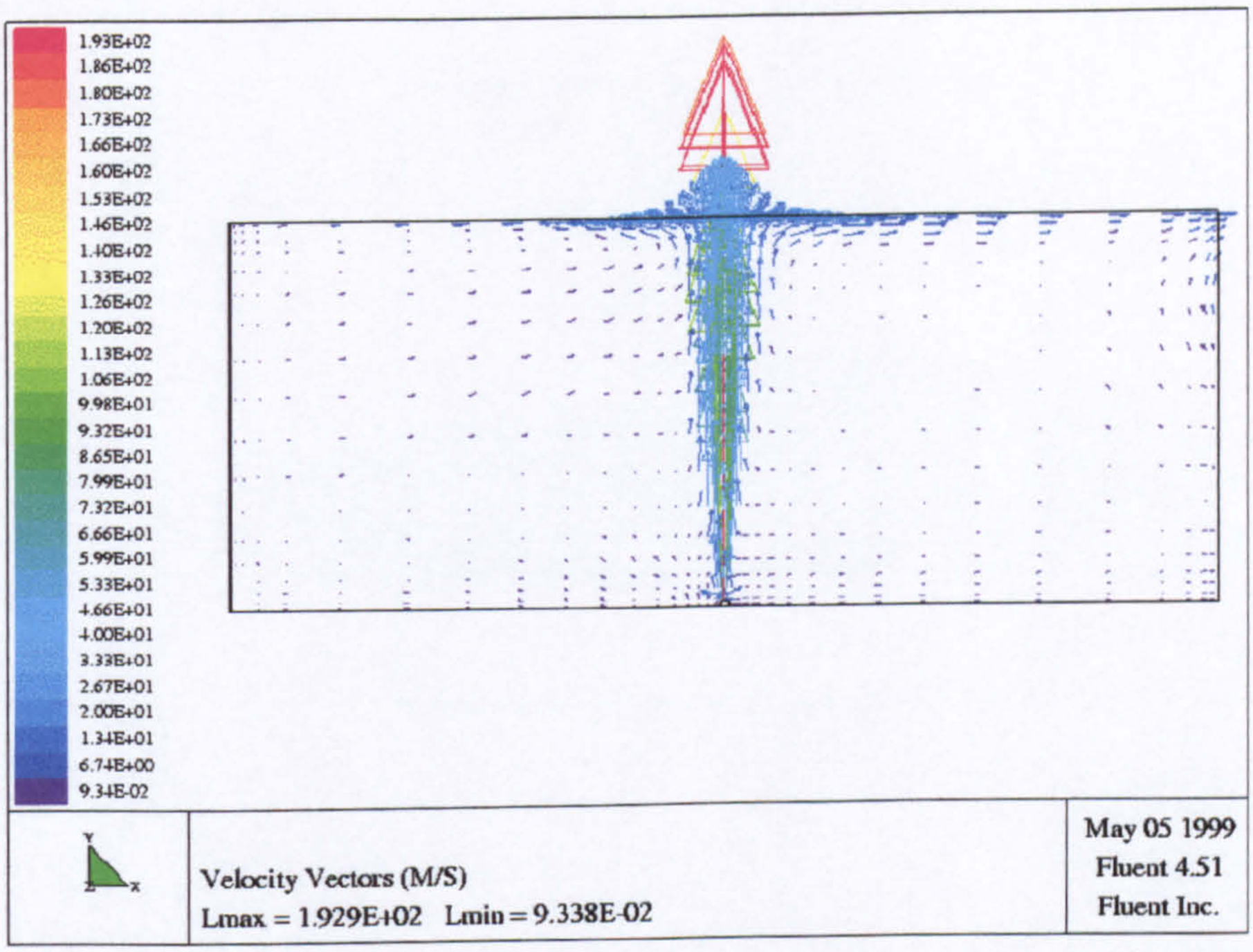

Figure (8.17). Predicted velocity vector of the jet fire section at longitudinal x-y plane at the centre of the jet fire.

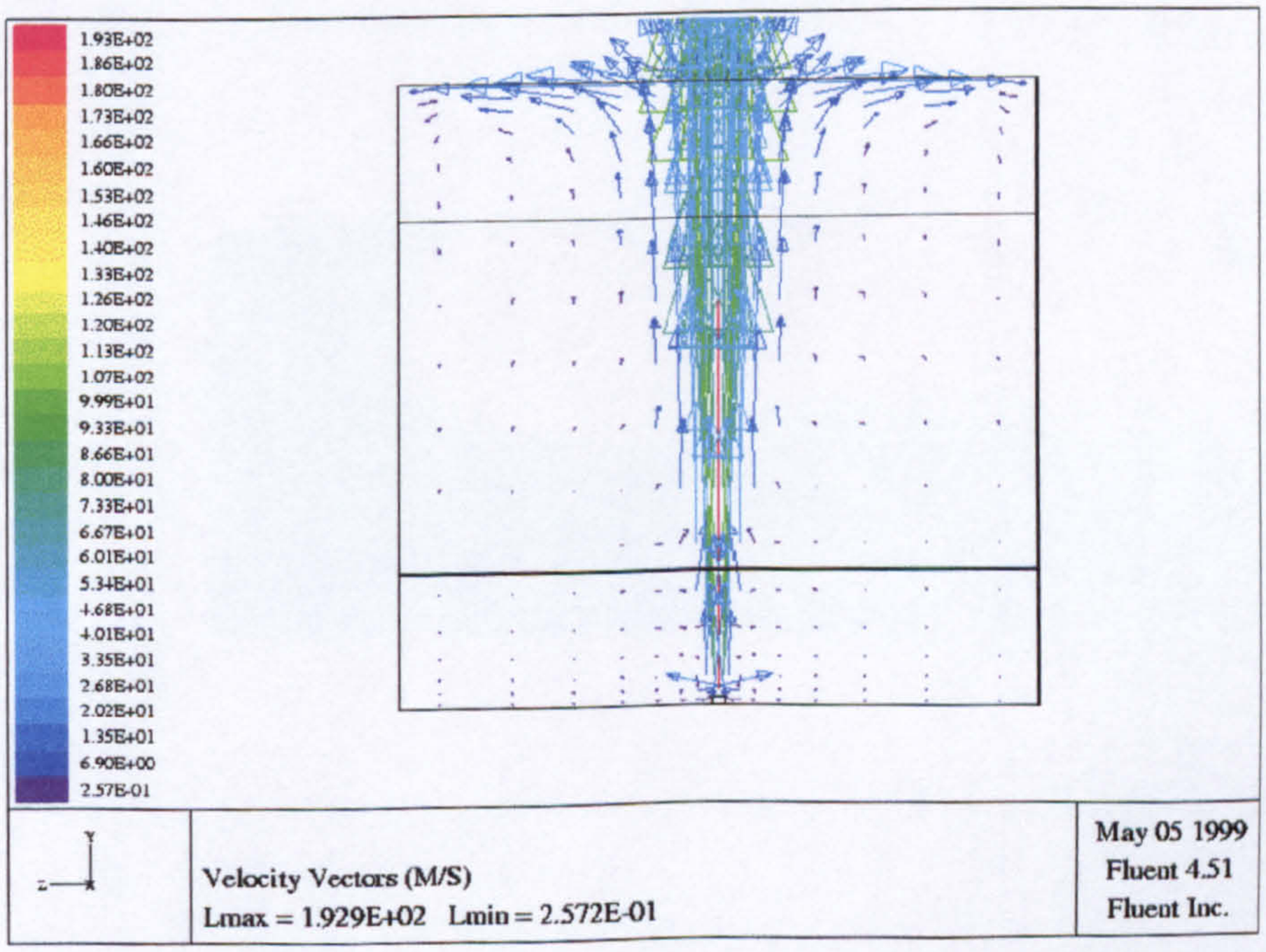

Figure (8.18). Predicted velocity vector of the jet fire section at lateral y-z plane at the centre of the compartment.

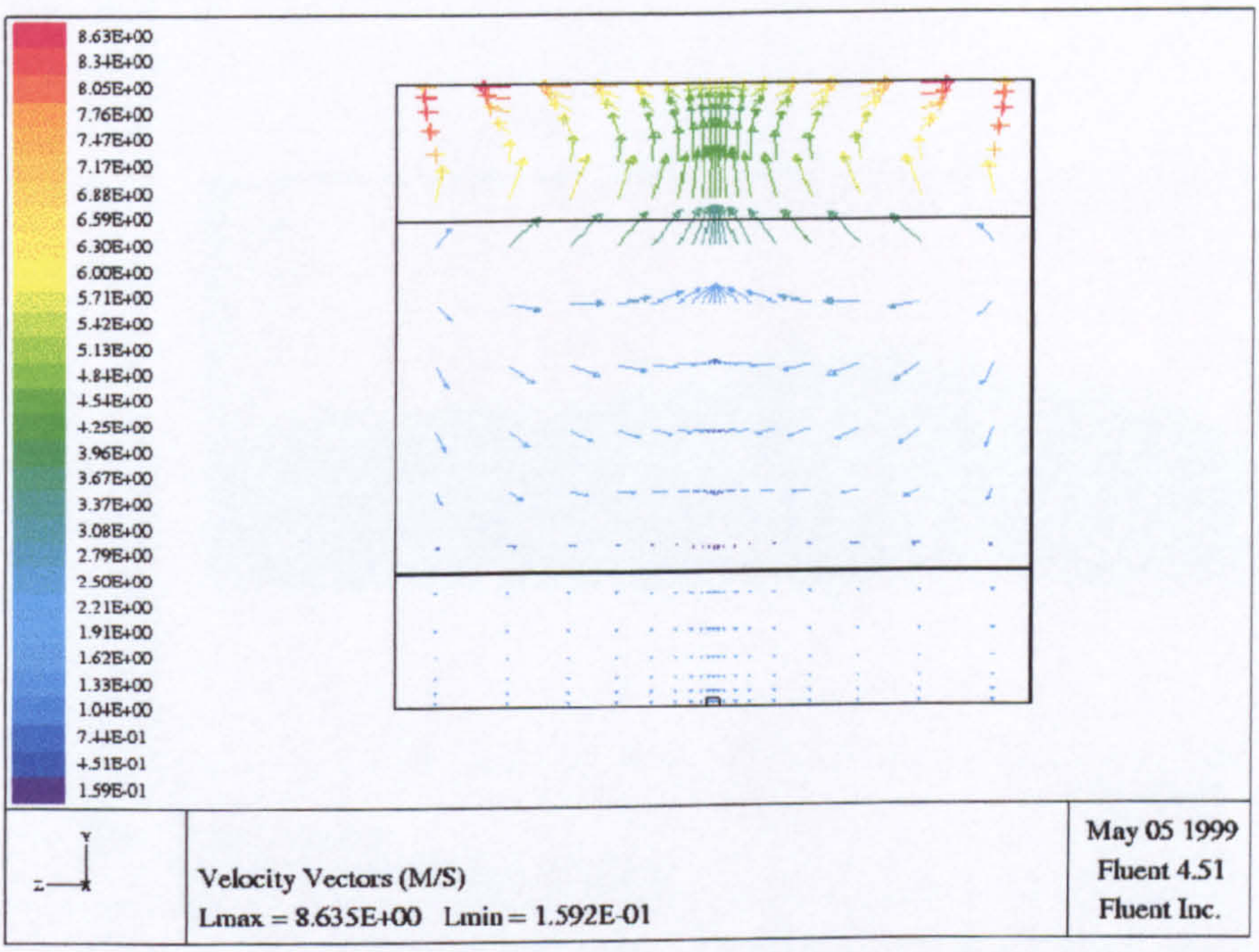

Figure (8.19). Predicted velocity vector of the jet fire section at lateral y-z plane 1.3 cm from the baffle, showing the inlet and exit flow.

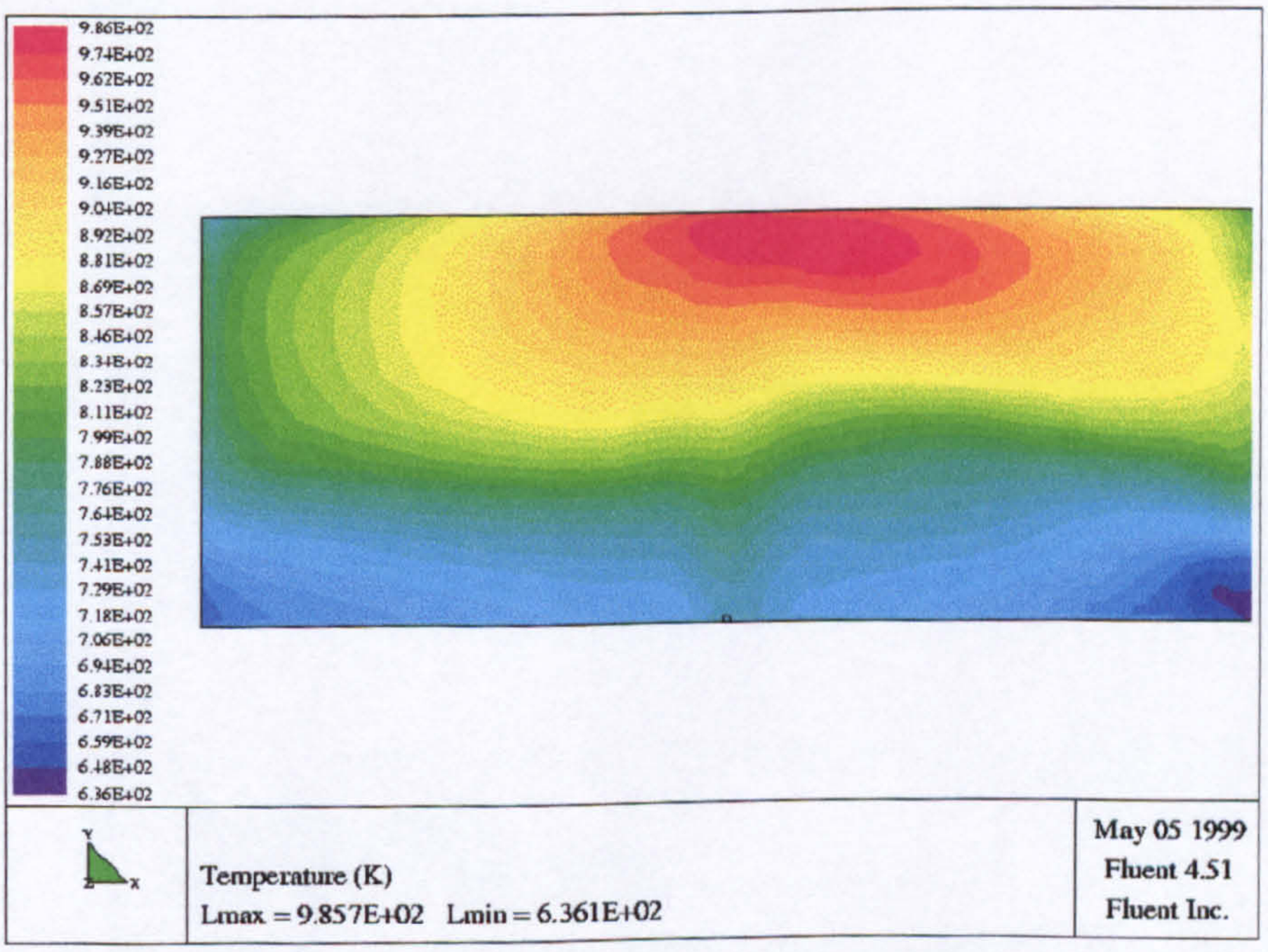

Figure (8.20). Predicted temperature filled contours of the side wall in longitudinal x-y plane when radiation sub-model and h_{ext} = 10 W/m^2 K has been used.

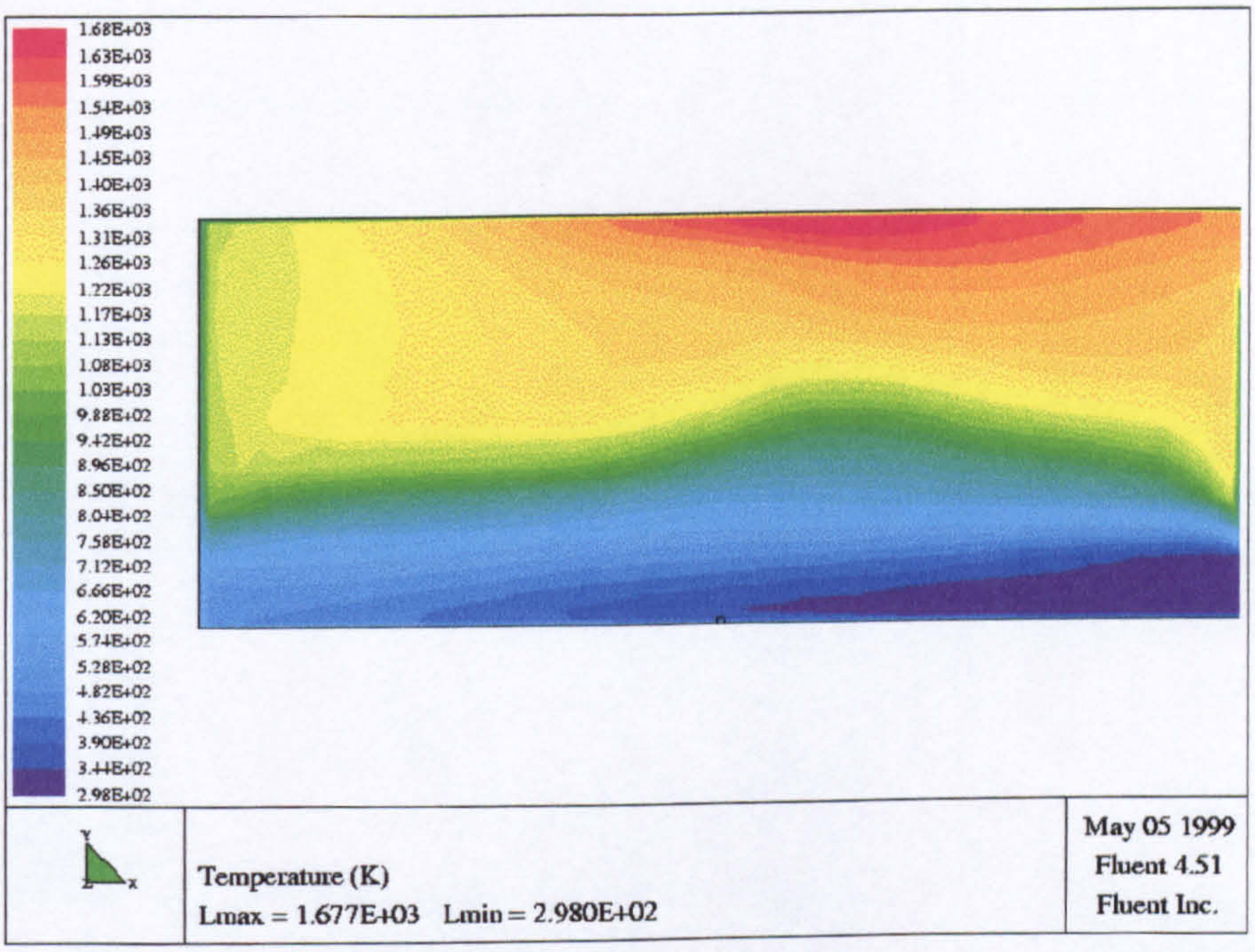

Figure (8.21). Predicted temperatures filled contours of slice in the longitudinal x-y plane near the side wall when radiation sub-model and h_{ext} = 10 W/m^2 K have been used.

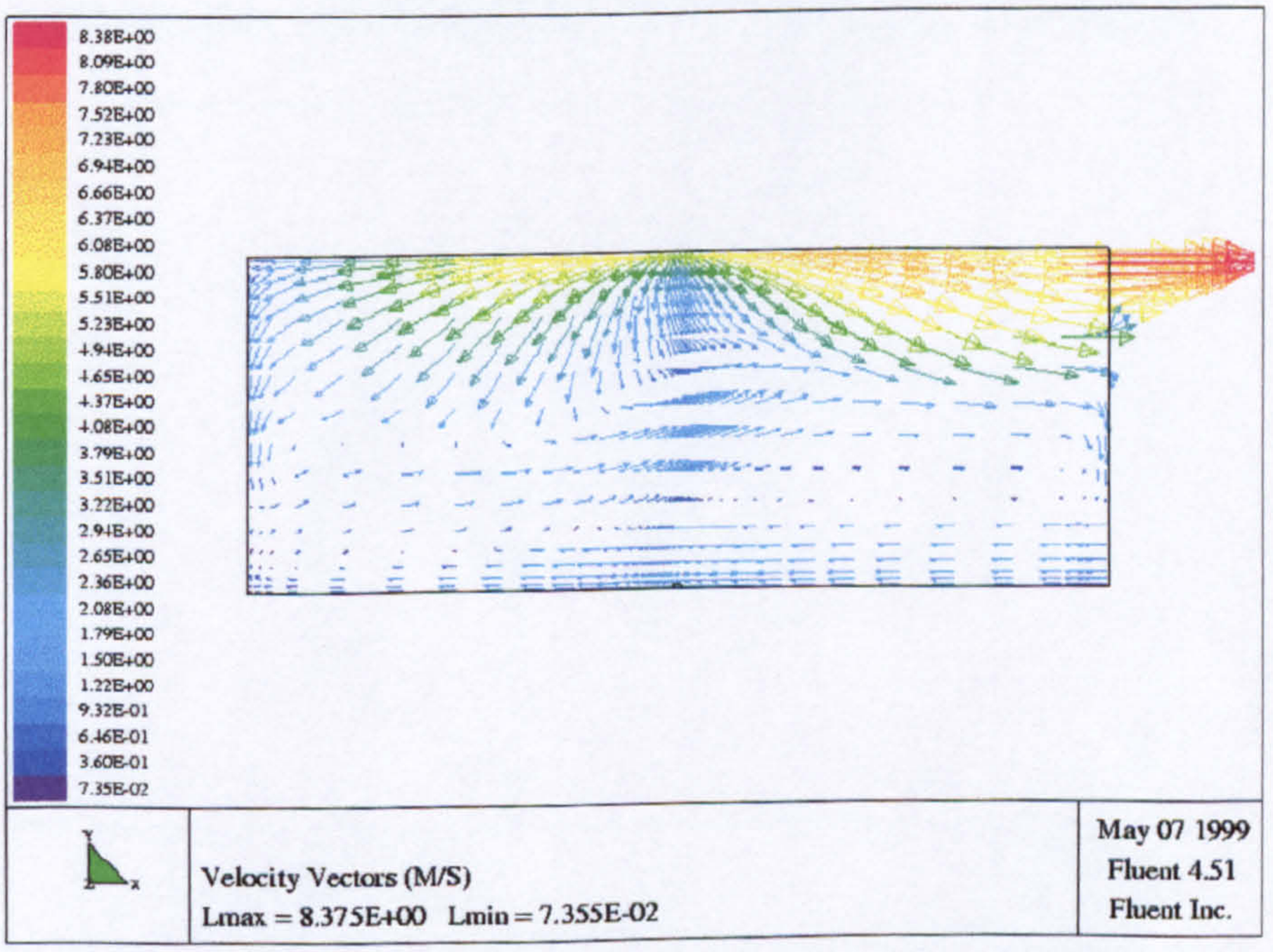

Figure (8.22). Predicted velocity vector at longitudinal x-y plane 15 cm (1 cell) from the side wall, showing the inflow direction and velocity in the bottom right and outflow velocity and direction at the top right corner.

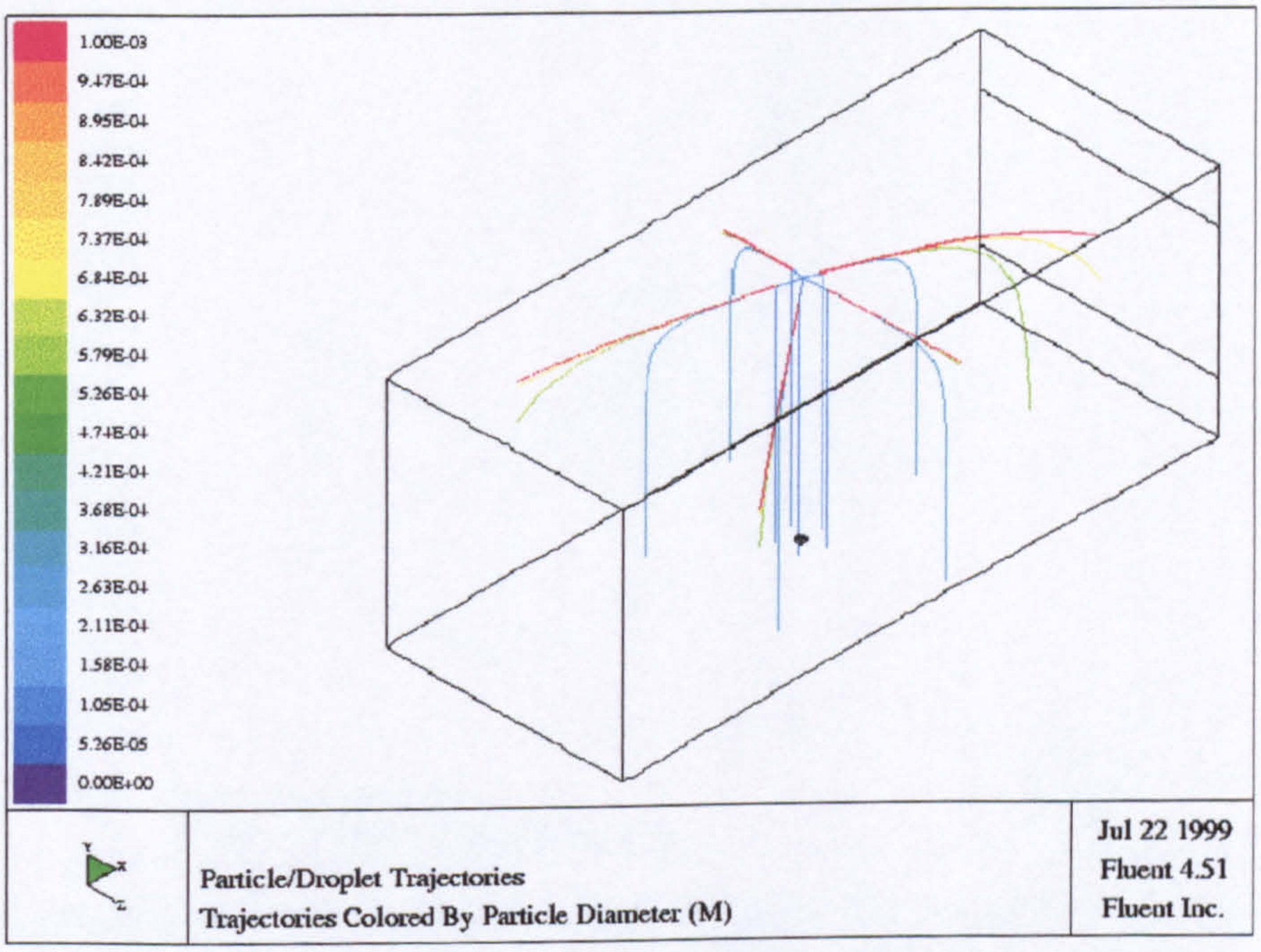

Figure (8.23). Predicted trajectories of water droplets injected from one spray located in the centre of the compartment for 150° spray angle (with out fire).

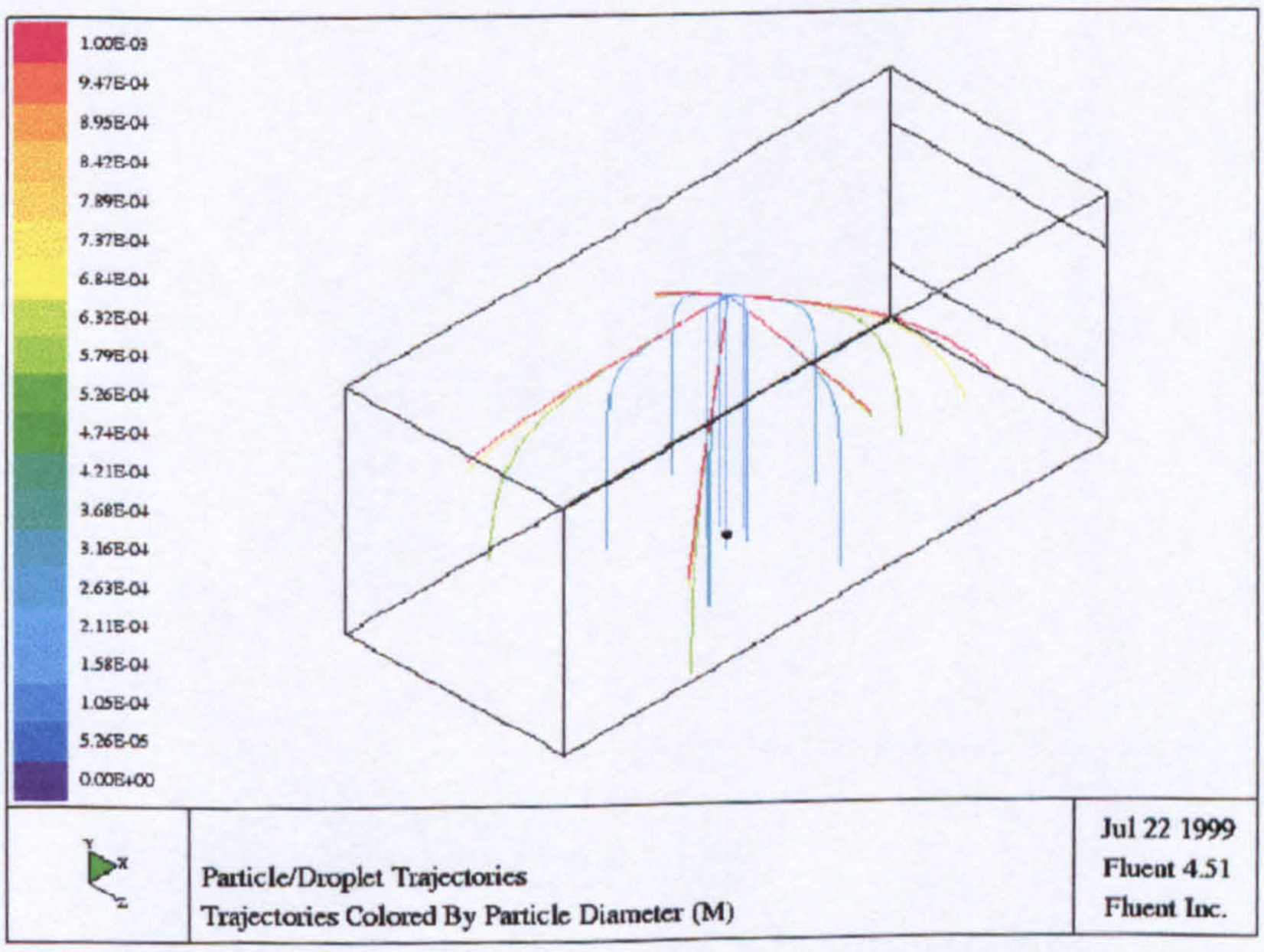

Figure (8.24). Predicted trajectories of water droplets injected from one spray located in the centre of the compartment for 120° spray angle (with out fire).

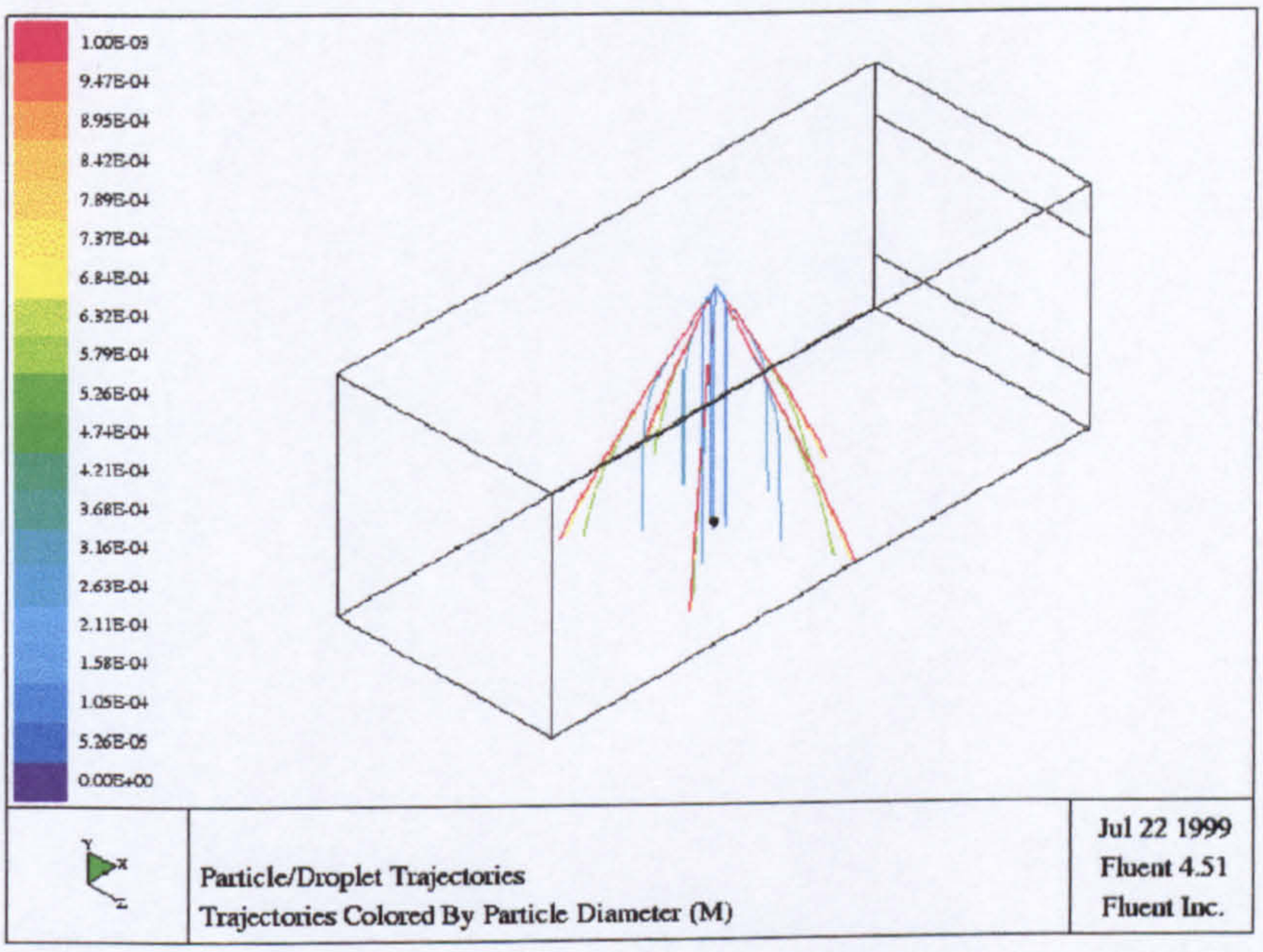

Figure (8.25). Predicted trajectories of water droplets injected from one spray located in the centre of the compartment for 60° spray angle (with out fire).

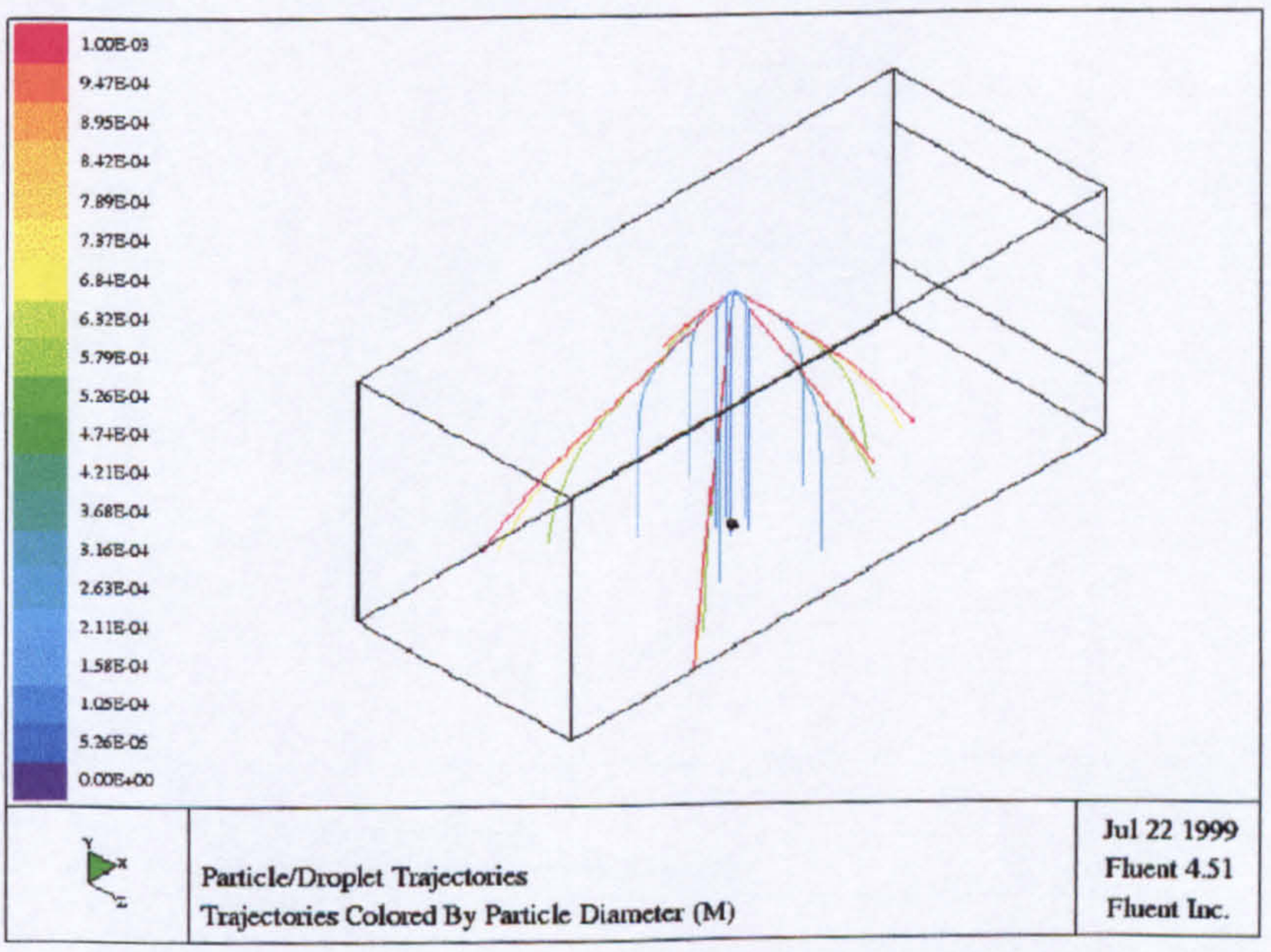

Figure (8.26). Predicted trajectories of water droplets injected from one spray located in the centre of the compartment for 90° spray angle (with out fire).

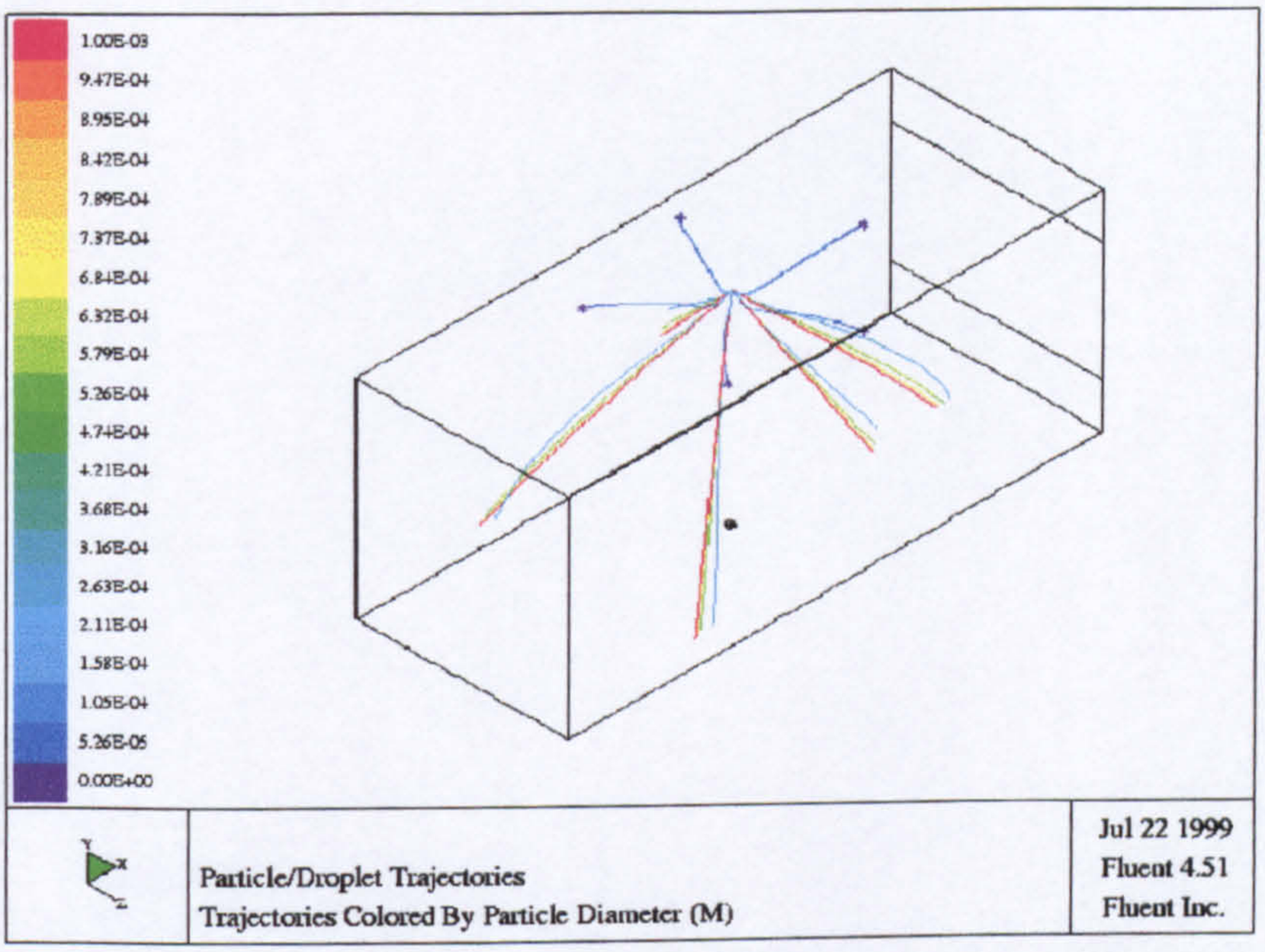

Figure (8.27). Predicted trajectories of water droplets injected over the jet fire for water flow rate of 90 lit/min, 90° spray angle and $\bar{d} = 386$ μm (COMP23).

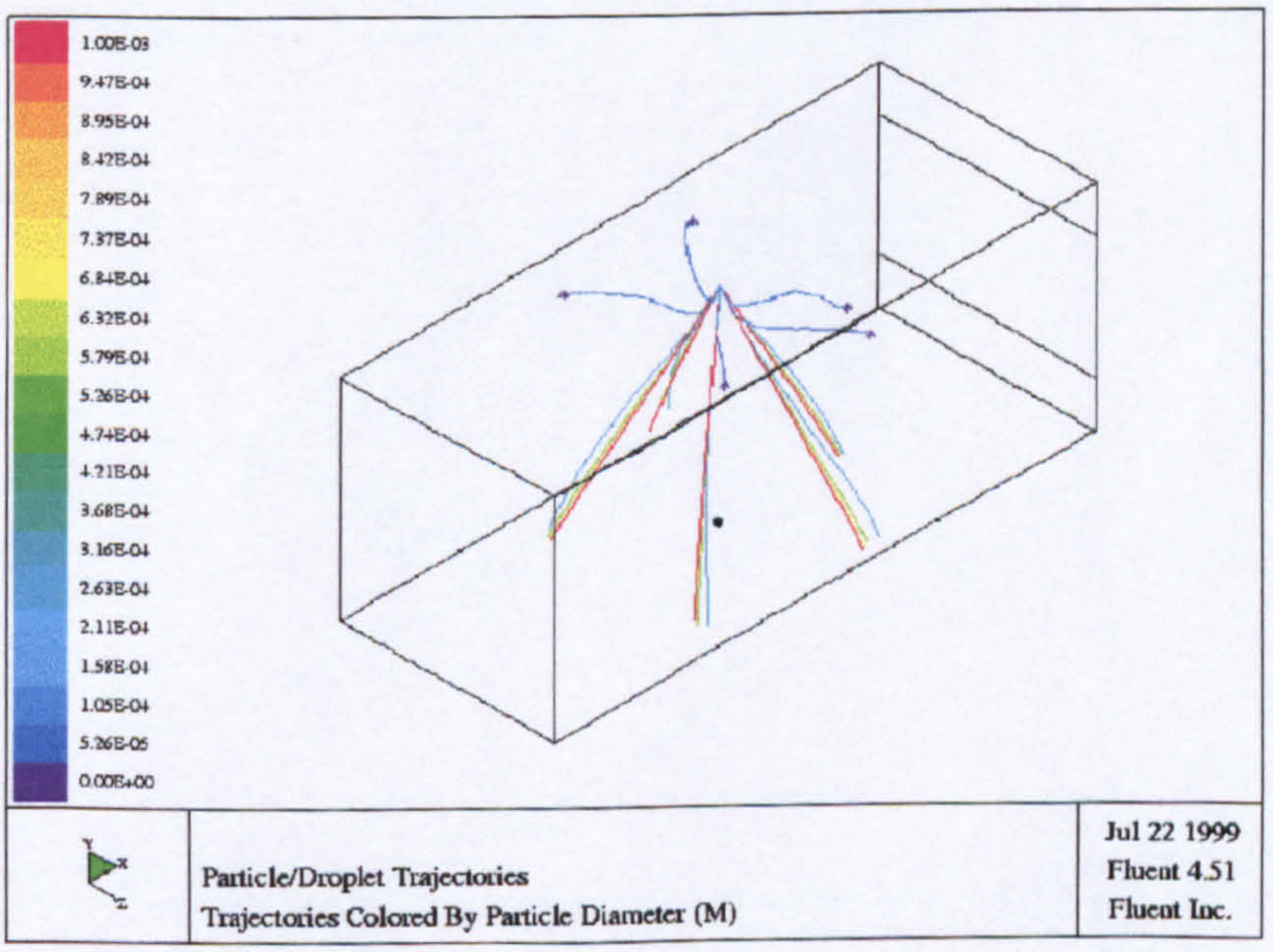

Figure (8.28). Predicted trajectories of water droplets injected over the jet fire for water flow rate of 90 lit/min, 60° spray angle and $\bar{d} = 335$ μm (COMP16).

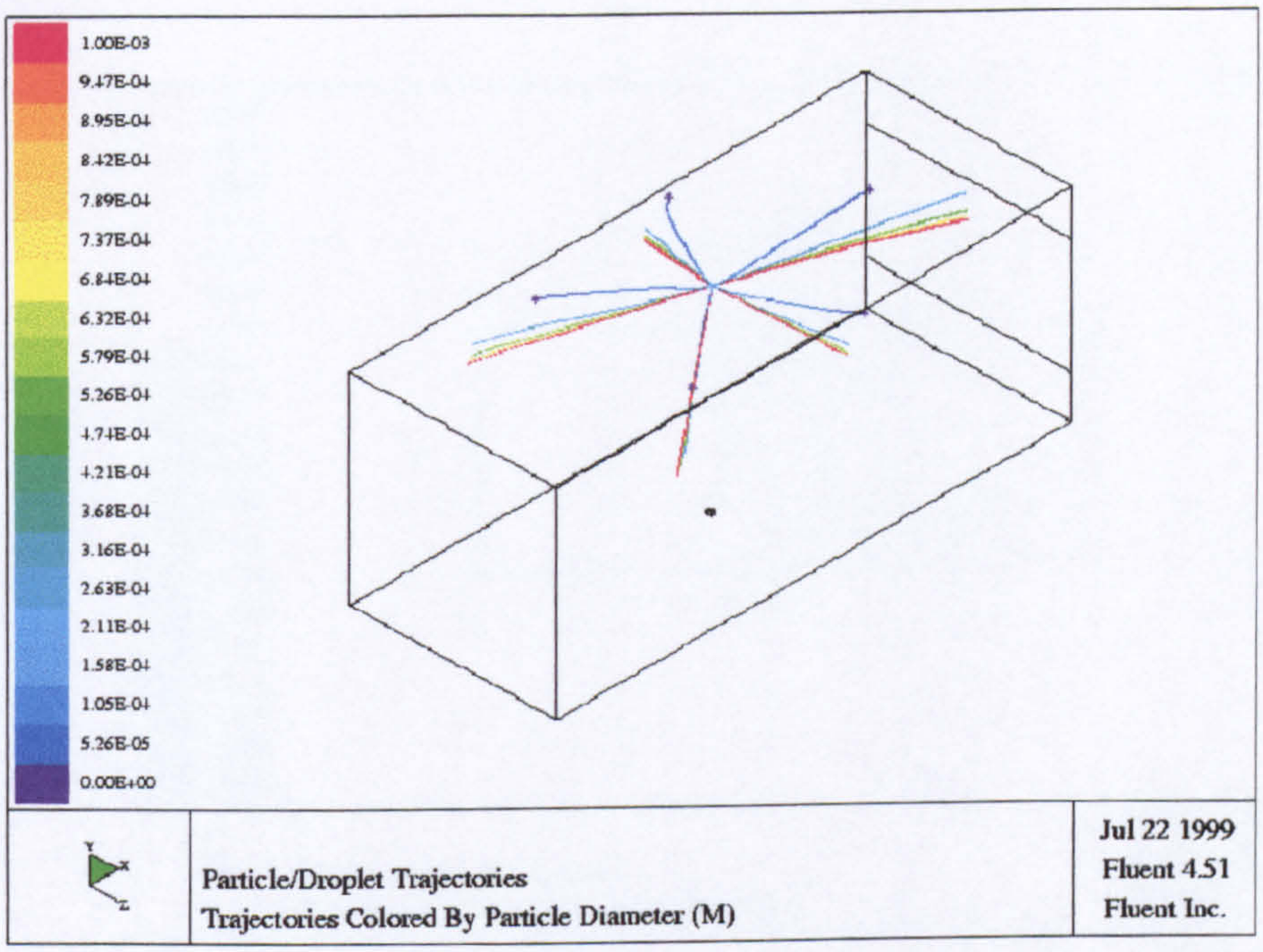

Figure (8.29). Predicted trajectories of water droplets injected over the jet fire for water flow rate of 54 lit/min, 150° spray angle and $\bar{d} = 417$ μm (COMP3).

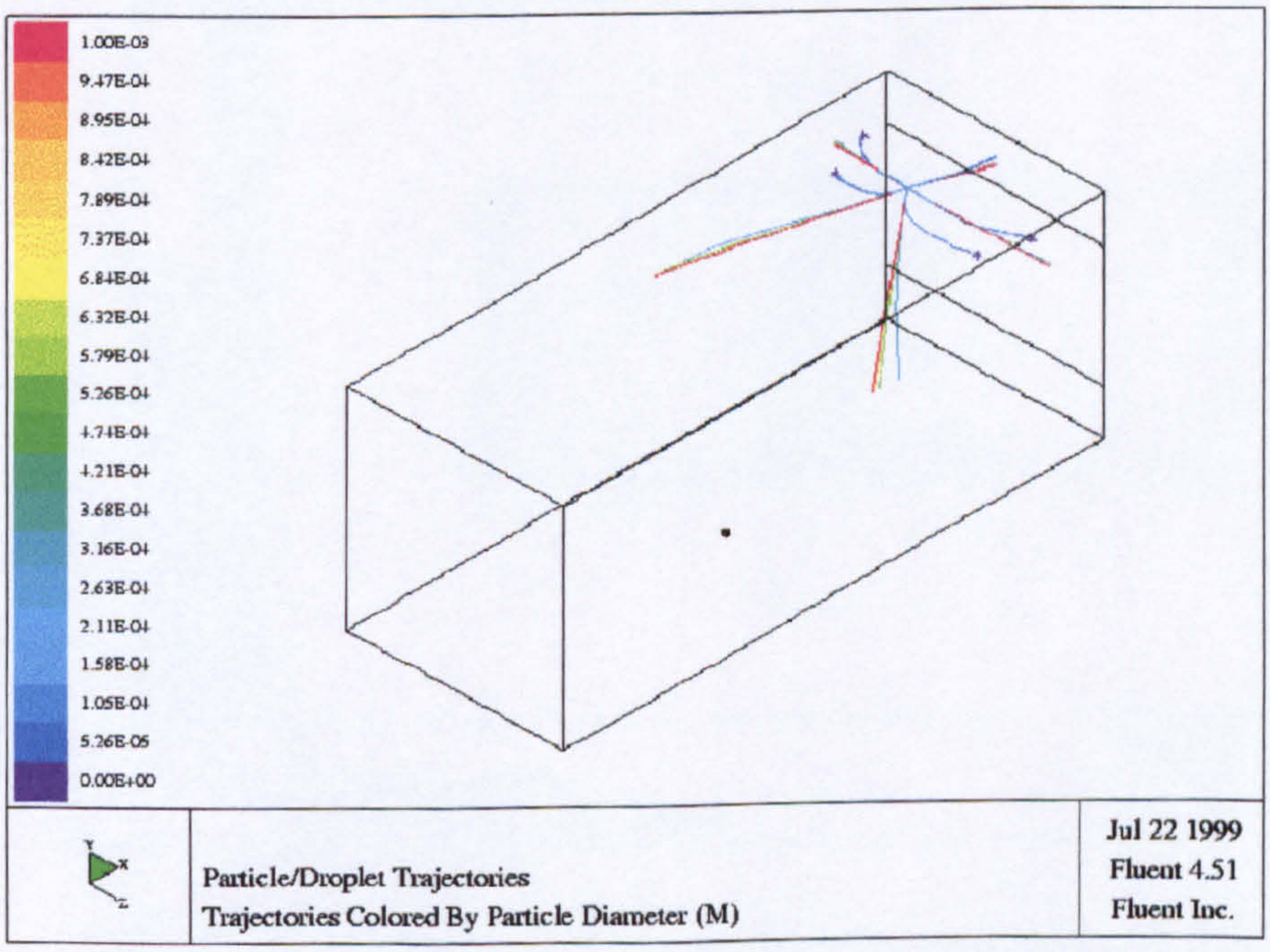

Figure (8.30). Predicted trajectories of water droplets injected from one spray located in front spray location for water flow rate of 54 lit/min, 150° spray angle and $\bar{d} = 417$ μm (comp38).

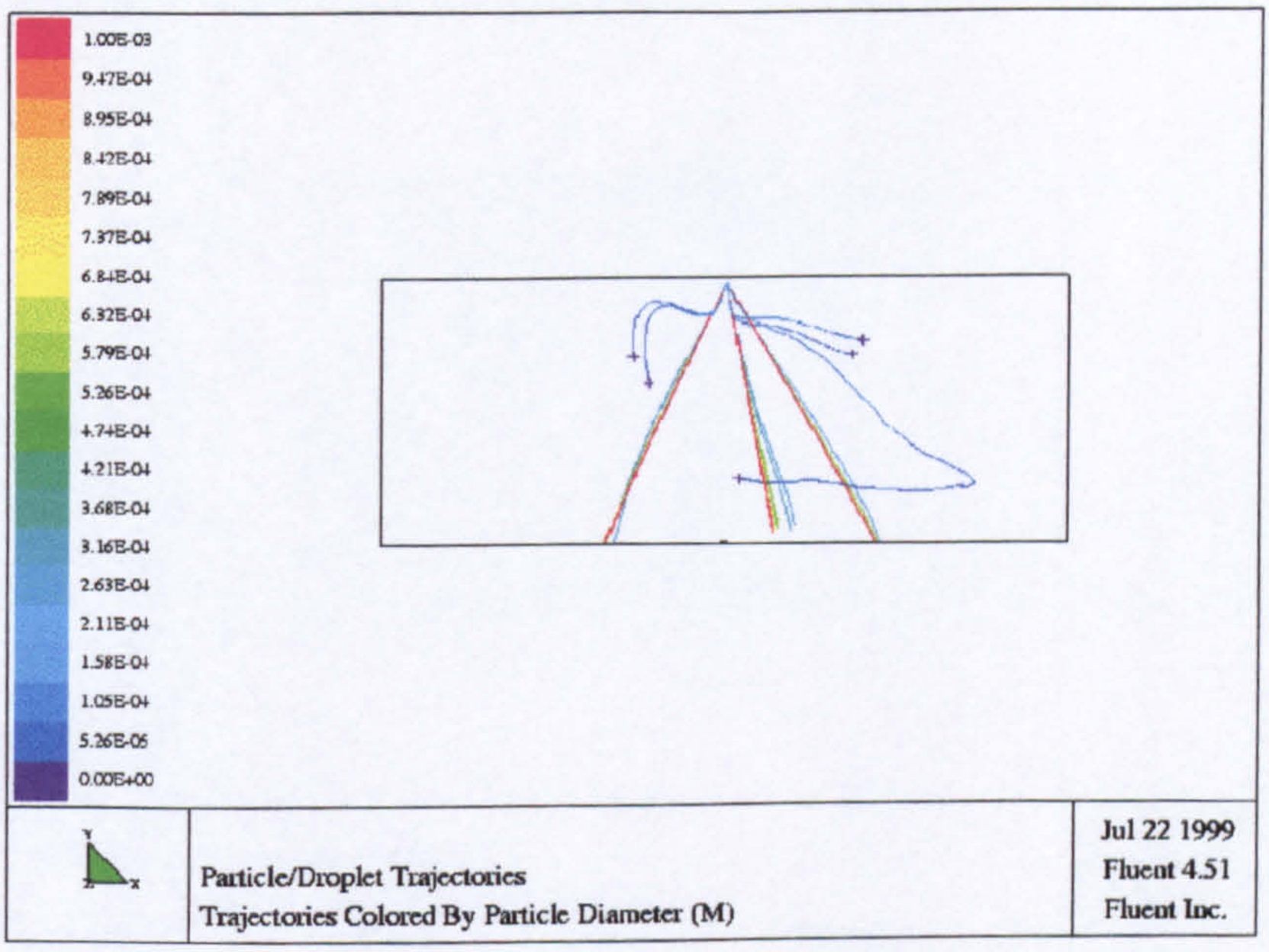

Figure (8.31). Predicted trajectories of water droplets injected from one spray located in the centre of the compartment for 60° spray angle (COMP17).

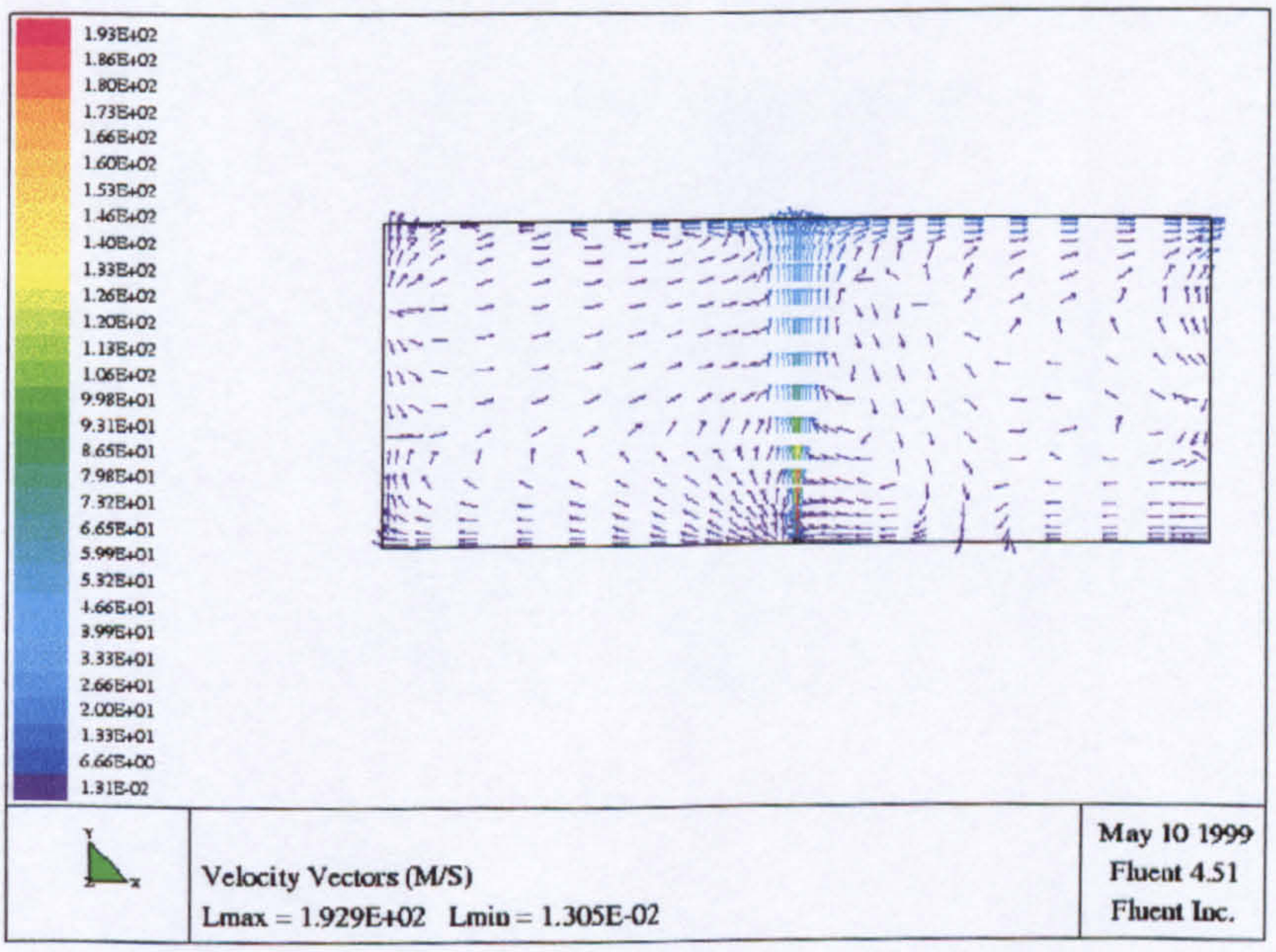

Figure (8.32). Predicted velocity vectors after the water spray activation for 90 lit/min (COMP16).

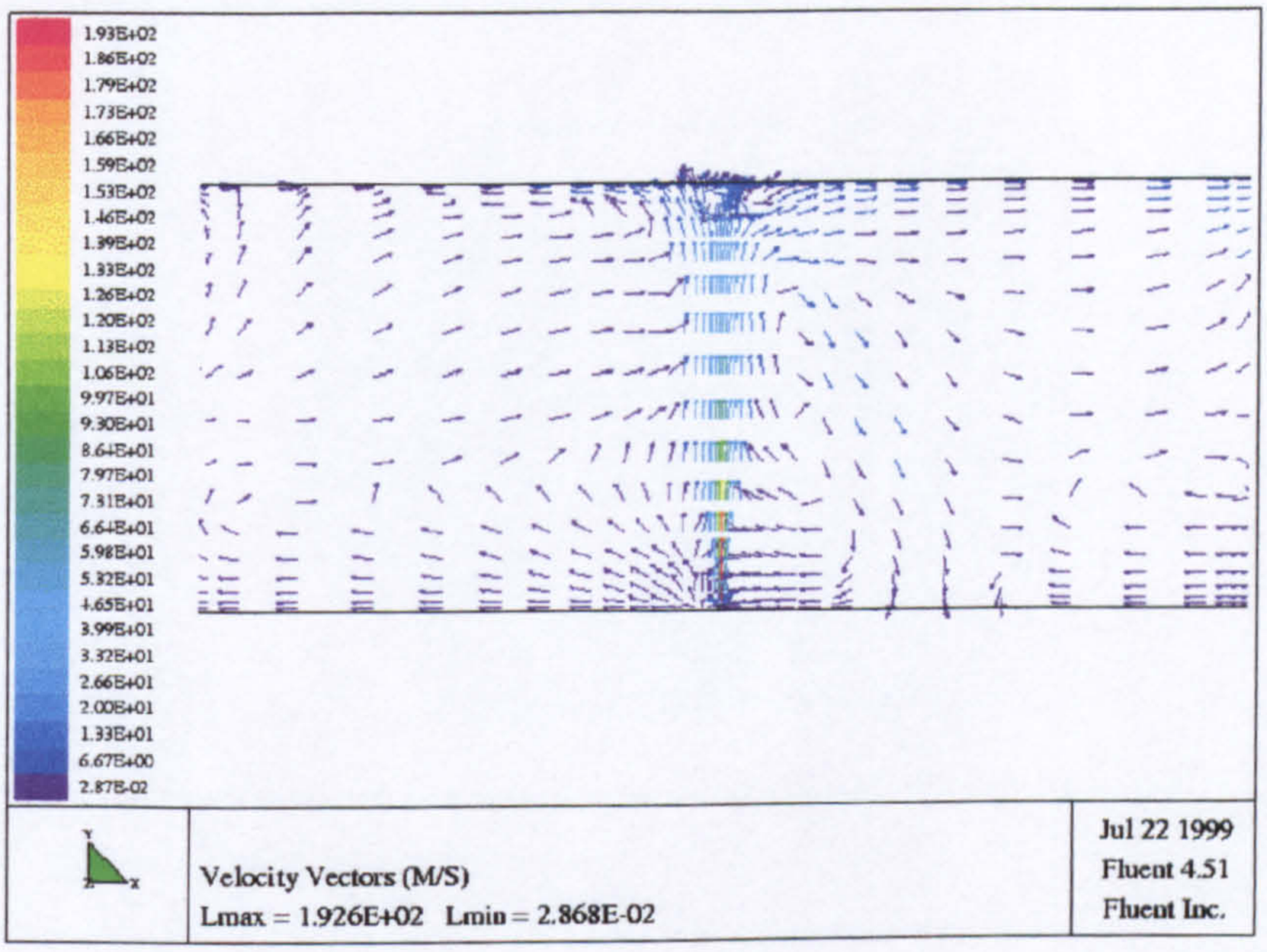

Figure (8.33). Predicted velocity vectors after the water spray activation for 36 lit/min (COMP12).

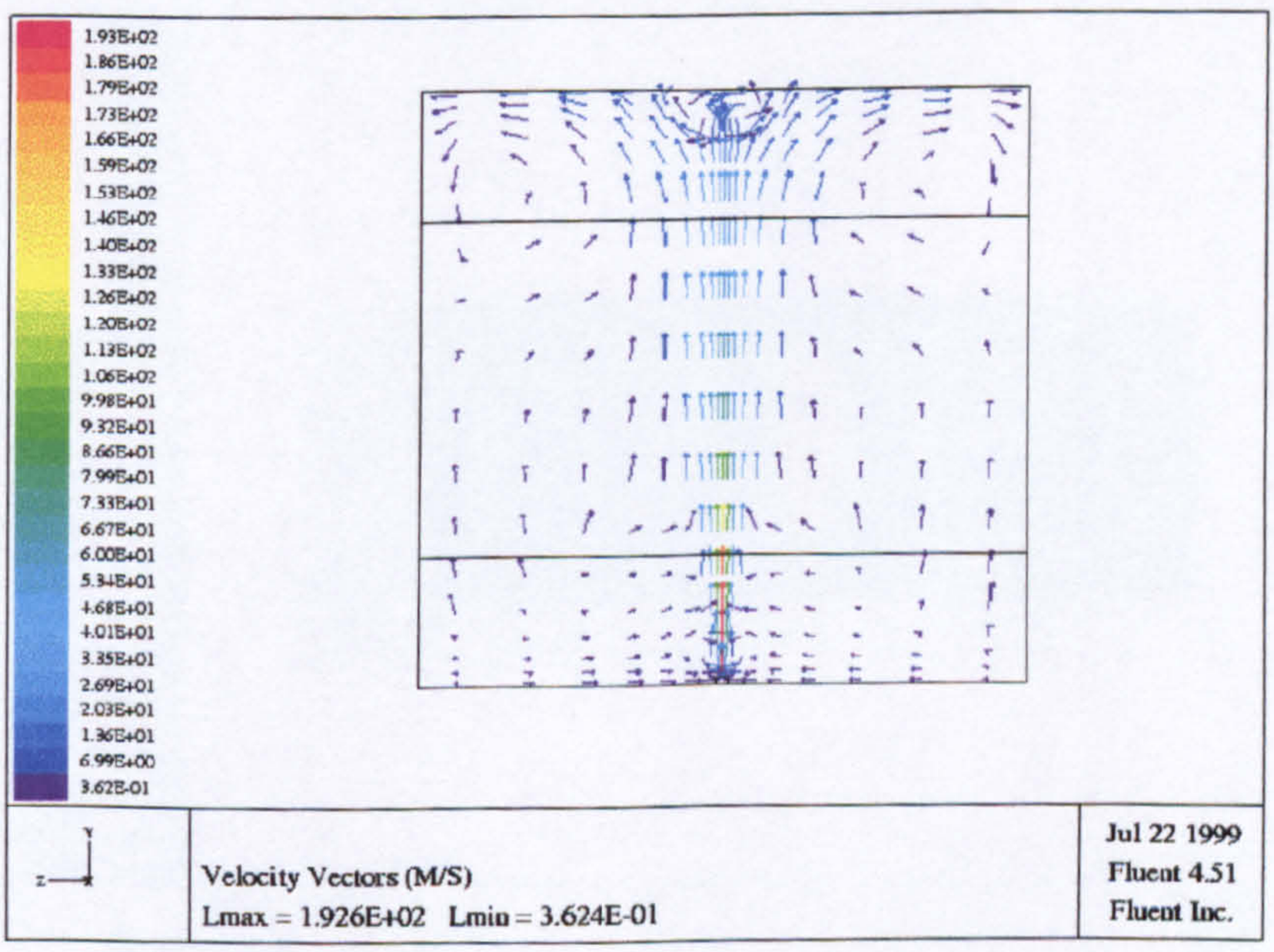

Figure (8.34). Predicted velocity vectors at lateral y-z plane through the compartment centre when 90 lit/min water spray activated, (COMP16).

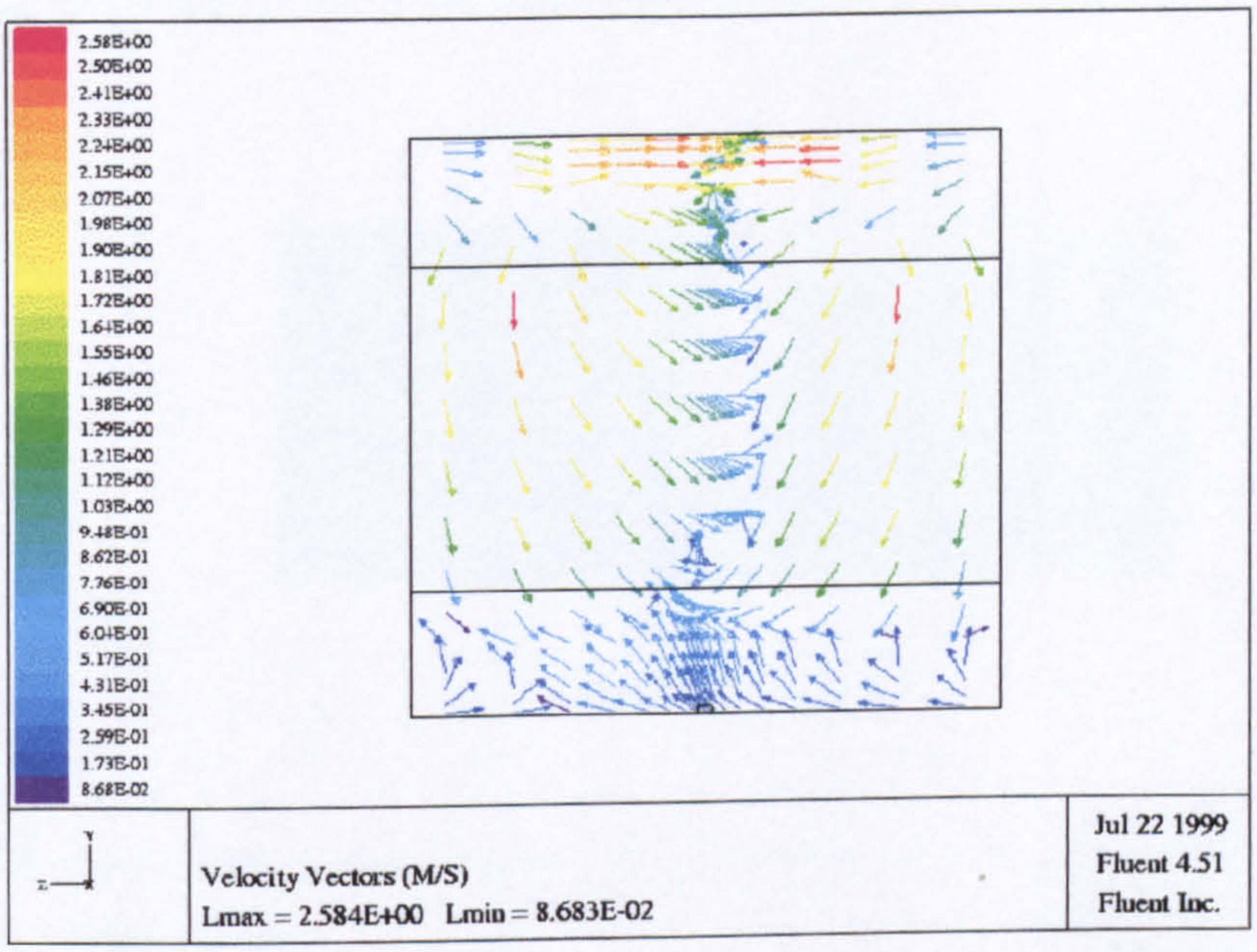

Figure (8.35). Predicted velocity vectors at the back wall when 72 lit/min water flow rate used, (COMP51).

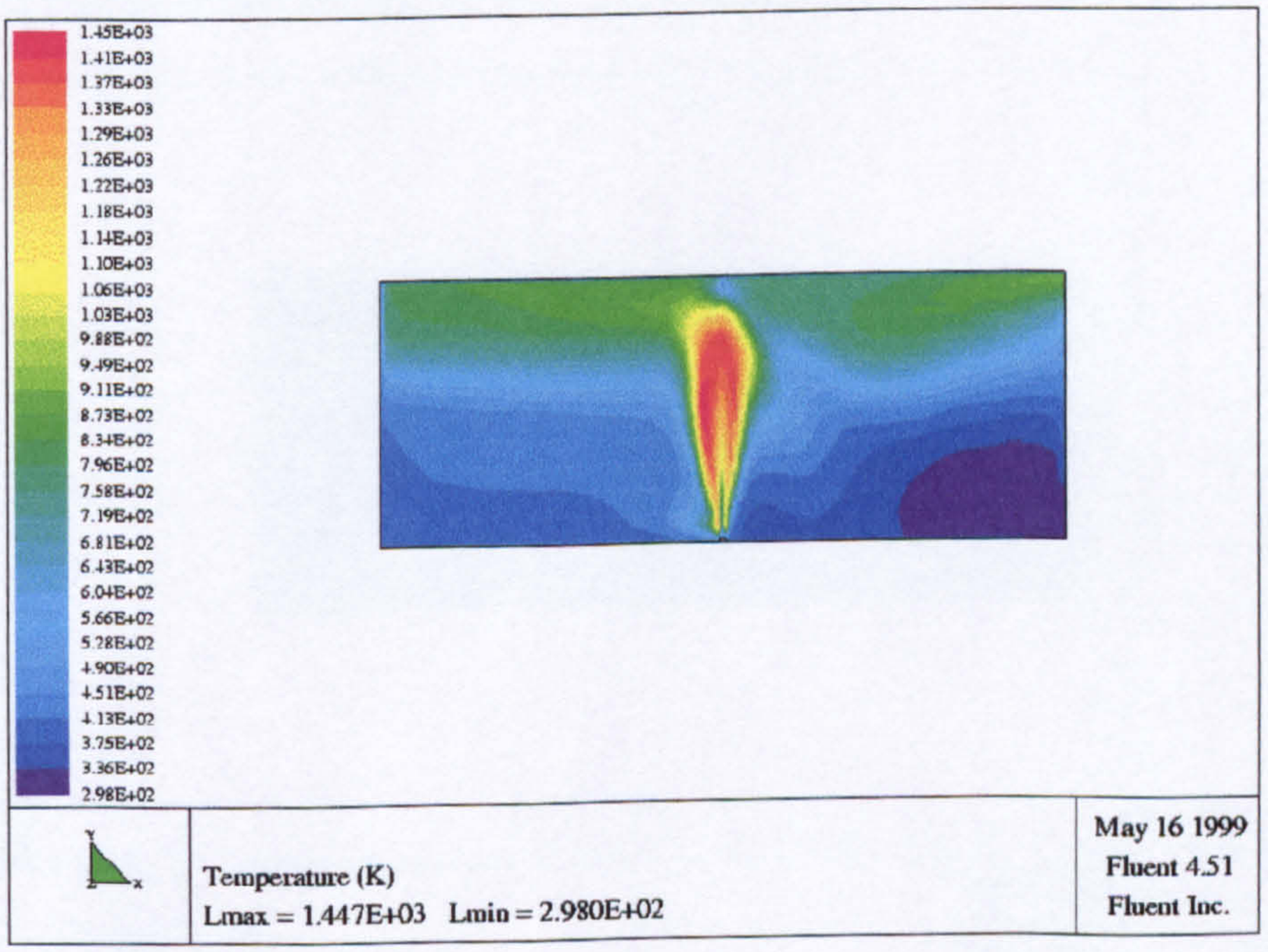

Figure (8.36). Predicted temperatures filled contour which show the reduction in the flame length, (COMP18).

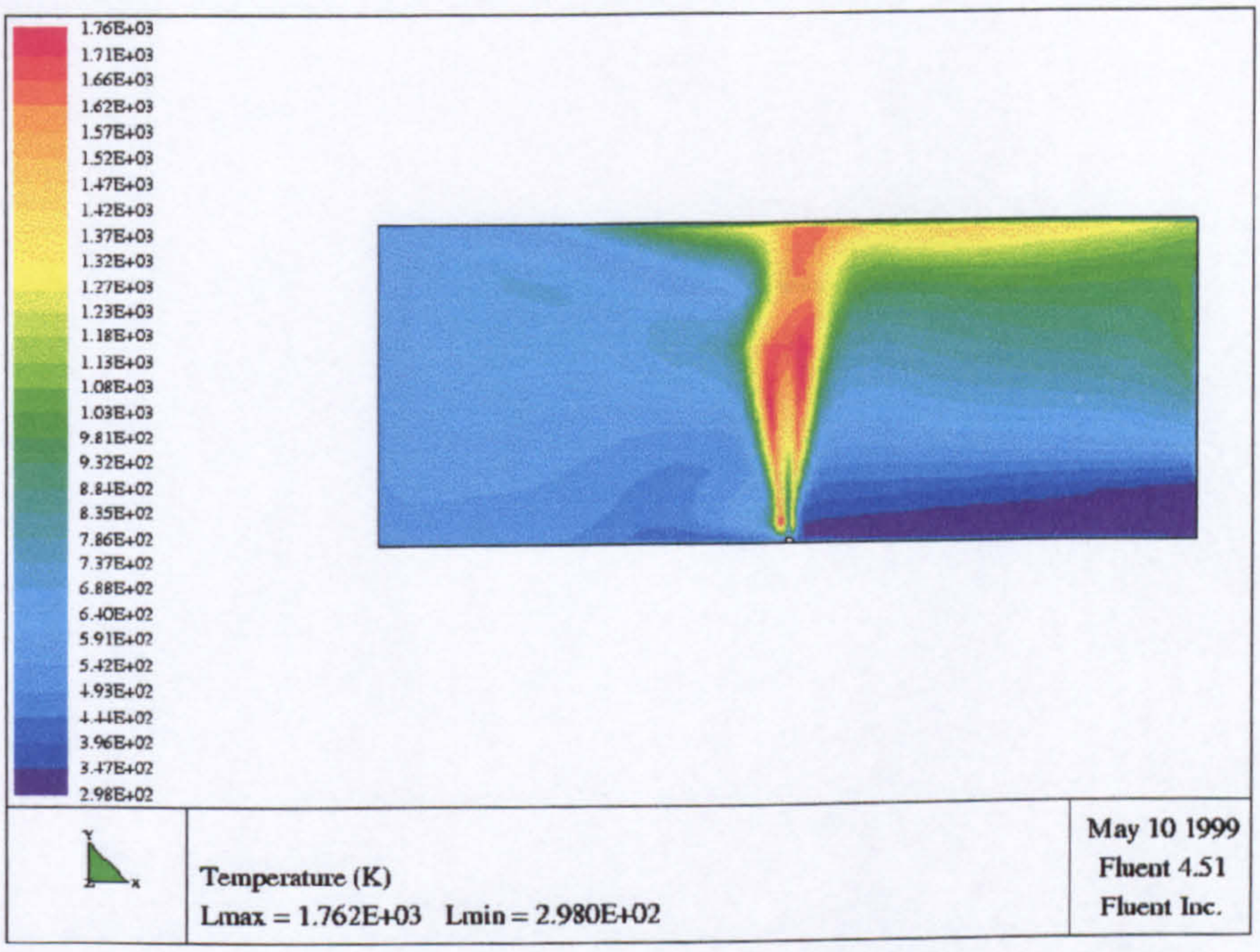

Figure (8.37). Predicted filled contours temperatures for 54 lit/min water flow rate discharged from one spray located at the back of the compartment, (COMP10).

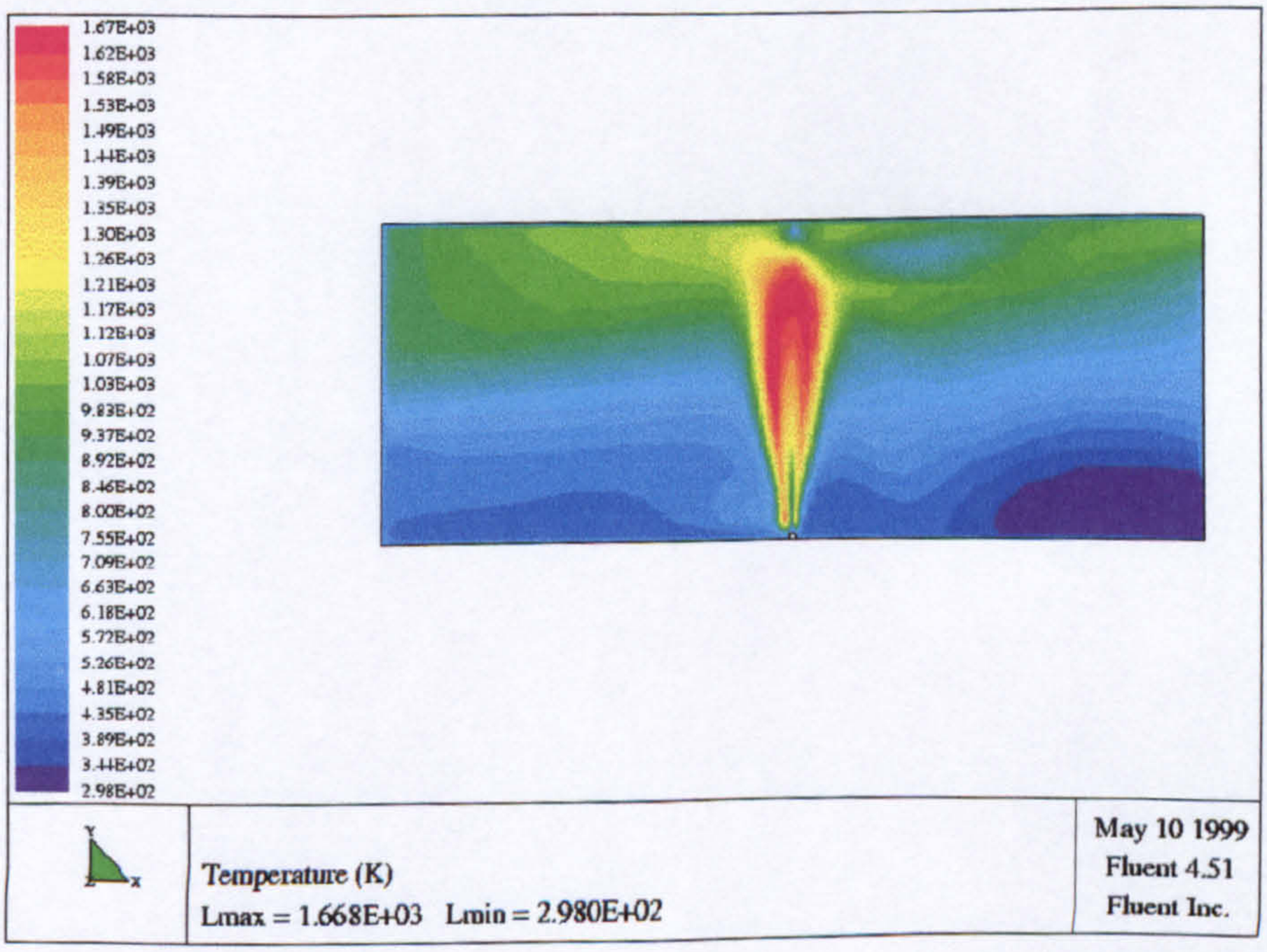

Figure (8.38). Predicted filled contours temperatures for 72 lit/min water flow rate discharged from one spray located in the centre of the compartment, (COMP14).

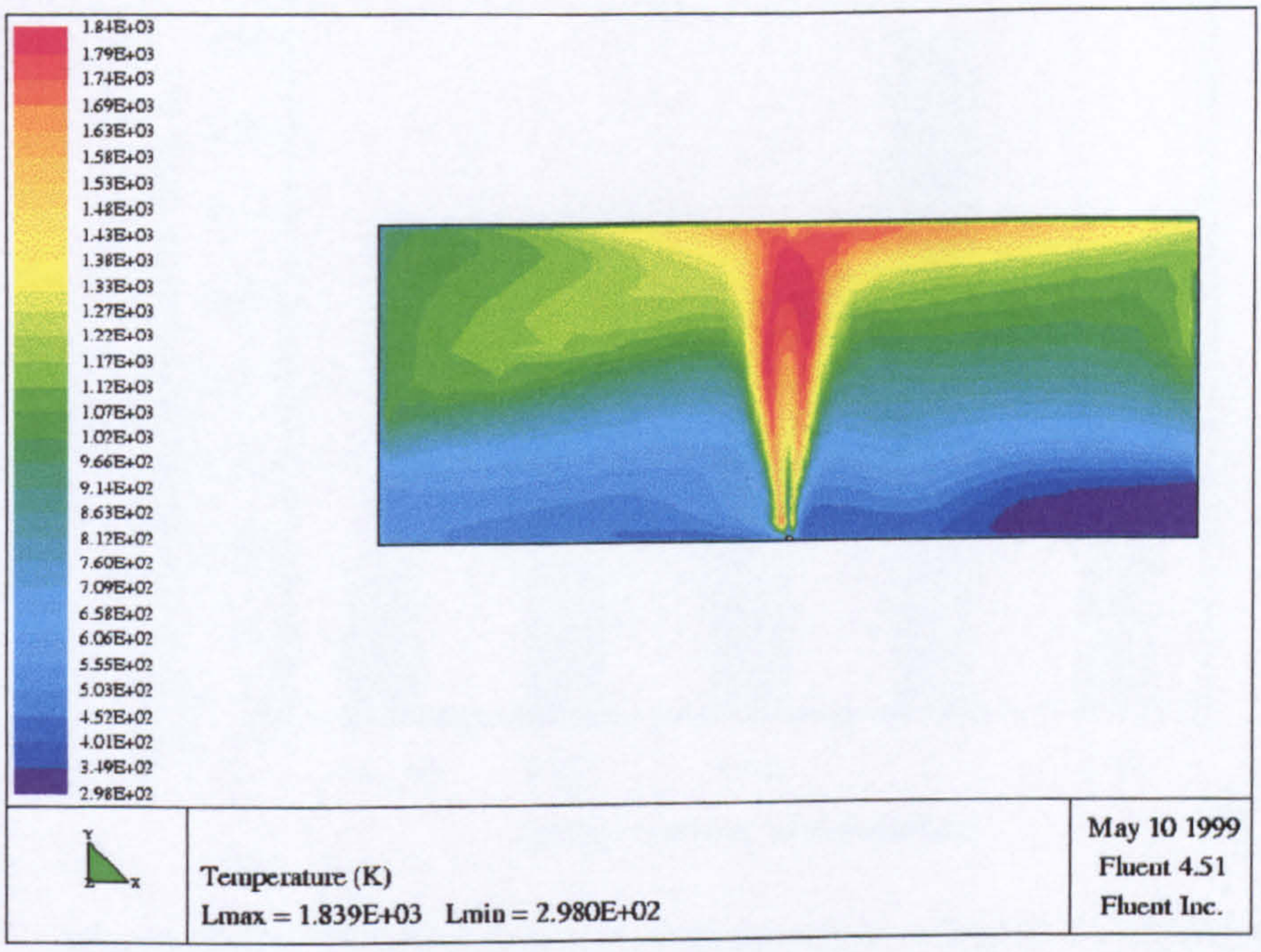

Figure (8.39). Predicted filled contours temperatures for 36 lit/min water flow rate discharged from one spray located in the centre of the compartment, (COMP12).

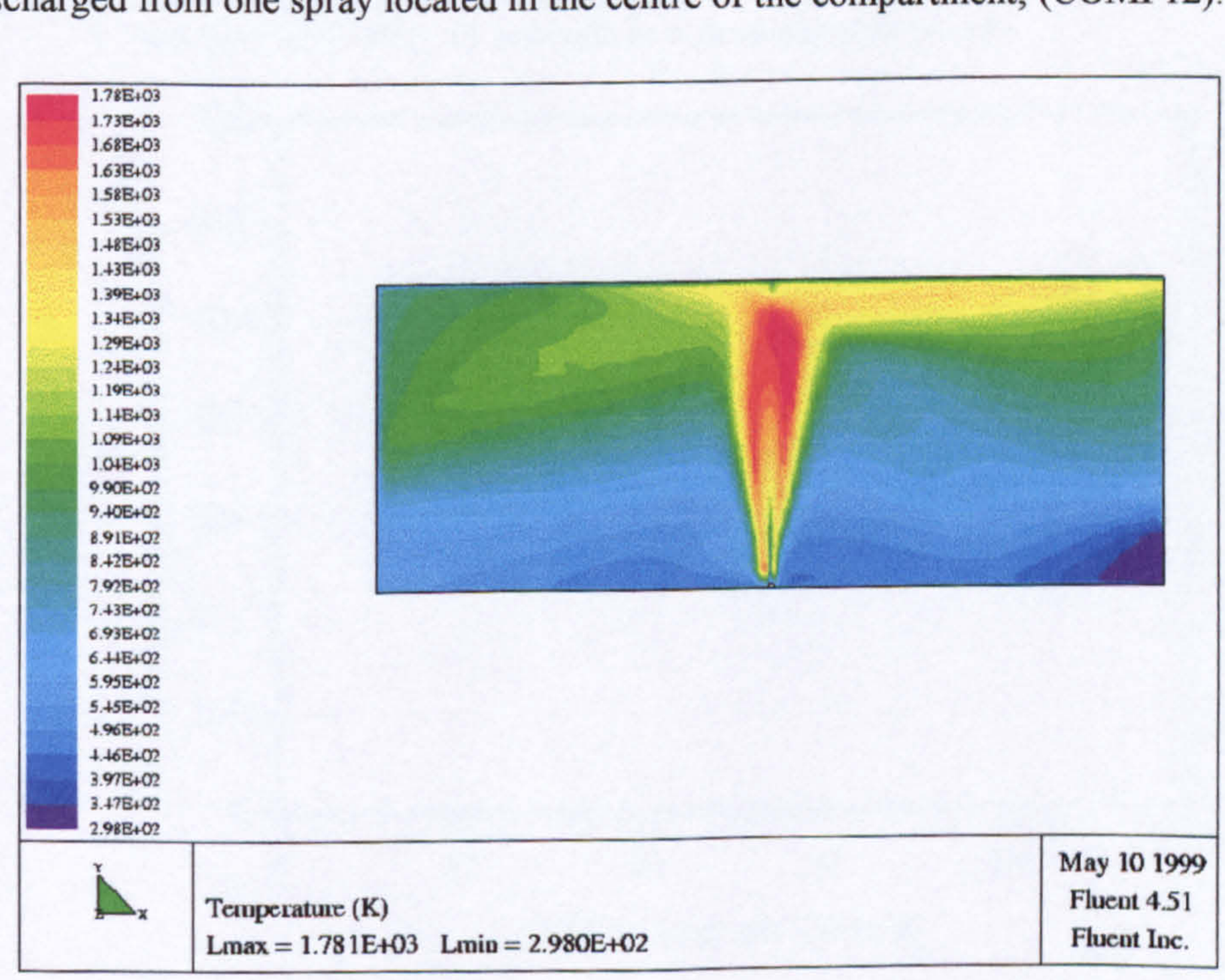

Figure (8.40). Predicted filled contours temperatures for 54 lit/min water flow rate discharged from one spray located in the centre of the compartment, (COMP21).

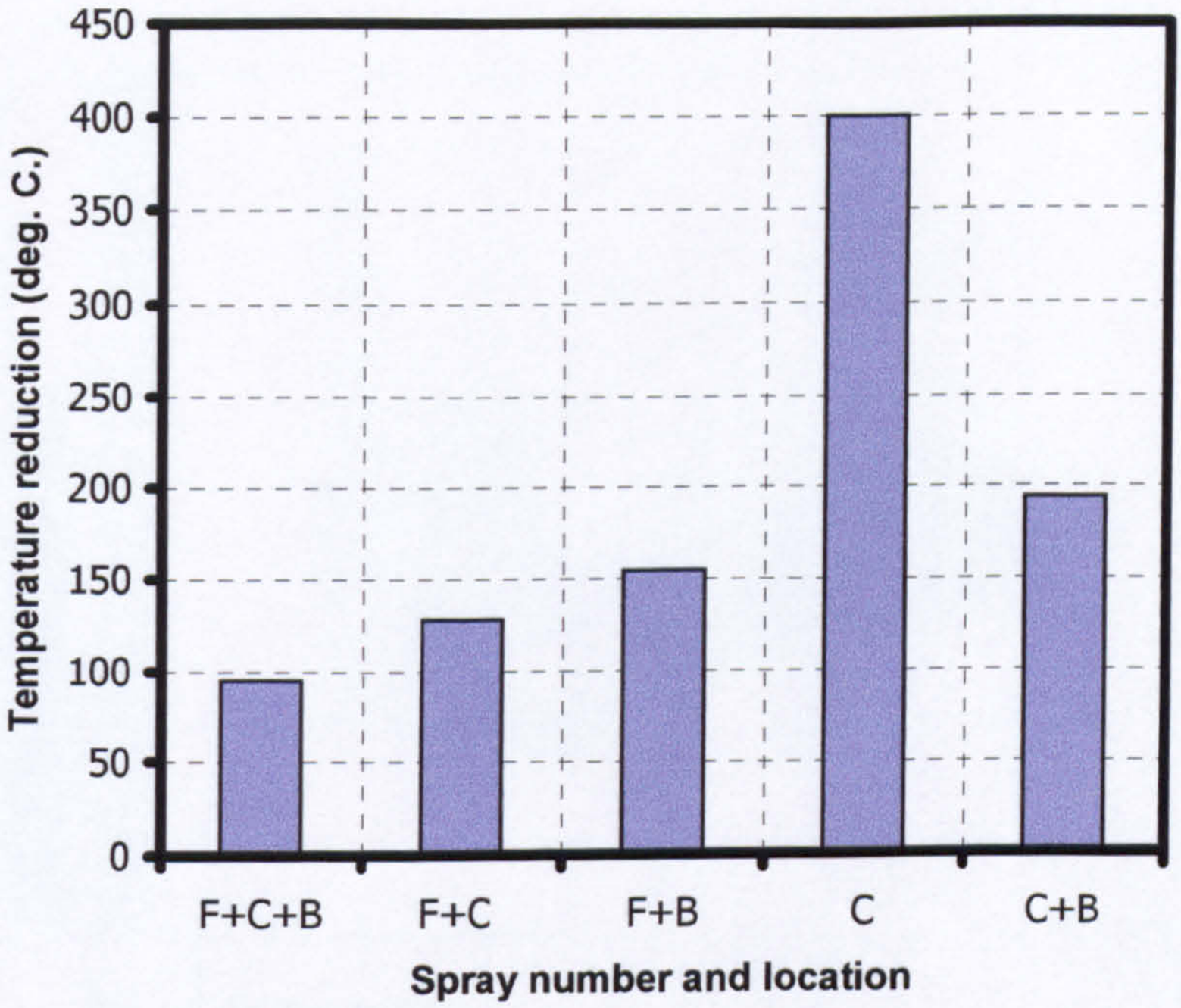

Figure (8.41). Predicted average gas temperature reduction for different spray locations and numbers when 72 lit/min water flow rate has been used while keeping the other parameters constant at 150° spray angle. The average temperature reduction at location 'C' was predicted after 11 seconds in a time-dependent case.

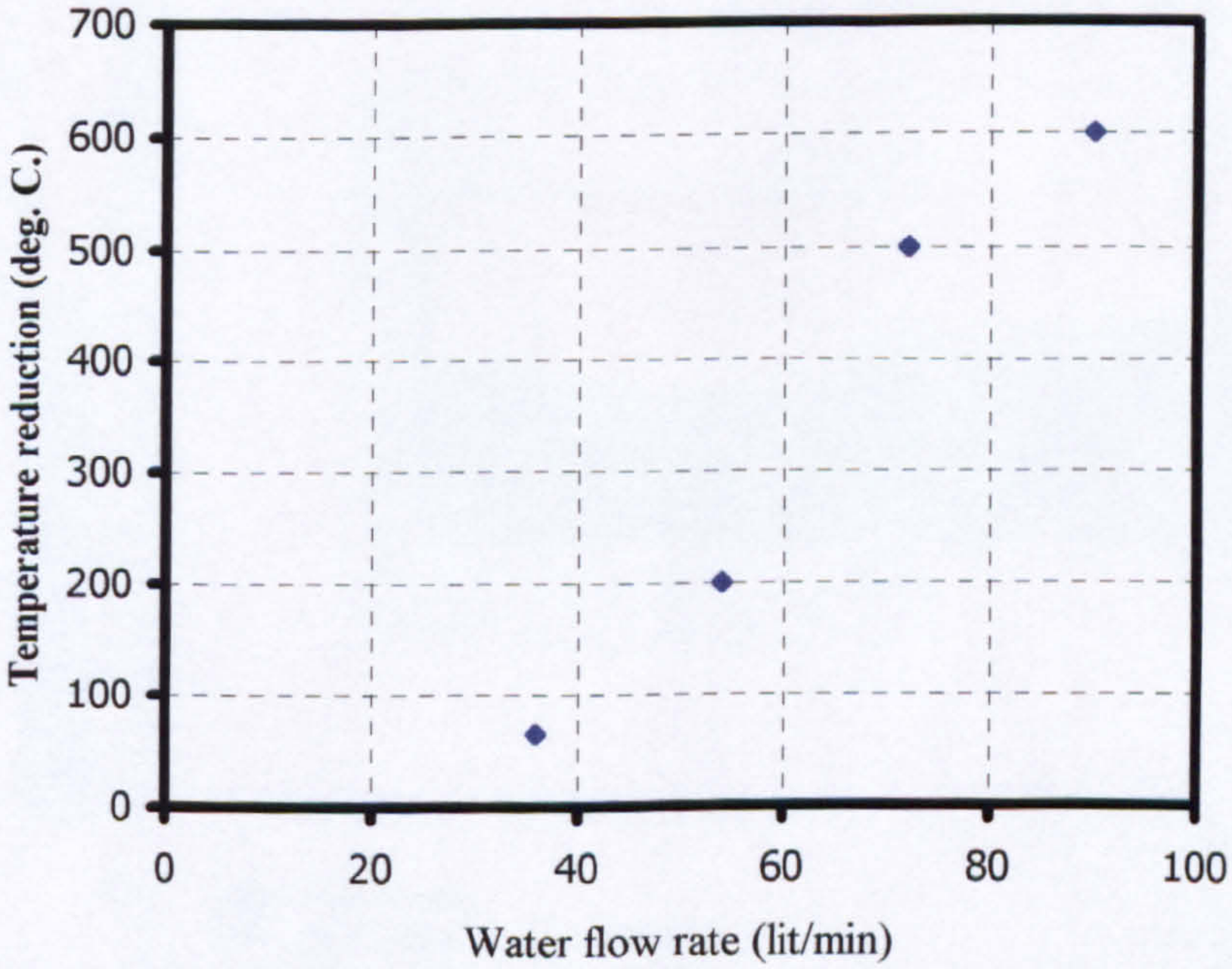

Figure (8.42). Predicted average gas temperatures reduction for different water flow rates at 60° spray angle in a steady state cases.

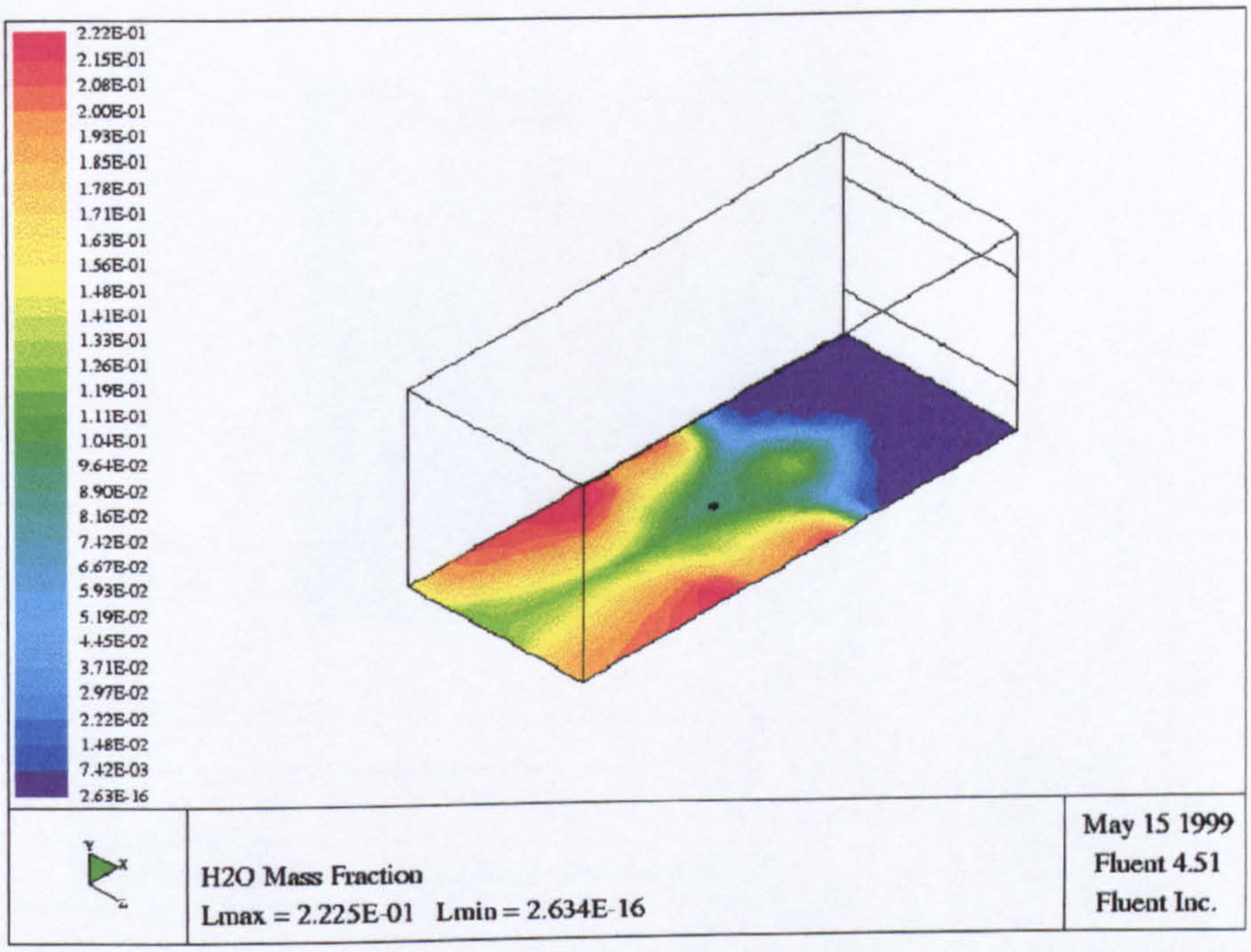

Figure (8.43). Predicted filled contours of water mass fraction at the floor from 90 lit/min flow rate, (COMP16).

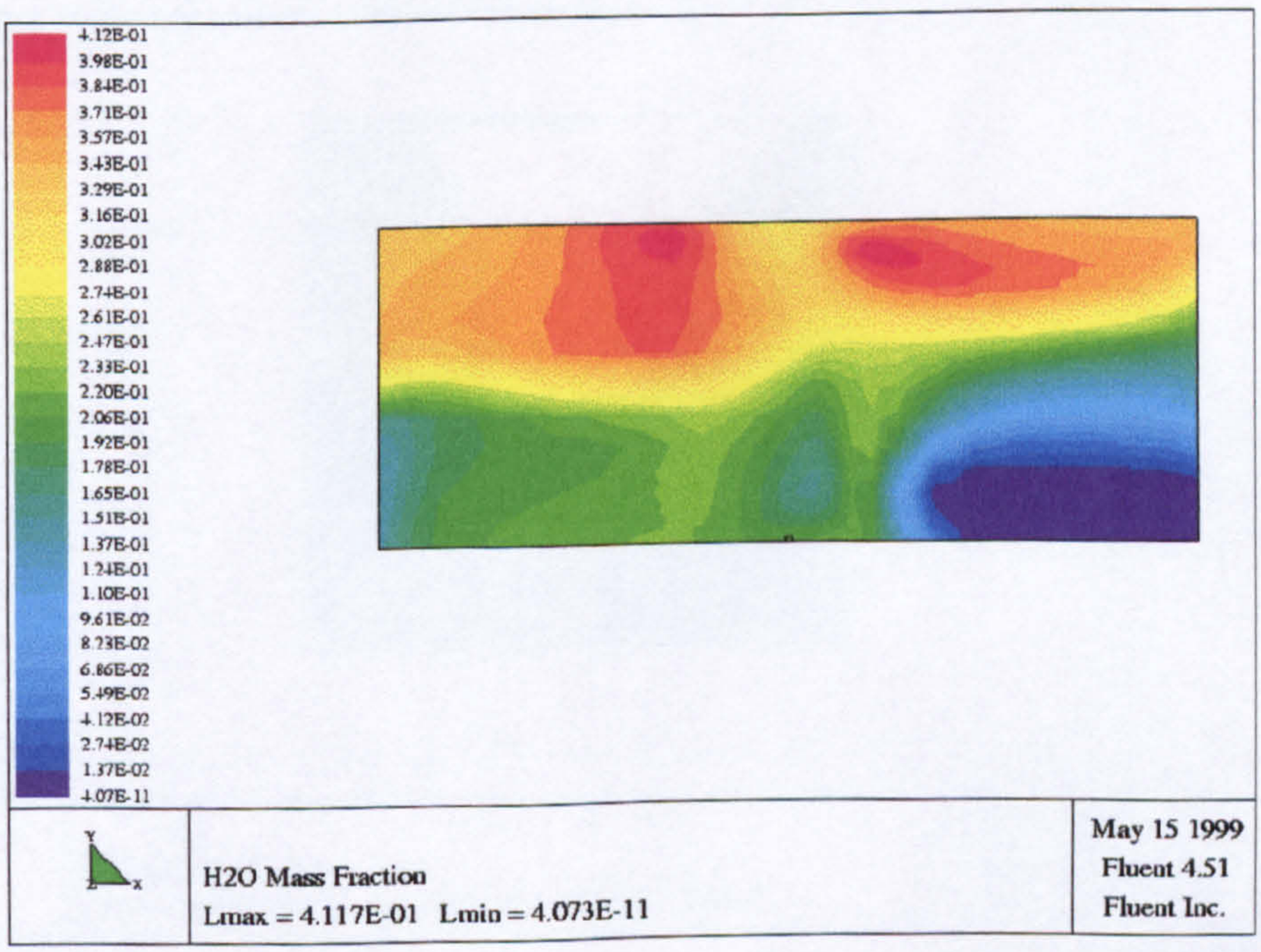

Figure (8.44). Predicted filled contours of the water mass fraction on the walls from 90 lit/min flow rate, (COMP16).

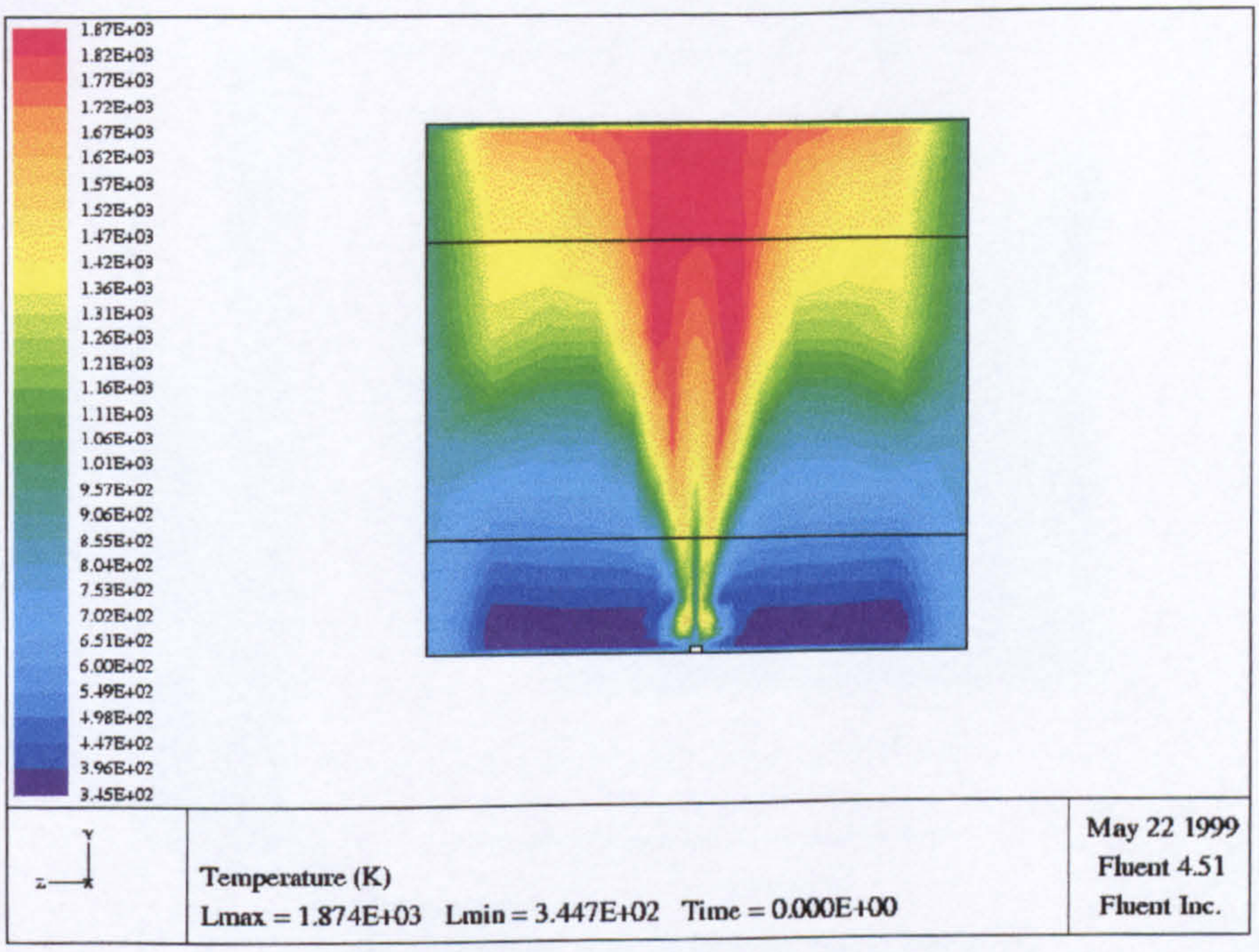

Figure (8.45). Predicted filled contours temperatures before water spray activation (time=0 S).

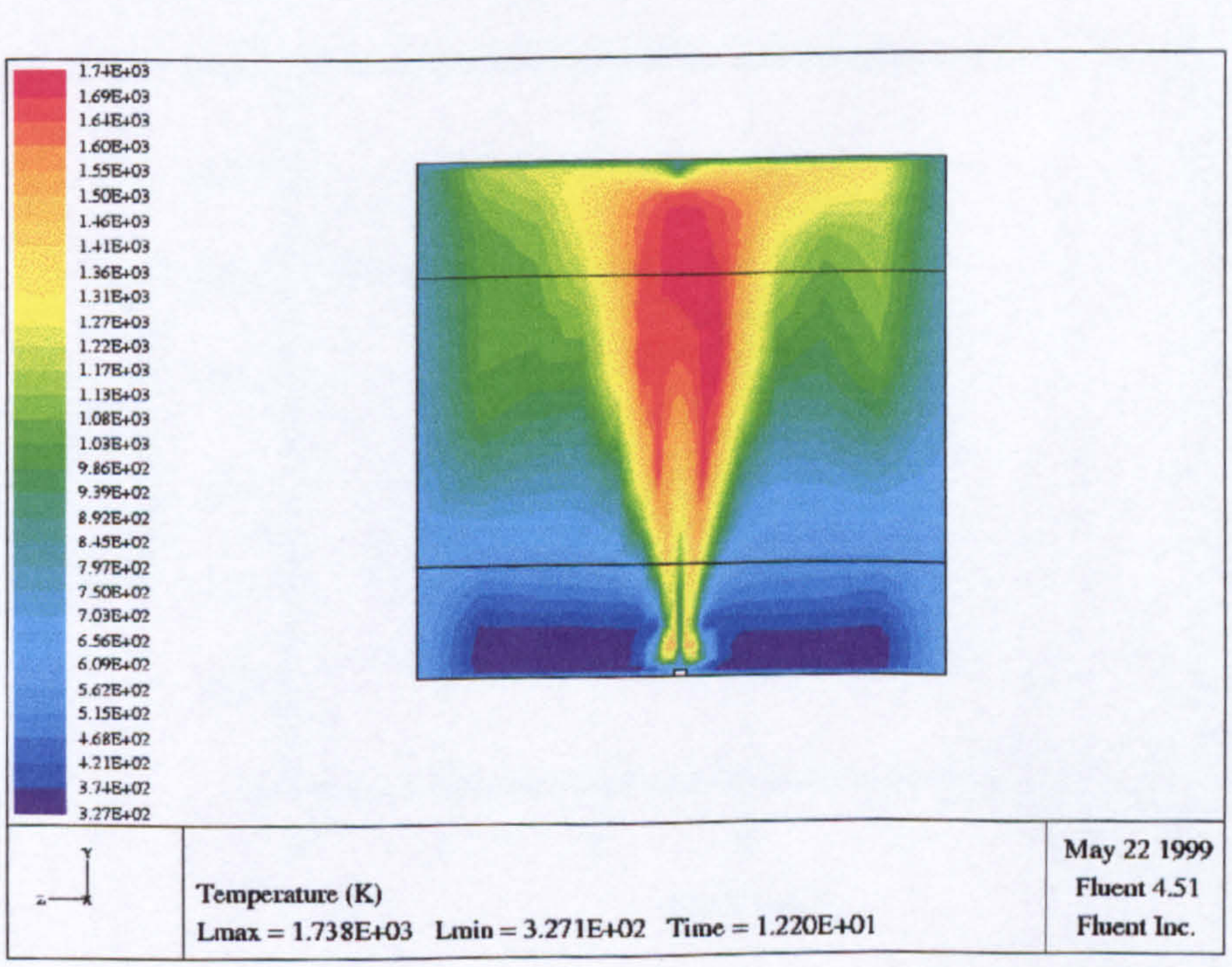

Figure (8.46). Predicted filled contours temperatures after water spray activation (time = 12 S) for one spray nozzle located centrally with 72 lit/min water flow rate.

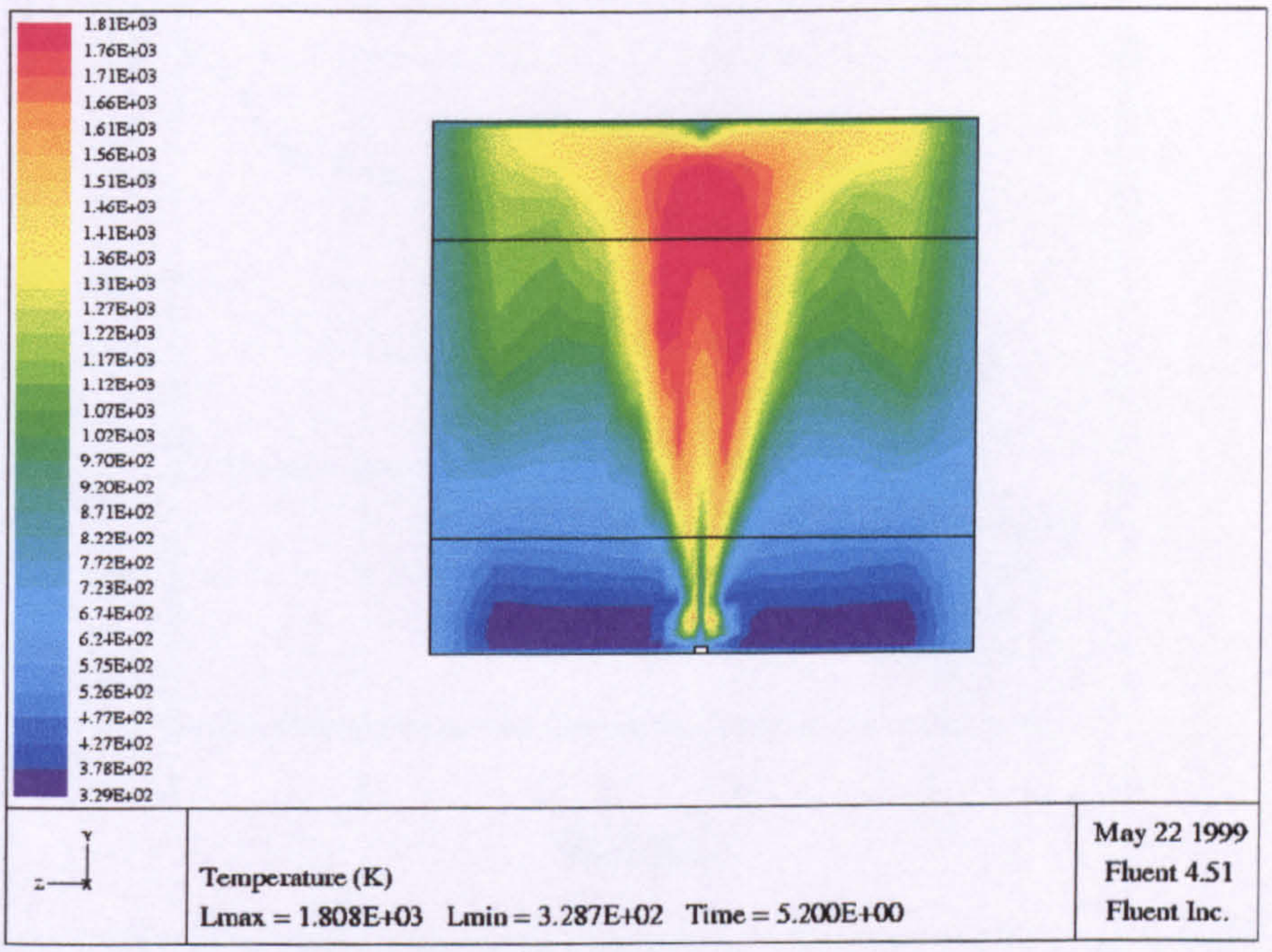

Figure (8.47). Predicted filled contour temperatures after water spray activation (time = 5 S) for one spray nozzle located centrally with 72 lit/min water flow rate.

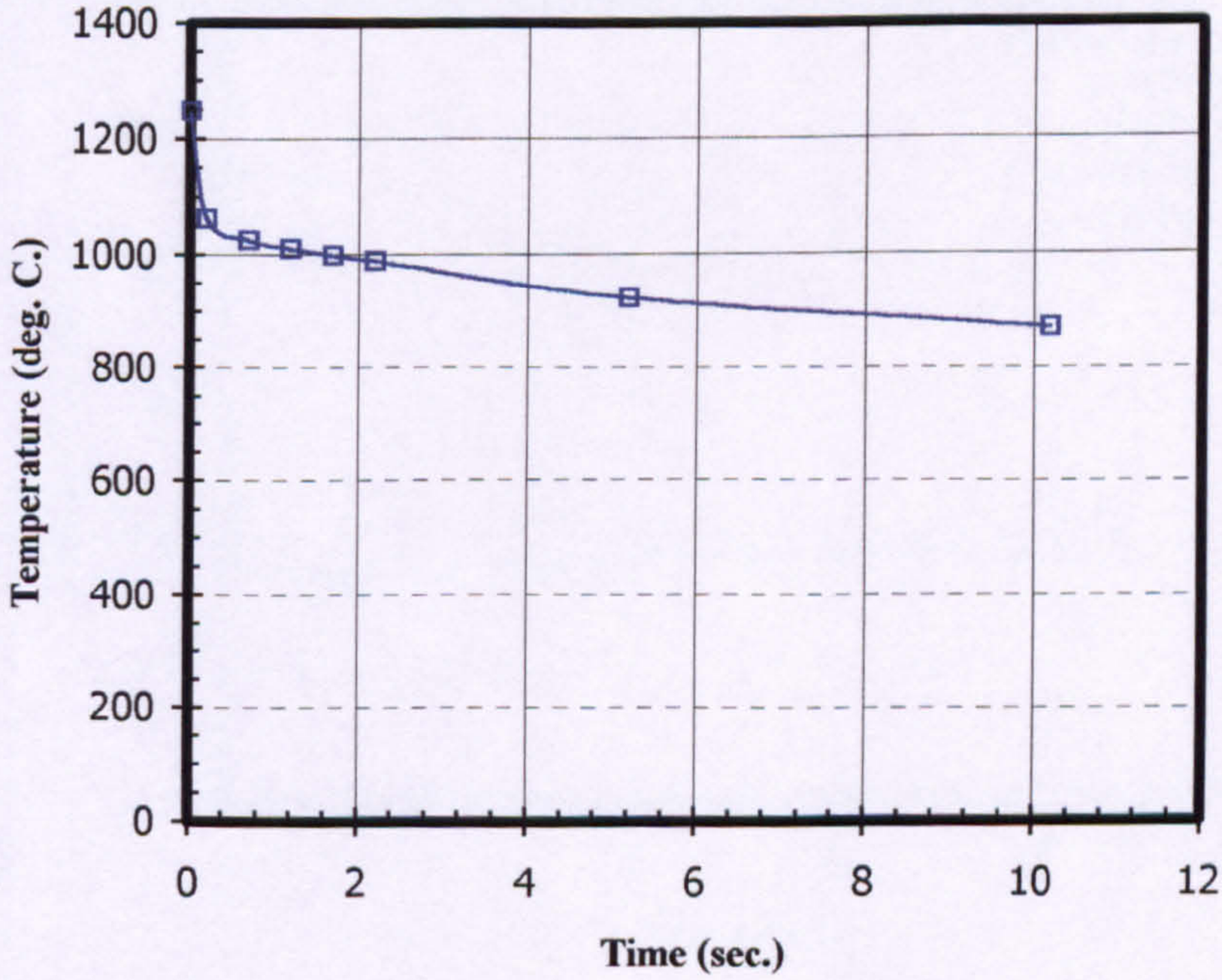

Figure (8.48). Predicted average temperature for time-dependent case with one spray 150° nozzle with 72 lit/min water flow rate (CMP4).

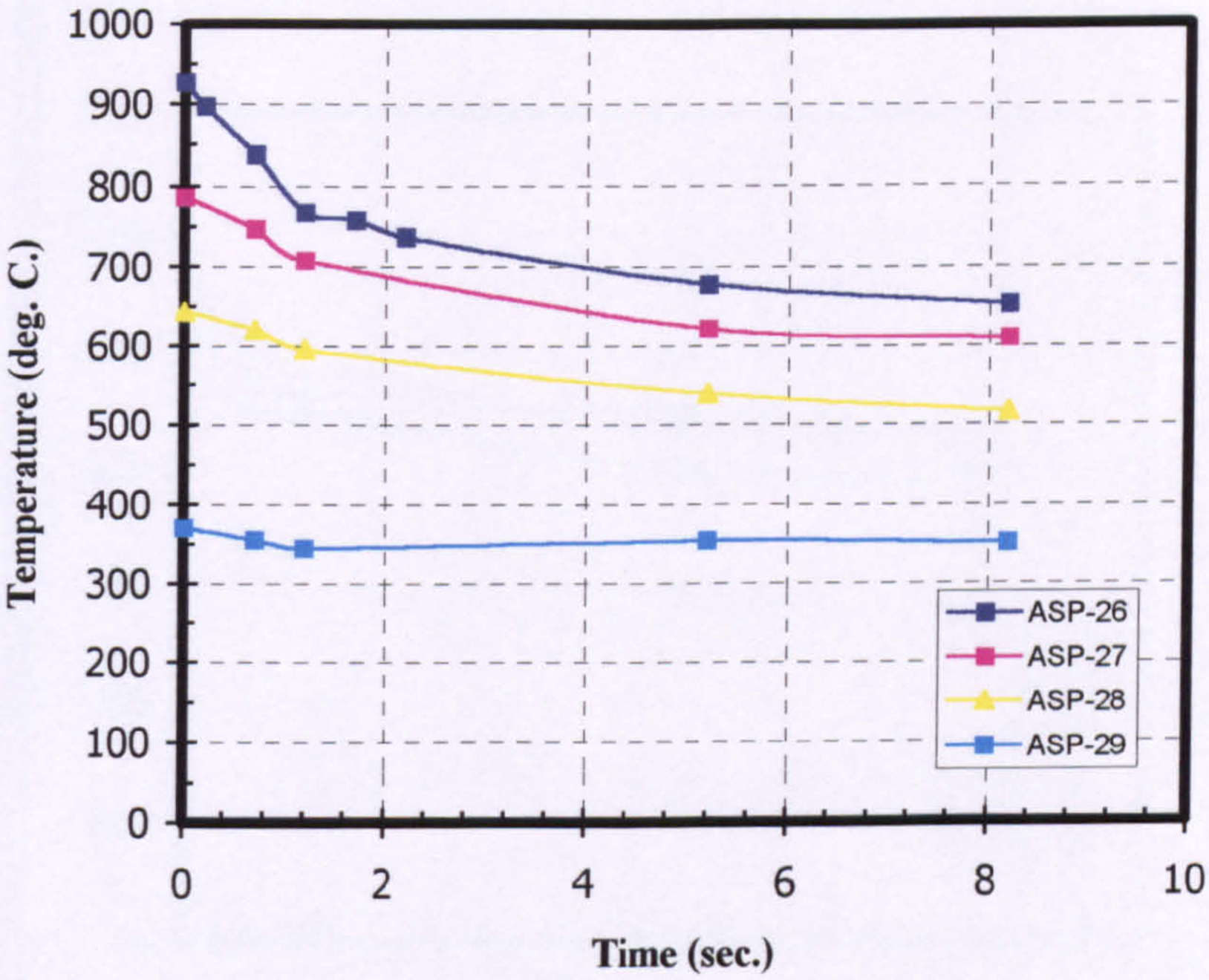

Figure (8.49). Predicted temperature versus time when one spray nozzle has been used with 72 lit/min water flow rate, (COMP4).

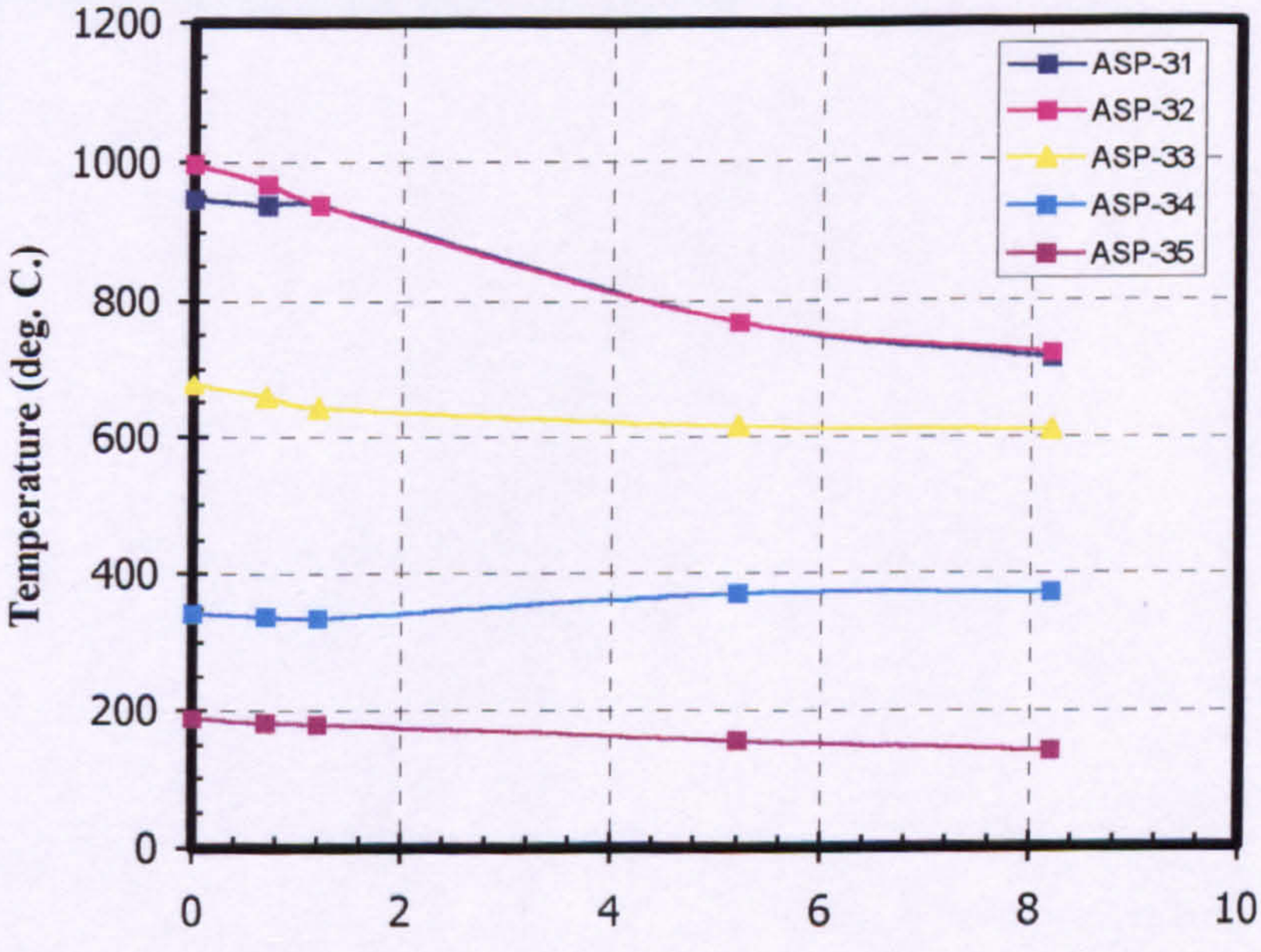

Figure (8.50). Predicted temperature versus time when one spray nozzle has been used with 72 lit/min water flow rate, (COMP4).

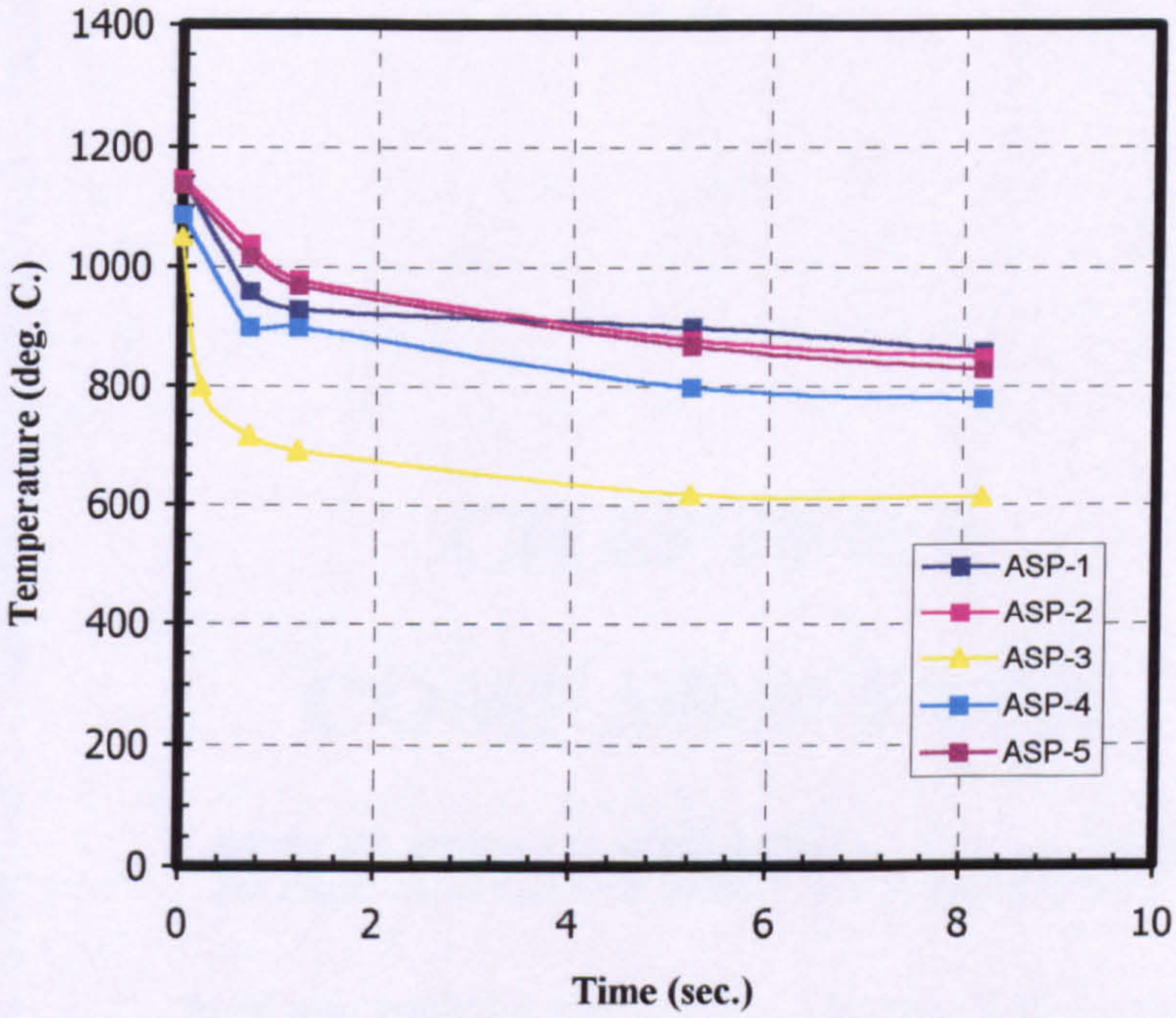

Figure (8.51). Predicted temperature versus time when one spray nozzle has been used with 72 lit/min water flow rate, (COMP4).

CHAPTER 9

COMPARISON OF EXPERIMENTAL AND NUMERICAL RESULTS

9.1 INTRODUCTION

Numerical modelling was validated against programmes of experiments carried out in the 35 m^3 steel compartment. Steady state without water spray (one phase) and with water spray (two phases) and time-dependent (transient) two-phase simulations were chosen for final validation purposes.

In order to be able to have confidence in the predictions made by the model, the steady state and the time varying gas temperatures at the thermocouples locations ASP-1 to 5 and ASP-26 to 35 were monitored. From these locations and the arrangement of the numerical grid used some coincident positions were chosen for

comparison purpose. The comparison between predicted and experimental data of each test in the steady state case can be made using three different figures .
Identical conditions were modelled to that used in the experiments to give the best similarity between predicted and measured results.

9.2 STEADY STATE COMPARISON

Direct comparisons between measured data and the FLUENT predictions of the temperature distribution at different locations along the compartment are made in Figures (9.1) to (9.8).
Predicted gas temperature in the compartment shows a steady increase from floor to ceiling, in good agreement with the experiment. Temperatures measured at two vertical thermocouples strings situated 1 meter either side of the jet fire nozzle on the central plane, and comprising 5 thermocouples each are compared with predictions in Figures (9.1) and (9.2).
Detailed data of the gas temperature distribution at the compartment opening is compared with the numerical results obtained by the FLUENT code in Figure (9.3). The mean gas temperature readings measured at five thermocouples locations of the compartment upper opening for the last two minutes are presented and compared with the data predicted when steady state conditions were reached in the same locations. The figure shows the predicted gas temperature is in good agreement with the measured data from the compartment outlet.
Measurements from three thermocouples located at the vertical centreline of the back wall are compared with the predicted temperature in Figure (9.4). Overall agreement can be seen to be reasonably good, although wall temperatures close to the floor are predicted somewhat high. On the other hand, Figure (9.5) shows the measured temperature from four wall thermocouples located at the horizontal centreline of the

ceiling, and the predicted temperature for the same locations. From the figure the predicted temperature in the centre of the ceiling directly above the jet nozzle was higher than measured temperatures by 160° C. The most pronounced discrepancy between measured and predicted temperatures occurs at the location above the jet nozzle. With increasing distance from the jet nozzle, the predicted gas temperature distribution is in better agreement with the data. This is almost certainly due to the treatment of heat losses to the boundaries assumed to be prescribed by a fixed heat transfer coefficient of 55 W/m^2 K. One factor which might cause this discrepancy between the measured and the predicted data is due to both numerical and measured error which contributes to this disagreement. Another reason for this discrepancy is that, at high temperatures, the products of combustion are partially dissociated into a number of atomic, molecular and free species. As each dissociation is endothermic (absorbs energy rather than releases it), this will tends to depress the final temperatures.

Wall surfaces temperature predictions are compared in Figures (9.6) to (9.10) with measurements for both Southeast and Northwest walls. Whereby Figures (9.6) and (9.7) illustrated comparison between predicted and measured wall temperatures on vertical line at distance from the compartment opening at the Southeast wall at 4.467 and 1.520 metres, respectively.

The predicted and measured wall temperature distributions at the Northwest wall are compared in Figure (9.8).

Temperature contours as estimated by five wall thermocouples in the experiment when steady state condition has been reached for the Northwest wall are shown in Figure (9.9). On the other hand, a contours plot has been made as well for the comparable wall location with same conditions shown in Figure (9.10). These two figures of contours plot show that relatively good agreement between FLUENT prediction and the experimental data of wall temperatures can be achieved; they also demonstrate the temperature distribution on the walls.

The average temperature of the gas at the location where the flue gas temperature was measured for the experimental study was 989° C. This was in good agreement (about 4% less) with the predicted temperature which was 1030C.

Overall properties and some point determinations are compared in table (9.1). The observation from the O_2 and CO_2 percentage experimental data reasonably agreed with the predicted concentrations.

It was observed from the predicted and measured compartment surfaces temperatures shown in table (9.1) that there was greater heat loss in the experiments than in the prediction. This can be attributed to the facts that the exact compartment structure conditions were not known, and heat transfer from the structure elements and compartment to the outside atmosphere was based on assumptions. Also the uniformity of the heat transfer coefficient and emissivity used may have contributed to the difference.

Property	Prediction	Measured
Exit gas temperature	1030° C	989° C
Exit O2 concentration	2.09 %	1.88 %
Exit CO2 concentration	12.50 %	12.03 %
Ceiling temperature	679° C	641° C
Floor temperature	520° C	200° C
Southeast wall temperature	554° C	545° C
Northwest wall temperature	556° C	548° C
Back Wall Temperature	513° C	483° C

Table (9.1). Summary of the averaged predicted and measured values for some data at steady state.

The results in table (9.1) show that the steady state model predictions are in excellent agreement with measurement.

In general agreement is seen to be excellent although both the measurement and the numerical calculation errors can make contributions to this disagreement.

9.3 WATER SPRAY MODELLING

The comparison results of the water spray extinguishment are displayed through the same locations and positions as for steady state single phase fire scenario in section (9.2).

The steady state water spray extinguishment comparison will be made on selected cases to represent coverage for the different parameters used, low and high water flow rate, small and large spray angle and spray number and spray locations. Some of the time dependent prediction were compared as well.

9.3.1 STEADY STATE COMPARISON

When no extinguishment occurred after the water spray activation and the burning continued, this is considered as two phase steady state.

The results presented in Figure (9.11) and Figure (9.12) depict the temperature variation at the five locations at the Northeast string and upper opening, following spray activation for COMP13 which has 54 lit/min and one spray nozzle located centrally. From these, very interesting facts concerning the spreading of the spray in the compartment can be observed. Spray nozzle with 60° spray angle reduce the temperature of the middle and lower layers more than that of the upper layers. The

prediction point below the ceiling which corresponds to ASP-26 in the measurement is hardly affected by applying the narrow cone spray. However, this location is predicting higher temperature than respective measured thermocouple. Therefore, the decrease in gas temperature remote from the spray trajectories is, as expected, not as steep as the one in the spray region. The gas temperature comparisons, shown in Figure (9.11), are at the location near the upper opening, 0.38 metre below the ceiling. After the spray activation in this test, the conditions used in COMP13 were not able to extinguish the fire, and steady state condition was reached, which made part of the flame burn at the upper opening. This caused the thermocouple at the opening to register higher temperature readings as can be seen in Figure (9.11). The results show that the prediction are in good agreement with the measurement, except in Figure (9.12) where FLUENT over predicted the temperature near the ceiling.

The resulting comparisons of predicted and measured data for COMP21 are shown in Figures (9.13) and (9.14). From these comparisons, it can be observed that the right trend has been obtained for all five monitoring locations throughout the compartment. In this test the spray angle used was 90 degree and had larger coverage area than COMP13. As a result, the temperature reduction at the compartment opening was more than COMP13.

Figure (9.15) plots all measured temperatures versus the predicted temperatures from all the Northeast string, from one spray located centrally which has 54 lit/min water flow rate and 150° spray angle nozzle.

In Figure (9.16) the predicted and measured temperature of water spray extinguishment for COMP28 at the compartment opening is plotted . COMP28 has one spray nozzle located in the centre of the compartment with 54 lit/min water flow rates and 120 degree spray angle. On the other hand comparison COMP38 was made between predicted and measured results shown in Figures (9.17) and (9.18) for the front positioned spray with 54 lit/min and 150° spray angle.

Figures (9.19) to (9.21) show comparison between predicted and measured wall and ceiling temperatures when three spray 150° nozzles were used with 90 lit/min total water flow rate.

As indicated in above Figures, (9.13) to (9.21), the results show that the two-phase steady state model prediction is in good agreement with the measurement.

9.3.2 TIME DEPENDENT COMPARISON

A further comparison between the predicted and measured temperatures for some of the tests which represent extinguished tests was made.

The transient variations of the temperatures predicted at the thermocouple locations ASP-2, ASP-26 and ASP-33 are shown in Figures (9.22) to (9.24), together with the experimentally determined values. The test used was for one spray nozzle located centrally with 72 lit/min water flow rate.

Figure (9.24) shows that after 8 seconds the predictions are much closer to measurements.

Although temperature predictions are decreasing in time and follow the measured trend, the temperature difference between predicted and measured data could be accounted for in the coarseness of the grid existing around these locations, which makes it difficult to specify the coincidental locations of thermocouples used experimentally. Another important reason is the limitation for the modelling of the spray geometry and distributions. However, FLUENT user's manuals (1996) raises and points out limitation and skepticism about using time dependent models with dispersed phase simulation.

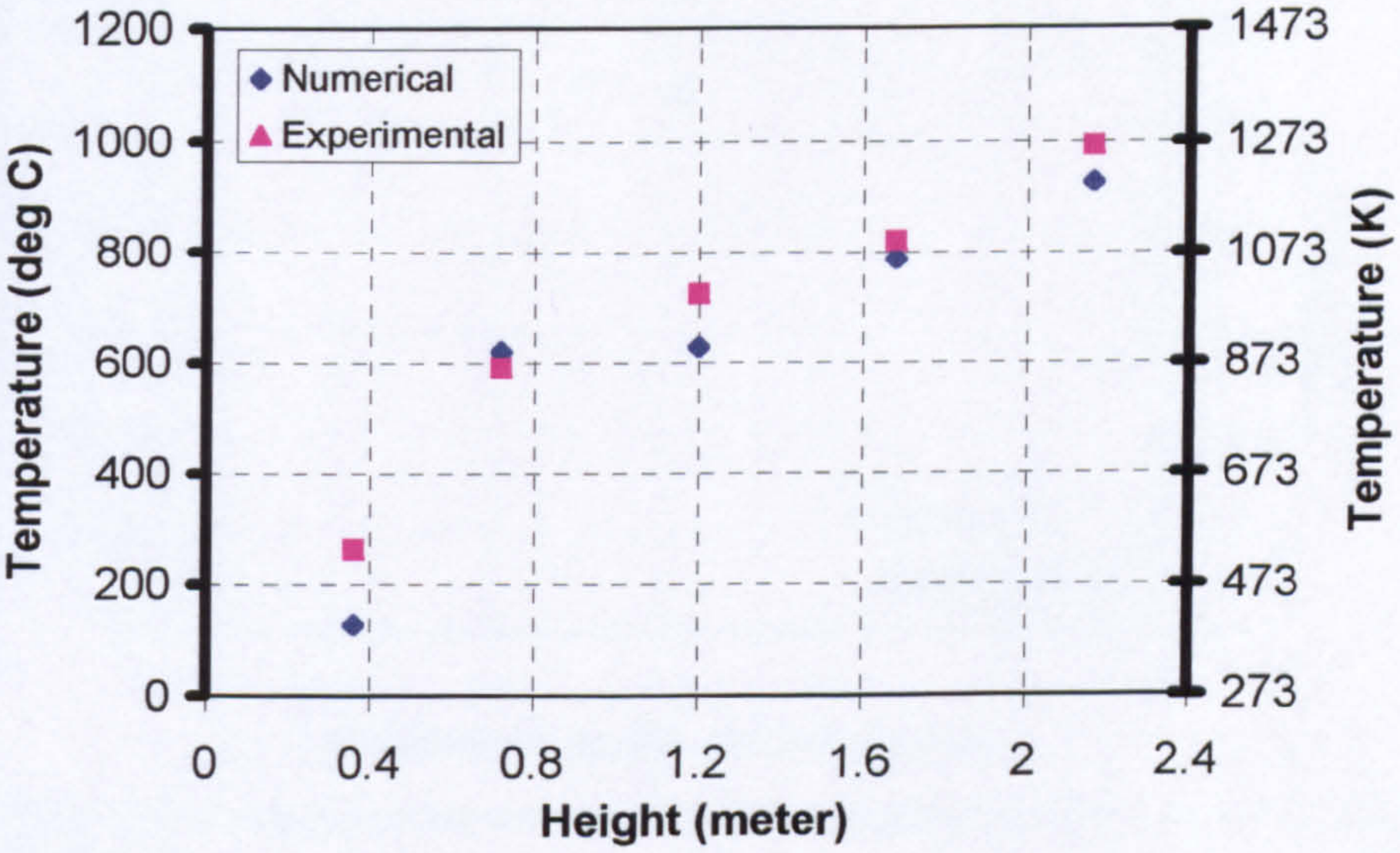

Figure (9.1). Comparison between predicted and measured temperatures at the Northeast string (ASP-26 to 30).

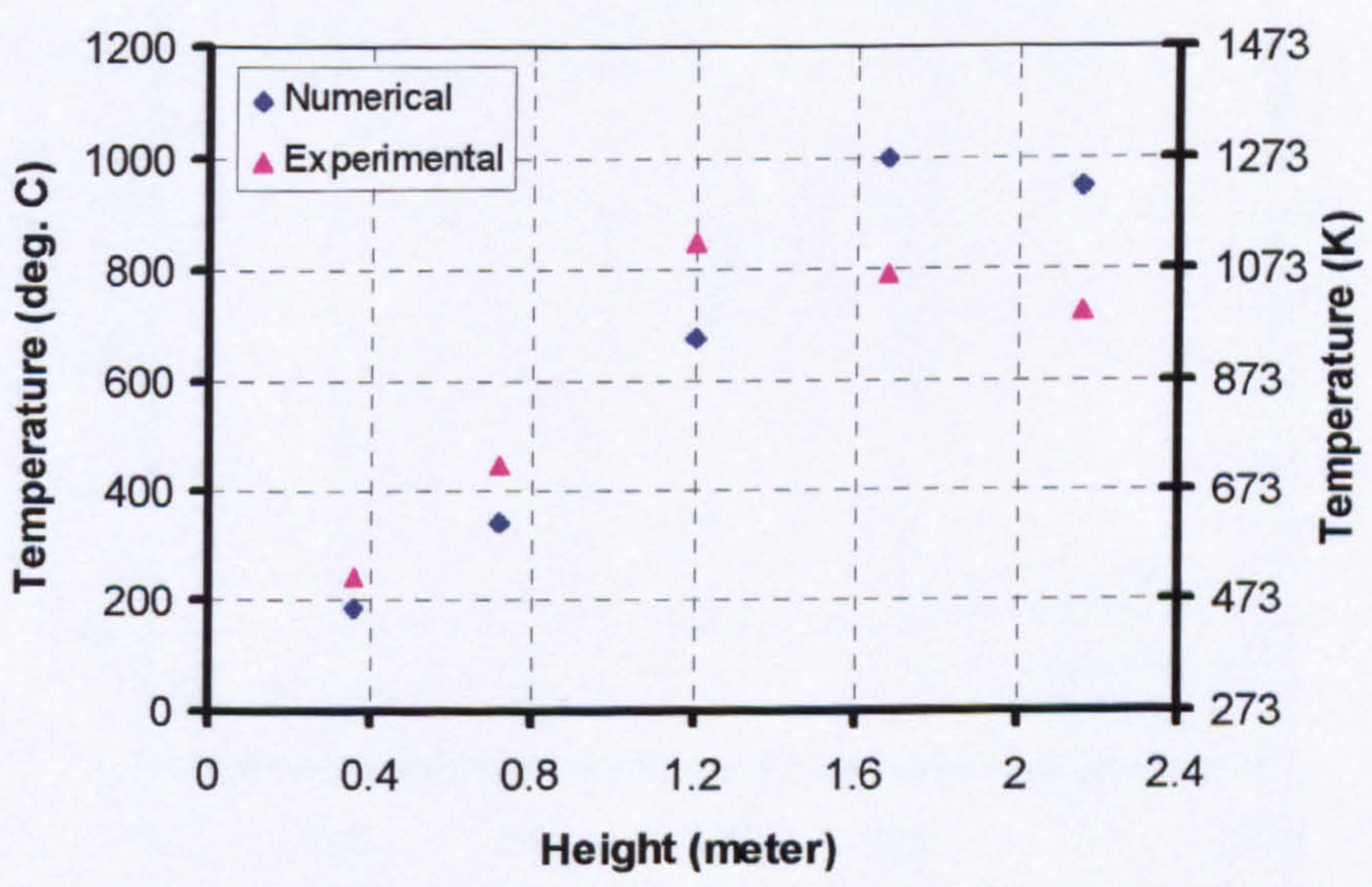

Figure (9.2). Comparison between predicted and measured temperatures at the Southwest string (ASP-31 to 35).

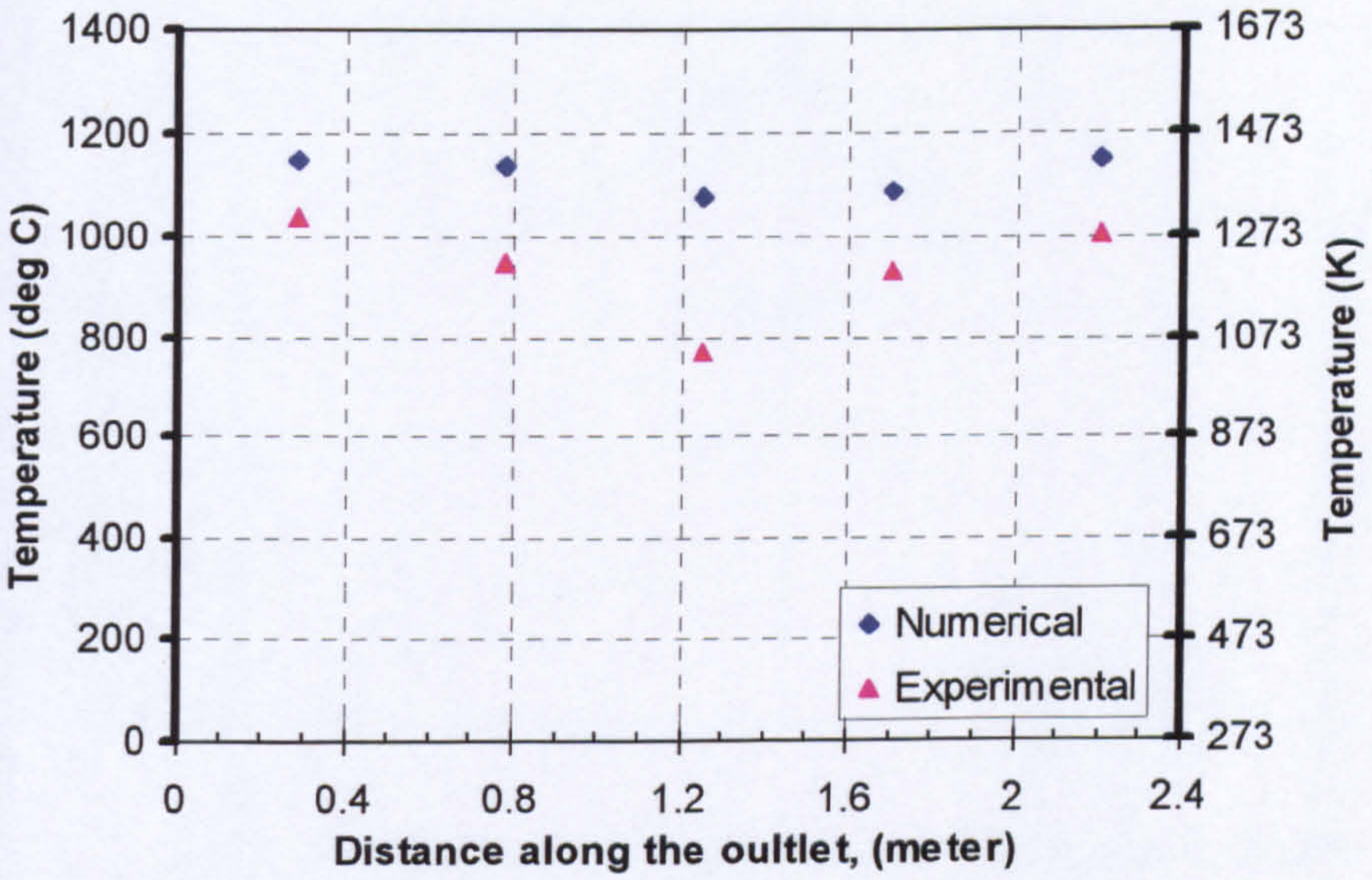

Figure (9.3) Comparison between predicted and measured temperatures at the outlet (ASP-1 to 5).

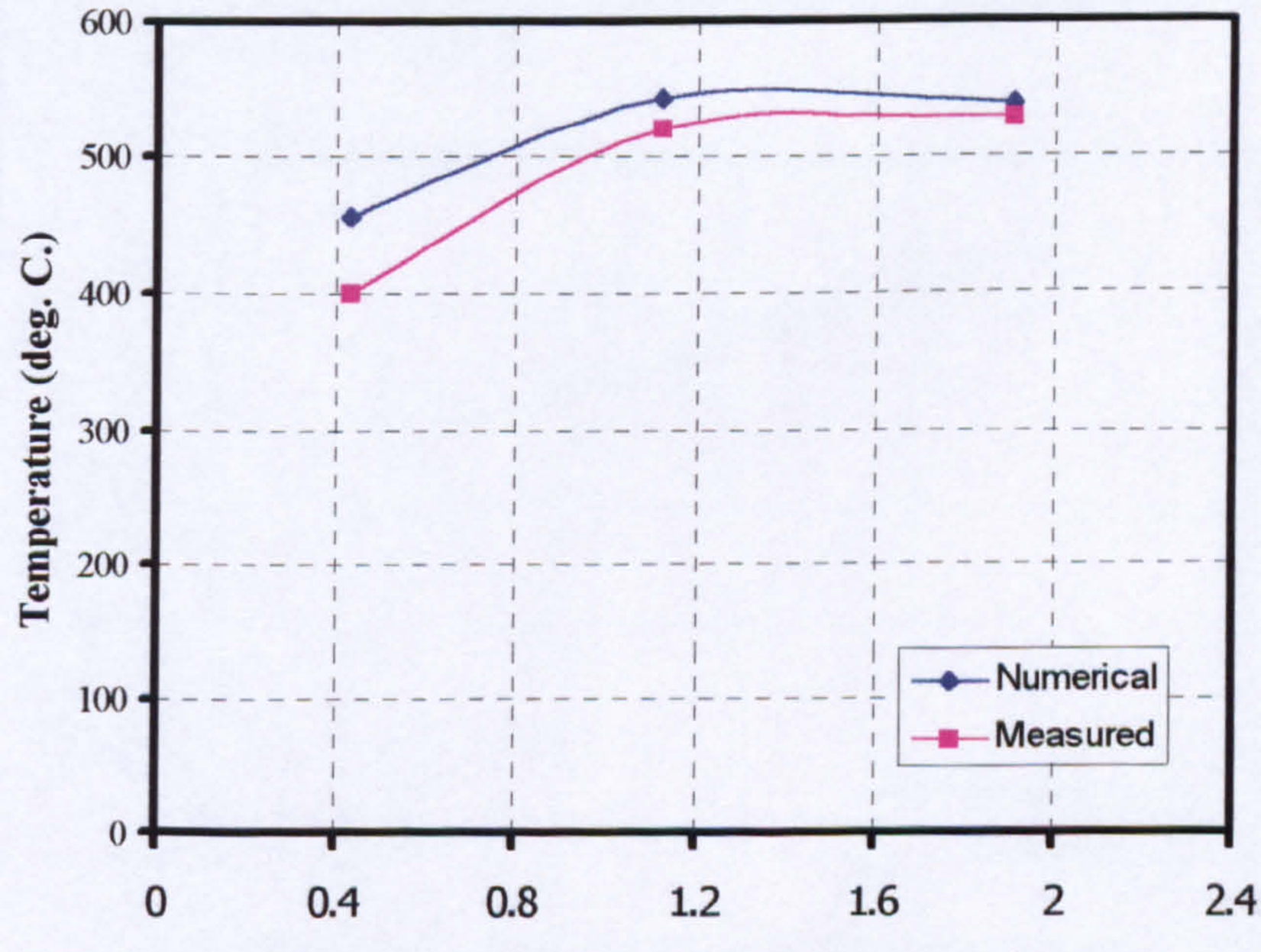

Figure (9.4) Comparison of predicted and measured back wall temperature (steady state) (W-6 to W-8).

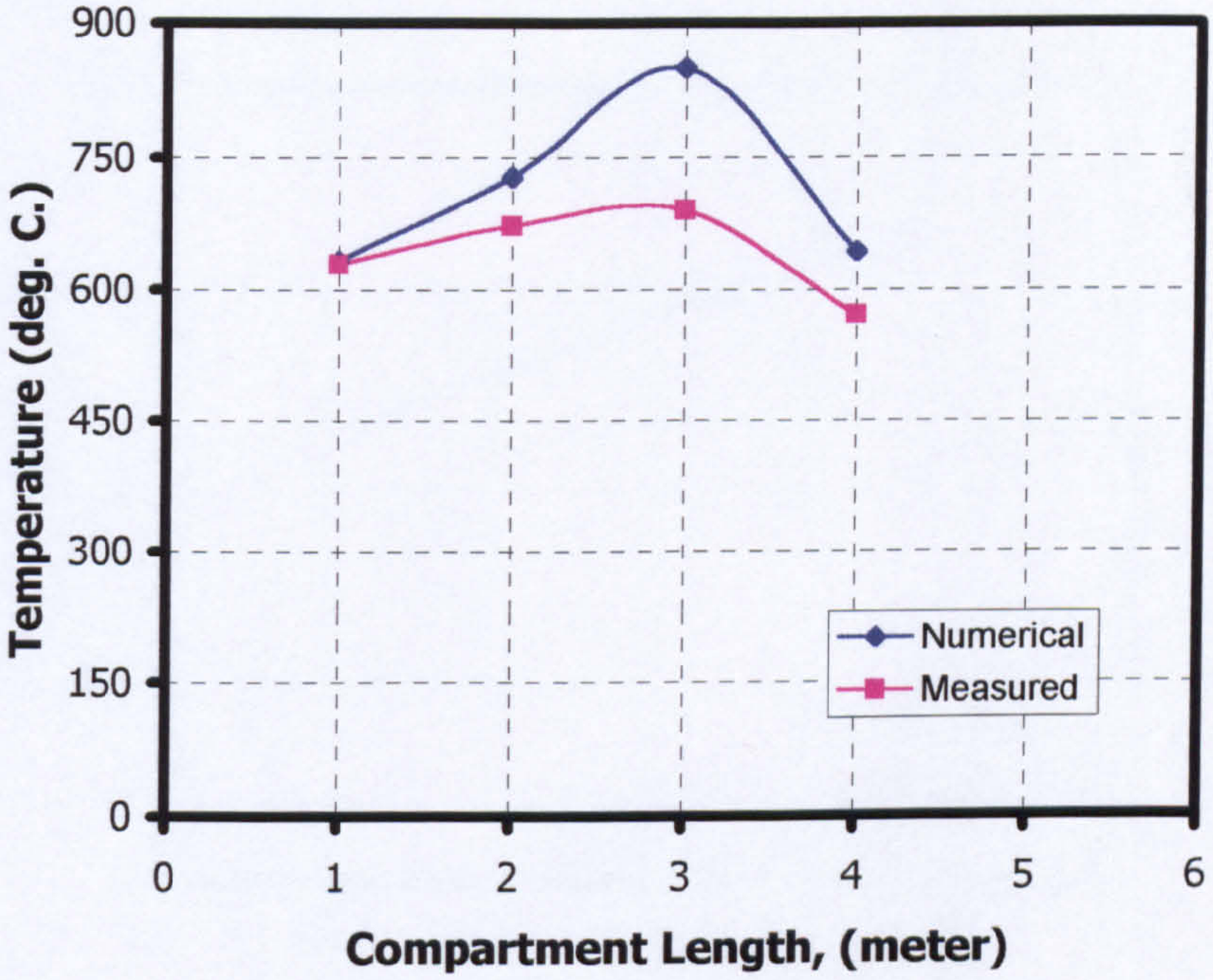

Figure (9.5) Comparison of predicted and measured wall temperature (steady state) at the roof (W-1 to W-4).

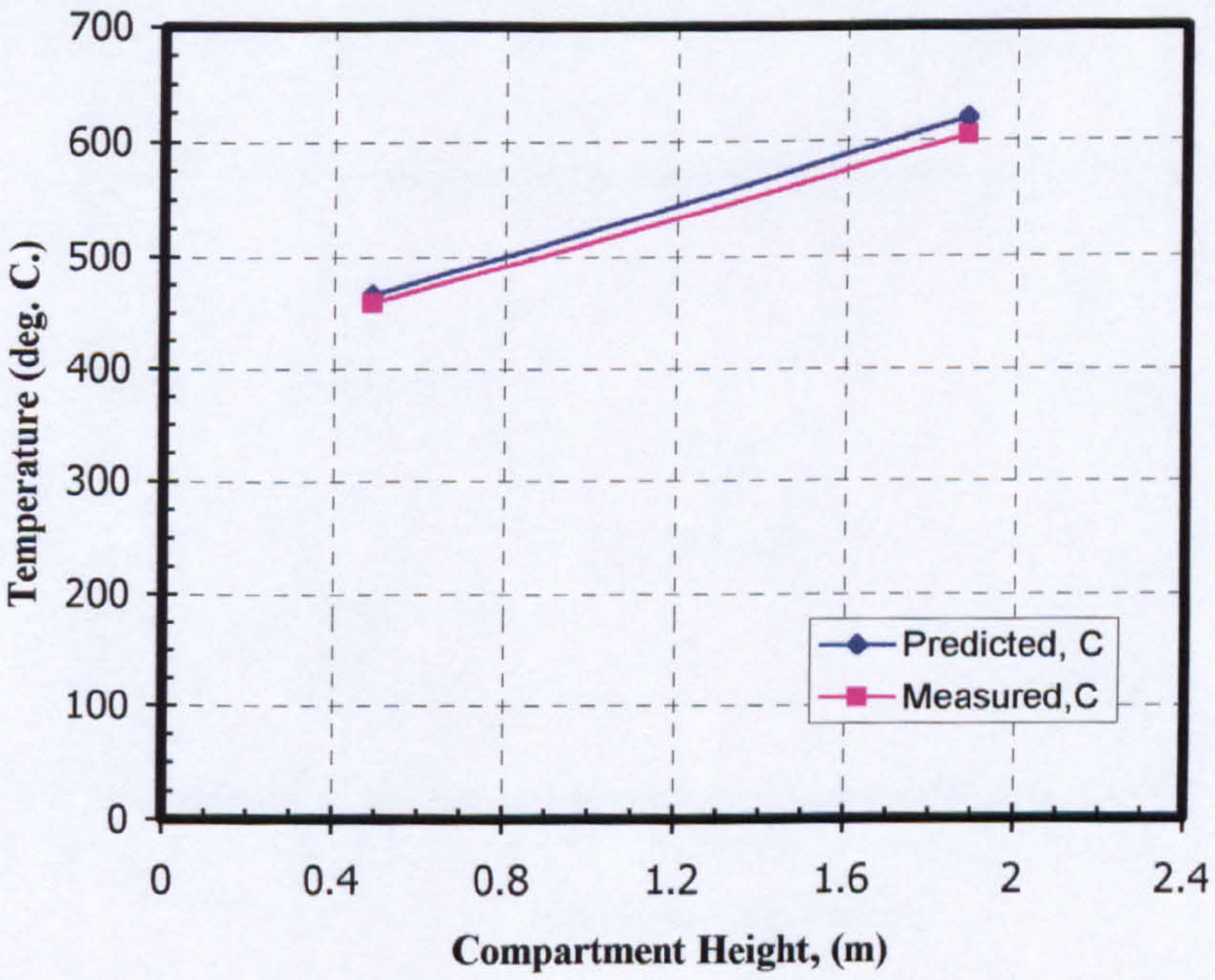

Figure (9.6) Comparison of predicted and measured wall temperatures (steady state) at the SE wall (w-11 and w-13).

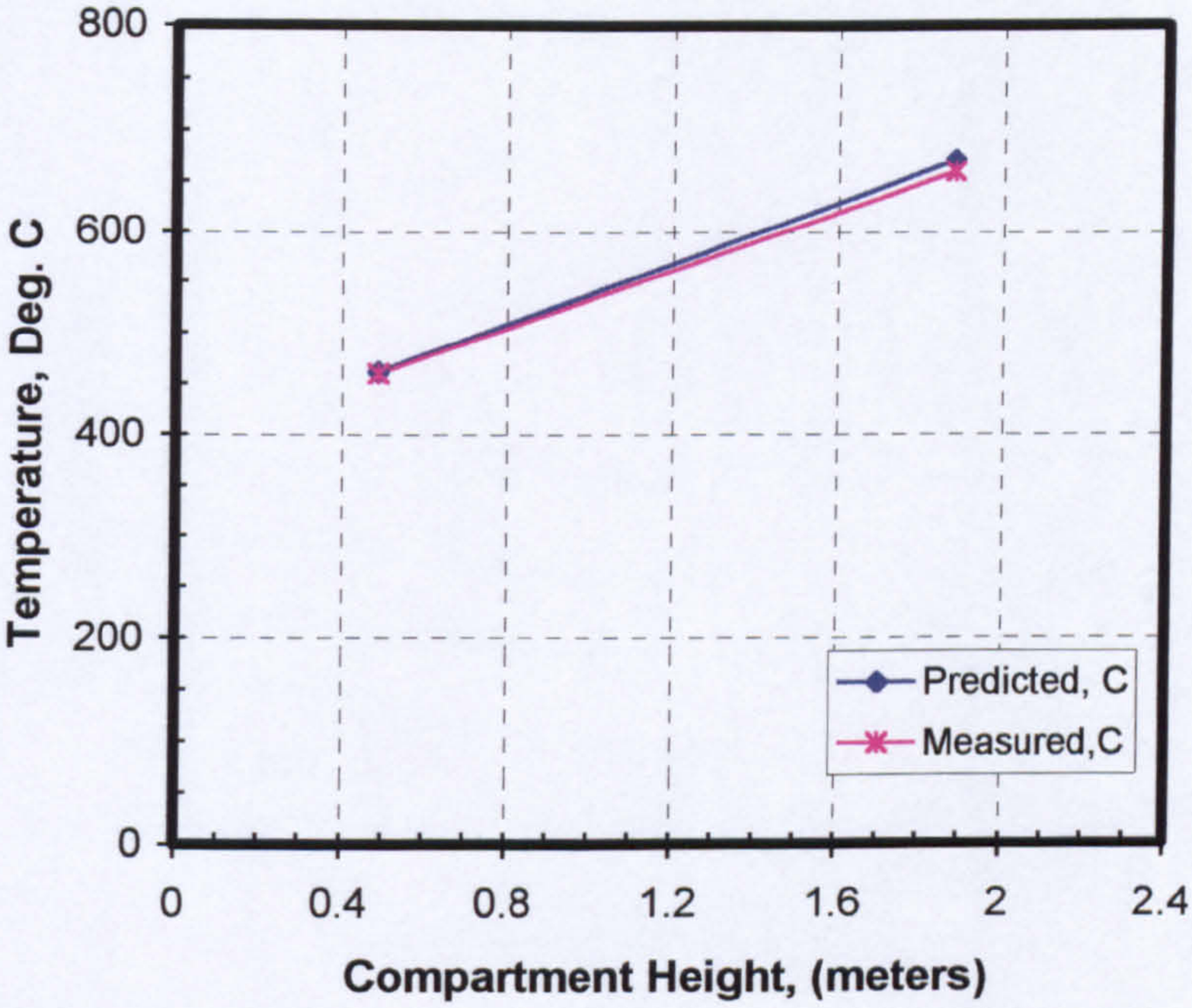

Figure (9.7) Comparison of predicted and measured wall temperatures (steady state) at the Southeast wall (w-12 and w-14).

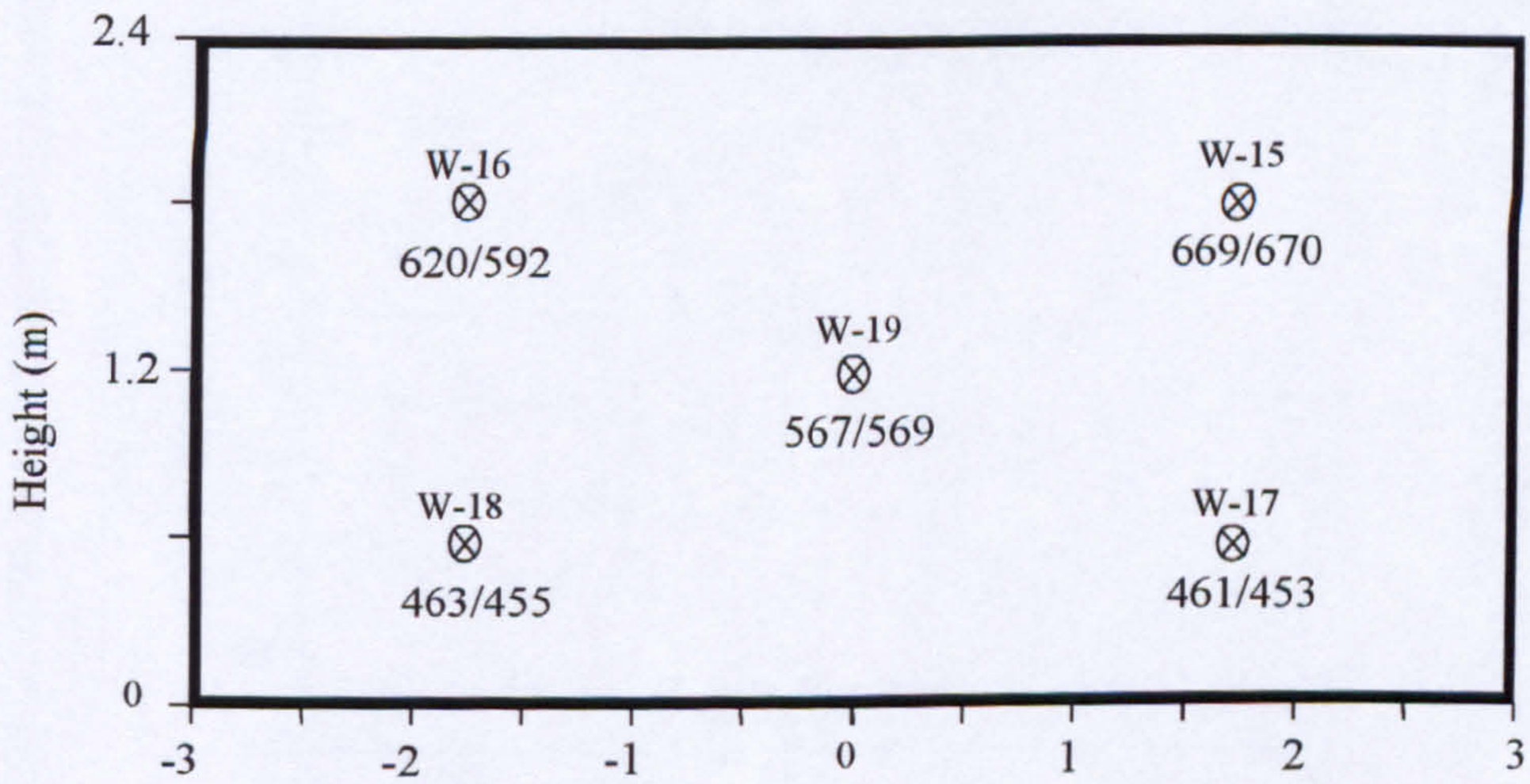

Figure (9.8) Comparison of experimental and predicted Northwest wall temperatures (predicted/measured, °C).

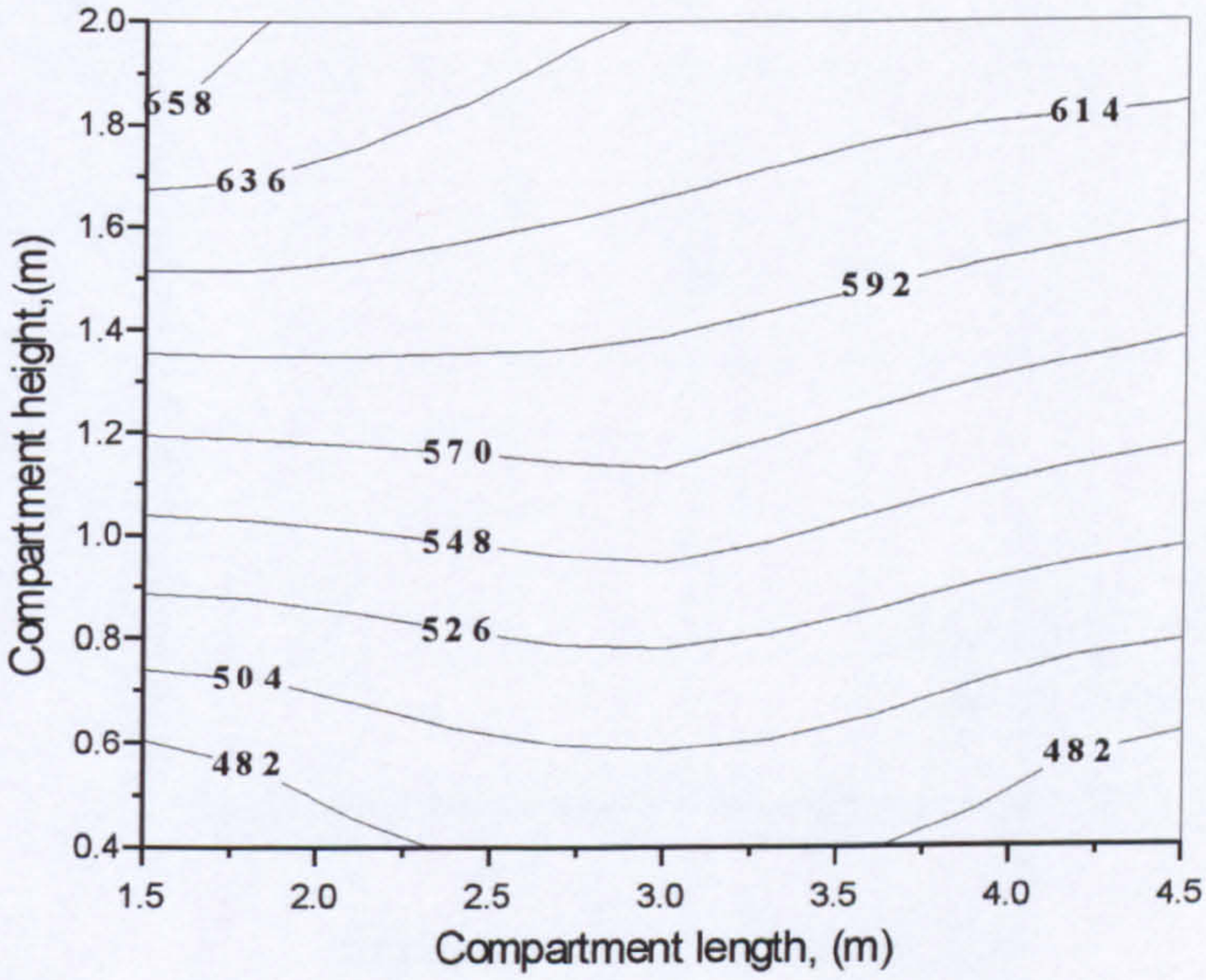

Figure (9.9) Shows measured Southeast wall temperatures contours

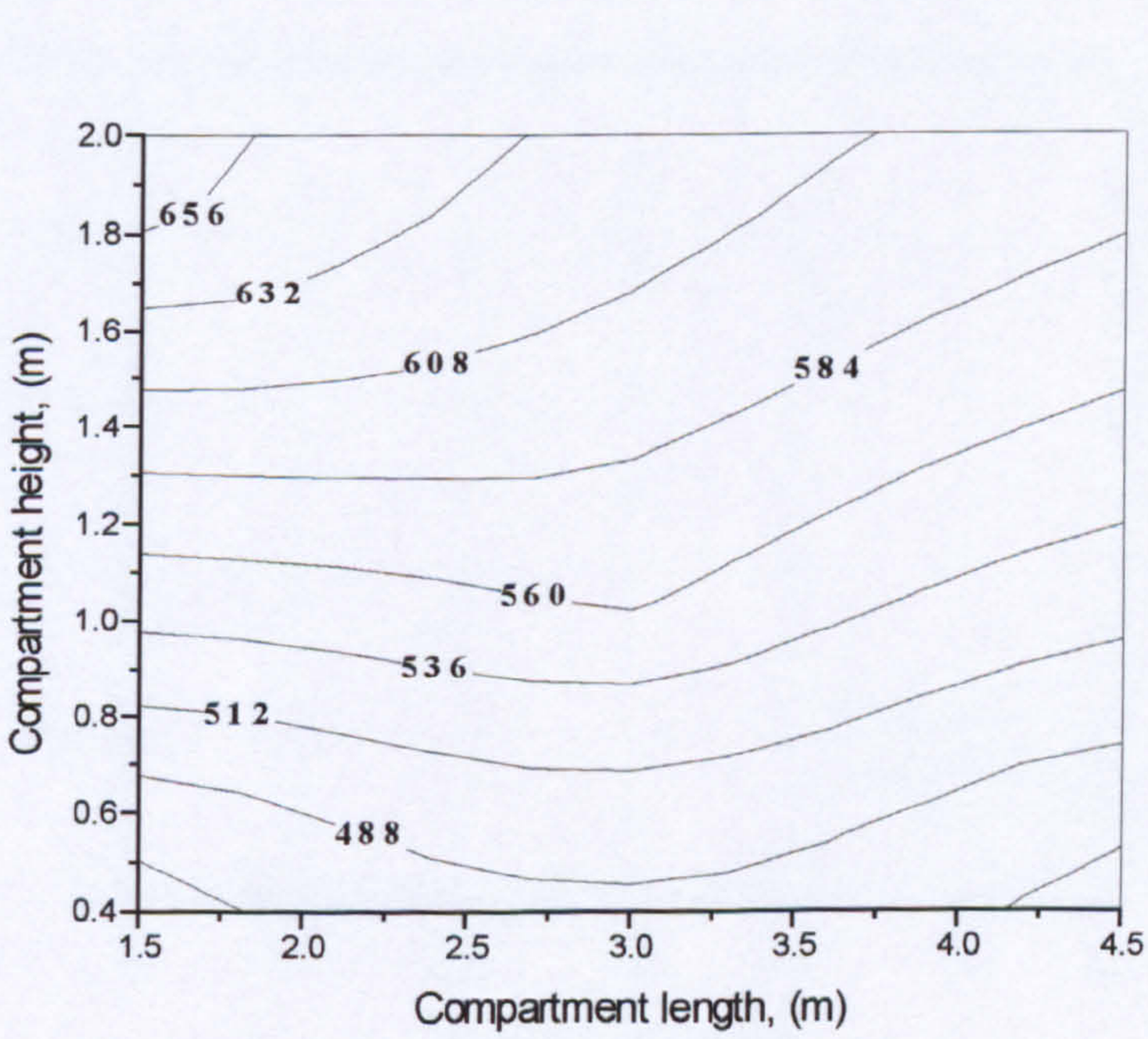

Figure (9.10) Shows predicted wall temperature contours for the same location of the Southeast wall in the experiment.

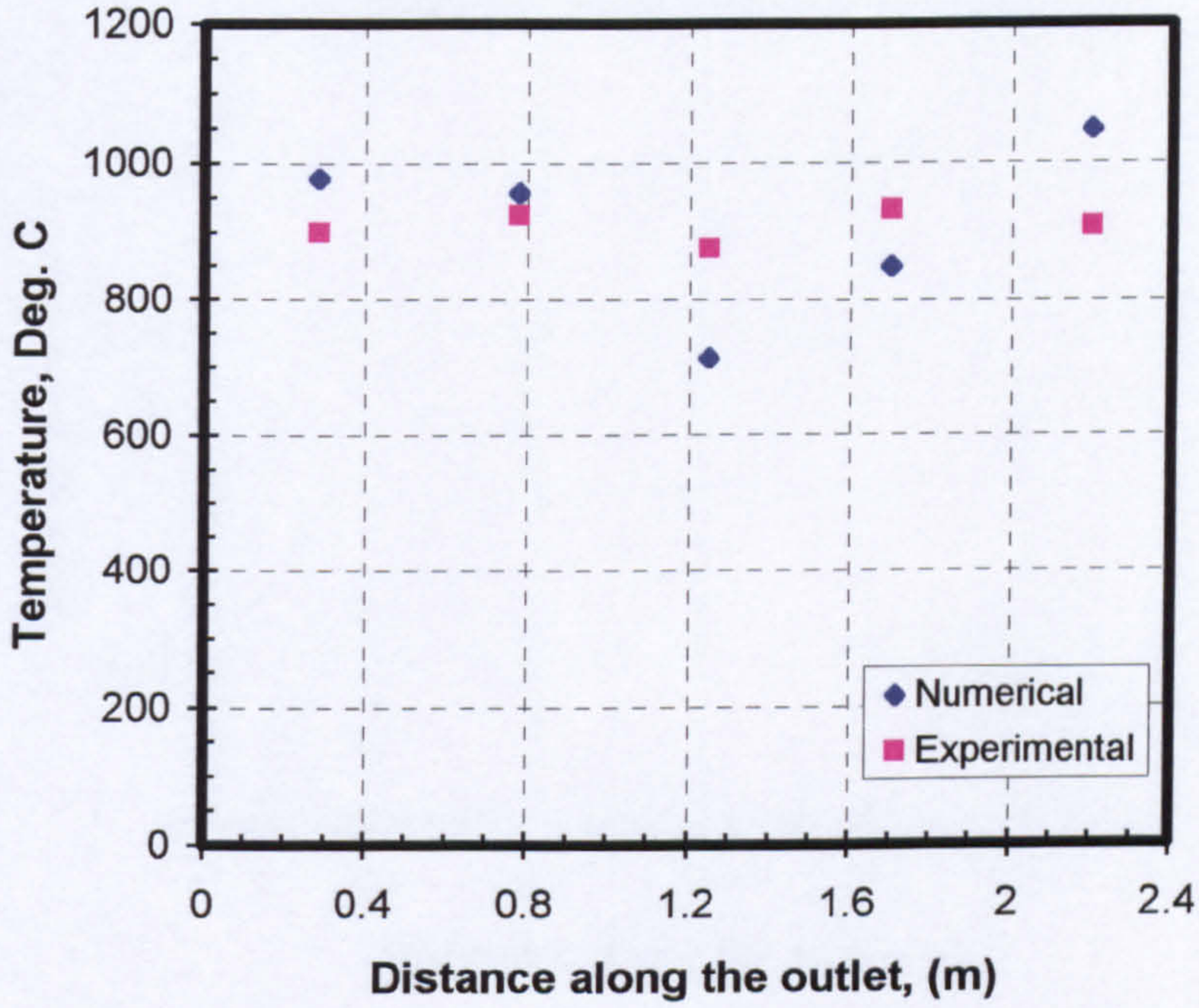

Figure (9.11) Comparison between predicted and measured steady state temperature at ASP1-5 for 54 lit/min, one spray located centrally at 60° spray angle (cmp13).

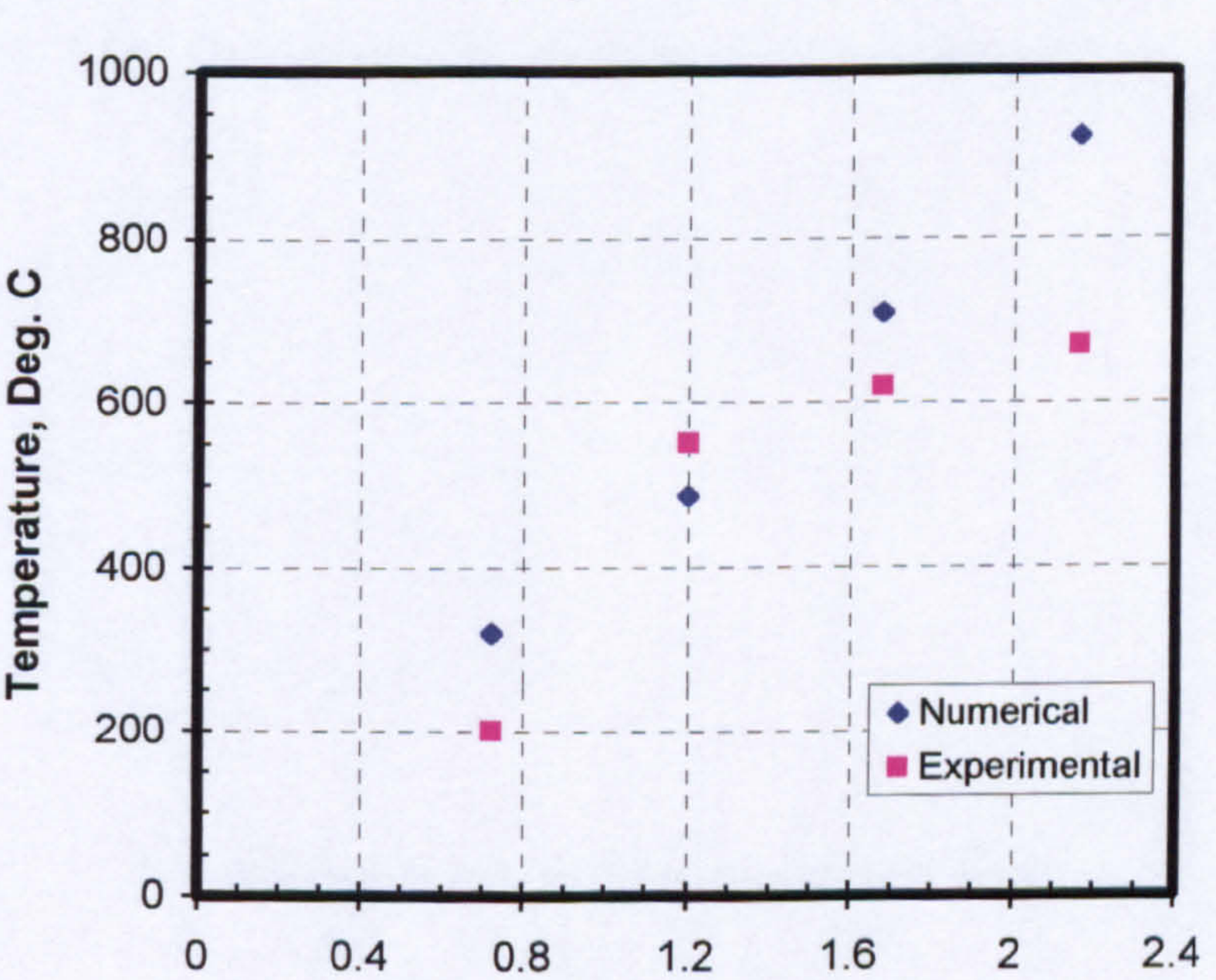

Figure (9.12) Comparison between predicted and measured steady state temperature at ASP26-30 for 54 lit/min, one spray located centrally at 60° spray angle (cmp13).

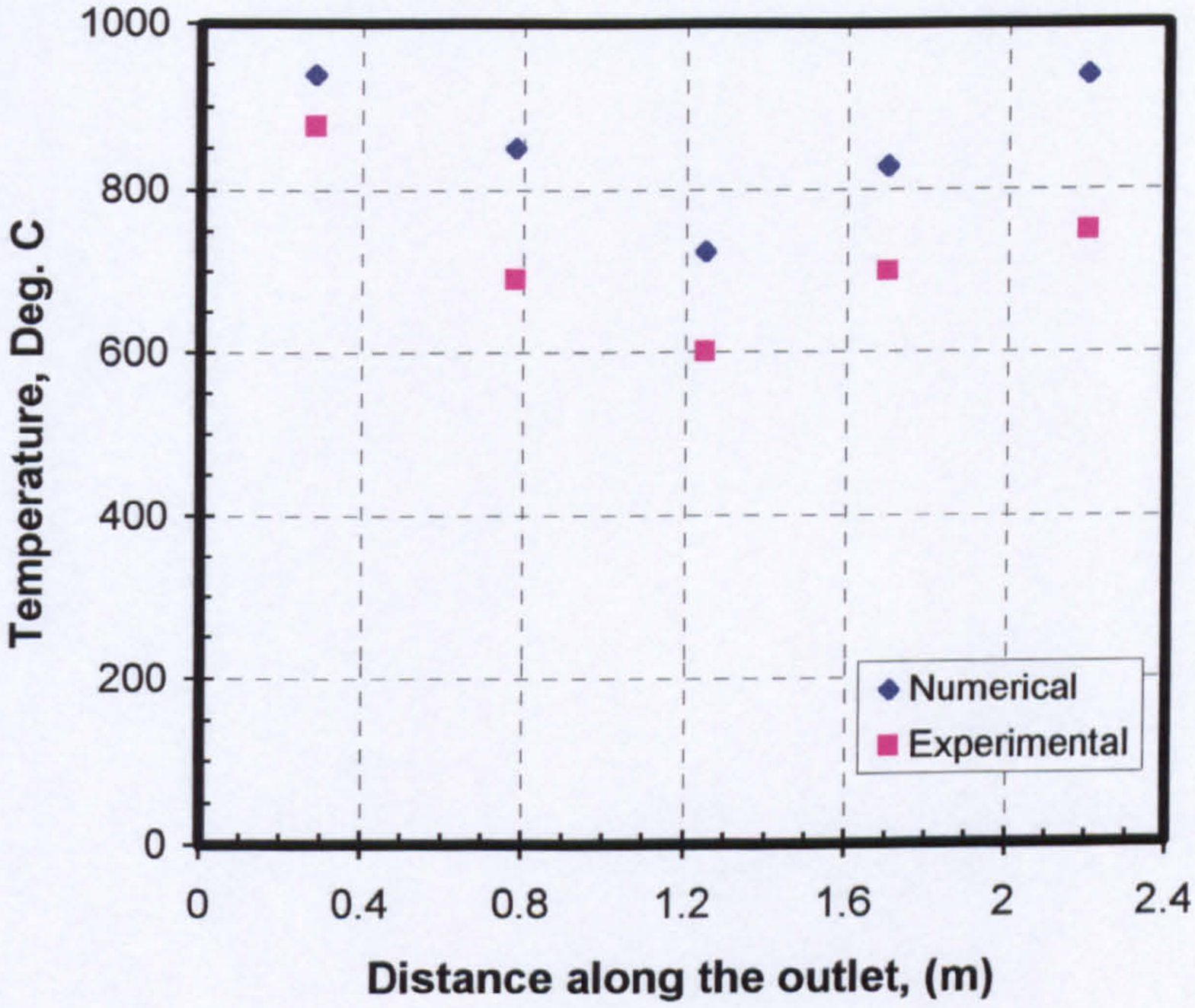

Figure (9.13) Comparison between predicted and measured steady state temperature at ASP1-5 for 54 lit/min, one spray located centrally at 90° spray angle (cmp21).

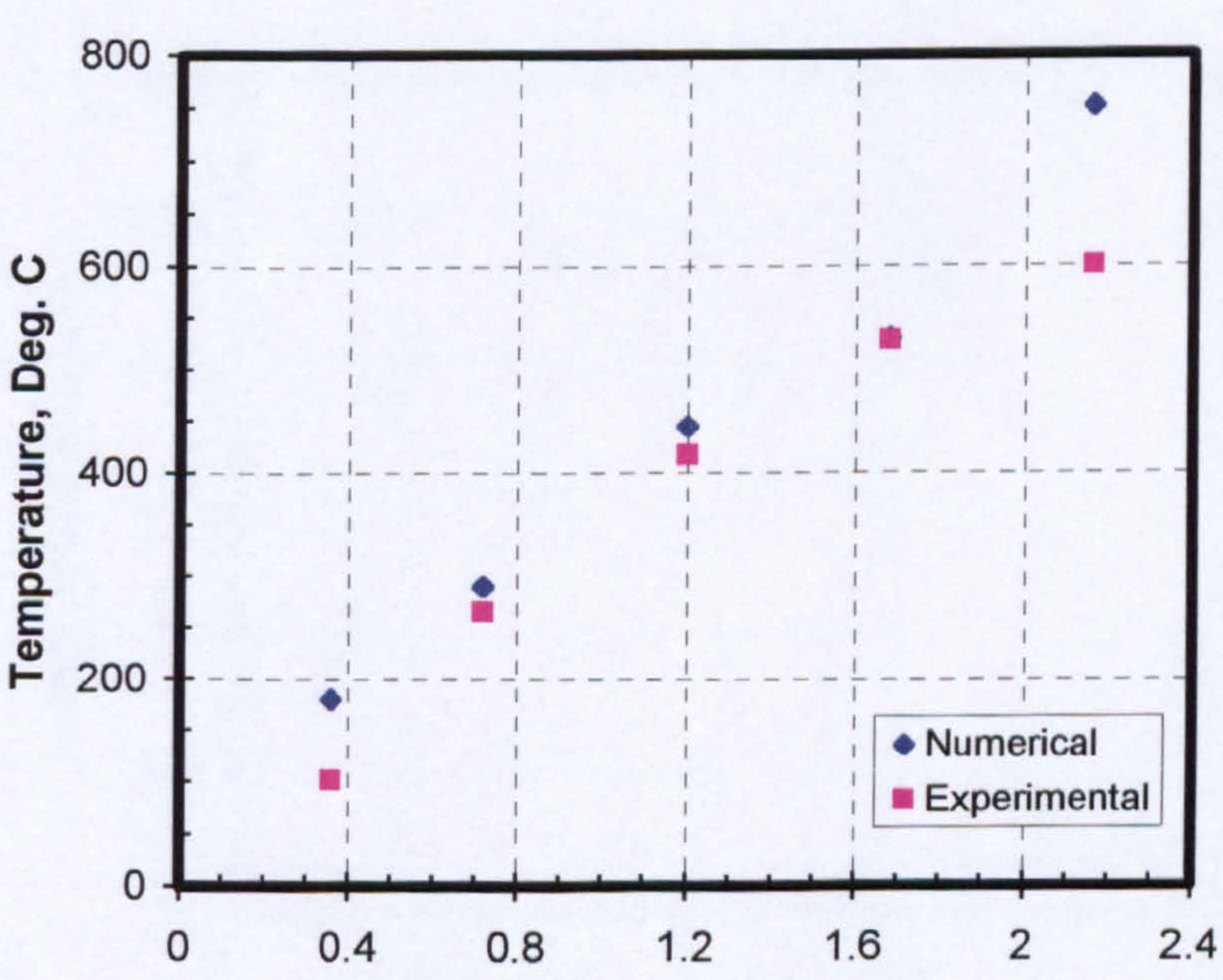

Figure (9.14) Comparison between predicted and measured steady state temperature at ASP26-30 for 54 lit/min, one spray located centrally at 90° spray angle (cmp21).

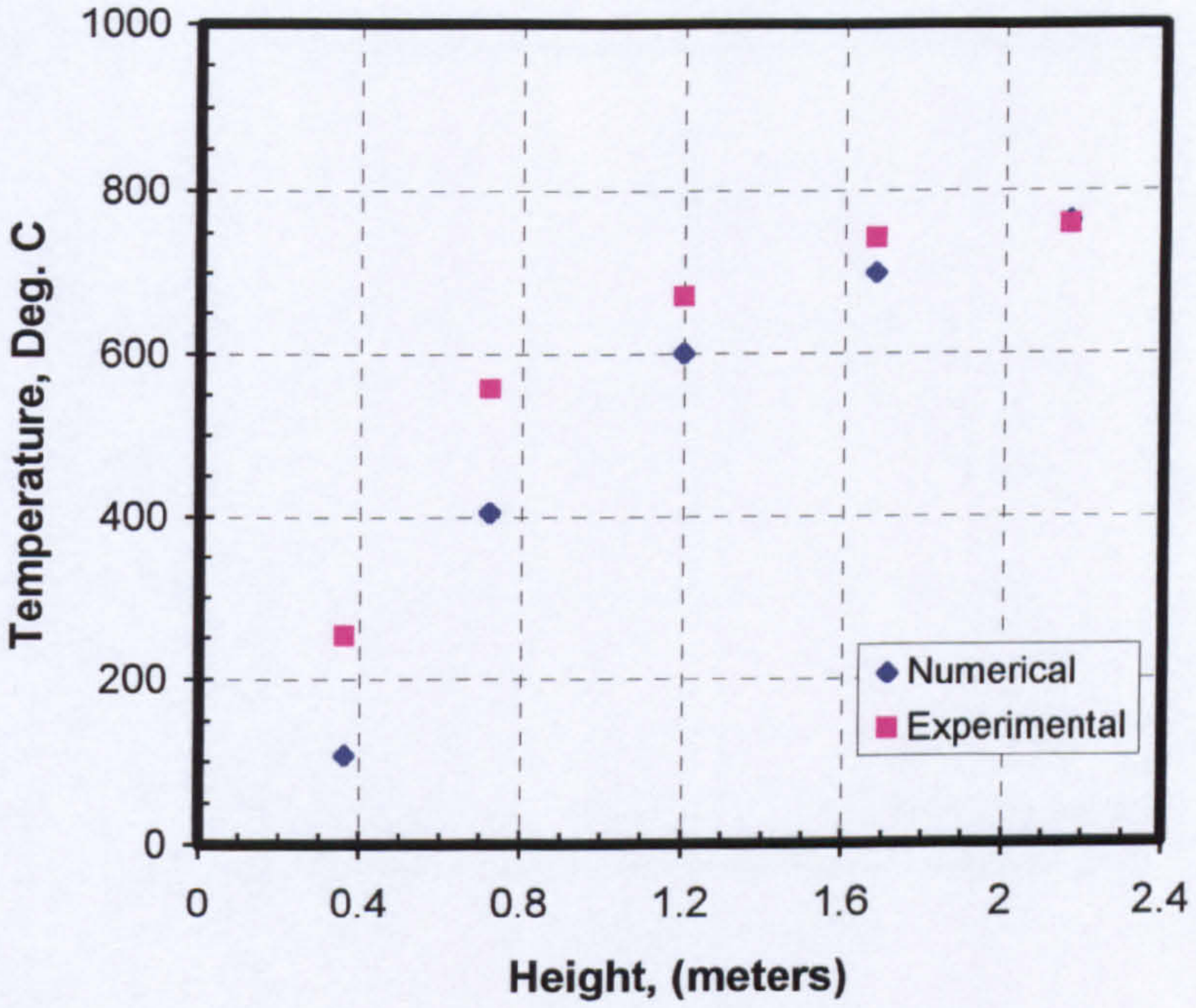

Figure (9.15) Comparison between predicted and measured steady state temperature at ASP26-30 for 54 lit/min, one spray located centrally at 150° spray angle (cmp3).

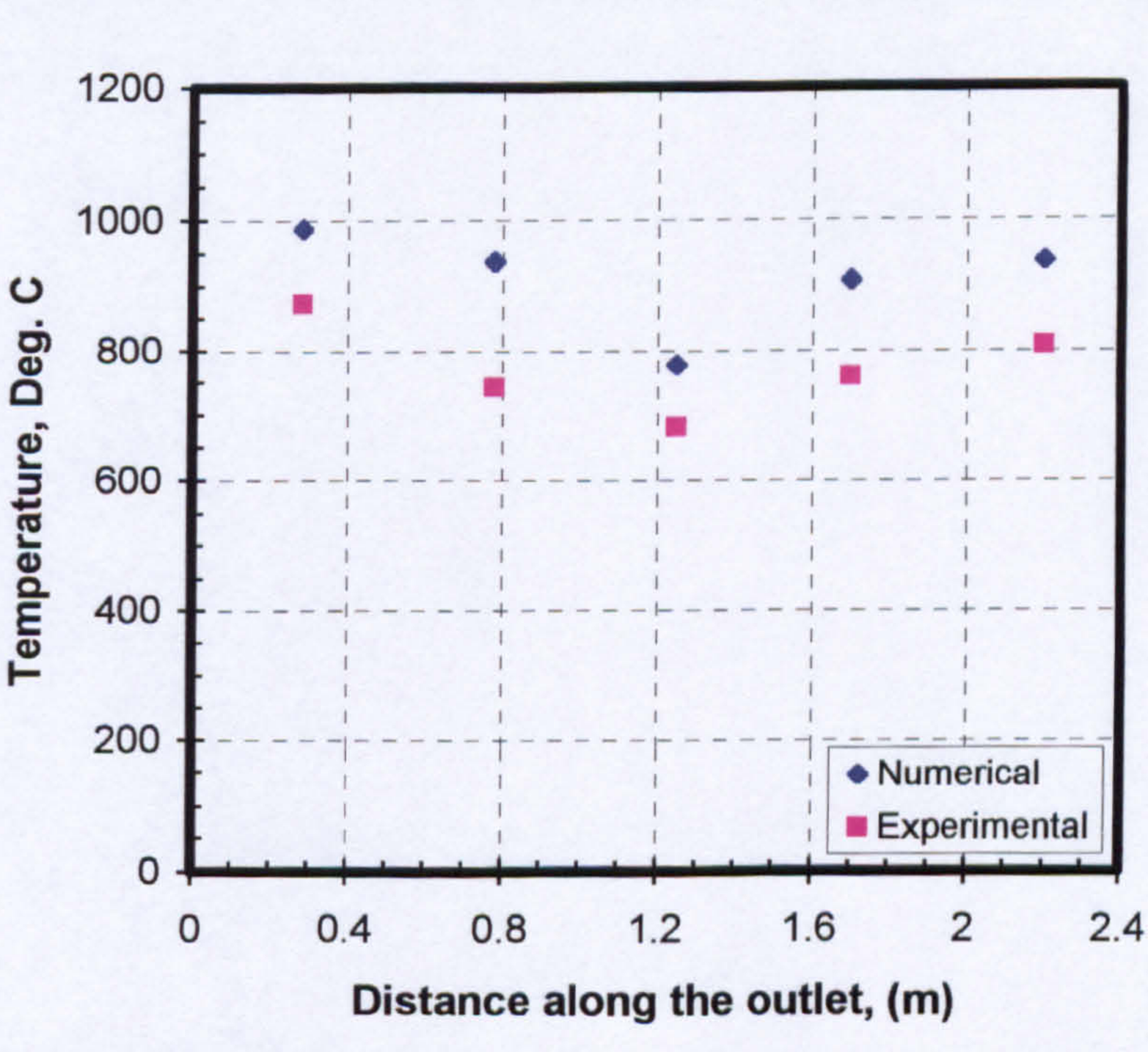

Figure (9.16) Comparison between predicted and measured steady state temperature at ASP1-5 for 54 lit/min, one spray located at the centre of the compartment (cmp28).

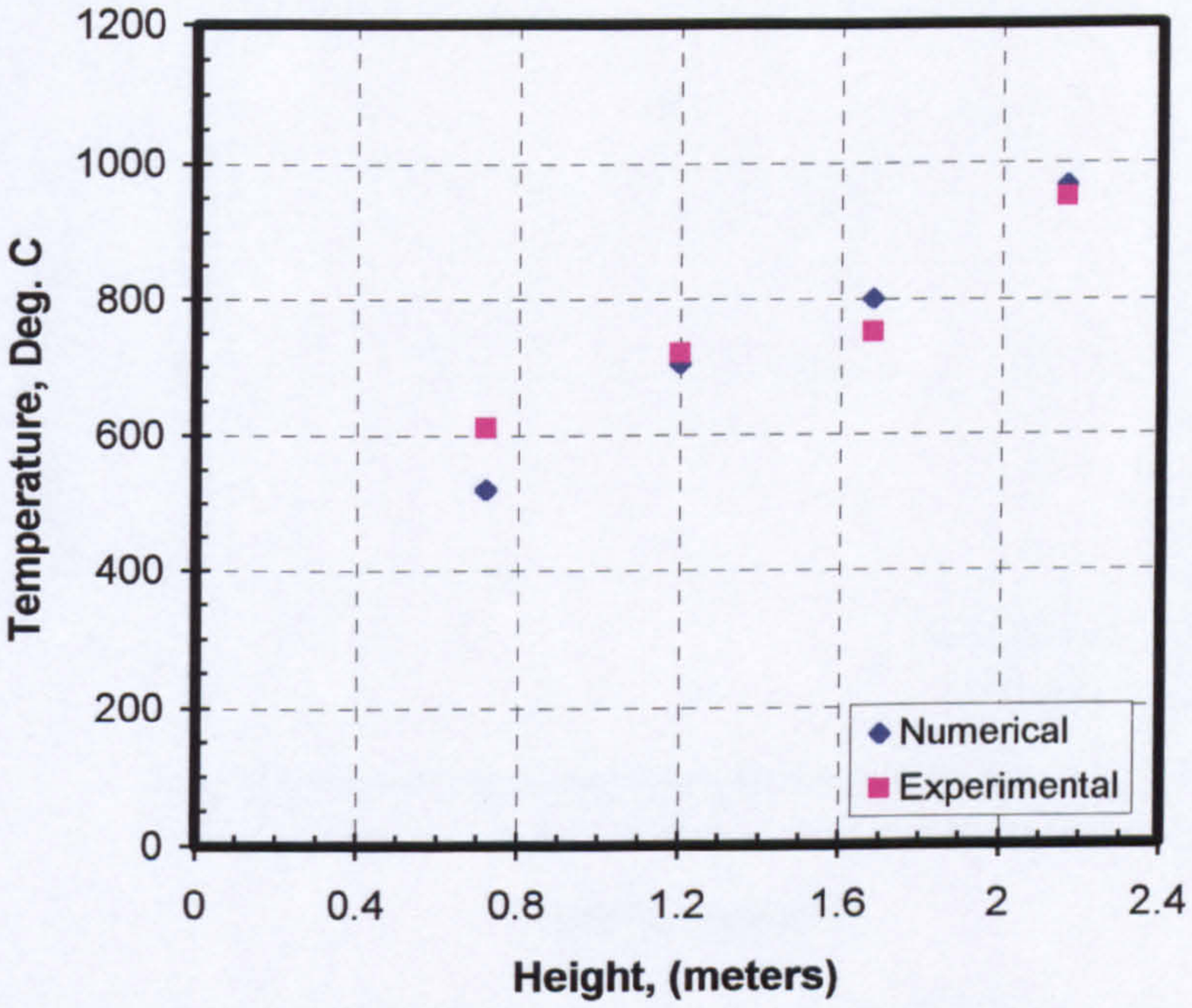

Figure (9.17) Comparison between predicted and measured steady state temperature at ASP26-30 for 54 lit/min, one spray located at the front of the compartment (cmp38).

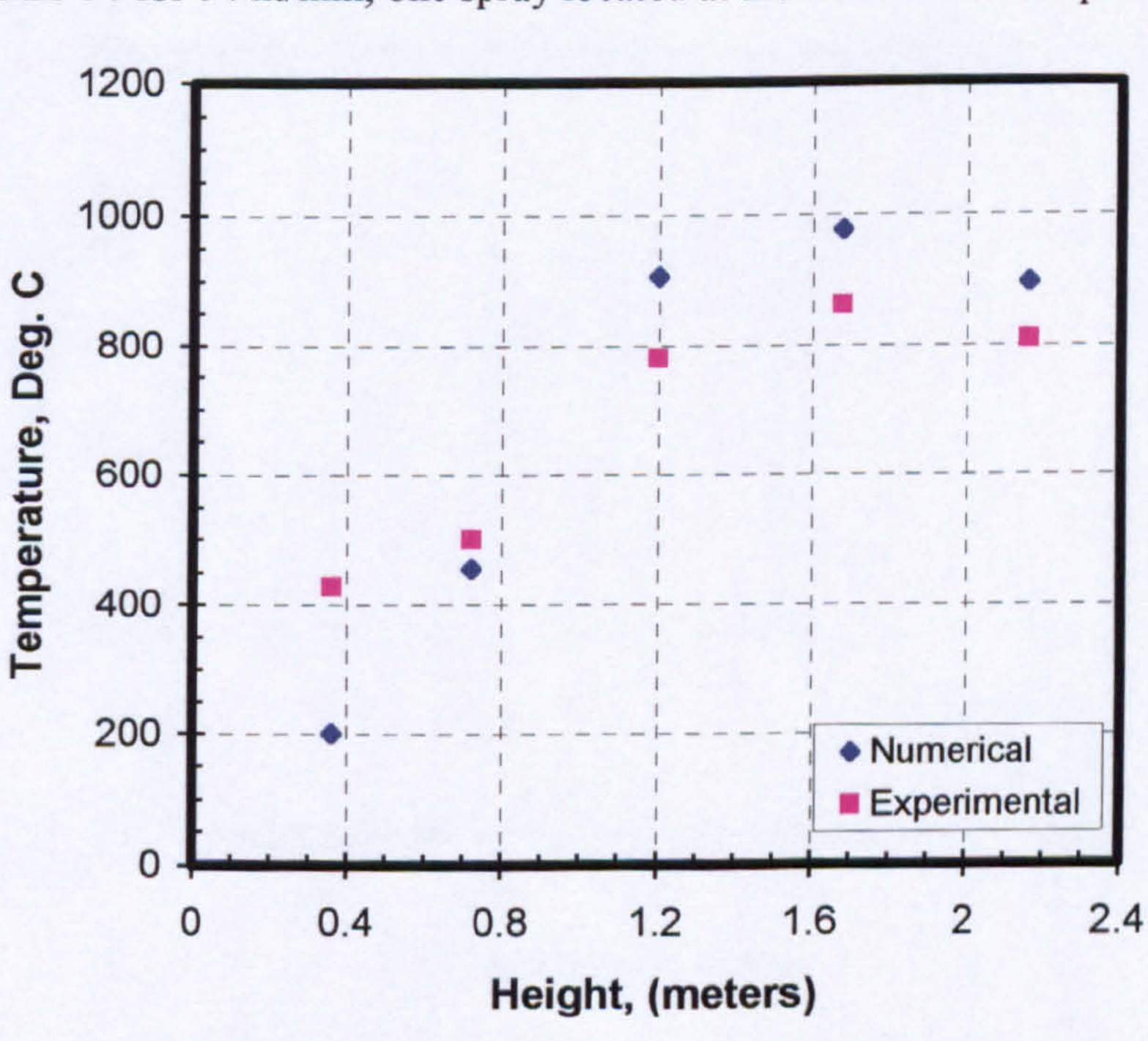

Figure (9.18) Comparison between predicted and measured steady state temperature at ASP31-35 for 54 lit/min, one spray located at the front of the compartment (cmp38).

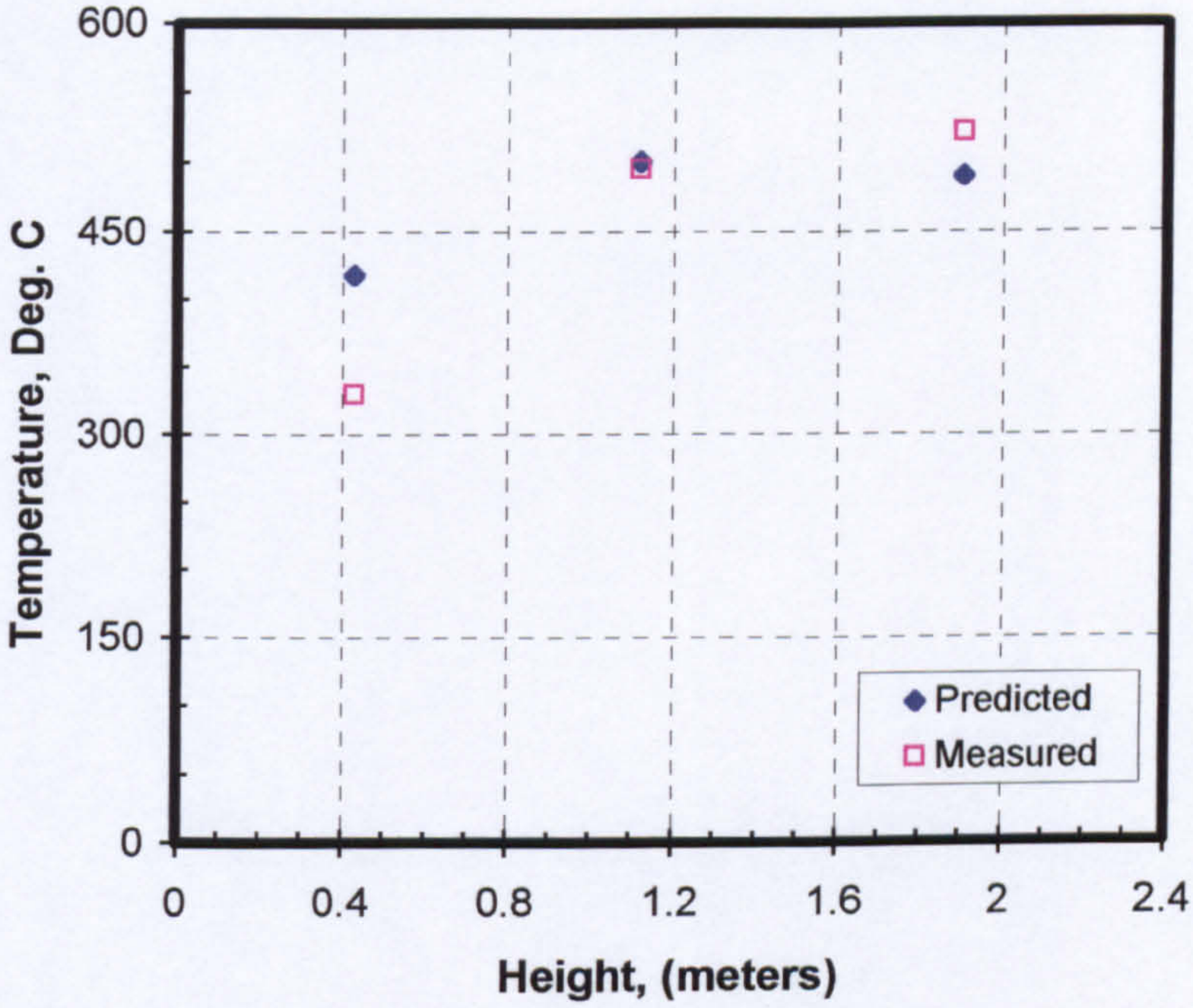

Figure (9.19). Predicted and measured back wall temperature comparison for three sprays used with total water flow rate of 90 lit/min and 150° spray angle, (COMP58).

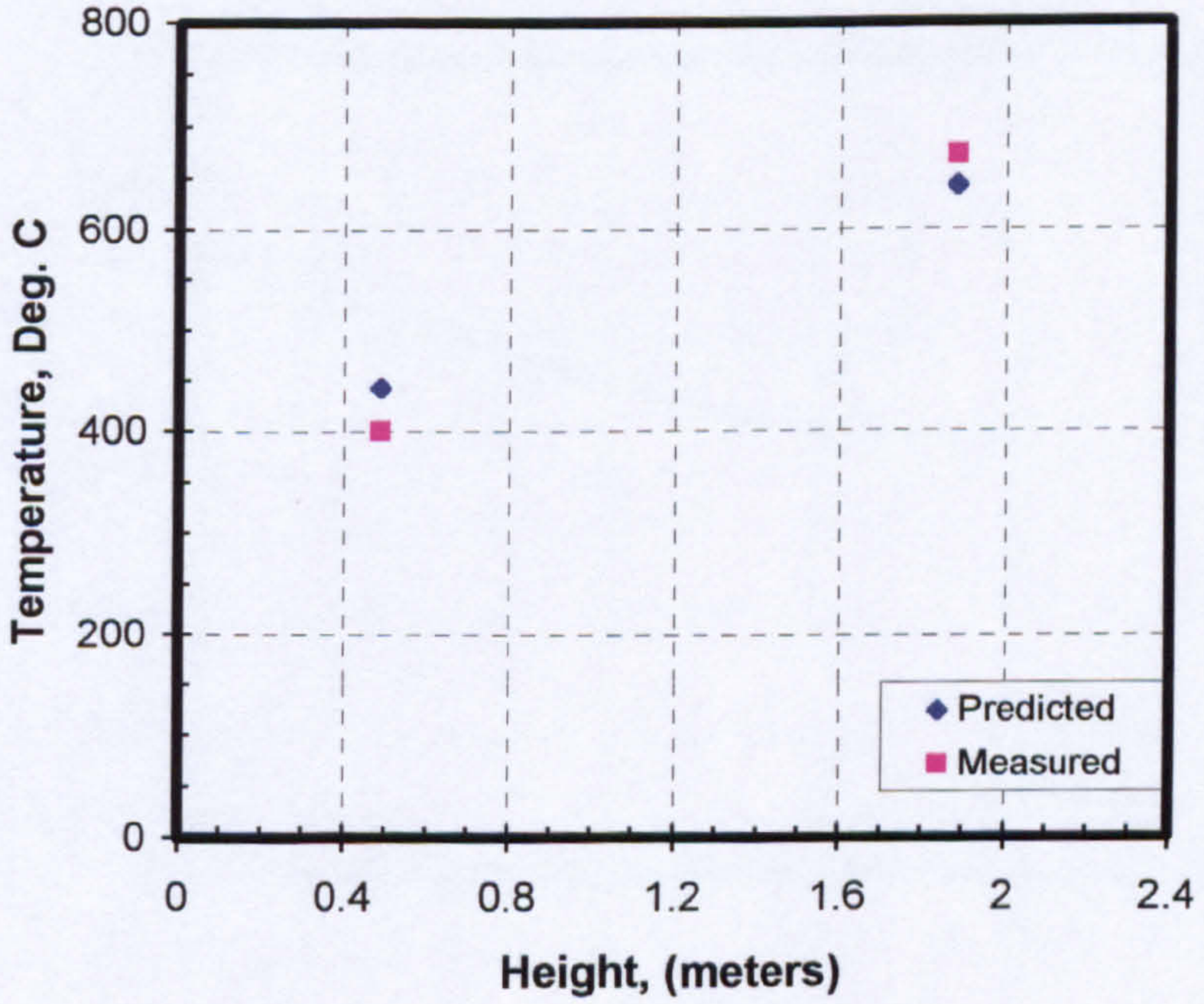

Figure (9.20) Predicted and measured Northwest wall temperature comparison at 1.5 m from the opening for three sprays used with total water flow rate of 90 lit/min and 150° spray angle, (COMP58).

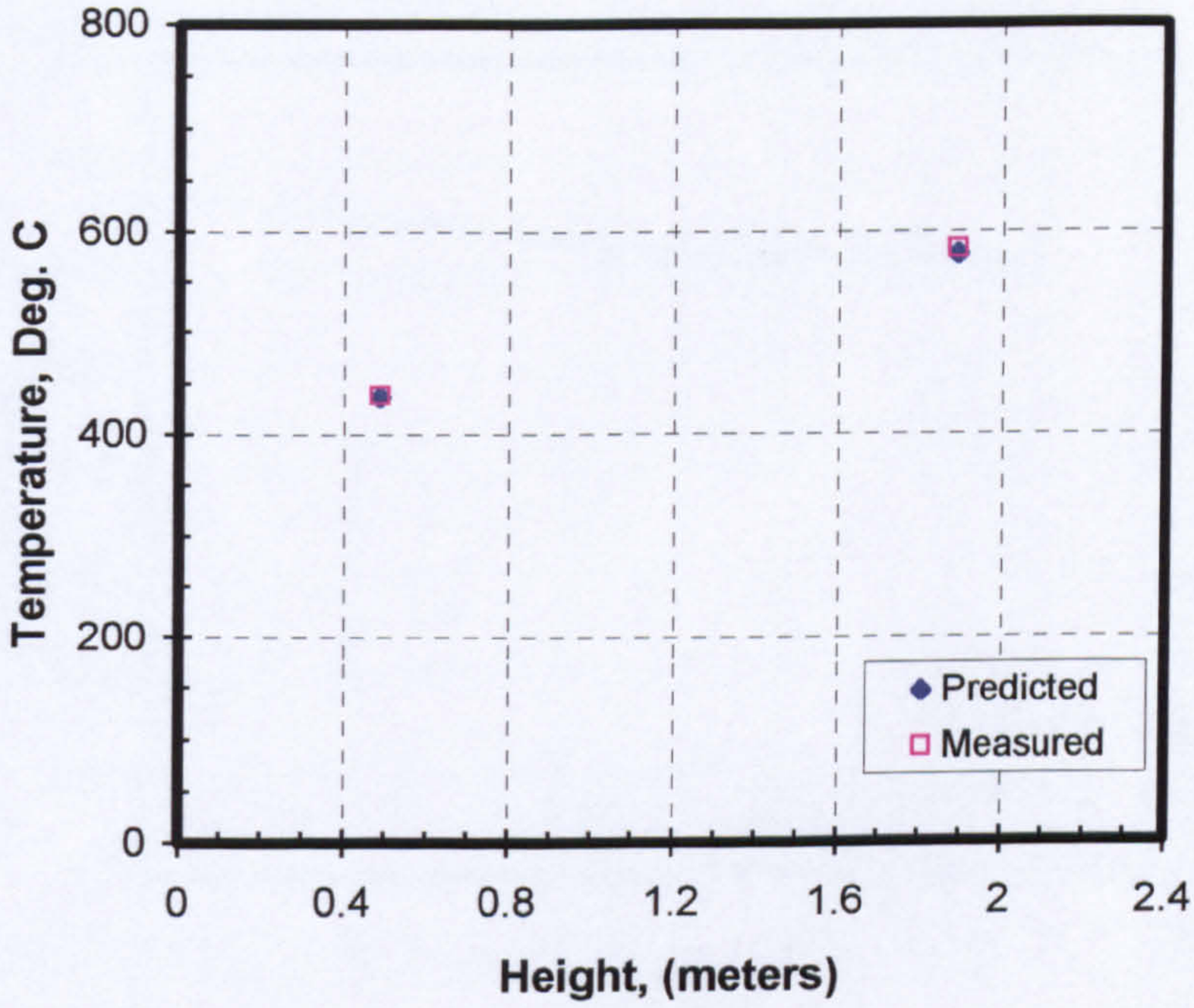

Figure (9.21) Predicted and measured Northwest wall temperature comparison at 4.5 m from the opening for three sprays used with total water flow rate of 90 lit/min and 150° spray angle, (COMP58).

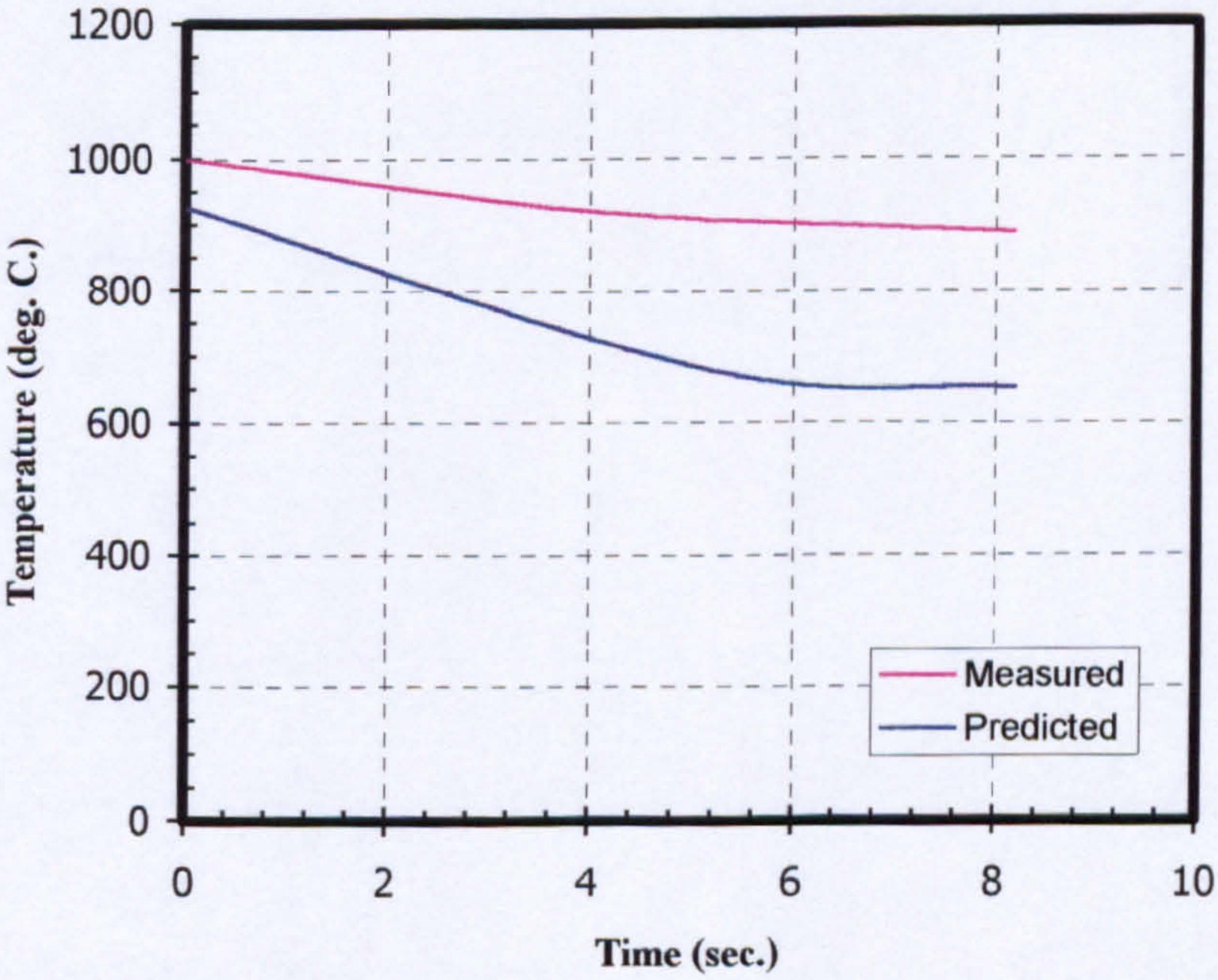

Figure (9.22) Predicted and measured ASP-26 temperature comparison for one spray 150° nozzle used with total water flow rate 72 lit/min (COMP4).

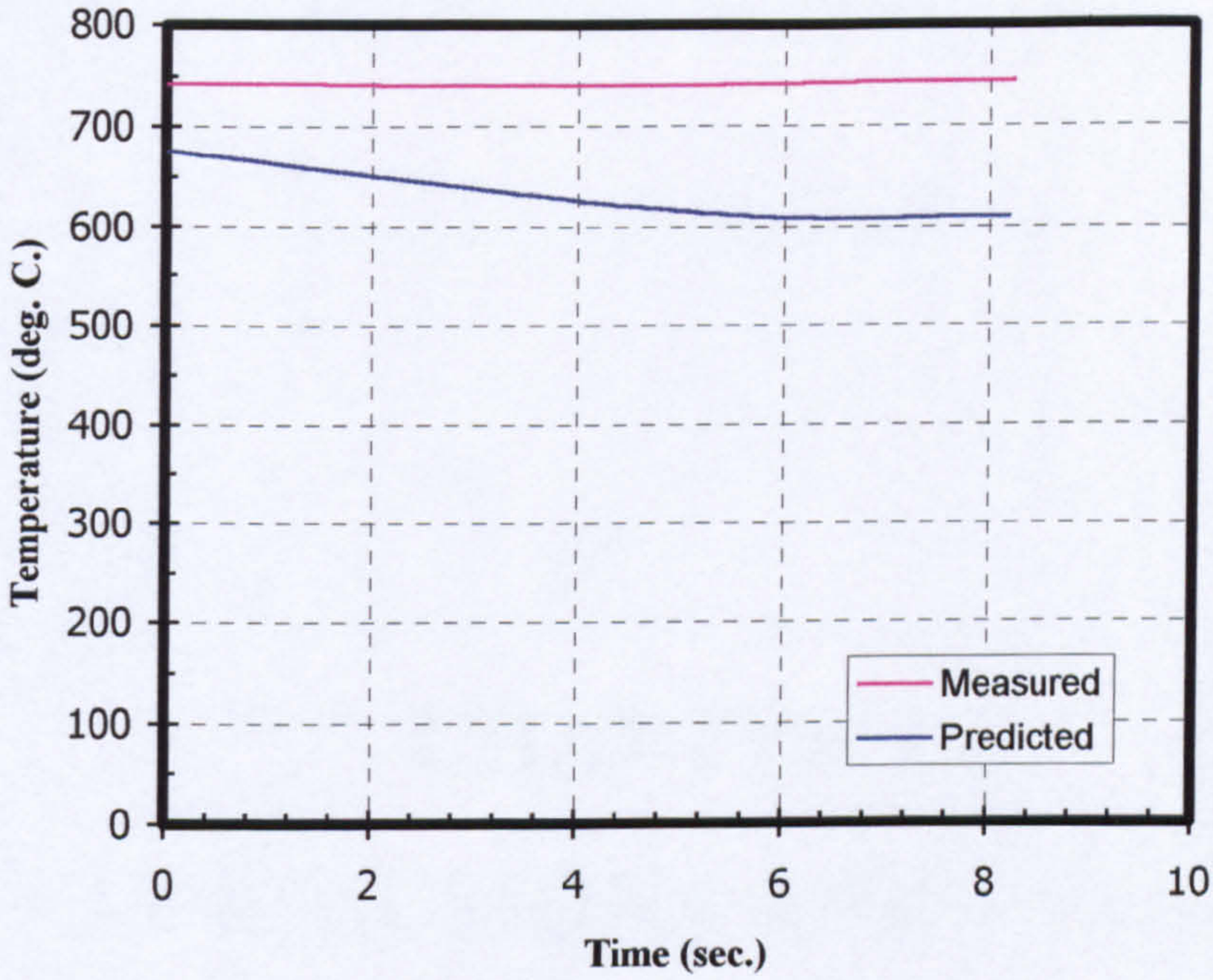

Figure (9.23) Predicted and measured ASP-33 temperature comparison for one spray 150° nozzle used with total water flow rate 72 lit/min (COMP4).

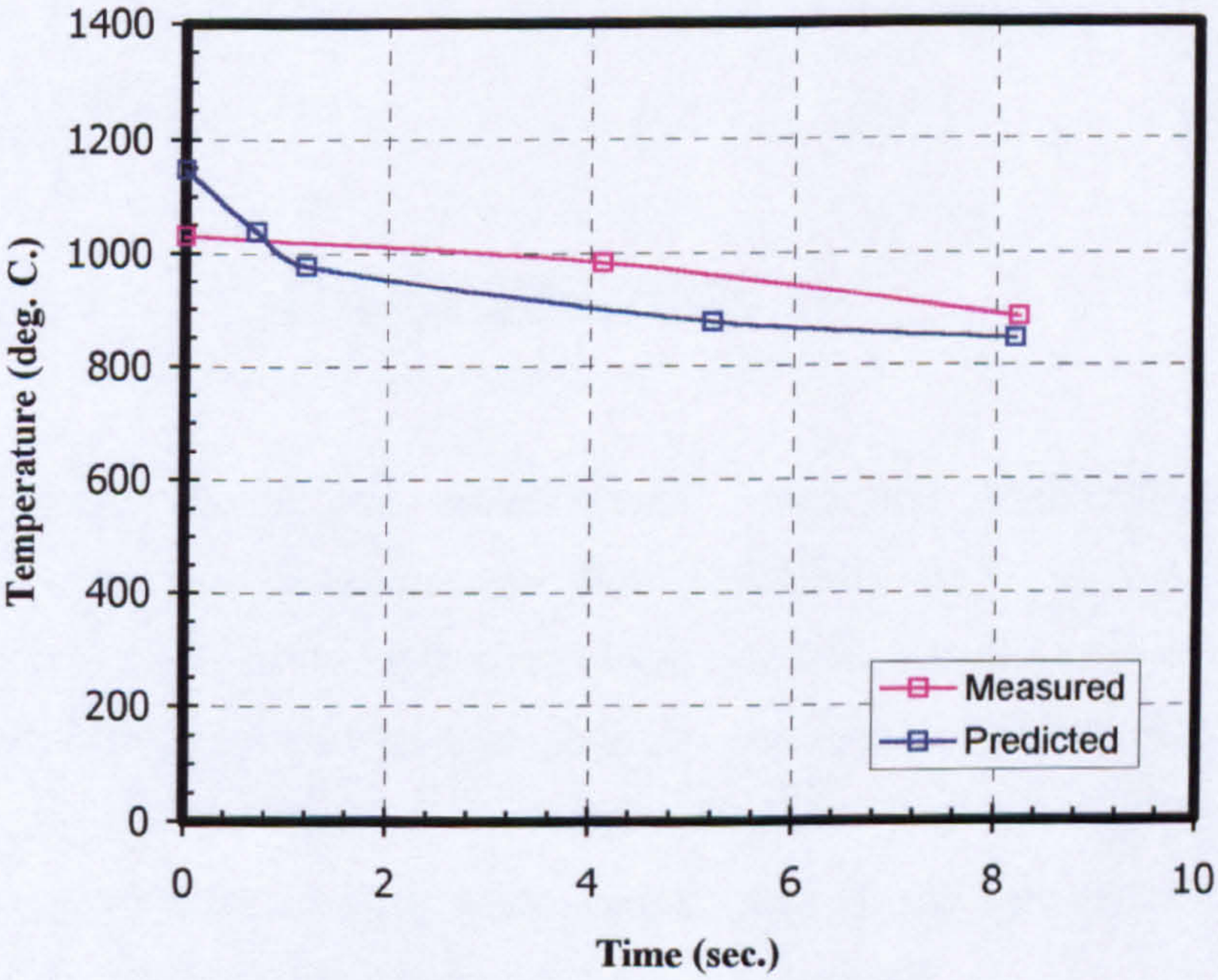

Figure (9.24) Predicted and measured ASP-2 temperature comparison for one spray 150° nozzle used with total water flow rate 72 lit/min (COMP4).

CHAPTER 10

CONCLUSIONS AND FUTURE WORK

10. 1 CONCLUSIONS

An experimental and computational work was conducted to study the behaviour and the temperature distribution of a jet fire in a compartment, to produce CFD model with combustion and heat transfer, and to determine the relationship between the extinguishing effectiveness of water spray and droplet size and distribution, and the location of the spray nozzle regarding the jet fire nozzle position. A large-scale compartment jet fire suppression rig was used and modified to simulate the offshore compartment.

10.1.1 JET FIRE WITHOUT WATER SPRAYS

Case studies representing compartment jet fire were examined. They showed that the flow of the high momentum jet can induce a very powerful recirculation flow in the compartment. The temperature distribution predictions of the gases and of the compartment surfaces made were in good agreement with experimental measurements. Correct trends in gas temperature changes were obtained.

The discrete transfer radiation model (DTRM) and heat transfer at the compartment surfaces was used in the modelling. Implementation of these models improved the accuracy of the prediction, in comparison with the adiabatic condition. The radiation model (DTRM) was computed for 6 and 8 rays, fired from the solid surface of each boundary cell. The results showed that the radiation calculation was the same in both cases. Therefore, six was used for both θ and ϕ, which reflects a compromise between computational economy, uniformity and accuracy of coverage. Applying a radiation correction factor at the compartment opening was recognised to be very critical to the accuracy of the radiation calculation and prediction of the temperature in the compartment, which takes into account the influence of the temperature of the gas beyond the inlet and outlet boundaries, and corrects these temperatures.

The heat transfer at the walls was applied by using the combined external convective and external radiation boundary conditions. A simplified approach was used to estimate the heat transfer coefficient.

The DTRM radiation model and heat transfer at the compartment surfaces showed that nearly a 20% temperature reduction resulted when compared with

the adiabatic conditions, and this was a closer match to what was actually observed.

The model developed showed that the FLUENT prediction procedure is capable of producing the main features of the three-dimensional flow field, and of predicting the steady state temperature distribution in the compartment with good accuracy.

10.1.2 JET FIRE WITH WATER SPRAY

The water spray was activated experimentally when the 5 minutes pre-burn time was reached. In the simulation when the fire reached steady state, the water spray was activated, and computation was continued iteratively until the two-phase converged to another steady state.

In order to supply data for spray characterisation in the numerical modelling, droplet size measurements with four different types of spray nozzle were made. The results from droplets measurements showed that in each case increasing the water flow rate decreased the water spray droplets diameter at constant spray angle. In the other hand, it was found that high dependence on droplet size with spray angle occurred and the higher the spray angle, the smaller the droplet size produced at constant water flow rate.

A simple approach for modelling the water spray in the CFD was used. As only limited number of droplets can be tracked computationally, the spray droplet distribution needs to be discretised. The spray is represented by five groups of droplets. Different water droplet sizes and similar water flow rate

was assigned for each group in order to get a uniform distribution. Each spray in the model was simulated using twenty-five injections. The model was completed by assigning the spray angle, droplet discharge velocity and spray location. The water particles were introduced into the gas phase flow computation every 5 iterations to balance conservation equations (mass, momentum and energy). Large numbers of iterations were allowed until both water spray and continuous phase flow reached a steady state simultaneously.

The drop in temperatures after water spray activation is characteristic of all thermocouples location inside the compartment, and is reflected in reduced temperature at the outlet opening as well. However, the absorption of heat from a fire by a water spray is definitely a function of a water discharge rate and mean droplets size.

The minimum water flow rate resulting in extinguishment of a jet fire in a compartment is strongly dependent on several variables such as spray angle and mean droplet diameter. A 150° spray angle was found to be the most effective in achieving temperature reductions because it produced the smaller droplet sizes. However, the minimum amount of water required for effective extinguishment of a 4.5 MW propane jet fire was determined for the different extinguishing arrangements. To extinguishing the jet fire from a single spray nozzle, the minimum water flow rate was about 72 lit/min for the nozzle type K50 150D, with a 150° spray angle, located centrally directly above the jet fire nozzle. The extinguishment time was found to be 12 seconds for the 35 m^3 compartment. For three spray nozzles the minimum amount of water flow rate was found to be 108 lit/min. In the case of the two spray nozzles setup the

total water flow rate needed was in the range of 90 lit/min, for the spray located centrally and in the front of the compartment. This result shows that it may be possible to extinguish a jet fire with water spray without a direct hit but with higher water flow rate. However, for controlling the jet fire, the minimum amount of water flow rate was found for each spray angle used (60, 90,120 and 150°) and for each spray nozzle arrangement. It showed that the minimum amount of water required for controlling jet fire was 36 lit/min found at 150° spray angle when one spray nozzle was used. The maximum water flow rate required to control the jet fire before extinguishment could occur was found to increase with the decrease of the spray angle. It reached 90 lit/min at 60° spray angle. For the different spray number and location at 150° spray angle, the minimum amount of water required for controlling jet fire was found to be 72 lit/min when two spray nozzles were used and located at the front and centre of the compartment. A higher water flow rate of 90 lit/min was required for controlling the other two spray nozzles arrangements.

The limited number of nozzles and test conditions does not allow a too general conclusion to be drawn. It was found that the minimum extinguishing water flow rate per spray depends on the location of flame with respect to the spray heads and number of spray nozzles activated, e.g. minimum water flow rate from one spray nozzle located above the flame was 72 lit/min; from two spray nozzles located above the flame and in the front of the compartment it was 45 lit/min and from three spray nozzles with one of them located above the flame 36 lit/min. To make a comparison with existing standards it is necessary to simplify the above observations, because these minimum water flow rates to extinguish the jet fire were based on specific fire-spray arrangements. If the

simplification is made by accounting for the different fire locations with regards to the spray heads the resulting scenario will be as follows. When the arrangements change these minima may not be enough to extinguish the fire. Therefore, in order to extinguish the jet fire which could issue from any position in the compartment, all the three spray nozzles in the compartment should be activated at a flow rate per spray head typical of the minimum rate found for one spray above the flame, i.e. 72 lit/min; this gives a total flow rate of 15 lit/min/m^2. This result can be compared with one of the most used guidelines for design of an extinguishment or fire control system which showed agreement with NFPA-15 (NFC code, 1994) and NFPA-750 (NFC Code, 1997). The result, which is 15 lit/min/m^2, falls within normal NFPA range which applied to most flammable gases as ranging from 8.1 to 20.4 lit/min/m^2.

When a spray systems design is to be made, consideration should be taken of the areas around the vent or any opening, because near the vent there will be an external flame. So more care should be given to that area. In addition, using a spray nozzle at a location near the opening will help extinguishment because the water droplets will be carried with the air entrained and the spray will create a water curtain which will obstruct the air entrainment and will limit the combustion gases from leaving the compartment.

From the tests it is observed that the extinguishing effectiveness of the water spray decreased with increasing droplet diameter. In the tests, the optimum Sauter mean diameter found was 190 μm (SMD), with at least 15 m/s water velocity at the exit. Therefore, nozzles that produce the highest velocity and the largest number of small droplets will be the most successful.

The spray angle effect when used with a jet fire is not still understood, because in this study different spray angles used produced different droplets sizes when the water flow rate and the other conditions were constant; the larger the spray angle, the smaller the droplets sizes produced were. Therefore, to find out the parameters of the extinguishing effectiveness when the water flow rate, spray number and location conditions were fixed, it was not clear that the reduction of the temperature was due to either the spray angle or the different droplet sizes produced with this type of spray angle. Nevertheless, a larger spray angle of 150° gave the maximum overall temperature reduction and is recommended to be used since it gave a larger coverage area and smaller drops sizes at any flow rate used.

The present study shows that the current version of the CFD code (FLUENT) is able to provide a satisfactory and practical means of modelling jet fire and extinguishment processes and is a very competent tool for predicting flow patterns within a confined volume. It is clear that present CFD codes with combustion are now able to provide us with details of the factors which control the steady state behaviour of confined fires and allow a mechanistic approach to the study of the dynamics of extinguishment.

Correlation between the predicted and observed wall temperature data could be improved further by accounting for the non-uniformity of steel temperature, heat transfer from the enclosure to the surroundings and by using a better estimate of the coefficient of heat transfer.

The water discharge rate and the median drop size of the water spray were recognised as important parameters in the cooling of compartment fires by

water spray. The stable temperature stratification within the compartment was disturbed by the injected water spray, and as a result, the mixing process and churning up of the layers appeared to cause an increase in the temperatures in the lower level of the compartment. Time dependent calculations provide a valuable insight into the changes taking place during the extinguishment process and indicate that time scales are consistent with observed values in field experiments.

The results have demonstrated the capabilities of the present prediction technique in modelling the mitigation of a compartment jet fire. It is encouraging to see that the numerical results indicated the correct trends. The computational and experimental study of the mitigation of the compartment jet fire and extinguishment by water spray reveals some interesting data. Computational fluid dynamic modelling using radiation and surface heat transfer provides a good representation of measured temperatures.

The relatively good agreement with experiments has shown that the model reproduces the water spray fire interaction with considerable accuracy. However, to predict fire extinguishment phenomenon more accurately, a computer model which accounts for effect of radiation on the droplets and spray interaction with the surface of the compartment should be developed.

This success increases confidence in the use of this CFD package for further simulation to reveal essential information about the ability of a water spray system to mitigate a compartment jet fire. Testing such a system experimentally needs a lot of auxiliary equipment and delicate instruments with high accuracy, which increases the cost of the experiment. The CFD

technique was introduced and verified as an alternative option. Therefore, the CFD results bring some confidence in its use as a design tool to improve and extend previous knowledge about the mitigation of compartment jet fires.

The test programme has shown, for at least the scenarios investigated, the promise and potential capabilities of the water spray systems as a fire suppression system for compartment jet fires. There is however still much to be learned for proper system design, engineering and reliability.

10.2 RECOMMENDATIONS FOR FUTURE WORK

1. The resolution in data logging system is 4 seconds, and the best estimate of extinguishing time is 4 seconds. This time is considered large for the extinguishing time in which so much action could happen in this period. Therefore, a data logging system with finer resolution should be used for further study.

2. In the experiments, it has been observed that it is difficult to get parameters such as droplets size, water flow rate and spray angle independent from other parameters. Therefore, similar study but with parameters independent of one another should be used by providing the proper facility.

3. Further study should be made by investigating some other variations to the different parameters to investigate the effect of the heat release rate

on the characterisation of the spray system. Therefore, studying the effect of the spray characterisation based on these variables should give insight into the fire-spray interaction and could provide general engineering conclusions.

4. The jet nozzle location is a very important parameter which influences the size and strength of the combustion recirculation zone on the extinguishing effectiveness and quality. Therefore, further study which takes into account the jet nozzle locations would provide very valuable information.

5. Ventilation is a critical parameter which affects the stability and the combustion efficiency inside the compartment as well as the flow field of the combustion gases. Since this study kept the ventilation parameter as a constant, studying the effect of the ventilation on the extinguishing effectiveness would be very useful.

6. In this study, the amount of CPU time involved to simulate a time dependent case is clearly unacceptable. Very careful investigations for the time dependent model in CFD and further research which focuses on investigating time dependent cases is needed, in order to reduce this CPU time.

7. Studying the rate of evaporation and the distribution of water in the experiments will give insight into the effectiveness of the systems used. These can be investigated by placing many small cylindrical buckets on the compartment floor with weighing facility.

8. In this study reasonable agreement has been achieved between the experimental results and the steady state CFD model predicted results for fire conditions in an offshore compartment module. Further research focusing on validating the CFD time dependent model under realistic jet fire conditions is recommended.

9. Since the wind speed and direction will affect the behaviour of the jet fire, future research should take into account the wind speed and direction as a variable parameter in studying the mitigation of compartment jet fires.

REFERENCES

Angus Fire, (1991), "Thermospray medium velocity water spray nozzle", Product information sheet, No. 102/4/91.

ASTM E799-92, (1998), "Standard Practice for Determining Data Criteria and Processing for Liquid Drop Size Analysis", American Society For Testing And Materials.

Alpert, R.L. (1984) "Calculated Interaction of Sprays With Large-Scale Buoyant Flows", Transaction of the ASME, 106, 310-317.

Alpert, R. L., (1985),"Numerical modelling of the interaction between automatic sprinkler sprays and fire plumes" Fire Safety Journal, Vol. 9, pp157-163.

Bachalo, William D., (1980), "Method for measuring the size and velocity of spheres by dual-beam light-scatter interferometry", Applied Optics, Vol. 19, No. 3, pp. 363-370.

Back, G.G., (1996), "Full Scale test of water mist fire suppression systems for navy shipboard machinery spaces", INTERFLAM'96, Seventh international fire science and engineering conference, Cambridge, England 26-28 March 1996, pp 435-444.

Bayvel, L. and Orzechowski, Z., (1993), "Liquid Atomization", Taylor & Francis, ISBN 0-89116-959-8.

Bennet, J. F., Cowely, L. T., Davenport, J. N. and Rowson, J. J., (1991), "Large scale natural gas and LPG jet fires", Final Report to the CEC, Report TNER.91.022, Shell Research Ltd., Thorton Research Centre, Thorton, UK.

Berlemont, A., Grancher, M. and Gouesbet, G., (1991),"On the Lagrangian simulation of turbulence influence on droplet evaporation", Int. J. Heat Mass Transfer, Vol. 34, 2805-2812.

Beyler, C.L. (1997), "The Interaction of Fire and Sprinklers" Sponsored by US Department of Health Education and Welfare and National Institute of Standard and Technology, Gaithersburg, MD, USA, NBS-GCR-78-121.

Bill, R.G. (1993) "Numerical Simulation of Actual Delivered Density (ADD) Measurements", Fire Safety Journal, 20, pp. 227-240.

Bill, R.G. (1997) "Fine-Spray (Water Mist) Protection of Shipboard Engine Rooms", Fire Safety Journal, vol. 29, No. 4, pp 318-336.

Braidech, M. M., Neale, J. A., Matson, A. F. and Dufour, R. E., (1955), "The mechanism of extinguishment of fire by finely divided water", Underwriters Laboratories Inc. for the National Board of Fire Protection, N.Y., Research Report No. 10, pp 73.

Brightwell, H. M. and Chamberlain, G. A., (1997), "Large scale compartment fires: Experimental details and data obtained in test COMP15", Offshore Technology Report - OTO 95 012, Health and Safety Executive.

Burgoyne, J. H. and Richardson, J. F., (1949), "Extinguishing burning liquids by the application of non-inflammable gases and liquids", Fuel, Vol. 28, pp 150-158.

Butz, J. R. and Carey, R., (1992), "Application of fine water mists to fire suppression", Halon Alt. Tech. Conf., May 12-14, 1992.

CCP, (1994), " Guidelines for Evaluating the Characteristics of Vapor Cloud Explosion, Flash Fires and BLEVEs", Centre for Chemical Process Safety of the American Institute of Chemical Eng., American Institute of Chemical Engineers-AIchemE, First Edition, ISBN 0-8169-0474-X.

Chamberlain, G.A. (1994) "An Experimental Study of Large Scale Compartment Fires", Trans. I Chem E., 72 (B), pp 211-219.

Chigier, N., (1983), "Drop Size and Velocity Instrumentation", Prog. Energy Combust. Sci., Vol. 9, pp. 155-177.

Chow, W.K. and Fong, N.K. (1991) "Numerical Simulation on Colling of the Fire-Induced Air Flow by Sprinkler Water Sprays", Fire Safety Journal, **17**, 263-290.

Chow, W. K. and Fong, N. K., (1993), "Application of Field Modelling Technique to Simulate Interaction of Sprinkler and Fire-Induced Smoke Layer", Comb. Sci. and Tech., Vol. 89, pp. 101-151.

Coppalle, A., Nedelka, D. and Bauer, B., (1993), "Fire protection: water curtains", Fire Safety Journal, Vol. 20, pp 241-255.

Cote, Arthur E. and Linville, Jim L., (1991)," Fire Protection Handbook", National Fire Protection Association, Seventeenth Edition, ISBN 0-87765-378-X.

Cowley, L. T., (1992), " Behaviour of Oil and Gas Fires In the Presence of Confinement and Obstacles", Health and Safety Executive, Offshore Technology Information OTI 92 597, Second Edition.

Cox, G. and Kumar, S. (1987), "Field Modelling of Fire in Forced Ventilated Enclosures" Comb. Sci. and Tech., 52, pp 7-23.

Cox, Geoffrey, (1995), "Combustion fundamentals of fire", Academic Press, ISBN 0-12-194230-9, First edition.

David R. Lide, (1997), "CRC handbook of chemistry and physics", Boca Raton, London, 77th ed., ISBN 0849304776.

DiNenno, P., et. al., (1988), "The SFPE Handbook of Fire Protection Engineering" National Fire Protection Association and Society of Fire Protection Engineers, First Edition.

Downie, B., Polymeropoulos, C. and Gogos, G. (1995), "Interaction of water mist with a buoyant Methane diffusion flame" Fire Safety Journal, **24**, 359-381.

Drysdale, Dougal., (1985),"An introduction to fire dynamics", John Wiley and Sons ltd., First edition, ISBN 0471906131.

Fletcher, D.F., Kent, J. H., Apte, V. B. and Green, A. R., (1994), "Numerical Simulations of Smoke Movement from a Pool Fire in a Ventilated Tunnel", Fire Safety Journal, Vol. 23(3), pp. 305-325.

FLUENT Manual, (1996),"FLUENT user's guide ", Fluent Incorporated, Lebanon, USA.

Foster, P. J., (1999), "Private Communication".

Fthenakis, V. M., Schatz, K. W., Rohatig, U. S. and Zakkay, V., (1993),"Computation of flow fields induced by water spraying of an uniformed gaseous plume", ASME Trans. Heat Transfer, Vol. 115, pp. 742-750.

Galea, E. R. and Markatos, N. C., (1987), "A review of mathematical modelling of aircraft cabin fires", Applied Mathematical Modelling, Vol. 11, pp. 162-176.

Galea, E. R. and Markatos, N. C., (1989), "Forced and natural venting of aircraft cabin fires-A numerical simulation", 73rd symposium on aircraft fire safety, Portugal, May 1989, pp. 17-1 to 17-9.

Gameiro, V. M. (1995),"Fine Water Spray Fire Extinguishing System- A Viable Halon Alternative", NIST, R9500251, pp 71-84.

Hanauska, C. P. and Back, G.G. (1993),"Halon: Alternative Fire Protection Systems-An Overview of Water Mist Fire Suppression System Technology" International CFC and Halon Alternatives Conference Proceedings, October 20-22, 1993, Washington, DC, pp 820-829.

Heskestad, G., Kung, H. K. and Todtenkopf, N.F. (1976)"Air Entrainment Into Water Sprays and Spray Curtains", ASME 76-WA/FE-40.

Hinkley, P. L., (1986), "The effect of smoke/fire venting on the opening of sprinklers", Fire Safety Journal, Vol. 11, pp. 211.

Hinkley, P. L., (1989), "The effect of smoke venting on the operation of sprinklers subsequent to the first", Fire Safety Journal, Vol. 14, pp. 221.

Hoffmann, N.A. and Galea, E. R. and Markatos, N. C., (1989), "Mathematical Modelling of Fire Sprinkler systems", Applied Mathematical Modelling, Vol. 13, pp. 298-306.

Hoffman, Nicole Andrea, (1990), "Computer simulation of fire-sprinkler interaction", PhD Thesis, Centre of Numerical Modelling and Process Analysis, School of Mathematics, Statistics and computing, Thames Polytechnic, London.

Hoffmann, N. A. and Galea, E. R., (1991),"On the Eulerian-Eulerian approach to fire-sprinkler modelling", J. Fire Protect. Engng, Vol. 3, pp. 123-136.

Hoffmann, N.A. and Galea, E. R. (1993) "An Extension of the Fire-Field Modelling Technique to Include Fire Sprinkler Interaction--- **II.** The Simulations", Int. J. Heat Mass Transfere, **36(6)**, 1445-1457.

Hottel, H.C. and Hawthorne, W.R. (1949)"Diffusion in Laminar Flame Jets,"3rd Symp. on Comb. Flame and Explosions, pp.254-266.

ILO, (1990), " Major Hazard Control: a Practical Manual", International Labour Office, Second Edition, ISBN 92-2-106432-8.

Jackman, L. A., Nolan, P. F. and Morgan, H. P., (1992), " Characterization of Water Drops From Sprinkler Sprays", Proceedings of First International Conference on Fire Suppression Research, Brandforsk and Nist, Stockholm and Boras-Sweden, May 5-8, 1992.

Jackman, L. A., Glocking, J. L. D. and Nolan, P. F., (1993), "Water sprays: Characteristics and effectiveness" Halon Alternatives Technical Working Conference, May 11-13, 1993, pp 263-273.

Jones, W. P. and Whitelaw, J. H., (1992), "Calculation methods for reacting turbulent flows: a review", Combustion and Flame, Vol. 48, pp. 1-26.

Jones, A. and Thomas, G.O., (1993), "The Action of Water Sprays On Fires And Explosions: A Review of Experimental Work", Trans IChemE, Vol. 71, Part B, pp 41-49.

Jones, A. and Nolan, P., (1995) "Discussion on the Use of Fine Water Sprays or Mists for Fire Suppression", Journal of Loss Prevention in the Process Industries, 8 (1), pp 17-22.

Kerrison, L., Galea, E. R., Hoffman, N. and Patel, M. K., (1994 a), "A comparison of a FLOW3D based fire field model with experimental room fire data", Fire Safety Journal, Vol. 23, pp. 387.

Kerrison, L., Mawhinney, R. N., Galea, E. R., Hoffman, N. and Patel, M. K., (1994 b), "A comparison of two fire field model with experimental room fire data", Proc. Fourth Int. Symp. On Fire Safety Science, IAFSS, p. 13.

Kim, M. B., Jang, Y. J. and Yoon, M. O, (1997)," Extinction Limit of a Pool Fire With a Water Mist", Fire Safety Journal, Vol. 28, No. 4, pp 295-306.

Kumar, S., Gupta, A. K. and Cox, G., (1991), "Effects of Thermal Radiation on the Fluid Dynamics of Compartment Fires", Proc. Third Int. Symp. On Fire Safety Science, Elsevier, pp. 345.

Kung, H. K. (1977) "Cooling of Room Fires by Sprinkler Spray", Journal of Heat Transfer, 99, pp 353-359.

Ladouceur, H.D., Fleming, J.W. and Brown, E. F., (1996)," Fire Suppression By Water Mist--A Numerical Study", 1995 fall technical meeting, the eastern states section of the combustion institute, October 16-18, 1995.

Lapple, C.E. and Shepherd, C.B., (1940),"Calculation of Particle Trajectories", Industrial and Engineering Chemistry, 32, 5, May 1940, pp 605-617.

Lees, Frank P., (1991), " Loss Prevention in the Process Industries: Hazard Identification, Assessment and Control", two volume, Butterworth-Heinemann, ISBN 0-408-10697-2, First edition.

Lees, Frank P., (1996), " Loss Prevention in the Process Industries: Hazard Identification, Assessment and Control", two volume, Butterworth-Heinemann, ISBN 0-7506-1547-8, Second edition.

Lefebvre, Arthur H., (1989), "Atomization and Sprays", Hemisphere, ISBN 0 891 166 03.

Lev, Y. (1991) " Water Protection of Surfaces Exposed to Impinging LPG Jet Fires", J. Loss Prev. Process Ind., 4, pp 252-259.

Lewis, M.J, Moss, M.B. and Rubini, P.A. (1997)," CFD Modelling of Combustion and Heat Transfer In Compartment Fires" Fire Safety Science-Proceedings of the Fifth International Symposium, 2-5 March 1997, Australia.

Liu, Fengshan, (1990), "New development in pulverised coal combustion: Numerical modelling of radiative heat transfer and experimental test of a novel burner technique", PhD Thesis, University of Sheffield.

Log, T., (1996),"Radiant heat attenuation in fine water sprays", INTERFLAM'96. Seventh international fire science and engineering conference, Cambridge, England 26-28 March 1996, pp 425-434.

Magnussen, B. F., and Hjertager, B. H., (1976), "On Mathematical Models of Turbulent Combustion with Special Emphasis on Soot Formation and Combustion", 16th Symp. (Int.) on Combustion, Cambridge, MA, Aug. 15-20, 1976.

Markatos, N. C., Pericleous, K. A. and Cox, G. (1986), "Mathematical Modelling of buoyancy-Induced Smoke Flow in Enclosures", International Journal of Heat Transfer, 25 (1), pp 63-75.

Markatos, N. C., Pericleous, K. A. and Cox, G. (1986b), "A novel approach to the field modelling of fire", PCH PhysicoChemical Hydrodynamics, Vol. 7, No.2/3, pp 125-143.

Mawhinney, J. R., (1992) "Fine Water spray fire suppression project", First international conference on fire suppression research proceedings, Stockholm and Boars, Sweden, May 5-8, 1992, pp 109-128.

Mawhinney, J. R., (1993a) "Design of Water Mist Fire Suppression Systems for Shipboard Enclosures", International Conference On Water Mist Fire Suppression Systems Proceedings, Boras, Sweden, November 4-5, 1993, pp 19-44.

Mawhinney, J. R., (1993b) " Engineering Criteria for Water Mist Fire Suppression Systems", Water Mist Fire Suppression Workshop, National Institute of Standard and Technology, March 1-2, 1993, Gaithersburg, Maryland, pp 37-74.

Mawhinney, J. R., (1994a) "Water Mist Suppression Systems May Solve an Array of Fire Protection Problems " NFPA Journal, vol. 88, No. 1, pp 46-50.

Mawhinney, R. N., Galea, E. R., Hoffman, N. and Patel, M. K., (1994b), "A critical comparison of a PHOENICS based fire field model with experimental compartment fire data", J. Fire Prot. Engr., Vol. 4 (6), pp. 137.

Mawhinney, J. R., Dlugogorski, B.Z. and Kim, A.K., (1995), " A Closer Look at the Fire Extinguishing Properties of Water Mist", Fire Safety Science-Proceedings of the Fourth International Symposium, 2-5 March 1995, pp 47-60.

Mawhinney, J. R. and Richardson, J. K., (1996) " State-of-the art Review of Water Mist Fire Suppression Research and Development " NRC of Canada and Hughes Associates, internal Report.

Mawhinney, J. R, (1996),"The role of fire dynamics in design of water mist fire suppression systems" INTERFLAM'96. Seventh international fire science and engineering conference, Cambridge, England 26-28 March 1996.

Mawhinney, R. N., (1996), "Fire- Sprinkler spray interaction modelling using an Euler-Lagrange approach", INTERFLAM'96. Seventh international fire science and engineering conference, Cambridge, England 26-28 March 1996.

Mawhinney, J. R. and Richardson, J. K., (1997) " A Review of Water Mist Fire Suppression Research and Development "Fire Technology, Vol. 33, no. 1, First Quarter 1997, p. 54-90.

McAdams, W. H., (1954), "Heat Transmission", McGraw-Hill Publishing.

McCaffrey, B.J. (1984) "Jet Diffusion Flame Suppression Using Water Spray", Comb. Sci. and Tech., 40, 107.

McCaffrey, B.J. (1989) "Momentum Diffusion Flame Characteristics and the effect of Water Spray", Comb. Sci. and Tech., 63, pp 315-335.

Mehta, U. B., (1991), "Some Aspects of Uncertainty in Computational Fluid Dynamics Results" Transactions of the ASME-Journal of Fluids Engineering, Vol. 113, pp. 538-543.

Morgan, H. P., (1979), "Heat Transfer from a buoyant smoke layer beneath a ceiling to a sprinkler spray", Fire and Materials, Vol. 3, pp. 27-33.

Morsi, S. A. and Alexander, A. J., (1972), "An Investigation of Particle Trajectories in Two-Phase Flow Systems," J. Fluid Mech., Vol. 55, part 2, pp 193-208.

Mugele, R.A., and Evans, H.D., (1951),"Droplet Size Distribution in Sprays", Industrial and Engineering Chemistry, vol. 43, part 1, No. 6, pp1317-1324.

Mullikin, H.F., (1941), "Gas temperature Measurement and the high-velocity thermocouple", Temperature- Its Measurement and Control in Science and Industry; pp 775-804. (Reinhold, 1941).

Nam, S. (1993)" Numerical Simulation of Actual Delivered Density of Sprinkler Spray Through Fire Plumes", Fluid Mechanics and Heat Transfere in Sprays, ASME, 270, 57-65.

Nam, S., (1996), "Development of a computational model simulating the interaction between a fire plume and a sprinkler spray", Fire Safety Journal, Vol. 26, pp. 1-33.

Nam, S. (1999)" Numerical Simulation of the Penetraion Capability of Sprinkler Spray", Fire Safety Journal, Vol. 32 (4), pp. 307-329.

Nash, P., (1975),"The Essentials of Sprinkler and Other Water Spray Fire Protection Systems", Fire Prevention, 1975:108, pp 15 -26.

Ndubizu, C., Motevalli, V. and Tatem, P. (1996),"Study of the Suppression Mechanisms of Small Flames by Water Mist", Naval Research Laboratory.

NFPA, (1994), "National Fire Code-NFPA 15: Standard for water spray fixed systems for fire protection", National Fire Protection Association, USA.

NFPA, (1997), "National Fire Code-NFPA 750: Standard on the installation of water mist fire protection systems", National Fire Protection Association, USA.

Novozhilov, V., Fletcher, D. F., Moghtaderi, B. and Kent, J. H., (1996), "Numerical Simulation of Enclosed Gas Fire Extinguishment by a Water spray", J. Applied Fire Science, Vol. 5(2), pp. 135-146.

Orr, E., (1996), "The use of water mist as a fire and explosion suppressant", Heriot-Watt University, Edinburgh, thesis.

Ott, S., (1993), "Measurements of temperatures, radiation and heat transfer in natural gas flames, Final Report of the JIVE project, Risø-R-703(EN), Risø National Laboratory.

Patankar, S. V., (1980), "Numerical Heat Transfer and Fluid Flow", Hemisphere Publishing Corp., Washington, DC.

Perry, Robert H. and Green, Don, (1984), "Perry's Chemical Engineers' Handbook", McGraw Hill International, Sixth Edition.

Persaud, M.A., Chamberlain, G.A. and Cuinier, C., (1997), "A Model For Predicting the Hazards From Large Scale Compartment Jet Fires", Proceedings of the Hazards XIII, Manchester, 22-24 April 1997, pp 163-173.

Peters, N. and Williams, F. A., (1983), "Lift off characteristics of turbulent jet diffusion flames", AIAA, vol. 21, pp 423-429.

Phylaktou, R., (1996), "Fire and Explosion, Short course", University of Leeds, 25-29 September 1996.

Ranz, W. E., and Marshall, W. R., (1952), "Evaporation from Drops, Part I", Chem. Eng. Prog., Vol. 48 (3), pp 141-146.

Rasbash, D.J., Rogowski, Z.W, and Stark, G.W.V., (1956),"Properties of Fires of Liquids", Fuel, 35, 1956, pp 94-107.

Rasbash, D.J. and Rogowski, Z.W, (1957),"Extinction of Fires in Liquids by Cooling with Water Sprays", Combustion and Flame, 1(1957), pp 453-466.

Rasbash, D.J., et al, (1960), "Mechanisms of Extinction of Liquid Fires with Water Sprays", Combustion and Flame, 4(1960), pp 223-234.

Rasbash, D.J., (1961), "Heat transfer between water sprays and flames of freely burning fires", Proceedings of the symposium on the Interaction between fluids and particles, London, IchemE.20-22 June 1962.

Rasbash, D.J., (1964), "The Extinction of Fires by Water Sprays", Fire Research Abstract, 1964, 4(1), pp 28-53.

Rasbash, D.J., (1985), "The Extinction of fire with plain water: A review", Fire Safety Science- Proceedings of the first international symposium, 1985.

Ravigururajan, TS, and Beltran, MR, (1989), "A model for attenuation of fire radiation through water droplets", fire safety journal, 1989, vol.15, no.2, pp.171-181.

Rogers, G. F. C., (1921), "Thermodynamic and transport properties of fluids", 5th ed. (1995), Basil Blackwell, Oxford, ISBN 0631197036.

Shell Report, (1974), "Shell development of the Atkinson suction pyrometer", EMGR.0032.74.

Simcox, S., Wilkes, N. S. and Jones, I. P., (1989), "Computer simulation of the flows of hot gases from the fire at King's Cross Underground Station", I. Mech. E. Seminar:

The King's Cross Underground Fire: Fire Dynamics and Organisation of Safety, MEP Publishing, Leamington Spa, UK.

Sinnott, R. K., (1996), "Coulson & Richardson's Chemical Engineering: Chemical Engineering Design", Butterworth-Heinemann, Volume 6, second edition, ISBN 0-7506-2557-0.

SINTEF NBL, (1994), "Fine water spray system-extinguishing tests in medium and full scale turbine hood", Norwegian Fire Research Laboratory, STF25 A94036, December 1994.

Smithells, C. J., (1983), "Metals Reference Book", 5th edition, Butterworth-Heinemann, London, ISBN 0408710535.

Spalding, D. B., (1971), "Mixing and chemical reaction in steady, confined turbulent flames", 13th Symp. on combustion, The Combustion Institute, Pittsburgh, PA.

Swithenbank, J., Beer, J. M., Abbott, D., and McCreath, C. G., (1976), "A Laser Diagnostic Technique for the Measurement of Droplet and Particle Size Distribution", Paper 76-69, 14th Aerospace science Meeting, Washington, D. C., January 26-28, 1976, American Institute of Aeronautics and Astronautics.

Thomas, M., (1992), "UK Home Office Research Into Domestic Fire Fighting", First International Conference On Fire Suppression Research, Stockholm and Boars, Sweden, May 5-8, pp 283-289,

Tien, C.L., Lee, K. Y. and Stretton, A. J., (1988), "Radiation heat transfer" Chapter 1-5 in the SFPE Handbook of Fire Protection Engineering, National Fire Protection Association and Society of Fire Protection Engineers, First Edition.

Ural, E. A., and Bill Jr., R. G., (1995),"Fire Suppression Performance Testing of Water Mist Systems for Combustion Turbine Enclosures", *Proc. Halon Options, Technical Working Conf.*, University of New Mexico, NMERI, Albuquerque, NM, 9-11 May, 1995.

Vervalin, C. H., (1987), " Fire Protection Manual for Hydrocarbon Processing Plants", Volume one, Third Edition, Gulf Publishing Company, ISBN 0-87201-333-2.

Vervalin, C. H., (1987), " Fire Protection Manual for Hydrocarbon Processing Plants", Volume Two, Second Edition, Gulf Publishing Company. ISBN 0-87201-288-3.

Waters, R., (1986),"Air and smoke movement within a large enclosure", Numerical simulation of fluid flow and heat-mass transfer process, pp. 135-147.

Welty, J.R., Wicks, C.E. and Wilson, R.E., (1984)"Fundamentals of Momentum, Mass and Heat Transfer", 3rd ed., pp81, Wiley Press.

Wicks, P. J. and Cole, S. T., (1995),"European Research in Accidental Release Phenomena", International conference and workshop on modelling and mitigating the

consequences of accidental releases of hazardous materials, New Orleans, Louisiana, 26-29 September, 1995, ISBN 0816 906 602.

Wighus, R. (1991a) " Active Fire Protection-Extinguishment of Enclosed Gas Fires With Water Sprays", STF25 A91028.

Wighus, R. (1991b) " Extinguishment of Enclosed Gas Fires With Water Spray" Fire Safety Science-Proceedings of the Fifth International Symposium, Edinburgh, Scotland.

Wighus, R. (1992), "Fire Suppression Research in Norway", First international conference on fire suppression research proceedings, Stockholm and Boars, Sweden, May 5-8, 1992.

Wighus, R., Aune, R., Drangsholt, G. and Stensaas, J. P., (1993),"Full scale water mist experiments" *Proc. Int. conf. On Water Mist Fire Suppression Systems*, Swedish National Testing and Research Institute, Boras, Sweden, 4-5 November 1993.

Wighus, R. (1995) "Engineering Relations For Water Mist- Fire Suppression Systems" SINTEF, STF25 A95042.

Woodburn, P. J. and Britter, R. E., (1996 a), "CFD simulation of a tunnel fire-Part I", Fire Safety Journal, Vol. 26, pp. 35-62.

Woodburn, P. J. and Britter, R. E., (1996 b), "CFD simulation of a tunnel fire-Part II", Fire Safety Journal, Vol. 26, pp. 63-89.

Yang, Z., (1989), "Numerical simulation of incompressible and compressible flow", PhD thesis, University of Sheffield.

You, H. Z., Kung, H. C. and Han, Z., (1986), "Spray cooling in room fires", NIST, NBS-GCR-86-515.

Yuen, M.C., (1974)," Behavior of Water Droplets in Fire Plume", Conference for fires safety for buildings: Research practice needs, Airlie House, Airlie, Virginia, July 18-20, 1973.

APPENDIX I

Published papers:

1. Alageel, K., Ewan, BCR and Swithenbank, J. (1996), "Experimental and Modelling Studies of Compartment Jet fire Suppression Using Water Spray" 1996 Annual Conference on Fire Research, Building and Fire Research Laboratory, National Institute of Standard and Technology, NISTIR 5904,Gaithersburg, MD.

2. Alageel, K., Ewan, BCR and Swithenbank, J. (1998), "Numerical Modelling Studies of Compartment Jet fire Suppression Using Water Spray" 1998, IChemE Research Event, 7-8 April, NewCastle, England.

This was accepted for oral and poster presentation. The poster presentation won the overall first prize of the IChemE Resarch Event.

3. Alageel, K., Ewan, BCR and Swithenbank, J. (1998), "Mitigation of Compartment Jet fire Using Water Spray" 1998 Annual Conference on Fire Research, Building and Fire Research Laboratory, National Institute of Standard and Technology, NISTIR 6242, Gaithersburg, MD.

NUMERICAL MODELLING STUDIES OF A COMPARTMENT JET FIRE USING WATER SPRAY

K Alageel, BCR Ewan, J Swithenbank
Department of Chemical and Process Engineering, University of Sheffield, Mappin Street, Sheffield, S1 3JD

The research work presented here addresses the problem of the suppression of a compartment jet fire by water sprays. This involved studying the interaction between water spray and a turbulent jet flame inside a compartment of dimension 6×2.4×2.4 m. The fuel used for the jet fire was propane emerging from a 1.5 cm diameter vertical nozzle and at a mass flow rate of 0.1 kg/s. Using a CFD code with combustion, the time dependent behaviour of the droplet dynamics was studied as well as its effect on the fire's temperature, O_2 consumption and species concentration. The results obtained have a relevance to the design and operation of offshore modules. The study can be divided into two main stages. The first dealt with the modelling of the turbulent confined jet fire and the flow of the combustion gases produced within a compartment, whilst the second involved the introduction of the cold water droplets through different spray head arrangements for different parameters.

Results show that present CFD codes are able to make sensible predictions about the stratified nature of the flow during steady state burning and also predict the behaviour of temperature and species concentration during the extinguishment process on a time dependent basis.

Keywords: Compartment fire, Jet fire, Water spray, Fire extinguishment.

INTRODUCTION

The safe design and operation of process plants requires an ability to predict hazard consequences reliably. A particular hazard is a jet fire arising in a confined space such as may exist on offshore gas and oil production platforms or land based gas facilities, the particular concern being the capability of such fires to produce large amounts of soot and carbon monoxide.

Industries continue to seek efficient and cost-effective means of protecting their plants and personnel from the hazards of fires. Following disasters, which occurred in the past, the need for effective mitigation systems has, once again, been highlighted. Mitigation systems involving agents such as halons, which are perceived to be environmentally damaging, are currently out of favour and interest has revived in the use of water sprays.

The main objective of the study is to investigate the interaction of the water sprays with a jet fire in an underventilated (confined) space, using CFD. In order to achieve the above objective, it is necessary to produce a workable CFD model of a confined jet which is representative of conditions which might exist offshore.

For this purpose a compartment has been chosen since this represents a geometry which has been the subject of a number of experimental and analytical studies.

COMPARTMENT GEOMETRY AND OPERATING CONDITIONS

The compartment dimensions were those of a standard container being 6m in length by 2.4m high and 2.4m in width. In order to extend the computation space beyond the

Experimental and modelling studies of Compartment Jet Fire Suppression Using Water Spray

K. Alageel , BCR Ewan and J Swithenbank

Chemical Engineering and Fuel Technology

Mechanical and Process Engineering Department

University of Sheffield

Mappin Street

Sheffield, S1 3JD, UK

The safe design and operation of process plants requires an ability to predict hazard consequences reliably. A particular hazard is a jet fire that might arise from the ignition of an accidental release of pressurised gas or liquid. Mitigation systems involving agents such as Halon, which are perceived to be environmentally damaging, are currently out of favour and interest has revived in the use of water sprays.

The objective of this study is to assess the effect of fine water spray droplets on a propane jet fire which burns at 0.1 kg/s inside a compartment 6 m long, 2.5 m wide and 2 m high (fig.1). The total volume is 30 m^3 with reduced ventilation to simulate accidental fires in offshore modules. The vertical jet nozzle size is 1.5 cm. in diameter.

Mathematical modelling was done by using the computational fluid dynamics programme FLUENT. The modelling approach used divided the domain of interest (i.e. the compartment) into a number of discrete cells (25000) and the conservation equations was solved for each cell to obtain the field variables such as the fluid density, species concentrations, and temperature. The geometry was specified to be open at one end with induced ventilation arising from the jet entrainment.

In the initial stages of this study, the modelling of the development of the jet fire and the associated movement of combustion products within closed system of inter-connected compartment was carried out. This was followed by the development of the model for the dispersion of water spray droplets.

The simulation starts by first running the code without combustion to do the cold flow calculations in the compartment. Following that, the jet fire is ignited and the calculation was resumed until the dispersion of water spray is activated, the code tracks the flow of water droplets in the compartment and the interaction between the droplets in terms of mass, momentum and heat transfer. The water flow rates used in the studies were 0.05, 0.075,0.1, 0.15 or 0.2 kg/s in each time for different spray(s) locations.

For propane flame, fuel dilution due to water evaporation decreased the CO_2 and CO production rate and the O_2 depletion rate, figures 2-6. Less hydrocarbons were burned and the hydrocarbon percentage was observed to increase as the water application rate was increased with further increase in the water application rate, dilution effects become dominant and the flame gets extinguished.

The result shows that, for this study, oxygen depletion is not the main cause of extinguishment as there is still enough oxygen in the compartment to sustain the combustion.

The result of this work will be validated with experimental result.

MITIGATION OF COMPARTMENT JET FIRE USING WATER SPRAY

K Alageel, BCR Ewan, J Swithenbank
Department of Chemical and Process Engineering, University of Sheffield, Mappin Street, Sheffield, S1 3JD, UK

INTRODUCTION

The main objective of the study is to investigate the interaction of the water sprays with a jet fire in an underventilated (confined) space, using CFD. In order to achieve the above objective, it is necessary to produce a workable CFD model of a confined jet which is representative of conditions which might exist offshore.
For this purpose a compartment has been chosen since this represents a geometry which has been the subject of a number of experimental and analytical studies.

COMPARTMENT GEOMETRY AND OPERATING CONDITIONS

The compartment dimensions were those of a standard container being 6m in length by 2.4m high and 2.4m in width. In order to extend the computation space beyond the actual compartment, in the manner recommended for example by Markatos (1), the compartment was situated within a larger chamber, allowing the cells at the compartment opening to be live. This outer environment provided the source for combustion air and an outlet for all the gases to exit, without imposing restrictions to the flow into and out of the compartment.
Propane gas is injected into the compartment through a 1.5 cm diameter nozzle of length 25 cm situated on the floor of the compartment and at its centre. Air is provided from the outer environment chamber into the region of the compartment opening and at low velocity to enable the compartment to entrain as much as is required for combustion.
The propane gas jet entrains air into the compartment, and so the flow rate of air into the domain defined by the outer chamber needed to be several times the stoichiometric quantity needed for combustion. This outer air supply flow velocity was around 0.3m/s and the propane velocity at the jet nozzle was equal to 250 m/s.

TWO-PHASE MODELLING

In order to combat fire it is necessary to understand the nature of the interaction between the hot combustion products and the liquid water. Factors which need to be considered include water flow rate, spray pattern, droplet size and the number and location of spray heads.
It is important also to find out the maximum amount of water that can be discharged from an appropriate spray head in order not to flood the compartment and cause water damage.
The simulation started by studying the effects of a single spray located at different positions in the roof of the compartment. This will give a chance to better understand the fire-spray interaction and evaluate the best spray(s) location to be used to carry out a more detailed investigation. The total water flow rate for each of these arrangements was varied from 0.1 to 3.3 kg/s and the velocities of the droplets used varied between 5 and 25 m/s. The mean droplet diameters could be chosen within the range from 100 to 600 μm. Finally the spray angle used for each of the spray heads is represented by 5 injection directions with each direction having the possibility of an independently defined size and velocity range.
Three spray locations were examined. In the first, a single spray is located above the propane nozzle. The remaining two placed on the front/rear axis and 2.0m on each side of the centre.

RESULT AND DISCUSSION

Initially, the steady state behaviour of the compartment fire was evaluated and used as the starting condition for the subsequent two phase calculation. Prior to the spray activation, the fire plume was able to rise straight upwards and spread outwards along the ceiling. For the case of a single spray located above the propane jet and at a low flow rate less than 1 kg/s, two major flows were apparent after the solution fully developed. The first, generated by the water spray, was downwards whilst the second, generated by the fire, was along the ceiling. These two currents met towards the centre of the compartment, aiding the mixing and cooling process.
The value for temperature used in the calculations throughout this paper, is the average temperature from the upper two-third of the compartment. Because of the configuration of the inlet to the compartment, realistic values of temperature are only obtained above this cooler inlet region.
From the modelling of different spray locations, the results show that less water is needed to extinguish the flame in the case of a single spray located centrally above the jet nozzle. For most flow rate, this location also gave lowest temperatures as shown in Figure 4. Subsequent modelling therefore used a single spray located in the centre of the compartment above the jet nozzle.
Figure 1 shows the average temperature in the compartment as function of mean droplet diameter of 100, 200, 300, 400, 500 and 600 μm. The curve is nearly parabolic and the lowest temperature was found with mean droplet diameters of 300 μm. Subsequent modelling was therefore carried out using mean diameters of 300 μm. It is likely that the minimum arises from

Appendix II

FLUENT setup and input parameters

```
*-----------------------------------------------*I
I  LICENSED BY AND THE PROPERTY OF FLUENT INC., I
I-----------------------------------------------*I
I                                                I
I  FFFFF  L      U   U  EEEEE  N   N  TTTTT      I
I  F      L      U   U  E      NN  N    T        I
I  FFFF   L      U   U  EEEE   N N N    T        I
I  F      L      U   U  E      N  NN    T        I
I  F      LLLLL   UUU   EEEEE  N   N    T        I
I                                                I
I-----------------------------------------------I
I  OUTPUT PRODUCED BY VERSION  4.52              I
*-----------------------------------------------*I
```

```
************************************************************
*                                                          *
*           FLUENT (V4.52) Fluid Flow Modeling             *
*                                                          *
*     Copyright (C) 1984, 1989, 1991, 1995 by Fluent Inc.  *
*      All rights reserved.  Use of this code is subject   *
*       to the terms of the software license agreement.    *
*        Use, reproduction, or disclosure by the U.S.      *
*       Government is subject to restrictions set forth    *
*         in Government Contracts with Fluent Inc. as      *
*              governed by FAR 52.227.19(c)(2).            *
*                                                          *
*           FLUENT is a registered trademark of:           *
*                                                          *
*                        Fluent Inc.                       *
*                   Centerra Resource Park                 *
*                     10 Cavendish Court                   *
*                Lebanon, New Hampshire  03766  USA        *
*                        (800) 445-4454                    *
************************************************************
*     Number of Cells and Species Dynamically Allocated    *
************************************************************
```

- UNITS SYSTEM -

INDEX	PROPERTY	UNITS	S.I. CONVERSION FACTOR
1	DIMENSIONLESS	DIM	1.000E+00
2	MASS	KG	1.000E+00
3	LENGTH	M	1.000E+00
4	TIME	S	1.000E+00
5	VELOCITY	M/S	1.000E+00
6	FORCE	N	1.000E+00
7	ACCELERATION	M/S2	1.000E+00
8	ENERGY	J	1.000E+00
9	POWER	W	1.000E+00
10	MASS FLOW RATE	KG/S	1.000E+00
11	TEMPERATURE	K	1.000E+00
12	ENTHALPY	J/KG	1.000E+00
13	PRESSURE	PA	1.000E+00
14	DENSITY	KG/M3	1.000E+00
15	VISCOSITY	KG/M-S	1.000E+00
16	K.E. OF TURBLNCE	M2/S2	1.000E+00
17	K.E. DISS. RATE	M2/S3	1.000E+00
18	SPEC. HEAT CAP.	J/KG-K	1.000E+00
19	THERMAL CONDUCT.	W/M-K	1.000E+00
20	DIFFUSIVITY	M2/S	1.000E+00
21	ACTIVATION ENRGY	J/KMOL	1.000E+00
22	ANGLE	RAD	1.000E+00
23	HEAT FLUX	W/M2	1.000E+00
24	PARTICLE DIAM.	M	1.000E+00
25	MOMENTUM TR RATE	KG-M/S2	1.000E+00
26	HEAT TRANSF COEF	W/M2-K	1.000E+00
27	PERMEABILITY	M2	1.000E+00
28	(INTERNAL MISC.)	-	1.000E+00
29	VOLUME. FLOWRATE	M3/S	1.000E+00
30	AREA	M2	1.000E+00
31	ARRHENIUS FACTOR	CONSISTENT UNITS	1.000E+00
32	INERTIAL FACTOR	/M	1.000E+00
33	VOL. HEAT RATE	W/M3	1.000E+00
34	ABSORB./SCATTER.	/M	1.000E+00
35	ANGULAR VELOCITY	RAD/S	1.000E+00
36	MOL. SIZE PARM.	A	1.000E+00

37	PRESSURE GRAD.	PA/M	1.000E+00
38	VORTICITY	/S	1.000E+00
39	MUSHY ZONE CON.	KG/M3/S	1.000E+00
40	SURFACE TENSION	N/M	1.000E+00
41	SURF. TEN. GRAD.	N/M/K	1.000E+00
42	CONTACT RESIST.	M2-K/W	1.000E+00
43	VOLUME	M3	1.000E+00
44	NUCLEI CONC.	10^15/M3	1.000E+00
45	TORQUE	N-M	1.000E+00
46	SCALAR-1	UDS-1-DIM	1.000E+00
47	SCALAR-2	UDS-2-DIM	1.000E+00
48	SCALAR-3	UDS-3-DIM	1.000E+00
49	SCALAR-4	UDS-4-DIM	1.000E+00
50	SCALAR-5	UDS-5-DIM	1.000E+00
51	SCALAR-6	UDS-6-DIM	1.000E+00
52	SCALAR-7	UDS-7-DIM	1.000E+00
53	SCALAR-8	UDS-8-DIM	1.000E+00
54	SCALAR-9	UDS-9-DIM	1.000E+00
55	SCALAR-10	UDS-10-DIM	1.000E+00
56	SCALAR-11	UDS-11-DIM	1.000E+00
57	SCALAR-12	UDS-12-DIM	1.000E+00
58	SCALAR-13	UDS-13-DIM	1.000E+00
59	SCALAR-14	UDS-14-DIM	1.000E+00
60	SCALAR-15	UDS-15-DIM	1.000E+00
61	SCALAR-16	UDS-16-DIM	1.000E+00
62	SCALAR-17	UDS-17-DIM	1.000E+00
63	SCALAR-18	UDS-18-DIM	1.000E+00
64	SCALAR-19	UDS-19-DIM	1.000E+00
65	SCALAR-20	UDS-20-DIM	1.000E+00
66	SCALAR-21	UDS-21-DIM	1.000E+00
67	SCALAR-22	UDS-22-DIM	1.000E+00
68	SCALAR-23	UDS-23-DIM	1.000E+00
69	SCALAR-24	UDS-24-DIM	1.000E+00
70	SCALAR-25	UDS-25-DIM	1.000E+00
71	SCALAR-26	UDS-26-DIM	1.000E+00
72	SCALAR-27	UDS-27-DIM	1.000E+00
73	SCALAR-28	UDS-28-DIM	1.000E+00
74	SCALAR-29	UDS-29-DIM	1.000E+00
75	SCALAR-30	UDS-30-DIM	1.000E+00
76	SCALAR-31	UDS-31-DIM	1.000E+00

77	SCALAR-32	UDS-32-DIM	1.000E+00
78	SCALAR-33	UDS-33-DIM	1.000E+00
79	SCALAR-34	UDS-34-DIM	1.000E+00
80	SCALAR-35	UDS-35-DIM	1.000E+00
81	SCALAR-36	UDS-36-DIM	1.000E+00
82	SCALAR-37	UDS-37-DIM	1.000E+00
83	SCALAR-38	UDS-38-DIM	1.000E+00
84	SCALAR-39	UDS-39-DIM	1.000E+00
85	SCALAR-40	UDS-40-DIM	1.000E+00
86	SCALAR-41	UDS-41-DIM	1.000E+00
87	SCALAR-42	UDS-42-DIM	1.000E+00

- GEOMETRY -

RECTANGULAR CARTESIAN COORDINATES

NI = 80 NJ = 38 NK = 40

--- GRID GENERATION INPUTS ---

X-GRID SEGMENT INFORMATION

SEGMENT	START-POINT	LENGTH	# CELLS	WEIGHTING-FACTORS START-POINT	END-POINT
1	0.0000E+00	3.0000E+00	38	0.0000	12.5000
2	3.0000E+00	1.7700E-02	2	0.0000	0.0000
3	3.0177E+00	2.9973E+00	38	12.5000	0.0000

Y-GRID SEGMENT INFORMATION

SEGMENT	START-POINT	LENGTH	# CELLS	WEIGHTING-FACTORS START-POINT	END-POINT
1	0.0000E+00	2.4000E+00	36	5.0000	5.0000

Z-GRID SEGMENT INFORMATION

WEIGHTING-FACTORS

SEGMENT	START-POINT	LENGTH	# CELLS	START-POINT	END-POINT
1	0.0000E+00	1.2000E+00	18	0.0000	8.8900
2	1.2000E+00	1.7700E-02	2	0.0000	0.0000
3	1.2177E+00	1.1973E+00	18	8.8900	0.0000

- CHEMICAL SPECIES DEFINITIONS -

TOTAL NUMBER OF CHEMICAL SPECIES = 5
NUMBER OF GAS PHASE SPECIES = 5
NUMBER OF SURFACE SPECIES = 0
NUMBER OF SPECIES EQUATIONS SOLVED = 4

SPECIES NUMBER	SPECIES NAME	SPECIES TYPE
1	C3H8	GAS PHASE
2	O2	GAS PHASE
3	CO2	GAS PHASE
4	H2O	GAS PHASE
5	N2	GAS PHASE - (NOT SOLVED)

- REACTION STOICHIOMETRY DEFINITION -

SPECIES NAME	REACTION NO. 1
C3H8	1.000E+00
O2	5.000E+00
CO2	-3.000E+00
H2O	-4.000E+00
N2	0.000E+00

- REACTION RATE CONSTANTS -

PARAMETER	REACTION NO. 1
TYPE	GAS PHASE
LAW	ARRH./MIX.
ARRHENIUS	
PRE-EXP.	1.000E+12
ACTIVATION	
ENERGY	1.000E+08
TEMP. EXP.	0.000E+00
CONSTANT-A	4.000E+00
CONSTANT-B	5.000E-01
SPEC. EXP.	
C3H8	1.000E+00
O2	1.000E+00

- MULTI-GRID PARAMETERS -

MAXIMUM NO. OF FINE GRID ITERATIONS: 30
MAXIMUM NO. OF ITERATIONS PER LEVEL: 500
COARSE GRID SPACING IN I-DIRECTION: 2
COARSE GRID SPACING IN J-DIRECTION: 2
COARSE GRID SPACING IN K-DIRECTION: 2
MONITOR MG SOLVER: NO
MAX.-MG-LEVEL: 4

- VELOCITY BOUNDARY CONDITIONS -

ZONE	U-VEL.	V-VEL.	W-VEL.	NORMAL
W1	0.00E+00	0.00E+00	0.00E+00	N/A
WJ	0.00E+00	0.00E+00	0.00E+00	N/A
IA	-1.05E+00	0.00E+00	0.00E+00	N/A
IJ	0.00E+00	1.93E+02	0.00E+00	N/A

- TURBULENCE BOUNDARY CONDITIONS -

- TWO EQUATION MODEL -

ZONE	TURB.-INTEN.	CHAR.-LENGTH
W1	SET	SET
WJ	SET	SET
IA	1.000E+01	6.000E-01
IJ	1.000E+01	1.500E-02

- CHEMICAL SPECIES BOUNDARY CONDITIONS -

ZONE	C3H8	O2	CO2	H2O
W1	LINK CUT	LINK CUT	LINK CUT	LINK CUT
WJ	LINK CUT	LINK CUT	LINK CUT	LINK CUT
IA	0.00E+00	2.30E-01	0.00E+00	0.00E+00
IJ	1.00E+00	0.00E+00	0.00E+00	0.00E+00

- TEMPERATURE BOUNDARY CONDITIONS -

ZONE	TEMPERATURE
W1	EXT. RAD/H-T
WJ	HEAT FLUX
IA	2.9800E+02
IJ	2.9800E+02

- SPECIAL TEMPERATURE BOUNDARIES -

ZONE	HEAT FLUX BOUNDARY	HEAT FLUX VALUE	EXT. H-T BOUNDARY	EXTERNAL HEAT TRANSFER COEFF.	EXT. TEMP.
W1	N	N/A	Y	1.0000E+01	2.9500E+02
WJ	Y	0.0000E+00	N	N/A	N/A

EXT. RAD

ZONE	BOUNDARY	T-INFINITY	EXT. EMISS.
W1	Y	2.9500E+02	8.0000E-01
WJ	N	N/A	N/A

- BODY FORCE -

IMPROVED TREATMENT OF BODY FORCE IN DISCRETE EQNS.- YES
INCLUDE BODY FORCE TERMS IN VELOCITY INTERPOLATION- YES

GRAVITATIONAL ACCELERATIONS :

X = 0.000E+00
Y =-9.810E+00
Z = 0.000E+00

REFERENCE DENSITY LOCATION :

I = 2
J = 2
K = 2

- TURBULENCE MODEL CONSTANTS -

C1 = 1.440E+00
C2 = 1.920E+00
CMU = 9.000E-02

- WALL FUNCTION TURBULENCE MODEL CONSTANTS -

WALL ZONE	CAPPA	ELOG
W1	4.187E-01	9.793E+00
WJ	4.187E-01	9.793E+00

- ZONAL EMISSIVITIES (RADIATION MODEL) -

ZONE	EMISSIVITY

W1	8.0000E-01
WJ	8.0000E-01
O	1.0000E+00
IA	1.0000E+00
IJ	1.0000E+00

- ZONAL RADIATION BOUNDARY TEMPERATURE CORRECTION -

ZONE	CORRECTION
O	2.0000E-01
IA	1.0000E+00
IJ	1.0000E+00

- DISCRETE TRANSFER RADIATION MODEL CONSTANTS -

CARBON DIOXIDE SPECIES = CO2
WATER VAPOR SPECIES = H2O
WEIGHTED SUM OF GRAY GASES MODEL
COMPUTED MEAN BEAM LENGTH = 1.805E+00
NUMBER OF RADIATING SURFACES= 3582
NUMBER OF RAYS IN THETA = 6
NUMBER OF RAYS IN PHI = 6

- USER DEFINED PHYSICAL MODELS -

DRAG ON PARTICLES - NO

- USER DEFINED PROPERTIES -

FLUID VISCOSITY - NO
FLUID DENSITY - NO
FLUID SPECIFIC HEAT - NO
FLUID THERMAL CONDUCTIVITY - NO

```
 TURBULENT VISCOSITY          - NO
 ABSORBTION COEFFICIENT       - NO
 SCATTERING COEFFICIENT       - NO

- USER DEFINED SOURCE TERMS -

 X-MOMENTUM EQUATION              - NO
 Y-MOMENTUM EQUATION              - NO
 Z-MOMENTUM EQUATION              - NO
 PRESSURE CORRECTION EQUATION     - NO
 TURBULENT K.E. EQUATION          - NO
 TURB. K.E. DISSIPATION EQUATION  - NO
 ENTHALPY EQUATION                - NO
 SPECIES EQUATIONS                - NO

- USER STARTUP SUBROUTINE IS NOT ACTIVE -

- USER DEFINED REAL VARIABLES -

       USPAR1 =  0.00000E+00          USPAR2 =  0.00000E+00
       USPAR3 =  0.00000E+00          USPAR4 =  0.00000E+00
       USPAR5 =  0.00000E+00          USPAR6 =  0.00000E+00
       USPAR7 =  0.00000E+00          USPAR8 =  0.00000E+00
       USPAR9 =  0.00000E+00          USPA10 =  0.00000E+00
       USPA11 =  0.00000E+00          USPA12 =  0.00000E+00
       USPA13 =  0.00000E+00          USPA14 =  0.00000E+00
       USPA15 =  0.00000E+00          USPA16 =  0.00000E+00
       USPA17 =  0.00000E+00          USPA18 =  0.00000E+00
       USPA19 =  0.00000E+00          USPA20 =  0.00000E+00

- USER DEFINED INTEGER VARIABLES -

       IUFLG1 =        0              IUFLG2 =        0
```

```
          IUFLG3 =        0                IUFLG4 =        0
          IUFLG5 =        0                IUFLG6 =        0
          IUFLG7 =        0                IUFLG8 =        0
          IUFLG9 =        0                IUFL10 =        0
          IUFL11 =        0                IUFL12 =        0
          IUFL13 =        0                IUFL14 =        0
          IUFL15 =        0                IUFL16 =        0
          IUFL17 =        0                IUFL18 =        0
          IUFL19 =        0                IUFL20 =        0

 - PROPERTY CALCULATION OPTIONS -

   COMPOSITION DEPENDENT VISCOSITY                        -  NO
   COMPOSITION DEPENDENT THERMAL CONDUCTIVITY              -  NO
   COMPOSITION DEPENDENT SPECIFIC HEAT                    - YES
   ANY PROPERTY COMPUTED USING KINETIC THEORY              -  NO
   ENABLE USER SPECIFIED MIXING LAWS                      -  NO

- DENSITY IS COMPUTED FROM THE IDEAL GAS LAW
- THE OPERATING PRESSURE = 1.0132E+05

- SPECIES MOLECULAR WEIGHTS -

   SPECIES        MOLECULAR
    NAME           WEIGHT
----------     ------------
C3H8             4.4000E+01
O2               3.2000E+01
CO2              4.4000E+01
H2O              1.8000E+01
N2               2.8970E+01

- MIXTURE VISCOSITY DEFINITION -

 - VISCOSITY DEFINITION
```

```
VISCOSITY   =   1.720E-05
 - SPECIFIC HEAT DEFINITION FOR C3H8
    CP       = - 4.195E+00 + 6.442E+00*T**1 - 2.800E-03*T**2 + 5.000E-07*T**3
 - SPECIFIC HEAT DEFINITION FOR O2
    CP       =   6.924E+02 + 4.647E-01*T**1 - 1.000E-04*T**2 + 1.000E-08*T**3
 - SPECIFIC HEAT DEFINITION FOR CO2
    CP       =   5.613E+02 + 8.064E-01*T**1 - 2.000E-04*T**2 + 2.000E-08*T**3
 - SPECIFIC HEAT DEFINITION FOR H2O
    CP       =   1.276E+03 + 1.294E+00*T**1 - 3.000E-04*T**2 + 2.000E-08*T**3
 - SPECIFIC HEAT DEFINITION FOR N2
    CP       =   7.688E+02 + 5.050E-01*T**1 - 1.000E-04*T**2 + 1.000E-08*T**3
   ENTHALPY REFERENCE TEMPERATURE =   2.9800E+02

     MIXING RULE FOR SPECIFIC HEAT
     IS MASS FRACTION WEIGHTED

- MIXTURE THERMAL CONDUCTIVITY DEFINITION -

    - THERMAL CONDUCTIVITY DEFINITION

        K       =   2.500E-02

   - FORMATION ENTHALPY INFORMATION -

     SPECIES        FORMATION        REFERENCE
      NAME          ENTHALPY        TEMPERATURE
   ----------    ------------     ------------
       C3H8       -1.0390E+08       2.9815E+02
```

O2	0.0000E+00	2.9815E+02
CO2	-3.9370E+08	2.9815E+02
H2O	-2.4190E+08	2.9815E+02
N2	0.0000E+00	2.9815E+02

- BINARY DIFFUSION COEFFICIENT DEFINITION -

BINARY DIFFUSION COEFFICIENT FOR C3H8 IN THE MIXTURE :

DIJ = 2.880E-05

BINARY DIFFUSION COEFFICIENT FOR O2 IN THE MIXTURE :

DIJ = 2.880E-05

BINARY DIFFUSION COEFFICIENT FOR CO2 IN THE MIXTURE :

DIJ = 2.880E-05

BINARY DIFFUSION COEFFICIENT FOR H2O IN THE MIXTURE :

DIJ = 2.880E-05

- SECOND PHASE SOLUTION CONTROL PARAMETERS -

MAXIMUM NUMBER OF STEPS	- 5000
STEP LENGTH FACTOR	- 2.000E+01
COEFFICIENT OF RESTITUTION FUNCTION OF ANGLE	- NO
COEFFICIENT OF RESTITUTION	- 1.000E+00
NUMBER OF WALL REFLECTIONS ALLOWED PER CELL	- 25
SELECT RUNGA-KUTTA METHOD	- NO
SELECT DETAILED TRACKING REPORT	- NO
SELECT STEP-BY-STEP TRACKING REPORT	- NO
ALLOW INJECTIONS TO HAVE DIFFERENT PROPERTIES	- NO
SECOND PHASE SAMPLING PROBE ENABLED	- NO
THERMOPHORESIS FORCE ENABLED	- NO

PARTICLE TRACKING TAKES PLACE EACH 5 ITERATIONS

MEAN PATH USED FOR PARTICLE TRACKING

- PARTICLE/DROPLET BOUNDARY CONDITIONS -

ZONE	BOUNDARY CONDITION
W1	ESCAPE
WJ	ESCAPE
O	ESCAPE
IA	ESCAPE
IJ	ESCAPE

- PARTICLE LAWS ACTIVATED FOR USER-DEFINED HISTORY -

INERT	- YES
VAPORIZE	- NO
BOILING	- NO
DEVOLAT	- NO
BURNOUT	- NO
INERT (LAW 6)	- YES
USER LAW 7	- NO
USER LAW 8	- NO
USER LAW 9	- NO
USER LAW 10	- NO

- SECOND PHASE PARTICLE/DROPLET PROPERTIES -

PARTICLE DENSITY	= 1.000E+03
BOILING POINT	= 3.730E+02
LATENT HEAT OF VAPORIZATION	= 2.250E+06
VAPORIZATION TEMPERATURE	= 3.000E+02
FRACTION VOLATILE COMPONENT	= 1.000E+00
HEAT OF PYROLYSIS	= 0.000E+00

- TEMPERATURE DEPENDENT PROPERTIES -

- SPECIFIC HEAT

CP = 4.180E+03

- THERMAL CONDUCTIVITY

K = 7.800E-02

- BINARY DIFFUSION COEFFICIENT

DIJ = 2.600E-05

- VAPOR PRESSURE

T	VAP. PRESS.
2.5600E+02	1.3300E+02
2.7500E+02	7.0605E+02
2.8500E+02	1.4027E+03
2.9600E+02	2.8100E+03
3.0700E+02	5.3220E+03
3.1500E+02	8.2050E+03
3.2500E+02	1.3623E+04
3.4000E+02	2.7347E+04
3.5600E+02	5.3428E+04
3.7300E+02	1.0132E+05

EVAPORATING/BOILING SPECIES = H2O

- SECOND PHASE INITIAL CONDITIONS -

INJECT		INITIAL VALUES								
NO	TYPE	(X)	(Y)	(Z)	(U)	(V)	(W)	(T)	(DIAM)	(MFLOW)

1	DROPLET	3.018E+00	2.350E+00	1.218E+00	1.930E+01	-5.200E+00	0.000E+00	2.980E+02	1.000E-04	7.247E-02
2	DROPLET	3.018E+00	2.350E+00	1.218E+00	1.930E+01	-5.200E+00	0.000E+00	2.980E+02	3.250E-04	1.236E-01
3	DROPLET	3.018E+00	2.350E+00	1.218E+00	1.930E+01	-5.200E+00	0.000E+00	2.980E+02	5.500E-04	4.012E-02
4	DROPLET	3.018E+00	2.350E+00	1.218E+00	1.930E+01	-5.200E+00	0.000E+00	2.980E+02	7.750E-04	3.706E-03
5	DROPLET	3.018E+00	2.350E+00	1.218E+00	1.930E+01	-5.200E+00	0.000E+00	2.980E+02	1.000E-03	1.006E-04
6	DROPLET	3.018E+00	2.350E+00	1.218E+00	5.970E+00	-5.200E+00	1.834E+01	2.980E+02	1.000E-04	7.247E-02
7	DROPLET	3.018E+00	2.350E+00	1.218E+00	5.970E+00	-5.200E+00	1.834E+01	2.980E+02	3.250E-04	1.236E-01
8	DROPLET	3.018E+00	2.350E+00	1.218E+00	5.970E+00	-5.200E+00	1.834E+01	2.980E+02	5.500E-04	4.012E-02
9	DROPLET	3.018E+00	2.350E+00	1.218E+00	5.970E+00	-5.200E+00	1.834E+01	2.980E+02	7.750E-04	3.706E-03
10	DROPLET	3.018E+00	2.350E+00	1.218E+00	5.970E+00	-5.200E+00	1.834E+01	2.980E+02	1.000E-03	1.006E-04
11	DROPLET	3.018E+00	2.350E+00	1.218E+00	-1.563E+01	-5.200E+00	1.140E+01	2.980E+02	1.000E-04	7.247E-02
12	DROPLET	3.018E+00	2.350E+00	1.218E+00	-1.563E+01	-5.200E+00	1.140E+01	2.980E+02	3.250E-04	1.236E-01
13	DROPLET	3.018E+00	2.350E+00	1.218E+00	-1.563E+01	-5.200E+00	1.140E+01	2.980E+02	5.500E-04	4.012E-02
14	DROPLET	3.018E+00	2.350E+00	1.218E+00	-1.563E+01	-5.200E+00	1.140E+01	2.980E+02	7.750E-04	3.706E-03
15	DROPLET	3.018E+00	2.350E+00	1.218E+00	-1.563E+01	-5.200E+00	1.140E+01	2.980E+02	1.000E-03	1.006E-04
16	DROPLET	3.018E+00	2.350E+00	1.218E+00	-1.563E+01	-5.200E+00	-1.140E+01	2.980E+02	1.000E-04	7.247E-02
17	DROPLET	3.018E+00	2.350E+00	1.218E+00	-1.563E+01	-5.200E+00	-1.140E+01	2.980E+02	3.250E-04	1.236E-01
18	DROPLET	3.018E+00	2.350E+00	1.218E+00	-1.563E+01	-5.200E+00	-1.140E+01	2.980E+02	5.500E-04	4.012E-02
19	DROPLET	3.018E+00	2.350E+00	1.218E+00	-1.563E+01	-5.200E+00	-1.140E+01	2.980E+02	7.750E-04	3.706E-03
20	DROPLET	3.018E+00	2.350E+00	1.218E+00	-1.563E+01	-5.200E+00	-1.140E+01	2.980E+02	1.000E-03	1.006E-04

21	DROPLET	3.018E+00	2.350E+00	1.218E+00	5.970E+00	-5.200E+00	-1.830E+01	2.980E+02	1.000E-04	7.247E-02
22	DROPLET	3.018E+00	2.350E+00	1.218E+00	5.970E+00	-5.200E+00	-1.830E+01	2.980E+02	3.250E-04	1.236E-01
23	DROPLET	3.018E+00	2.350E+00	1.218E+00	5.970E+00	-5.200E+00	-1.830E+01	2.980E+02	5.500E-04	4.012E-02
24	DROPLET	3.018E+00	2.350E+00	1.218E+00	5.970E+00	-5.200E+00	-1.830E+01	2.980E+02	7.750E-04	3.706E-03
25	DROPLET	3.018E+00	2.350E+00	1.218E+00	5.970E+00	-5.200E+00	-1.830E+01	2.980E+02	1.000E-03	1.006E-04

- SOLUTION CONTROL PARAMETERS -

SOLVER MARCHING DIRECTION	- K-DIRECTION
SOLVER SWEEP DIRECTION	- I-DIRECTION
ALTERNATE SWEEP DIRECTION	- YES
SOLUTION METHOD	- SIMPLE
ALLOW PATCHING OF BOUNDARY VALUES	- NO
CONVERGENCE/DIVERGENCE CHECK ON	- YES
MINIMUM RESIDUAL SUM	- 1.000E-03
MINIMUM ENTHALPY RESIDUAL	- 1.000E-06
NORMALIZE RESIDUALS	- YES
CONTINUITY CHECK	- YES

- INTERPOLATION SCHEME ON CELL FACES -

FOR DENSITY	- UPWIND
FOR PRESSURE	- MOMENTUM WEIGHTED
FOR VELOCITY	- LINEAR
TEMPERATURE CHANGE LIMITER	- 1.000E+00
REYNOLDS STRESS TURBULENCE MODEL	- NO
RNG TURBULENCE MODEL	- NO
INCLUDE BUOYANCY TERMS IN TURB. MODEL	- NO
MONITOR SOLVER	- NO

```
      COMPRESSIBLE FLOW                          - NO
      SUPERSONIC INFLOW                          - NO
      SUPERSONIC OUTFLOW                         - NO
      FIX VARIABLE OPTION ENABLED                - NO
      SET PRESSURE REFERENCE LOCATION            - NO
      VISCOUS DISSIPATION                        - NO
      INCLUDE SPECIES DIFF. EFFECTS IN ENTH.     - NO

      DIFFERENCING SCHEME  - POWER LAW

      REFERENCE PRESSURE LOCATION :
        I =    2
        J =    2
        K =    2
```

VARIABLE	SOLVED	BLOCK CORRECT	NO. SWEEPS	UNDERRELAX 1	UNDERRELAX 2	RESIDUAL AT ***** ITERATIONS
PRESSURE	YES	NO	5	5.0000E-01	5.0000E-01	2.0408E-04
U-VELOCITY	YES	NO	1	2.0000E-01	2.0000E-01	9.4858E-06
V-VELOCITY	YES	NO	1	2.0000E-01	2.0000E-01	4.1064E-05
W-VELOCITY	YES	NO	1	2.0000E-01	2.0000E-01	8.7923E-06
TURB. K.E.	YES	NO	1	2.0000E-01	2.0000E-01	1.5791E-04
K.E. DISS.	YES	NO	1	2.0000E-01	2.0000E-01	5.1716E-04
ENTHALPY	YES	NO	1	2.0000E-01	2.0000E-01	1.2239E-05
C3H8	YES	NO	1	2.0000E-01	2.0000E-02	1.1373E-04
O2	YES	NO	1	2.0000E-01	2.0000E-02	3.5901E-05
CO2	YES	NO	1	2.0000E-01	2.0000E-02	2.2352E-05
H2O	YES	NO	1	2.0000E-01	2.0000E-02	1.1179E-05
PROPERTIES	YES	N/A	N/A	N/A	N/A	N/A
VISCOSITY	N/A	N/A	N/A	2.0000E-01	2.0000E-01	N/A
TEMPERATURE	N/A	N/A	N/A	3.0000E-01	3.0000E-01	N/A
RADIATION	YES	N/A	N/A	N/A	N/A	N/A
2ND PHASE	N/A	N/A	N/A	3.0000E-01	3.0000E-01	N/A

```
      RADIATION SOLVED EVERY   10 ITERATIONS

      MAXIMUM NUMBER OF DTRM ITERATIONS =     10
```

DTRM ITERATION TOLERANCE = 1.0000E-03

- TIME DEPENDENCE -

TIME STEP LENGTH (SECONDS)	= 1.0000E-01
MAXIMUM NUMBER OF ITERATIONS PER STEP	= 500
MINIMUM RESIDUAL SUM (TO TRIP STEP)	= 1.0000E-03
MINIMUM ENTHLAPY RESIDUAL (TO TRIP STEP)	= 1.0000E-06
AUTO SAVE	= YES
NUMBER OF TIME STEPS BETWEEN SAVES	= 5

Appendix III

FLUENT Residuals Report

```
                    ..........................NORMALIZED RESIDUALS.........................
 NITER      (P)       (U)       (V)       (W)       (E)       (D)       (H)      (SPECIES)
132993  7.172E-05 6.1E-06 7.4E-06 3.7E-06 8.4E-06 9.9E-06 7.1E-05 (S1)- 5.2E-04
132994  7.177E-05 6.1E-06 7.4E-06 3.7E-06 8.4E-06 9.9E-06 7.1E-05 (S2)- 3.5E-04
132995  7.206E-05 6.1E-06 7.4E-06 3.7E-06 8.4E-06 1.0E-05 7.1E-05 (S3)- 2.1E-04
132996  7.151E-05 6.1E-06 7.4E-06 3.7E-06 8.4E-06 1.0E-05 7.1E-05 (S4)- 2.1E-04
132997  7.152E-05 6.1E-06 7.4E-06 3.7E-06 8.5E-06 1.0E-05 7.1E-05 (S1)- 5.2E-04
132998  7.122E-05 6.1E-06 7.4E-06 3.7E-06 8.5E-06 1.0E-05 7.1E-05 (S2)- 3.5E-04
132999  7.109E-05 6.1E-06 7.4E-06 3.7E-06 8.5E-06 1.0E-05 7.1E-05 (S3)- 2.1E-04
133000  7.092E-05 6.1E-06 7.4E-06 3.7E-06 8.5E-06 1.0E-05 7.1E-05 (S4)- 2.1E-04
133001  7.106E-05 6.1E-06 7.4E-06 3.7E-06 8.5E-06 1.0E-05 7.1E-05 (S1)- 5.2E-04
133002  7.114E-05 6.1E-06 7.4E-06 3.7E-06 8.6E-06 1.0E-05 7.1E-05 (S2)- 3.5E-04
133003  7.078E-05 6.1E-06 7.4E-06 3.7E-06 8.6E-06 1.0E-05 7.1E-05 (S3)- 2.1E-04
133004  7.069E-05 6.1E-06 7.4E-06 3.7E-06 8.6E-06 1.0E-05 7.1E-05 (S4)- 2.1E-04
133005  7.051E-05 6.1E-06 7.4E-06 3.7E-06 8.6E-06 1.0E-05 7.1E-05 (S1)- 5.2E-04
133006  7.033E-05 6.1E-06 7.3E-06 3.7E-06 8.6E-06 1.0E-05 7.1E-05 (S2)- 3.5E-04
133007  7.049E-05 6.1E-06 7.3E-06 3.7E-06 8.6E-06 1.0E-05 7.1E-05 (S3)- 2.1E-04
133008  7.035E-05 6.1E-06 7.3E-06 3.7E-06 8.6E-06 1.1E-05 7.1E-05 (S4)- 2.1E-04
133009  7.029E-05 6.1E-06 7.3E-06 3.7E-06 8.7E-06 1.1E-05 7.1E-05 (S1)- 5.2E-04
133010  7.015E-05 6.1E-06 7.3E-06 3.7E-06 8.7E-06 1.1E-05 7.1E-05 (S2)- 3.5E-04
133011  7.015E-05 6.1E-06 7.3E-06 3.6E-06 8.7E-06 1.1E-05 7.1E-05 (S3)- 2.1E-04
133012  7.020E-05 6.1E-06 7.3E-06 3.6E-06 8.7E-06 1.1E-05 7.1E-05 (S4)- 2.1E-04
                    ..........................NORMALIZED RESIDUALS.........................
 NITER      (P)       (U)       (V)       (W)       (E)       (D)       (H)      (SPECIES)
133013  7.016E-05 6.1E-06 7.3E-06 3.6E-06 8.7E-06 1.1E-05 7.1E-05 (S1)- 5.2E-04

COMMANDS AVAILABLE FROM *MAIN*:
   READ-CASE-FILE                  READ-CASE-DATA
   READ-DATA-FILE                  EXPERT
   FORMATTED-FILES                 SETUP-1
   CALC-1                          PATCH
   SETUP-2                         LINE-PRINT
   VIEW-ALPHA                      WRITE-CASE-FILE
   WRITE-CASE-DATA                 WRITE-DATA-FILE
   WRITE-RADIATION-FILE            READ-RADIATION-FILE
   OPTIONS                         VIEW-GRAPHICS
   UNIVERSAL-FILE                  QUIT
   HELP
ENTER HELP (COMMAND) FOR MORE INFORMATION.
(*MAIN*)-
```